

Draft Final Report

**DETERMINE OPTIMUM DEPTHS OF DRILLED SHAFTS
SUBJECT TO COMBINED TORSION AND LATERAL
LOADS USING CENTRIFUGE TESTING**

UF Project No.: 4910450472312

WPI No.: 406300

Contract No.: BC-354, RPWO #9

Submitted to:

Mr. Richard Long

Research Center

Florida Department of Transportation

605 Suwannee Street, MS 30

Tallahassee, FL 32399-0450

(904) 488-8572

Mr. Peter Lai, PE

Florida Department of Transportation

605 Suwannee Street, MS 5L

Tallahassee, FL 32399

(904) 488-8911



**UNIVERSITY OF
FLORIDA**

Department of Civil and Coastal Engineering, College of Engineering

365 Weil Hall, P.O. Box 116580, Gainesville, FL 32611-6580

Tel: (352) 392-8697 SunCom: 622-8697 Fax: (352) 392-3394

April 2003

1. Report No. Draft Final Report		2. Government Accession No.		3. Recipient's Catalog No.	
4. Title and Subtitle Determine Optimum Depths of Drilled Shafts Subject to Combined Torsion and Lateral Loads Using Centrifuge Testing				5. Report Date April 2003	
				6. Performing Organization Code	
7. Author(s) M. C. McVay, R. Herrera and Z. Hu				8. Performing Organization Report No. 4910-4504-723-12	
9. Performing Organization Name and Address University of Florida Department of Civil and Coastal Engineering 365 Weil Hall / P.O. Box 116580 Gainesville, FL 32611-6580				10. Work Unit No. (TRAIS)	
				11. Contract or Grant No. BC354, RPWO #9	
12. Sponsoring Agency Name and Address Florida Department of Transportation Research Management Center 605 Suwannee Street, MS 30 Tallahassee, FL 32301-8064				13. Type of Report and Period Covered Draft Final Report September 22, 1999 – March 20, 2003	
				14. Sponsoring Agency Code	
15. Supplementary Notes Prepared in cooperation with the Federal Highway Administration					
16. Abstract <p>Eighty centrifuge tests were conducted on high mast sign/signal structures (mast arm, pole, drilled shaft). The foundations, drilled shafts, were constructed in dry and saturated sands under three different soil densities (loose, medium, and dense). Two different methods of construction were employed: casing and wet-hole (bentonite slurry). The foundations, cement grout with steel reinforcement, were installed and spun up in the centrifuge while still fluid, allowing the soil stresses around the shafts to equilibrate to field (prototype) values. The sign/signal structures were laterally loaded at three different points: 1) pole; 2) mid mast arm; and 3) mast arm tip. Loading on the pole applied no torque to the foundation, whereas loading on the mast arm applied increased values of torque.</p> <p>With loading on the pole (no torque: 30 tests), soil failure was observed for short shafts (length to diameter: L/D ratio < 5), whereas long shafts (L/D > 5) exhibited shaft failure (flexure). Broms predicted the long shafts lateral capacities well, but over predicted (un-conservative) the short shaft response. P-Y methods (Reese, et al.) with a nonlinear shaft representation, predicted both the short and long shaft response.</p> <p>For loading on the mast arm (i.e. lateral loading with torque), torsional resistance was predicted quite satisfactorily by axial skin friction models (FHWA, etc.). The torsional resistance was found independent of lateral load magnitude, as well as soil properties (i.e., sand density, strength, etc.). However, the lateral resistance of the shafts was found significantly affected by the applied torque on the foundation. General monographs on reduction of lateral resistance as a function of torque to lateral load ratio were developed.</p> <p>In the case of wet-hole construction with bentonite slurry, little if any influence on lateral or torsional response was found, if the slurry cake thickness was limited to 0.5 in prior to grouting. If the cake was allowed to thicken, reductions in torsional resistance by as much as fifty per cent were noted for thick cake (3.0 in).</p> <p>Finally, a Mathcad file was developed to predict both lateral and torsional capacities of high mast sign/signal pole structures.</p>					
17. Key Words Drilled shaft Torque and lateral loading Centrifuge testing Dry and saturated sands			18. Distribution Statement No restrictions. This document is available to the public through the National Technical Information Service, Springfield, VA, 22161		
19. Security Classif. (of this report) Unclassified		20. Security Classif. (of this page) Unclassified		21. No. of Pages 377	22. Price

TABLE OF CONTENTS

	<u>page</u>
LIST OF TABLES	v
LIST OF FIGURES	vi
CHAPTERS	
1 INTRODUCTION	1
1.1 General	1
1.2 Purpose and Scope	2
2 CURRENT HIGH MAST DESIGN	4
2.1 Physical Size of Pole, Mast Arm, and Embedment Depth.....	4
2.2 Analysis of High Mast Sign	6
2.2.1 Design of Laterally Loaded Shafts – No Torque	6
2.2.1.1 Broms’ method.....	7
2.2.1.2 P-Y method	11
2.2.2 Current Torsional Design Methods in the State of Florida – No Lateral Load.....	17
2.2.2.1 Structures Design Office Method	17
2.2.2.2 District 5 method	19
2.2.2.3 District 5 method–O’Neill & Hassan.....	20
2.2.2.4 District 7 method	22
2.2.3 Coupled Torsional and Lateral Loading.....	22
2.3 Experimental Model of Prototype.....	24
2.3.1 Length to Diameter Ratio	27
2.3.2 Pole and Mast Arm Dimensions and Loading.....	27
2.3.3 Definition of Failure for Single Mast Arm Traffic Signs.....	28
2.3.4 Florida Soils	28
3 TESTING EQUIPMENT.....	30
3.1 Centrifuge Background	30
3.1.1 Theory of Similitude	31
3.1.2 Slip Rings and Rotary Union.....	35
3.1.3 Omega Amplifier.....	38
3.2 Model Container and New Instrumentation Platform.....	38
3.3 Test Equipment	39
3.3.1 Linear Variable Differential Transformers.....	40
3.3.2 Load Cell	41
3.3.3 Pneumatic Cylinders.....	41
3.3.4 Data Acquisition System	41

3.3.5	Data Acquisition Software	42
4	CENTRIFUGE TESTING.....	44
4.1	Edgar Test Sand	44
4.2	Concrete Grout Mix	46
4.3	Drilled Shaft Foundation.....	47
4.4	Shafts Constructed in Dry Sands with a Casing	51
4.4.1	Dry Sand Placement in the Centrifuge.....	51
4.4.2	Testing Program: Parameters Varied	53
4.4.3	Testing Process.....	53
4.4.3.1	Model preparation.....	53
4.4.3.2	Testing of the model and data recorded.....	58
4.5	Shafts Constructed in Saturated Sand	59
4.5.1	Mineral Slurry and Cake Formation.....	59
4.5.2	Sand Placement, Saturation, and Wet-hole Shaft Construction.....	62
4.5.3	Testing Program: Parameters Varied	66
4.5.4	Influence of Slurry Cake on Capacity	66
5	TEST RESULTS	70
5.1	Introduction	70
5.2	Lateral Load on Pole with No Torsion.....	71
5.2.1	Measured Experimental Results.....	72
5.2.2	Predicted Lateral Result with No Torsion.....	73
5.3	Lateral Load with Torque	78
5.3.1	Measured Torque-Lateral Load Results	79
5.3.1.1	Influence of Length to Diameter Ratio	84
5.3.1.2	Influence of Soil Density on Torque-Lateral Tests ..	88
5.4	Combined L/D, Strength and Torque to Lateral Load Ratio	88
5.5	Comparison with Field Load Test and Current Design Methods	92
5.6	Proposed Design Guideline.....	95
6	EXPERIMENTAL RESULTS IN SATURATED SAND.....	105
6.1	Introduction	105
6.2	Lateral Loading at Top of Pole	106
6.3	Lateral Loading Along the Mast Arm.....	108
7	EXPERIMENTAL RESULTS IN SATURATED SAND.....	120
7.1	Introduction	120
7.2	Lateral Model for Drilled Shaft Subject to Torque.....	120
7.3	Mathcad File Overview	126
7.4	Mathcad Input Parameters	127
7.4.1	Drilled Shaft Properties	127
7.4.2	Loading Conditions	130

7.4.3	Cohesionless Soil Properties	130
7.4.4	Cohesive Soil Properties	131
7.5	Mathcad Drilled Shaft Moment Capacity	132
7.6	Mathcad Computational Procedures and Programming	133
7.6.1	Soil Property Array and Slices	133
7.6.2	Loading Condition Parameters	134
7.6.3	Cohesionless Soil Computations	135
7.6.4	Cohesive Soil Computations	135
7.6.5	Shear and Moment Equilibrium	136
7.6.6	Torque Modified Shear and Moment	138
7.6.7	Shear Forces Along Shaft Length	139
7.6.8	Torsional Capacity of the Shaft.....	139
7.7	Mathcad Output.....	140
7.7.1	Numerical Output	140
7.7.2	Graphical Output	141
8	CONCLUSIONS AND RECOMMENDATIONS	144
	REFERENCES	148
	APPENDICES	
A	Centrifuge Results on Dry Sand (Raw Data).....	A-1
B	Centrifuge Test on Dry Sand (Reduced Data).....	B-1

LIST OF TABLES

<u>Table</u>	<u>page</u>
2.1 Typical Dimensions of Single Mast Arm Traffic Signs.....	4
2.2 Constant Soil Modulus vs. Relative Density.....	12
2.3 SPT Blow Count vs. Constant Soil Modulus.....	13
3.1 Centrifuge Scaling Relationships.....	35
4.1 Determination of e_{max}	44
4.2 Determination of e_{min}	45
4.3 Average Unit Weight and Angle of Internal Friction.....	46
4.4 Sand Raining Device.....	52
4.5 Summary of Centrifuge Test Program.....	54
4.6 Centrifuge Tests in Saturated Sand with Wet-hole Construction.....	67
5.1 Lateral Load Data Statistical Analysis.....	72
5.2 Centrifuge Lateral Load Results and LPILE, FB-PIER, and Broms' Predictions.....	74
5.3 Torsional-Lateral Load Tests Statistical Analysis.....	80
5.4 Centrifuge Torque Results, FDOT and Tawfiq-Mtenga Predictions.....	94
5.5 Proposed Modifiers.....	99
6.1 Saturated Sand Unit Weights and Properties Tested.....	105
6.2 Measured and Predicted Ultimate Load on Pole.....	108
6.3 Measured and Predicted Lateral Load on Shafts in Saturated Sand.....	119
7.1 Summary of Ultimate Shear (kips) available at Top of Pole, Dry Sand.....	124
7.2 Measured and Predicted Ultimate Load on Pole, Saturated Sand.....	124
7.3 Summary of Ultimate Shear (kips).....	125

LIST OF FIGURES

<u>Figure</u>	<u>page</u>
2.1 Scanned Image of High Mast Sign Elevation Plan from FDOT Design Plans.....	5
2.2 Failure Modes for Free-Headed Piles: (a) Long Pile; (b) Short Pile.....	8
2.3 Short Free Head Piles in Cohesionless Soil: (a) Distribution of Deflections; (b) Soil Reactions; and (c) Bending Moment	9
2.4 Cohesionless Soil Ultimate Lateral Resistance – Long Pile	10
2.5 P-Y Curves for Static and Cyclic Loading of Sand.....	15
2.6 Blow Count vs. Friction Angle and Relative Density	16
2.7 k vs. Relative Density	16
2.8 Initial Drilled Shaft and Pole Models.....	25
2.9 Pole and Mast Arm Assembly Parts	26
3.1 The UF Geotechnical Centrifuge.....	31
3.2 Slip Rings, Rotary Union, and Connection Board	36
3.3 Solenoids	37
3.4 Plan View of New Instrumentation Platform in the Centrifuge	39
3.5 LVDTs, Load Cell, Sign Pole and Mast Arm	40
3.6 Data Acquisition Board	42
3.7 Output Screen from LabVIEW.....	43
4.1 Sieve Analysis Results	45
4.2 Concrete Compressive Strength Testing	47
4.3 Model of Typical Structure and Foundation ($L/D = 3$).....	48
4.4 Slotted Steel Cylinder with Spiral Reinforcement	49
4.5 Complete Model (arm, pole, shaft) After Testing	50
4.6 Sand Raining Device	52
4.7 Plastic Tube Insertion.....	55
4.8 Vacuuming Sand from Casing.....	56
4.9 Measuring Depth to Bottom of Shaft	56
4.10 Pouring the Grout	57
4.11 Traffic Light Model Placement	57
4.12 Insitu Slurry Viscosity Determination.....	60
4.13 Different Thicknesses of Slurry Cake: (a) the slurry cake after 15 min. of spinning; and (b) the slurry cake after 3 hours of spinning	61
4.14 Preparing the Saturated Dense Specimen.....	62
4.15 Inserting the Plastic Tube	63

4.16	Slurry Placed in Wet-hole Method of Construction	63
4.17	Process of Grouting the Slurry Filled Construction Hole	65
4.18	Placement of Model Pole, Mast Arm and Reinforcement.....	65
4.19	Comparison of Test Results Among Different Thicknesses of Slurry Cakes	69
5.1	Testing Set-up.....	71
5.2	Measured vs. FB-PIER for Medium Dense Sand.....	75
5.3	Measured vs. FB-PIER for Medium Loose Sand	76
5.4	Measured vs. FB-PIER Prediction for Loose Sand	77
5.5	Measured Resistance for 35-ft Embedded Shafts.....	81
5.6	Measured Resistance for 25-ft Embedded Shafts.....	82
5.7	Measured Lateral Resistance for 15-ft Embedded Shafts	83
5.8	Measured Lateral Resistance for 35-ft Embedded Shafts	85
5.9	Measured Lateral Resistance for 25-ft Embedded Shafts	86
5.10	Measured Lateral Resistance for 15-ft Embedded Shafts	87
5.11	Torque vs. Top of Foundation Rotation, Medium Dense Sand.....	89
5.12	Torque vs. Top of Foundation Rotation, Medium Loose Sand.....	90
5.13	Torque vs. Top of Foundation Rotation, Loose Sand	91
5.14	Schematic of Field Load Test.....	92
5.15	Loss of Capacity Graphs for Mid Mast Loading.....	96
5.16	Loss of Capacity Graphs for Arm Tip Loading.....	97
5.17	Percent Reduction in Lateral Load Capacity	98
5.18	Modifier Prediction vs. Centrifuge Results for Medium Dense Sand.....	100
5.19	Modifier Prediction vs. Centrifuge Results for Medium Loose Sand.....	101
5.20	Modifier Prediction vs. Centrifuge Results for Loose Sand	102
5.21	Loss of Capacity vs. Torque to Lateral Load Ratio	104
6.1	Loading Applied Top of Pole with No Torque	107
6.2	Embedment = 25 ft, Loose Sand, Load Applied Mid Mast Arm	109
6.3	Embedment = 25 ft, Loose Sand, Load Applied at Arm Tip	110
6.4	Embedment = 25 ft, Dense Sand, Load Applied Mid Mast Arm.....	111
6.5	Embedment = 25 ft, Dense Sand, Load Applied at Arm Tip	112
6.6	Embedment = 35 ft, Loose Sand, Load Applied Mid Mast Arm	113
6.7	Embedment = 35 ft, Loose Sand, Load Applied at Arm Tip	114
6.8	Embedment = 35 ft, Dense Sand, Load Applied Mid Mast Arm.....	115
6.9	Embedment = 35 ft, Dense Sand, Load Applied at Arm Tip	116
7.1	Proposed Soil Pressure Acting on Pile/Shaft	121
7.2	Mathcad File – A Portion of Input Data Layout with Problem Sketch.....	128

7.3	Mathcad File Drilled Shaft and Loading Conditions Input Parameters Sheet	129
7.4	Mathcad File View of Soil Properties Input Along with Sketch.....	131
7.5	Typical Subroutine Logic Used to Build Property Array, Results are Shown to the Right of the Subroutine.....	134
7.6	Subroutine Used to Determine Soil Type and Compute Ultimate Soil Resistance.....	137
7.7	Torque Modified Shear and Moment Computations.....	138
7.8	Mathcad Numerical Output Sheet	140
7.9	Graphical Output Plotting Layout Showing Soil/Shaft Shear Response Associated with Applied Torque.....	142
7.10	Graphical Output Plotting Layout Showing Ultimate Slice Forces Along Shaft Length Associated with Applied Torque	143

CHAPTER 1 INTRODUCTION

1.1 General

As a result of Hurricane Andrew, the Florida Department of Transportation (FDOT) has mandated that all structures designed from central Florida south must withstand one hundred and twenty mile per hour (mph) winds. In addition, all high mast lighting and sign structures within five miles of the coast must be supported with cantilever mast arms attached to poles connected to deep foundations (drilled shafts). However, due to the structure's shape (inverted L), significant lateral and torsional loads may develop on the foundation.

The current practice for the design of the drilled foundations is to treat the lateral and torsional load as separate, i.e., uncoupled. In the case of lateral resistance, either Brom's or a Winkler (i.e., p-y) approach is used to obtain the shaft's diameter and minimum cutoff elevation. Next, a torsional analysis of the foundation is performed (FDOT Structures Design Office, District 5, and District 7 methods: Chapter Two) to ensure that the cutoff elevation is sufficient to carry the torque. If not, the shaft length is increased to carry the design torque.

Recently, both experimental (Tawfiq, 2000) and analytical studies (Tawfiq, 2000; Duncan, 1997) have suggested that torque loads influence the shaft's lateral resistance. In the case of the Florida study (Tawfiq, 2000), three full-scale torsional load tests were conducted. One of the field tests did not fail (constructed with dry hole method), one

failed at a very low torque (wet hole with significant slurry cake), and the last failed at the expected torque. The latter study concluded that the current FDOT design methods were conservative (Tawfiq, 2000).

1.2 Purpose and Scope

Due to the significant lack of experimental data, the FDOT contracted with the University of Florida to conduct multiple centrifuge tests on drilled shafts subject to combined lateral and torsional loading (i.e., sign pole, etc.). The initial study was to vary the shafts embedment ratios (L/D), soil properties, and lateral load placement (i.e., torque/lateral load ratio) in dry sands using steel casings in construction. The latter tests were considered to be optimum, resulting in the highest lateral and torsional resistance with minimal influence of construction. A total of fifty-four centrifuge tests were performed under twenty-seven (2 repetitions) different conditions (load application, shaft length, soil density, etc.).

Subsequently, a supplement to the original work was implemented to study the influence of construction and water table. To characterize typical field installation, both mineral (bentonite) and polymer (KB) slurries were to be investigated. As noted in earlier field work (Tawfiq, 2000), torsional resistance of a drilled shaft was significantly impacted by the thickness of slurry cake during construction. Consequently, thirty-five additional centrifuge tests were performed studying the influence of shaft length, soil density, and load location under a variety of conditions in saturated sands.

Based on the experimental centrifuge database, the current FDOT design of drilled shafts subject to torque and lateral load was to be validated/modified. Since FDOT's current lateral design (Broms) required monographs (charts) to interpret between

short (soil failure) and long (pile failure) shafts, a Mathcad file was to be written to perform the analysis. In the case that Broms lateral or FDOT torsional capacity methods were changed/modified, then the Mathcad file was to be changed/modified such that it could subsequently be used for design.

CHAPTER 2
CURRENT HIGH MAST DESIGN

2.1 Physical Size of Pole, Mast Arm, and Embedment Depth

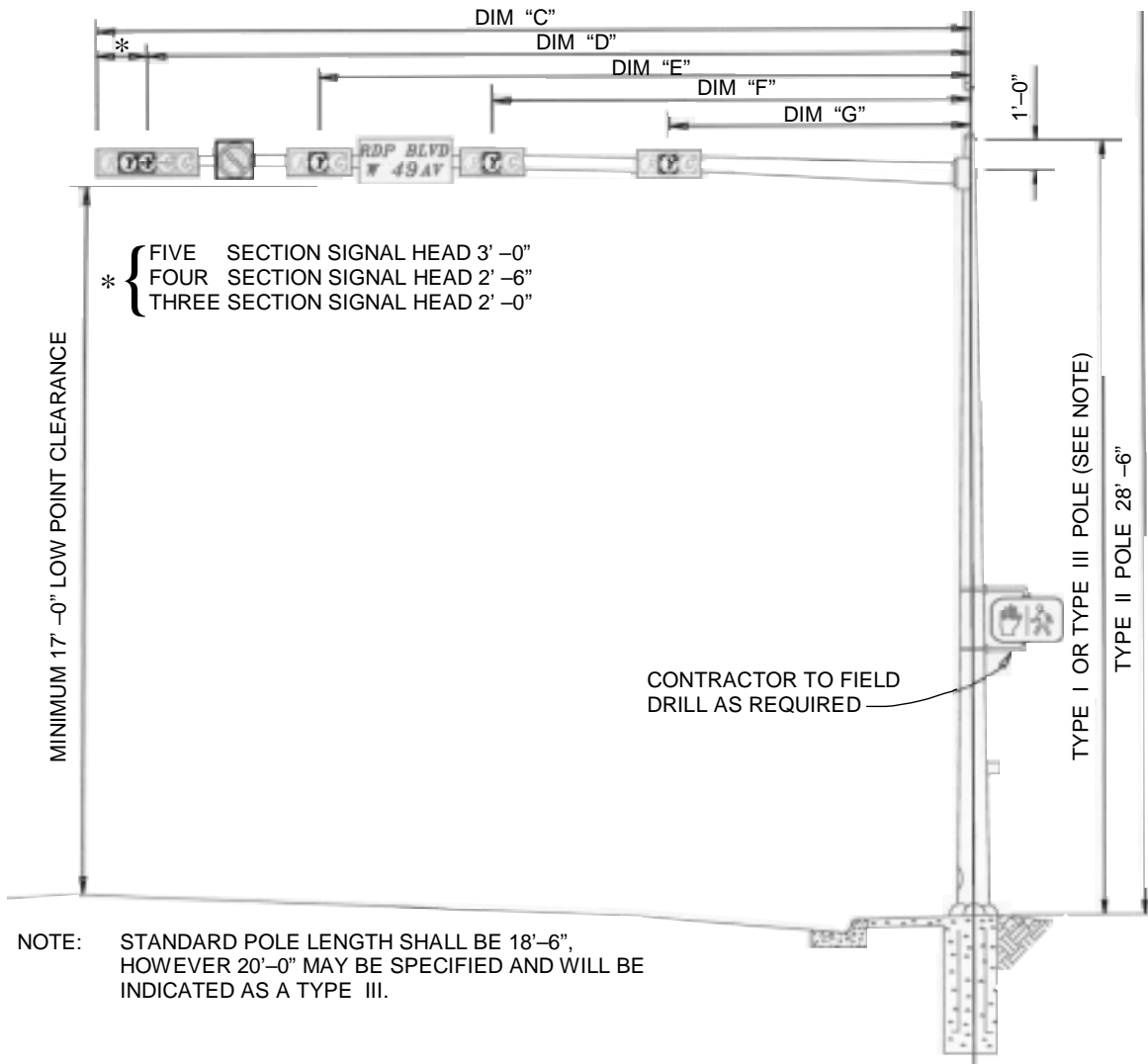
Typical dimensions of mast arms for traffic signs may vary from state to state and even from district to district within the same state. Table 2.1 shows some typical ranges in dimensions for single mast arm signs resting on drilled shaft foundations. The latter were obtained from construction plans provided by the Florida Department of Transportation Structures Design Office, and the Miami Dade County Public Works Office.

Table 2.1 Typical Dimensions of Single Mast Arm Traffic Signs

Pole Height (ft)		Mast Arm Length (ft)		Shaft Diameter (ft)		Shaft Embedment (ft)	
From	To	From	To	From	To	From	To
18	28.5	15	50	3	5	10	35

Figure 2.1 shows a typical pole, mast arm, and foundation (drilled shaft) with dimensions. Note that sizes (diameter, cross-section, etc.) vary depending on distance spanned and loading.

Since pole heights and mast arm lengths varied, it was decided to select a representative system and vary the load placement. For testing, a prototype structure with a pole height of 20 feet (ft) and a mast arm length of 30 ft was considered representative of high mast signs in the Central and North Florida areas.



TRAFFIC MAST ARM & ORIENTATION DETAIL

Figure 2.1 Scanned Image of High Mast Sign Elevation Plan from FDOT Design Plans.

Similarly, the foundation selected for modeling was a drilled shaft of 5 ft in diameter with embedment depths of 15, 25, and 35 ft. The foundation diameter may be considered on the high end of constructed shafts, but it was decided that failure of the larger systems could lead to significant damage and loss of life.

2.2 Analysis of High Mast Sign

As identified earlier, the analysis and design of a high mast sign involves both torsion and lateral forces acting on the foundation. The latter is an area where neither substantial research nor experimental field-testing has been performed. Moreover, it is not known whether the application of torsion decreases the lateral resistance of a drilled shaft or vice versa. Since current design (discussed in Section 2.3.2) treats lateral and torsional loading separate, a typical design does employ a high factor of safety due to uncertainty. A brief overview of lateral load design and torsional loading design of drilled shafts is presented, along with the combined method of Tawfiq-Mtenga (2000).

2.2.1 Design of Laterally Loaded Shafts – No Torque

One of the main advantages of using drilled shafts over pile foundations is their ability to withstand larger lateral loads due to their larger available diameters. They are used extensively as supports for bridge piers and abutments, as well as communication towers. However, their use is not limited to heavy structures. Due to their ease of installation, they typically support overhead sign structures, single and double mast-arm traffic lights, and even noise walls. Analysis of the lateral capacity of a foundation must be performed as part of its overall design. Reese and O'Neill (1999) present the following objectives for lateral load design:

- Determine the necessary penetration of the drilled shaft to carry the computed loads at the shaft head without undergoing excessive movement.
- Determine the necessary diameter, steel schedule and mechanical properties of the concrete to resist the bending moment, shear and axial

thrust that will be imposed on the drilled shaft by the lateral loads in combination with axial loads.

- Determine the deformations and/or stiffnesses of the drilled shaft in lateral translation and rotation in order to model the effects of foundation deformation on the performance of the structure.

Several methods are currently available to analyze drilled shafts under lateral loading, such as the “Equivalent Cantilever Method” (Davisson 1970), “Characteristic Load Method” (Duncan et al., 1994), which is based on a parametric analysis of numerous P-Y method solutions (O’Neill and Reese, 1999), and “Broms’ Method” (Broms, 1964a, 1964b, 1965). The latter method is commonly used because of its relative simplicity of analysis (an example of Broms’ method is presented below). In addition to Broms’ method, computer programs which employ P-Y methods or finite elements may be utilized to validate the simpler methods. Programs such as FB-PIER, or LPILE, can be used for such purposes. For complete coverage of lateral design refer to FHWA publication “Handbook on Design of Piles and Drilled Shafts under Lateral Load,” FHWA-IP-84-11, July, 1984.

2.2.1.1 Broms’ method. Broms (1964) introduced a simplified method for computing the lateral capacity of short pile/shafts in soils subject to lateral load alone (i.e., no torque). The ultimate lateral resistance is calculated assuming that failure takes place in either the soil (Fig. 2.2b) or with the formation of a plastic hinge within the pile/shaft (Fig. 2.2a).

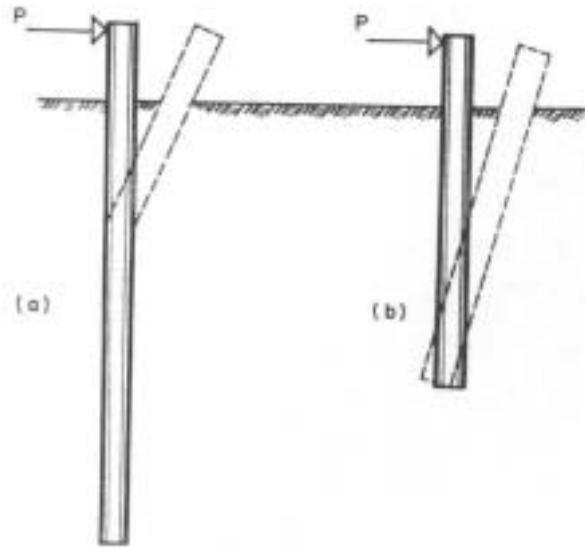


Figure 2.2 Failure Modes for Free-Headed Piles: (a) Long Pile; (b) Short Pile (Broms 1964).

In the case of the short pile, the assumed pressure distribution, Fig. 2.3b, acting on the pile/shaft in cohesionless soil is given by

$$Q = 3 D \gamma Z K_p \quad (\text{Eq. 2.1})$$

where D is the diameter of the pile/shaft, z is the depth below ground surface, γ is the unit weight, and K_p is the passive earth pressure coefficient. Note that the pressure distribution (Fig. 2.3b) in the vicinity of the pile/shaft bottom is simplified (i.e., no stress reversal) with the use of a large concentrated point load.

Based on moment equilibrium at the bottom of the shaft, the load P_{ult} may be computed as a function of soil properties and geometry. Broms gave the following solution:

$$P_{ult} = \frac{\gamma D L^3 K_p}{2 (e + L)} \quad (\text{Eq. 2.2})$$

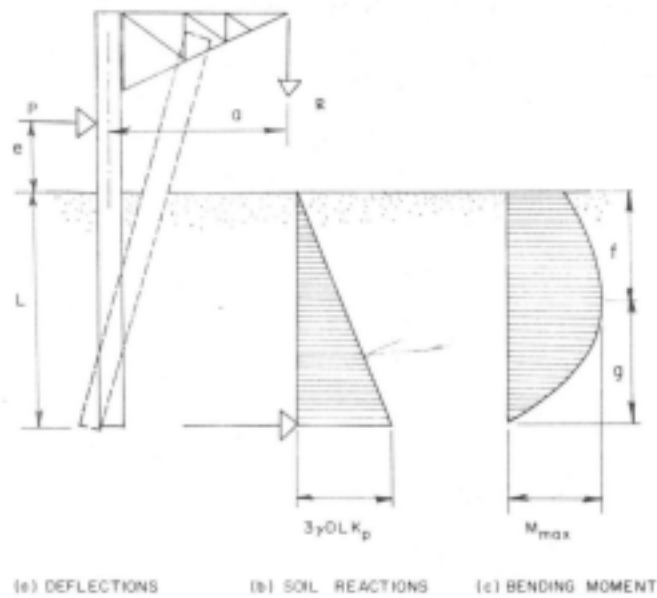


Figure 2.3 Short Free Head Piles in Cohesionless Soil: (a) Distribution of Deflections; (b) Soil Reactions; and (c) Bending Moment (after Broms, 1964).

The location of maximum moment (Fig. 2.3c), f , may be determined as:

$$f = \sqrt{\frac{L^3}{3(L+e)}} \quad (\text{Eq. 2.3})$$

Note that f is a function of the shaft's length and vertical load location, but is independent of soil properties.

In the case of longer shafts (Fig. 2.2a), the soil resistance increases, as well as the maximum moment in the shaft. At a sufficient embedment, the shaft's maximum moment capacity is reached, whereupon a plastic hinge (continued rotation with no increase in moment) forms (Fig. 2.2a). Assuming a linear increasing soil resistance (Eq. 2.1), Broms (1964) presented an implicit equation for P_{ult} (power function), as well as its solution (numerical) in a monograph (Figure 2.4).

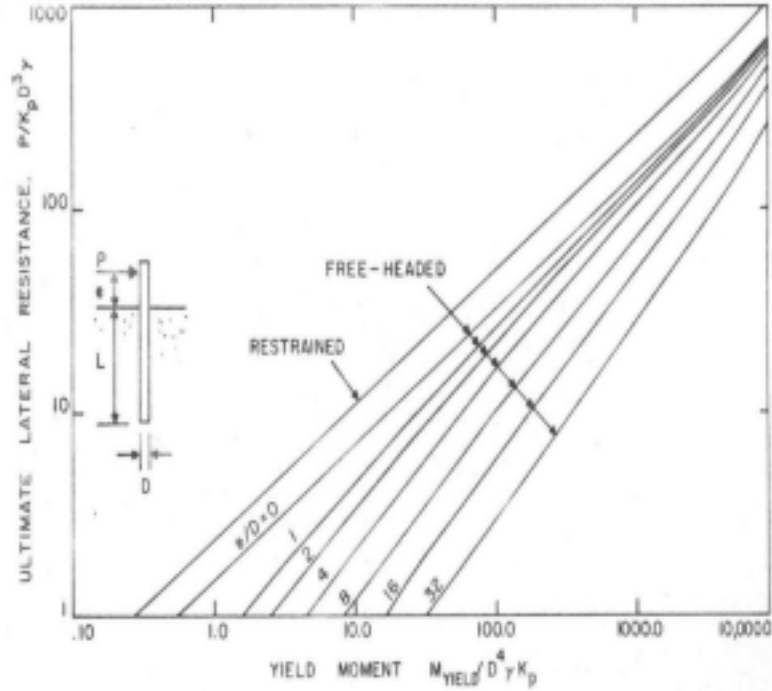


Figure 2.4 Cohesionless Soil Ultimate Lateral Resistance – Long Pile (Broms, 1964)

M_{yield} (Fig. 2.4) is the ultimate or yield moment of the pile/shaft's cross-section. For this work an analytical solution was obtained by first determining depth of plastic hinge, X_c as:

$$X_c = \frac{B}{2A} + \frac{1}{2}e^2 \frac{A}{B} - \frac{1}{2}e \quad (\text{Eq. 2.4a})$$

where:

$$A = \gamma D K_p \quad (\text{Eq. 2.4b})$$

$$B = \left[\left[4M - Ae^3 + 2\sqrt{-2M(-2M + Ae^3)} \right] A^2 \right]^{\frac{1}{3}} \quad (\text{Eq. 2.4c})$$

and M is the yield or ultimate moment of the cross-section, which for this study (5-ft diameter shaft) was approximately 10 m-MN (7300 ft-kips). Note, the depth of the ultimate moment, X_c , is dependent on soil properties (K_p , and γ), whereas for a short

pile, f , (Eq. 2.3) is not. The analytical expression for the ultimate force, P_{ult} , for a free head condition may be computed using Eq. 2.4a as:

$$P_{ult} = \frac{3}{2} \gamma D K_p X_c^2 \quad (\text{Eq. 2.5})$$

In terms of shaft/pile design, the user needs to select the lower P_{ult} value obtained from Eq. 2.2 or 2.5. In the case of short shafts, Eq. 2.2 will control, whereas, for long shafts, Eq. 2.5 will govern. The latter is evident from the influence of L on P_{ult} in Eq. 2.2, but its disappearance in both X_c (Eq. 2.4a) and P_{ult} (Eq. 2.5).

2.2.1.2 P-Y method. A P-Y curve represents the lateral resistance (soil), load per length of shaft (P) for a given lateral displacement (Y) at a given depth on the shaft. The lateral resistance, P (F/L), for a given lateral displacement is the resultant force (integration of radial stress around perimeter of pile/shaft) per unit length of pile/shaft. Its development is based on the flexible foundation approach, used in the shallow “mat” foundations (Teng, 1962) design. The approach is considered more accurate than its predecessor (rigid method), and introduced the concept of soil-structure interaction employing a subgrade modulus E_s , to represent the soil stiffness. This “flexible” method modeled the soil-structure interface as a “bed of springs” on which the foundation rested. The model allowed for non-uniform pressure distribution by permitting the springs under higher load to deform further. The earliest use of springs to represent the interaction between soil and foundation is attributed to Winkler (1867), and hence the name, Winkler Model, or Beam on Elastic Foundation analysis. The main disadvantage of the Winkler Model is that every spring is assumed to behave linearly, and to act independently from other springs, ignoring the interaction between them.

In lateral load design of deep foundations, the Winkler soil model was applied vertically along the soil-structure interface. The stiffness of the springs (i.e., the soil modulus of horizontal subgrade reaction E_s), is represented in the following manner;

$$E_s = p/y \quad (\text{Eq. 2.6})$$

where, p = the soil reaction per unit length of drilled shaft (F/L)

y = lateral deflection (L).

For cohesionless soils, the variation of E_s with depth is expressed by the following relationship;

$$E_s = n_h * z \quad (\text{Eq. 2.7})$$

where, n_h = constant modulus of subgrade reaction, k (F/L³)

z = any point along pile/drilled shaft embedment. (L).

Suggested values of n_h (sometimes called k) may be found in the literature. The following in Table 2.2 are values recommended in the help section of the computer program LPILE Plus 3.0.

Table 2.2 Constant Soil Modulus vs. Relative Density

Relative Density	Loose	Medium	Dense
Submerged Sand	20 pci 5,430 KPa/m	60 pci 18,300 KPa/m	125 pci 33,900 KPa/m
Sand above WT	25 pci 8,790 KPa/m	90 pci 24,430 KPa/m	225 pci 61,000KPa/m

Johnson and Kavanagh (1968) proposed the following relationship (see Table 2.3) between the constant soil modulus and Standard Penetration Test blow count (N);

Table 2.3 SPT Blow Count vs. Constant Soil Modulus

N-Value	8	10	15	20	30
Nh (pci)	9.8	15	27	35	53.2

Since the soil reaction vs. deflection relationship for soils is nonlinear, the Winkler model required some modification. The shortcomings of the method (spring linearity and independence) are overcome by the introduction of the nonlinear springs or limit pressures for the P-Y curves. The pile/drilled shaft is divided into n intervals, with a node at the end of each interval. Soil is modeled as a series of non-linear springs located at each node, the flexural stiffness of each interval is defined by the appropriate EI, and the load deformation properties of each spring is defined by a P-Y curve (Coduto, 2001). The behavior of a pile/drilled shaft can be analyzed by using the equation of an elastic beam supported on an elastic foundation, and is given by the following equation;

$$EI (d^4y/dx^4) + p = 0 \quad (\text{Eq. 2.8})$$

where, E = modulus of elasticity of drilled shaft (F/L²)

I = moment of inertia of drilled shaft section (L⁴)

p = soil reaction (F/L).

An important difference between the Winkler model and the P-Y method is that the Winkler model considers only compressive forces between the foundation and the soil, whereas the lateral soil load acting on a deep foundation is the result of compression on the leading side, shear friction on the two adjacent sides, and possibly some small compression on the back side (Tawfiq, 2000). Thus, it is misleading to think of the P-Y curve as a compression phenomenon only (Briaud et al. 1983, and Smith, 1989).

In present day practice laterally loaded piles and shafts are modeled using beam theory to represent the drilled shaft and uncoupled, non-linear load transfer functions (P-Y curves) to represent the soil (O'Neill and Murchison, 1983). The following paragraphs present in general terms two of the four semi-empirical methods found in O'Neill and Murchison's 1983 paper "Evaluation of P-Y Relationships in Cohesionless Soils."

The most commonly used P-Y curve for sand was introduced by Reese, Cox, and Koop in (1974) and is used in COM624, LPILE, and FB-PIER. Each P-Y curve is constructed at a desired depth (Fig. 2.5), and consists of three segments, defined by two straight lines with a parabola between them. The initial slope is determined by multiplying n_h times the depth at which a P-Y curve is desired. The ultimate soil resistance is determined from the lesser value obtained from the following two equations;

$$p_u = \gamma z [D(K_p - K_a) + zK_p \tan\phi \tan\beta] \quad (\text{Eq. 2.9a})$$

$$p_u = \gamma Dz(K_p^3 + 2K_o K_p^2 \tan\phi + \tan\phi - K_a) \quad (\text{Eq. 2.9b})$$

where p_u = ultimate soil resistance per unit of depth

z = depth

γ = unit weight of soil (buoyant or non buoyant as appropriate)

K_a = Rankine active coefficient

K_p = Rankine passive coefficient

K_o = at-rest earth pressure coefficient

ϕ = angle of internal friction

$\beta = 45 + \phi/2$.

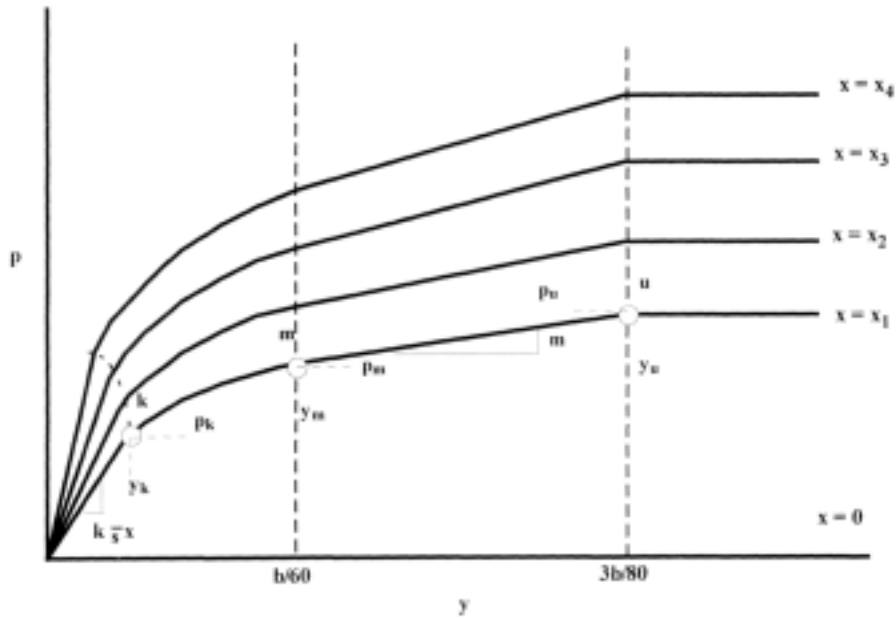


Figure 2.5 P-Y Curves for Static and Cyclic Loading of Sand (after Reese, et al., 1974).

The value of p_m (beginning of second linear segment of the curve) is determined from empirical charts, while the values of y_m and y_u are ratios of the pile diameter. The point (y_k, p_k) is determined from an empirical relationship involving y_m , y_u , p_m , and p_u . Typically, the blow count, N , from the Standard Penetration Test is used to estimate the soil's angle of internal friction, ϕ and its relative density, D_r (Figure 2.6). The soil's relative density, D_r , is then used to estimate the soil subgrade modulus, k (Figure 2.7).

O'Neill and Murchison (1983) P-Y curve for sand is employed in the API design guidelines. It follows a similar procedure to obtain an ultimate soil resistance p_u .

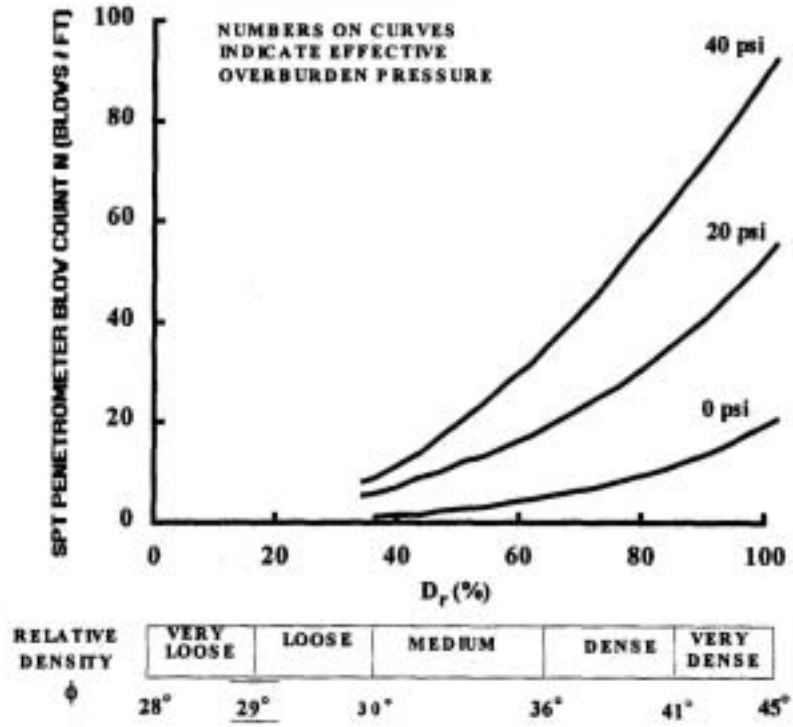


Figure 2.6 Blow Count vs. Friction Angle and Relative Density.

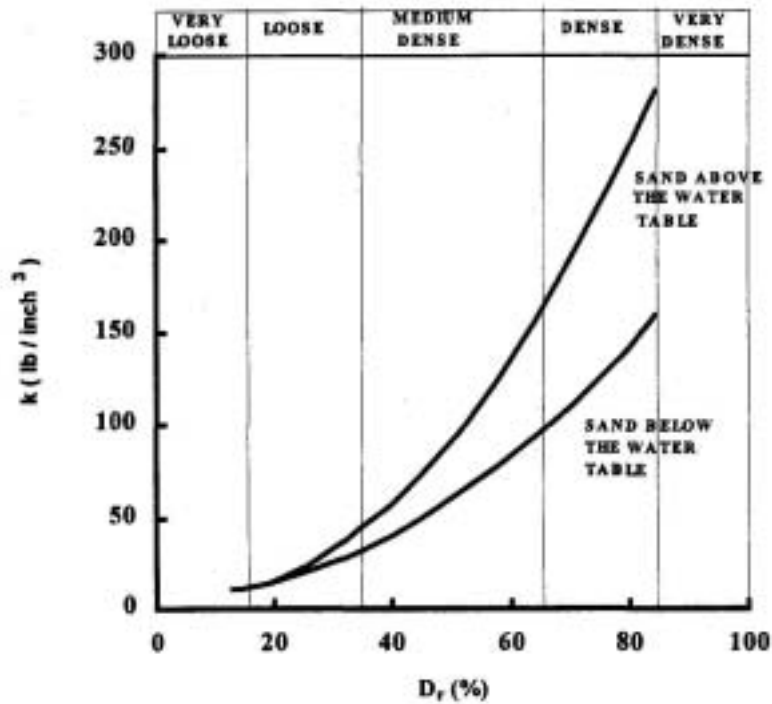


Figure 2.7 k vs. Relative Density

However, the P-Y curves are defined with one mathematical function, through the following equation.

$$p = \eta A p_u \tan \eta [(kz / A \eta p_u) * y] \quad (\text{Eq. 2.10})$$

where, η = a factor used to describe pile shape; = 1.0 for circular piles

$A = 0.9$ for cyclic loading

$A = 3 - 0.8 z/D$ 0.9 for static loading

D = shaft diameter

p_u = ultimate soil resistance per unit of depth

$k = E_s$ = modulus of lateral soil reaction (F/L).

2.2.2 Current Torsional Design Methods in the State of Florida – No Lateral Load

The State of Florida Department of Transportation has currently three methods of estimating the torsional capacities of drilled shaft foundations;

- Structures Design Office Method
- District 5 Method
- District 7 Method

Each method has a different approach to the determination of the soil-structure torsional unit skin friction, as well as tip friction values. A brief discussion follows of each.

2.2.2.1 Structures Design Office Method. This method is used to determine torsional resistance in both cohesive and cohesionless soil. It is also feasible to analyze

stratified layers as long a value of resistance is obtained for each separate layer and then summed for a total. The analysis for cohesionless soil is as follows:

Side torsional resistance (F-L) is based on Coulombic Friction using at rest stress state (i.e., $K_0 \sigma_v'$):

$$T_s = (K_0 * \gamma * 0.5L^2) * \pi * D * \tan \delta * 0.5D \quad (\text{Eq. 2.11})$$

where, T_s = side torsional resistance, ft-lbs

K_0 = at rest lateral earth pressure coefficient

γ = effective soil unit weight, lb/ft³

L = length of drilled shaft foundation, ft

D = diameter of drilled shaft foundation, ft

δ = soil-structure friction angle which is set equal to the internal friction angle of the soil for drilled shaft foundations (Tawfiq et al., 2000).

The shaft's base torsional resistance is given by:

$$T_b = W * \tan \delta * 0.33 * D \quad (\text{Eq. 2.12})$$

where, T_b = base torsional resistance, ft-lbs

W = weight of drilled shaft foundation, lbs

D = diameter of drilled shaft foundation, ft

δ = soil-structure friction angle which is set equal to the internal friction angle of the soil for drilled shaft foundations (Tawfiq et al., 2000).

Total shaft torsional resistance is

$$T_{\text{total}} = T_s + T_b \quad (\text{Eq. 2.13})$$

An example of the application of the method is as follows;

Parameters used: $K_o = 0.426$
 $\phi = 35$ degrees
 $\delta = 35$ degrees
 $L = 35$ ft
 $D = 5$ ft
 $\gamma = 98.34$ pcf
 $W = 96214$ lbs.

Next, the Structures Design Office Method, side torsional resistance, T_s , is computed as:

$$T_s = (K_o \gamma 0.5L^2) \pi D \tan \delta 0.5D$$

$$T_s = 7.063 * 10^5 \text{ ft-lbs}$$

Base torsional resistance:

$$T_b = W \tan \delta 0.33D$$

$$T_b = 1.112 * 10^5 \text{ ft-lbs}$$

And finally, total torsional capacity is given as:

$$T = T_s + T_b = 8.174 * 10^5 \text{ ft-lbs}$$

2.2.2.2 District 5 method – SHAFTUF. District 5 proposes three ways of determining total torsional resistance, the first of which is by obtaining the ultimate skin friction (Q_s) from a program developed in the University of Florida, called SHAFTUF.

Then the side torsional resistance is computed as:

$$T_s = Q_s * (D/2) \quad (\text{Eq. 2.14})$$

And the base torsional resistance is found from:

$$T_b = 0.67 * (W + A_y) * \tan(0.67) * (D/2) \quad (\text{Eq. 2.15})$$

where, A_y = vertical loading upon the drilled shaft, lbs.

And, finally, the total torsional resistance is given as:

$$T_{\text{total}} = T_s + T_b \quad (\text{Eq. 2.16})$$

2.2.2.3 District 5 method – O’Neill and Hassan. The second and third approaches District 5 proposes for the determination of torsional resistance, is based on O’Neill and Hassan method. It differs only in the equations used to estimate the unit skin friction, f_s , and is based on the Standard Penetration Test blow count (N);

The unit skin friction is obtained by the following relationship;

$$f_s = \sigma * \beta \quad (\text{Eq. 2.17})$$

where, σ = effective vertical stress at mid-layer

β = load transfer ratio

and,

$$\text{If } N_{60\text{-uncorrected}} \geq 15 \quad \beta_{\text{nominal}} = 1.5 - 0.135 * (z)^{0.5} \quad 1.2 \geq \beta_{\text{nominal}} \geq 0.25$$

$$\text{If } N_{60\text{-uncorrected}} < 15 \quad \beta = (N/15) * \beta_{\text{nominal}}$$

where z = depth from ground surface to mid-layer.

The side friction force is computed from:

$$Q_s = \pi * D * L * f_s \quad (\text{Eq. 2.18})$$

And the base resistance from

$$Q_b = 0.67 * (W + A_y) * \tan \delta \quad (\text{Eq. 2.19})$$

The total torsional resistance (torque) is:

$$T_{\text{total}} = Q_s * (D/2) + Q_b * (D/2) \quad (\text{Eq. 2.20})$$

The following is an example of the O'Neill & Hassan $-\beta$ Method, using the same parameters as the earlier Structures Design Office example, with a vertically loading of $A_y = 4437.2$ lbs, typical vertical loading (Tawfiq et al., p.15).

First, the vertical stress, σ , is computed, along with unit skin friction,

$$\sigma = \gamma(L/2) = 1.721 * 10^3 \text{ psf}$$

$$\beta = 1.5 - [0.135 * ((L/2))^{0.5}]$$

$$f_s = \sigma * \beta = 1.61 * 10^3$$

Next, the total side friction is found,

$$Q_s = \pi * D * L * f_s = 8.849 * 10^5 \text{ lbs}$$

Then the shaft's base resistance for torsional loading is determined,

$$Q_b = 0.67 * (W + A_y) \tan \delta = 4.722 * 10^4 \text{ lbs}$$

And finally, the total torsional capacity is computed,

$$T = [Q_s * (D/2)] + [Q_b * (D/2)] = 2.333 * 10^6 \text{ ft-lbs}$$

2.2.2.4 District 7 method. District 7 method is the “ α ” method, which is generally used to determine resistance of shafts and piles embedded in cohesive soils.

The unit skin friction f_s is determined from the following relationship;

$$f_s = \alpha * C + \sigma_v * K * \tan \delta \quad (\text{Eq. 2.21})$$

where, α = adhesion factor ($\alpha = 1$ for sands)

C = average cohesion for stratum of interest ($C = 0$ for sands)

σ_v = effective vertical stress on the segment of the shaft

δ = effective friction angle at the soil concrete interface (0.5ϕ to 0.67ϕ)

K = coefficient of lateral earth pressure.

The base resistance force is found from,

$$Q_b = (3/8) * (W + A_y) * \tan \delta \quad (\text{Eq. 2.22})$$

And the torsional base resistance is given as

$$T_b = Q_b * (0.67 * D) \quad (\text{Eq. 2.23})$$

The torsional side friction is

$$T_s = \pi D * L * f_s * D/2 \quad (\text{Eq. 2.24})$$

And the total torque resistance is

$$T_{\text{total}} = T_b + T_s \quad (\text{Eq. 2.25})$$

2.2.3 Coupled Torsional and Lateral Loading

A method, which takes into account the combined influence of lateral and torsional forces on a foundation, is the Tawfiq-Mtenga (2000) method. Based on the

subgrade reaction (Reese and Matlock, 1956, Matlock and Reese, 1960), the method predicts torsional resistance as a function of lateral deflection rather than ultimate lateral capacity (Tawfiq, 2000). The method employs the “Winkler soil model,” where the elastic soil medium is replaced by a set of elastic springs. The springs are characterized through P-Y springs, i.e., lateral load, soil reaction per unit length (p), vs. lateral deflection (y). The following expressions describe the relationship used for the initial slope of the P-Y curve in cohesionless soil:

$$p = k_h * y \quad (\text{Eq. 2.26})$$

and,

$$k_h = n_h * x \quad (\text{Eq. 2.27})$$

where, n_h = the constant modulus of subgrade reaction.

The latter expressions apply to cohesionless soils and normally consolidated clays, where strength increases with depth due to overburden pressure. The following steps are required (Tawfiq, 2000, p. 158);

1. Calculate the load, moments for the mast arms
2. Transfer the loads and the moments to the drilled shaft
3. Determine the resultant lateral force and overturning moment
4. Using the subgrade reaction method determine the soil pressure along the shaft
5. Distribute the lateral pressure around the shaft perimeter at specified depths
6. Obtain the resultant pressure around the shaft perimeter at specified depths
7. Set the threshold lateral pressure using Rankine’s method along the shaft depth
8. Integrate the net soil pressure along the shaft; and

9. Determine the maximum torsional resistance using:

$$\text{Maximum torsional resistance: } \tau = p_h * \tan\delta \quad (\text{Eq. 2.28})$$

where, p_h = integrate the net soil pressure along the shaft (Step 8)

δ = soil-shaft angle of friction = ϕ = soil angle of friction.

Results obtained by the Tawfiq-Mtenga method will be presented later.

2.3 Experimental Model of Prototype

As discussed in Section 2.1, the pole height and mast arm length vary for single mast arm traffic signs, depending on the number of lanes at the intersection. For experimental testing, a pole height of 20 ft, and a mast arm length of 30 ft was selected. The latter measurements are considered representative of the typical range of heights and lengths used in the state of Florida.

The model was constructed to mirror the prototype dimensions and characteristics as closely as practical. However, tapered members were not used since the taper effect would not alter the results obtained during testing. A steel hollow section was used for the pole model due to failure of smaller solid sections. The mast arm was modeled with a solid aluminum section due to weight issues and ease of constructability. Several iterations were undertaken to obtain the proper model for testing. A brief discussion is presented below on the model development.

Initially, the structure model (pole and mast arm) was constructed out of solid cylindrical pieces of steel. The pole extended all the way to the bottom of the foundation and rested on a thin piece of Styrofoam as can be seen in Figure 2.8. The purpose of the Styrofoam was to support the pole and ensure it resided in the shaft not the soil. The

concrete was fluid when the centrifuge was spun up to allow the soil stresses to replicate the prototype values. However, the steel shaft had insufficient moment capacity (Fig. 2.8) and it was replaced with an aluminum pipe. With the aluminum, the Styrofoam piece was not required due to its reduction in weight. However, the section had insufficient yield strength to sustain the stresses applied by the lateral loads.



Figure 2.8 Initial Drilled Shaft and Pole Models.

Next a hollow steel section, pipe was selected for the pole, and a solid steel section for the mast arm. Performance of the pole section was satisfactory, however, when testing at the smaller length to diameter ratio (i.e., L/D equal to three), the weight of the mast arm was found to be generating a moment on the foundation, which was high enough to bring the entire structure out of alignment.

Finally, the pole was modeled with a hollow steel section that extended to the bottom of the foundation (Fig. 2.9). The portion of the steel that was embedded into the foundation had four continuous slots cut into it to reduce its steel ratio in the concrete. The mast arm was modeled with an aluminum solid section. All model dimensions were constructed by dividing the prototype heights and lengths by the number of gravities at which the model would be tested (45 for all tests). Prototype dimensions for a 20-ft high pole and 30-ft long mast arm are scaled to 5.3 inches and 8 inches, respectively.

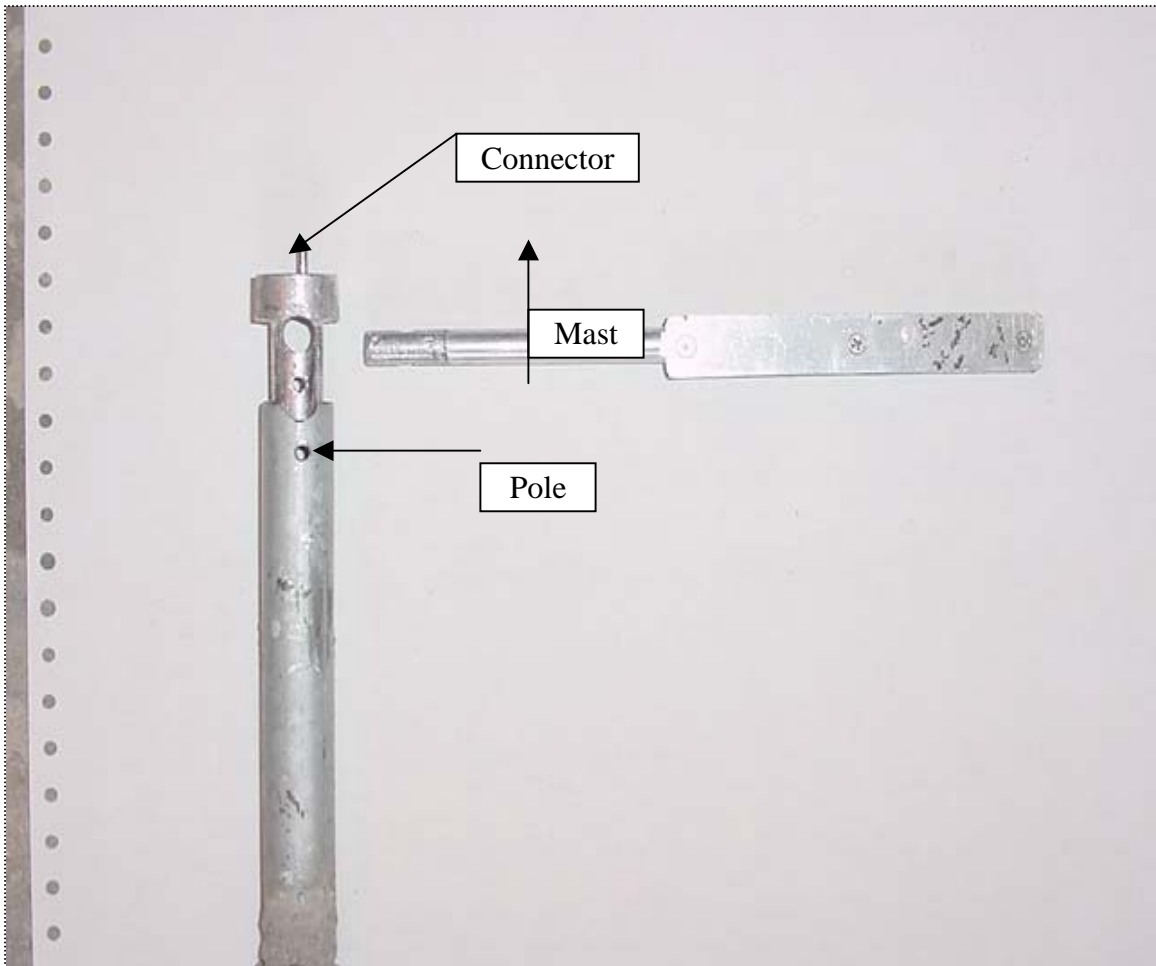


Figure 2.9 Pole and Mast Arm Assembly Parts.

2.3.1 Length to Diameter Ratio

Table 2.1 presents typical shaft diameter and embedment lengths used in the state of Florida. During the testing phase, scaled models of 5-ft prototype diameter were tested in the centrifuge. The 5-ft prototype diameter shaft was also must easier to construct in comparison to smallest diameter (30-in.) in the specifications. The length to diameter ratios used for testing were 3, 5, and 7, based on the values from Table 2.1, and were selected to represent the relatively wide range of embedments used for high mast signs. The objective for studying different L/D ratios was to determine the influence of L/D ratio on shaft capacity for different torque to lateral load ratios, under different soil densities.

2.3.2 Pole and Mast Arm Dimensions and Loading

Table 2.1 also presented typical values found in the specifications for construction of single mast arm traffic signs. Based on this information, a single value was chosen for each member (i.e., pole and mast arm). After numerous discussions, a prototype dimension of the pole was set at 20 ft and mast arm of 30 ft in length. A flat member was attached to the mast arm to provide a wider area for the load cell to take readings as load was applied. Figure 2.9 shows the pole and mast arm assembly parts.

Loading was applied at three different locations on the pole and mast arm. The first application of the load was to the top of the pole at its centerline (i.e., no torsion), simulating a lateral load test on the foundation. For the second phase of testing, combined torsion and lateral loading, the load was applied at two different locations along the mast arm. For “Mid Mast Arm” tests, the load was applied $3^{7/8}$ inches from the center of the foundation model. The latter distance translates to 14.5 ft in prototype

dimensions. The third point of load application was $5^{1/8}$ inches from center along the mast arm, or 19.22 ft from the center of the foundation in the prototype dimensions. The latter would be more representative of longer cantilever mast arms. It should be noted that moving the load application point along the mast arm, increases the torque on the foundation, for a given lateral load.

2.3.3 Definition of Failure for Single Mast Arm Traffic Signs

Two general types of failure can occur on a single mast arm traffic sign at the foundation level. The first is excessive lateral deflection at the top of the foundation. The latter causes the pole to lean, and any connected masts arms would swing down potentially interfering with vehicles passing beneath. Movements on the order of 12 inches at the top of foundation could result in vertical mast arm tip movements of 2.25 ft (rigid body rotation), potentially interfering passing vehicles.

The second mode of failure involves rotation (due to torsion) of the foundation and the superstructure, with limited lateral deflection. In this latter case serviceability is the issue. It is expected that a rotation of 15 degrees of pole and foundation would negate the intended function of the sign, i.e., it would be extremely difficult to read. Also, it would impair the motorist's concentration, which may become a hazard to other vehicles and pedestrians.

2.3.4 Florida Soils

A general subsurface profile of central and north Florida consists of two soil layers. The first is clean to silty fine sand that extends to depths ranging from 20 to 60 ft. The underlying layer is generally sandy silt to silty clay with traces of shell fragments

and occasional pockets of organic material. Underlying the clayey layer, a soft rock formation is generally encountered, consisting of limestone with sporadic cavities filled with silty to clayey sands.

Typical embedment depths for the drilled shafts supporting high mast signs do not go beyond the sandy layer described above. For this reason the material chosen for testing had to be granular cohesionless material with an angle of internal friction representative of typical Florida soil (30 to 38 degrees). The selection of the material used for testing is discussed in the following chapter.

CHAPTER 3 TESTING EQUIPMENT

3.1 Centrifuge Background

The UF centrifuge used in this study was constructed in 1987 as part of a project to study the load-deformation response of axially loaded piles and pile groups in sand, Gill (1988). Throughout the years several modifications have been undertaken to increase the payload capacity of the centrifuge. Currently, electrical access to the centrifuge is provided by four 24-channel electrical slip-rings and the pneumatic and hydraulic access is provided by a three port hydraulic rotary union. The rotating-arm payload on the centrifuge is balanced by fixed counterweights that are placed prior to spinning the centrifuge. Aluminum C channels carry, i.e., support both the pay-load and counter-weights in the centrifuge.

On the pay-load side (Figure 3.1), the aluminum C channels support the swing-up platform, through shear pins. The latter allows the model container to rotate as the centrifugal force increases with increasing revolution speed (i.e., rpm). The platform (constructed from A36 steel), and connecting shear pins were load tested with a hydraulic jack in the centrifuge. The test, concluded that both the swing up platform and shear pins were safe against yielding if the overall pay-load capacity was less than 12.5 tons (Molnit 1995).



Figure 3.1 The UF Geotechnical Centrifuge.

3.1.1 Theory of Similitude

Laboratory modeling of prototype structures has seen a number of advances over the decades. Of interest are those, which reduce the cost of field-testing as well as reduce the time of testing. Additionally, for Geotechnical Engineering, the modeling of insitu stresses is extremely important due to soils' stress dependent nature (stiffness and strength). One way to reproduce the latter accurately in the laboratory is with a centrifuge.

A centrifuge generates a centrifugal force, or acceleration based on the angular velocity that a body is traveling at. Specifically, when a body rotates about a fixed axis each particle travels in a circular path. The angular velocity, ω , is defined as dq/dt , where q is the angular position, and t is time. From this definition it can be implied that every point on the body will have the same angular velocity. The period T is the time for one revolution, and the frequency f is the number of revolutions per second (rev/sec). The relation between period and frequency is $f = 1/T$. In one revolution the body rotates 2π rads or

$$\omega = 2\pi \div T = 2\pi f \quad (\text{Eq. 3.1})$$

The linear speed of a particle (i.e., $v = ds/dt$) is related to the angular velocity, ω , by the relationship $\omega = dq/dt = (ds/dt)(1/r)$ or

$$v = \omega r \quad (\text{Eq. 3.2})$$

An important characteristic of centrifuge testing can be deduced from Eqs. 3.1 and 3.2: all particles have the same angular velocity, and their speed increase linearly with distance from the axis of rotation (r). Moreover, the centrifugal force applied to a sample is a function of the revolutions per minute (rpm) and the distance from the center of rotation. In a centrifuge, the angle between the gravitational forces, pulling the sample towards the center of the earth, and outward centrifugal force is 90 degrees. As the revolutions per minute increase so does the centrifugal force. When the centrifugal force is much larger than the gravitational force the normal gravity can be neglected. At this point the model will in essence feel only the “gravitational” pull in the direction of the

centrifugal force. The earth's gravitational pull (g) is then replaced by the centrifugal pull (a_c) with the following relationship;

$$\text{Centrifugal acceleration} \quad a_c := r \cdot \left(\frac{\pi \cdot \text{rpm}}{30} \right)^2 \quad (\text{Eq. 3.3})$$

$$\text{where} \quad \text{rpm} := \frac{30}{\pi} \cdot \sqrt{\frac{a_c}{r}} \quad (\text{Eq. 3.4})$$

$$\text{Scaling factor;} \quad N := \frac{a}{g} \quad (\text{Eq. 3.5})$$

$$N := \frac{\sqrt{a_c^2 + g^2}}{g} \quad (\text{Eq. 3.6})$$

$$\text{if } a_c \gg g, \quad N := \frac{a_c}{g} \quad (\text{Eq. 3.7})$$

where a equals the total acceleration

g equals the normal gravitational acceleration

a_c equals the centrifugal acceleration

rpm number of revolutions per minute

r equals distance from center of rotation.

The scaling relationship between the centrifuge model and the prototype can be expressed as a function of the scaling factor, N (Eq. 3.5). It is desirable to test a model that is as large as possible in the centrifuge, to minimize sources of error (boundary effects, etc.), as well as grain size effects with the soil. With the latter in mind, and requiring the characterizing of foundation elements with 15 to 35 ft of embedment in the

field, the following rationale was employed to determine the appropriate centrifuge g level and angular speed ω .

The maximum height of the sample container was 12 inches, the longest foundation to be modeled (35 ft embedment) if tested at 45 gravities would require a model depth of 9.33 inches, which would ensure that the bottom of the foundation model had two inches of soil beneath (i.e., minimizing end effects). Spinning the centrifuge at higher or lower gravities would imply the model would either have to be smaller, or too large to fit in the container.

Knowing that the desired scaling factor N, was 45 gravities, and that the distance from the sample center of mass to the centrifuge's center of rotation was 1.3 meters (51.18 inches), it is possible to then compute the angular speed of the centrifuge, ω from Eq. 3.3,

$$\omega := \frac{30}{\pi} \cdot \sqrt{\frac{45 \cdot 9.81 \frac{\text{m}}{\text{s}^2}}{1.3 \text{ m}}} = 176 \text{ rev/min} = 2.93 \text{ rev/sec}$$

The actual Scaling factor, N from Eq. 3.6 is:

$$N := \frac{\sqrt{(45 \cdot 9.81)^2 + 9.81^2}}{9.81 \frac{\text{m}}{\text{s}^2}} = 45.01$$

Based on Eq. 3.5, a number of important model (centrifuge) to prototype (field) scaling relationships have been developed (Bradley, 1984). Shown in Table 3.1 are those, which apply to this research.

Table 3.1 Centrifuge Scaling Relationships (Bradley, 1984)

Property	Prototype	Model
Acceleration (L/T^2)	1	N
Dynamic Time (T)	1	1/N
Linear Dimensions (L)	1	1/N
Area (L^2)	1	1/N ²
Volume (L^3)	1	1/N ³
Mass (M)	1	1/N ³
Force (ML/T^2)	1	1/N ²
Unit Weight (M/L^2T^2)	1	N
Density (M/L^3)	1	1
Stress (M/LT^2)	1	1
Strain (L/L)	1	1
Moment (ML^2/T^2)	1	1/N ³

Based on Table 3.1, two of significant importance is:

- Linear Dimension are scaled 1/N (prototype length = N*model length)
- Stresses are scaled 1:1.

The first significantly decrease the size of the experiment, which reduces both the cost and time required to run a test. The second, ensure that the insitu field stresses are replicated which controls both stiffness and strength of the soil.

3.1.2 Slip Rings and Rotary Union

A total of 96 channels are available in the centrifuge through four slip rings (24 channels each) mounted on the central shaft, Figure 3.2. Each channel may be accessed

from the top platform above the centrifuge, and used to obtain readings from instrumentation being used to monitor the model, or the centrifuge itself.



Figure 3.2 Slip Rings, Rotary Union, and Connection Board (left)

For this particular research, several channels were used to send voltages (power-in), and obtain readings (signal-out) from a 250-lb load cell, three Linear Variable Differential Transducers (LVDT's to measure deformation), and one camera. Power was also supplied, through slip rings to solenoids, which controlled air supply to the air pistons (point load source, etc), and to an Omega Amplifier (discussed later), which boosted the signal (LVDTs, etc) coming out. To minimize noise, cross talk, etc., low

voltage out devices was kept on different sets of slip rings than the higher voltage power input. For instance, the voltage-in for the load cell was 5 volts, however, the signal (voltage-out) coming from the instrument ranged from 0 to 20 millivolts.

The pneumatic port on the hydraulic rotary union was used to send air pressure to the air pistons acting on the model. The air line was then connected on the centrifuge through a set of solenoids, Figure 3.3, located close to the center of rotation. Solenoids have the advantage that they may be operated independently of each other, allowing the application of air pressure to a large number of pistons in any combination required. The solenoids required an input voltage of 24 volts of direct current and opened or closed valves depending if voltage was supplied or not.



Figure 3.3 Solenoids.

3.1.3 Omega Amplifier

As discussed previously, signal from a number of instrumentation (e.g., load cells, pressure transducers) may be in the millivolt range, which is very susceptible to interference (spurious electrical noise). For this reason, the signal from the load cell was amplified before being sent up the slip-rings to the data acquisition board located above and outside of the centrifuge. The amplifier used was an Omega DMD465 signal conditioning module, capable of amplifying signal up to 250 times. If higher amplification is required, it has the option of using an external resistor to attain amplification of up to 1,000 times the original voltage. The amplifier uses a 115 volts input, which was kept separate (different slip-ring) from all other wiring in the centrifuge. It amplified the signal from the load cell from 0 to 20 millivolts, to 0 to 5 volts (250 times), and resulted in an output noise of only 0.5 millivolts, which is considered negligible. The amplifier was attached as close as possible to the center of rotation of the centrifuge in order to avoid malfunction as well as minimize centrifugal forces on the device during testing.

3.2 Model Container and New Instrumentation Platform

The model container used for this project is the same used to test laterally loaded pile groups (McVay et. al 1996). It was constructed out of aluminum 6061 alloys in a rectangular shape having inside dimensions of 10 inches (width) by 18 inches (length), by 12 inches (height). The sample container was designed to contain a triangular distributed soil pressure of 60 psi at the base of the container (Molnit 1995).

For this study, a new instrumentation, and loading platform was designed and constructed. The new platform, shown in Figure 3.4, is capable of supporting three

LVDT's and two air pistons (the load cell was attached to the tip of the larger air piston). It was built of medium strength aluminum and connected to the model container by aluminum angles that were bolted to the sides of the soil container.



Figure 3.4 Plan View of New Instrumentation Platform in the Centrifuge.

3.3 Test Equipment

Initially, two air pistons, two linear variable differential transformers and a 1000-lb load cell were used for load and deflection monitoring on the model. However, the load cell was replaced for a more accurate 250-lb device, and a third LVDT was added to in order to measure deflections at the top and bottom of the pole, as well as rotation of the mast arm. A brief description of the individual instruments follows.

3.3.1 Linear Variable Differential Transformers

Three LVDT's were used to obtain readings of deformation at the mast arm (LVDT No. 1), at the top of the pole (LVDT No. 2), and at the bottom of the pole, just above the top of foundation (LVDT No.3), Figure 3.5. The LVDT is an electro-mechanical device that produces an electrical output proportional to the displacement of a separate movable core. This set-up eliminates the need for friction corrections since the rod is essentially floating between the coils. All Three LVDT's used were two-inch travel, DC operated model GCD 121-1000 Schaevitz with an excitation voltage of 15 VDC 30mA.

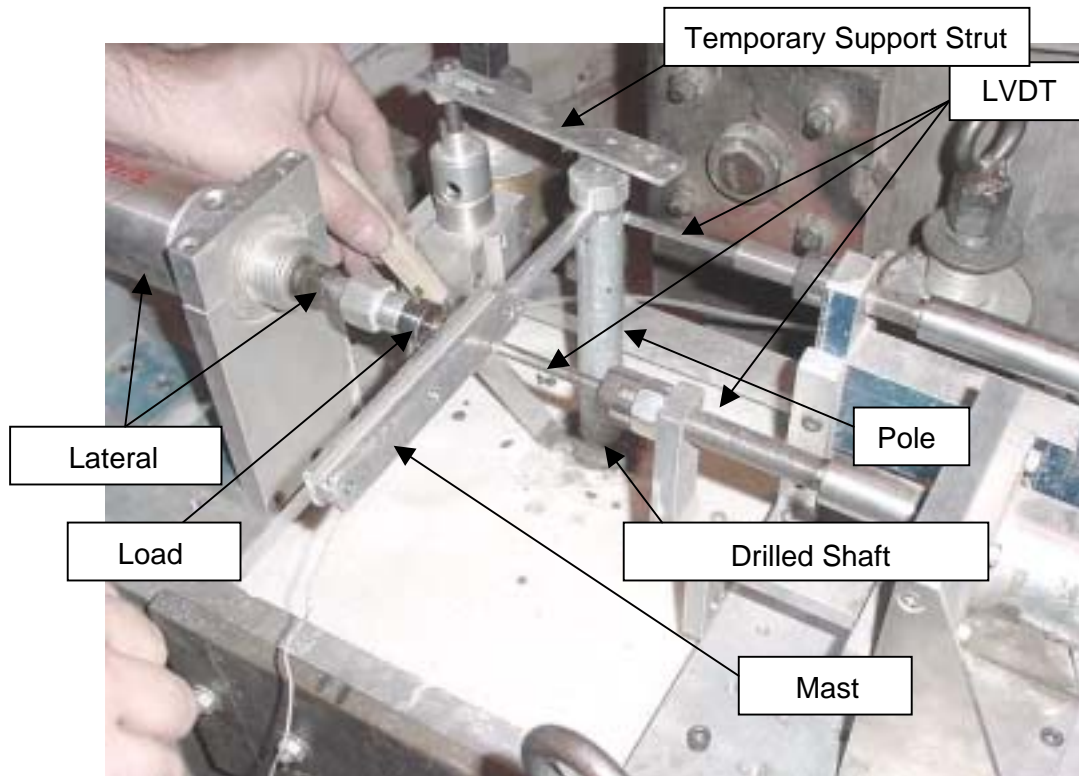


Figure 3.5 LVDTs, Load Cell, Sign Pole and Mast Arm.

3.3.2 Load Cell

A 1,000-lb load cell was initially used for testing, but it soon became apparent that the maximum readings would not surpass the 200-pound (lb) range. To obtain reliable and precise readings from the instrument, a 250-lb cell was subsequently used. Its signal was amplified before being sent through the slip rings to the data acquisition system. The load cell used was an OMEGA-LCFA miniature tension and compression cell that requires a 10-volt DC input.

3.3.3 Pneumatic Cylinders

Two double acting universal mounting type pneumatic air cylinders (Figure 3.5) were used during testing. Bronze rods with threaded tips, which reside inside a stainless steel housing, are extended or contracted by air pressure. The two cylinders used had one inch and two-inch maximum rod travel. The cylinder with the shorter travel was used to keep the pole and mast arm assembly in place while the concrete mix hydrated in flight. The air cylinder with the longer travel had the load cell threaded on its tip, and was used to provide lateral force to the pole or mast arm.

3.3.4 Data Acquisition System

A new data acquisition system was used for this particular research. Selection of a new pc data acquisition board was based on input voltage, sampling speed, number of required channels, signal resolution, cost, and compatibility with LabVIEW (data acquisition software).

Hardware known to be compatible with the data acquisition software was the National Instruments E-Series boards, which provided a wide selection of high-speed PCI boards. An overview of the capabilities of the board (Figure 3.6) is presented below:

- Family: NI6034E
- Product Name: PCI-6034E
- BUS: PCI
- Analog Inputs: 16 SE/8 DI
- Sampling Rate(S/s): 200,000 Samples per second
- Input Resolution (bits): 16
- Input Range (V):
- Input Gains: 1, 10, 100
- Digital I/O: 8
- Counter/Timers: 2 DAQ-STC – 24bit, 20Mhz
- Trigger: Digital.



Figure 3.6 Data Acquisition Board.

3.3.5 Data Acquisition Software

All of measured signals (LVDTs and Load Cells) were sent from the centrifuge through the pc's data acquisition card and read with the data acquisition software, LabVIEW. LabVIEW allows the programmer to display results from instrumentation by

intuitively assembling block diagrams, VIs, which represent instruments, analysis, printing, etc. The advantages of the new software are its high speed, windows compatibility, real time calculation of data input, and the ease with which the program can be modified to fit future research requirements. Figure 3.7 displays the LabVIEW window for monitoring the instrumentation for the project tests.

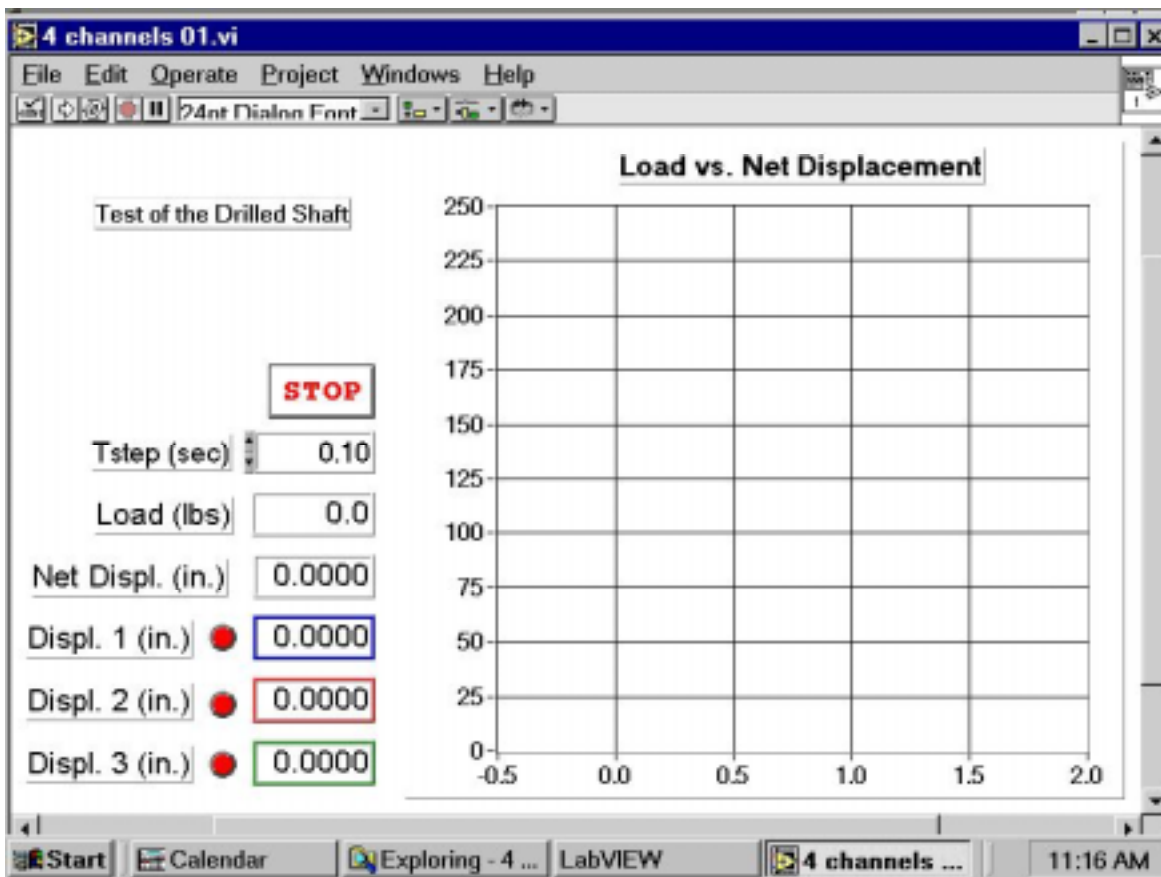


Figure 3.7 Output Screen from LabVIEW.

CHAPTER 4
CENTRIFUGE TESTING

4.1 Edgar Test Sand

The soil initially tested for this project was a silty-sand collected from a site approximately one mile north of the Gainesville Airport. After conducting two triaxial consolidated drained tests, and a series of direct shear tests, the material was discarded due to its high internal angle of friction (40 degrees). The latter was believed to be atypical for Florida where angles of friction between 32 and 38 degrees are generally encountered. Subsequently, another site in north Florida (Edgar mine: commercial wholesaler) was tested and found acceptable. Figure 4.1 shows grain size curves from a number of samples taken from the wholesaler’s bags. The soil was classified as SP in the Unified Soil Classification System, i.e., fine sand.

As with any sand, its strength and stiffness is controlled by its relative density or unit weight and moisture content. To establish the latter, the sand’s maximum (Table 4.1) and minimum void ratio (Table 4.2) with corresponding unit weight was determined.

Table 4.1 Determination of e_{max}

Weight of Mold (g)	Weight of Soil (+) Mold	Weight of Soil (g)	Dry Soil Unit Weight (pcf)	Void Ratio e_{max}
3732.5	7771.0	4038.5	89.0	0.82
3732.5	7740.0	4007.5	88.4	0.83
3732.5	7600.0	3867.5	85.3	0.90
Average			87.6	0.85

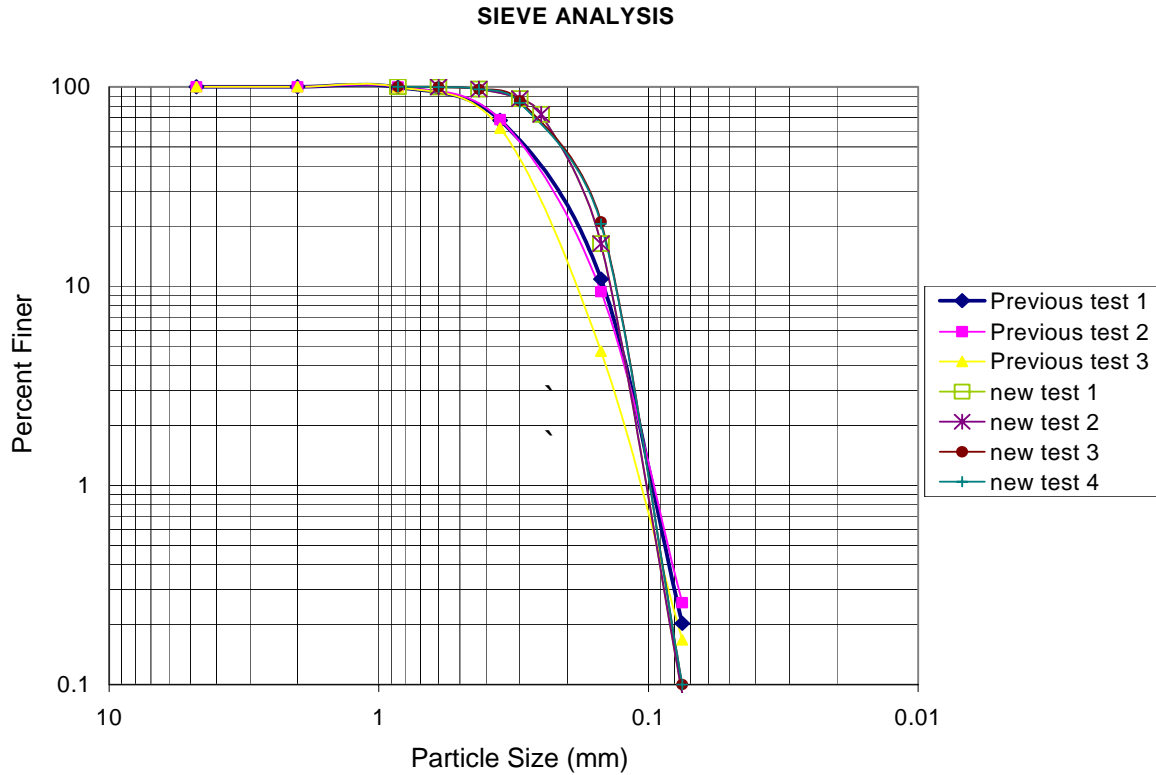


Figure 4.1 Sieve Analysis Results.

Table 4.2 Determination of e_{min}

Weight of Mold (g)	Weight of Soil (+) Mold	Weight of Soil (g)	Dry Soil Unit Weight (pcf)	Void Ratio e_{min}
3732.5	8377.0	4644.5	102.4	0.58
3732.5	8435.0	4702.5	103.7	0.56
3732.5	8281.0	4548.5	100.3	0.61
Average			102.1	0.58

Next a series of direct shear tests were performed on the Edgar Sand at different dry unit weights. Table 4.3 shows the increase in the sand's angle of internal friction, ϕ , with dry unit weight.

Table 4.3 Average Unit Weight and Angle of Internal Friction

Average Unit Weight (pcf)	Friction (ϕ)
91.4	32.6
94.2	34.2
97.1	35.8
99.0	37.0

4.2 Concrete Grout Mix

In order to characterize a typical drilled shaft installation, it was required for the foundation grout to be liquid, or semi-liquid during the initial phase of the centrifuge flight, at least until full acceleration on the model had been achieved. The latter would ensure that the expected prototype stresses around the shaft walls would occur in the model prior to the grout (i.e., shaft concrete) hydration similar to the field.

A series of different grout fluidity tests were run on several different mix combinations. In the case of the dry sand experiments, the final mix selected for use was twenty percent water, twenty-seven percent *Quickrete*, and fifty-three percent Quick Cement, with a hydration time of approximately four hours. For the saturated sand experiments with bentonite slurry, the grout mix was changed (strength issues in the saturated sand). A Rapid Road Repair mix from Quickrete worked the best. A high-range water reducer and an accelerator additive were used to increase the early strength and workability of the concrete. For the saturated sands the grout mix was as follows: 500 g Rapid Road Repair, 50 g sand (between sieve #7 and #10), 65 g water, 3 ml high-range water reducer, 11 ml accelerator. Both mixes had a 1000 psi unconfined compression strength (Figure 4.2) after five hours of curing time. The centrifuge

experiments were maintained at the forty-five gravities for the latter time until the grout in the shafts had developed its strength prior to lateral load testing.



Figure 4.2 Concrete Compressive Strength Testing.

4.3 Drilled Shaft Foundation

As identified in Chapter 2, the centrifuge tests were to be performed on a 20-ft pole with a 30-ft connecting mast arm. The pole was to be supported by a 5-ft diameter drilled shaft embedded 15-ft, 25-ft, and 35-ft below ground surface, based on typical shaft lengths in Florida, i.e., shown in Table 2.1.

As discussed in Chapter 3, “Theory of Similitude,” the constructed model had to be 45 times smaller than the prototype and subject to a series of scaled loads with different load application points. The final model design consisted of an 8-inch long solid aluminum cylinder for the mast arm, and a 5.3-inch high hollow steel cylinder for the model pole. The whole structure rested on a drilled shaft foundation, 1.33 inches in diameter. Model drilled shaft embedments were 4, 6.6, and 9.3 inches below the top of the sand, respectively. Figure 4.3 shows a complete mast arm, pole and drilled shaft after testing.



Figure 4.3 Model of Typical Structure and Foundation ($L/D = 3$).

To characterize the steel reinforcement in the drilled shaft, the steel pole was extended all the way to the bottom of the foundation. Slots, Figure 4.4, were subsequently cut into the embedded section, reducing the steel ratio to typical values. In addition, a steel wire was wrapped around the longitudinal reinforcement to model shear reinforcement. The latter also provided confinement to the concrete while the foundation was tested.

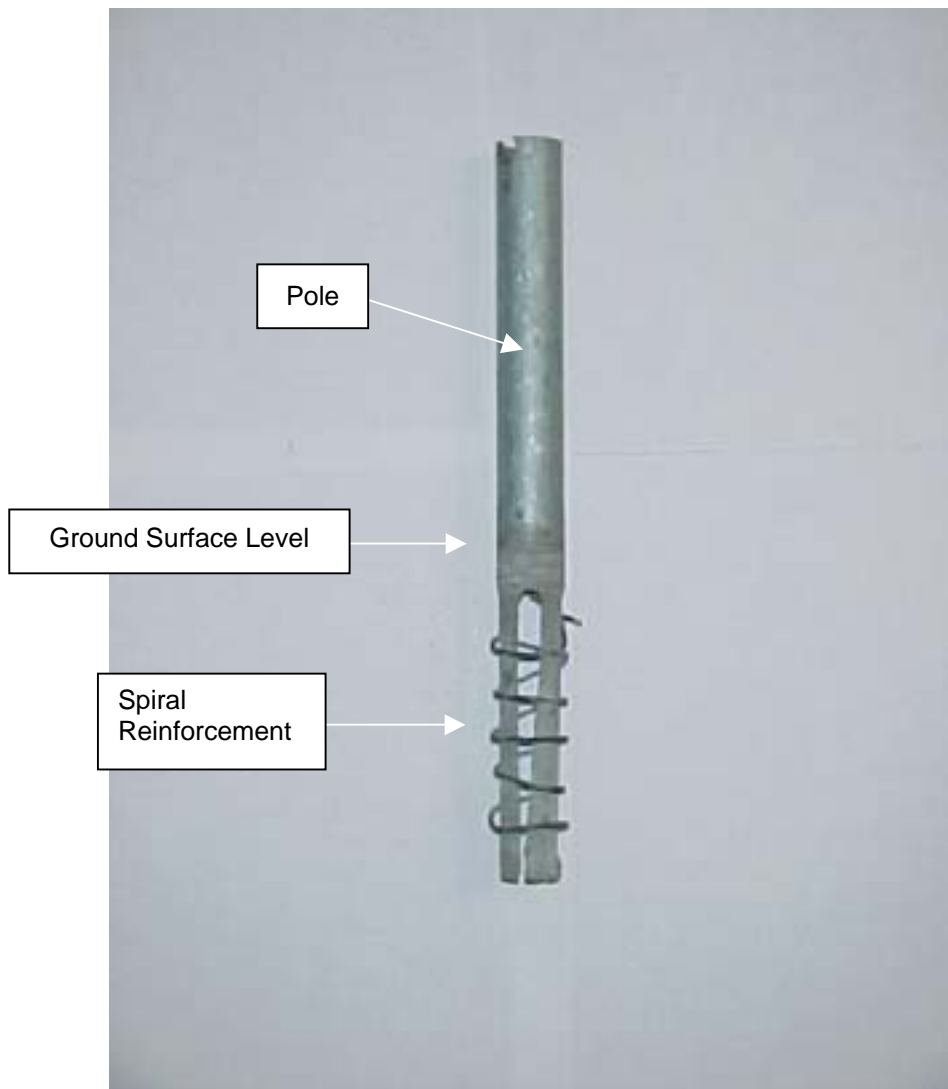


Figure 4.4 Slotted Steel Cylinder with Spiral Reinforcement.

Shown in Figure 4.5 is a shaft, which was tested in the centrifuge, removed and subsequently taken apart. The concrete was separated from the steel reinforcement with great difficulty revealing the spiral reinforcement. Note also, the mast arm and its connection to the pole.

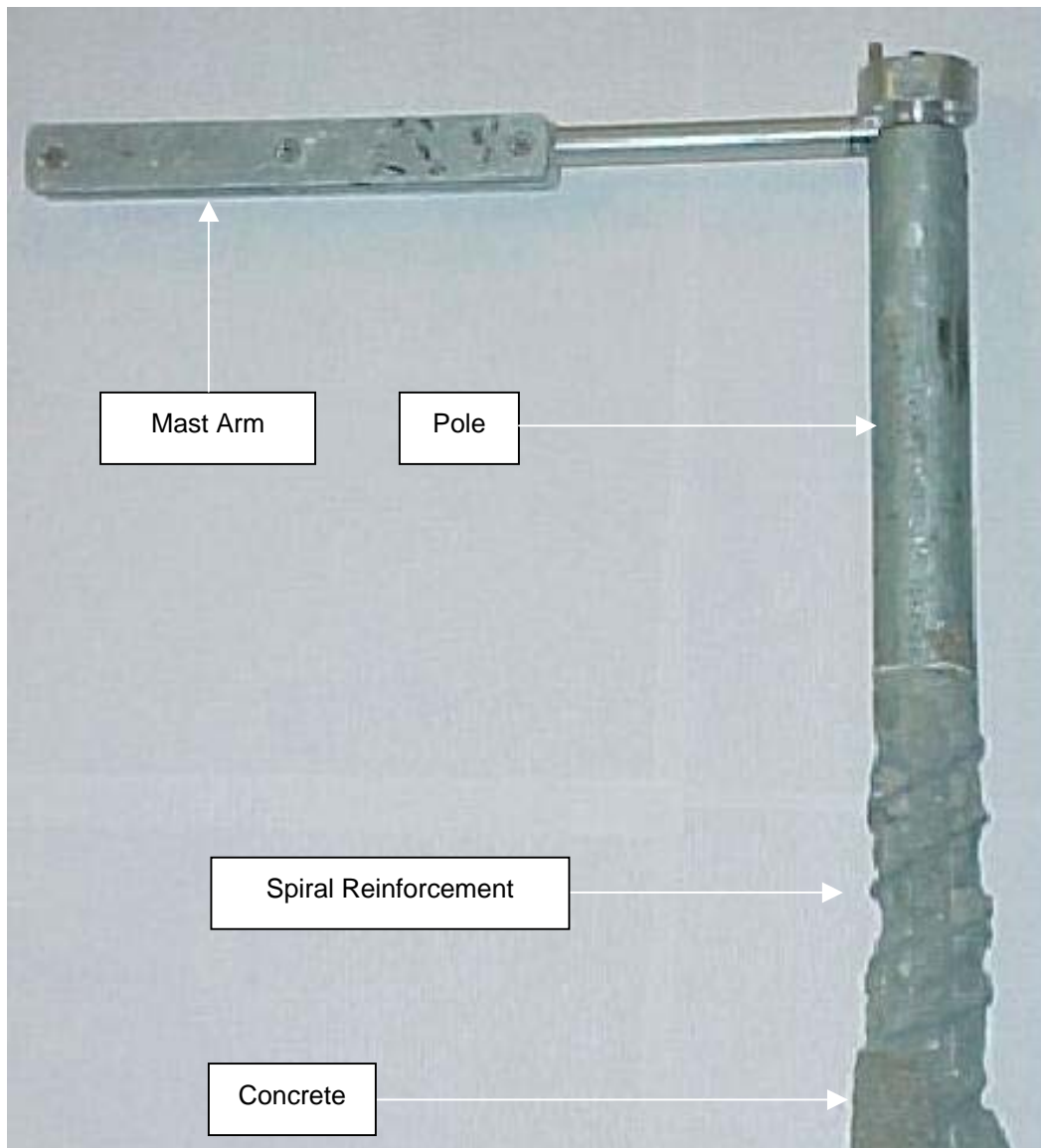


Figure 4.5 Complete Model (arm, pole, shaft) After Testing.

4.4 Shafts Constructed in Dry Sands with a Casing

Generally, drilled shafts may be constructed by one of three different ways in the field: 1) dry, 2) wet (slurry: mineral or polymer) or 3) with a casing. Typically, stiff clays are installed dry (i.e., only with an auger), whereas sands especially if they are below the water table are constructed either with slurry or a temporary casing. Of concern with slurry construction are its effects on a shaft's axial or torsional resistance. Consequently, the initial effort (fifty-four tests) involved shafts constructed with a casing. The latter studied only the effects of load/torque ratio, soil strength, etc., i.e., not shaft construction (i.e., slurry head, viscosity, etc.).

4.4.1 Dry Sand Placement in the Centrifuge

As with previous centrifuge research (McVay 1998), sand raining was used to prepare the soil sample in the centrifuge container. The latter entailed the use of a set of wooden boxes of the same dimensions as the sample container with screens attached to their bottom. The sand was then poured into the top box and allowed to rain down into the centrifuge container, Figure 4.6. By stacking different number of boxes on top of each other, the fall height could be adjusted and different relative densities obtained. After numerous tests, three different drop heights were selected. The average results from each drop were recorded and tabulated in Table 4.4. The sand varied from medium loose to medium dense with soil strengths given in Table 4.3 based on unit weight.



Figure 4.6 Sand Raining Device.

Table 4.4 Sand Raining Results

Drop Height (in)	Total Weight (lbs)	Weight of Sand (lbs)	Unit Weight (pcf)	Average Unit Weight (pcf)
21	275.8	102.3	91.67	92.07
	276.7	103.2	92.47	
33	280.5	107	95.88	95.88
	280.5	107	95.88	
44.5	283	109.5	98.12	98.34
	283.5	110	98.57	

4.4.2 Testing Program: Parameters Varied

As identified earlier, centrifuge testing allows significant repetition of tests with a minimum loss of time and money compared to full-scale tests. Difference due to soil conditions, shaft lengths, load placement, etc. may all be studied. It is important, however, that repeatability of results be obtained when study the influence of one parameter, i.e., L/D, lateral load placement, soil density, etc. Consequently, a testing program was designed for at least two tests per data point, with 18 lateral load tests on the pole and 36 combined torsional & lateral force tests (loose on mast arm). It should be noted that a number of tests had to be repeated to give reproducible results. In six months of testing, 54 successful tests were performed on shafts constructed in dry sand with casing used to create and stabilize the shaft hole. Table 4.5 presents the test matrix for this research. It involved three different densities of sand, three different embedment depths, and three different load application points. A discussion of the testing process follows.

4.4.3 Testing Process

To ensure repeatable results a checklist was prepared and followed. The following paragraphs explain the procedures followed to prepare the sample as well as perform the experiments.

4.4.3.1 Model preparation. Silica-quartz sand was rained into the sample container, which was then weighed. From the known volume and weight of sand, the unit weight and corresponding relative density was checked; if not acceptable a new sample was prepared. Subsequently, the sand was evened out along the top of the container, the instrumentation platform was attached, and all the stands that hold the

Table 4.5 Summary of Centrifuge Test Program

Test No.	Prototype Foundation Diameter (ft)	Prototype Embedment length (ft)	Location of Applied Load			Soil Density (pcf)
			On the Pole	Mid. Mast Arm	Tip of Mast Arm	
1	5	35	*			98.34
2	5	35	*			98.34
3	5	35		*		98.34
4	5	35		*		98.34
5	5	35			*	98.34
6	5	35			*	98.34
7	5	25	*			98.34
8	5	25	*			98.34
9	5	25		*		98.34
10	5	25		*		98.34
11	5	25			*	98.34
12	5	25			*	98.34
13	5	15	*			98.34
14	5	15	*			98.34
15	5	15		*		98.34
16	5	15		*		98.34
17	5	15			*	98.34
18	5	15			*	98.34
19	5	35	*			95.88
20	5	35	*			95.88
21	5	35		*		95.88
22	5	35		*		95.88
23	5	35			*	95.88
24	5	35			*	95.88
25	5	25	*			95.88
26	5	25	*			95.88
27	5	25		*		95.88
28	5	25		*		95.88
29	5	25			*	95.88
30	5	25			*	95.88
31	5	15	*			95.88
32	5	15	*			95.88
33	5	15		*		95.88
34	5	15		*		95.88
35	5	15			*	95.88
36	5	15			*	95.88
37	5	35	*			92.07
38	5	35	*			92.07
39	5	35		*		92.07
40	5	35		*		92.07
41	5	35			*	92.07
42	5	35			*	92.07
43	5	25	*			92.07
44	5	25	*			92.07
45	5	25		*		92.07
46	5	25		*		92.07
47	5	25			*	92.07
48	5	25			*	92.07
49	5	15	*			92.07
50	5	15	*			92.07
51	5	15		*		92.07
52	5	15		*		92.07
53	5	15			*	92.07
54	5	15			*	92.07

instruments were checked for bolt tightness. Next, the sample in the container was lowered with a hydraulic lift onto the swing-up platform of the centrifuge. The container was then bolted onto the platform and all instrumentation and air cylinders were connected to their respective slip-ring blocks and pneumatic lines.

The LabVIEW software was started and initial readings from the instrumentation were taken. At this point, the air cylinders were also checked for proper functioning. Next, a thin transparent plastic tube at the scaled diameter and height was pushed into the soil (Figure 4.7) and all the sand inside it was vacuumed out (Figure 4.8). Subsequently, the embedded depth of the model was measured (Figure 4.9).

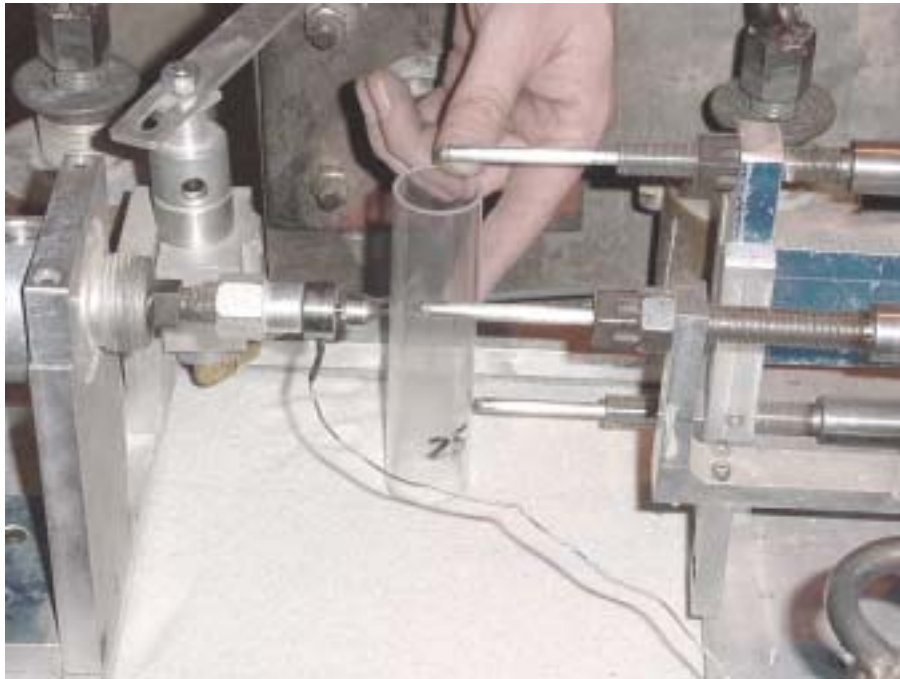


Figure 4.7 Plastic Tube Insertion.

Care was exercised in the vacuuming process, since the number of gravities in flight (N) magnifies small changes in the model. Next, the grout (i.e., prototype concrete) was placed (i.e., tremied) into the cased hole (Figure 4.10).

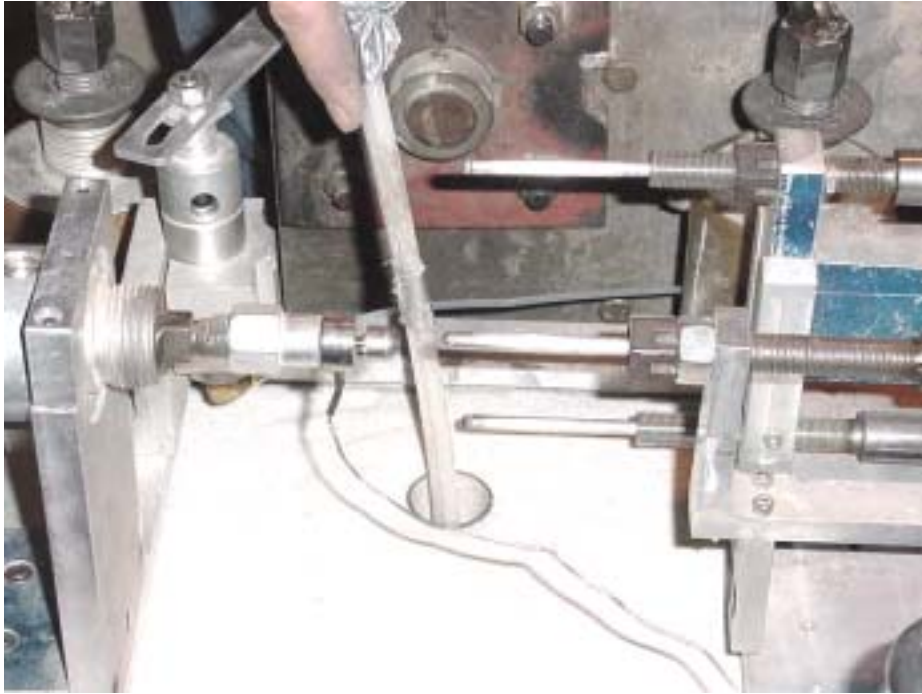


Figure 4.8 Vacuuming Sand from Casing.

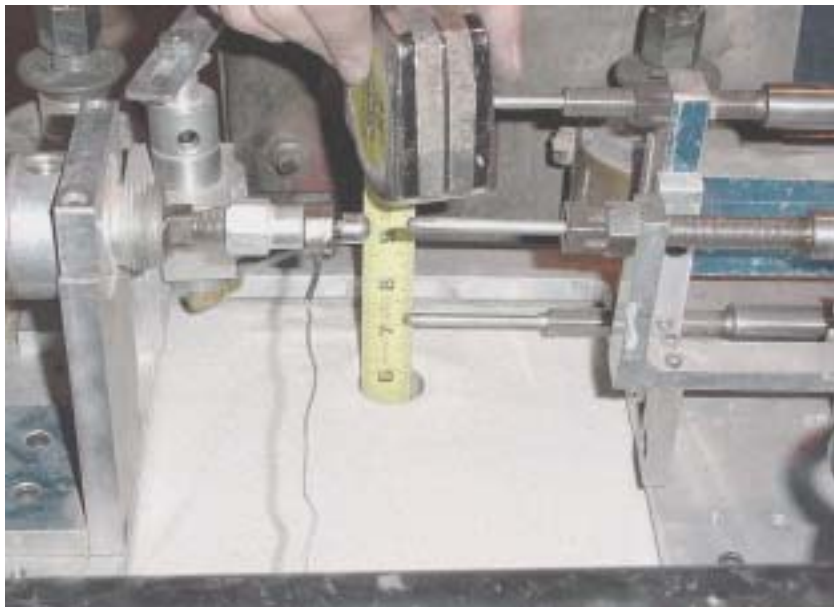


Figure 4.9 Measuring Depth to Bottom of Shaft.



Figure 4.10 Pouring the Grout.

Once the grout was poured, the plastic tube was slowly pulled out of the sand, and the complete traffic light model was pushed into the liquid grout foundation, Figure 4.11.

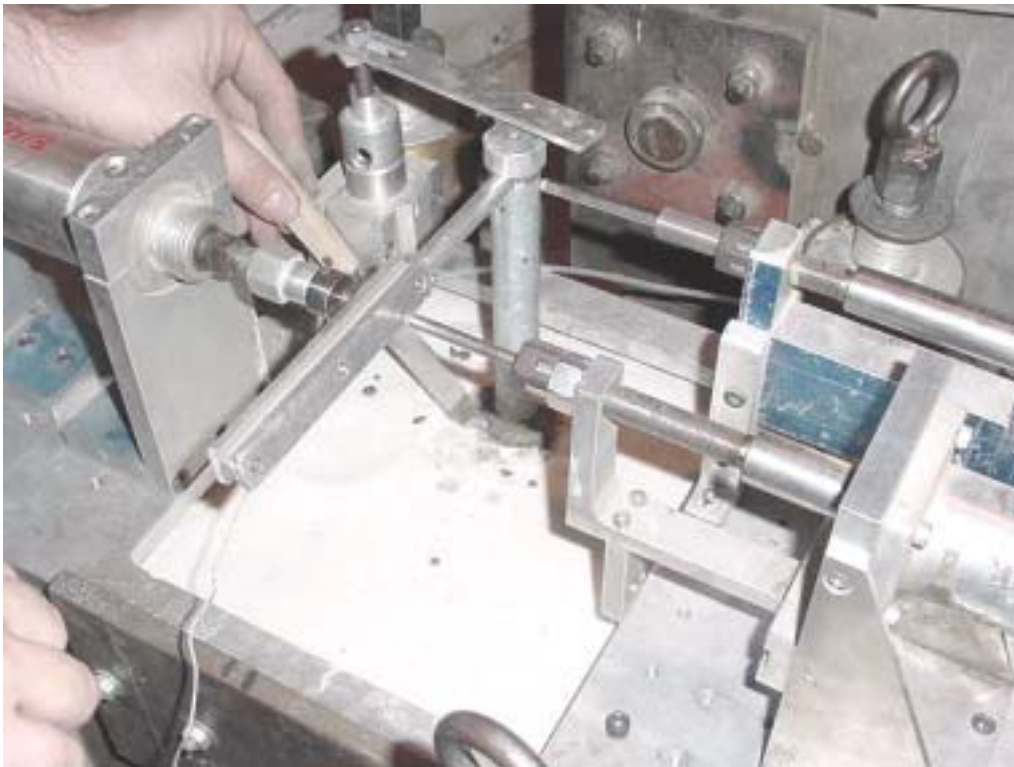


Figure 4.11 Traffic Light Model Placement.

A spatula was then used to remove any extra grout (i.e., prototype concrete) around the top of the shaft while it was still in a fluid state. Next, the cover was placed on the centrifuge and LabVIEW was checked again to see if all the LVDT's and the load cell were properly working. The main centrifuge switch was then switched on and the experiment was slowly brought up to a 30.17 Hz, which corresponds to 176 rpm's, or 45 gravities.

4.4.3.2 Testing of the model and data recorded. Once the traffic light model and its foundation were in place, and the centrifuge had been brought up to speed, a four-hour waiting time occurred to allow the grout to hydrate. Subsequently, the testing phase consisted of lifting the structure's temporary support (vertical air piston, Figure 4.11), and applying load to the pole, or at a point along the mast arm as stipulated in Table 4.5. Load application was performed at a consistent rate for every test. The testing phase was observed through a T.V. monitor, which was connected to a wireless color camera inside the centrifuge. LabVIEW readings were taken throughout the test.

Testing time (Load Application), i.e., after the grout hydration, was approximately one and a half minutes. Data reduction included plotting the load, mast arm displacement, top of pole displacement, and bottom of pole displacement vs. time. Other plots included mast arm, top of pole, and bottom of pole deflection vs. load, as well as torque versus displacement, and torque versus shaft rotation. Excel graphs obtained for all repeatable tests are included in the Appendices of the report.

4.5 Shafts Constructed in Saturated Sand

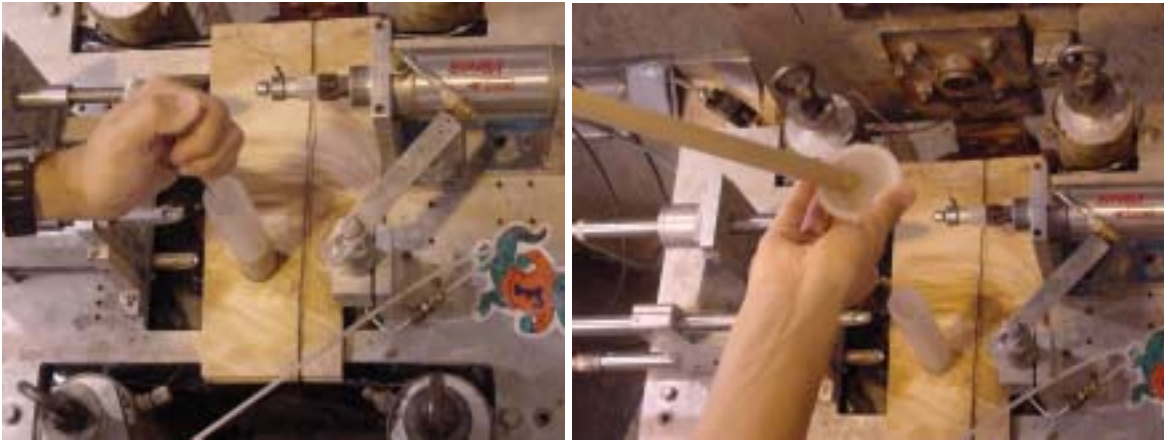
As part of a supplement to the original contract, a series of centrifuge tests were conducted on saturated sands employing the wet-hole method of construction. Saturated sands are representative of flooding conditions, which generally exist during a hurricane, and would have the lowest vertical and lateral effective stresses on a shaft. Also of interest was the influence of mineral or polymer slurries (i.e., used in shaft construction) on the shaft's lateral and torsional resistance. Since a shaft has never been constructed in a centrifuge with the wet-hole method of construction employing mineral slurry, the process (i.e., slurry cake, etc.) had to be developed.

4.5.1 Mineral Slurry and Cake Formation

The mineral slurry used in the wet-hole method of construction is usually selected from the montmorillonite (e.g., bentonite) family. The slurry is placed early in the construction process with a positive head (slurry height above ground water table). Due to the head difference, the water in the slurry permeates into the surrounding sand, depositing the clay mineral as a cake on wall of the hole. Due to the cake's low permeability, the remaining slurry in the hole will generate vertical and lateral (hydrostatic conditions) stresses on the wall of the hole preventing it from collapsing.

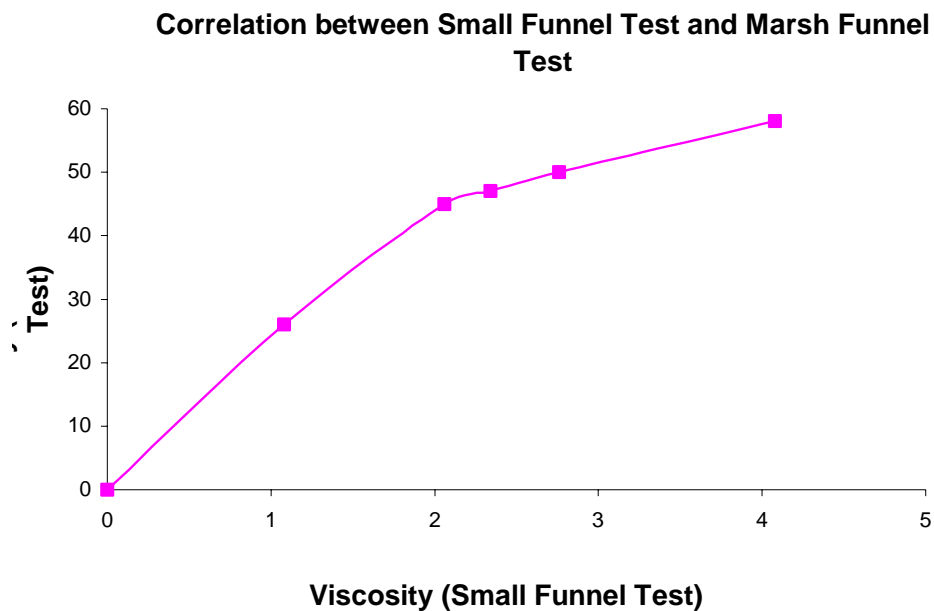
The thickness of a slurry cake is a function of slurry's viscosity, head, and time left in the hole. For this research, the slurry prior to placement had a viscosity of 43 sec (Marsh cone), and a unit weight of sixty-four lb per cubic foot. In order, to develop the wall cake characteristics, the centrifuge was spun for various times (15 min. to 3 hours), stopped, and the slurry's viscosity in the hole was tested. Since the Marsh Funnel Test could not be used due of the small volume of slurry in the hole, a new viscosity

measurement had to be developed. Methods such as a viscometer, a glass tube, and a small funnel were tried to measure the slurry's viscosity in the hole. It was found that the small funnel approach, Figure 4.12 (similar to Marsh cone) gave the most repeatable results. For instance, if the centrifuge was spun for 15 min., its Marsh viscosity was determined to be 45 sec, and after 3 hours of spinning, its viscosity was about 47 sec.



a) Insertion of Tube to Recover Slurry

b) Filling Small Funnel with Slurry



c) Determination of Slurry Viscosity

Figure 4.12 Insitu Slurry Viscosity Determination.

Since the thickness of the cake depends on the slurry head, typical and high water table elevations were of interest (worse case scenarios). It was decided that a head of 1 in (model), which equates to 4 ft in prototype or field was representative.

Of importance was the dynamic time measured in the centrifuge vs. the prototype (field). Similitude (Chapter 3) suggested that a model time of $1/N$ prototype value was needed. For instance, 15 min. in the centrifuge would equate to 11 hours in the prototype and three hours in the centrifuge should be equivalent to 6 days in the prototype. To test the latter, centrifuge tests were performed and the generated slurry cake thickness was measured. Shown in Figure 4.13a is the model's slurry cake thickness (0.012 in which is equivalent to 0.5 in. in prototype) after spinning 15 min. in the centrifuge. The model thickness of the slurry cake after spinning for 3 hours was 1/16 in. (Fig 4.13b), which is approximately 2.8 in. in the prototype. Consequently, the latter agreed very closely with the $1/N$ scaling relationship.



(a)

(b)

Figure 4.13 Different Thicknesses of Slurry Cake: (a) the slurry cake after 15 min. of spinning; and (b) the slurry cake after 3 hours of spinning.

4.5.2 Sand Placement, Saturation, and Wet-hole Shaft Construction

The experiments were performed on the saturated sand, the Edgar (Silica-quartz) sand with grain size distribution given in Fig. 4.1. The construction of the model started with the filling of centrifuge container with water. Subsequently, the sand was rained through the sieves shown in Fig. 4.6. However, as a result of the sand settling through the water, the sand had only a relative density, D_r , of 34% ($\gamma_d = 92.8$ pcf, $\gamma_t = 120.5$ pcf), (referred to as the loose sample). For the dense specimen (two densities considered), the loose sample in the centrifuge container was placed on a vibratory table (see Figure 4.14) and vibrated for thirty seconds. The resulting deposit had a relative density, D_r , of 69% ($\gamma_d = 99.2$ pcf, $\gamma_t = 124.5$ pcf), and is hereafter referred to as the dense specimen.



Figure 4.14 Preparing the Saturated Dense Specimen.

After the placement of the saturated sand in the centrifuge container (dense or loose), the shaft construction began. First a plastic tube (see Figure 4.15) was inserted into the saturated sand to the final depth of the shaft (ensured uniform hole size). Then, the sand within the tube was dug out with a spoon. Care was taken to ensure that the water level in the tube was kept a little higher than the ground level (water level). Next, slurry (see Figure 4.16) was poured into the bottom of the tube to displace the water, and the plastic tube (Figure 4.15) was slowly removed.

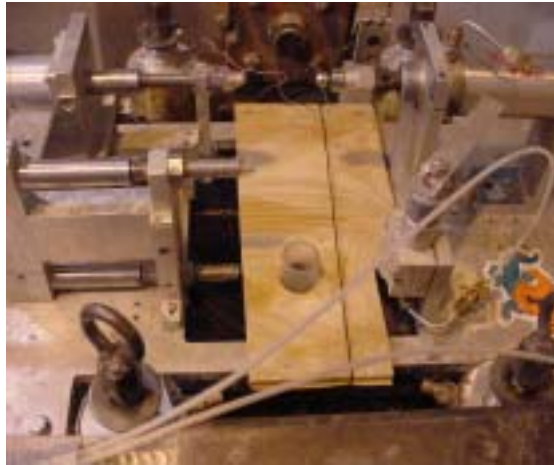


Figure 4.15 Inserting the Plastic Tube.



Figure 4.16 Slurry Placed in Wet-hole Method of Construction.

For this phase of construction, the slurry was maintained 4 in. higher than the ground level (water level). Next, the centrifuge container with slurry in construction hole was spun up to 10 g acceleration for 30 seconds. The latter caused the slurry head to drop to 1 in. The slurry within the hole was then refilled to 4 in. and the experiment was spun up to 45 g acceleration, for 15 min. to 3 hours depending on the test. When the centrifuge was stopped, the slurry head had dropped to 1 in. (3.75 ft prototype) above the water table.

After the spinning of the centrifuge at 45 g acceleration for the specified time, the centrifuge was stopped and the viscosity of the slurry in the construction hole was measured. The latter was accomplished by inserting a plastic pipe into the excavation (Figure 4.12a), removing a sample, filling the small funnel (Figure 4.12b) and timing the flow of slurry out of the small funnel. Using the relation between the small funnel and the Marsh Funnel Test (Figure 4.12c), the Marsh viscosity was determined.

Next, the concrete was placed in the slurry filled construction hole as follows: first, the grout was placed in a long plastic tube; then a rubber plug was put on the top of the tube, and tape was placed on the bottom of the tube to create a vacuum so the tube could be held vertical. Subsequently, the tube, filled with grout, was inserted into the bottom of the slurry excavation (Figure 4.17). Then the rubber plug at top of the tube (Figure 4.17) was removed, allowing the grout in the tube to flow out into the excavation. The concrete displaced the slurry (Figure 4.17), and the tube with grout was slowly lifted.

After placement of the concrete, the model pole, mast arm, and reinforcement was placed in the fluid grout (Figure 4.18a). Next, the top of the sign pole was attached to the vertical bimba air cylinder (Figure 4.18b) in order to keep the pole vertically aligned

during centrifuge spin up and grout hydration. Finally, the extra concrete (top of sand) was removed, and the computer software (LabVIEW, Figure 3.7) was zeroed.

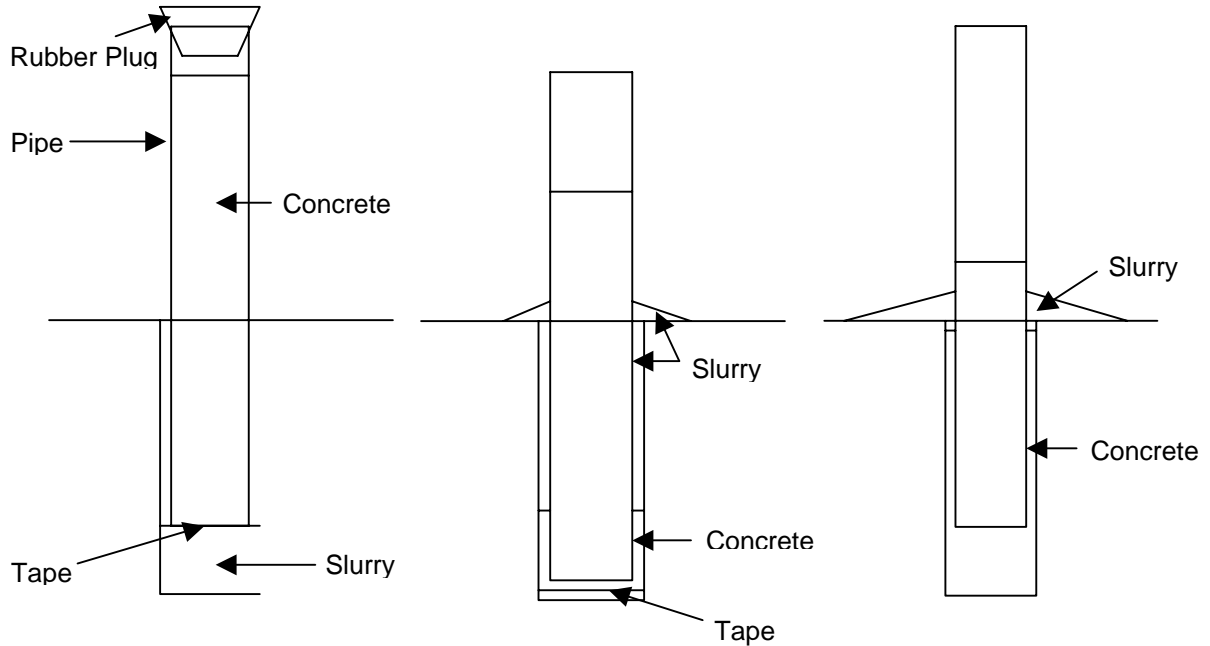


Figure 4.17 Process of Grouting the Slurry Filled Construction Hole.



a) Model Inserted in Fluid Grout

b) Instrumentation Attached to Model

Figure 4.18 Placement of Model Pole, Mast Arm and Reinforcement.

The centrifuge was spun at 176 rpm, equivalent to 45 g acting on the model. The experiment was spun for 5 hours so that the grout could hydrate and reach a strength of 1000 psi. After the elapsed five hours, the load test program initiated. First, the temporary support (small BIMBA air piston, Figure 4.18b) was lifted off the model. Next, a force was applied to either the pole or mast arm with the large BIMBA air piston (Figure 4.18b). Both displacements (top and bottom of pole, and end of mast arm) and forces were recorded with LabVIEW software. The same failure criteria (displacement and rotation) were used to end the test, i.e., lateral deflection at top of shaft of 12 inches and/or fifteen degrees of rotation of the shaft.

4.5.3 Testing Program: Parameters Varied

As part of the supplement to the original contract, centrifuge tests were to be performed on saturated sand using the wet-hole method of construction. Due to the significant decrease in both vertical and horizontal effective stresses with saturation, it was expected that the earlier short shafts ($L/D = 3$, $L = 5$ ft) would fail by torsion and would add little to the database. Consequently, the final loading variation (Table 4.6) was: eight lateral load tests on the pole and sixteen combined torsional and lateral force tests, with two repetitions per test. In terms of the soil and shaft lengths, Table 4.6, the tests involved two different densities of sand, and two different embedment depths. Again, each test was repeated twice to ensure accurate assessment of capacities.

4.5.4 Influence of Slurry Cake on Capacity

Of interest was the influence of the construction method on the combined lateral/torsional capacities of drilled shafts. As reported by Tawfiq (2000), shafts, which

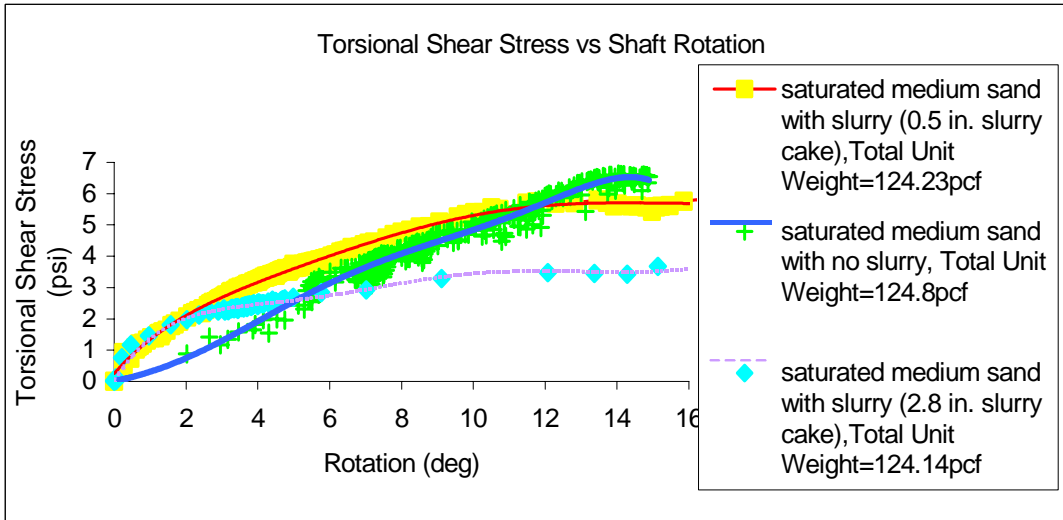
Table 4.6 Centrifuge Tests in Saturated Sand With Wet-hole Construction

Test No.	Prototype Foundation Diameter (ft)	Type of Slurry	Prototype Embedment Length (ft)	Location of Applied Load			Soil State	Date
				On the Pole	On the Mid Mast Arm	On the Tip of Mast Arm		
1	5	Bentonite	25	*			Loose	9/16/02 16:55
2	5	Bentonite	25	*			Loose	9/20/02 16:41
3	5	Bentonite	25		*		Loose	6/28/02 20:37
4	5	Bentonite	25		*		Loose	7/5/02 18:13
5	5	Bentonite	25			*	Loose	9/30/02 16:07
6	5	Bentonite	25			*	Loose	10/3/02 18:13
7	5	Bentonite	25	*			Dense	10/16/02 18:30
8	5	Bentonite	25	*			Dense	10/18/02 16:34
9	5	Bentonite	25		*		Dense	7/25/02 17:37
10	5	Bentonite	25		*		Dense	8/12/02 16:57
11	5	Bentonite	25			*	Dense	10/8/02 17:53
12	5	Bentonite	25			*	Dense	10/14/02 22:23
13	5	Bentonite	35	*			Loose	1/24/03 16:46
14	5	Bentonite	35	*			Loose	1/27/03 20:36
15	5	Bentonite	35		*		Loose	12/3/02 18:31
16	5	Bentonite	35		*		Loose	1/6/03 16:10
17	5	Bentonite	35			*	Loose	11/19/02 20:48
18	5	Bentonite	35			*	Loose	11/25/02 21:53
19	5	Bentonite	35	*			Dense	10/29/02 21:29
20	5	Bentonite	35	*			Dense	11/1/02 16:59
21	5	Bentonite	35		*		Dense	1/13/03 21:14
22	5	Bentonite	35		*		Dense	1/15/03 20:27
23	5	Bentonite	35			*	Dense	11/12/02 18:16
24	5	Bentonite	35			*	Dense	1/17/03 18:23

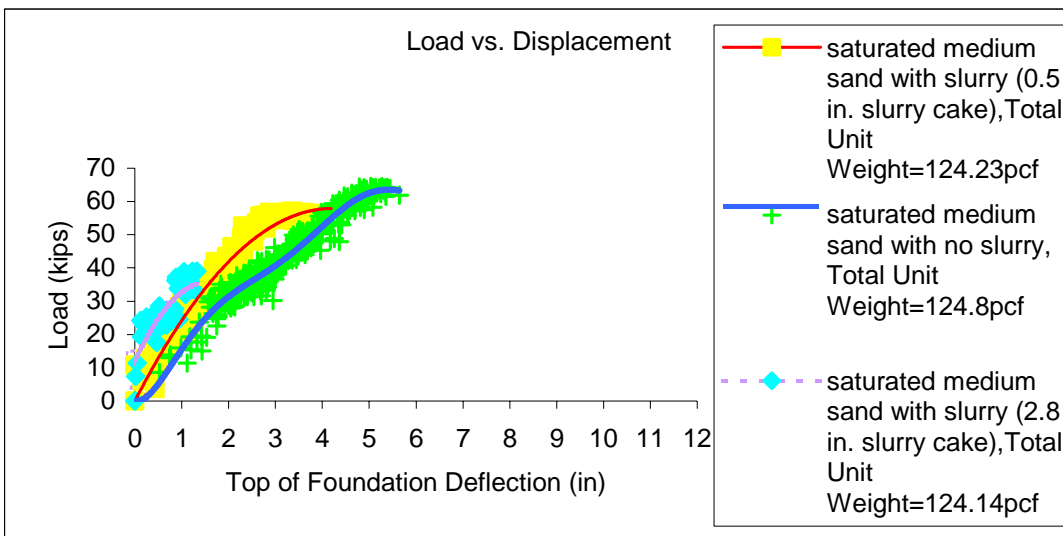
Note: The dry unit weight of loose sand is about 92.8 pcf (120.5 pcf in total unit weight)
The dry unit weight of dense sand is about 99.2 pcf (124.5 pcf in total unit weight).

were constructed under wet-hole method of construction, had significantly different capacities. Specifically, a shaft constructed with 3.0 in. of slurry cake, had half the capacity of a shaft constructed with 0.5 in. of slurry cake. With the latter in mind, a series of shafts (25-ft embedment) were constructed in saturated dense sand (unit weight = 124.2 pcf) under different construction techniques and tested under combined lateral/torsional loading (load applied at mid mast arm). The construction techniques investigated were 1) casing, i.e., no slurry, 2) slurry with 0.5 inch of cake, and 3) slurry with approximately three inches of slurry cake.

Shown in Figure 4.19 is both the lateral and torsional response of the shafts. Evident from the figures, all the shafts failed in torsional capacity (i.e., rotated more than fifteen degrees). The differences in construction are evident in Figure 4.19b, i.e., torsional shear stresses. The shafts constructed with the casing or with 0.5 in of slurry cake had little if any difference in torsional shear stress; however, the shaft constructed with 3 in. of slurry cake had a fifty percent reduction in capacity (similar to Tawfiq, 2000). Interestingly, the slurry cake thickness had little influence on the initial slope of the lateral response, Figure 4.19a. This was expected since the lateral resistance from soil, i.e., P-Y, is due to the sand not the slurry cake.



(a)



(b)

Figure 4.19 Comparison of Test Results Among Different Thicknesses of Slurry Cakes.

CHAPTER 5 EXPERIMENTAL RESULTS IN DRY SAND

5.1 Introduction

Fifty-four tests were conducted in the centrifuge on single mast arm traffic light poles, supported on drilled shaft foundations founded in dry sands. The work outlined in the original contract was to investigate the influence of combined lateral and torsional load on shaft response with minimal construction effects, i.e., dry sand with temporary casing.

The prototype dimensions studied were obtained from State of Florida specifications, Table 2.1, which was a mast arm length of 30 ft and a pole height of 20 ft. The foundation, a drilled shaft, had a diameter of 5 ft with variable length to diameter ratios: 3, 5, and 7. Each foundation was tested by applying a lateral load at one of three potential locations: top of the pole, at the center of the mast arm, or at the tip of the mast arm. Applying the lateral load along the mast arm, created a torque in addition to the lateral load on the foundation top. All tests were loaded until failure occurred. The latter was defined by one of two modes namely, excessive lateral deflection (larger than 12 inches) at top of foundation, or excessive rotation (equal to, or larger than 15 degrees).

The soil foundation for all fifty-four tests was a Florida fine sand, Edgar, classified as poorly graded (SP). It was placed in three relative densities, loose, medium and dense states. A discussion of shaft construction is available in Section 4.4.

Data obtained from each test included deflections on the mast arm, top and bottom of the pole, as well as the applied load. Figure 5.1 shows a traffic pole, mast arm, foundation, loading device (air piston), and LVDTs to measure movements along the pole.

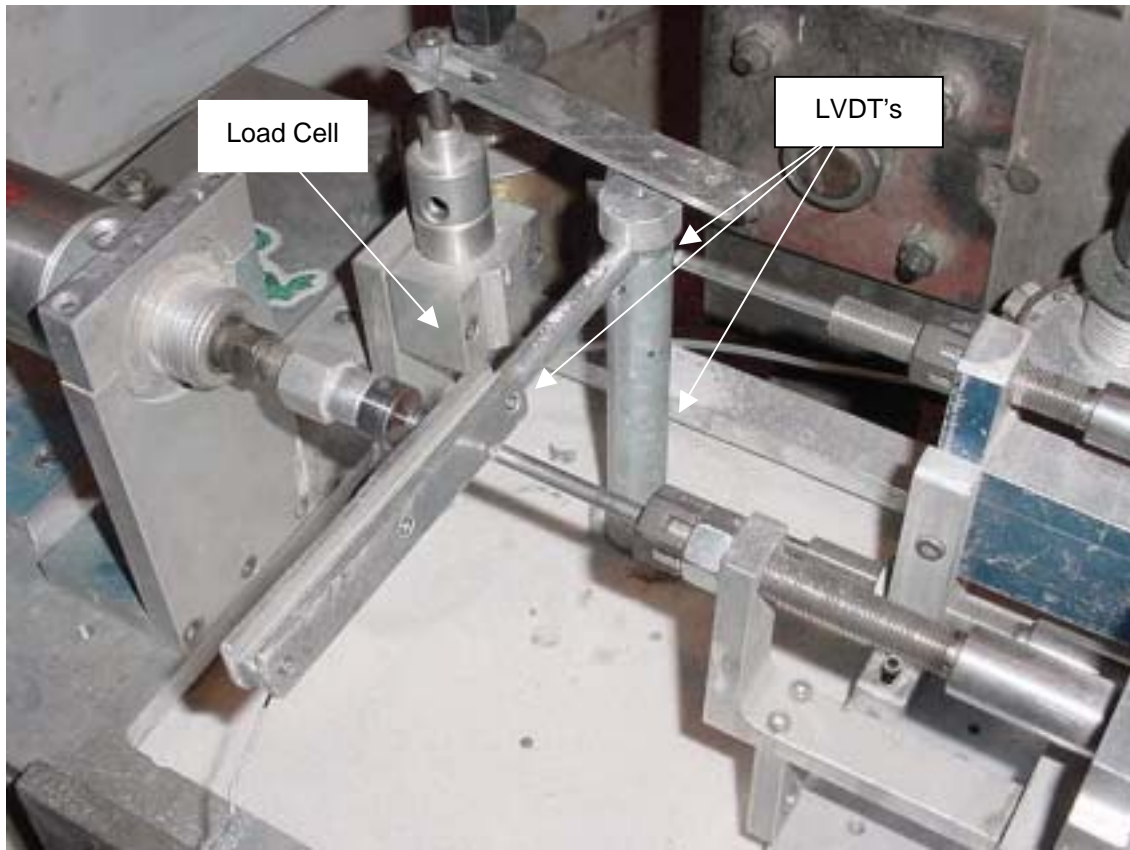


Figure 5.1 Testing Set-up.

5.2 Lateral Load on Pole with No Torsion

Lateral load tests were conducted by applying a load directly on the pole top, in line with the foundation's center. In prototype dimensions the load would have been located 20 ft above the foundation top, creating a lateral force and a moment at the top of the drilled shaft.

5.2.1 Measured Experimental Results

Eighteen lateral load tests were performed in the centrifuge with the load applied at the pole's top (Table 5.1). The latter accounts for different soil density (3), length to diameter ratio (3) and repeatability (2) of tests. The latter was performed to ensure the validity of test results. Subsequently, the results were statistically analyzed to check if the range in the tests was satisfactory, and that no further repetitions were required for any particular testing sequence. Prototype values are presented in Table 5.1 at one-inch of deflection at the foundation top, deflection at which certain signs of failure could be seen around the prototype structure such as cracking of the concrete. All of the values obtained for the coefficient of variance were below 0.4 indicating that the measured response was satisfactory.

Table 5.1 Lateral Load Data Statistical Analysis

Lateral Load Data Statistical Analysis					
L/D	Dr (%)	Lateral Load (kips)	Mean	Standard Deviation	Coefficient of Variance
3	29.14	19	25.2	5.0	0.20
	29.14	21			
	50.7	23			
	50.7	27			
	63.5	29			
	63.5	32			
5	29.14	47	56.2	12.4	0.22
	29.14	53			
	50.7	40			
	50.7	58			
	63.5	75			
	63.5	64			
7	29.14	80	101.7	25.9	0.25
	29.14	70			
	50.7	94			
	50.7	106			
	63.5	120			
	63.5	140			

5.2.2 Predicted Lateral Result with No Torsion

Current methods (Chapter 3) used to design and predict capacity or deflection of deep foundations include the use of sophisticated software, as well as hand solutions that can be implemented into spreadsheets for ease of calculation.

In particular, the P-Y used in the programs L-PILE, and FB-PIER (see Chapter 3), which have the capability of generating shear, bending, and deflection response of a foundation along its length, were used for comparison. In addition, the passive earth pressure approach of Broms' coded in an Excel spreadsheet was compared with the measured response. Comparison between measured (prototype centrifuge response) and predicted is given in Table 5.2.

Results from Table 5.2 show an excellent correlation between FB-PIER, LPILE 3.0 with centrifuge results. The comparison is based on deflections for given (measured) lateral loads. Broms' method as shown in Table 5.2 was slightly unconservative. The key parameter for the P-Y approach (i.e., FB-PIER & LPILE programs) was the constant modulus of subgrade reaction, k . Selection of this parameter was based on the soil unit weight achieved in the sample container, which gives relative density, D_r , which is correlated to k values given in the LPILE and FB-PIER manuals.

However, results from Table 5.2 are values at a single point along the load-deflection curve. For a better picture of how well FB-PIER compared to the measured response, Figures 5.2 to 5.4 show a comparison for six inches of deflection.

Each plot shows both a linear and nonlinear representation of the drilled shaft. For the nonlinear, the shaft reinforcement (steel ratio and placement), and concrete strength and modulus is represented with FB-PIER's nonlinear discrete element.

Table 5.2 Centrifuge Lateral Load Results and LPILE, FB-PIER, and Broms' Predictions

Shaft Embedment (ft)	Centrifuge Results Prototype deflection (in.)	Prototype Load (kips)	Soil γ (pcf)	Soil Modulus (k) (pci)	LPILE Predictions (in.)	LPILE Factor of Safety	FB-PIER Predictions (in.)	FB-PIER Factor of Safety	Broms Predictions (in.)	Broms Factor of Safety
15	1	30	98.34	35	1.4	1.4	1.37	1.4	0.99	1.0
25	1	70			0.9	0.9	0.91	0.9	0.64	0.6
35	1	130			1.1	1.1	1.02	1.0	1.01	1.0
15	1	25	95.88	30	1.3	1.3	1.29	1.3	0.88	0.9
25	1	50			0.7	0.7	0.75	0.7	0.52	0.5
35	1	100			0.9	0.9	0.85	0.9	0.82	0.8
15	1	18	92.07	25	1.1	1.1	1.12	1.1	0.68	0.7
25	1	50			0.9	0.9	0.89	0.9	0.55	0.6
35	1	75			0.7	0.7	0.73	0.7	0.66	0.7
					Average FS	1.0	Average FS	1.0	Average FS	0.8

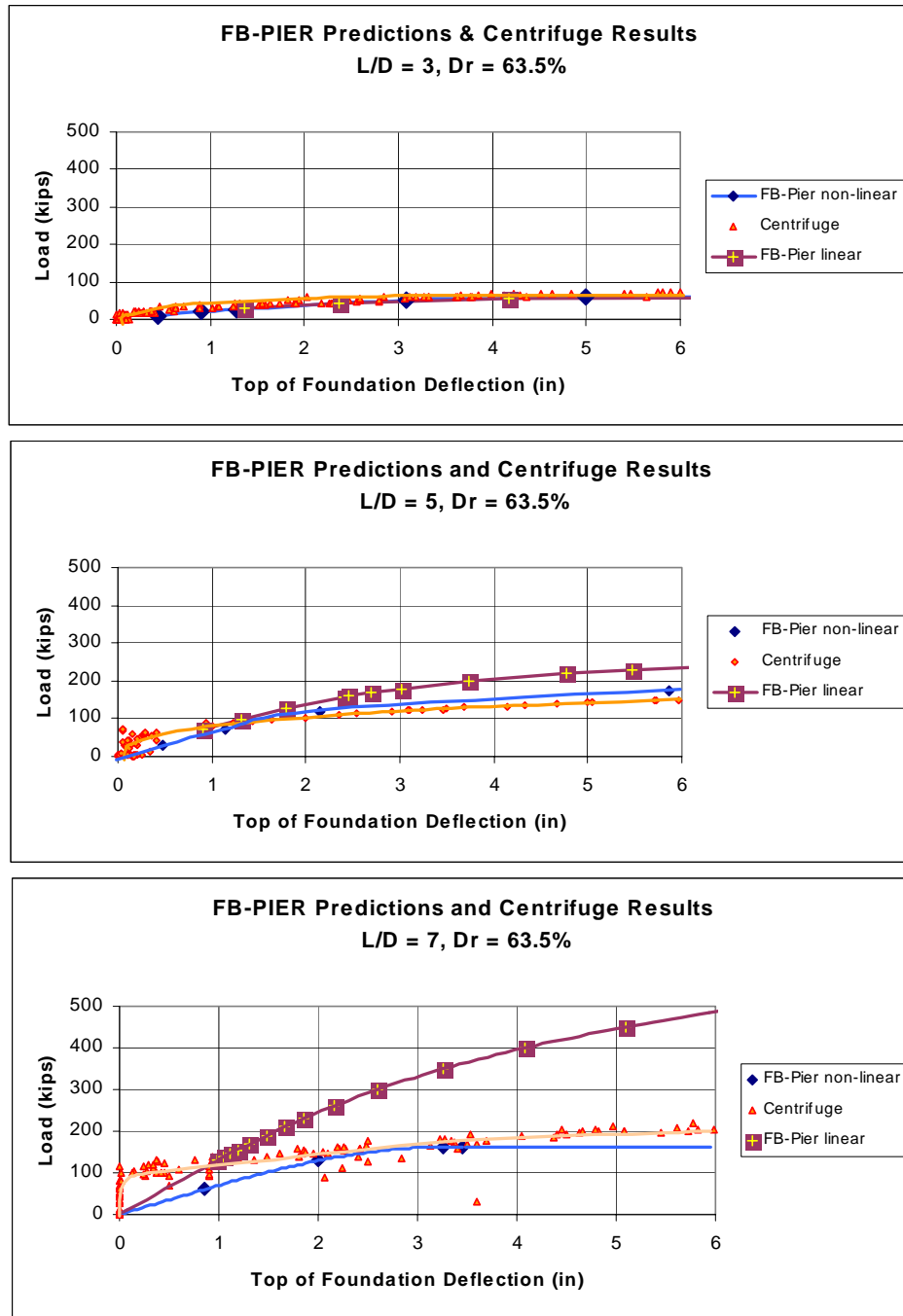


Figure 5.2 Measured vs. FB-PIER for Medium Dense Sand.

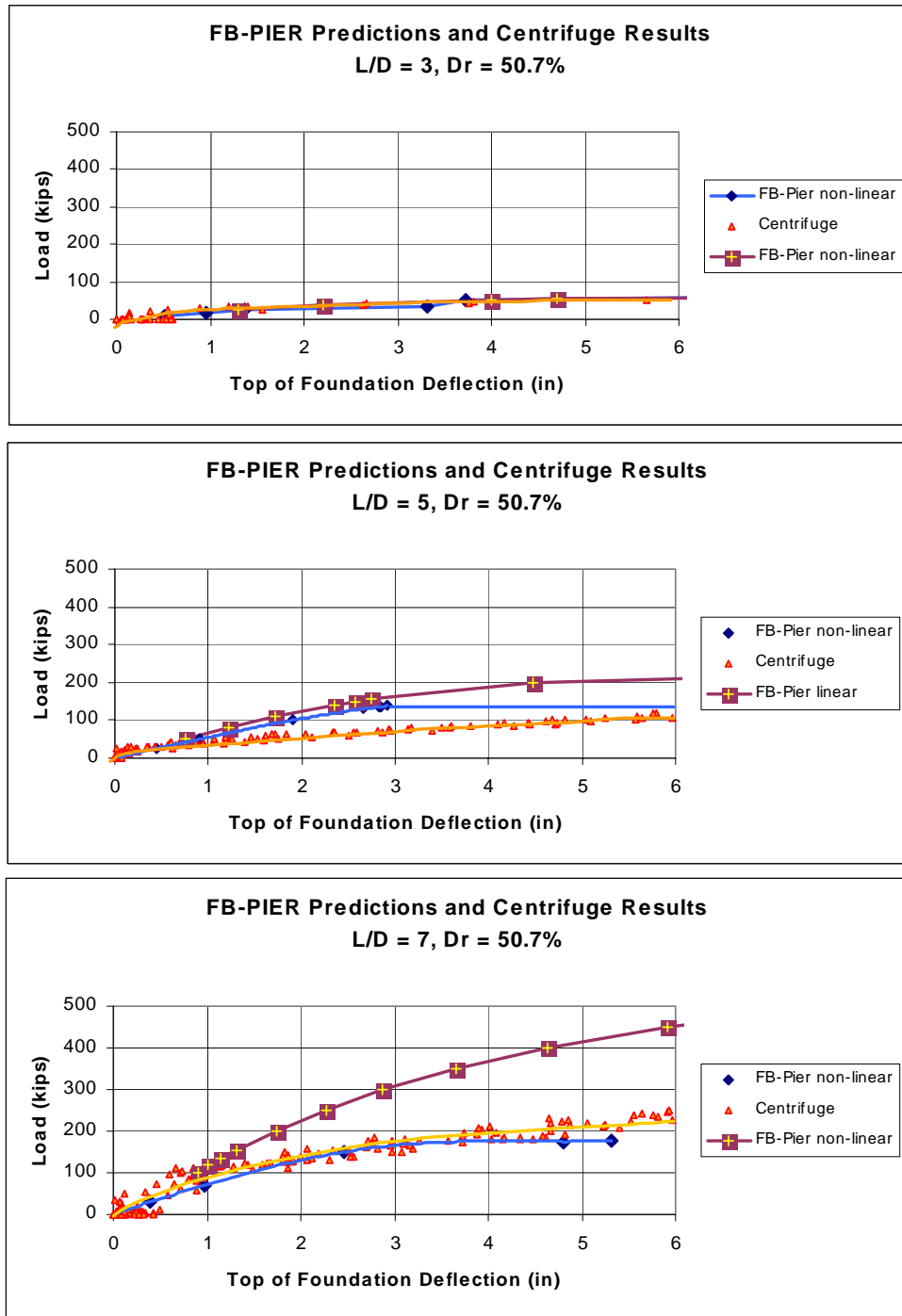


Figure 5.3 Measured vs. FB-PIER for Medium Loose Sand.

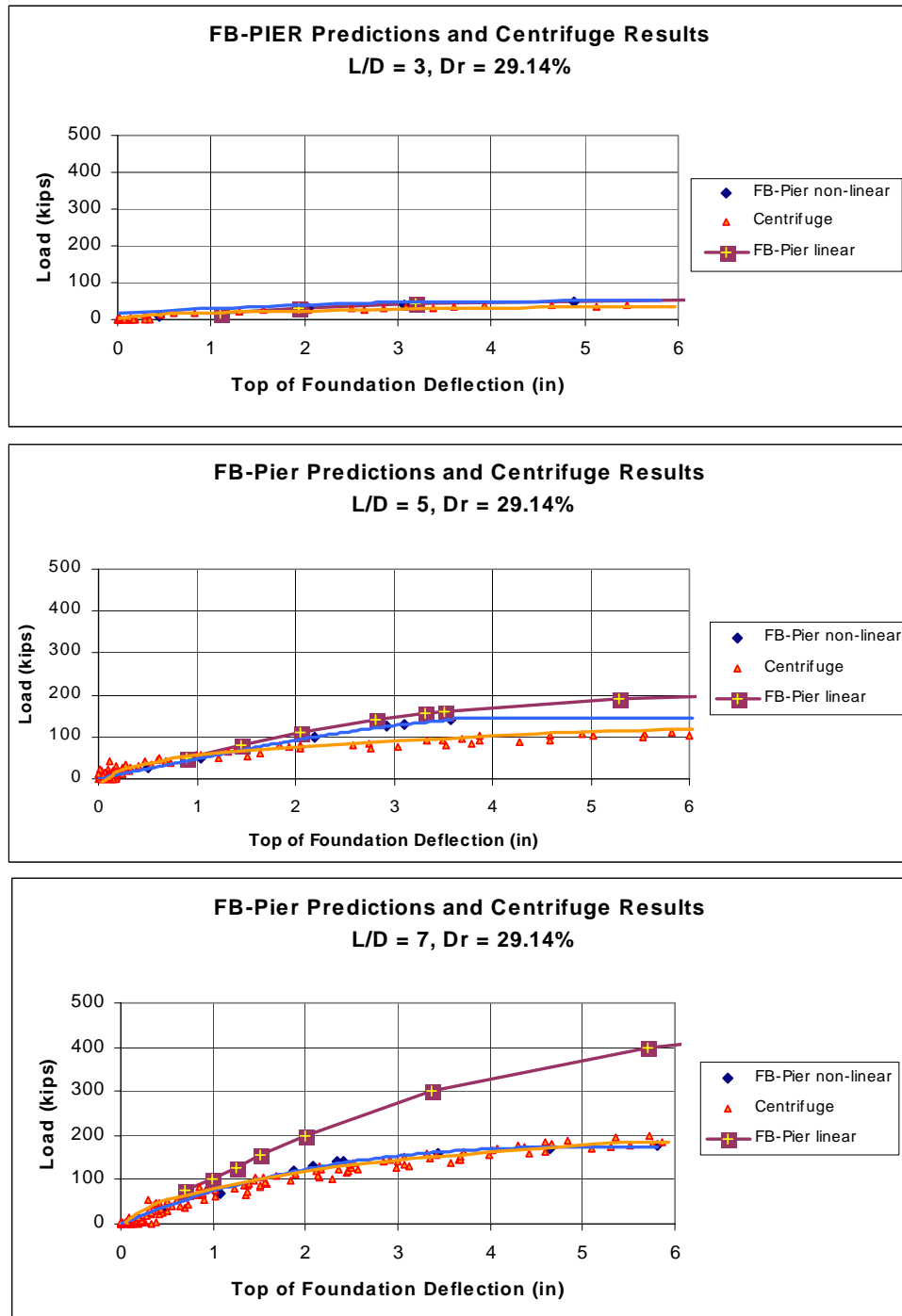


Figure 5.4 Measured vs. FB-PIER Prediction for Loose Sand.

Evident from the graphs the load-deformation behavior is governed not only by the soil, but the strength and stiffness of the foundation. This can be observed by the smaller increasing load capacity of the nonlinear drilled shaft with increased L/D ratios, i.e., 5 and 7. That is the short shafts, in this case 15 foot embedment, $L/D = 3$, can be modeled as linear objects since they behave as rigid bodies (i.e., rotate) and lateral deformation is due to soil failure. However, for long shafts, $L/D = 5$ and 7 there is a significant difference in lateral resistance for the linear and nonlinear representation. The latter suggest that the longer shafts are undergoing cracking within the soil mass, since along its length, a reversal in the direction of the shear forces occurs which is the location of maximum moment in the shaft. This point may be considered as a point of fixity beyond which little improvement in lateral resistance occurs by increasing drilled shaft length. Consequently, as can be observed by the non-linear shaft predictions, the ability of the computer program to model not only soil response but the structure as well is a necessity for shafts with L/D ratios in the range of 5 to 7.

5.3 Lateral Load with Torque

Behavior of deep foundations subject to lateral loads has been a widely studied topic among Geotechnical Engineers, however, literature discussing the influence of torsion on a deep foundation is relatively small in number. Furthermore, centrifuge research on the topic is even harder to find.

For this project, in addition to lateral load tests, a testing sequence consisting of combined lateral load plus torque was performed to determine its influence on the foundation capacity, as well as the influence of torque to lateral load ratio.

5.3.1 Measured Torque-Lateral Load Results

Torque-lateral load tests were performed by applying the load at one of two points along the mast arm, which imparts both a lateral load and a twisting force to the foundation top. The latter is representative of high mast lighting, signs and signals. To study the influence of torque to lateral load ratio, the load was moved along the mast arm. This would be representative of variable length mast arms.

Results from the torque-lateral load tests were statistically analyzed to identify any irregularities that may have occurred during testing. Values of coefficient of variance shown in Table 5.3 reveal that the testing sequence was satisfactory.

Next, plots (see Figures 5.5 to 5.7) of lateral load applied to the pole and at variable distance along the mast arm were constructed for variable embedded shaft lengths. The latter gives a direct measure of the influence on variable torque to lateral load ratios.

Evident from Figures 5.5 to 5.7 the lateral resistance of the foundation diminished as the lateral load moved out along the mast arm. That is by applying a torque in combination with a lateral loading the shafts' resistance is reduced overall. The latter may be explained from Rankine's passive Mohr circle. Rankine's passive resistance, P_p , used in assessing P_u for a P-Y curve in sand, assumes no shear stress on vertical planes.

With the addition of torque, a shear stress is developed on the vertical plane, which reduces the maximum horizontal stress, which will develop on a vertical plane. The latter is a result of a fixed size Mohr circle, i.e., circle is tangent to strength envelope, and an increasing shear stress on the vertical plane. The decrease in magnitude of maximum horizontal stress, i.e., σ_h (used in P-Y curve) is a direct function of applied

Table 5.3 Torsional-Lateral Load Tests Statistical Analysis

(Torsional-Lateral) Centrifuge Results Statistical Analysis on Test Repeatability							
Point of Load Application	Dr (%)	Length to Diameter Ratio	Prototype Torque (ft-kips)	Centrifuge Values of Unit Skin Friction (psf)	Mean Value of Unit Skin Friction	Standard Deviation	Coefficient of Variance
Arm Tip	63.5	3	710	1205.3	1279.6	389.0	0.304
	63.5		770	1307.2			
	50.7		660	1120.4			
	50.7		700	1188.4			
	29.14		590	1001.6			
	29.14		630	1069.5			
Mid Mast Arm	63.5	3	1180	2003.2			
	63.5		1250	2122.1			
	50.7		650	1103.5			
	50.7		630	1069.5			
	29.14		495	840.3			
	29.14		780	1324.2			
Arm Tip	63.5	5	1000	1018.6	1383.2	318.4	0.230
	63.5		1260	1283.4			
	50.7		1480	1507.5			
	50.7		1520	1548.3			
	29.14		1000	1018.6			
	29.14		1260	1283.4			
Mid Mast Arm	63.5	5	1750	1782.5			
	63.5		1850	1884.4			
	50.7		1375	1400.6			
	50.7		1740	1772.3			
	29.14		1050	1069.5			
	29.14		1010	1028.8			
Arm Tip	63.5	7	1900	1382.4	1503.6	437.2	0.291
	63.5		1950	1418.7			
	50.7		2150	1564.3			
	50.7		2250	1637.0			
	29.14		1800	1309.6			
	29.14		2200	1600.6			
Mid Mast Arm	63.5	7	3040	2211.8			
	63.5		3320	2415.5			
	50.7		1610	1171.4			
	50.7		1860	1353.3			
	29.14		1230	894.9			
	29.14		1490	1084.1			

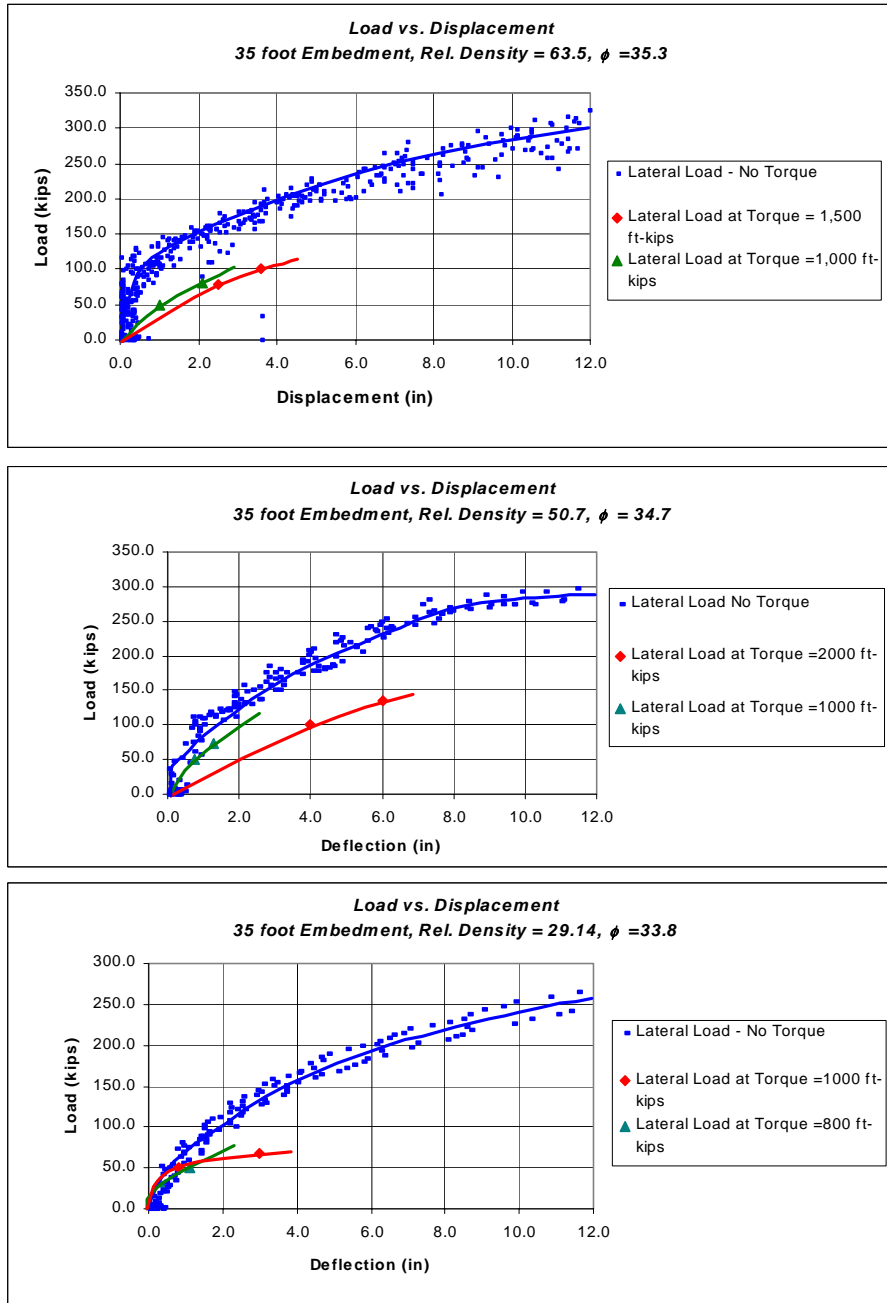


Figure 5.5 Measured Resistance for 35-ft Embedded Shafts.

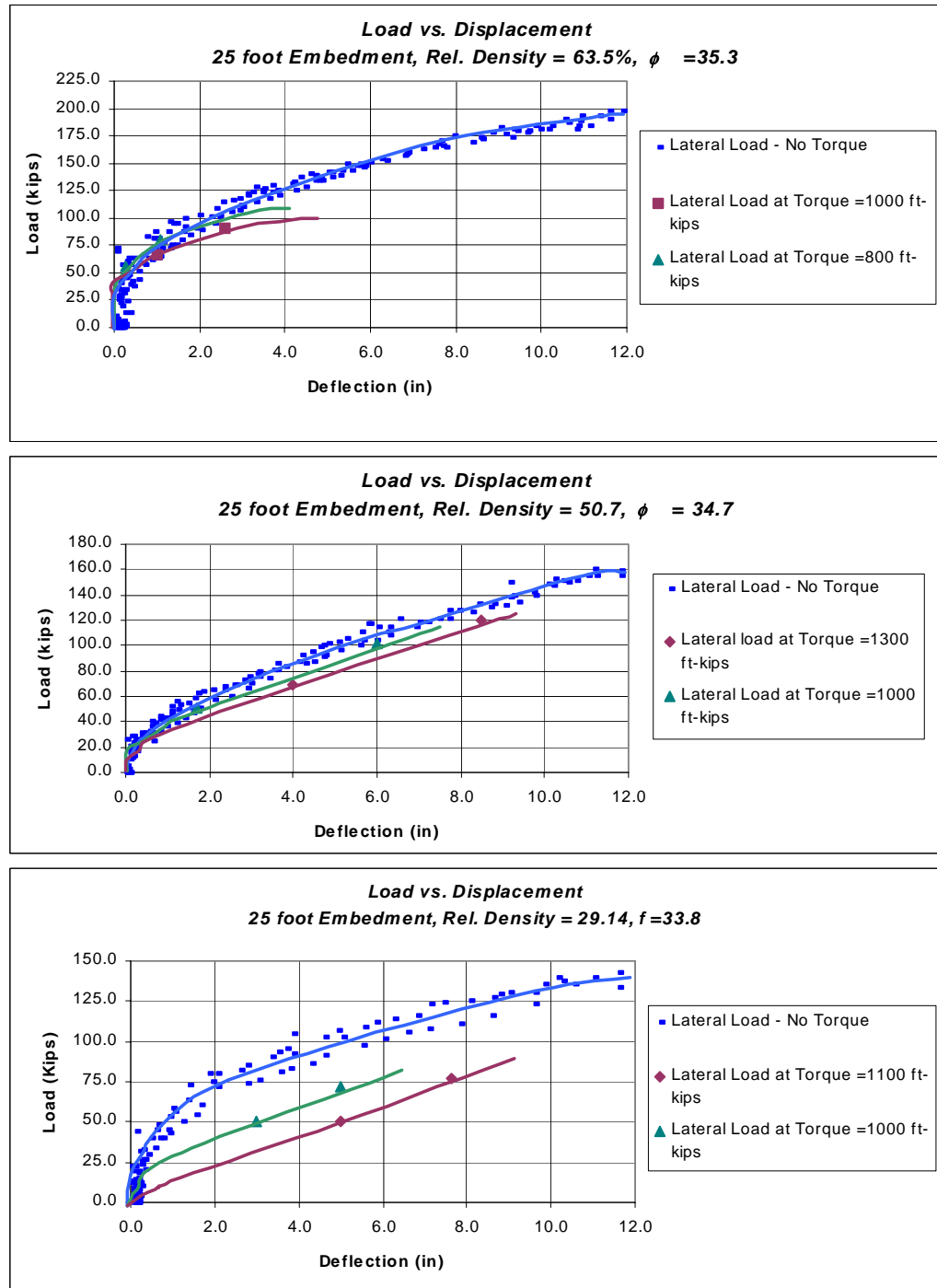


Figure 5.6 Measured Resistance for 25-ft Embedded Shafts.

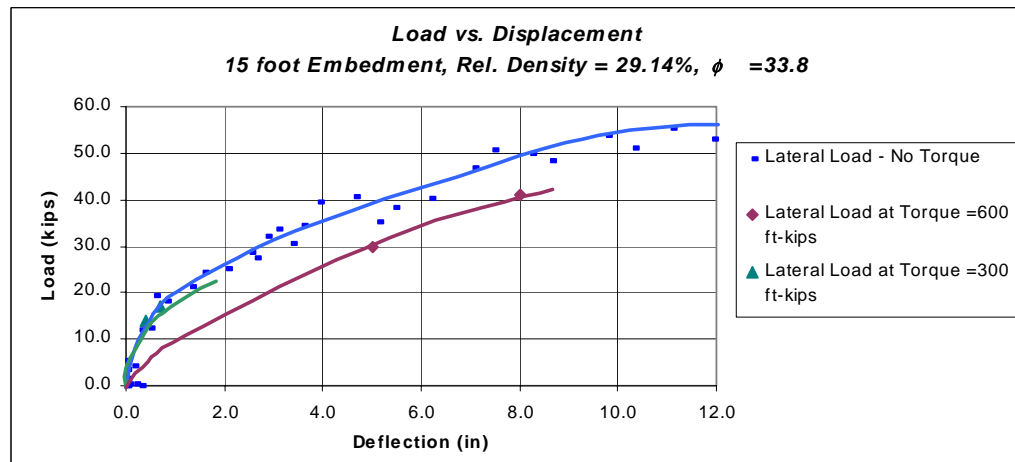
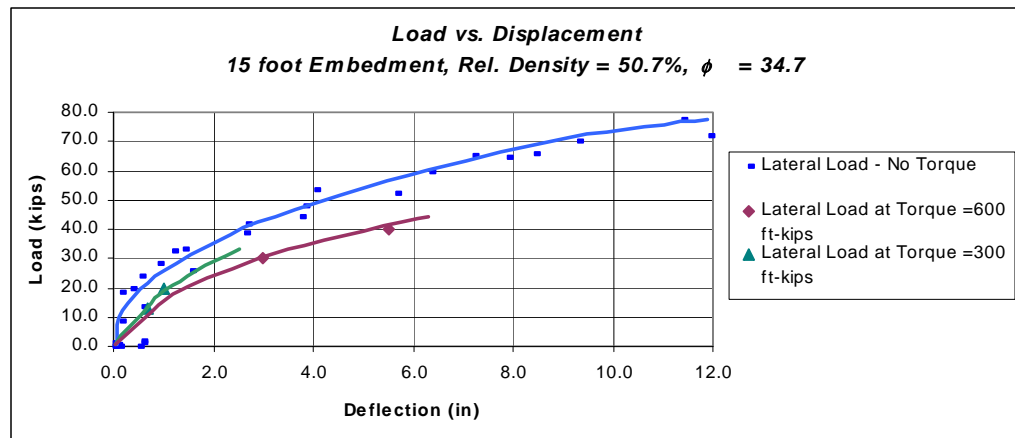
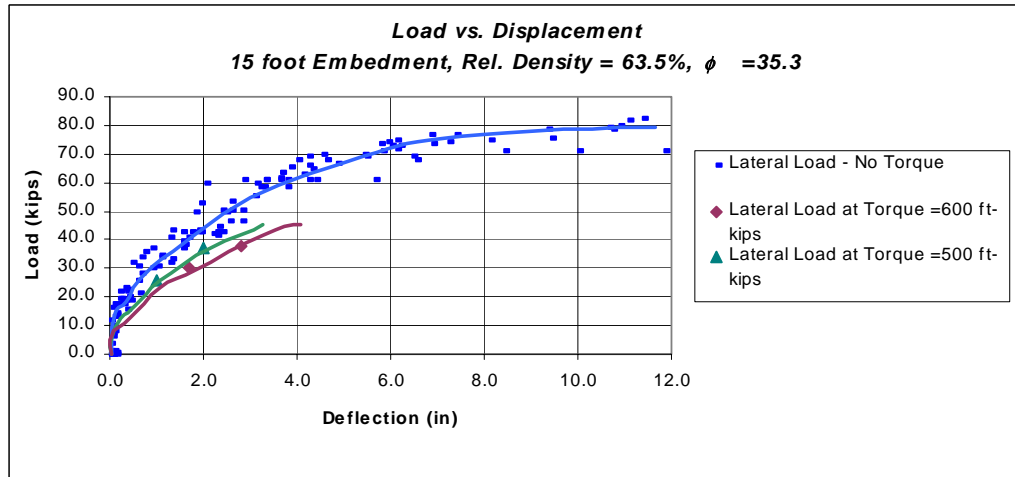


Figure 5.7 Measured Resistance for 15-ft Embedded Shafts.

torsional shear stress. Consequently, it is recommended that the P-Y or lateral resistance curves be adjusted based on torque or lateral load to torque ratio.

5.3.1.1 Influence of Length to Diameter Ratio. As identified earlier, drilled shaft foundations with a constant diameter and varying embedments behave differently as the ratio of embedment to diameter changes. The study the influence of L/D ratio on the combined torque with lateral load, the previous graphs were plotted with fixed vertical and horizontal axes for all L/D ratios (Figure 5.8 to 5.10). A constant y-axis value of 50 kips and x-axis value of 12-inches were employed to indicate the influence of the L/D ratio.

Two clear trends were identified from Figures 5.8 to 5.10. One, the shaft's resistance to lateral load and torque increased with soil density. And second, the influence of torsion on the lateral resistance of a drilled shaft increases as the L/D ratio increases. This behavior is attributed to the large effect of the drilled shaft's tip on small L/D ratio. That is shorter shafts have torsion being carried by the shaft's tip, whereas, for longer shafts, the torsion is being carried along the side of the shaft. The latter in turn reduces the lateral resistance, σ_p , or the magnitude of the P-Y curve at the top of the shaft which is providing the lateral resistance of the shaft.

To estimate the influence of tip resistance two torsion tests (Mid Mast Arm) were performed on shafts with L/D equal to 5 into soil with a relative density of 57.3 percent, where the tip of the foundation was rested over an oiled metal surface to allow rotation without friction. Results of the tests showed a 9 percent decrease in capacity, which was somewhat higher than expected, considering the tip area was only 4.76 percent of the

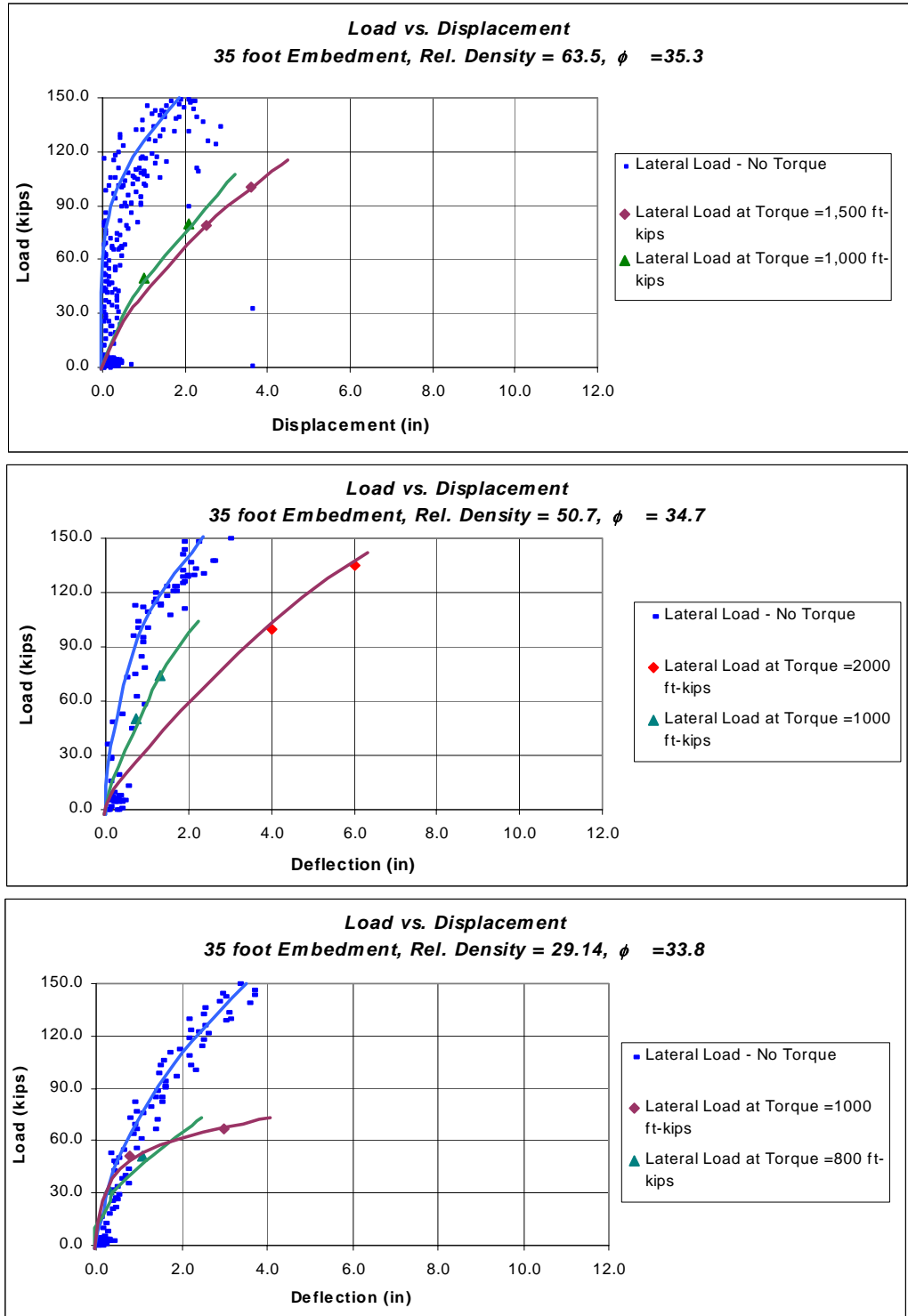


Figure 5.8 Measured Lateral Resistance for 35-ft Embedded Shafts.

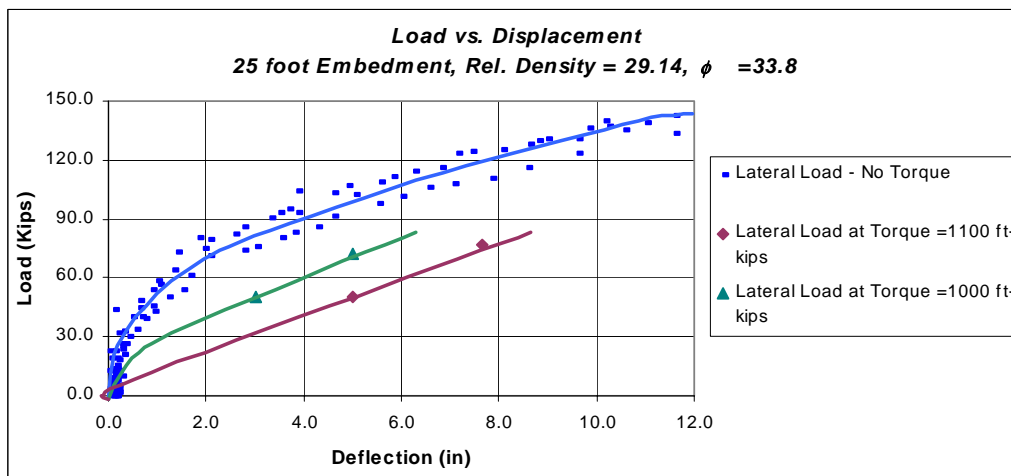
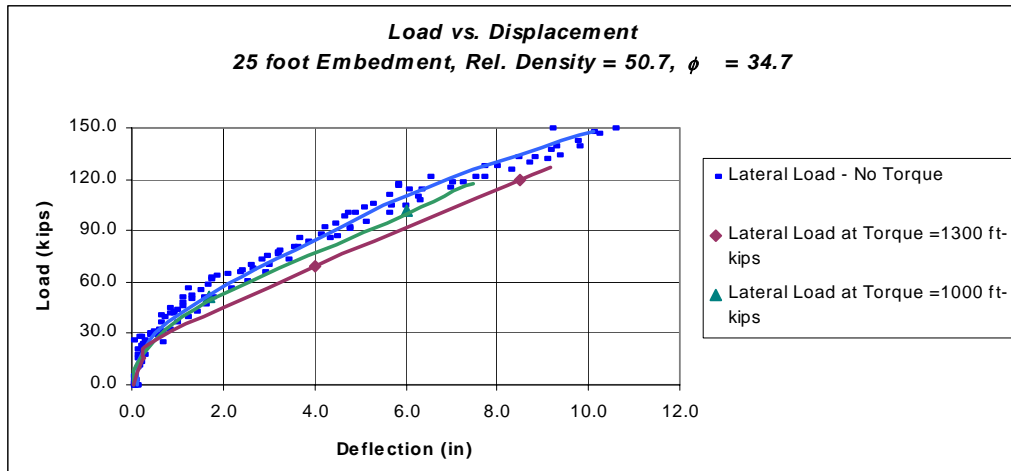
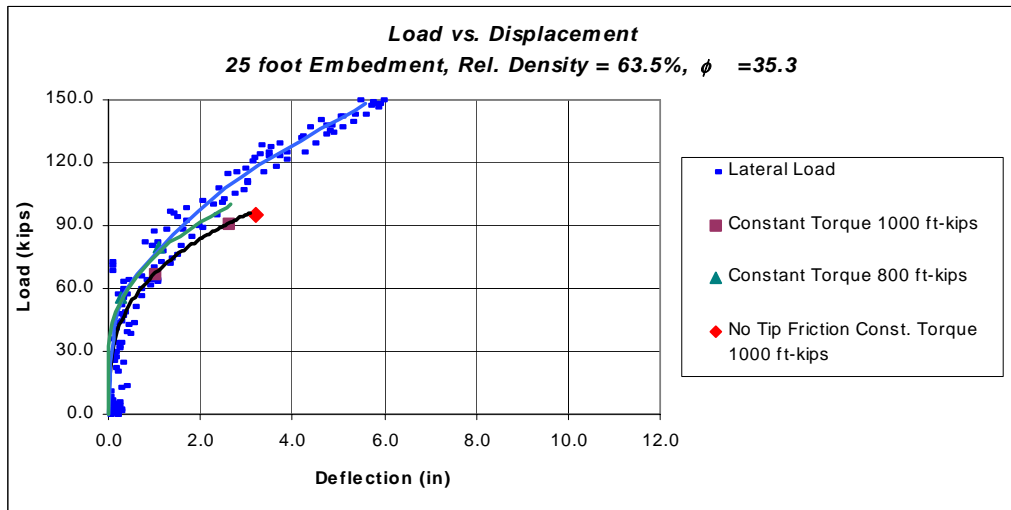


Figure 5.9 Measured Lateral Resistance for 25-ft Embedded Shafts.

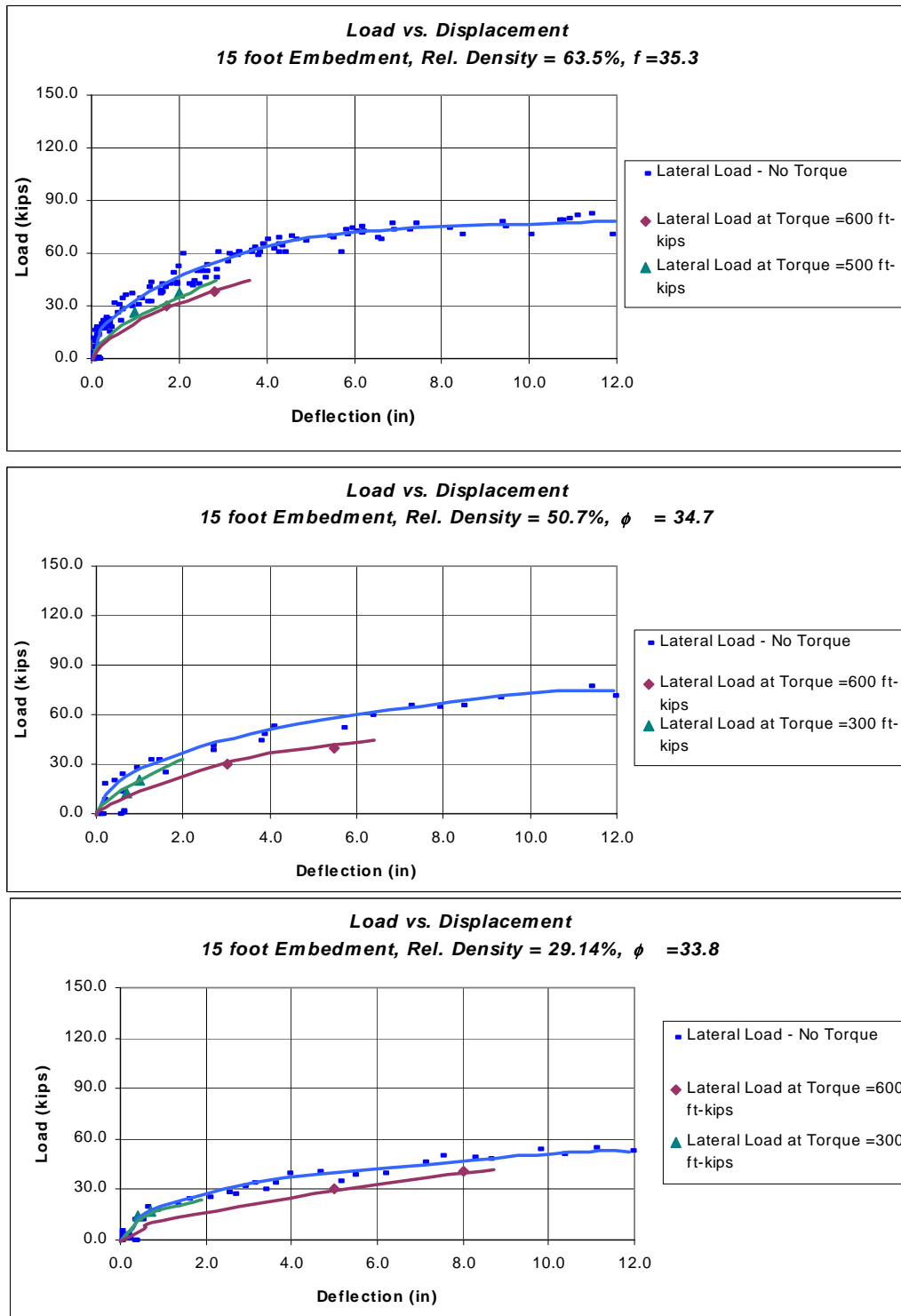


Figure 5.10 Measured Lateral Resistance for 15-ft Embedded Shafts.

total surface area in contact with the soil. Further tests, indicate that there is still considerable influence on capacity from tip resistance at L/D ratios up to five.

5.3.1.2 Influence of Soil Density on Torque-Lateral Tests. Next the data was analyzed for the influence of soil densities. Figures 5.11 to 5.13 vary L/D for constant soil densities. The values of torque in each plot were obtained by multiplying the force applied to the mast arm (load cell readings) by the distance from the center of the foundation. Rotation was obtained from LVDT readings. Evident from the figures, the influence of soil density is a major contributor to ultimate torque achieved. That is the higher the density, the higher value of ultimate torque. The graphs also reveal that a reversal of controlling influences. For samples tested in soil with a relative density of 63.5 percent, it is the mid mast arm tests that have the higher values of torque. However, for tests with a relative density of 29.14 percent (loose sand), the tests performed on the arm tip are the ones that exhibit the higher torque resistance.

5.4 Combined L/D, Strength and Torque to Lateral Load Ratio.

One clear trend observed throughout the testing is the increase in capacity with increasing soil density. However, the influence of length to diameter ratio varies as the ratio decreases, with the lower ratio (three) behaving as a linear member, and the higher ones clearly involving foundation strains that affect the load deformation curve as observed on the comparison graphs of FB-PIER vs. centrifuge results.

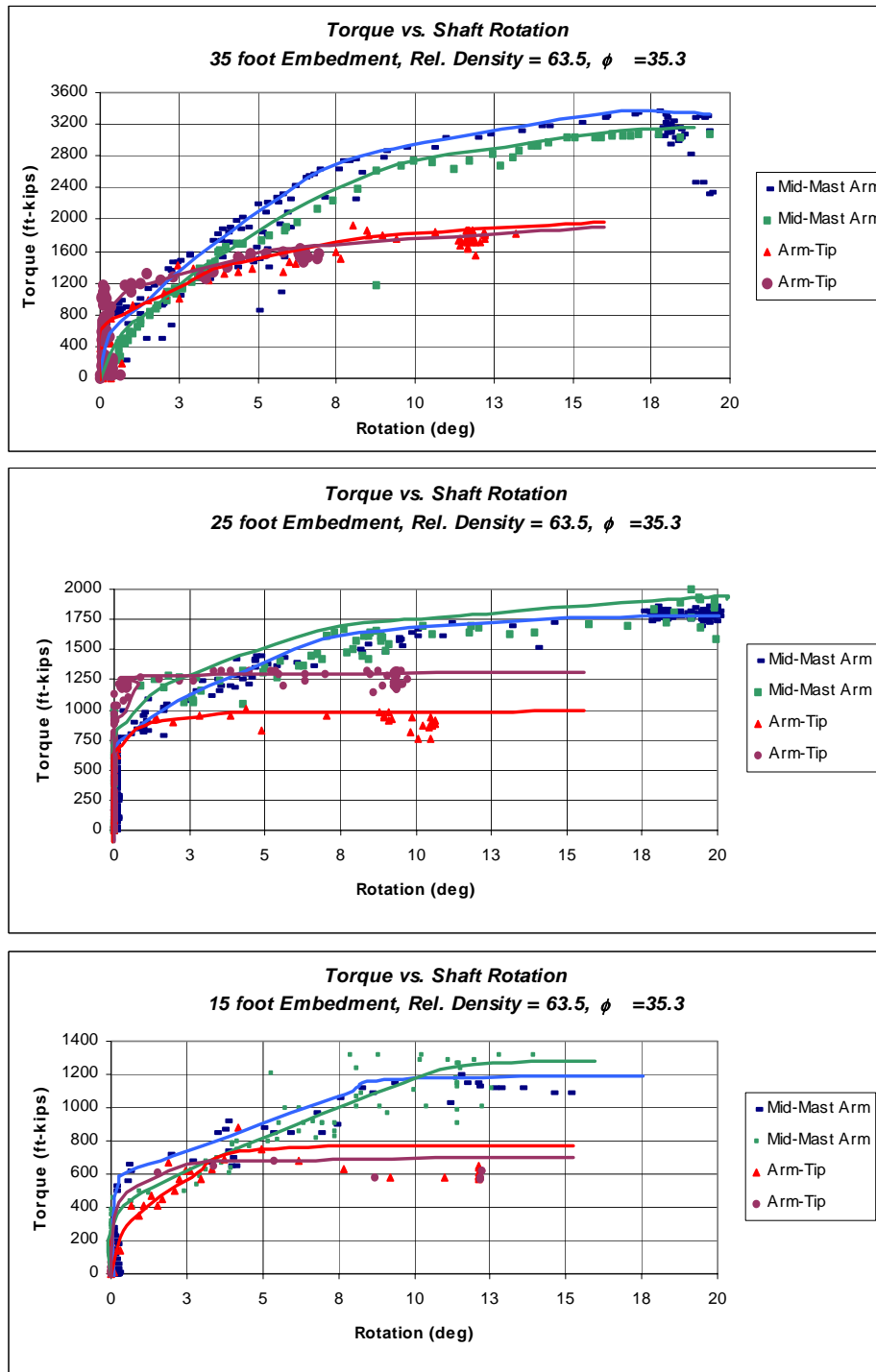


Figure 5.11 Torque vs. Top of Foundation Rotation, Medium Dense Sand.

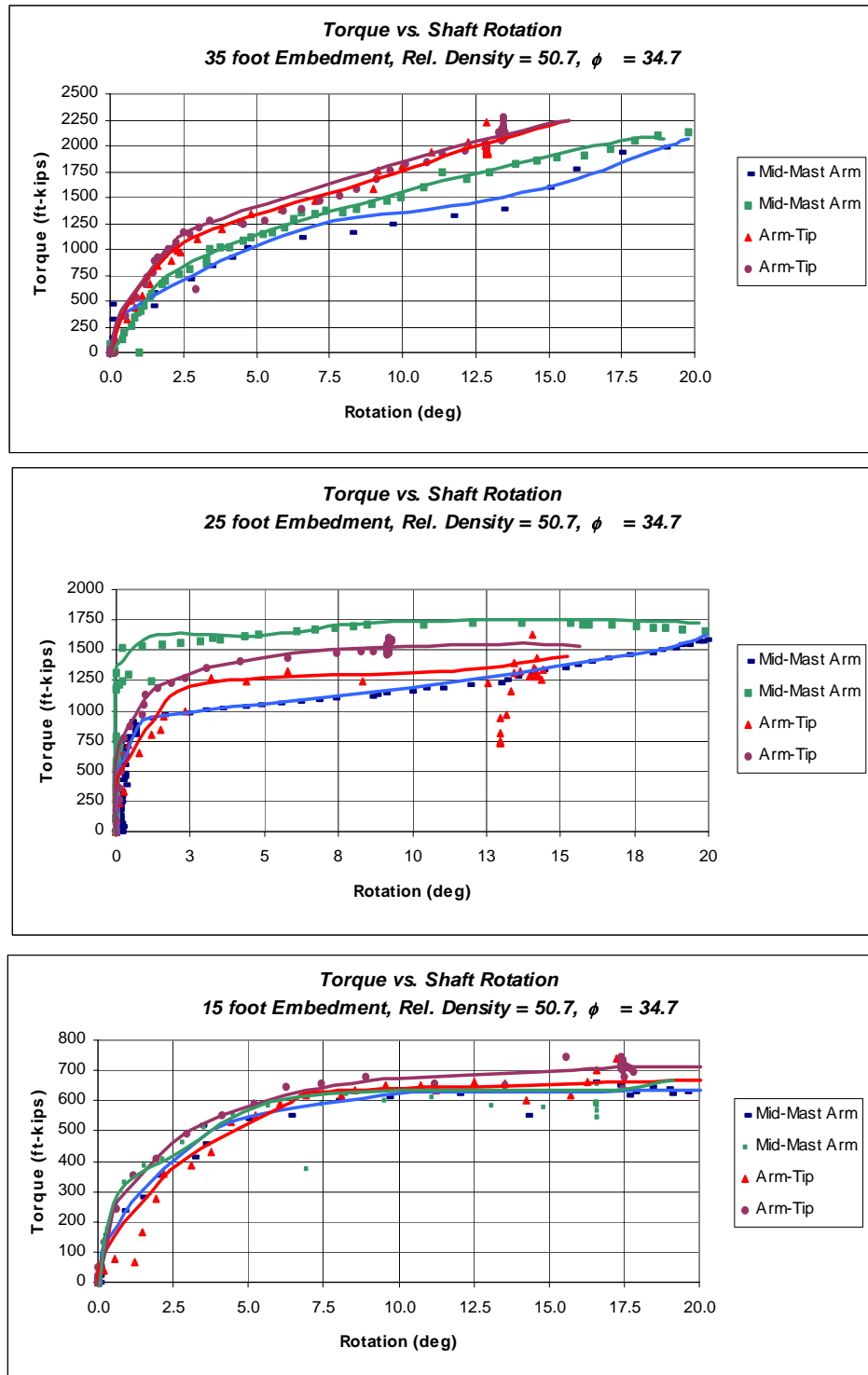


Figure 5.12 Torque vs. Top of Foundation Rotation, Medium Loose Sand.

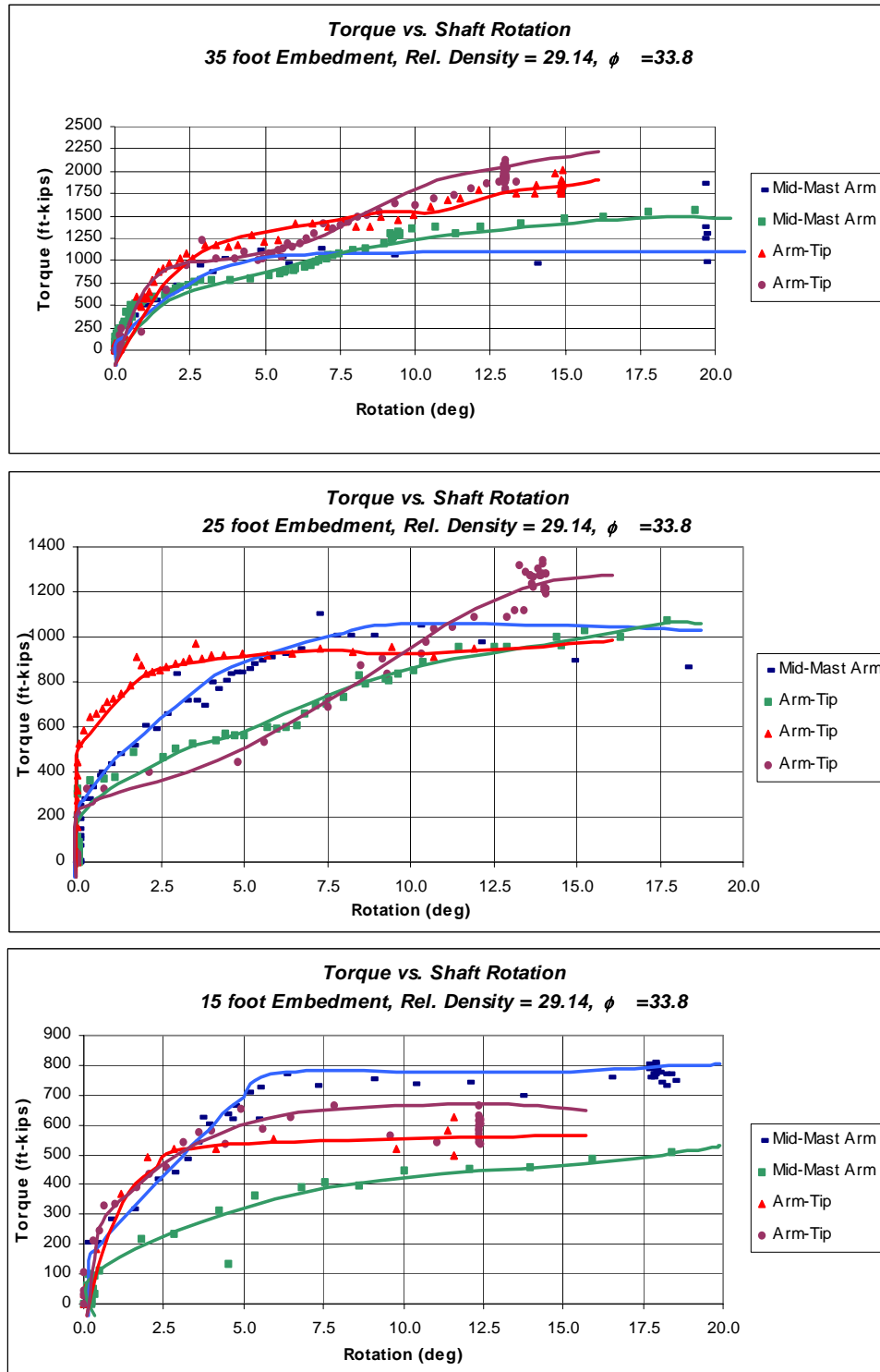


Figure 5.13 Torque vs. Top of Foundation Rotation, Loose Sand.

Results obtained from the addition of torque to the foundation top, were expected as far as the decrease in capacity is concerned, however, the results revealed that the reduction in capacity is greatest with the higher L/D ratios. The stronger influence on capacity of the tip of the drilled shaft is evident from this set of results

5.5 Comparison with Field Load Test and Current Design Methods

Full-scale field load testing of drilled shafts was performed by Tawfiq et al., at the Florida State University (FSU) campus under similar conditions to the ones pertaining this research. One end of a steel beam was connected to the top of a drilled shaft foundation, and was loaded to generate a torque and lateral load transfer to the foundation top as shown in Figure 5.14.

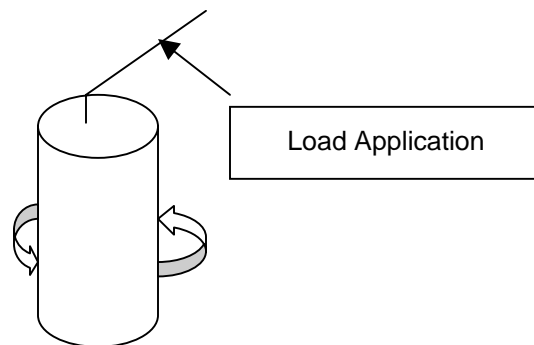


Figure 5.14 Schematic of Field Load Test.

One field test was conducted on a 4-ft diameter shaft with 20 ft of embedment into a silty sands to sandy silts with a relative density (D_r) of 72 percent. The relative density value was obtained by correlations of D_r against Standard Penetration Test blow counts, which were provided with the report. This shaft was cast by the dry method of construction, as were the centrifuge models.

The latter test would be most similar the centrifuge model test of a 5-ft diameter, 25-ft embedment drilled shaft with the 63.5 percent relative density. The field test was to be conducted until 15 degrees of rotation at the top of foundation were achieved. However, the field load test foundation cracked before any rotation was recorded. Approximately 480,000 ft-lbs of torque, which corresponds to 955 lbs/ft² of torsional unit skin friction, was applied. In the centrifuge model no visible cracking of the foundation was encountered, and rotation was initially recorded at approximately 1,000,000 ft-lbs of torque having developed 1018 lb/ft² of torsional unit skin friction. Consequently, it is believed that the full-scale tests with the dry method of construction did validate the minimum unit skin friction reported in the centrifuge tests. It should be noted that the wet hole method of tests conducted in the field were not used in this study due to their significant difference in resistance compared to the dry method. The FSU report did note a 1-inch cake between the shaft and the insitu soil which would significantly alter the shafts resistance.

Next, the data obtained from centrifuge testing was compared to the prediction methods identified in Chapter 3. Values of one inch of lateral deflection and 15 degrees of rotation were used for the comparison since these values were identified as failure.

The methods investigated were the Structures Design Office Method, District 5 Method, District 7 Method, and the Tawfiq-Mtenga Method. The results are presented below in Table 5.4.

Results from the methods are not as accurate as the ones obtained for the lateral load applied to sign poles. The latter may be a result of the lack of a large enough

Table 5.4 Centrifuge Torque Results, FDOT and Tawfiq-Mtenga Predictions

Shaft Embedment (ft)	Soil γ (pcf)	Soil ϕ (deg)	Centrifuge Results Prototype Torque* (ft-kips)	FB-PIER Predictions (ft-kips)	FB-PIER Factor of Safety	SDO** Predictions (ft-kips)	SDO** Factor of Safety	District 5 Predictions (ft-kips)	District 5 Factor of Safety	District 7 Predictions (ft-kips)	District 7 Factor of Safety	Dr. Tawfiq's Predictions (ft-kips)	Dr. Tawfiq Factor of Safety
15	98.34	36.3	870	492.0	1.8	178.0	4.9	282.5	3.1	168.0	5.2	225.0	3.9
25			1387.5	1234.0	1.1	441.0	3.1	727.0	1.9	423.3	3.3	371.0	3.7
35			2487.5	2207.0	1.1	819.0	3.0	1378.0	1.8	794.0	3.1	567.0	4.4
15	95.88	34.7	650	479.0	1.4	173.0	3.8	219.1	3.0	163.6	4.0	219.0	3.0
25			1475	1200.0	1.2	429.4	3.4	552.2	2.7	412.1	3.6	363.0	4.1
35			1993.8	2148.0	0.9	797.7	2.5	1036.0	1.9	772.9	2.6	560.0	3.6
15	92.07	33.8	636.3	459.0	1.4	166.4	3.8	170.6	3.7	156.9	4.1	208.0	3.1
25			1050	1150.0	0.9	411.5	2.6	387.0	2.7	394.8	2.7	356.0	2.9
35			1680	2059.0	0.8	764.1	2.2	662.0	2.5	740.1	2.3	543.0	3.1
*Value of Torque at 15° rotation				Average FS	1.18	Average FS	3.26	Average FS	2.59	Average FS	3.41	Average FS	3.52
**Structures Design Office													

database to fine-tune the prediction equations. All methods however, had factors of safety above 1.0, with FB-PIER having the most accurate predictions.

All methods used in the prediction of torsional capacity, with the exception of the Tawfiq-Mtenga method are independent of torque to lateral load ratio. The centrifuge results clearly show that the relationship between the two has an important effect on the ultimate resistance. In fact, the magnitude of the ratio will determine the capacity of the foundation.

5.6 Proposed Design Guideline

Having established that the data obtained during testing was adequate, the next step was to analyze the data to identify a set of modifiers that would allow the prediction of capacity of the foundation under a combination of torsional and lateral load.

Moreover, it was recognized that the modifiers had to mesh with the established pure lateral load vs. deflection relationship obtained from software such as FB-PIER or L-PILE. To identify the magnitude of the modifiers to be used in the determination of capacity under lateral-torsional loads, a relationship between lateral and torsional-lateral tests had to be established. It was recognized that such modifiers should take into account the soil density, length to diameter ratio, and point of load application. Figures 5.15 and 5.17 show the decrease in capacity for the lateral load's position.

Next, the decrease in lateral resistance was plotted versus L/D ratio as shown in Figure 5.17. Two inconsistencies were observed in these graphs. The first was the excessively high reduction in capacity for the Mid Mast Arm tests with a $D_r = 29.14$ percent at $L/D = 7$. The second was the irregular shape of the trendline joining the Arm Tip tests with $D_r = 50.7$ percent due to the value obtained at $L/D = 5$. However, all the

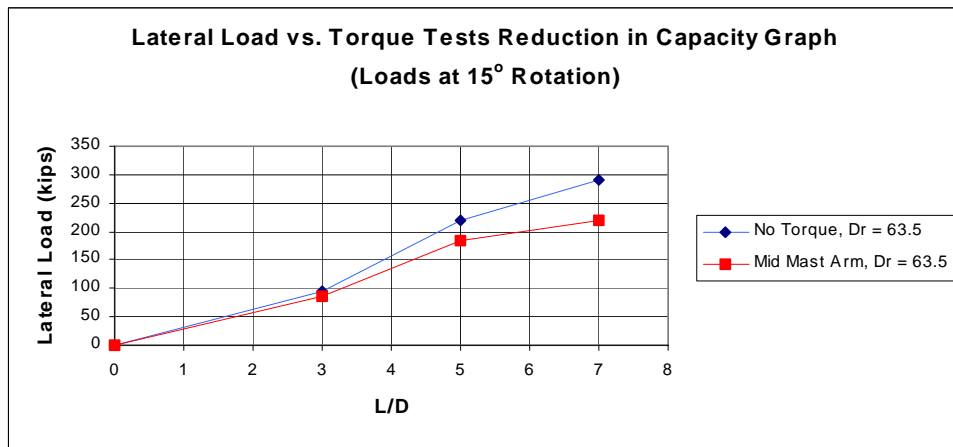
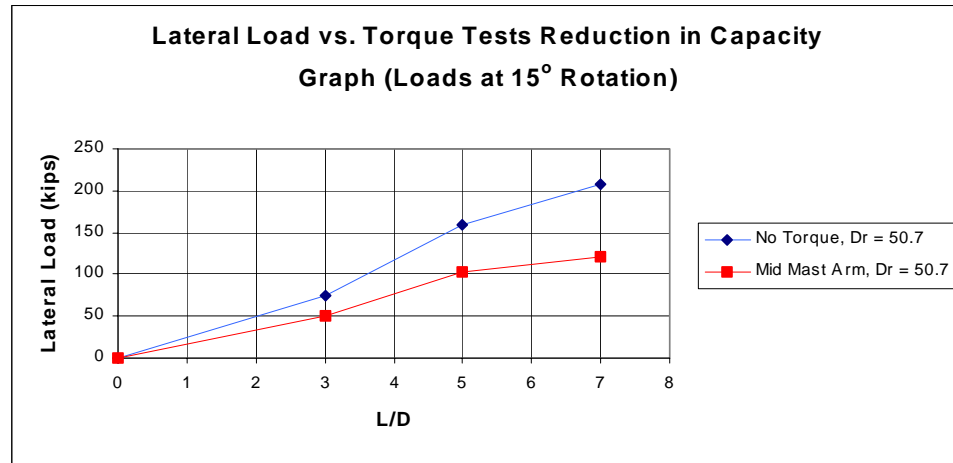
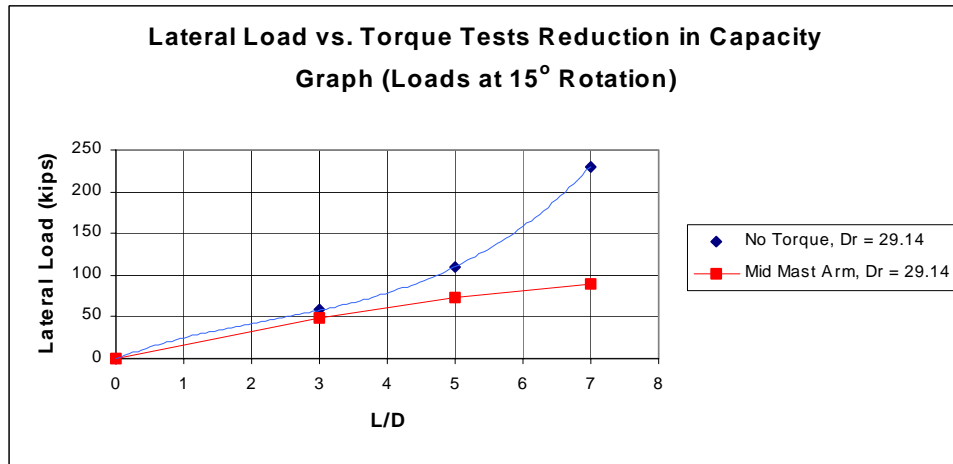


Figure 5.15 Loss of Capacity Graphs For Mid Mast Loading.

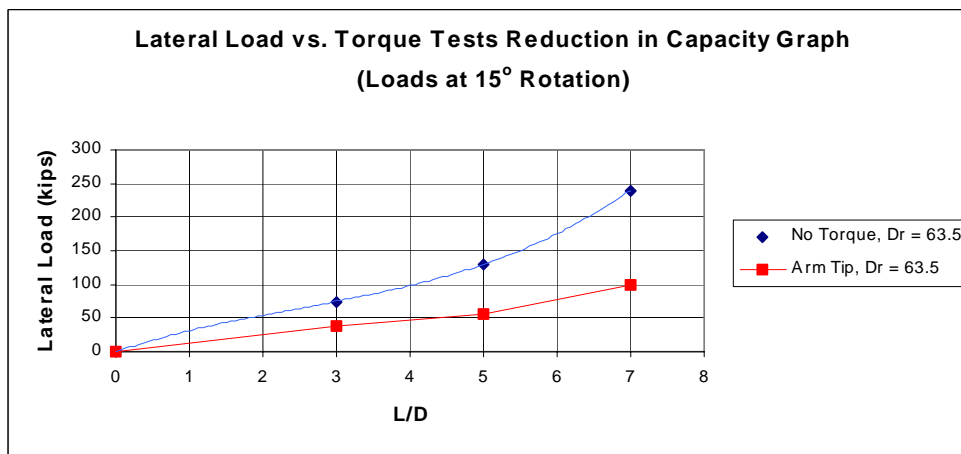
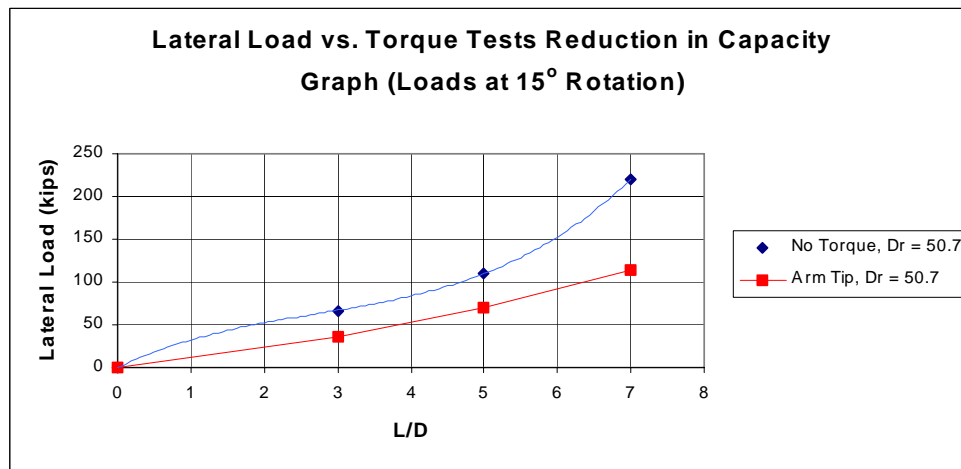
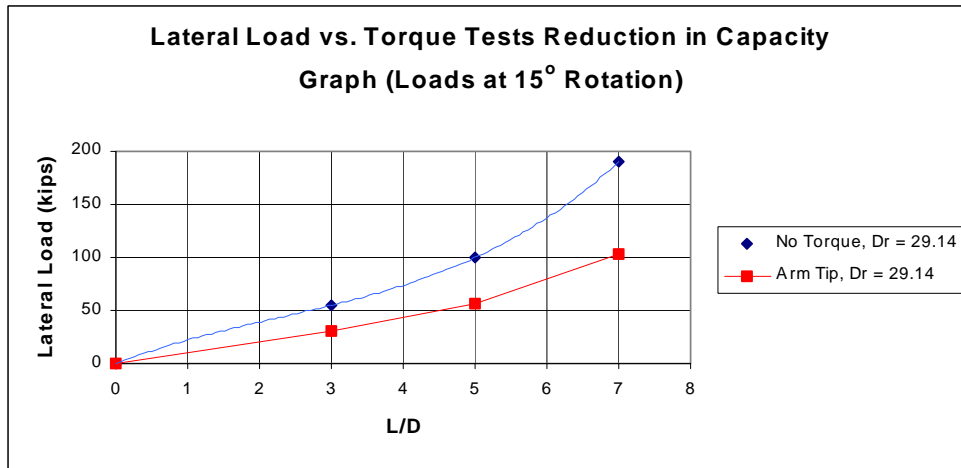


Figure 5.16 Loss of Capacity Graphs For Arm Tip Loading.

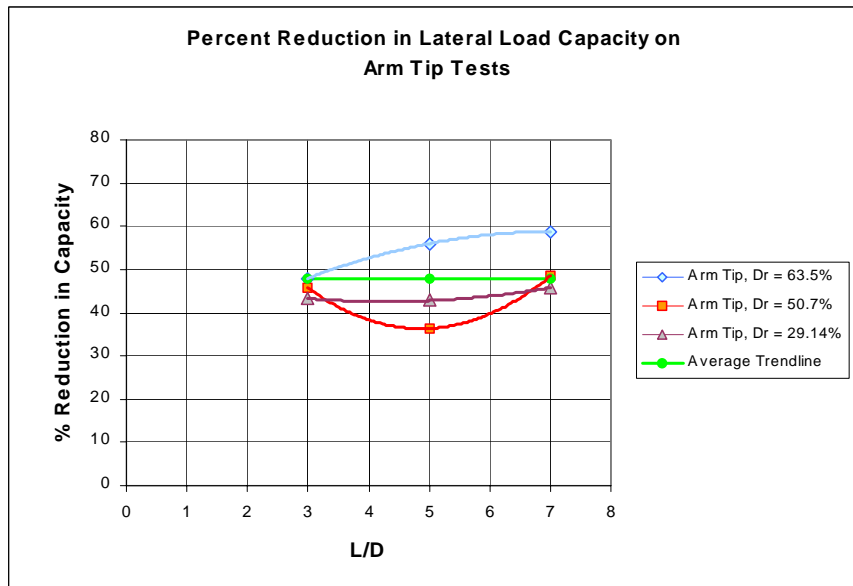
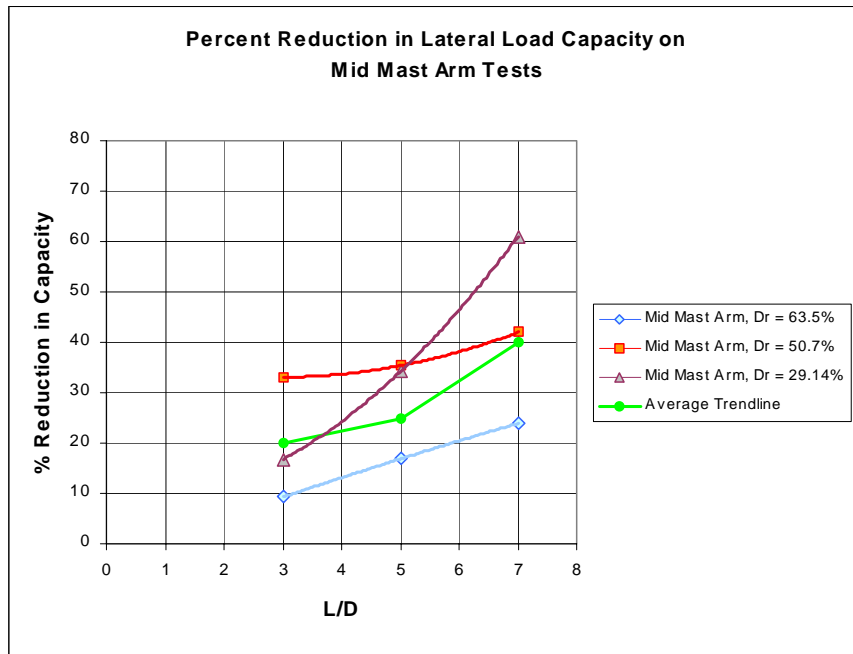


Figure 5.17 Percent Reduction in Lateral Load Capacity.

data was used in developing average trendlines based on load point application. Note, the magnitude of the points plotted on the graphs is determined by soil density, and the slope of the trendlines that join them is determined by the L/D ratio.

As expected the magnitude of decrease in capacity is largest for the Arm Tip tests in all soil densities (except for the Mid Mast Arm test with a $D_r = 29.14$ percent at $L/D = 7$). Also, the Mid Mast Arm tests reveal a dependency of results on L/D ratio. Consequently, the modifiers extracted from this graph were obtained by taking an average of the percent reduction points for each L/D ratio. The modifier extracted from the Arm Tip tests was taken to be a constant since the results do not indicate a strong dependency on L/D ratio. Table 5.5 summarizes the percent reduction values and modifiers obtained from Figure 5.17.

Table 5.5 Proposed Modifiers

L/D	% Reduction in capacity for different L/D ratios			Proposed modifiers used in the prediction of loss of capacity		
	3	5	7	3	5	7
Mid Mast Arm tests	20	25	40	0.8	0.75	0.6
Arm Tip tests	48	48	48	0.52	0.52	0.52

The modifiers were obtained by subtracting the percent reduction from unity. To verify the accuracy of the modifiers the actual test data was plotted and a series of curves representing the predicted capacities were superimposed on it. These graphs are presented Figure 5.18 to 5.20.

The trendlines are either directly over the test data or slightly below them, predicting a conservative value for capacity. Consequently, the graphs show the modifiers do a good job at predicting the decrease in capacity as a function of different embedment depths and varying soil densities.

However, the limitation of the modifiers is that they are only useful for predicting the decrease in capacity for two particular points of loading along the mast arm. These

points being the Mid Mast Arm tests, 14.5 ft away from the center of the foundation, and the Arm Tip tests, 20 ft away from the center of the foundation (measurements in prototype length). To obtain a prediction of capacity for loading at any point along the mast arm, the reduction given in Table 5.5 were plotted versus the torque to lateral load ratio in Figure 5.21. In this plot, 100 percent represents loading only on the pole.

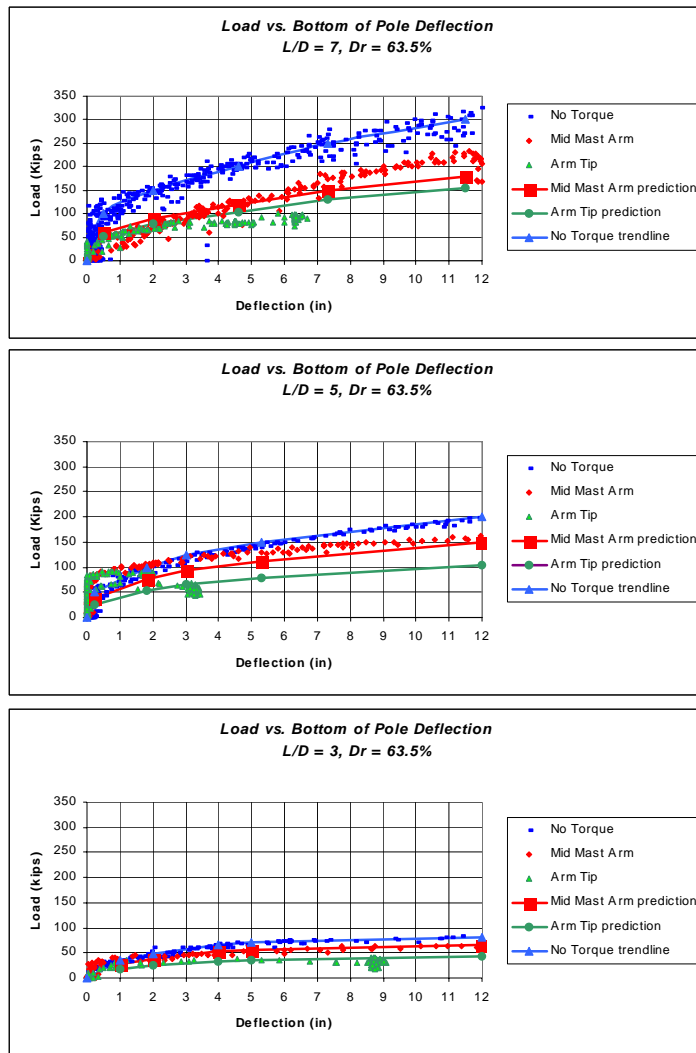


Figure 5.18 Modifier Prediction vs. Centrifuge Results for Medium Dense Sand.

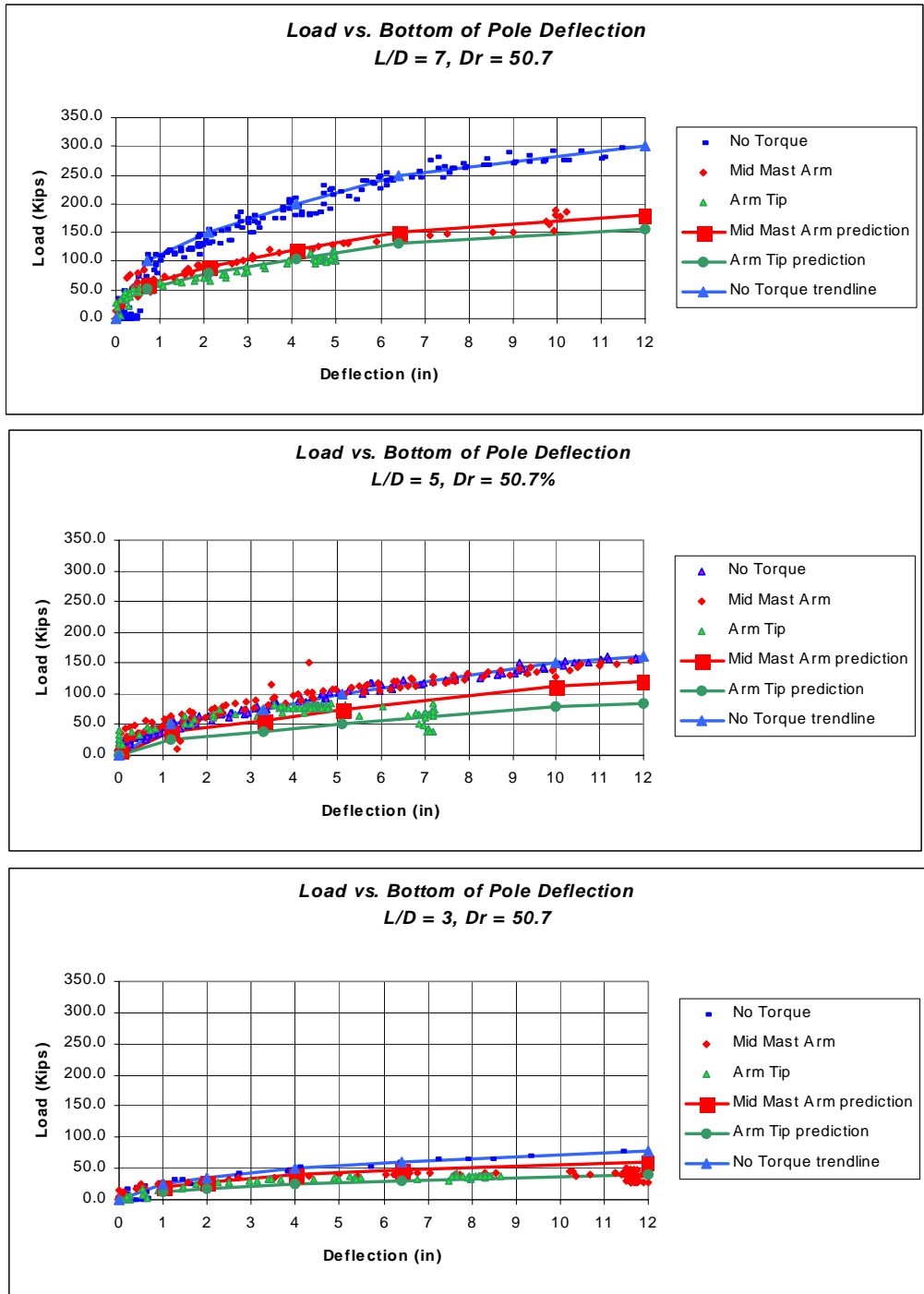


Figure 5.19 Modifier Prediction vs. Centrifuge Results for Medium Loose Sand.

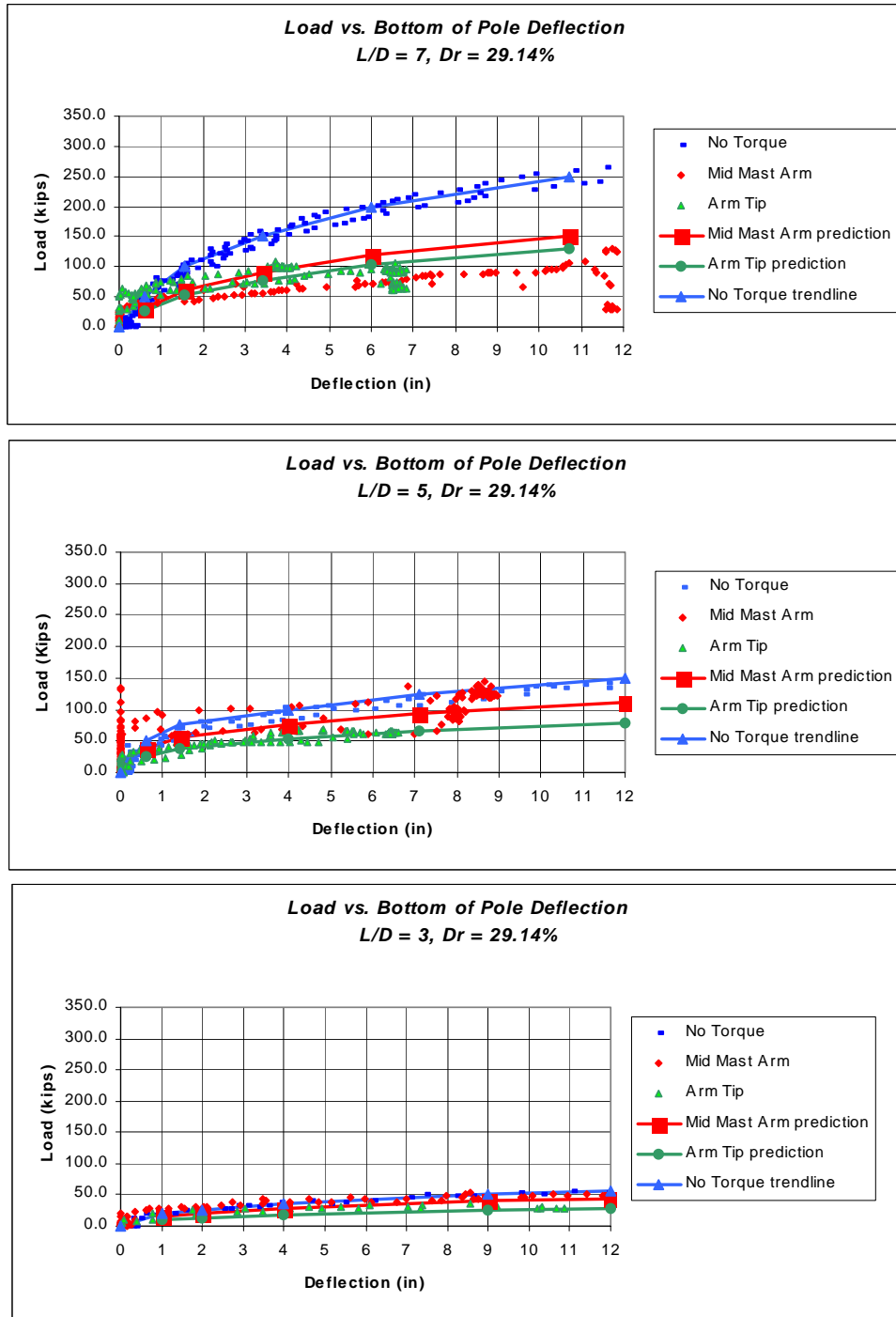


Figure 5.20 Modifier Prediction vs. Centrifuge Results for Loose Sand.

Subsequently, moving the load along the mast arm, represented by torque/lateral load ratio, reduces the lateral resistance as shown in Figure 5.21. The latter enables the designer to predict the decrease in lateral resistance capacity for a load applied at any point along the mast arm.

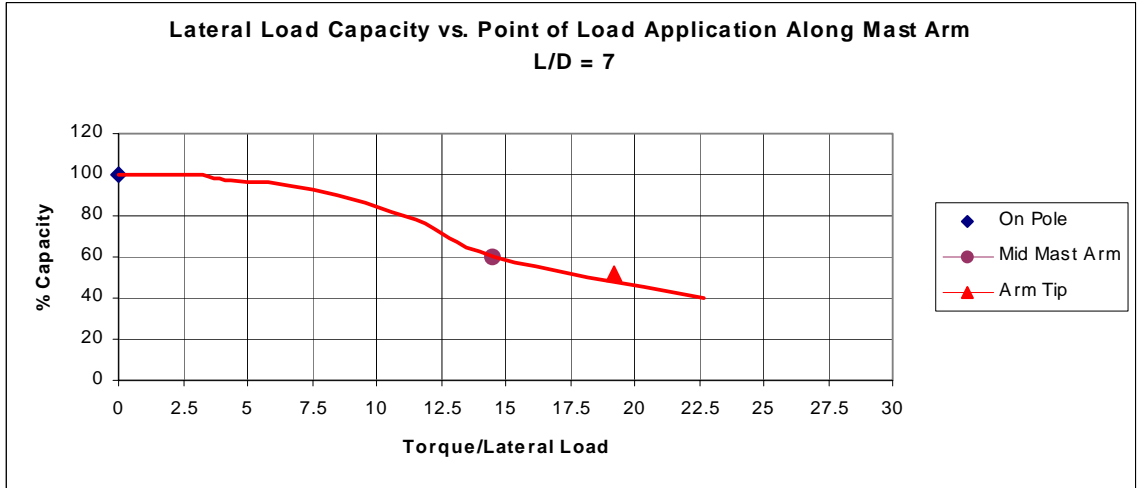
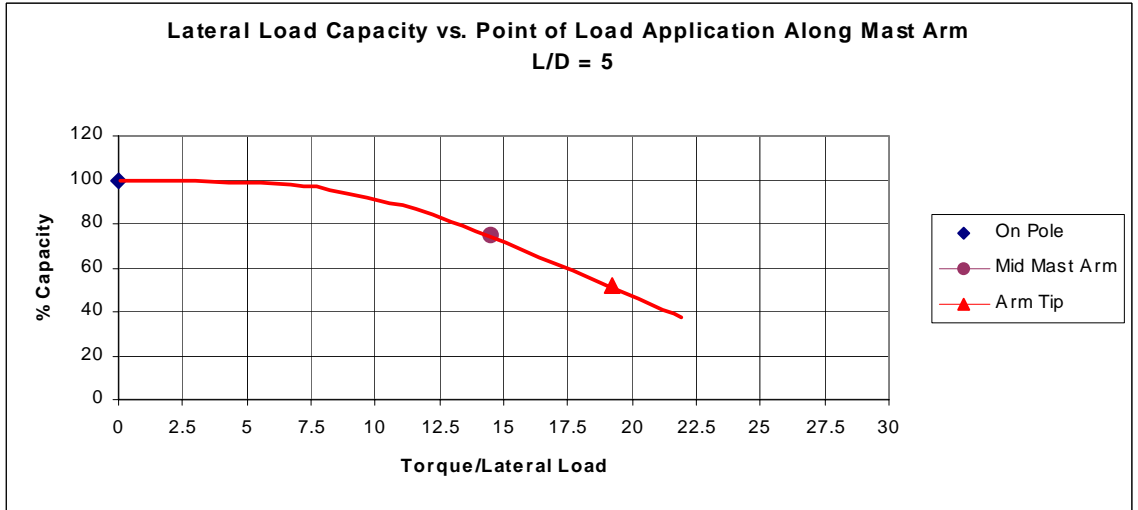
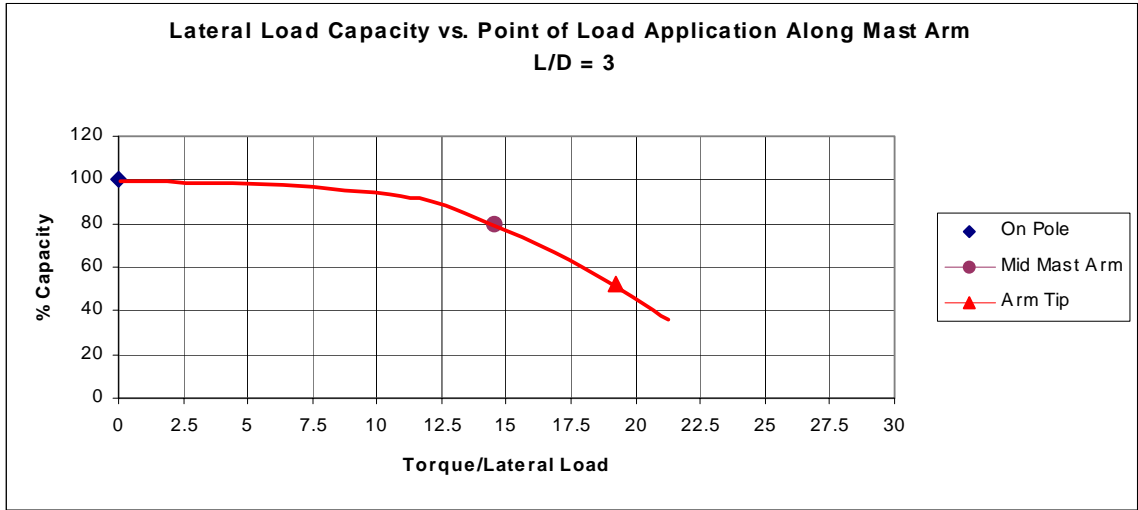


Figure 5.21 Loss of Capacity vs. Torque to Lateral Load Ratio.

CHAPTER 6
EXPERIMENTAL RESULTS IN SATURATED SAND

6.1 Introduction

Twenty-six centrifuge tests were conducted on single mast arm traffic light poles, supported on drilled shaft foundations cast in saturated sands (water table at ground surface). The original contract investigated the influence of combined lateral and torsional load on shafts constructed in dry sands; however, in a hurricane with the potential of flooding, a supplemental effort was undertaken to investigate saturated sand.

The prototype dimensions are those identified in Table 2.1, i.e., a mast arm length of 30 ft and a pole height of 20 ft. The foundation (drilled shaft) had a diameter of 5 ft and two different embedment lengths: 25 ft or 35 ft. Each foundation was tested by applying a lateral load at one of three potential locations: top of the pole, at the center of the mast arm, or at the tip of the mast arm. All tests were loaded until failure occurred. The latter was defined by one of two modes: excessive lateral deflection (larger than 12 in.) at top of foundation, or excessive rotation (equal to, or larger than 15 degrees).

The soil used in the experiments for all twenty-six tests was Edgar fine sand from Florida, classified as poorly graded (SP). It was placed in two different relative densities, loose and dense with properties given in Table 6.1.

Table 6.1 Saturated Sand Unit Weights and Properties Tested

Unit Weight of Saturated Sand (pcf)	Unit Weight of Dry Sand (pcf)	Void Ratio	Relative Density (%)	Friction Angle (ϕ)
120.5	92.8	0.80	34	33.6
124.5	99.2	0.68	69	38.0

All of the twenty-six tests were constructed with the wet-hole method of construction employing a mineral bentonite slurry (Section 4.5). Two of the tests varied the slurry cake thickness prior to grouting (Section 4.5); the other twenty-four tests kept the slurry cake thickness at 0.5 in. and varied the load application, shaft length, or soil density. For the twenty-four tests, eight applied the load to the top of the pole, and the other sixteen applied the load along the mast arm creating a torque.

A discussion of the tests with the load applied to the top of the pole is presented first, followed by the results with the load applied along the mast arm.

6.2 Lateral Loading at Top of Pole

Shown in Figure 6.1 is the load vs. displacement (ground surface) response of the pole under two different shaft embedment lengths and two different soil densities (loose and dense). As expected with the 25-ft embedment, increasing the soil density increases the shaft's lateral resistance. However, in the case of the 35-ft embedment, there was no increase in the ultimate capacity of the shaft. The soil resistance will increase as the soil relative density increases ($D_r = 34\%$ to $D_r = 69\%$). But, if the shaft's capacity is reached (see Broms' Equation 2.5) then increasing soil density or shaft length will have no effect on shear capacity of the shaft.

Shown in Table 6.2 is the both the measured and predicted ultimate capacity of foundations with the load applied to the top of pole (20 ft above ground). Broms and FB-Pier predictions are based on the saturated unit weights and soil strengths (angle of internal friction) given in Table 6.1. The ultimate moment capacity (6,758 ft-kips) of the cross-section (required by Broms) was obtained from FB-Pier's Moment interaction diagram with specified steel and concrete properties within cross-section. For Broms, the

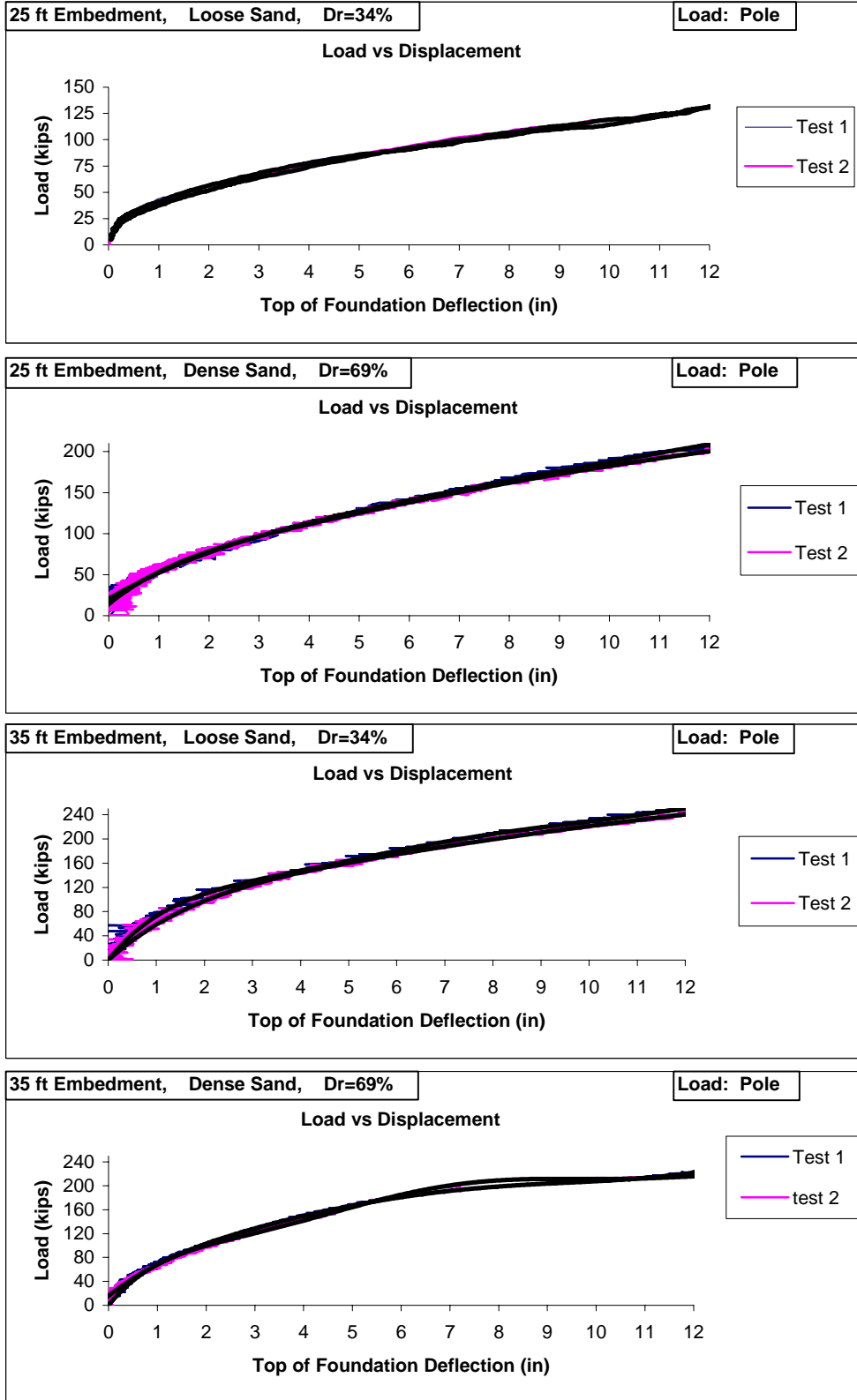


Figure 6.1 Loading Applied Top of Pole with No Torque.

Table 6.2 Measured and Predicted Ultimate Load on Pole

Relative Density (Dr: %)	Length to Diameter Ratio L/D	Measured Load (kips)	Broms Predicted Load (kips)	FB-Pier Predicted Load (kips)
34	5	132	175	141
69	5	203	226	190
34	7	240	238	240
69	7	220	246	225

solution for a short shaft (Eq. 2.2, soil failure) and long shaft (Eq. 2.5, shaft failure) were each computed, and the lower which controls failure, reported in Table 6.2. According to Broms, soil failure (Eq. 2.2) occurred for the L/D of 5 shafts, and shaft failure (Eq. 2.5) happened for the longer shafts (L/D=7). Evident from a comparison of measured to predicted (Broms, FB-Pier) response, Broms solutions for a short shaft (L/D = 5, or L = 25 ft) are un-conservative (twenty-five per cent). The latter may be attributed to Broms soil pressure distribution (Fig. 2.3). FB-Pier, which employs a P-Y soil resistance, gives less than a ten per cent error. It should also be noted that the construction method (bentonite slurry) had no effect on measured and predicted lateral capacities.

6.3 Lateral Loading Along the Mast Arm

Presented in Figures 6.2 through 6.9 are load vs. displacement, torque vs. rotation, torsional shear stress vs. displacement, and torsional shear stress vs. rotation for all the experiments with loading along the mast arm. Each figure presents experimental results varying just one parameter, i.e., point of load application (mid mast, and arm tip), soil densities (Dr = 34% and 69%), or shaft embedment depth (L/D = 5 and 7). For instance in Figure 6.2, two tests (repeatability) were performed on a shaft embedded 25 ft (L/D = 5) in a loose sand (Dr = 34%), with the load applied in the middle of its mast arm (i.e.,

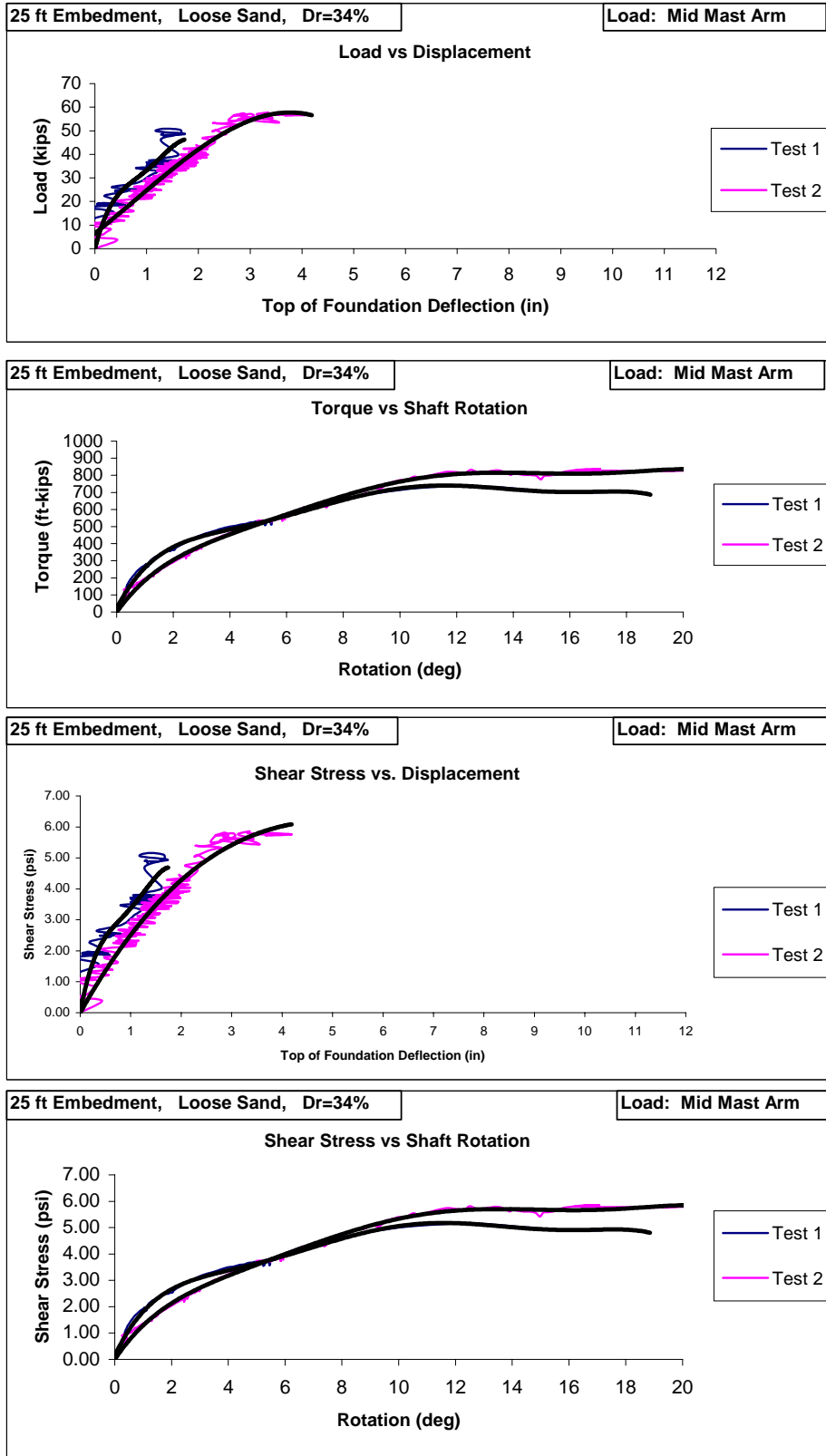


Figure 6.2 Embedment = 25 ft, Loose Sand, Load Applied Mid Mast Arm.

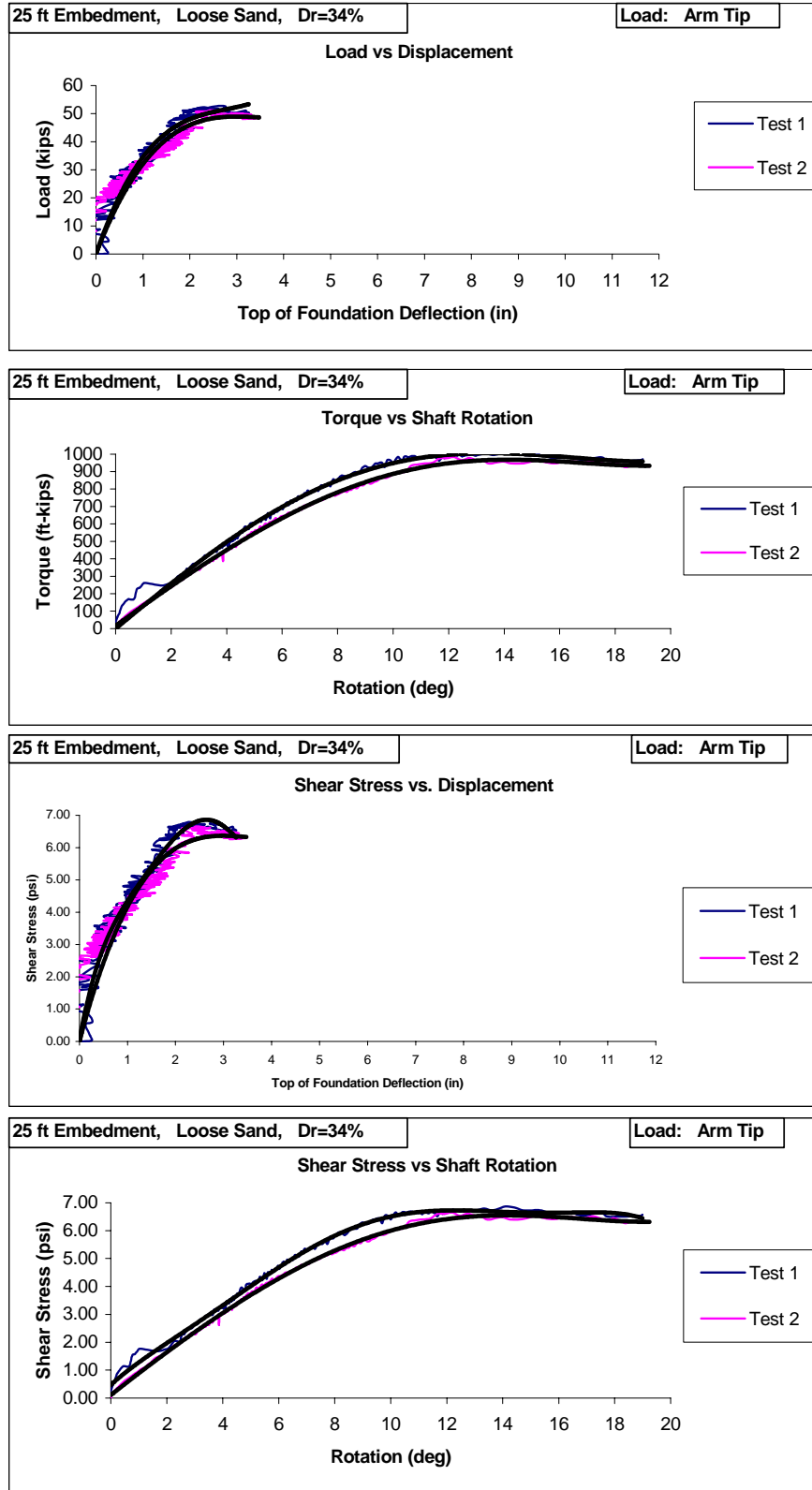


Figure 6.3 Embedment = 25 ft, Loose Sand, Load Applied at Arm Tip.

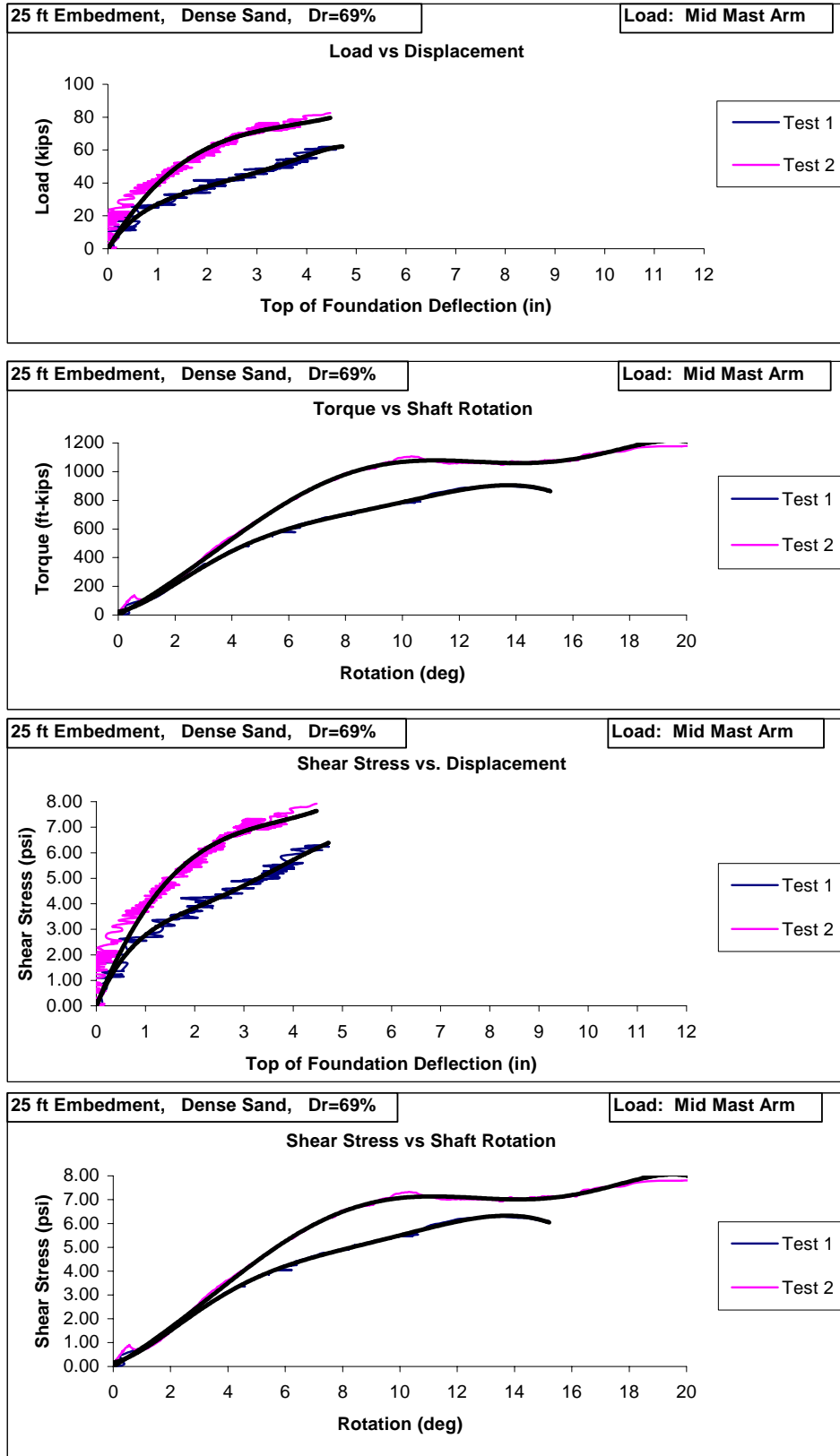


Figure 6.4 Embedment = 25 ft, Dense Sand, Load Applied Mid Mast Arm.

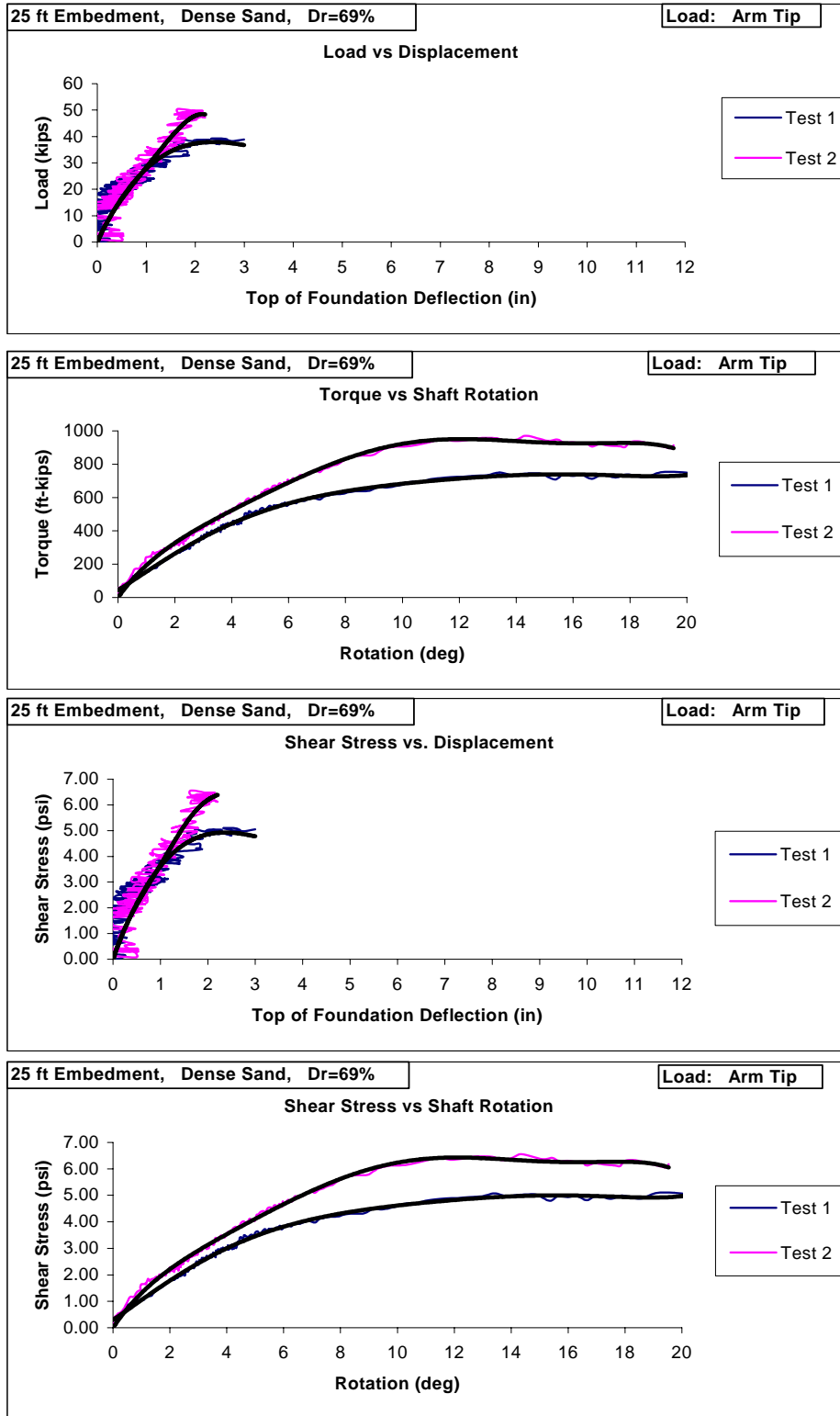


Figure 6.5 Embedment = 25 ft, Dense Sand, Load Applied at Arm Tip.

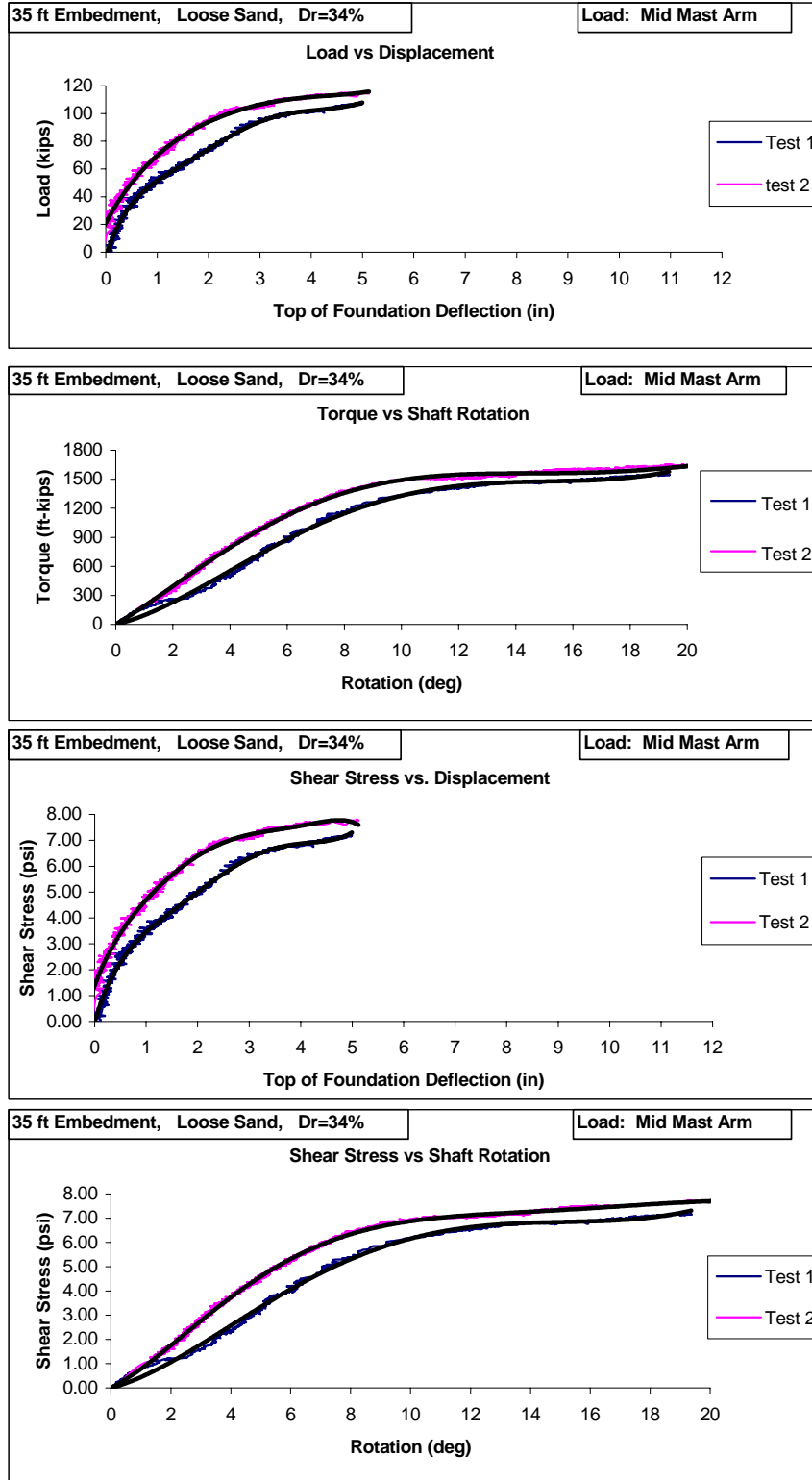


Figure 6.6 Embedment = 35 ft, Loose Sand, Load Applied Mid Mast Arm.

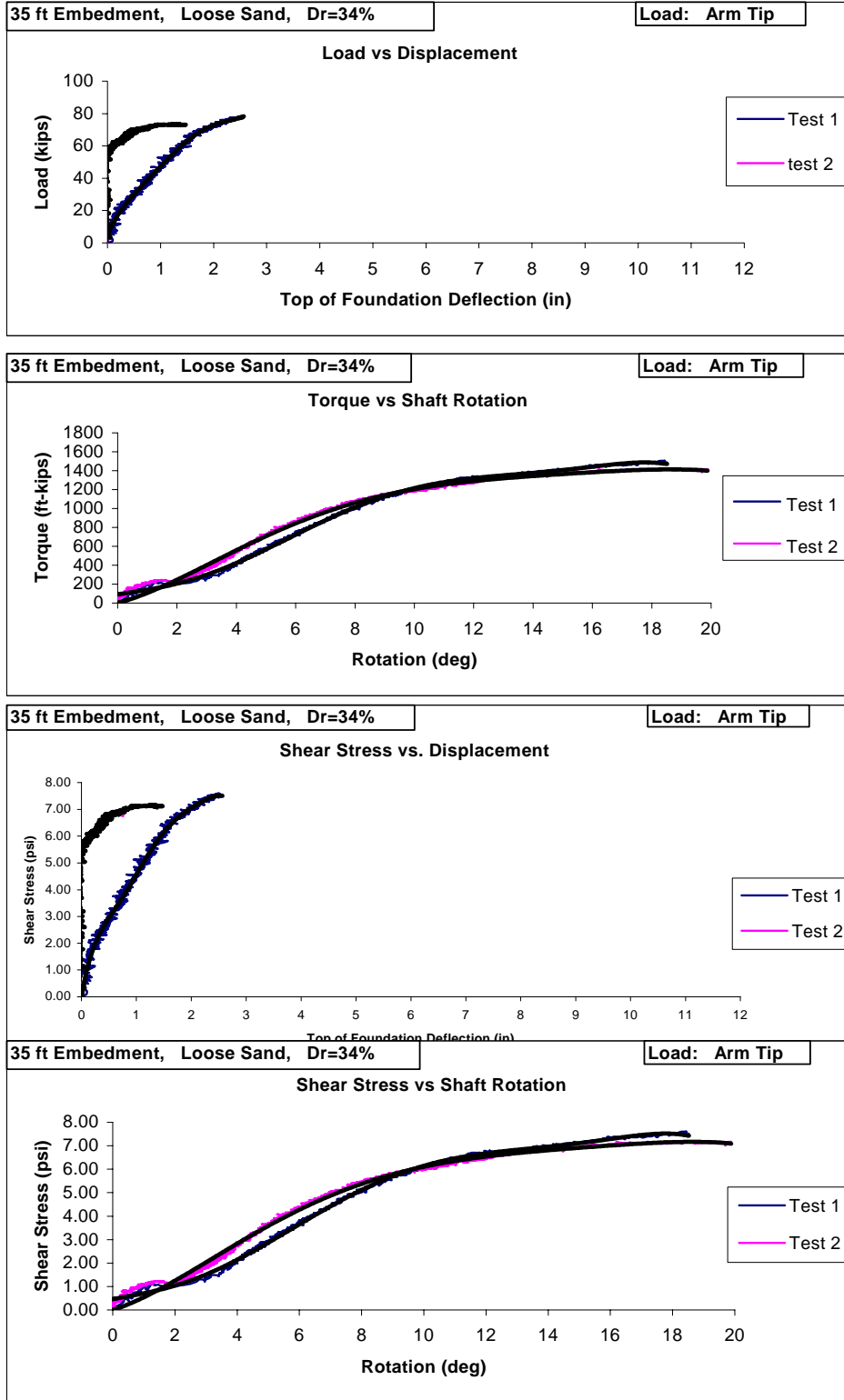


Figure 6.7 Embedment = 35 ft, Loose Sand, Load Applied at Arm Tip.

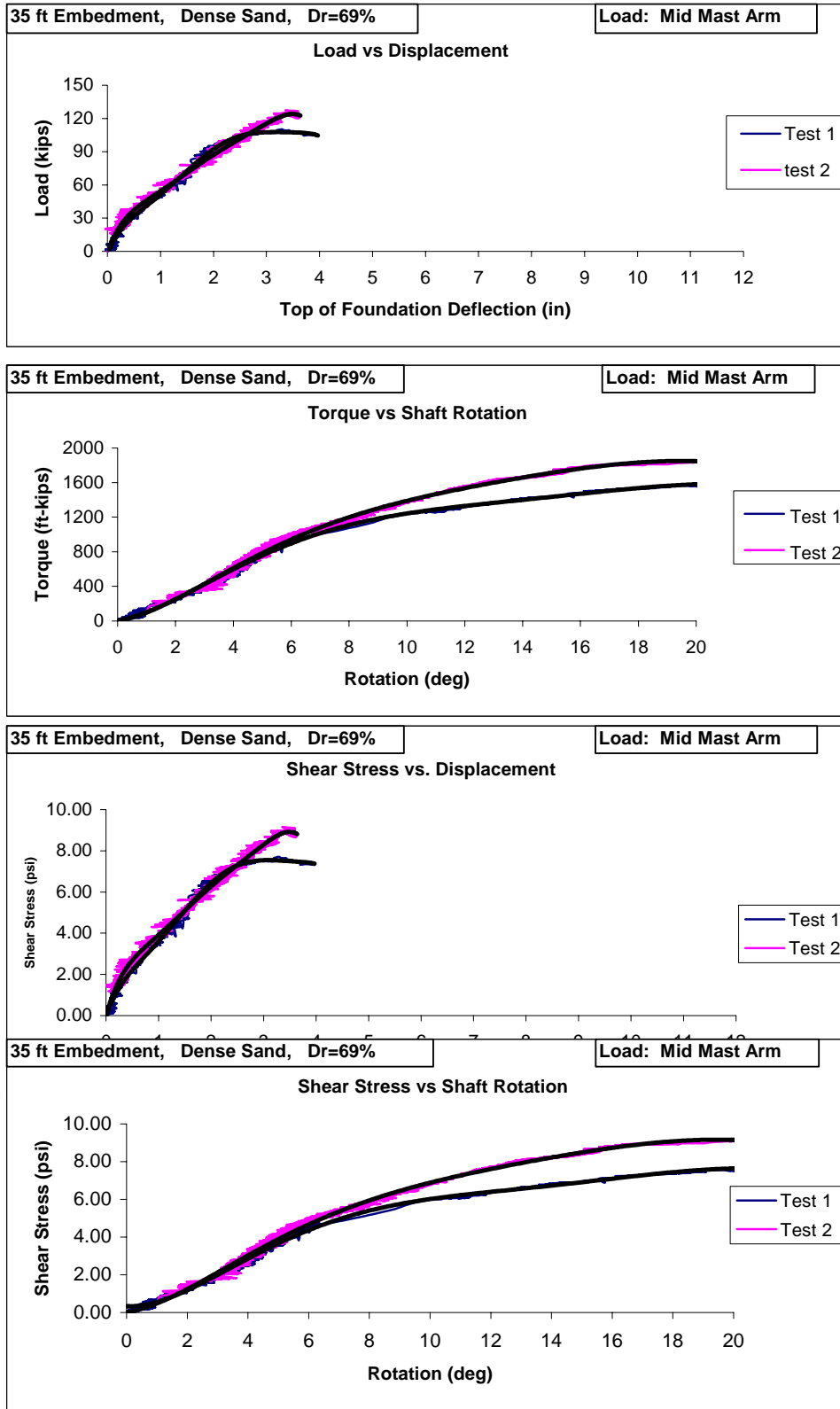


Figure 6.8 Embedment = 35 ft, Dense Sand, Load Applied Mid Mast Arm.

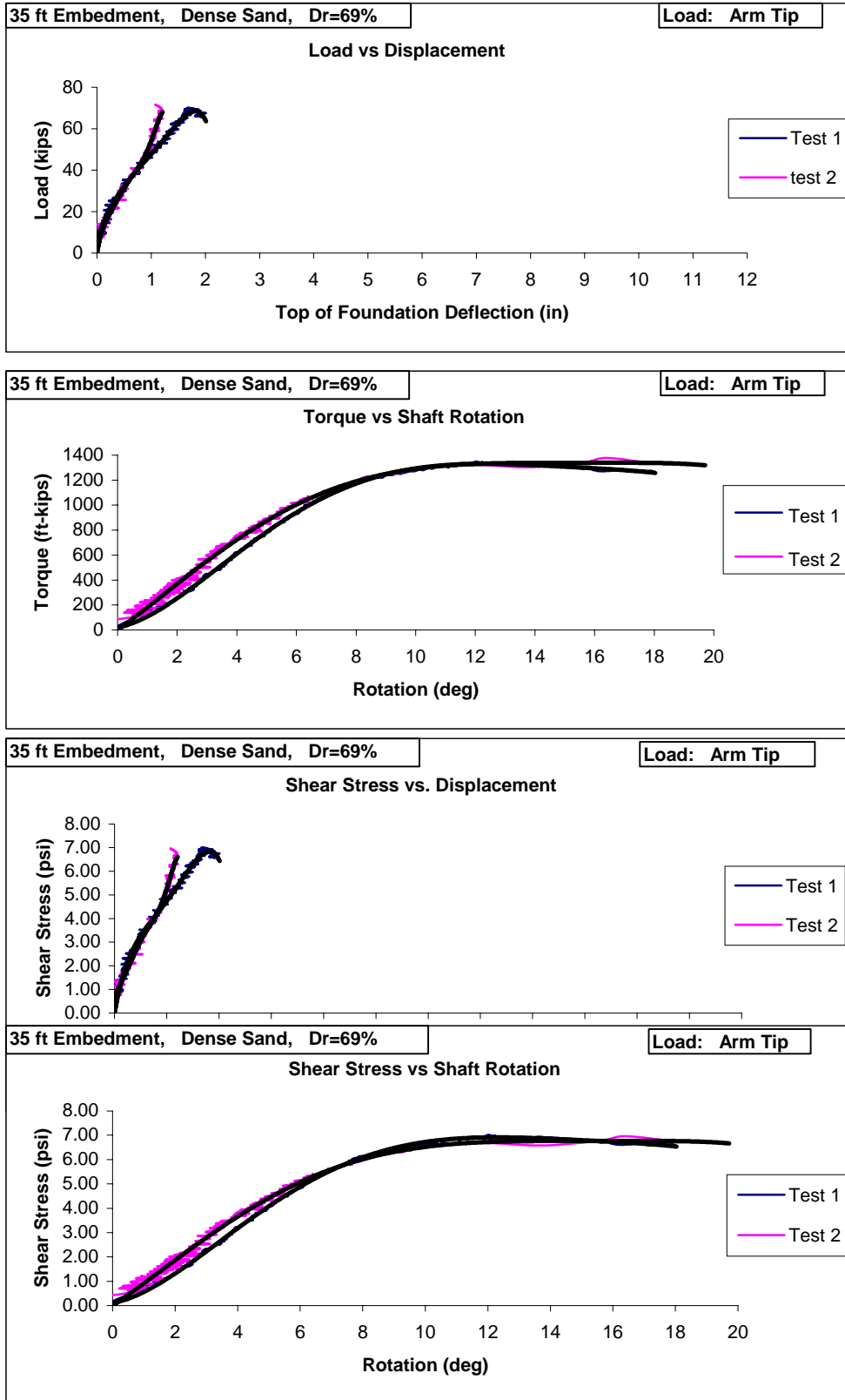


Figure 6.9 Embedment = 35 ft, Dense Sand, Load Applied at Arm Tip.

14.5 ft from pole). The top plot (Fig. 6.2) is the applied load vs. displacement (LVDT at top of footing). The next plot shows the Torque (load x distance from load to center of pole) vs. the rotation (obtained from LVDT on pole and mast arm) of the shaft. The bottom two plots in Figure 6.2 show the torsional shear stress versus displacement of the top of the shaft and rotation of the shaft. The torsional shear stress was obtained by dividing the applied Torque by the surface area and radius of the shaft.

Evident from all the figures (Figs. 6.2 through 6.9), the shafts failed by rotation (greater than fifteen degrees) instead of lateral displacement. The only experiment that had excessive lateral displacements (approximately six inches) was the 35-ft embedded shaft in loose sand with mid mast arm loading. The latter was expected since the torsional resistance of a shaft increases with depth and the applied torque ratio (torque/lateral load) was the smallest of those tested.

The sixteen rotation failures were attributed to the significant loss in vertical and horizontal effective stress in the saturated sand, which reduced the torsional resistance accordingly. The lateral soil resistance in the sand was also reduced, but since it had been more than sufficient to fail the shaft ($L/D = 5$, &7) in the dry, it was still sufficient to prevent lateral failure.

Using District 5, or FB-Pier method, the unit torsional shear stress, f_s , was computed with depth as follows:

$$f_s = \sigma' * \beta \quad (\text{Eq. 6.1})$$

where, σ' = vertical effective stress at mid-layer

β = load transfer ratio, and,

$$\beta_{\text{nominal}} = 1.5 - 0.135 * (z)^{0.5} \quad 1.2 \leq \beta_{\text{nominal}} \leq 0.25.$$

Next, the Torque resistance was computed from both the side and bottom of each shaft as:

$$T_s = \pi * D * L * f_s * (D/2) \quad (\text{Eq. 6.2})$$

$$T_b = \int \int f_s r^2 dr d\theta \quad (\text{Eq. 6.3})$$

$$T_{\text{total}} = T_s + T_b$$

where L = length of shaft

r = radius of shaft; and

D = diameter of shaft.

Finally, the predicted lateral load was found by dividing the total torque, T_{total} , by the distance along the mast arm that the load was applied. Table 6.3 shows a comparison of measured and predicted lateral loads.

Evident from a comparison of measured and predicted failure loads (rotation fifteen degrees), the District 5 or FB-Pier approach is always conservative and within twenty-five percent of failure. It should be noted that there was no trend in the error differences (e.g., dense sand having higher torque resistance) for all the tests. The latter method (District 5, FB-Pier) assumes no distinction (see Eq. 6.1) from soil properties (i.e., angle of internal friction, etc.), only shaft depth. The discussion of lateral failure of the 25-ft embedded shaft in loose sand with mid mast arm loading is presented in Chapter Seven.

Table 6.3 Measured and Predicted Lateral Load on Shafts in Saturated Sand

Point of Load Application	Relative Density (%)	Length to Diameter Ratio	Applied Lateral Load (kips)	Applied Torque (ft-kips)	Failure Mode	Measured Average Applied Lateral Load (kips)	Predicted Lateral Capacity (kips)	Ratio (Measured Load to Predicted Load)	Errors (Difference between Measured and Predicted) (Percentage)
Mid Mast Arm	69	5	61.4	890	Torsional	67.93	53	1.28	22%
	69		74.5	1080					
	34		51.0	740	Torsional	53.79	50	1.08	7%
	34		56.6	820					
Arm Tip	69	5	49.4	950	Torsional	43.96	40	1.10	9%
	69		38.5	740					
	34		50.2	965	Torsional	50.86	38	1.34	25%
	34		51.5	990					
Mid Mast Arm	69	7	99.3	1440	Torsional	107.93	92	1.17	15%
	69		116.6	1690					
	34		101.4	1470	Torsional-Lateral	105.52	86	1.23	18%
	34		109.7	1590					
Arm Tip	69	7	69.7	1340	Torsional	69.72	69	1.01	1%
	69		69.7	1340					
	34		72.8	1400	Torsional	73.10	65	1.12	11%
	34		73.4	1410					

CHAPTER 7 PROPOSED LATERAL AND TORSIONAL CAPACITY MODELS FOR DRILLED SHAFTS

7.1 Introduction

As identified in Chapters 5 and 6, a drilled shaft may fail by either rotation or lateral displacement or a combination of both depending on soil conditions (soil density, water table, etc.) and shaft geometry (length, reinforcement, etc.). Also shown in chapters five and six, the torsional resistance of a shaft is independent of lateral load and may be represented by the District 5 or FB-Pier model. In the case of lateral resistance, however, the lateral capacity of a shaft is dependent on the applied torque (see Fig. 5.21). Moreover, the reduction in a shaft's lateral capacity may be characterized through the ratio of torque to lateral load on the shaft. The latter reduction may be applied to Broms, P-Y, or any method, which estimates the lateral capacity of a shaft when the load is applied to the pole (i.e., no torque). Overall, shaft failure is controlled by the smaller of District 5 or FB-Pier model (torsion), or the torque modified (Fig 5.21) lateral resistance (Broms, P-Y, etc).

7.2 Lateral Model for Drilled Shaft Subject to Torque

As part of this research, a Mathcad file was written to design drilled shafts subject to combined lateral load with torque. Since Broms method was un-conservative for short shafts, used a simple soil pressure distribution, and could not handle multiple soil layers,

For sand, Reese et al. (1978), ultimate soil pressure as a function of depth was used for

$S_p(x)$:

$$S_p(x) = \gamma x \left[\frac{K_o x \tan \phi \sin \phi}{\tan(\beta - \phi) \cos \alpha} + \left(\frac{\tan \beta}{\tan(\beta - \phi)} \right) (D + x \tan \beta \tan \alpha) \right. \\ \left. + K_o x \tan \beta (\tan \phi \sin \beta - \tan \alpha) - K_a D \right] \quad (\text{Eq. 7.1})$$

where K_o = the at rest earth pressure coefficient, 0.4

γ = Buoyant unit weight, (F/L³)

β = 45 + $\phi/2$ (degrees)

α = $\phi/2$ (degrees); and

K_a = Rankine's active earth pressure coefficient.

In the case of clay, Gazioglu and O'Neill (1984) integrated soft and stiff clay representation for S_p was used:

$$S_p(x) = F \cdot N_p \cdot c \cdot D \quad (\text{Eq. 7.2})$$

where F = soil degradability factor, which is a function of failure strain and loading condition (sustained or cyclic)

N_p = ultimate lateral soil coefficient, which is a function of critical length

c = the soil's undrained shear strength, (F/L²)

D = the shaft diameter (L).

Since $S_p(x)$ may not vary linearly with depth (except between depths Z and L , Fig. 7.1), it is computed from incremental slices (typical: 50 slices, each with a width of $L/50$) along the length of the shaft/pile. Similar to the free earth support approach in sheet

piling, the soil pressure is assumed to vary linearly from a value of $S_p(Z)$ (soil in a passive state on left side of the wall) to a value of $S_p(L)$ (soil in a passive state on right side of the wall) at a depth L (see Fig 7.1). In between these locations, the wall's deflection is diminishing, goes to zero (at Z_c) and subsequently increases in the opposite direction. Depth Z_c (Fig. 7.1) is also the location of the pile/shaft's maximum shear. The two unknowns, Z and P_{ult} (force on Pole), are solved with force and moment equilibrium applied to the combined shaft and pole. From the resultant soil pressure, Z , and force P_{ult} , the shear and the moment distribution in the pile & shaft may be determined.

Generally, if the pile/shaft has an L/D ratio less than five, the moment in the pile/shaft will not exceed its ultimate value, M_{ult} . For such a case, the pile/shaft failure (i.e., limiting P_{ult}) is due to soil resistance. However, as the shaft's length increases, the moment in the pile/shaft will eventually equal its cross-sectional capacity (M_{ult}). Subsequently, a plastic hinge forms, and no increase in lateral resistance, P_{ult} , will occur when increasing the shaft's length. Nevertheless, the designer may still wish to increase the pile/shaft's length to resist torque. In the latter case, the full soil resistance (i.e., passive stress state, S_p) is not mobilized, especially at the bottom of the pile/shaft (insufficient lateral displacement). Consequently for equilibrium, the soil's passive pressure, S_p , needs to be adjusted downward, i.e., $R_m S_p$, as shown in Fig. 7.1. The values of R_m , Z , and P_{ult} are solved from the force, and moment equilibrium along with the moment capacity of the pile/shaft's cross-section.

Table 7.1 shows a comparison of P_{ult} predicted from the proposed method, along with Broms (Eqs. 2.2 or 2.5) and the centrifuge results for dry sands (Chapter 5) with loading on the pole. The maximum error between the proposed and measured response

is eighteen percent [L/D equal to five in the loose sand, $D_r = 29\%$], with average error of nine percent.

Table 7.1 Summary of Ultimate Shear (kips) Available at Top of Pole, Dry Sand

Soil	L/D=3			L/D=5			L/D=7		
	P_{ult} Meas.	P_{ult} Fig 7.1	P_{ult} Broms	P_{ult} Meas.	P_{ult} Fig 7.1	P_{ult} Broms	P_{ult} Meas.	P_{ult} Fig 7.1	P_{ult} Broms
29.1	50	49	78	150	178	228	275	272	280
50.7	55	54	84	165	164	247	290	275	282
63.5	70	56	89	205	210	260	300	297	284

Table 7.2 shows a comparison of P_{ult} predicted from the proposed method (Fig. 7.1), along with Broms (Eqs. 2.2 or 2.5) and the centrifuge results for saturated sands (Chapter 6) with loading on the pole. The maximum error between the proposed (Fig. 7.1) and measured response is eleven percent [L/D equal to five in the loose sand, $D_r = 34\%$], with average error of five percent.

Table 7.2 Measured and Predicted Ultimate Load on Pole, Saturated Sand

Relative Density (D_r : %)	Length to Diameter Ratio L/D	Measured Load (kips)	Broms Predicted Load (kips)	P_{ult} Fig 7.1 (kips)
34	5	132	175	147
69	5	203	226	200
34	7	240	238	240
69	7	220	246	227

In the case of loading on the mast arm (i.e., lateral load with torque), the lateral resistance, P_{ult} , of the pile/shaft decreases (for sands, Fig. 5.21). Since both the pile/shaft shear and P_{ult} are determined from the soil pressure (Fig. 7.1), the latter should also be adjusted through R_T (Fig. 7.1) from Fig 5.21 for sands.

In the case of dry sands subject to lateral load and torque (i.e., loading on mast arm), Table 7.3 presents both the measured (Chapter 5) and predicted failure shear forces

based on Figs. 7.1 and 5.21. The maximum error is twenty percent ($L/D = 3$, $Dr = 63.5\%$, mast tip load), with an average error of nine percent.

Table 7.3 Summary of Ultimate Shear (kips)

L/D ratio	Load App.	Dense, $Dr=63.5\%$		Medium, $Dr=50.7\%$		Loose, $Dr=29.1\%$	
		Meas. (kips)	Pred. (kips)	Meas. (kips)	Pred. (kips)	Meas. (kips)	Pred. (kips)
7	pole	300	297	290	275	275	272
	mid mast	210	180	180	167	140	165
	mast tip	130	143	130	136	120	134
5	pole	205	210	165	164	150	178
	mid mast	150	151	140	118	130	128
	mast tip	80	96	74	79	70	80
3	pole	70	56	55	54	50	49
	mid mast	55	45	45	43	45	39
	mast tip	25	26	25	25	20	23

For the saturated sands (Chapter 6), only one shaft had large lateral displacements (5 inches), the 35-ft embedded shaft in loose sand ($Dr = 34\%$) with loading on mid mast arm. Using the latter soil conditions (i.e., submerged unit weight, etc.), the predicted ultimate lateral capacity from Fig. 7.1 would be 145 kips. Since, an applied lateral load of 106 kips was placed when rotational failure (fifteen degrees) occurred, it is believed that an ultimate lateral capacity of 130 kips would be achieved at a lateral displacement of twelve inches, if larger rotation were allowed. The latter would only be in error by eleven percent, suggesting Figure 5.21 is valid for both dry and saturated deposits.

From comparisons with FB-Pier simulations, it was found the pressure distribution given in Fig 7.1 is accurate for shafts with L/D ratios up to eight (i.e., dense sands) or ten (i.e., loose sands). Shafts with longer lengths will develop inflection points, resulting in smaller lateral deflections and decreasing lateral pressure with increasing

depth. A discussion of the Mathcad file developed for FDOT and the proposed method follows.

7.3 Mathcad File Overview

There are three major components to the Mathcad file: 1) input parameters, 2) computation areas, and 3) output. Each of these components has multiple sections, which are used to perform specific functions. In the first section (input parameters) are unit definitions located inside the blue border, known as an “area”, directly under the file’s title block. This area can be viewed by double clicking on the blue border. The areas appear as borders in the Mathcad sheet. An area is an inserted space within the sheet that can be expanded or collapsed by double clicking on its border. The unit definitions area defines the engineering units associated with the subsequent computations. In this section the user also defines the input parameters of the shaft, soil and loading conditions. In the next section, computations are performed, data arrays are established and subroutines are executed. This section was broken into nine areas. Inside each of these areas the user will find parameter definitions, soil property arrays, soil resistance computations, flexural moment and torque modifier interpolations, etc. The computation areas are defined as follows:

- 1) Flexural Moment Interpolation
- 2) Soil Properties
- 3) Torque Multiplier Interpolation
- 4) Reese’s Cohesionless Analysis
- 5) Integrated Clay Analysis

- 6) Limit State Equilibrium
- 7) Torque Modified Shear and Moment
- 8) Shear Force in Shaft
- 9) Torsional Capacity of the Shaft

The Mathcad file along with numerical and graphical results will be presented. Refer to the Mathcad file for reference.

7.4 Mathcad Input Parameters

The input parameters required to perform a successful analysis are highlighted in yellow (see Figure 7.2). The picture shown in the top right side of the Mathcad sheet (Fig. 7.2) illustrates the basic design problem and identifies the structure, drilled shaft with two soil layers. Whenever possible, soil input parameters should be backed by laboratory tests or insitu tests that are standard of practice. It is necessary that the each of the soil parameters described herein have a suffix (1 or 2) that corresponds to the associated soil layer 1 or soil layer 2.

7.4.1 Drilled Shaft Properties

The drilled shaft properties define the foundation element's geometry and material properties. The diameter and length are used to define the L/D ratio, which is frequently used in subsequent computations, interpolations and programming conditional statements. The user can define the shaft length and diameter in common units of length. The elastic modulus of the drilled shaft, E_p , represents the combined material modulus of the reinforcing steel and concrete and can be inputted in common units of force per length squared (F/L^2). The shaft modulus is a function of the compressive strength of the

Required Input Is In Yellow**Drilled Shaft Properties:**

D := 60in	<i>Diameter of Drilled Shaft</i>
L := 25ft	<i>Length of Drilled Shaft embedded in Soil</i>
Ep := 4000000-psi	<i>Drilled Shaft Modulus</i>
p := 2.7%	<i>Ratio of Percent Cross-Sectional Area of Steel to Gross Cross-Sectional Area</i>

Loading Condition:

e := 20ft	<i>Location of Lateral Load (Vu_Top) above Ground Surface</i>
x := 0ft	<i>Location of Lateral Load (Vu_Top) along mast arm</i>

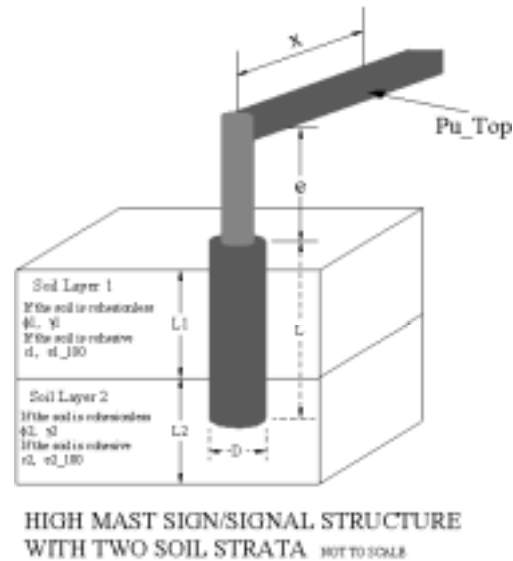
Soil Properties:**Soil Layer 1:****L1 := 50ft** *Stratum Thickness**Input nonzero values for cohesionless soils:***φ1 := 33.6deg** *Soil's Angle of Internal Friction in degrees***γ1 := 58.1pcf** *Soil's Moist Unit Weight (Average Bouyant Unit Weight if Ground Water Table is Encountered)**If soil stratum is COHESIVE input nonzero values for the following; OTHERWISE c1 MUST BE SET TO ZERO:***c1 := 0psf** *Undrained Shear Strength***ε1_100 := 0.0** *Strain at Failure from an Unconfined Compression Test***Soil Layer 2:****L2 := 50ft** *Stratum Thickness**Input nonzero values for cohesionless soils:***φ2 := 33.8deg** *Soil's Angle of Internal Friction in degrees***γ2 := 92.07pcf** *Soil's Moist Unit Weight (Average Bouyant Unit Weight if Ground Water Table is Encountered)**If soil stratum is COHESIVE input nonzero values for the following; OTHERWISE c2 MUST BE SET TO ZERO:***c2 := 2000psf** *Undrained Shear Strength***ε2_100 := .07** *Strain at Failure from an Unconfined Compression Test*

Figure 7.2 Mathcad File - A Portion of Input Data Layout with Problem Sketch.

concrete, f'_c , and the yield strength of the steel, f_y . Drilled shaft concrete typically has a compressive strength at 28 days of approximately 4 ksi, with a corresponding elastic modulus of approximately, 4000 ksi. The typical yield strength of the reinforcing steel is 60 ksi. The following equation provides a rule of thumb approach for computing the elastic modulus as a function of f'_c .

$$E_c = 57000\sqrt{f_{pc}} \quad (\text{Eq. 7.3})$$

where, f_{pc} is concrete compressive strength at 28 days.

It is recommended that laboratory tests, such as an unconfined compression test of the concrete, be performed to validate the material's performance under working loads.

The area ratio of steel to concrete, ρ is inputted as a percent. This value is used in conjunction with the shaft diameter to obtain the ultimate bending moment, M_{ult} of shaft's cross-section. The latter is used to adjust the soil resistance, R_m , in Figure 7.1.

Figure 7.3 shows the shaft input parameters.

DRILLED SHAFT DESIGN FOR HIGH MAST ARM SIGN/SIGNAL STRUCTURE

Required Input Is In Yellow

Drilled Shaft Properties:

D = 60in	<i>Diameter of Drilled Shaft</i>
L = 15ft	<i>Length of Drilled Shaft embedded in Soil</i>
Ep = 4000000 psi	<i>Drilled Shaft Modulus</i>
ρ = 8%	<i>Ratio of Percent Cross-Sectional Area of Steel to Gross Cross-Sectional Area</i>

Loading Condition:

e = 20ft	<i>Location of Lateral Load (Vu_Top) above Ground Surface</i>
x = 14.5ft	<i>Location of Lateral Load (Vu_Top) along mast arm</i>

Figure 7.3 Mathcad File Drilled Shaft and Loading Conditions Input Parameters Sheet.

7.4.2 Loading Conditions

The Mathcad file computes a point load acting at a user defined vertical height above the ground surface, e (Fig. 7.3), at a horizontal distance, x , along the mast arm. The user can assign e and x in any common units of length. Since the computed point load represents a uniform wind load on the mast arm, x , should be one-half of the loaded width. The distance e represents the height of the pole, and the distance x times the point load represents the applied torque on the foundation. The analysis can handle any height pole, but is limited to point load acting a horizontal distance not more than 21 ft along the mast arm measured from the centerline of the pole. The value of x is used for determining the torque lateral load modifier (R_T in Fig. 7.1; called TLM in Mathcad file).

7.4.3 Cohesionless Soil Properties

The required parameters are the soil's unit weight (γ), angle of internal friction (ϕ) and the stratum thickness for up to two soil layers, L1 or L2 (Figure 7.4). The assigned units for unit weight are force per length cubed. For convenience the units can be expressed as pcf. The user should enter the moist unit weight if no water table is encountered. If the water table is assumed to be at the ground surface then the user should enter the buoyant unit weight, or if a water table is encountered within a defined stratum thickness then the user should enter a weighted average unit weight. The friction angle is entered in degrees. Engineering judgment should be exercised conservatively when selecting friction angle since the final result is sensitive to relatively small changes in this parameter. It has been found from this research that as L/D ratios approach five that the mobilized failure wedge in a dry sand will be sufficient enough to induce bending failure of the drilled shaft section within the soil. Friction angle and unit weight

Soil Properties:

Soil Layer 1:

L1 := 50ft *Stratum Thickness*Input nonzero values for cohesionless soils:**φ1 := 33.6deg** *Soil's Angle of Internal Friction in degrees***γ1 := 58.1pcf** *Soil's Moist Unit Weight (Average Bouyant Unit Weight if Ground Water Table is Encountered)*If soil stratum is COHESIVE input nonzero values for the following; OTHERWISE c1 MUST BE SET TO ZERO:**c1 := 0psf** *Undrained Shear Strength***ε1_100 := 0.0** *Strain at Failure from an Unconfined Compression Test*

Soil Layer 2:

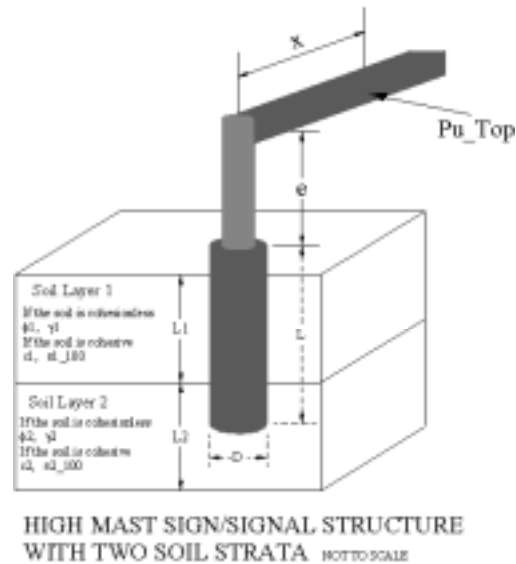
L2 := 50ft *Stratum Thickness*Input nonzero values for cohesionless soils:**φ2 := 33.8deg** *Soil's Angle of Internal Friction in degrees***γ2 := 92.07pcf** *Soil's Moist Unit Weight (Average Bouyant Unit Weight if Ground Water Table is Encountered)*If soil stratum is COHESIVE input nonzero values for the following; OTHERWISE c2 MUST BE SET TO ZERO:**c2 := 2000psf** *Undrained Shear Strength***ε2_100 := .07** *Strain at Failure from an Unconfined Compression Test*

Figure 7.4 Mathcad File View of Soil Properties Input Along with Sketch.

predominantly control the soil's resistance over the length of the shaft. The thickness of the stratum can be entered in common units of length.

7.4.4 Cohesive Soil Properties

The cohesive soil parameters (Fig 7.4) required to estimate the shaft's lateral capacity are undrained shear strength, c , strain at failure from an unconfined compression test, ϵ_{100} , and stratum thickness, L . **It is imperative that the user enters a value, a zero or nonzero, in the undrained shear strength placeholder is a cohesionless soil.** This parameter acts as a switch for the Mathcad file that is used to determine whether the soil

type is cohesive or cohesionless and for selecting the appropriate computational analysis associated with the soil type. If a nonzero value is entered in the placeholder for either c_1 or c_2 then a cohesive analysis is performed. Otherwise, if a value of zero or less is entered then a cohesionless soil analysis is performed.

7.5 Mathcad Drilled Shaft Moment Capacity

The area defined as Flexural Moment Interpolation is used for determining the moment capacity of the drilled shaft section, which controls the limiting soil pressure, R_m S_p (Fig. 7.1) acting on the shaft. This interpolation is based on over 300 runs (cases) of FB-Pier finite element program to determine drilled shaft moment capacity. The cases considered variation in shaft diameter, concrete compressive strength, and area and arrangement of steel. From discussions with the Florida Department of Transportation, the interpolation of the maximum moment of the cross-section assumes a minimum clear cover of six inches. The required user input parameters for interpolation are the gross shaft diameter, D , and the cross-sectional area ratio of steel to concrete, ρ . The interpolation is based on shaft diameters ranging from 24 to 60 inches, and area ratios ranging from 1% to 8% steel. Cases were developed in FB-Pier using these ranges and by varying f'_c from 3 ksi to 6 ksi and the arrangement of concentric bars from 8 up to 52 bars. The case studies revealed that f'_c had approximately a 5% influence of the interpolated result. Consequently, it was decided to use a fixed value of f'_c of 4.5 ksi with shaft diameters of 24, 36, 48 and 60 inches. The moment capacities were then computed using FB-Pier for ρ ranging from 1% to 8%. The number of bars arranged in a concentric circle also influenced the result by approximately 5% when varying the

number of bars from 8 to 52. The FB-Pier computed moments were obtained using a concentric bar arrangement of 24 bars. The generalized parameters, f'_c , and bar arrangement yield a final interpolated result that is within approximately 7 % of FB-Pier computations. The user can override the interpolated value by entering a computed maximum moment in the placeholder provided immediately after this area. The interpolated moment should be unfactored.

7.6 Mathcad Computational Procedures and Programming

The subsequent sections summarize the Mathcad subroutines written to handle the analysis for cohesionless and cohesive soils. The programming logic for handling different soil layers and manipulating soil parameters is also discussed.

7.6.1 Soil Property Array and Slices

In the area labeled as “SOIL PROPERTY ARRAY & SLICES” the number of slices along the length of shaft is determined and the storage of soil properties for each slice is performed. The Mathcad file will slice the shaft into four inch slices if the number of nodes is greater than 50; and, 2 inch slices if less than 50. The number of nodes is determined by first dividing the shaft length, into 4 inches.

The parameters used for computing soil resistance and slice forces are stored into arrays (Figure 7.5) that are passed through functions in subsequent file computations. The arrays appear in the following order: undrained shear strength, failure strain, vertical effective stress, and friction angle. Each array is constructed such that the property is stored in the appropriate soil layer by means of a conditional statement. The vertical effective stress array consists of two lines of computation, which represent the effective

stress of the initial shaft slice and the addition of effective stress due to subsequent slices starting at the top of the shaft (ground surface) and progressing to the shaft tip.

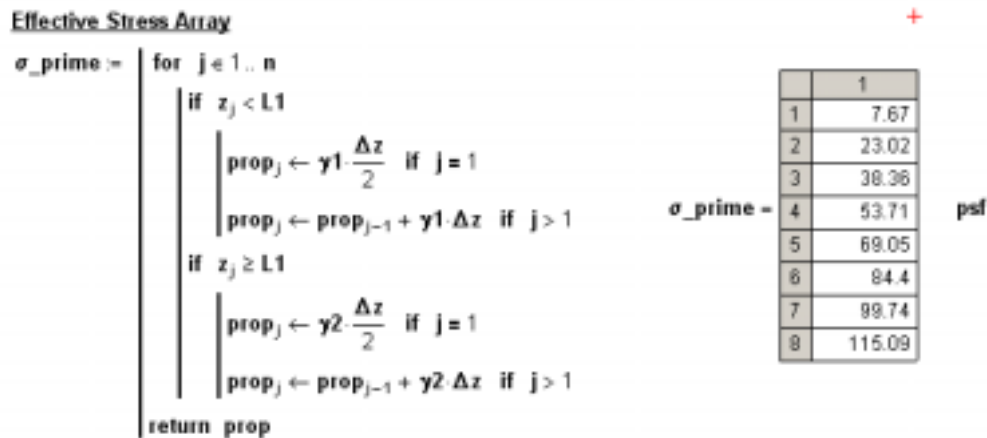


Figure 7.5 Typical Subroutine Logic Used to Build Property Array, Results are Shown to the Right of the Subroutine.

7.6.2 Loading Condition Parameters

Based on the loading conditions defined by the height (e) and horizontal distance (x) of the ultimate point load along the mast arm, a torque multiplier will be interpolated in the area defined as TORQUE MULTIPLIER INTERPOLATION. From the centrifuge results (Fig. 5.21), torque to lateral load reduction multipliers are stored in arrays for L/D ratios of 3, 5 and 7. For each L/D ratio, a multiplier is interpolated for discrete points along the mast arm; distances of 7.5 ft, 14.5 ft, and 21 ft from the centerline of the pole. A second interpolation is performed with respect to the user's L/D ratio to determine the final torque lateral load multiplier.

The interpolated torque lateral load multiplier is limited to L/D ratios between 3 and 7; and for a distance x of not more than 21 ft measured from the centerline of the

drilled shaft. The limit on L/D is based on the working range of drilled shafts of this type.

7.6.3 Cohesionless Soil Computations

For cohesionless soils, the slice forces are computed based on Reese, et al, 1974. The equation taken from Reese, et al. 1974 assumes wedge-type failure of the soil mass (Eq. 7.1). The soil/shaft interaction based on Teng, is based on rigid body behavior. The ultimate soil resistance is computed for each slice over the length of the pile. In the area labeled “SHAFT ANALYSIS – COHESIONLESS” are the computational procedures, interpolations and subroutines used to compute the ultimate slice forces.

At the top of this area are two areas defined as z_over_D and Ac_array . The coefficient for cyclic loading (Ac) is interpolated using these arrays in the subsequent function. To the right of the arrays is a table, which gives values of Ac for z/D ratios, after Reese, 1974. The x/D ratio represents the depth of slice to shaft diameter for which the ultimate slice force is being computed.

Next, a function defined as Pu_SAND is used to compute the ultimate slice force. The function arguments are friction angle, depth to mid-slice from the ground surface and effective vertical stress. The function is defined as a program that computes the ultimate slice force to a given depth and is based on Equation 7.1.

7.6.4 Cohesive Soil Computations

Immediately after the cohesionless soil area computations is an area labeled “INTEGRATED CLAY ANALYSIS”. The computations in this area determine the ultimate slice force for cohesive soils and are based on O’Neill and Gazioglu, 1984.

This method requires the elastic modulus of the soil, which is found based on a correlation proposed by Bannerjee and Davies (1978). This is the same correlation that FB-Pier uses to compute soil modulus.

The function's arguments are undrained shear strength, depth to mid-slice from the ground surface and the strain at the maximum deviator stress from an unconfined undrained triaxial test. The computations within the program that define the ultimate slice force function are based on Eq. 7.2. N , ultimate lateral soil resistance factor, in the equation is a function of the depth of the slice and the critical length of the shaft. The first five lines of programming are used to determine the critical length and it ensures that the critical length cannot be greater than the given shaft length. Also, N can never be greater than nine. Subsequently, the soil degradability factor (F_{cyc}) is determined by a subroutine, which uses conditional statements to interpolate the factor for cyclic loading.

Finally, line 8 computes the ultimate slice force; line 9 returns the computed value to the function $P_{ult_CLAY}(c_u, z, \epsilon_{failure})$.

7.6.5 Shear and Moment Equilibrium

The computation for determining the ultimate soil resistance and available shear and moment are performed in the area labeled "LIMIT EQUILIBRIUM COMPUTATIONS". The ultimate soil resistances are first computed in this area using a subroutine that recalls the appropriate soil parameter arrays and functions. The undrained shear strength parameter (c_u) sets the condition for either cohesionless or cohesive computation of the slice forces. If c_u for a particular slice (j) is less than or equal to zero then the Pu_SAND function is called and the friction angle, depth, and effective stress arrays are fed into this function for each slice (Figure 7.6). If c_u is greater than zero than

the Pult_CLAY function is called and the appropriate arrays are fed through it. The ultimate resistance of the soil is evaluated as Pu_Soil.

Compute Ultimate Soil Resistance

```

Pu_Soil :=
  for j ∈ 1..n
  | Pu_Slicej ← Pu_SAND( $\phi_j$ , zj,  $\sigma_{primej}$ ) if cuj ≤ 0
  | Pu_Slicej ← Pult_CLAY(cuj, zj, sfailurej) if cuj > 0
  return Pu_Slice

```

Figure 7.6 Subroutine Used to Determine Soil Type and Compute Ultimate Soil Resistance.

The subsequent function defined as Slice_Force(fact) performs a series of steps in order to compute each slice force along the length of the shaft. It determines the net pressure zones about the shaft by computing the depth from the ground surface to the point of force reversal. It then sums moments about the top of the shaft associated with each slice force in order to determine the out of balance moment. A subsequent function V(T) sums the slice forces in the horizontal direction based on the Slice_Force. The resulting out of balance shear computed by V(T) is the available shear force at a height of e acting on the pole (Vu_Top). This is the ultimate load that the system can sustain at the top of the pole. Next, the function M_Soil_ult(Pf) computes the maximum moment in the shaft that the soil can support. The subroutine, which defines this function, finds the point of zero shear by summing pressure distribution slice forces and then sums moments about this point.

Following the maximum moment due to the soil computation, a subroutine called ratio, computes a ratio of maximum moment due to shaft and that due to the soil (above).

The ratio has a value of one if section moment is equal to or greater than the maximum moment of the soil. It is less than one if $M_{\text{Section}}(\text{shaft})$ is less than $M_{\text{Soil_ult}}(\text{Slice_Force}(1.0))$ of soil. This moment ratio is applied to each ultimate slice forces (Fig. 7.1) thereby reducing the pressure distribution about the shaft. Consequently, the available shear required to balance the moments and horizontal forces of the system is reduced based on the flexural capacity of the drilled shaft section.

7.6.6 Torque Modified Shear and Moment

The area labeled “TORQUE MODIFIED SHEAR & MOMENT” applies the interpolated torque lateral load multiplier to the ultimate shear and moment calculated in the previous area. Two sets of equations for the shear forces and bending moments with and without the torque multiplier are displayed in this area (Figure 7.7). The torque lateral load multiplier is defined as TLM, V_u is the ultimate shear if no torque is applied, and V_{u_Top} is the ultimate shear when a torque is applied. M_u represents the maximum

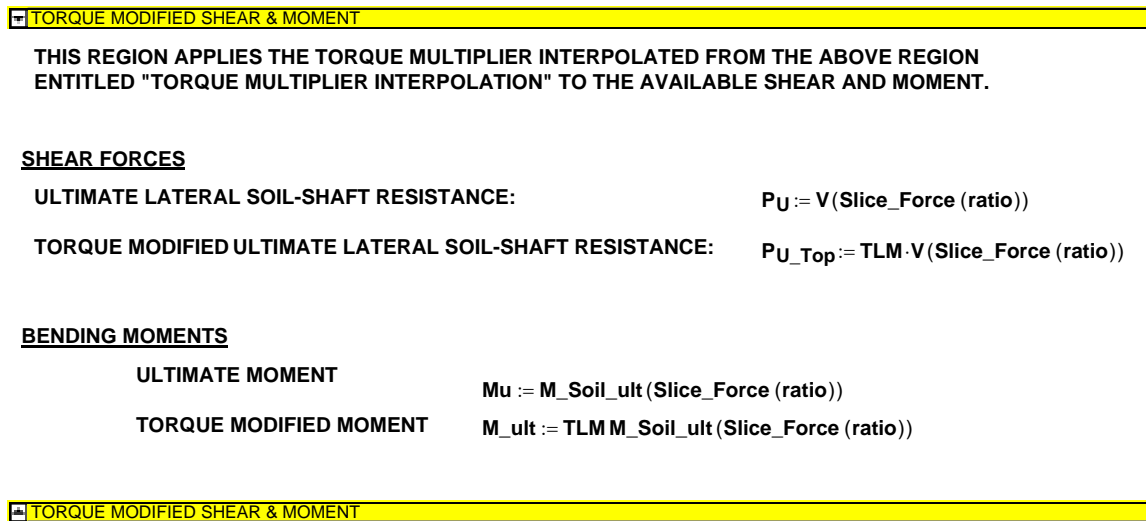


Figure 7.7 Torque Modified Shear and Moment Computations

moment that is induced by the soil wedge when no torque is applied, and M_{ult} is the maximum moment if torque is applied. This allows the user to directly observe the reduction effect torque has on lateral load capacity. The torque lateral load multiplier, much like the moment ratio described above, reduces the net pressure distribution. This behavior is directly related to observations from the centrifuge tests.

7.6.7 Shear Forces Along Shaft Length

The area defined as SHEAR FORCE ALONG SHAFT computes the shear force along the shaft length that is induced by the soil wedge. Through force equilibrium the shear forces associated with and without torque are summed in the horizontal direction. The shear forces computed in this area are plotted as part of the graphical output.

7.6.8 Torsional Capacity of the Shaft

For sands, the shaft's ultimate torsional shear capacity, f_s (stress), is given by Eq. 6.1 (i.e., District 5 and FB-Pier). For clays, the FHWA approach (O'Neill, 1995) for axial skin friction is used for the shaft's ultimate torsion shear capacity, f_s (stress), is $0.55 C_u$ (C_u = undrained shear strength of clay). The torque capacity, T_{total} , of the shaft is given through Equations 6.2 and 6.3 (force-length). The soils' "ultimate torsional soil resistance" (Figure 7.8) is obtained by dividing the shaft's torque capacity, T_{total} , by the distance along the mast arm, x (Fig. 7.2) the load is applied.

NUMERICAL OUTPUT

Maximum Available Shear Force on the Pole:

ULTIMATE TORSIONAL SOIL RESISTANCE:

$$P_{U_Torque} = 52.525 \text{ kip}$$

ULTIMATE LATERAL SHAFT RESISTANCE:

$$P_U = 201.985 \text{ kip}$$

TORQUE MODIFIED ULTIMATE LATERAL SHAFT RESISTANCE:

$$P_{U_Top} = 77.8 \text{ kip}$$

Maximum Moment in the Shaft Due to the Soil:

ULTIMATE MOMENT

$$M_u = 5.137 \times 10^3 \text{ kip}\cdot\text{ft}$$

TORQUE MODIFIED MOMENT

$$M_{ult} = 1.978 \times 10^3 \text{ kip}\cdot\text{ft}$$

Figure 7.8 Mathcad Numerical Output Sheet.

7.7 Mathcad Output

The Mathcad file provides both numerical and graphical output. The display of values and plots is intended to provide the user with information regarding soil/shaft interaction with respect to shear and moment at a maximum increment of four inches along the length of the shaft.

7.7.1 Numerical Output

The numerical output (Figure 7.8) consists of values for the ultimate torsional resistance of soil, ultimate lateral shaft resistance, and torque modified lateral shaft resistance, as well as, ultimate moment and torque modified moments, which are highlighted green. As explained in the previous section, the torque modified ultimate lateral and moment are ultimate values that are adjusted based on the torque applied

along the mast arm. If there is no torque applied to the mast arm then these values will equal the value given immediately above the green highlighted capacities.

The numerical output also consists of a set of six tables, which show values of soil/shaft shear response and magnitude of slice along the length of the shaft. Visible are the first 12 depth increments, which can be adjusted by the user by left clicking anywhere on a table and then clicking the up or down arrows to view the desired values.

7.7.2 Graphical Output

The graphical output (Figures 7.9 and 7.10) consists of plots of soil/shaft shear response and slice force along the shaft's length. Torque modified and unmodified values are plotted together on one graph and also individually on smaller graphs to the right of side of the graphical output sheet.

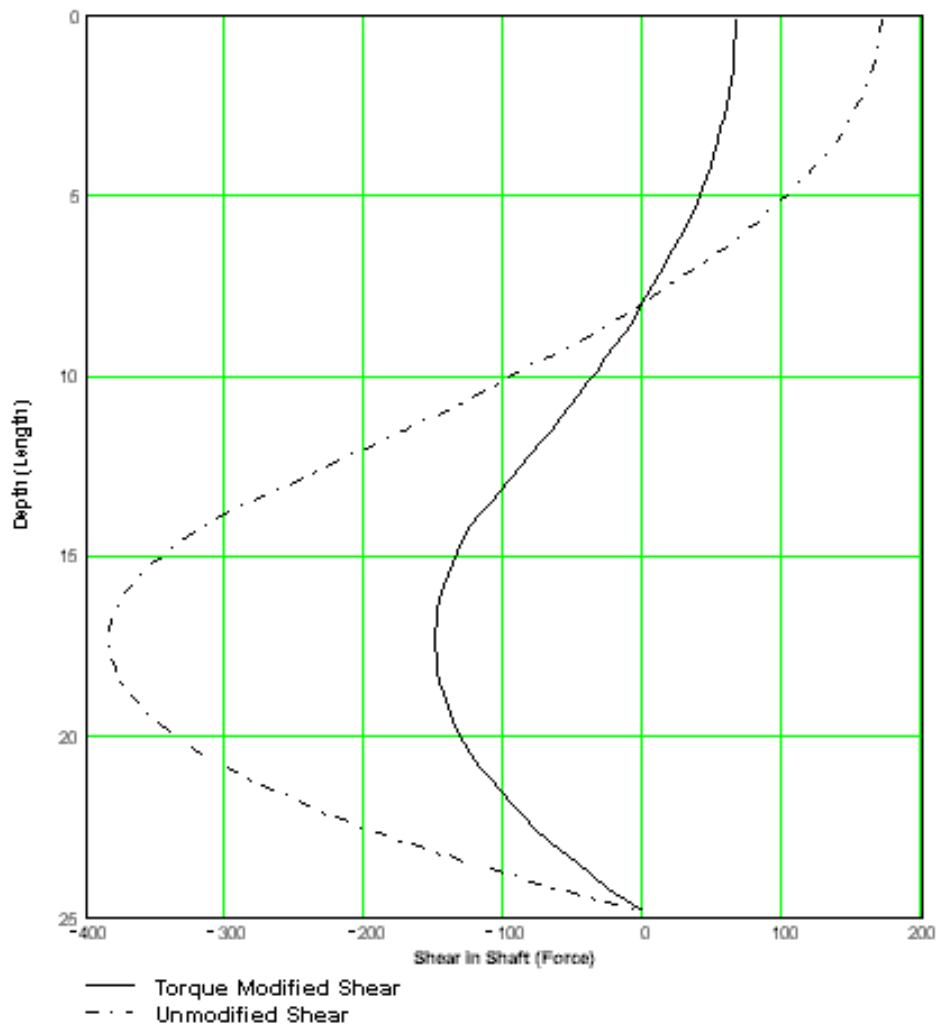
GRAPHICAL OUTPUT**Plot Soil/Shaft Shear Response Along Shaft Length**

Figure 7.9 Graphical Output Plotting Layout Showing Soil/Shaft Shear Response Associated with Applied Torque.

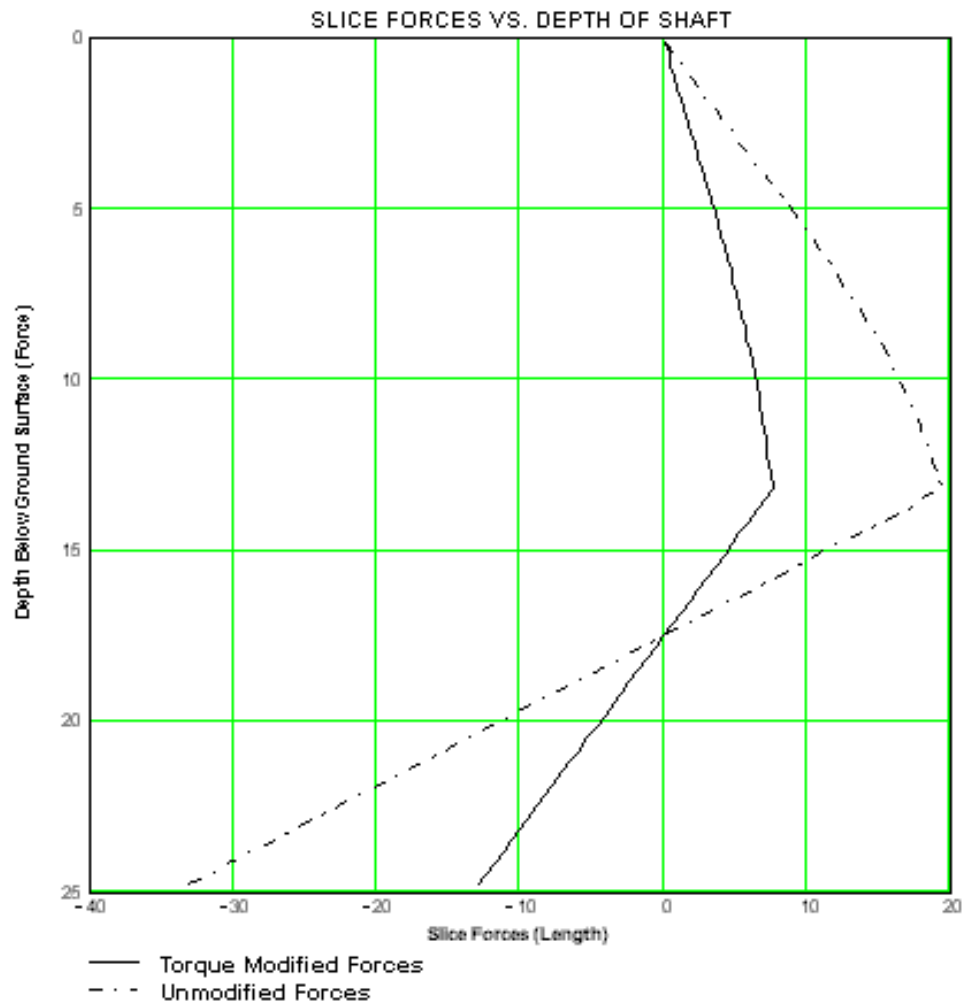
GRAPHICAL OUTPUT (Continued)**Plot of Slice Force Along Length of Shaft**

Figure 7.10 Graphical Output Plotting Layout Showing Ultimate Slice Forces Along Shaft Length Associated with Applied Torque.

CHAPTER 8 CONCLUSIONS AND RECOMMENDATIONS

The Florida Department of Transportation has mandated the use of high mast traffic signs/signals using mast arms attached to poles supported on drilled shafts as a result of Hurricane Andrew. Due to load location, significant torque and lateral loading may develop on the foundation. Of issue is the combined loading (load/torque) on the foundation since a few failures have been recorded in the field.

For this research, eighty centrifuge tests were performed on high mast traffic signs/signals. Testing was performed by applying the lateral load to the top of the pole, as well as along the mast arm. The latter generated torque in combination with lateral loading on the foundation. The models were constructed to 1:45 scale and tested in the University of Florida's Geotechnical centrifuge at 45 gravities, which replicate insitu field stresses.

For all experimental shafts, the concrete was constructed with cement grout and steel reinforcement, which extended up from the shaft to become the sign pole. All the shafts were placed and spun up in the centrifuge while the cement grout was fluid. The latter allowed the stresses in the soil around the shaft to equilibrate to field values. After four to five hours (cement grout hydrated), the lateral loading commenced.

The drilled shafts were installed in either dry or saturated fine sand (Edgar Florida) prepared at multiple densities (loose, medium, and dense) in both dry and saturated states. All of the shafts were constructed with either casing (dry sand) or with

wet-hole (saturated sand) method of construction. In the case of wet-hole, bentonite slurry was used to maintain hole stability; the influence of slurry cake thickness was investigated. It was concluded that if the slurry cake was kept below 0.5 in. (prototype: field), little if any influence on the shaft's torsional capacity was found. However, if the cake thickness approached 2.0 in. (field), then fifty percent reduction in torsional capacity of the shaft was observed.

In the case of loading on the pole (i.e., no torque), a shaft's lateral capacity increased with soil density and length to diameter (L/D) ratio ($L/D < 5$). Increasing a shaft's length to diameter ratio beyond five resulted in little if any lateral resistance due to flexure failure of the shaft. This behavior was predicted by FB-Pier, which matched the measured load vs. deflection for large movements. It was concluded that lateral resistance at small L/D ratios (i.e., close to three) was governed by soil density while longer shafts (i.e., deeper embedments), e.g. L/D ratios greater than 5, flexure strength of shaft controlled. It was generally observed (i.e., dry and saturated sands) that Broms ultimate capacity prediction was un-conservative for the short shafts ($L/D < 5$), but gave good prediction for long shafts ($L/D > 5$). The latter was attributed the magnitude of the assumed soil pressure distribution by Broms.

In the case of torsion on the drilled shaft, i.e., loading on the mast arm, all of the centrifuge experiments (dry and wet sand) revealed little if any influence of lateral loading on the torsional resistance of a shaft. A number of the current design methods used in the state of Florida were compared to measured response: the Structures Design Office method, District 7, District 5, FB-PIER, and the Tawfiq-Mtenga method. Results of the comparison (Table 5.4) revealed all of the Florida Department of Transportation

methods, including Tawfiq-Mtenga method are conservative, with FB-Pier giving the lowest F.S. 1.2. It was also observed for all of the saturated sand deposits, failure occurred through torsion (including $L/D = 7$) instead of lateral displacement. The latter was attributed to the significant reduction in vertical and horizontal effective stresses on the shaft due to a change from total unit weight to buoyant unit weight.

In the case of lateral capacity, the application of torque on the shaft had a significant impact on a shaft's ultimate lateral resistance. The latter reduction was very pronounced for high L/D ratios. Results were impacted little if any by soil density, but significantly by the torque to lateral load ratio. From all the lateral load tests with torque, it was possible to obtain a model, which predicts the decrease in lateral resistance as a function of soil density, L/D ratio and the torque to lateral load ratio (Fig. 5.21).

As part of this research a Mathcad was written to check design of drilled shaft subject to combined torsion and lateral loading. Since Broms method was unconservative for short shafts, employed a simple soil pressure distribution, and could not handle multiple soil layers, it was decided to implement a free earth support approach as put forward by Teng (1962). The limiting lateral soil stresses on the shaft (Fig. 7.1) are those used for in P-Y representations: Reese et al. (1978) for sand, and O'Neill et al. (1985) for clay. For short shafts, i.e., limit soil stress mobilized, maximum lateral loading on the pole is controlled by the soil properties. For longer shafts, the flexure capacity of the shaft limits the soil resistance (R_m : Fig. 7.1). When torque is applied to the pole (i.e., loading along the mast arm), the soil pressure on the shaft, is adjusted further downward (R_T : Fig 7.1) from Fig 5.21 as found with experimental data.

Since the experimental data revealed no influence of lateral loading on the torsional resistance of the shaft, the FHWA axial shear model (i.e., FB-Pier, District 5) model was also implemented in the Mathcad file. For all the experimental data, the Mathcad file was on average within twenty percent. A copy of the Mathcad file is supplied with the report.

Presently, a number of tests using polymer slurry are in the process of being completed (eight) on the saturated sand using the wet-hole method of construction. Preliminary results show similar response as the mineral slurry with less than 0.5 in. of slurry cake. It is proposed that a number of field tests be undertaken to independently verify the impact of torque on the lateral capacity of drilled shafts in dry sands.

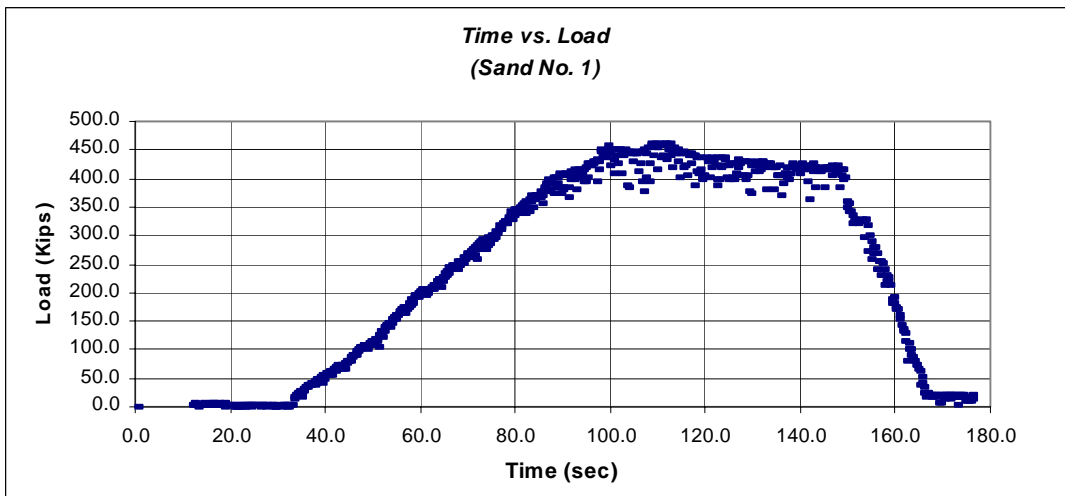
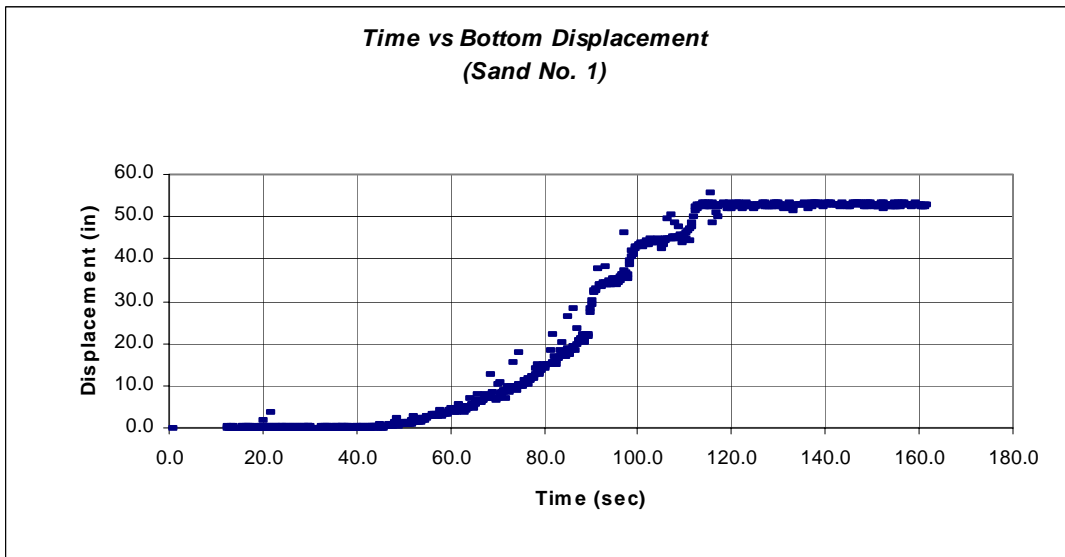
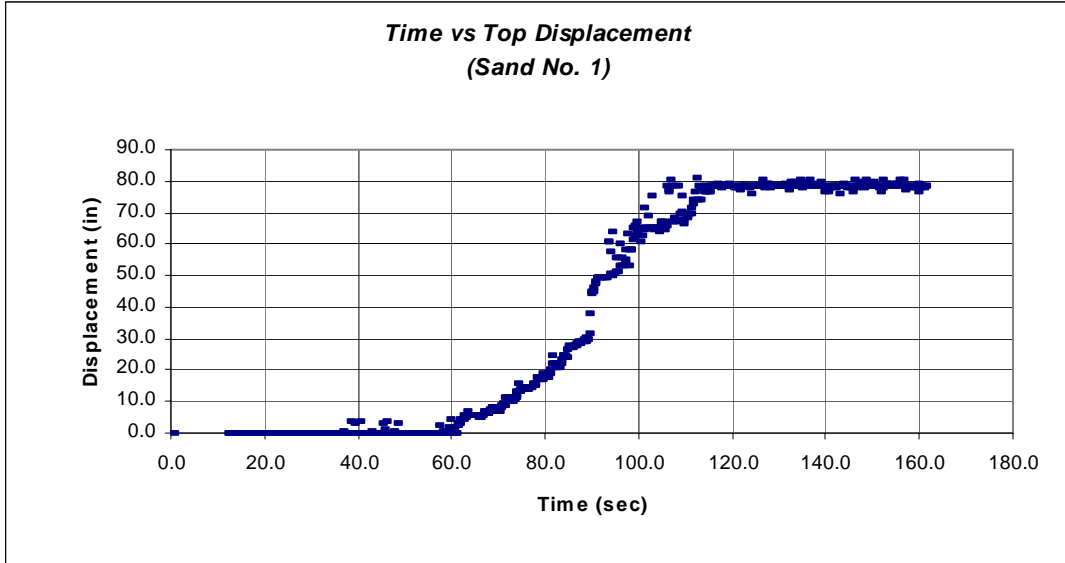
REFERENCES

- Broms, B., "Lateral Resistance of Piles in Cohesionless Soils," ASCE, *Journal of the Soil Mechanics and Foundation Division*, Vol. 90, No. SM3, May 1964, pp. 123-156.
- Reese, L.C., Cox, W.R., and Koop, F.D., "Analysis of Laterally Loaded Piles in Sand," *Proceedings, Sixth Annual Offshore Technology Conference*, Vol. 2, Houston Texas, May 1974, pp. 246-258.
- Reese, L.C., and O'Neill, M., *Drilled Shafts Student Workbook*, FHWA-HI-88-042, Federal Highway Administration, U.S. Department of Transportation, 1988.
- Tawfiq, K., "Drilled Shafts Under Torsional Loading Conditions," *Final Report to Florida Department of Transportation*, Contract # B-9191, June 2000, 185 pages.
- Teng, W.C., *Foundation Design*, Prentice-Hall Inc., Englewood Cliffs, NJ, 1962.

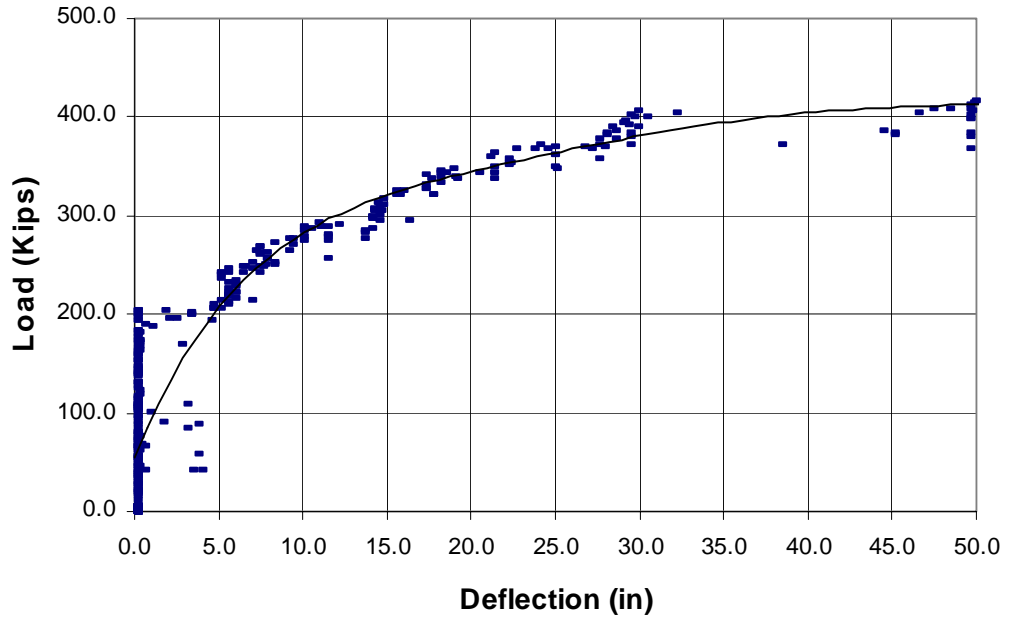
APPENDIX A
Centrifuge Results on Dry Sand (Raw Data)

Testing Sequence on Dry Sand

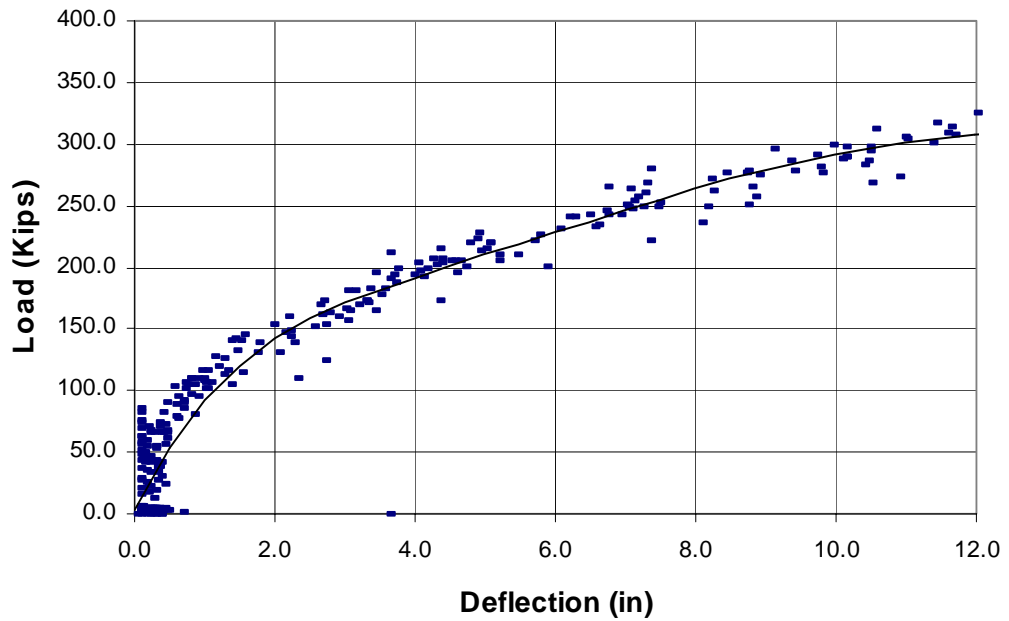
Test No.	Prototype Foundation Diameter (ft)	Prototype Embedment length (ft)	Location of Applied Load			Soil Density (pcf)
			On the Pole	Mid. Mast Arm	Tip of Mast Arm	
1	5	35	*			98.34
2	5	35	*			98.34
3	5	35		*		98.34
4	5	35		*		98.34
5	5	35			*	98.34
6	5	35			*	98.34
7	5	25	*			98.34
8	5	25	*			98.34
9	5	25		*		98.34
10	5	25		*		98.34
11	5	25			*	98.34
12	5	25			*	98.34
13	5	15	*			98.34
14	5	15	*			98.34
15	5	15		*		98.34
16	5	15		*		98.34
17	5	15			*	98.34
18	5	15			*	98.34
19	5	35	*			95.88
20	5	35	*			95.88
21	5	35		*		95.88
22	5	35		*		95.88
23	5	35			*	95.88
24	5	35			*	95.88
25	5	25	*			95.88
26	5	25	*			95.88
27	5	25		*		95.88
28	5	25		*		95.88
29	5	25			*	95.88
30	5	25			*	95.88
31	5	15	*			95.88
32	5	15	*			95.88
33	5	15		*		95.88
34	5	15		*		95.88
35	5	15			*	95.88
36	5	15			*	95.88
37	5	35	*			92.07
38	5	35	*			92.07
39	5	35		*		92.07
40	5	35		*		92.07
41	5	35			*	92.07
42	5	35			*	92.07
43	5	25	*			92.07
44	5	25	*			92.07
45	5	25		*		92.07
46	5	25		*		92.07
47	5	25			*	92.07
48	5	25			*	92.07
49	5	15	*			92.07
50	5	15	*			92.07
51	5	15		*		92.07
52	5	15		*		92.07
53	5	15			*	92.07
54	5	15			*	92.07

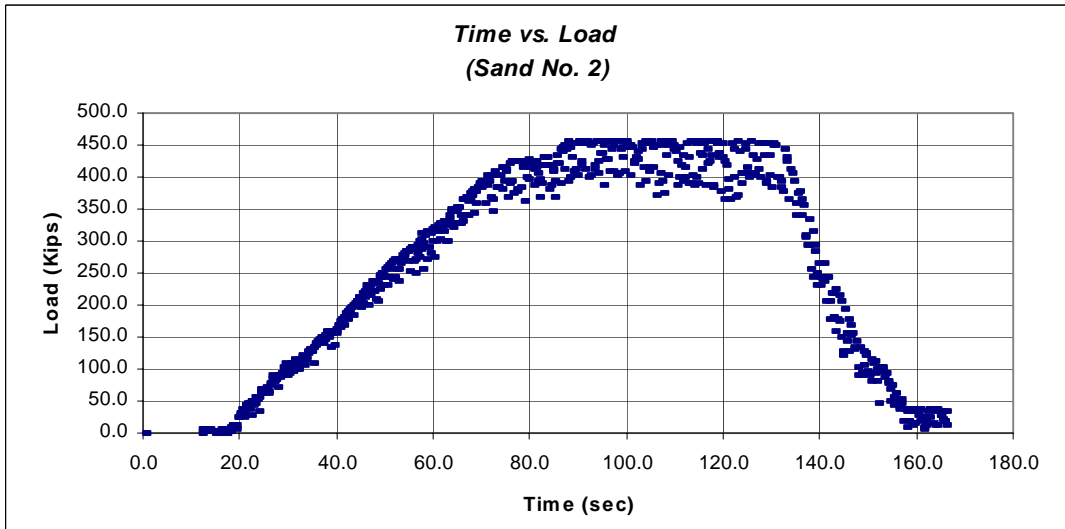
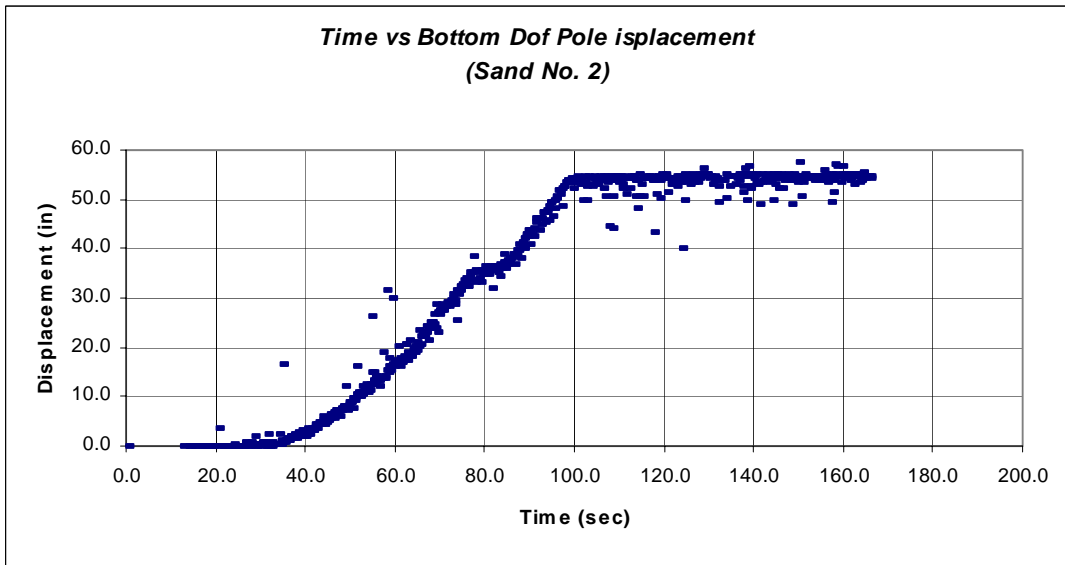
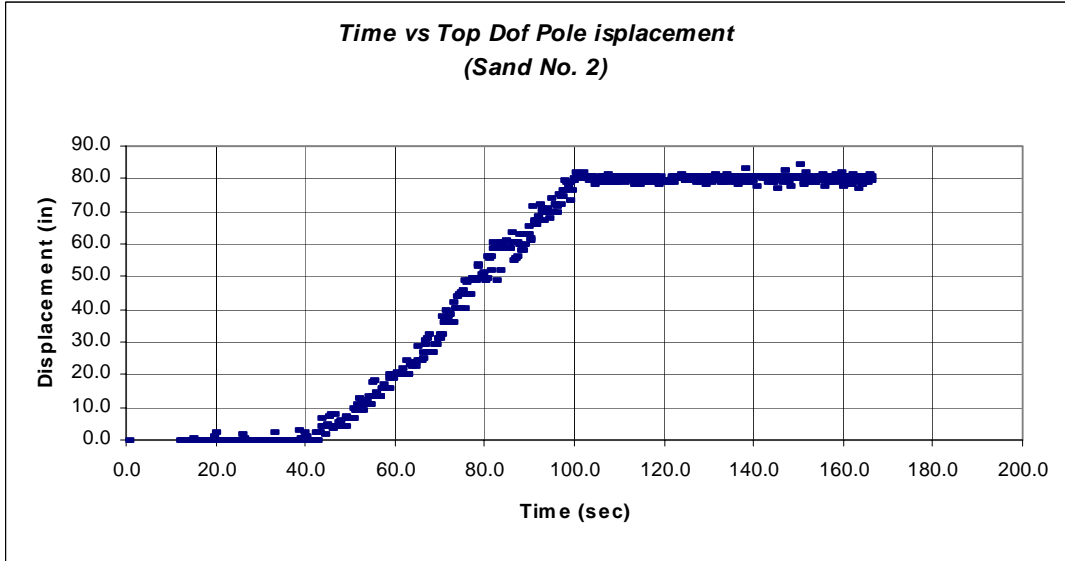


Load vs. Top of Pole Deflection
(Sand No. 1)

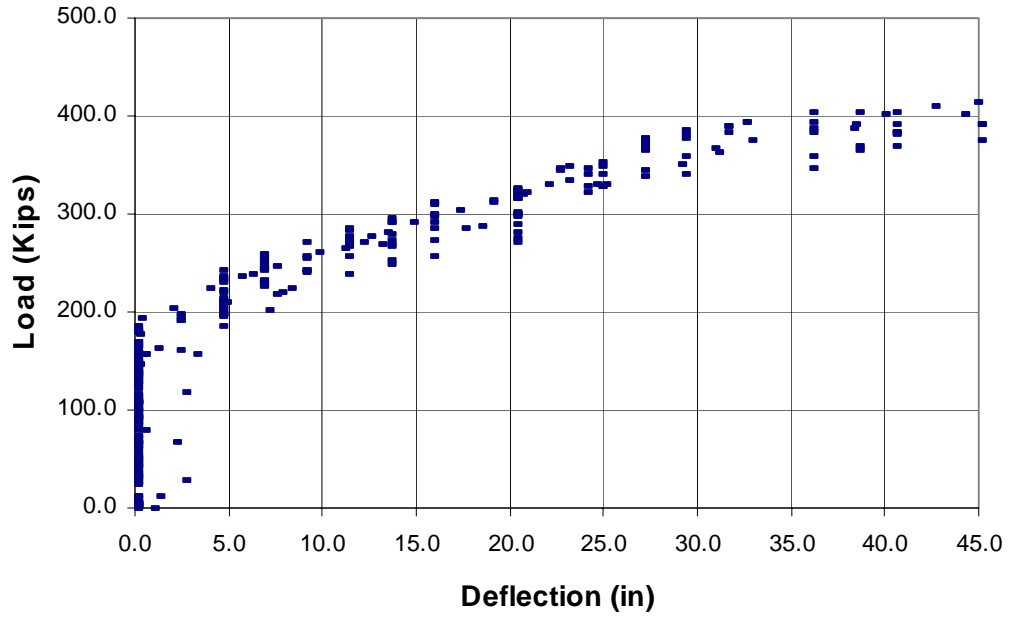


Load vs. Bottom of Pole Deflection
(Sand No. 1)

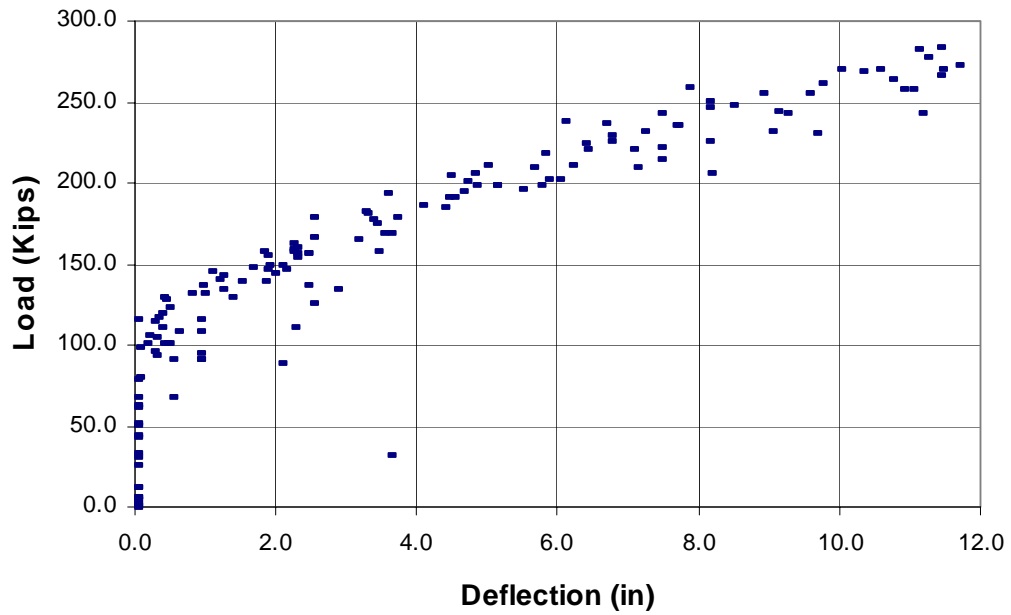


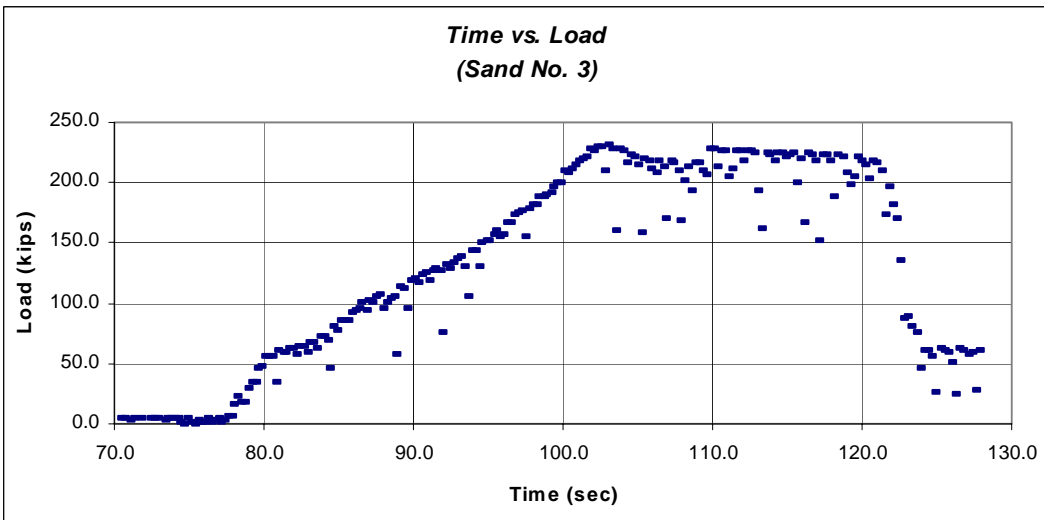
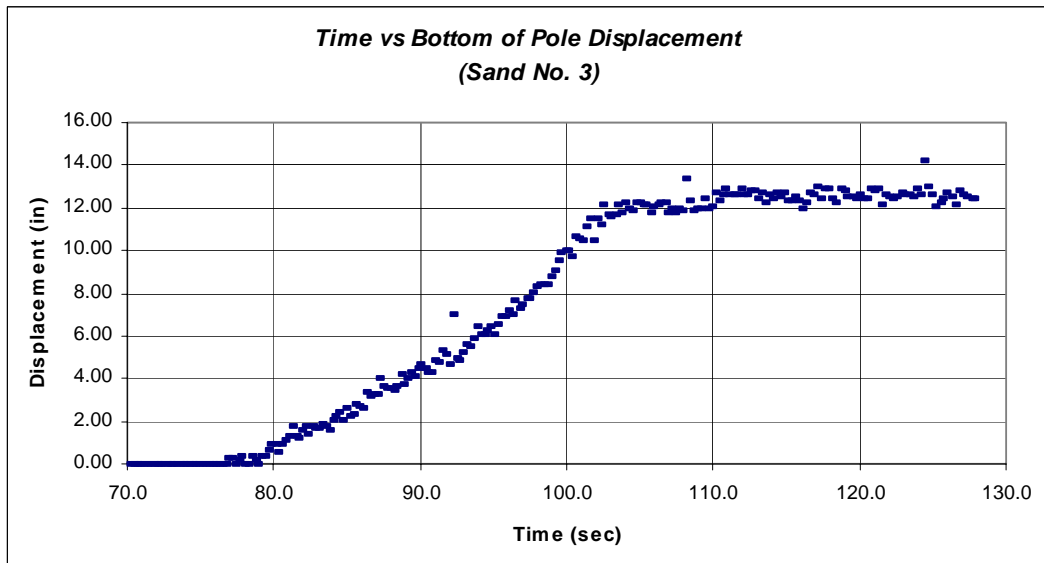
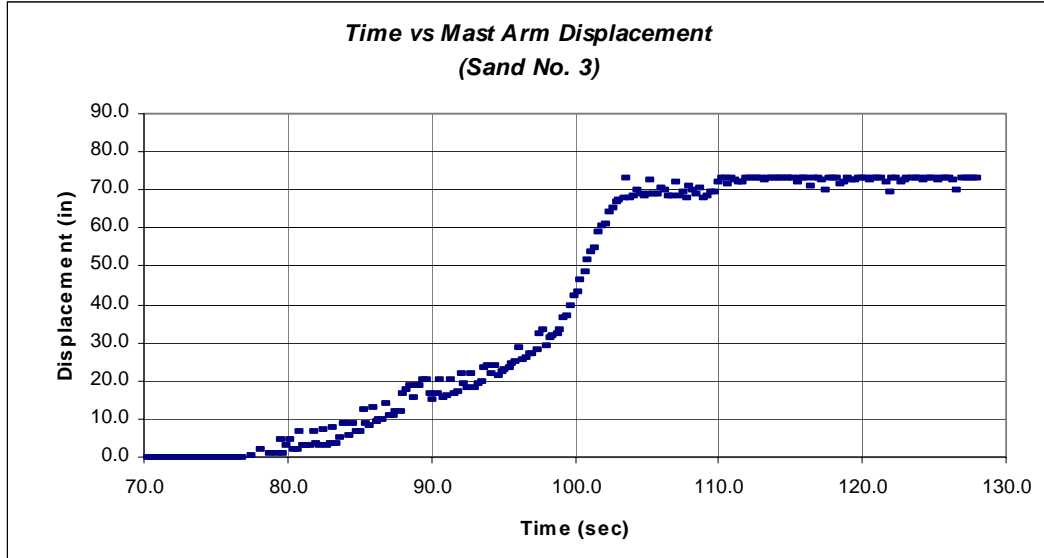


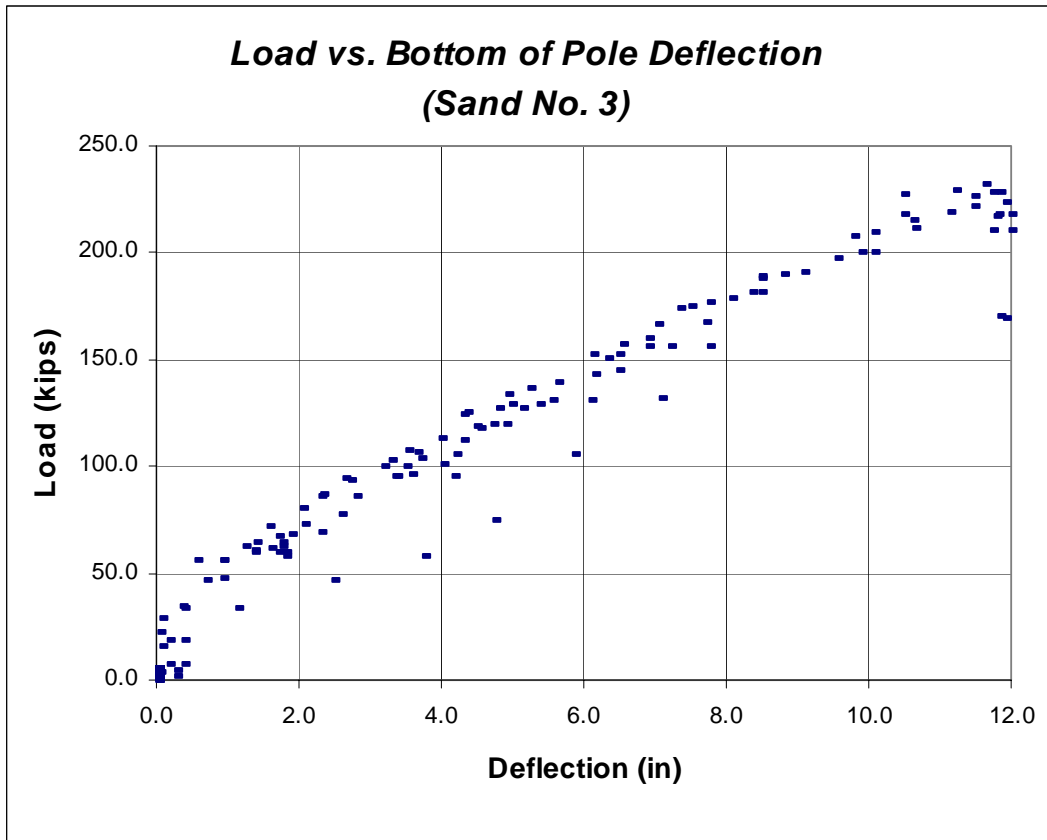
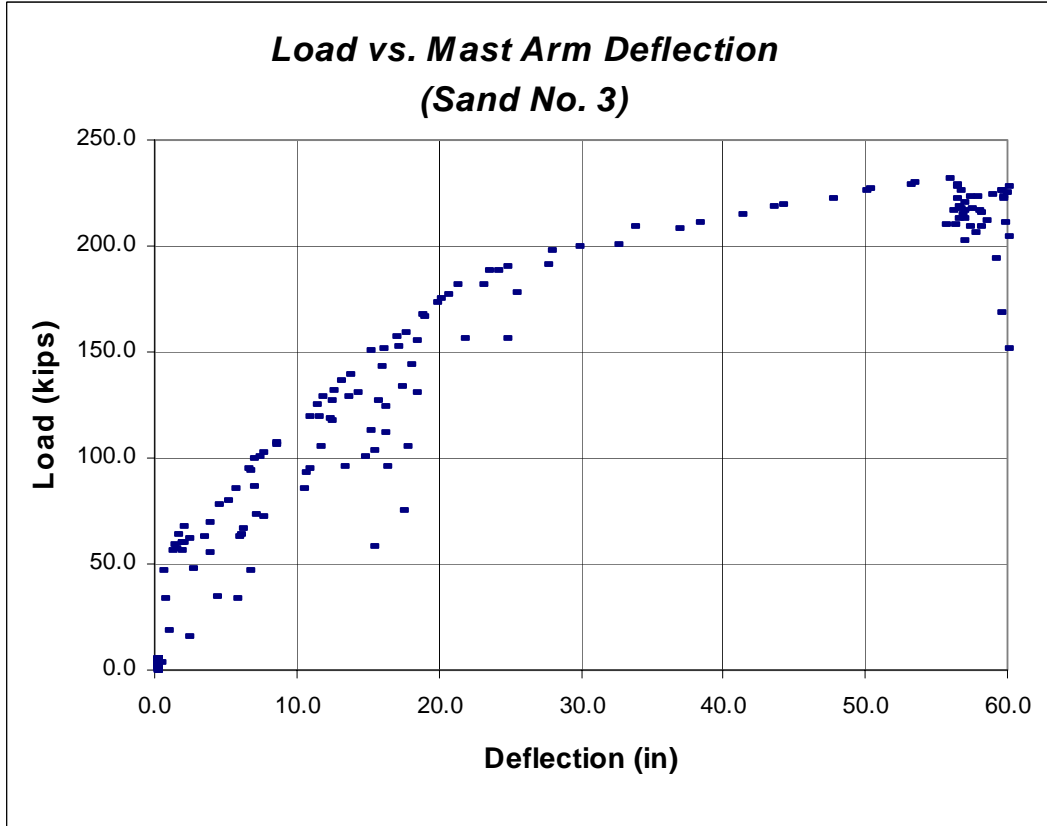
**Load vs. Top of Pole Deflection
(Sand No. 2)**

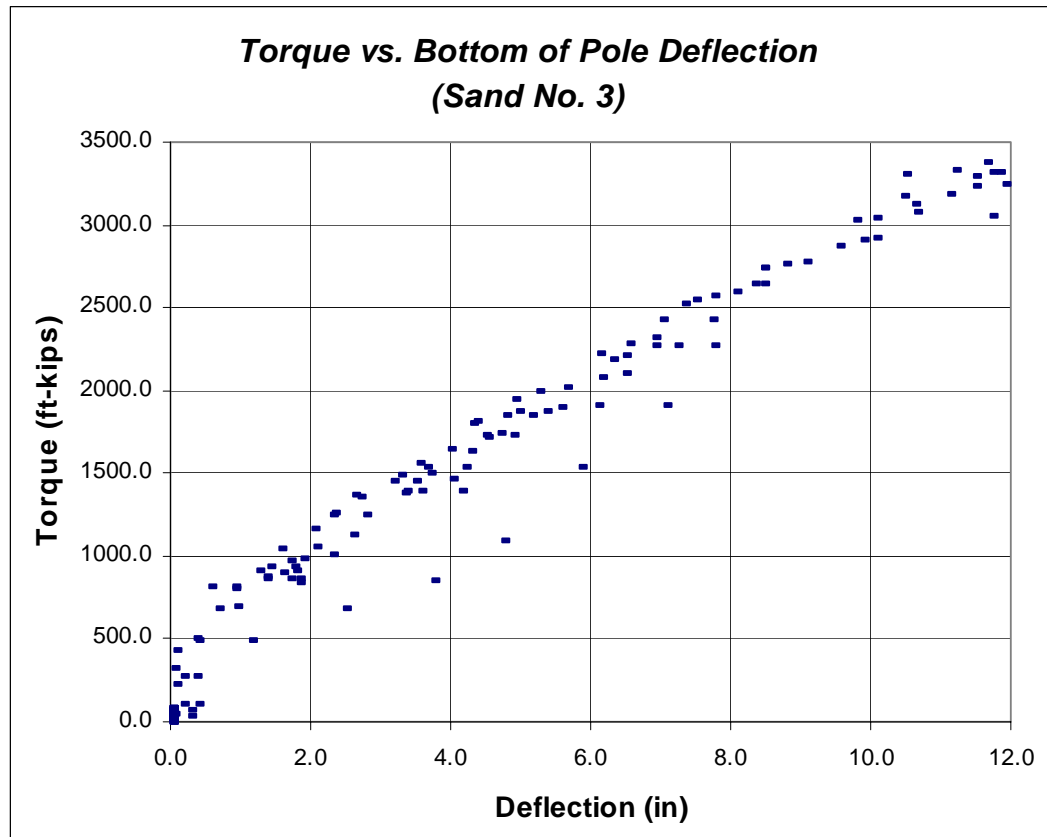
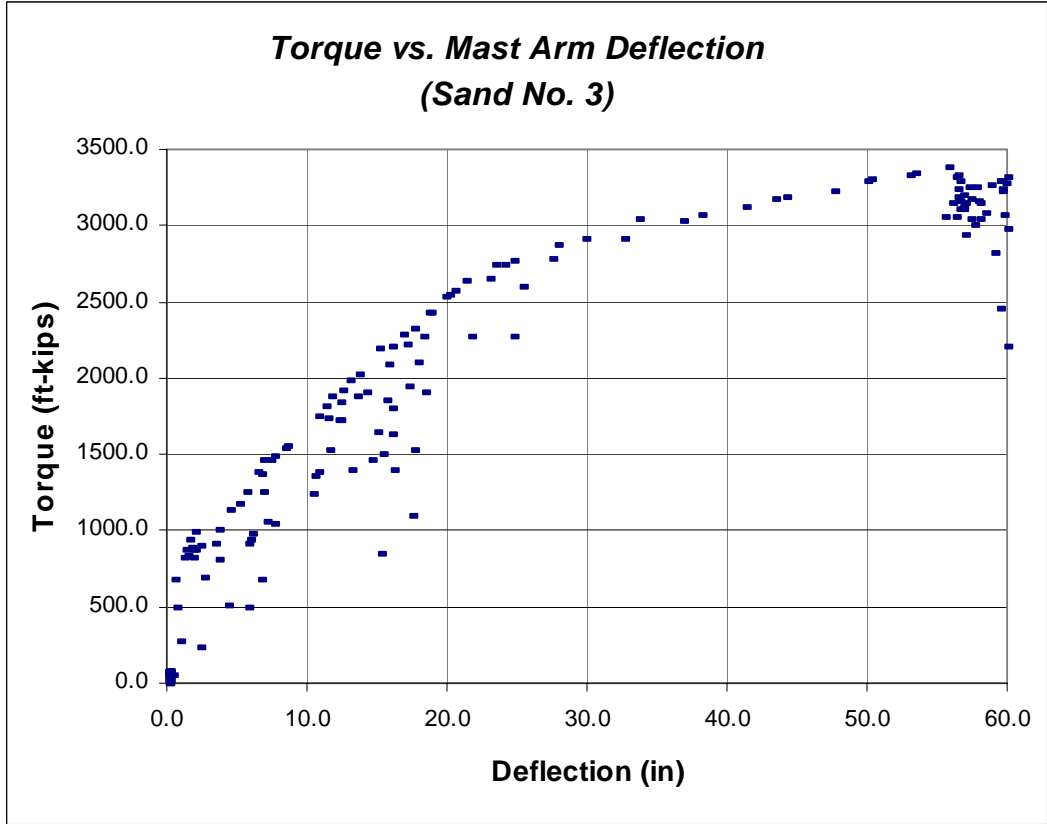


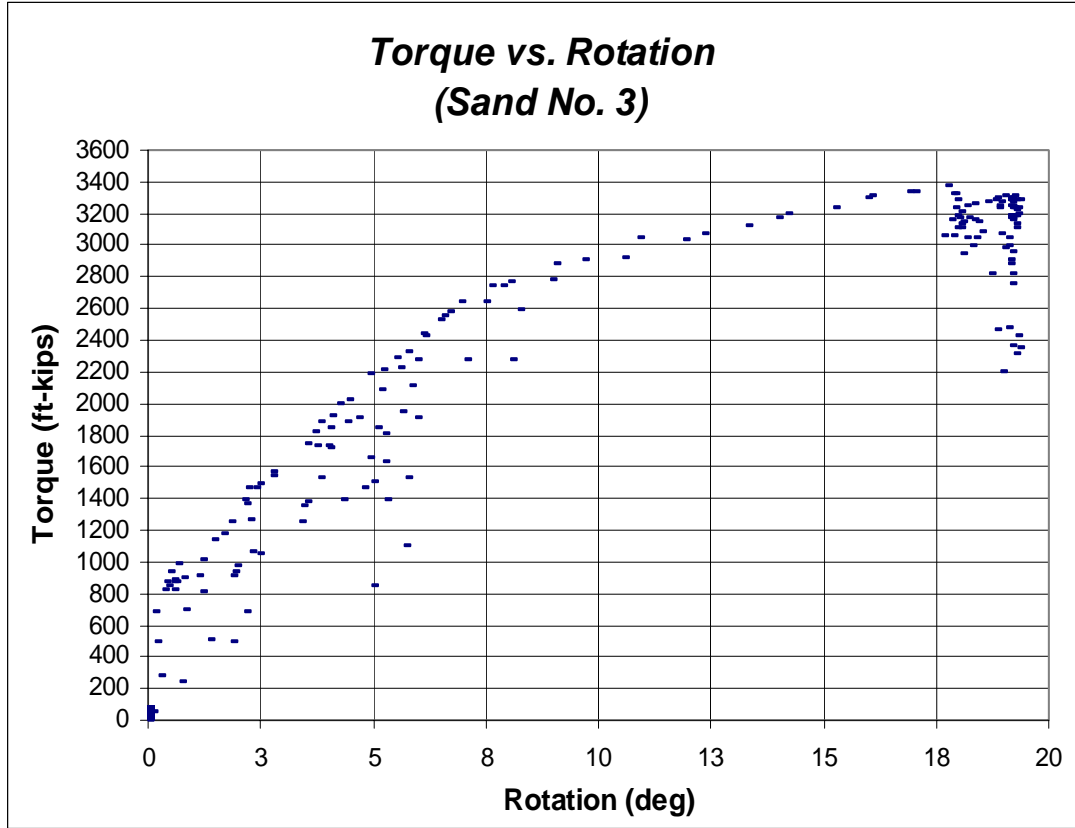
**Load vs. Bottom of Pole Deflection
(Sand No. 2)**

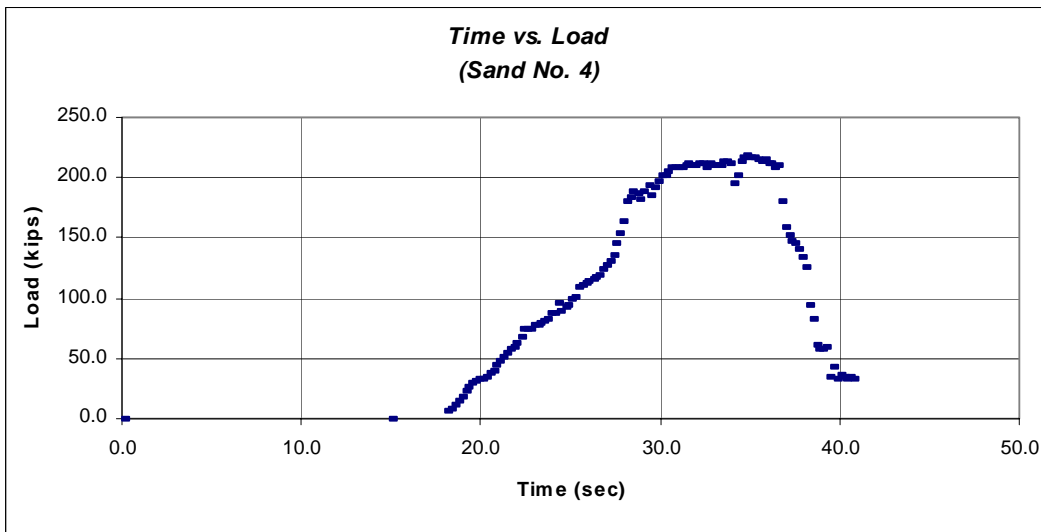
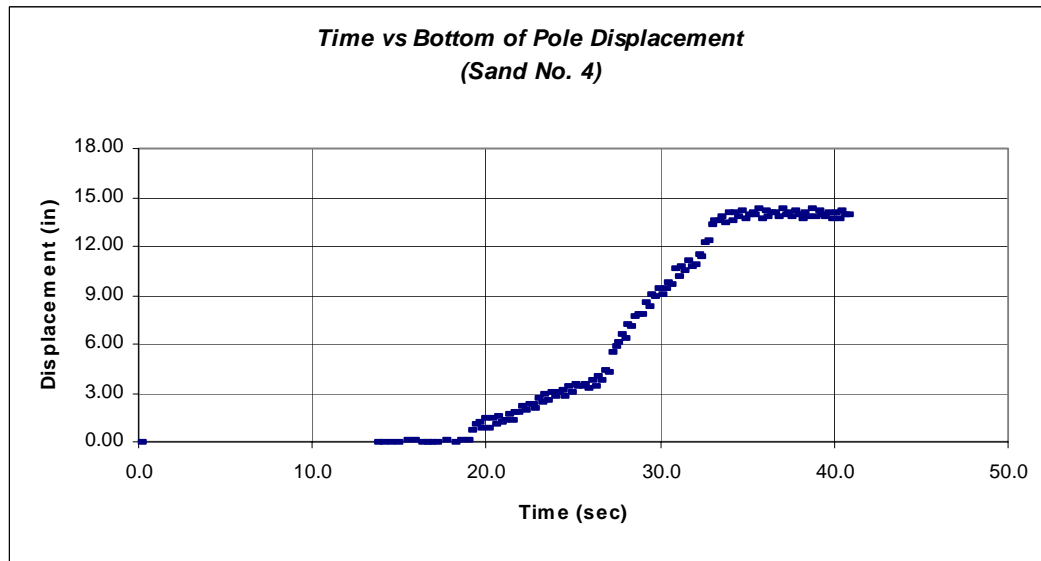
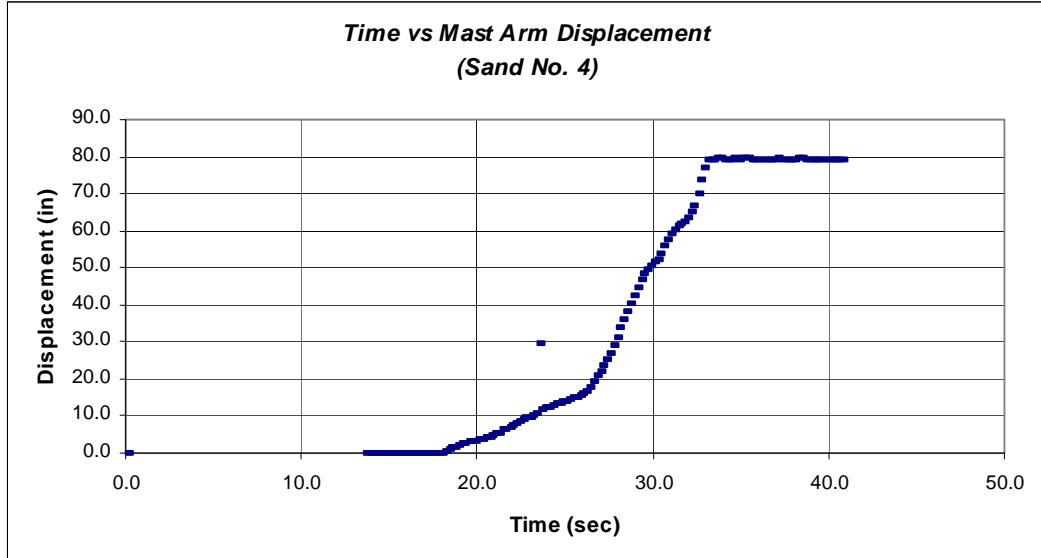


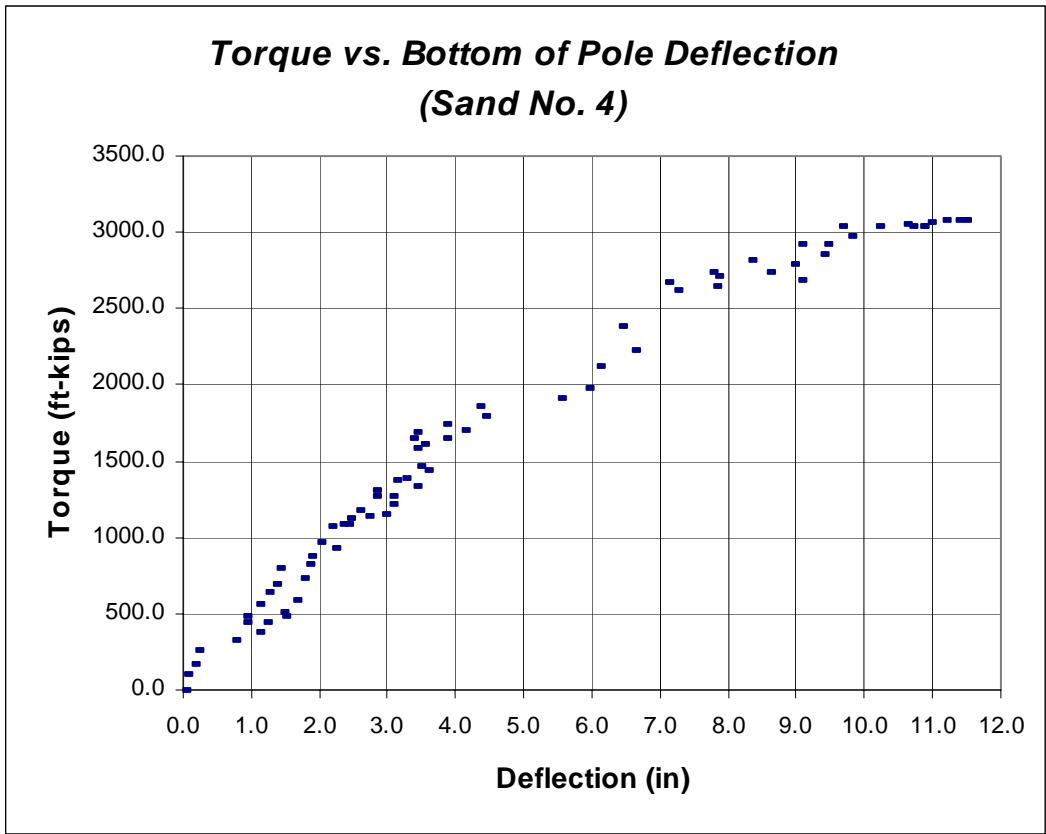
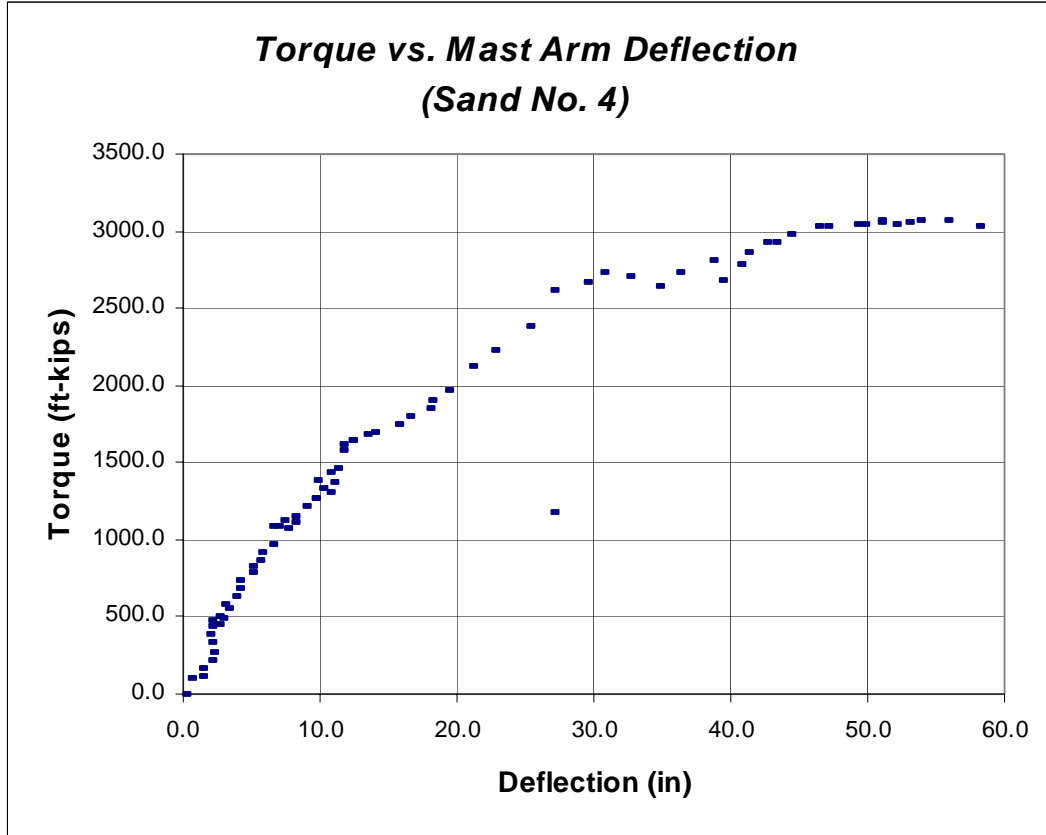


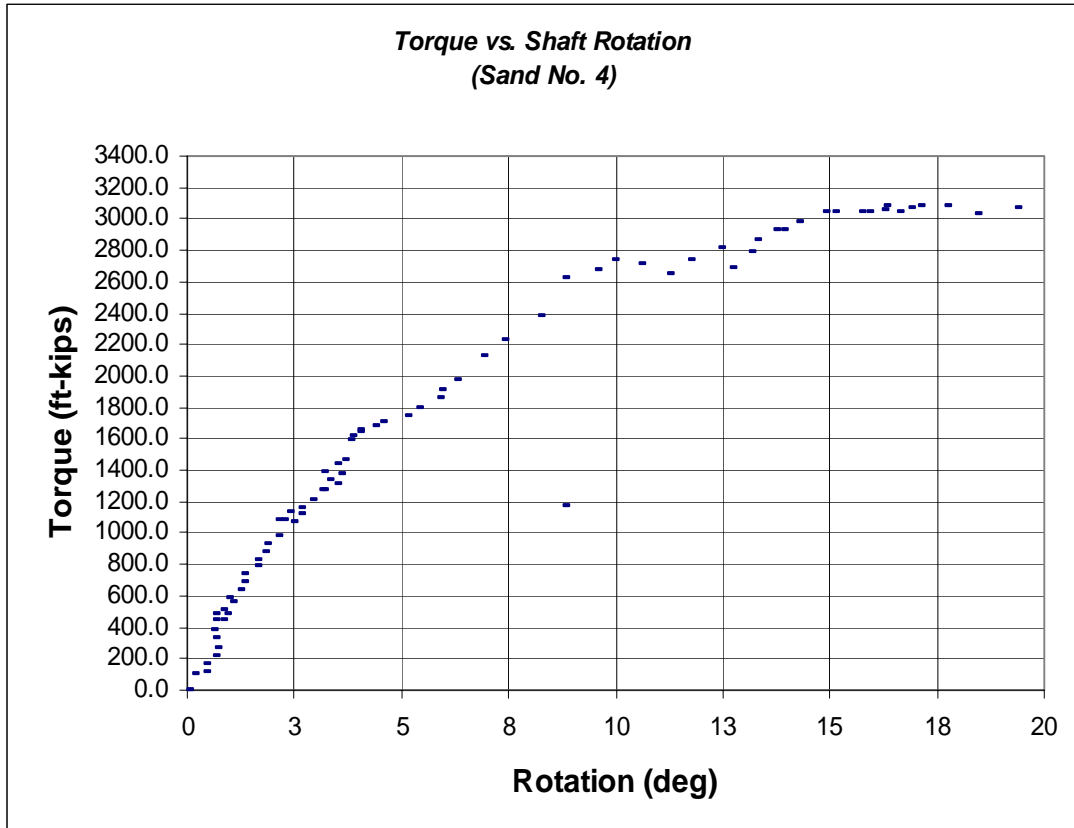


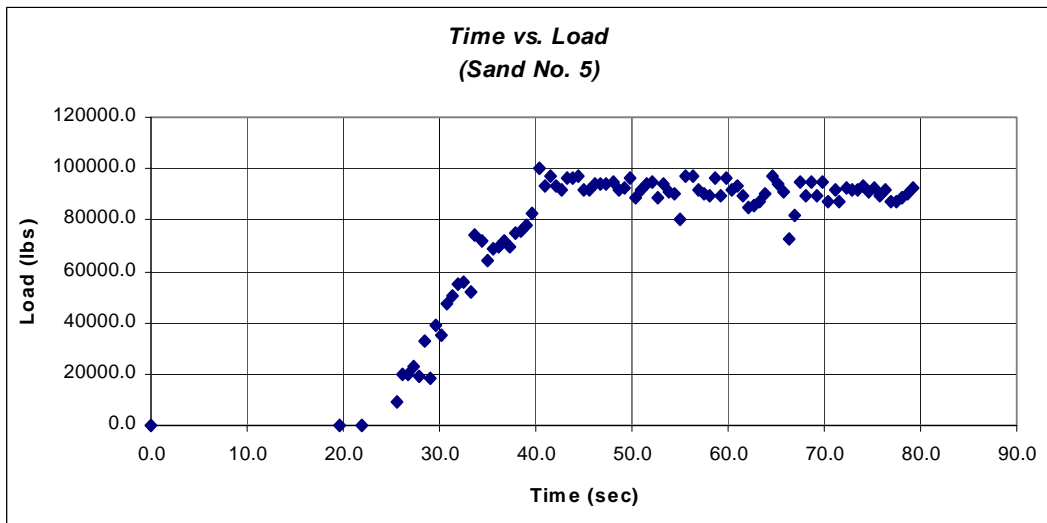
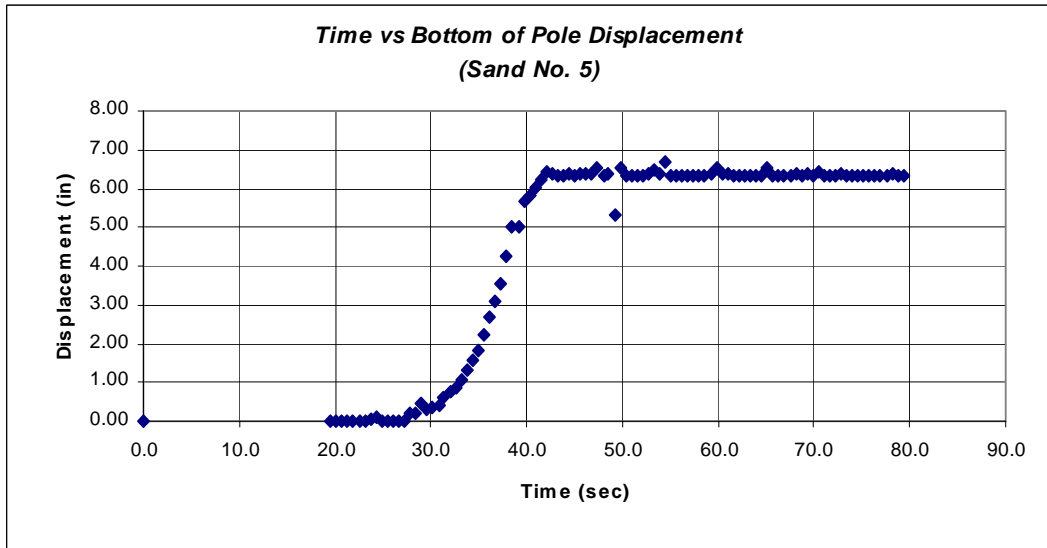
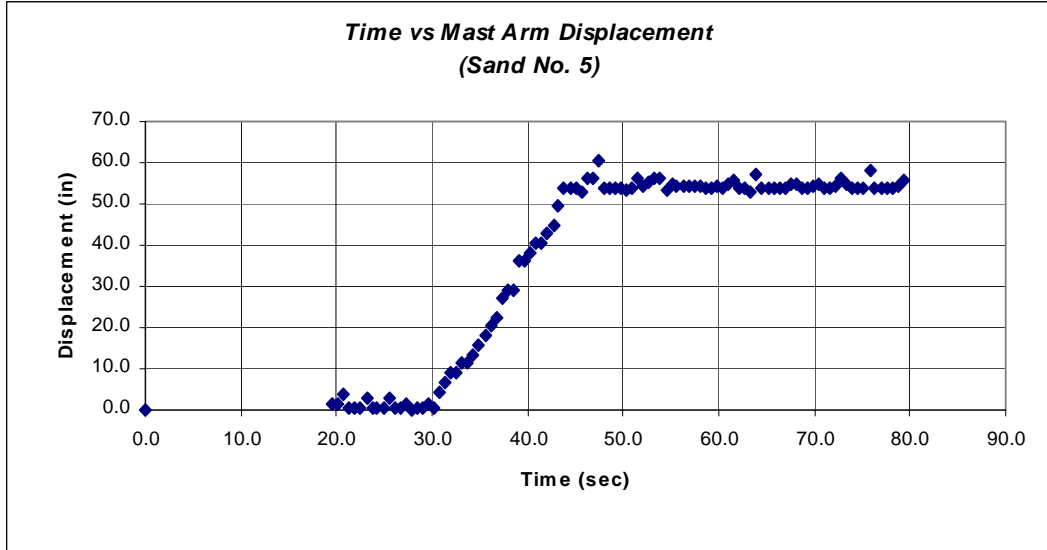


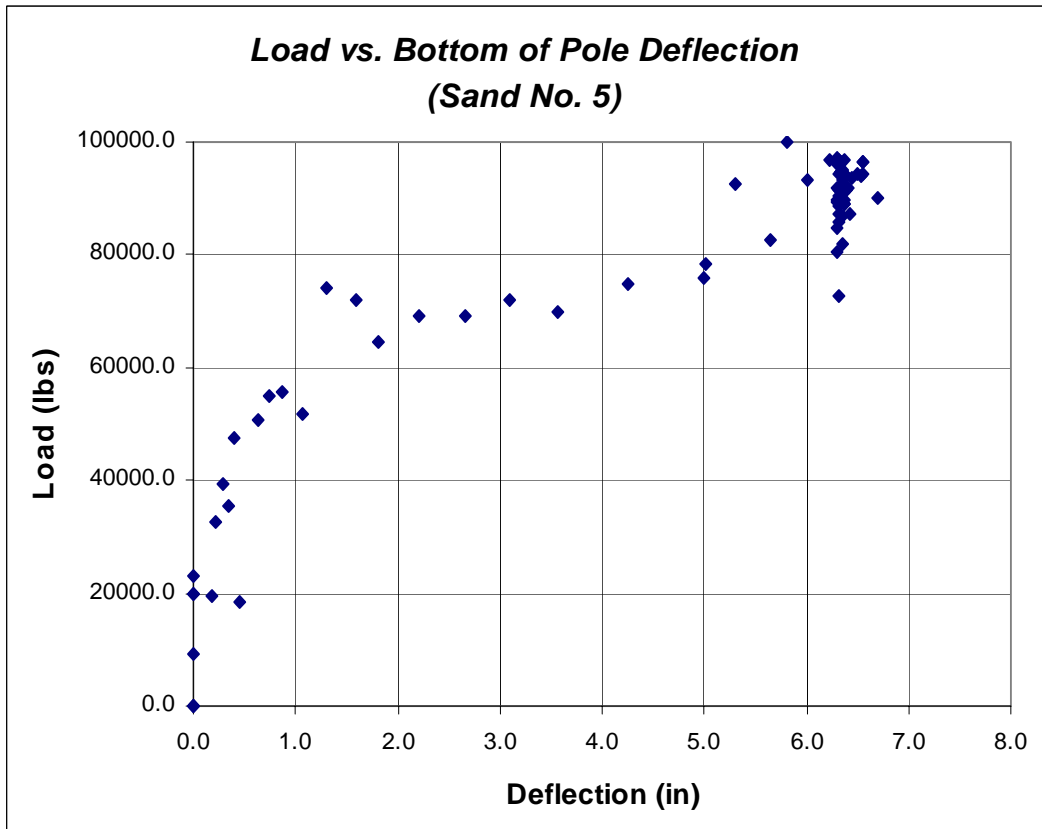
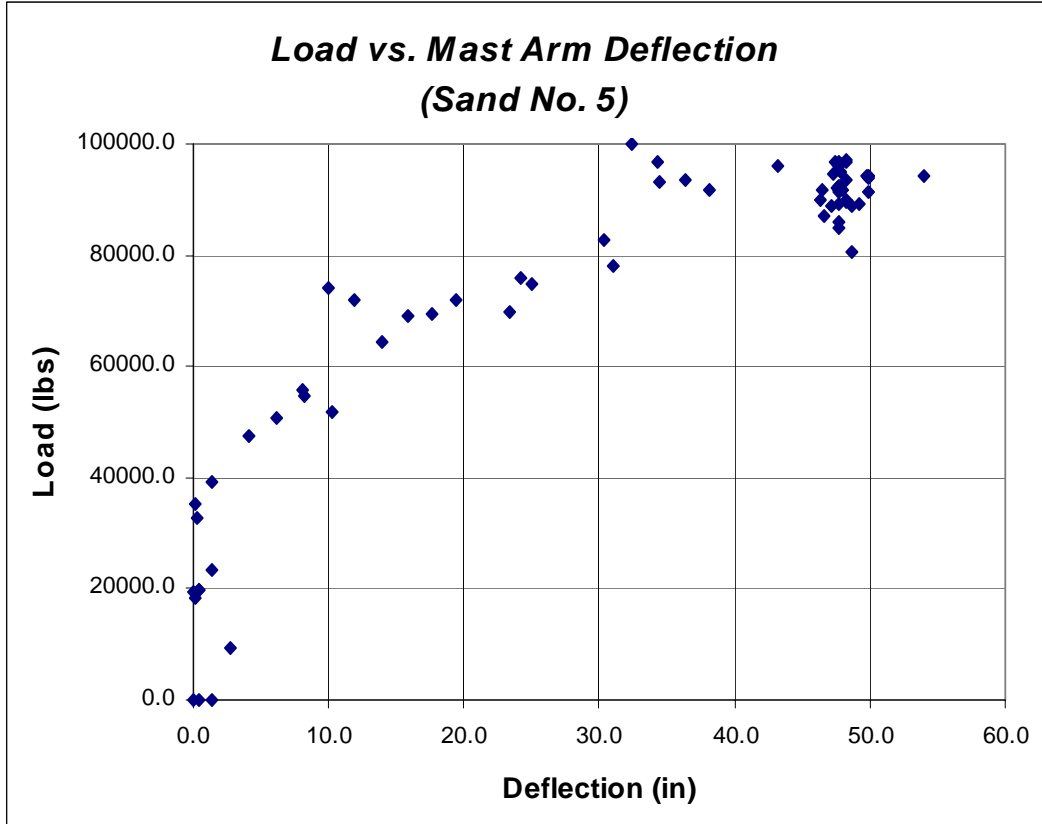


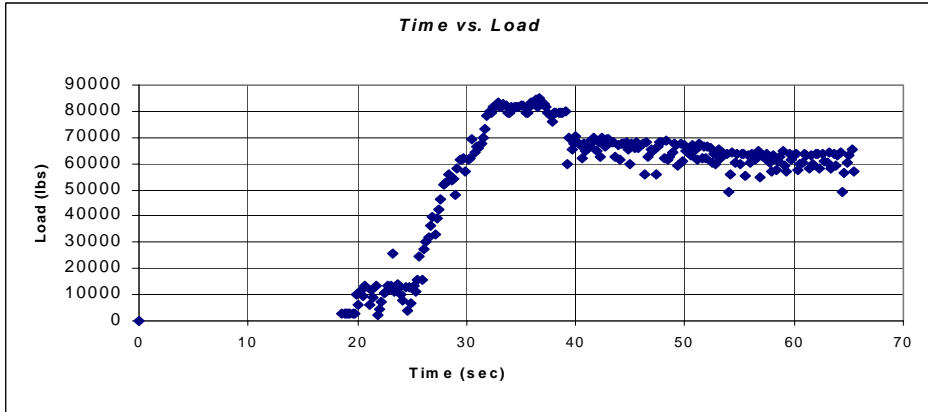
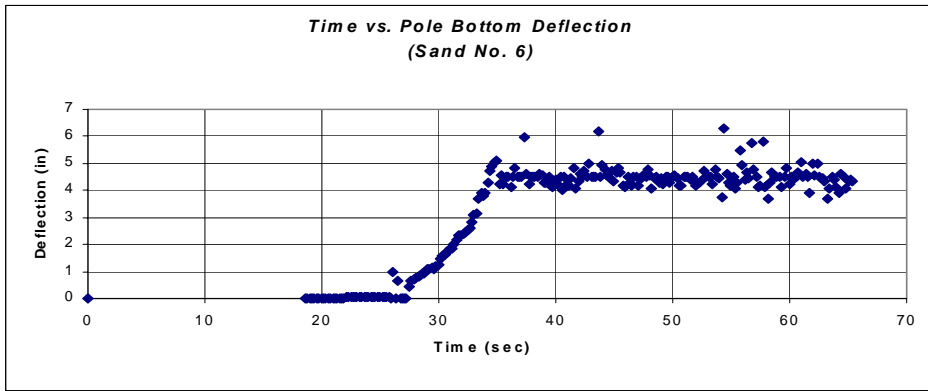
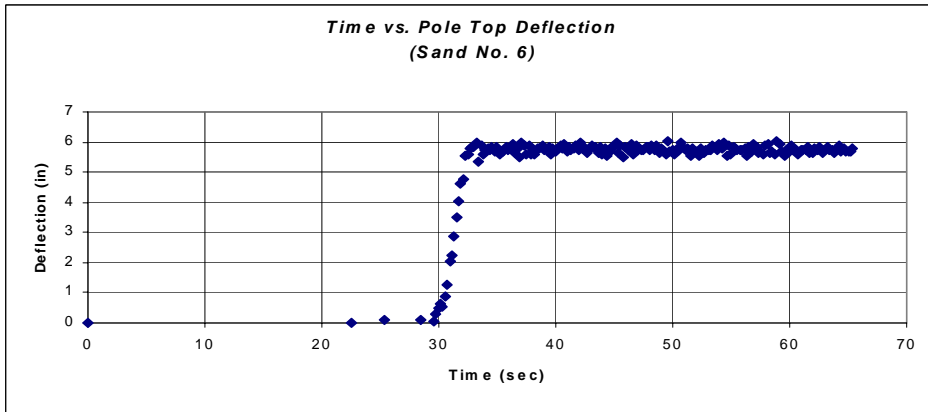
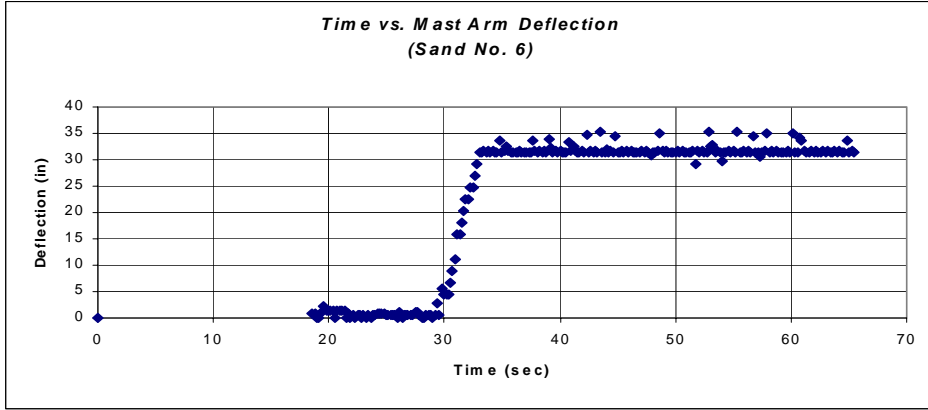


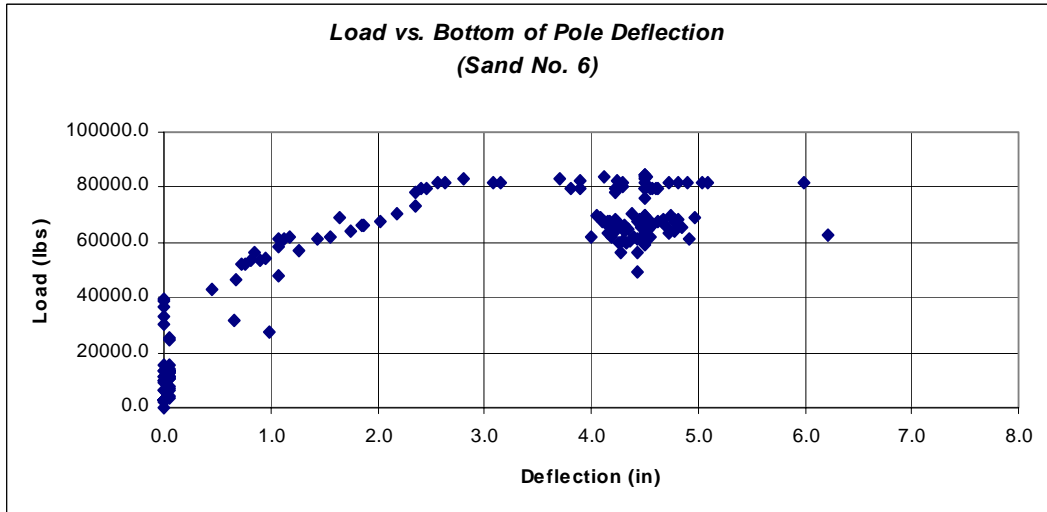
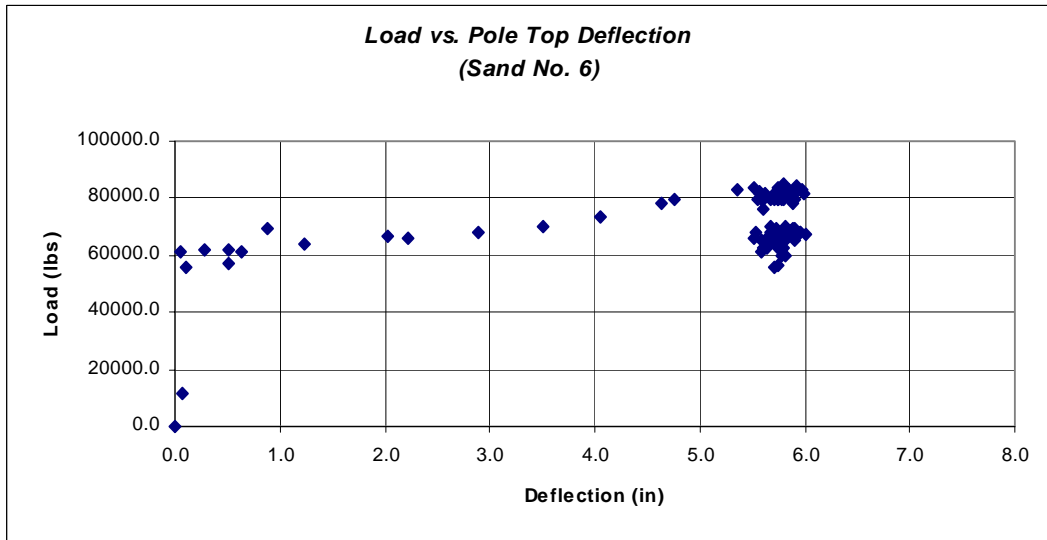
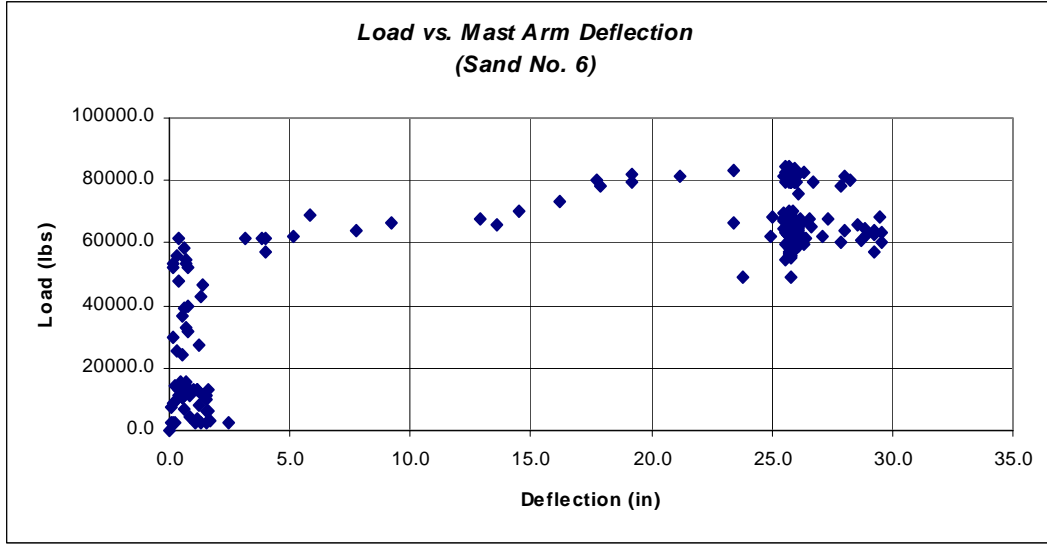


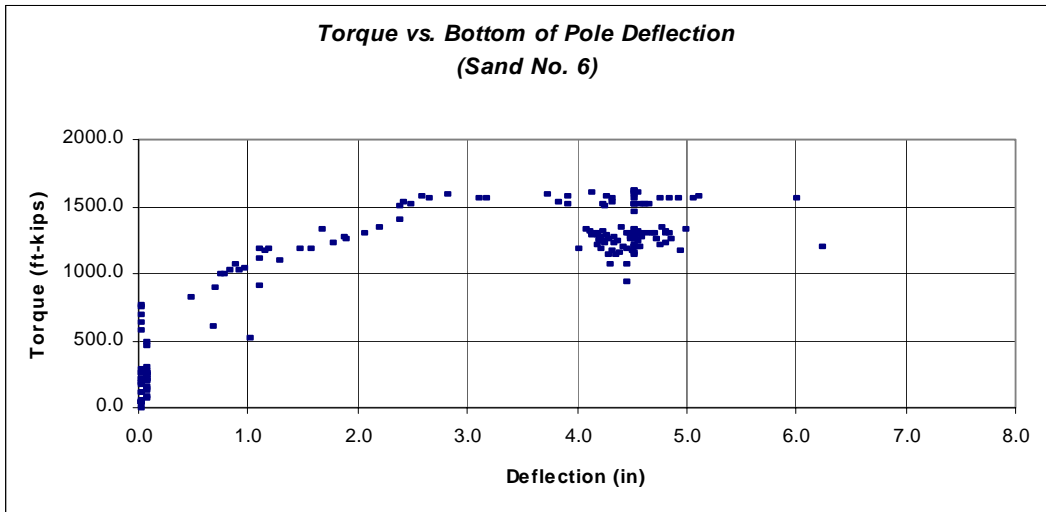
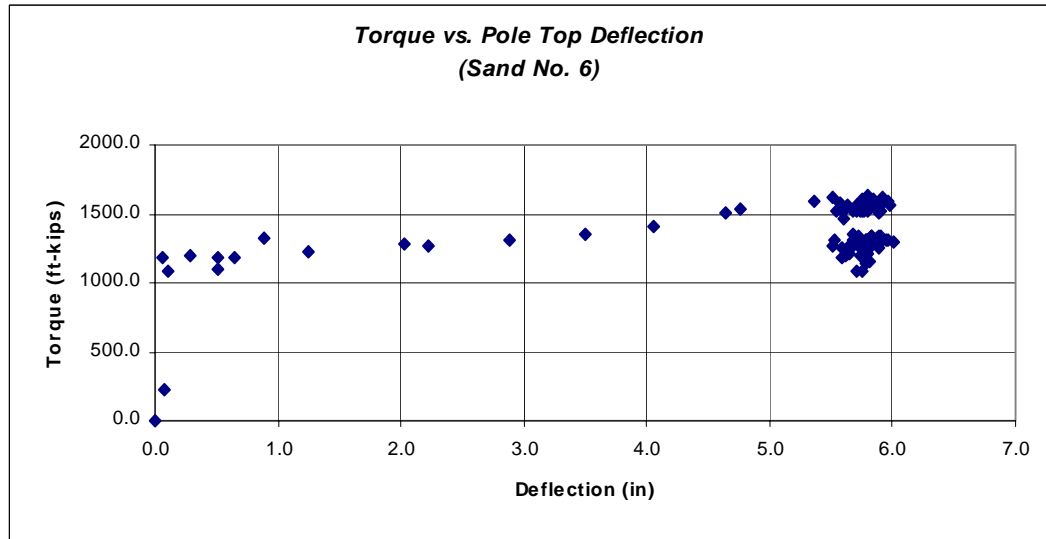
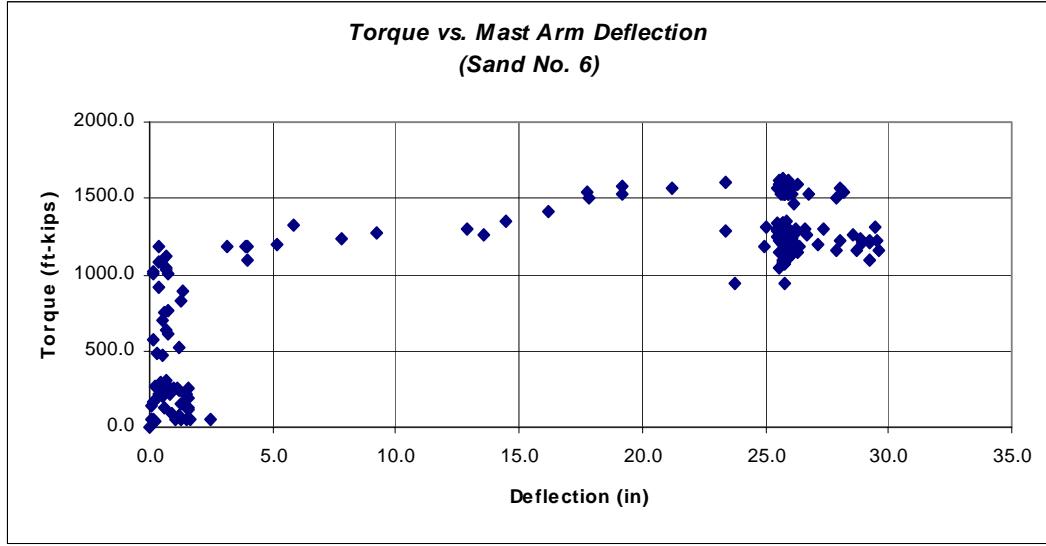


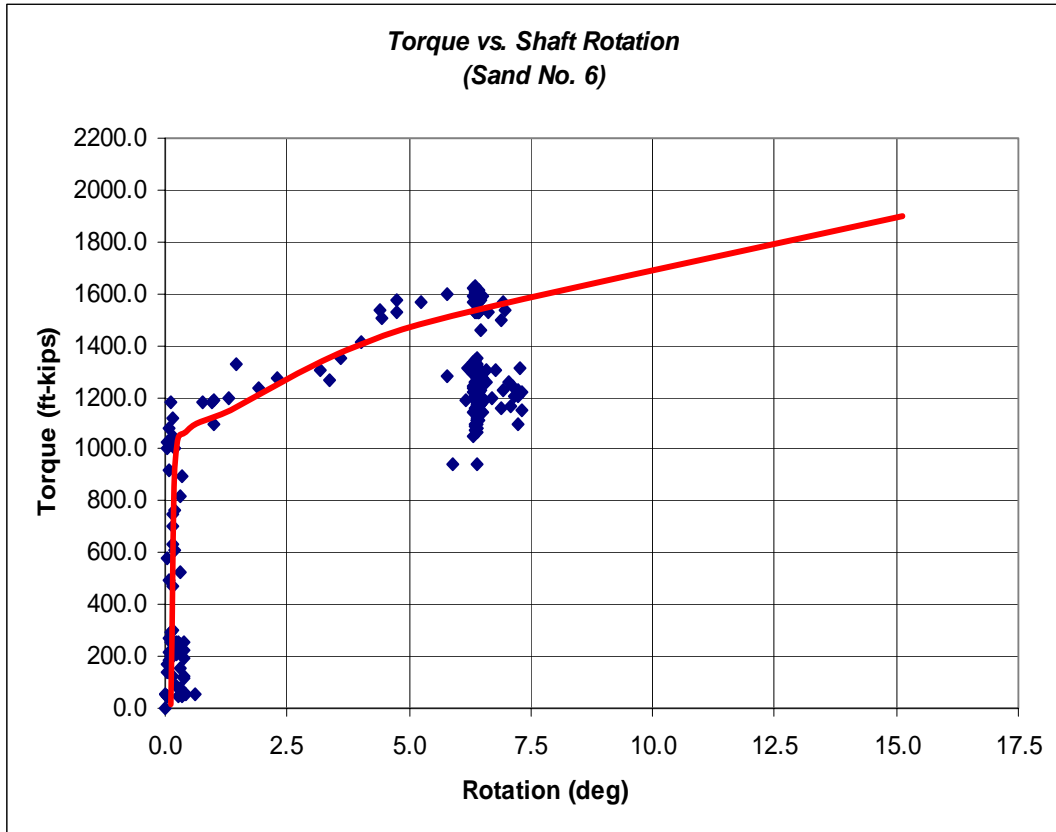


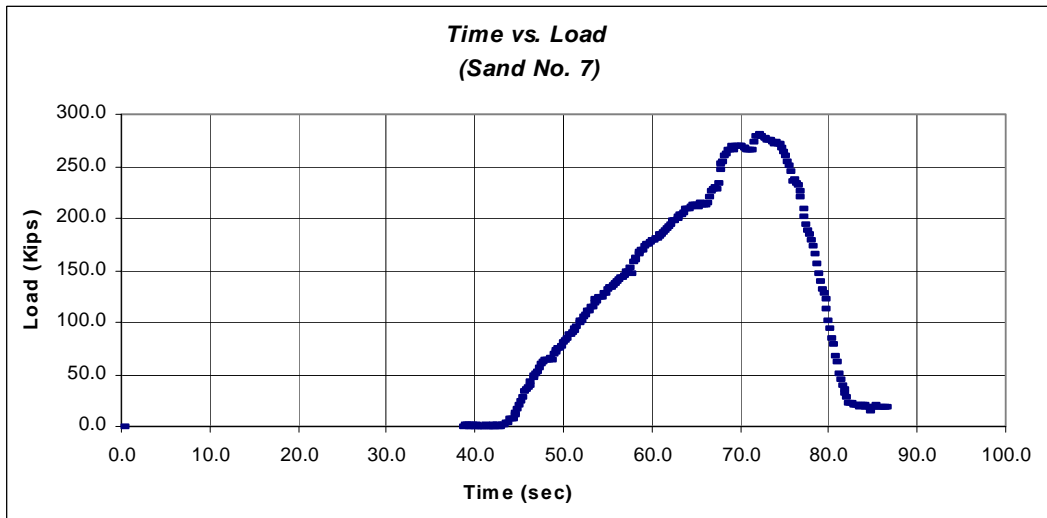
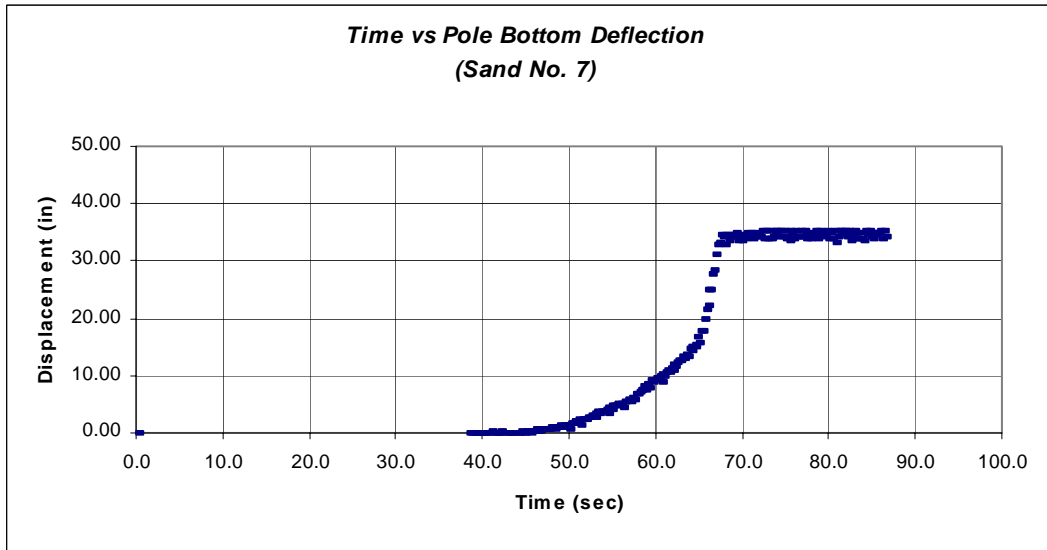
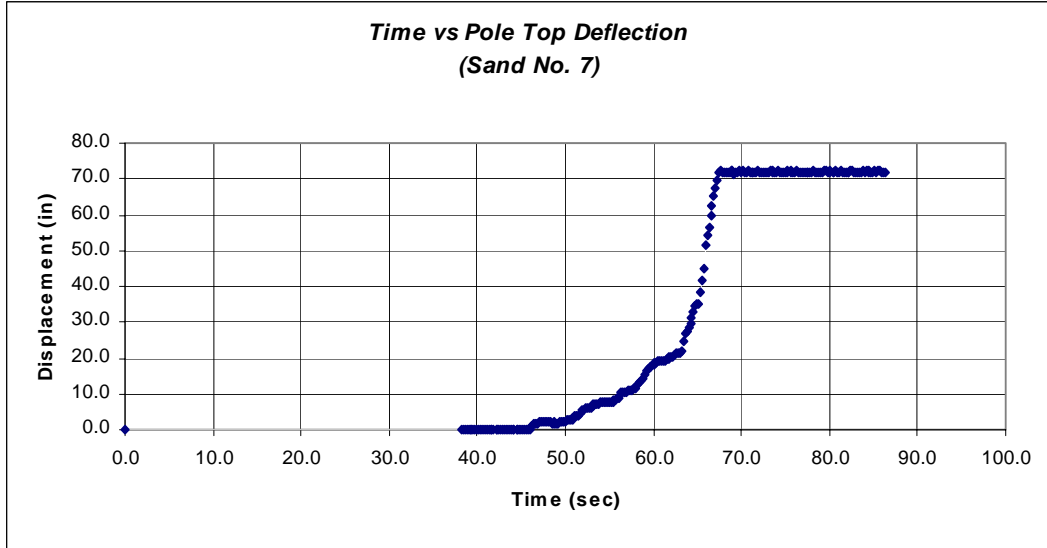


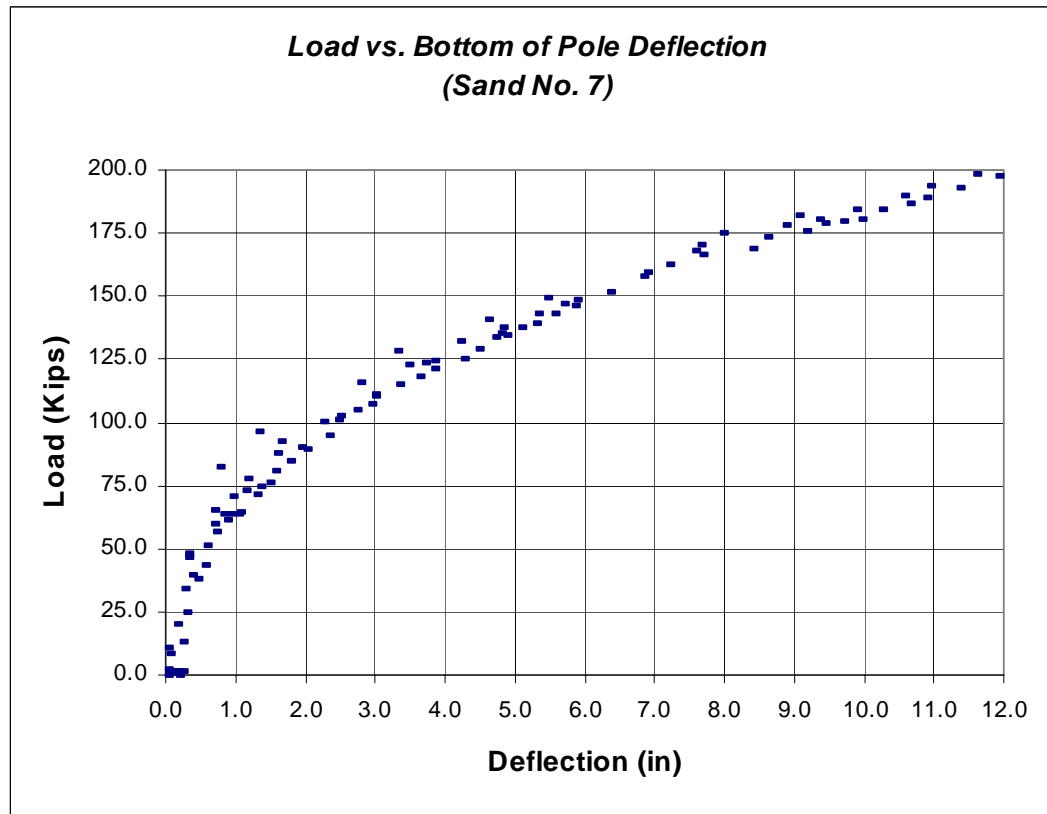
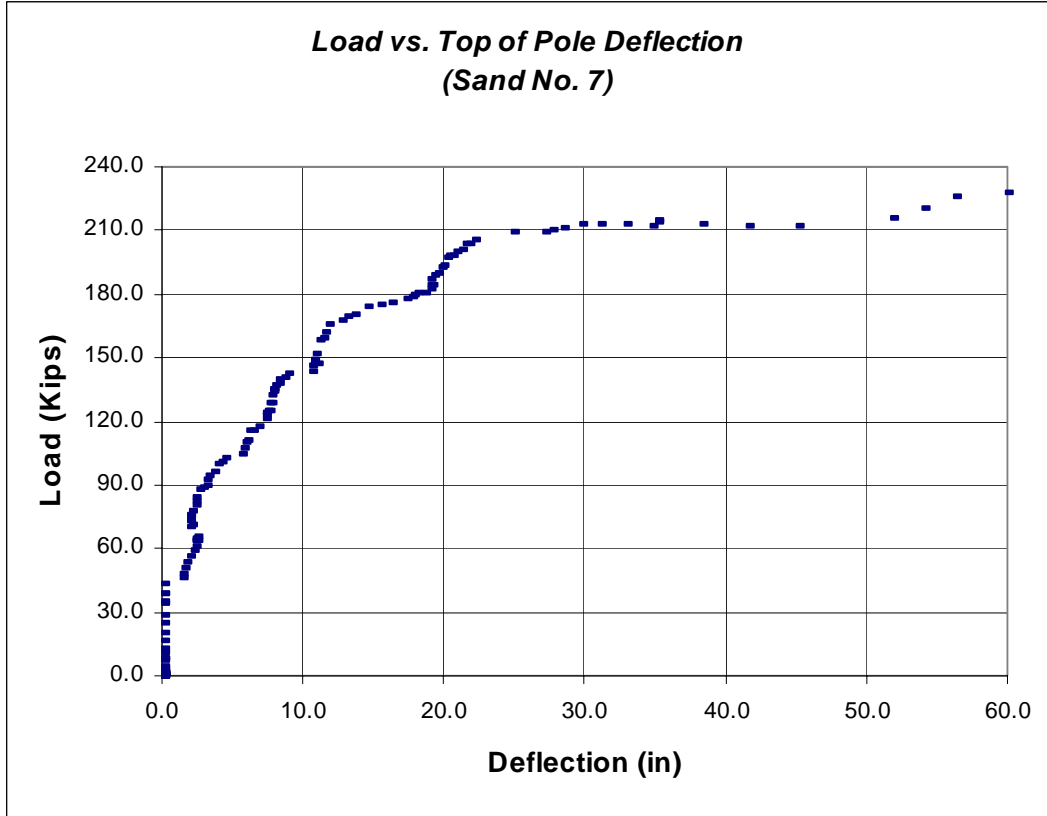


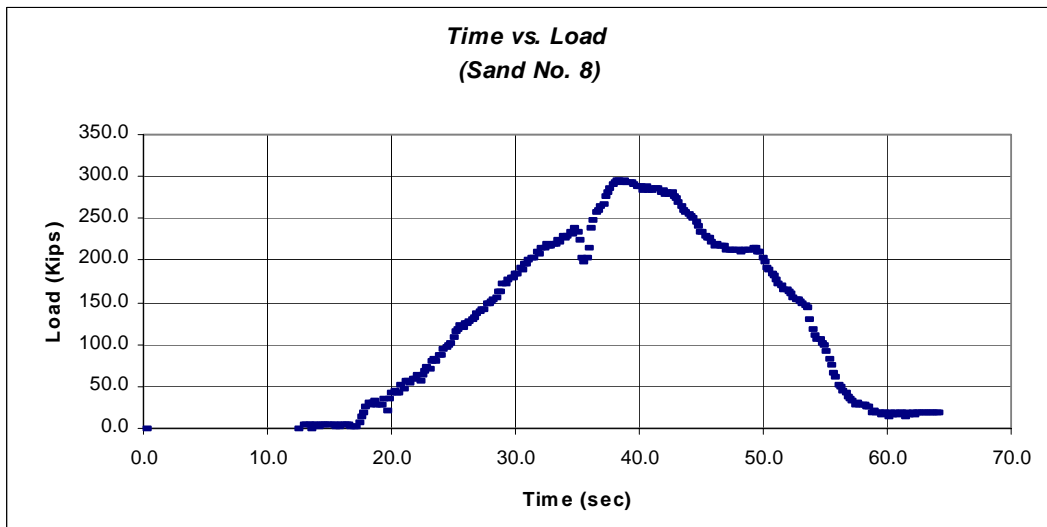
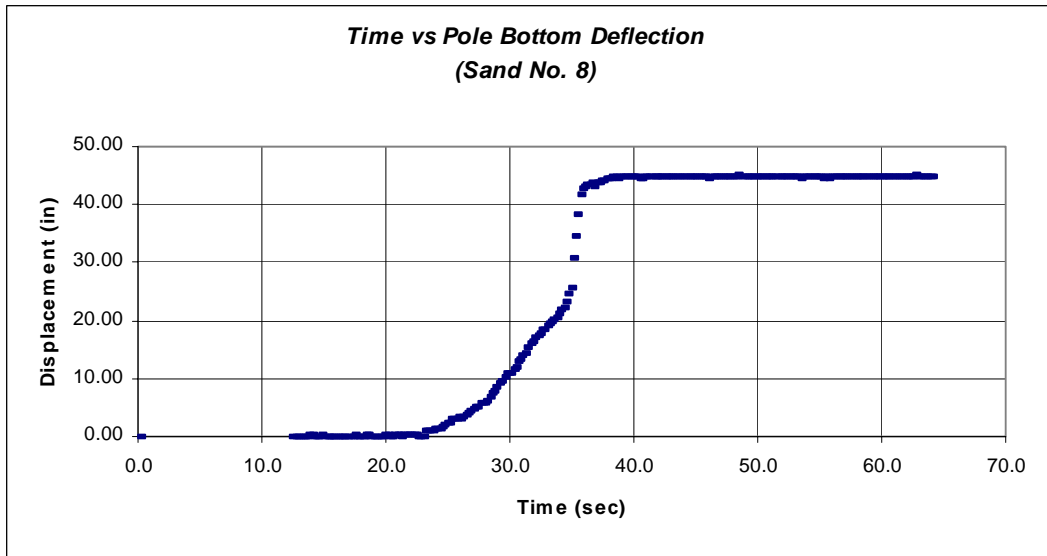
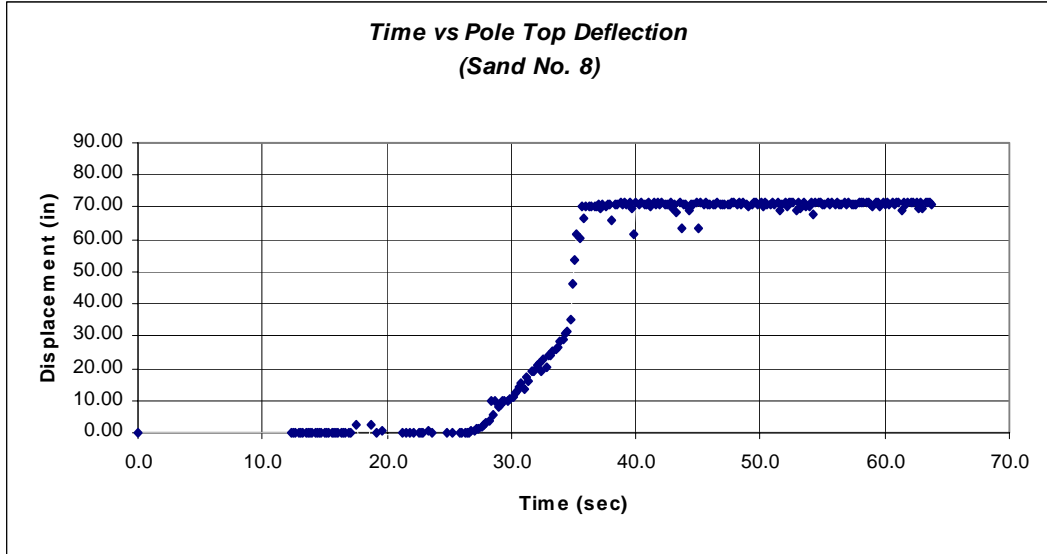




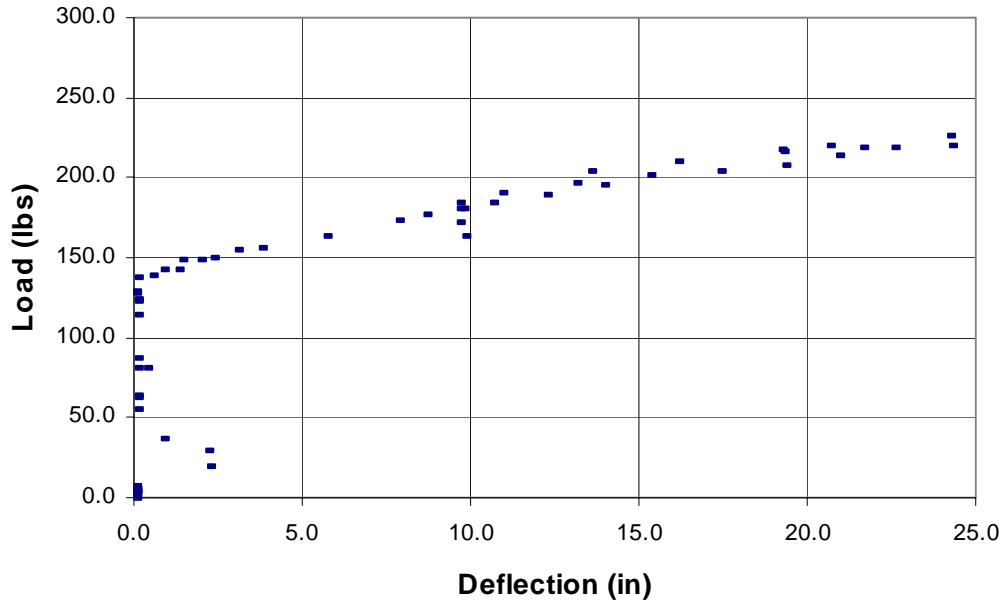




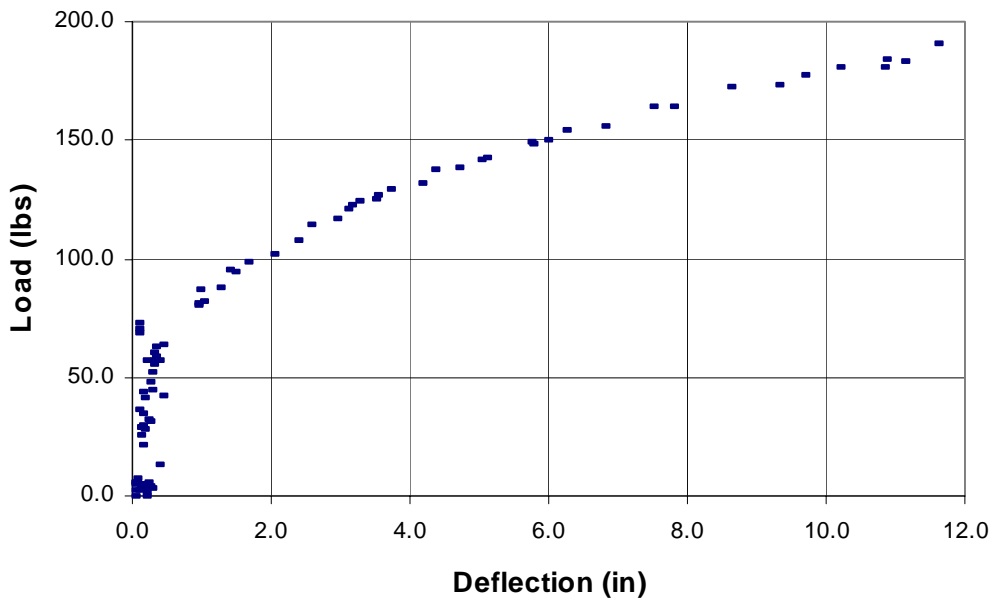


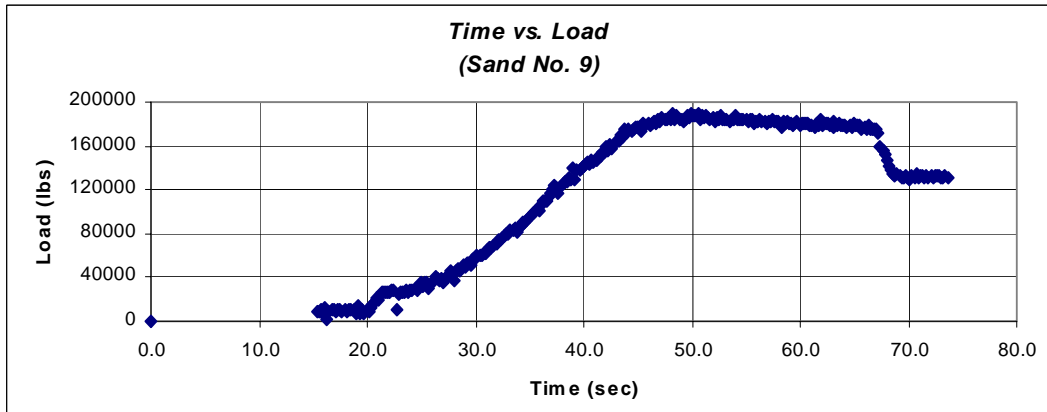
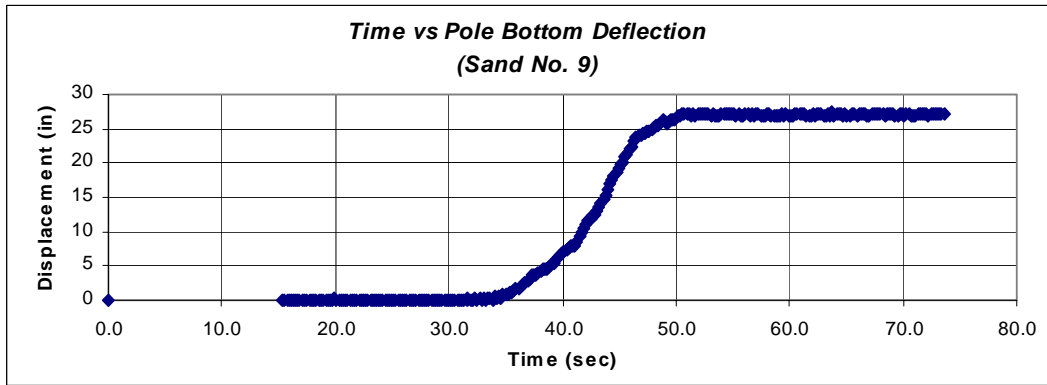
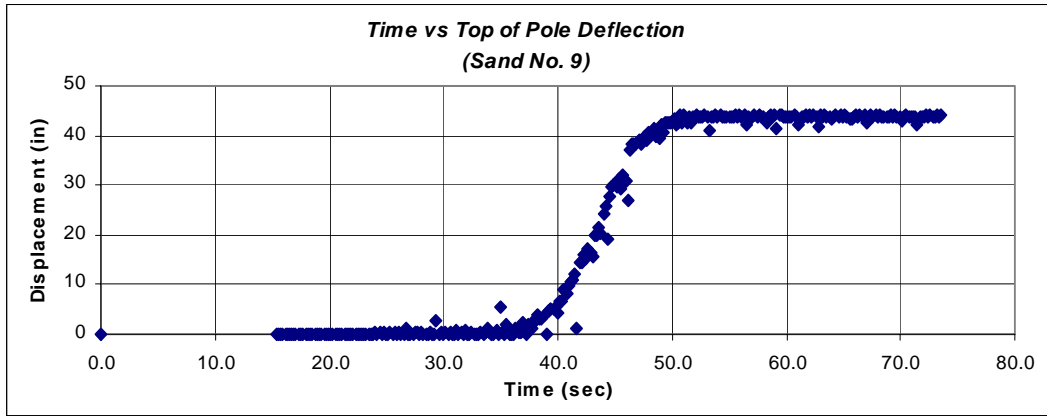
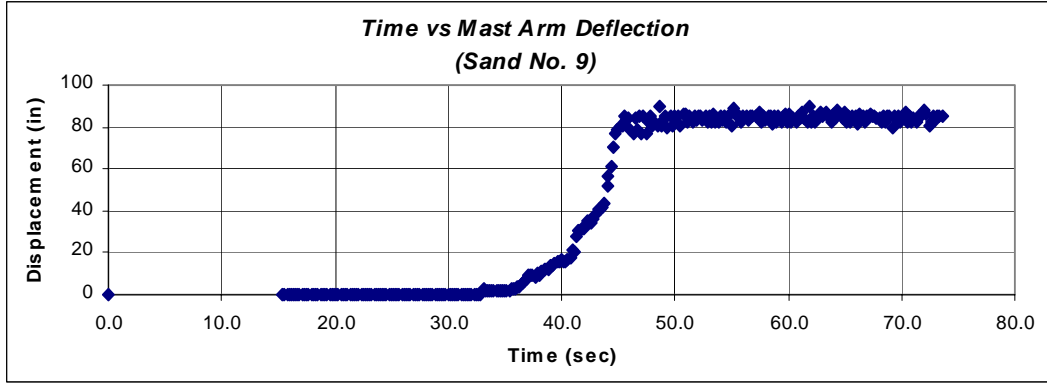


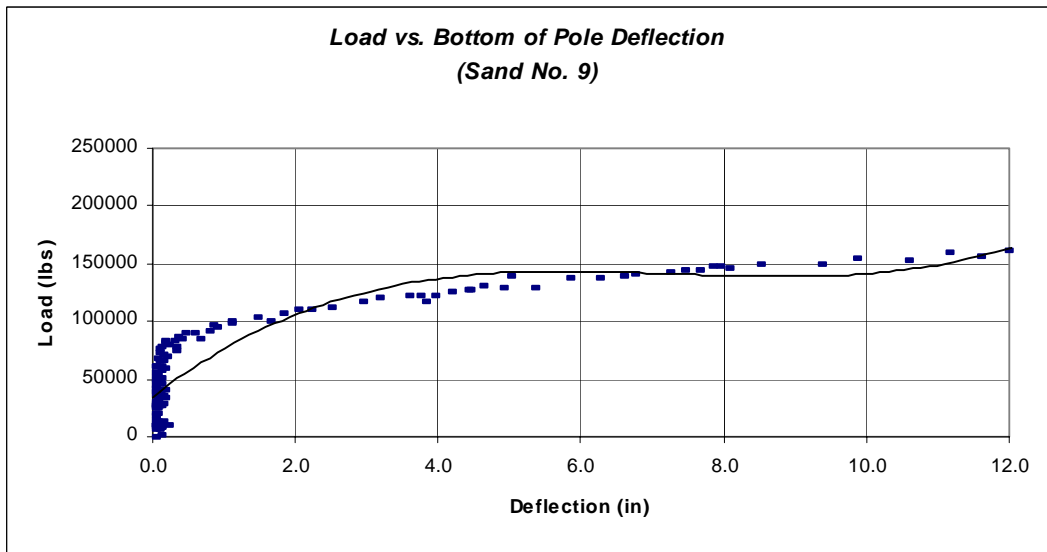
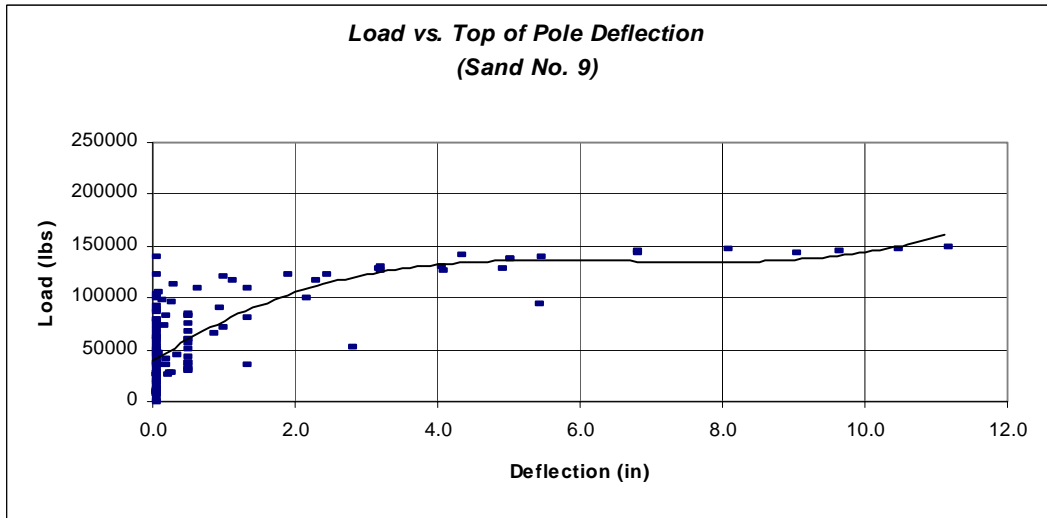
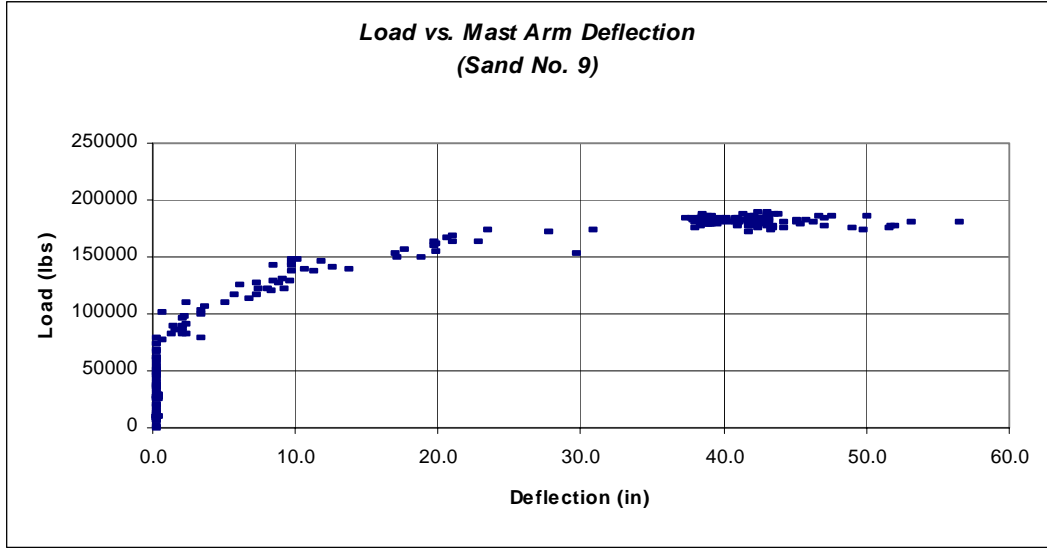
**Load vs. Top of Pole Deflection
(Sand No. 8)**

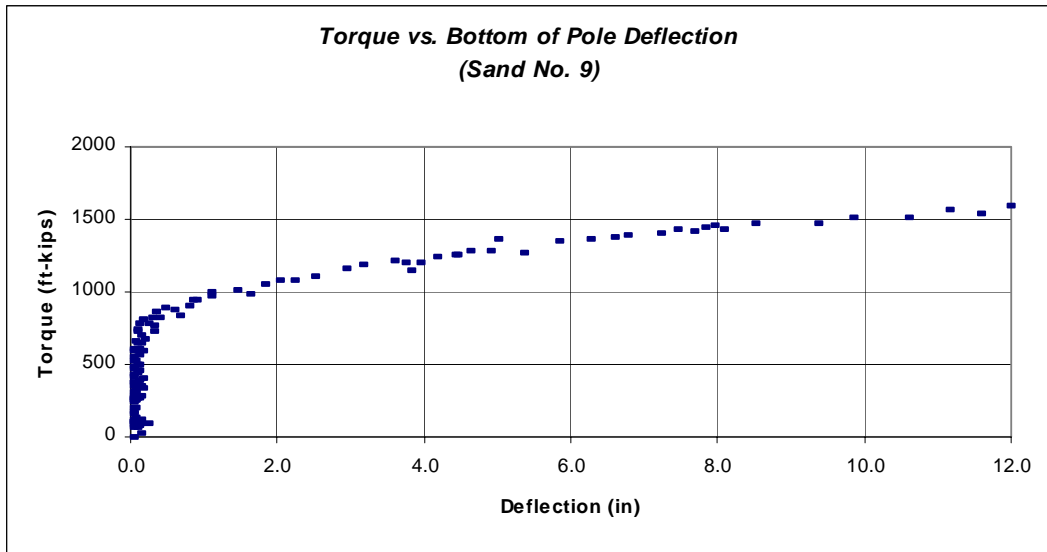
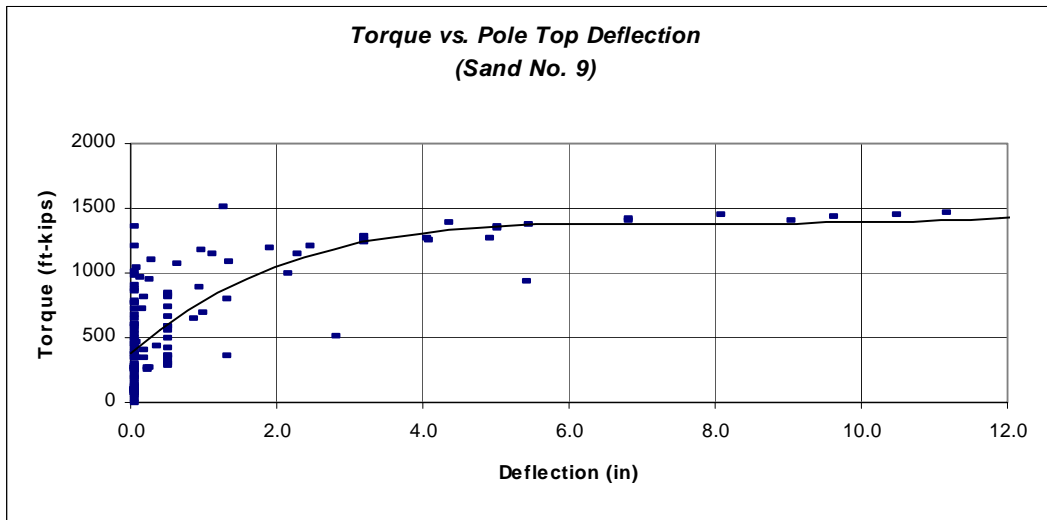
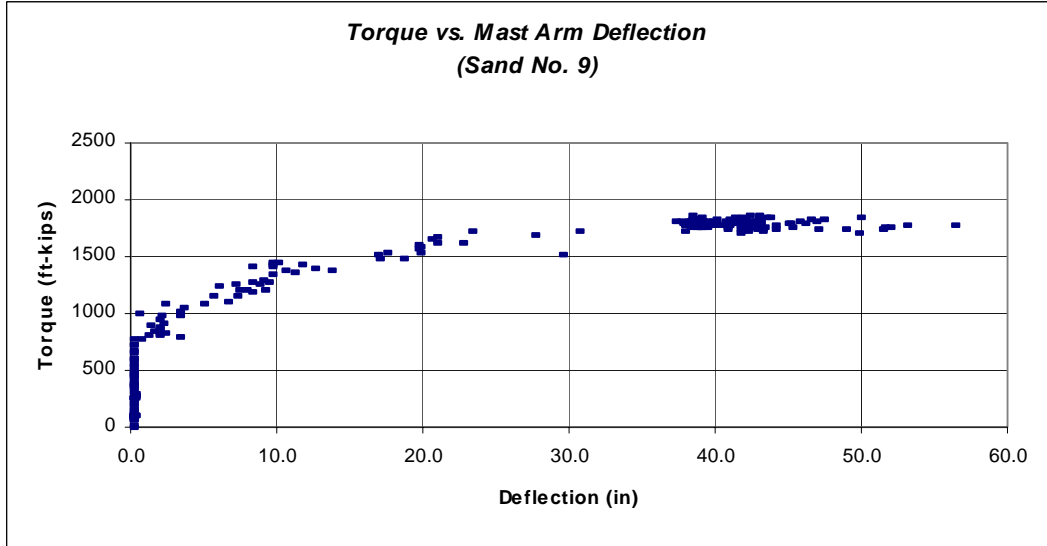


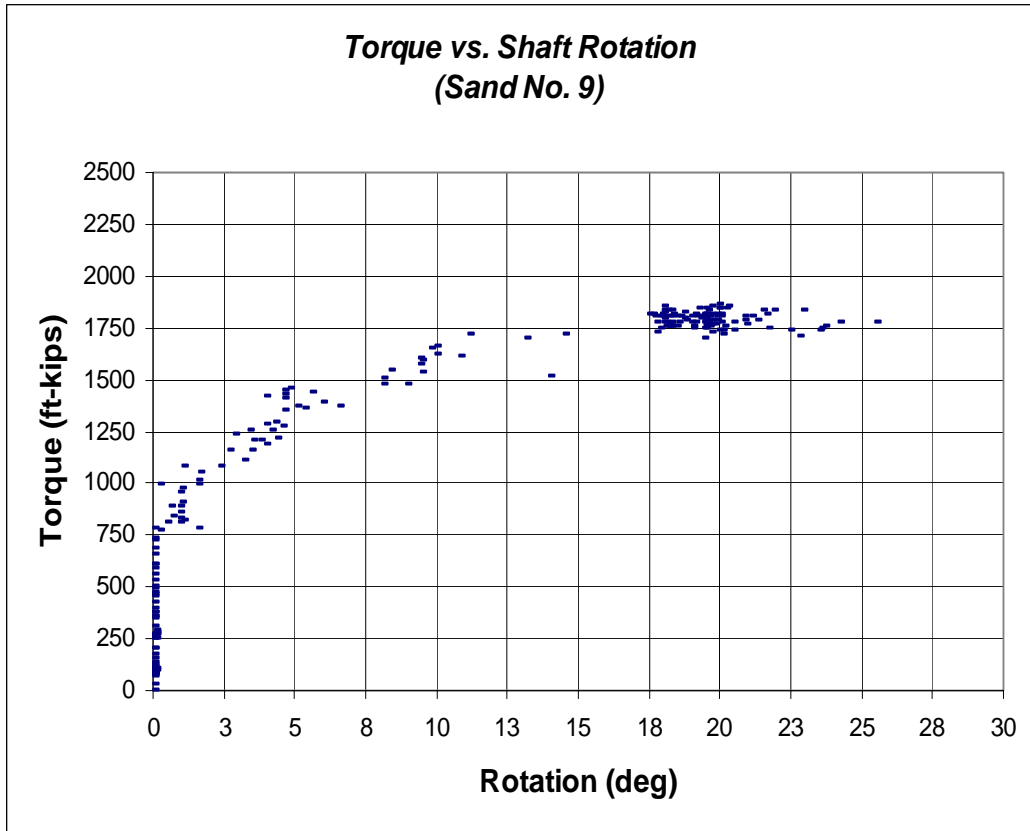
**Load vs. Bottom of Pole Deflection
(Sand No. 8)**

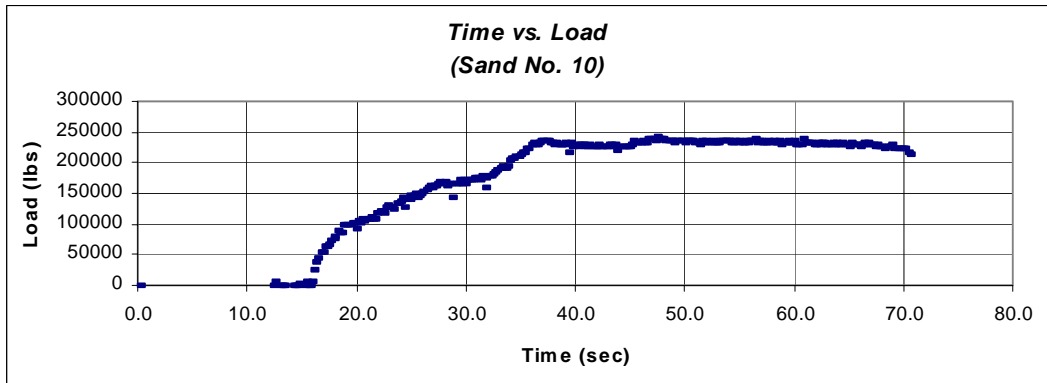
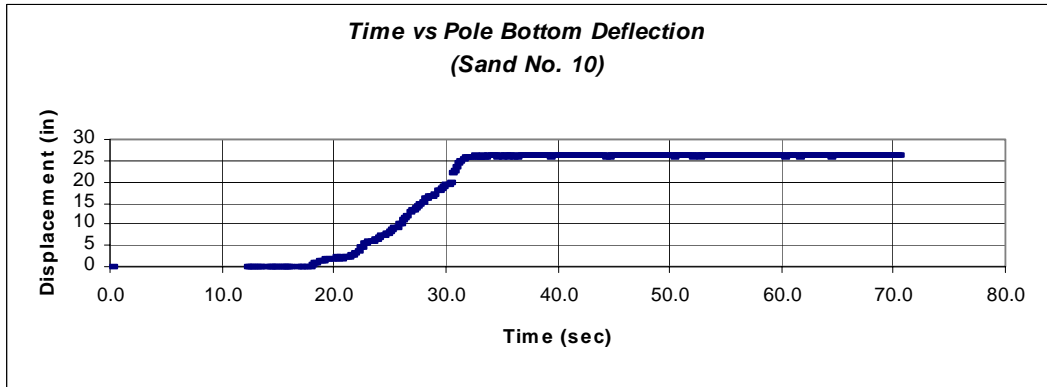
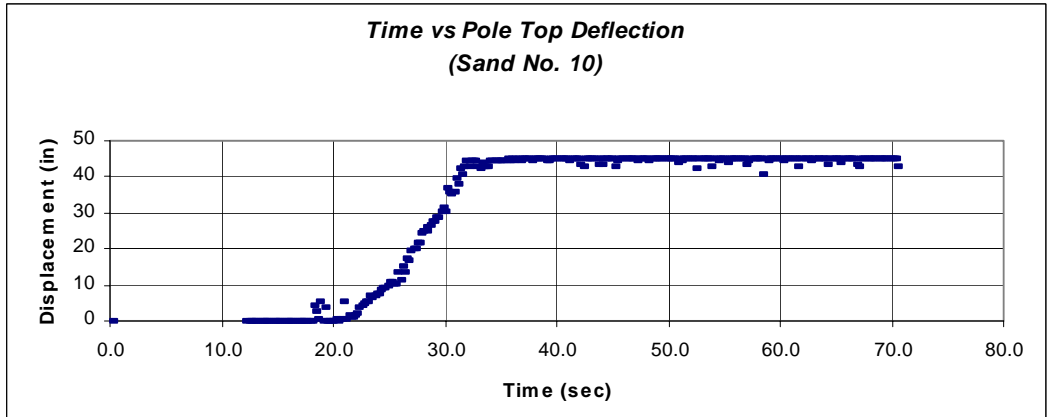
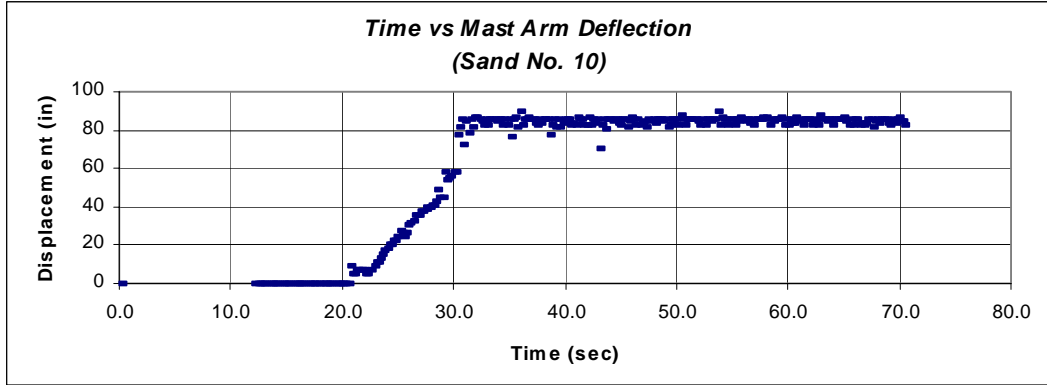


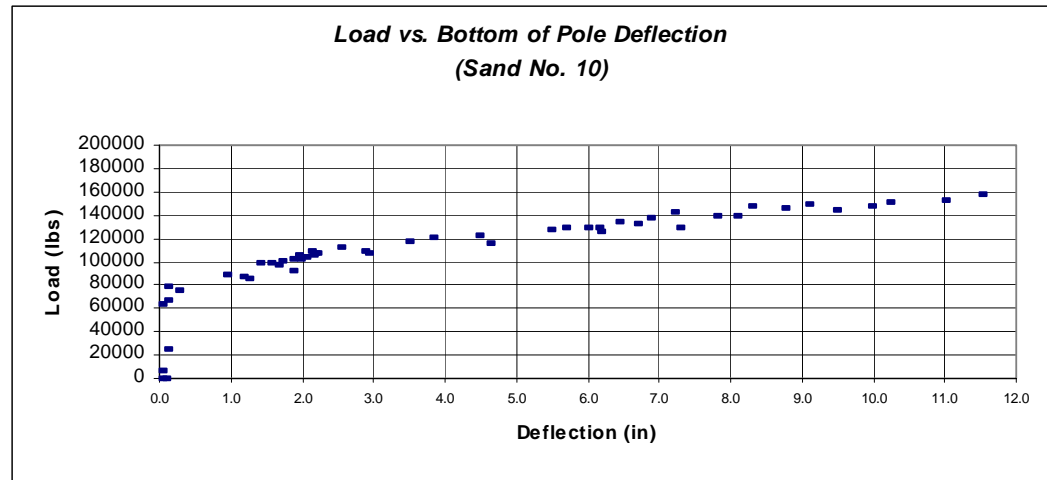
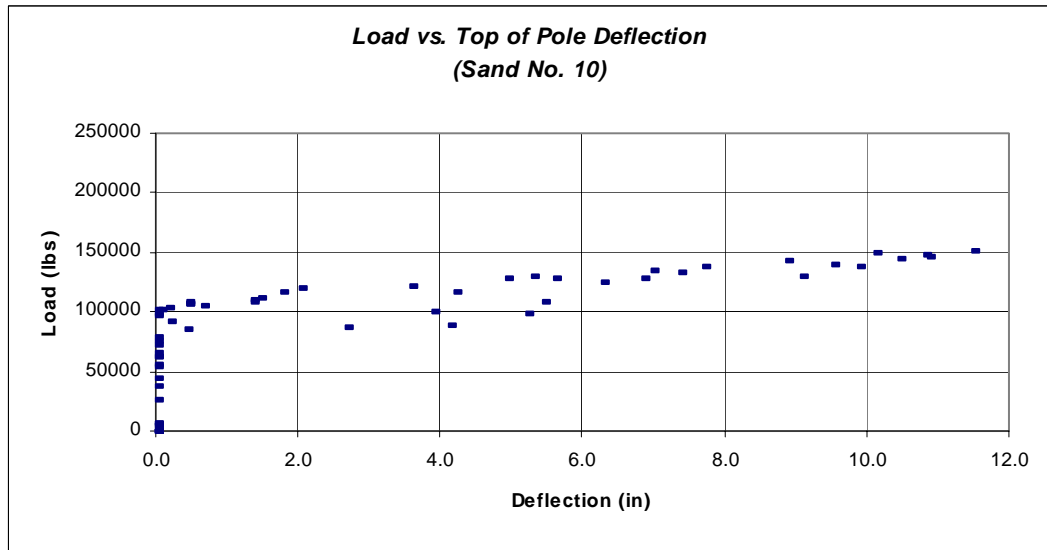
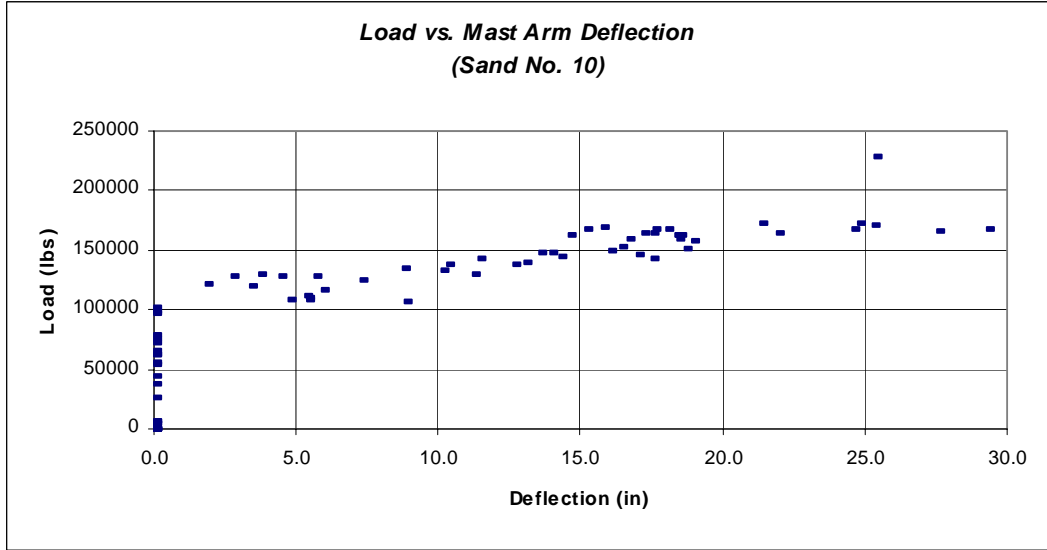


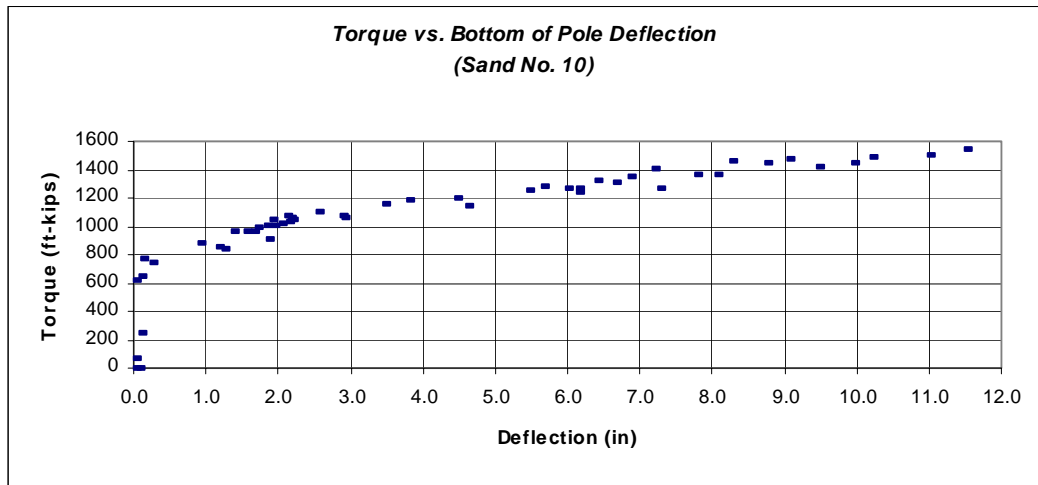
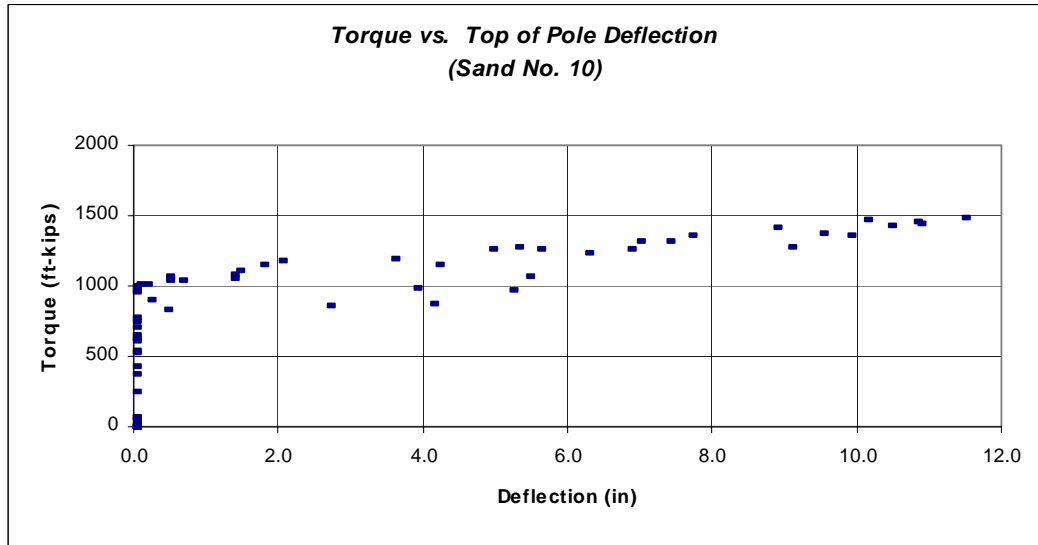
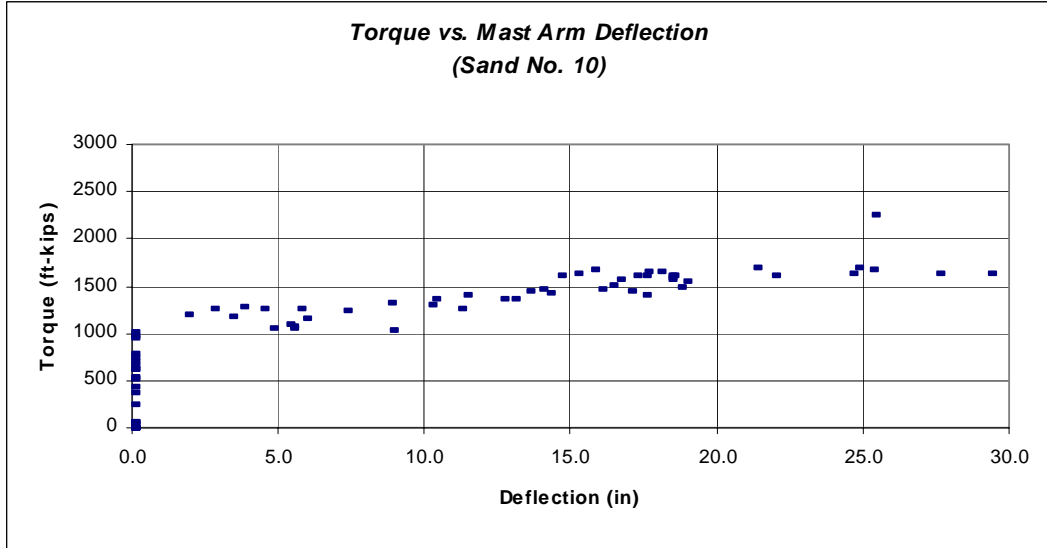


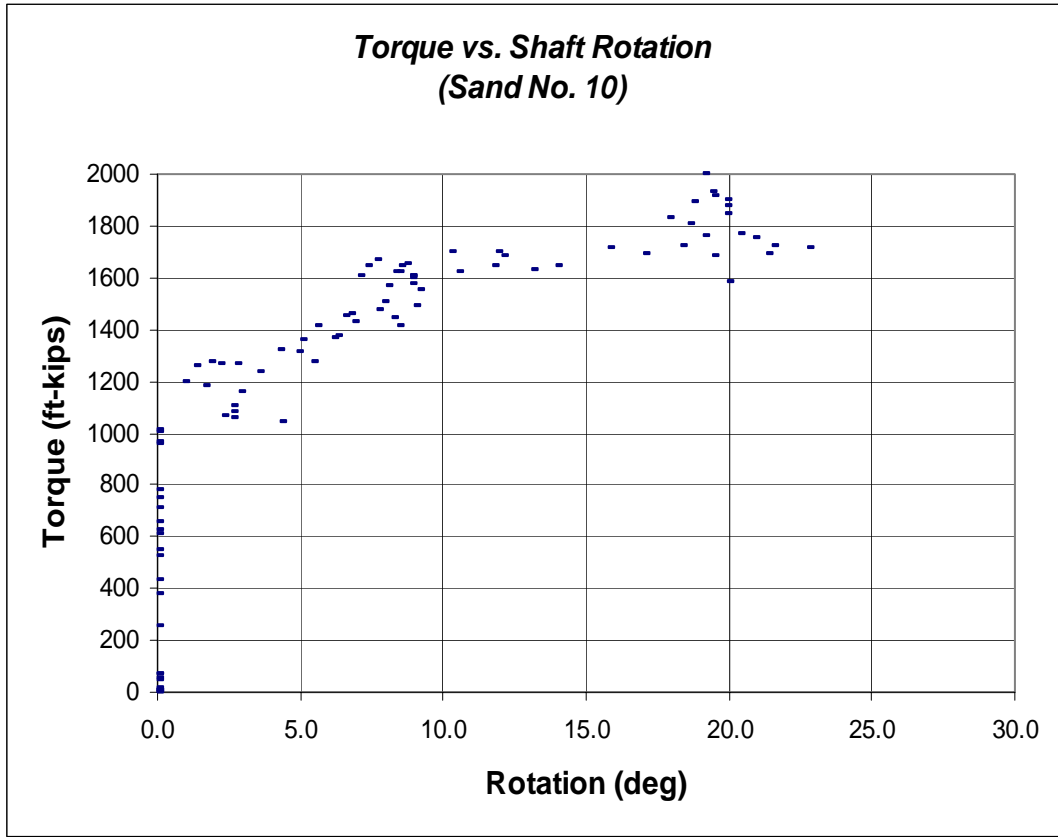


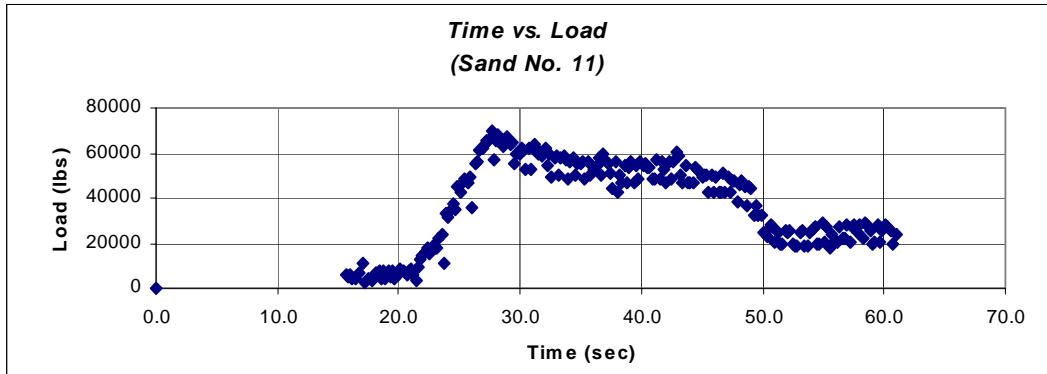
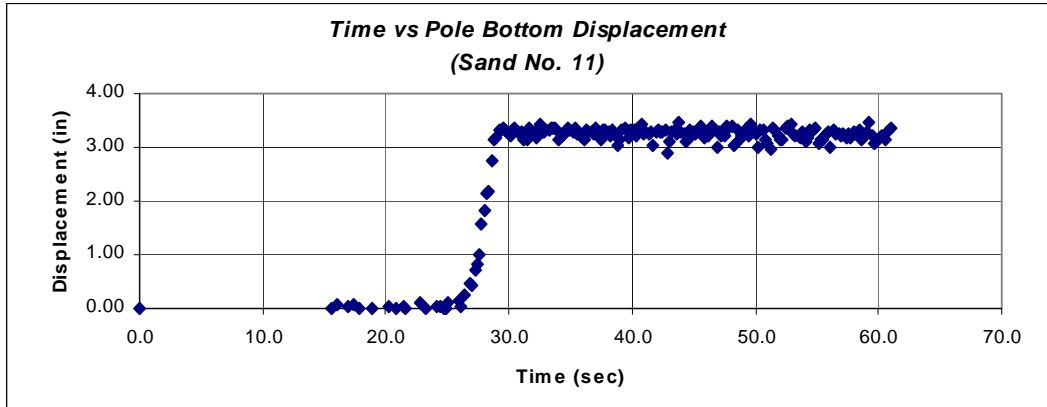
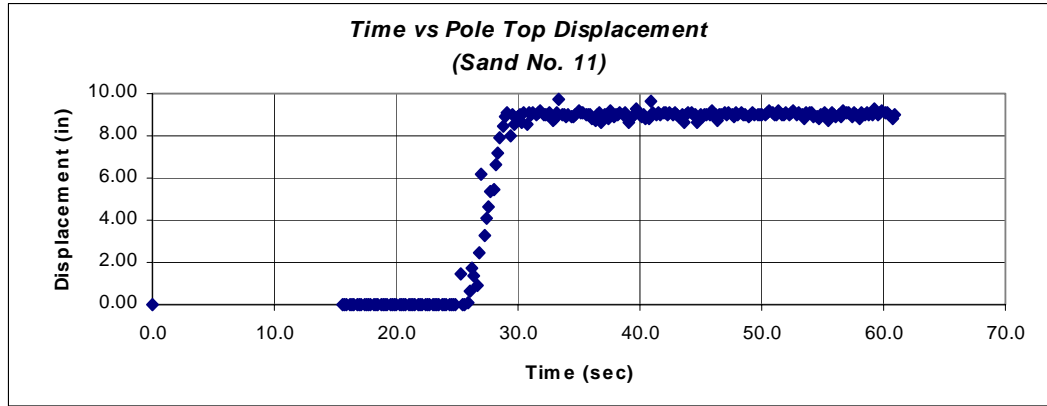
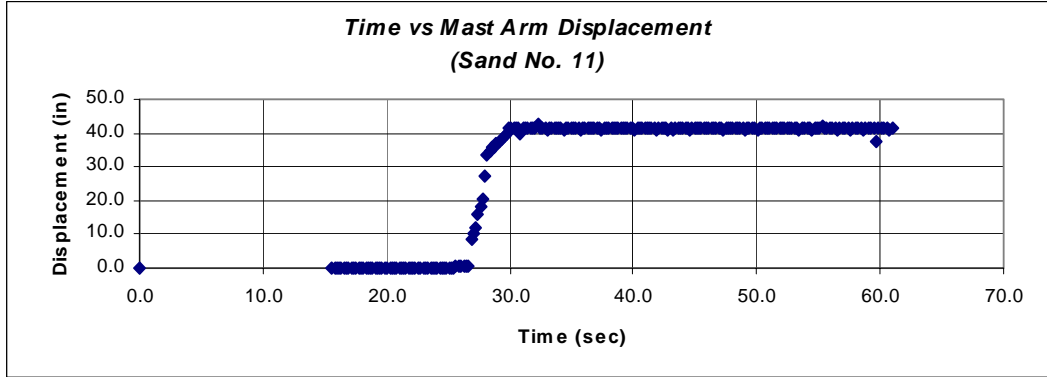


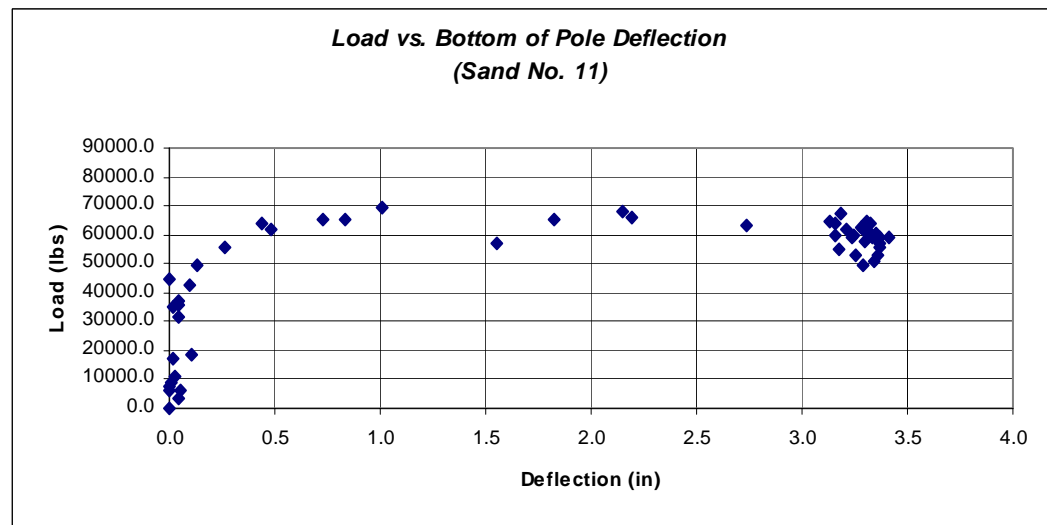
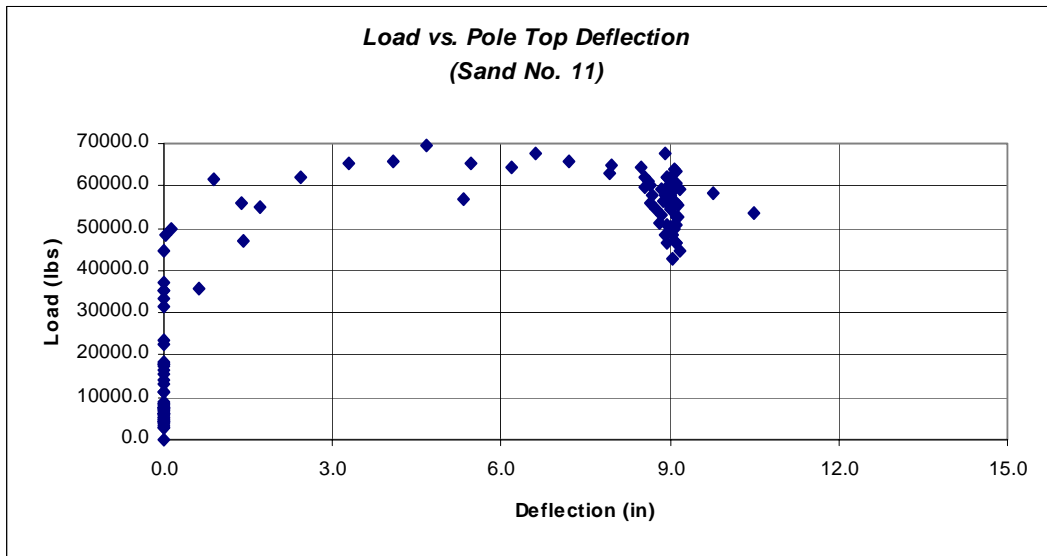
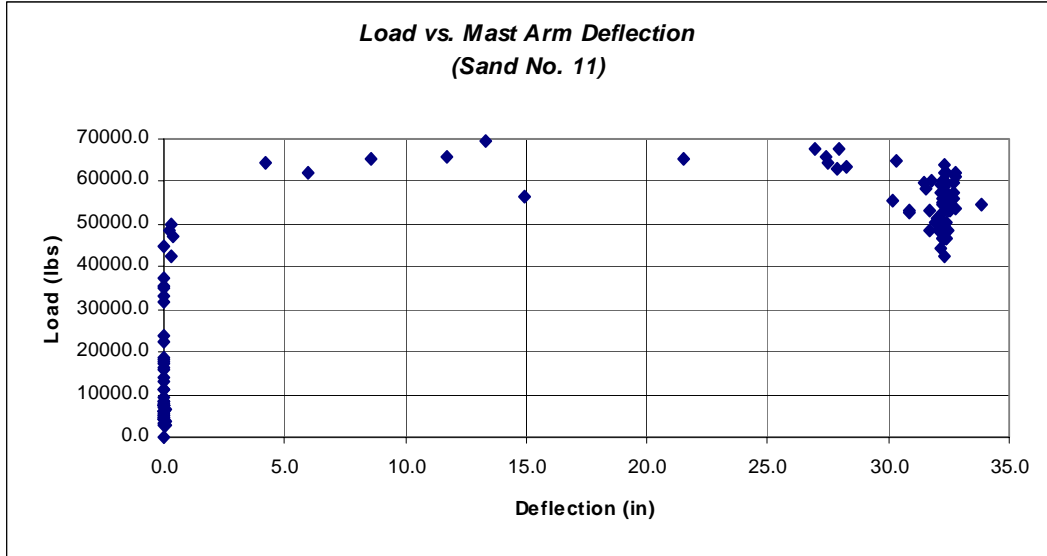


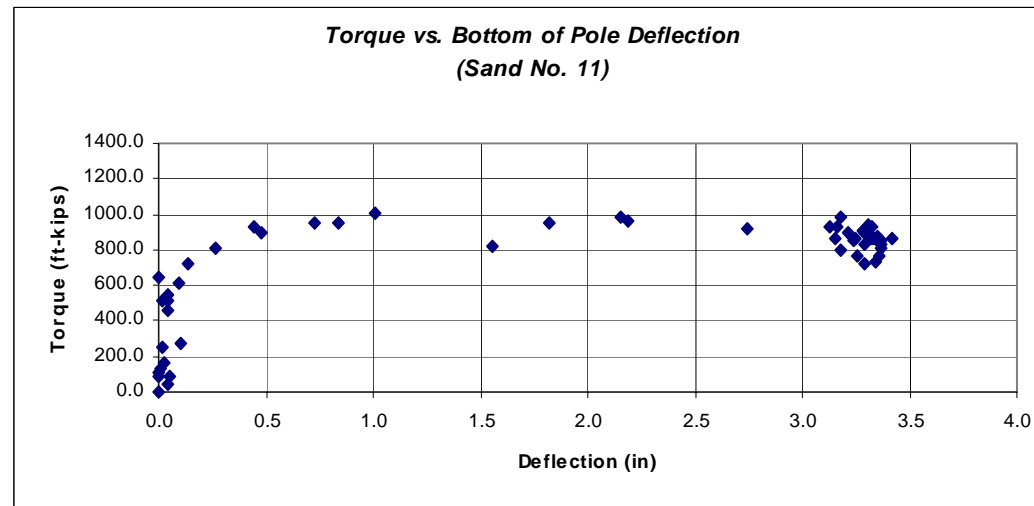
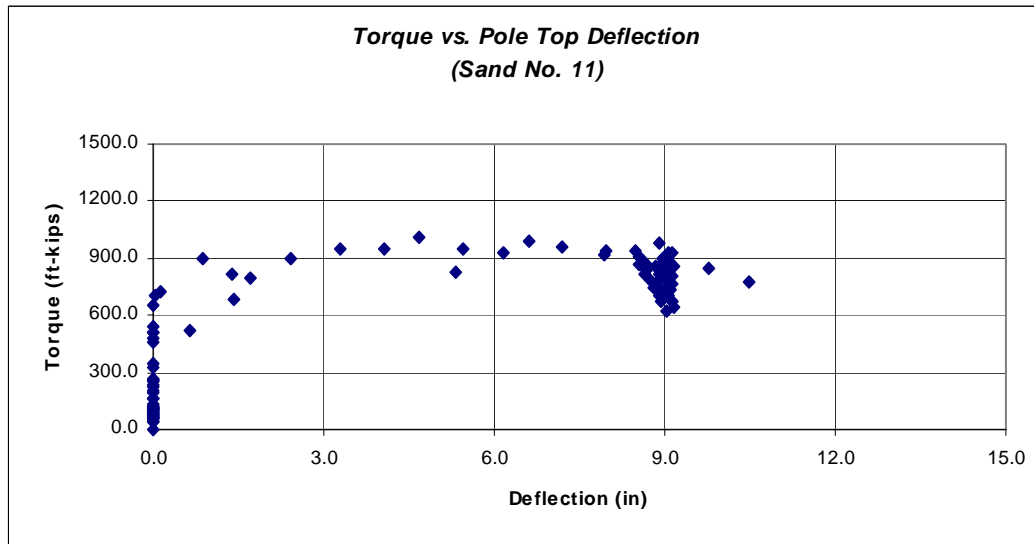
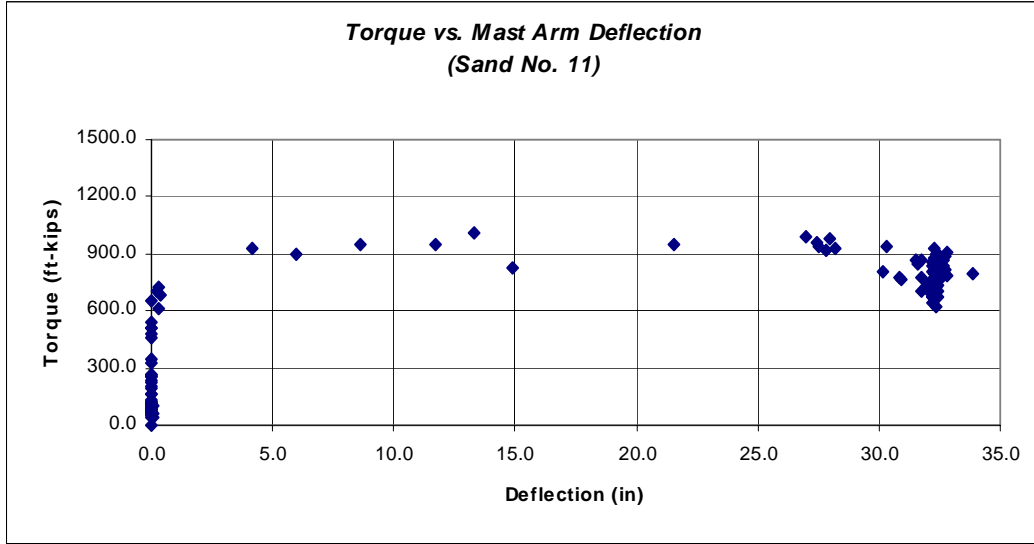


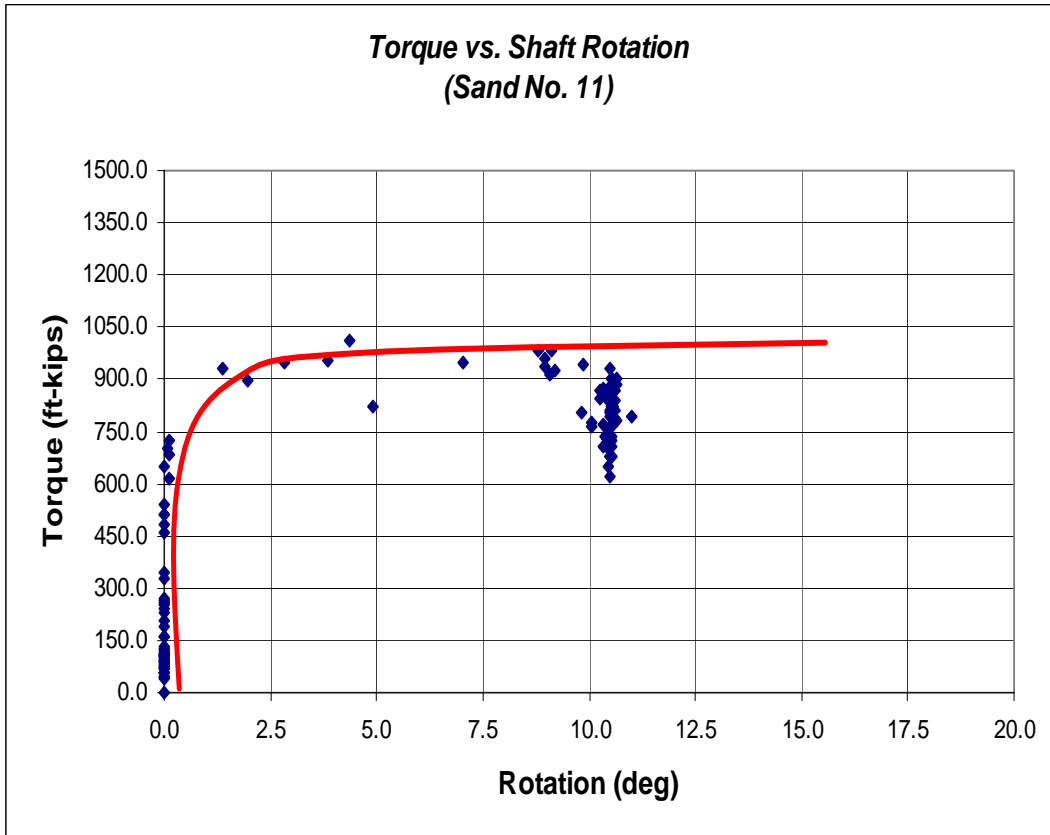


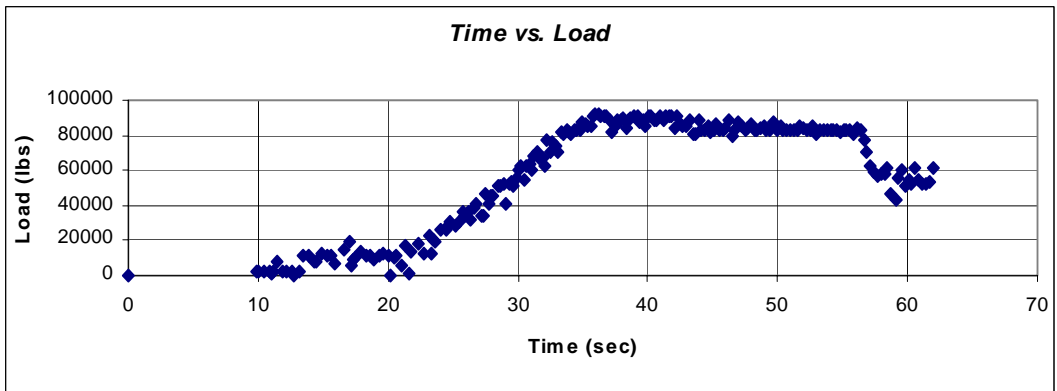
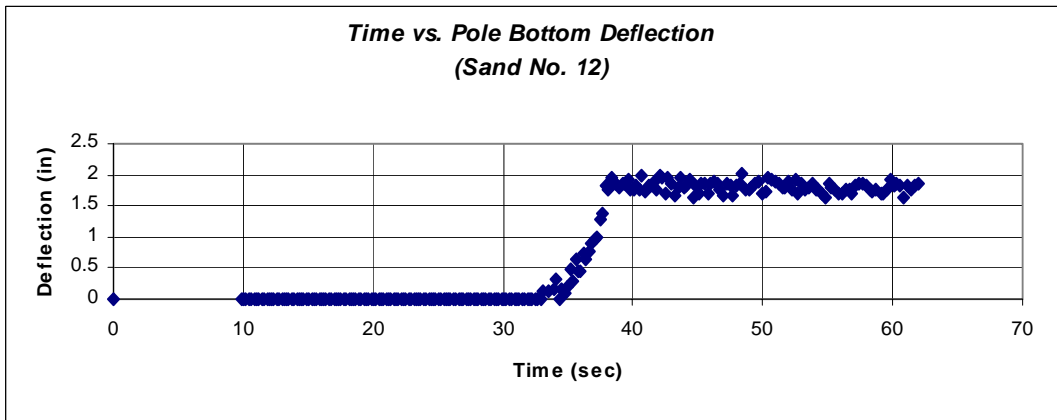
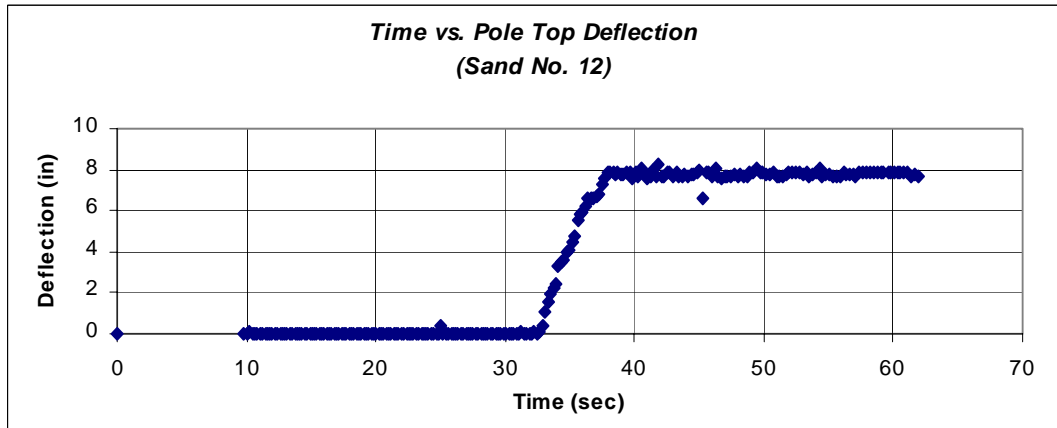
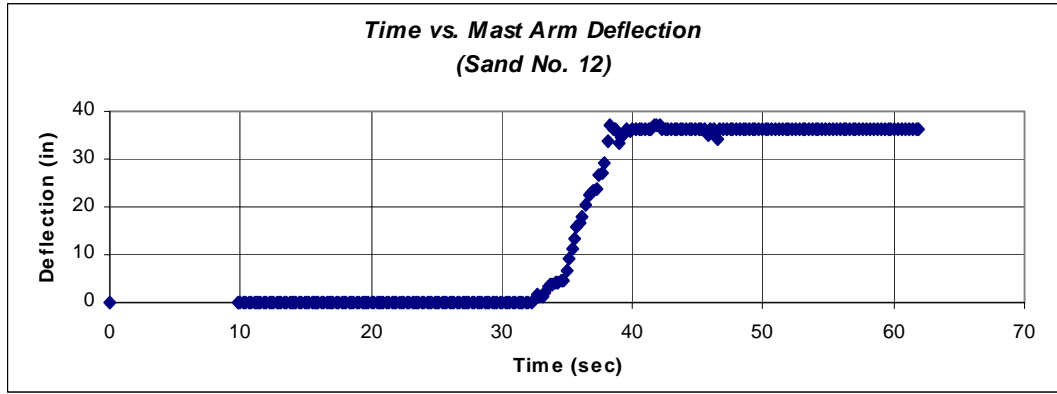


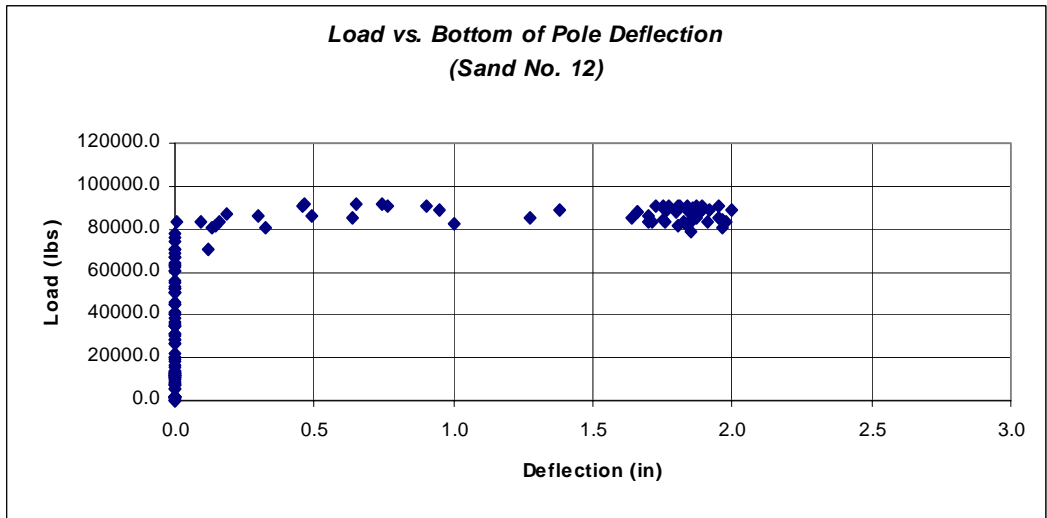
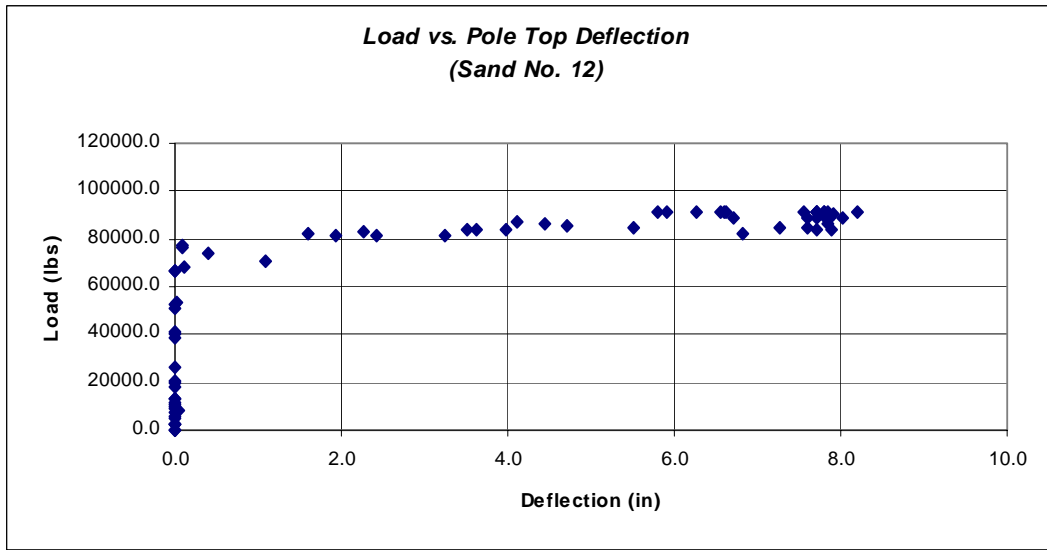
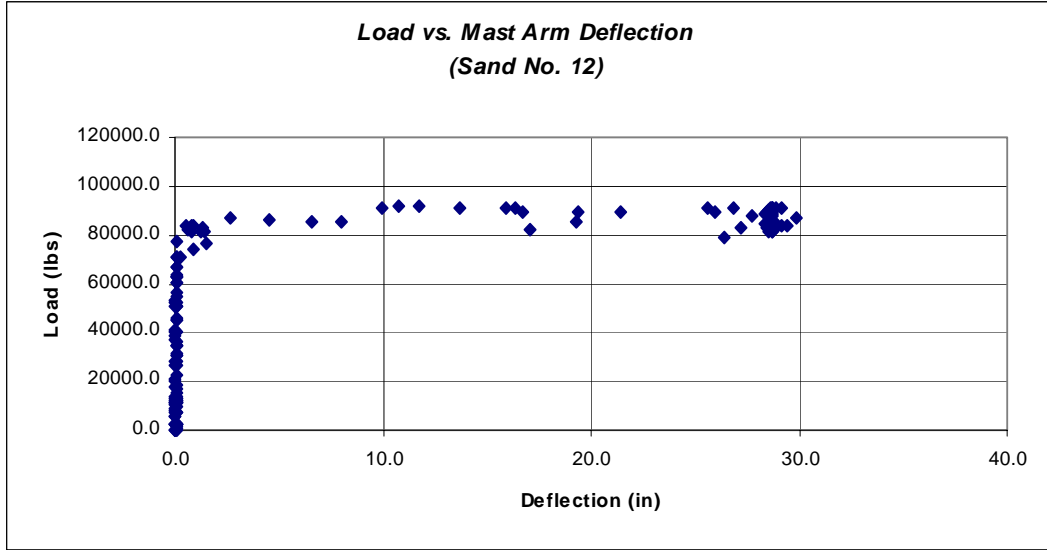


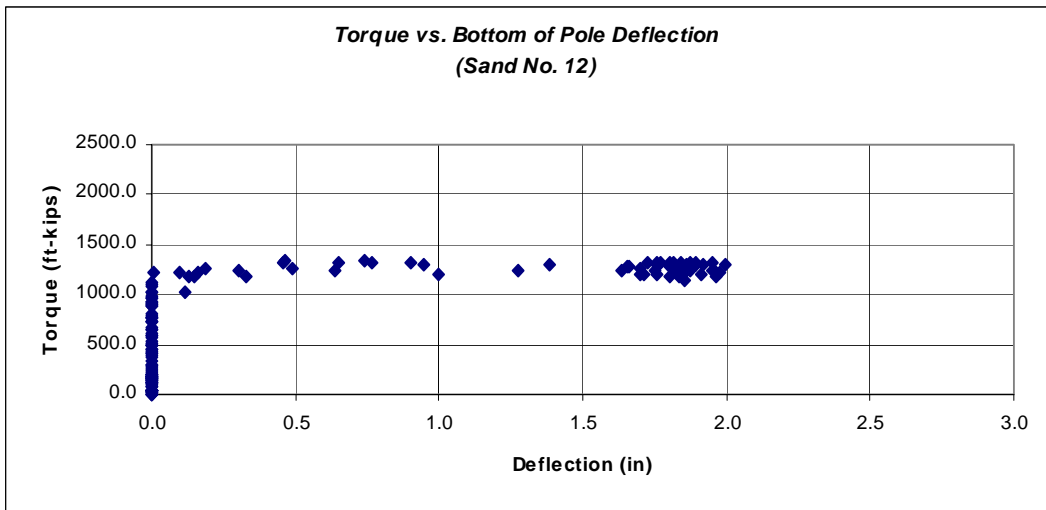
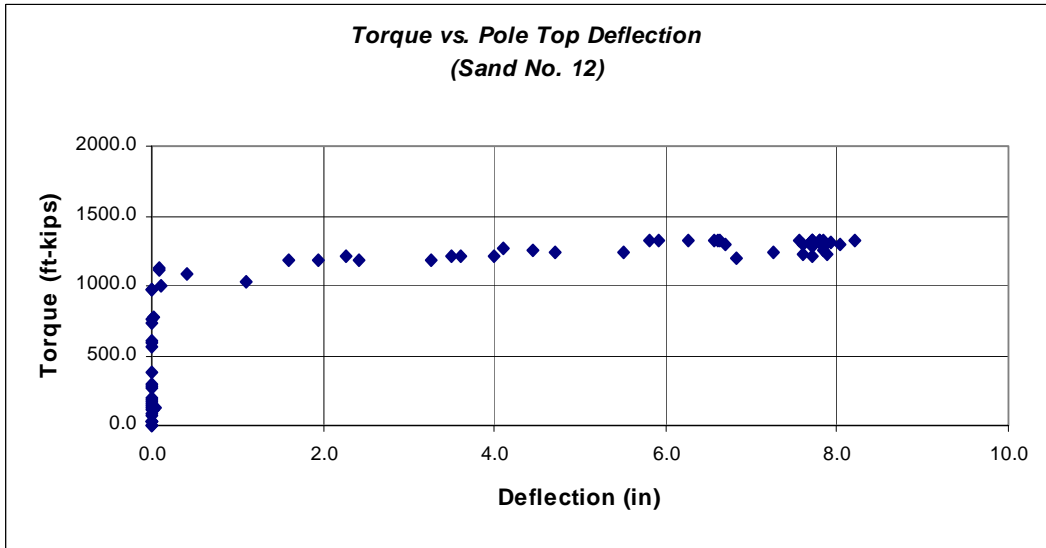
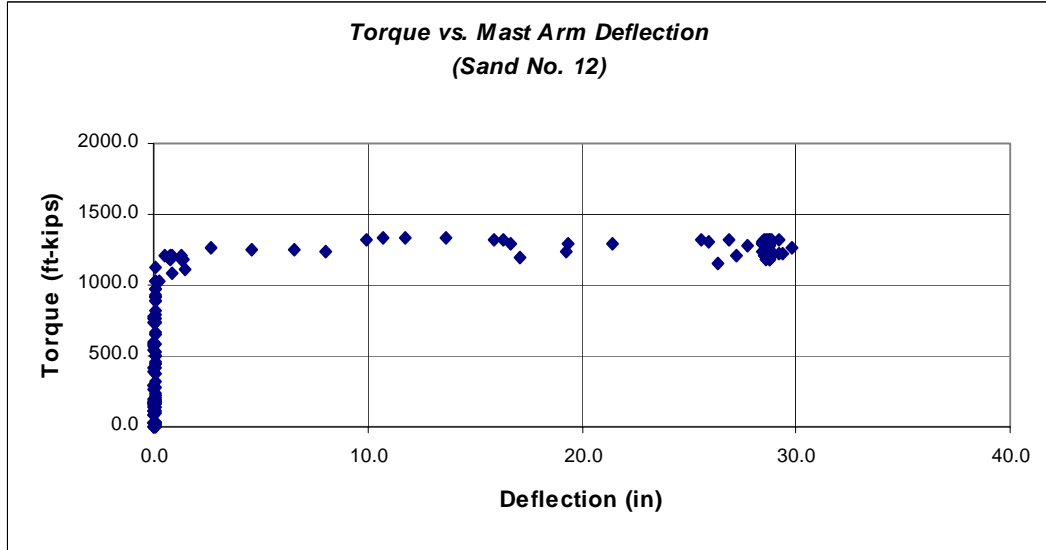


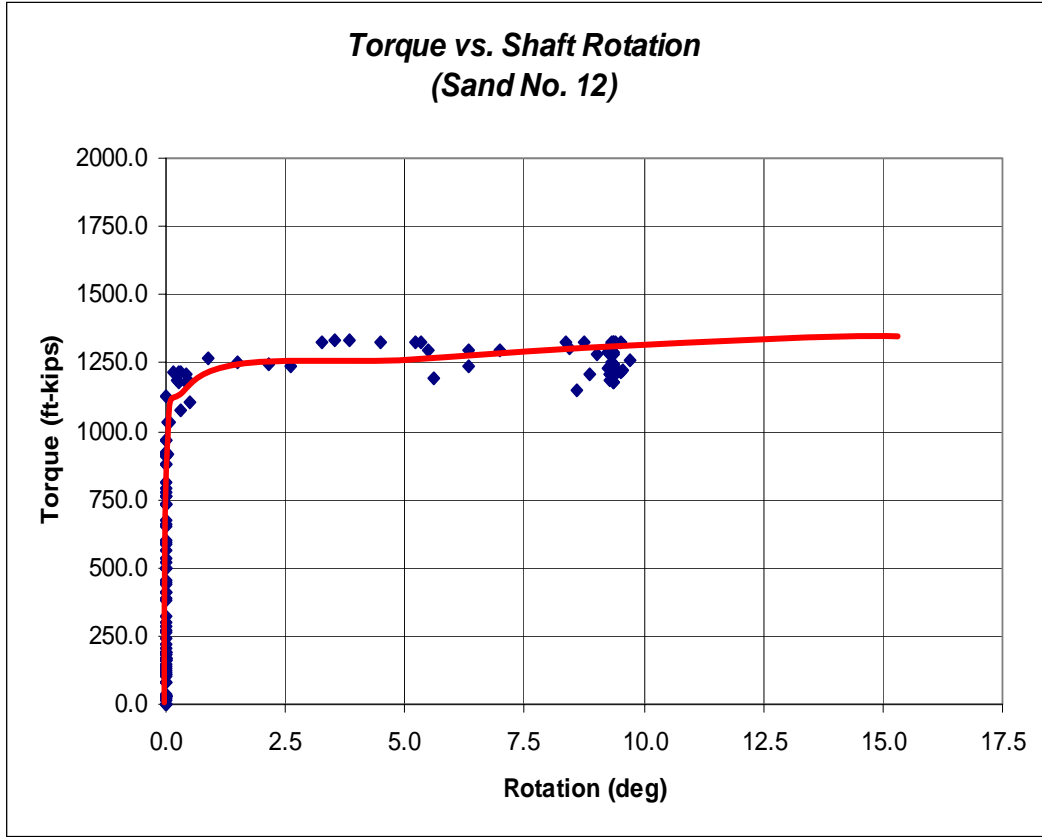


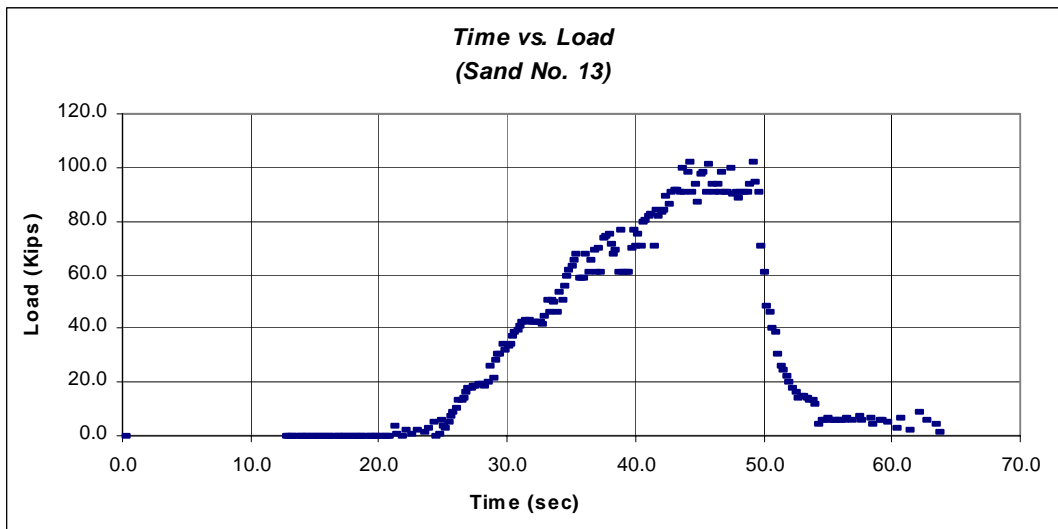
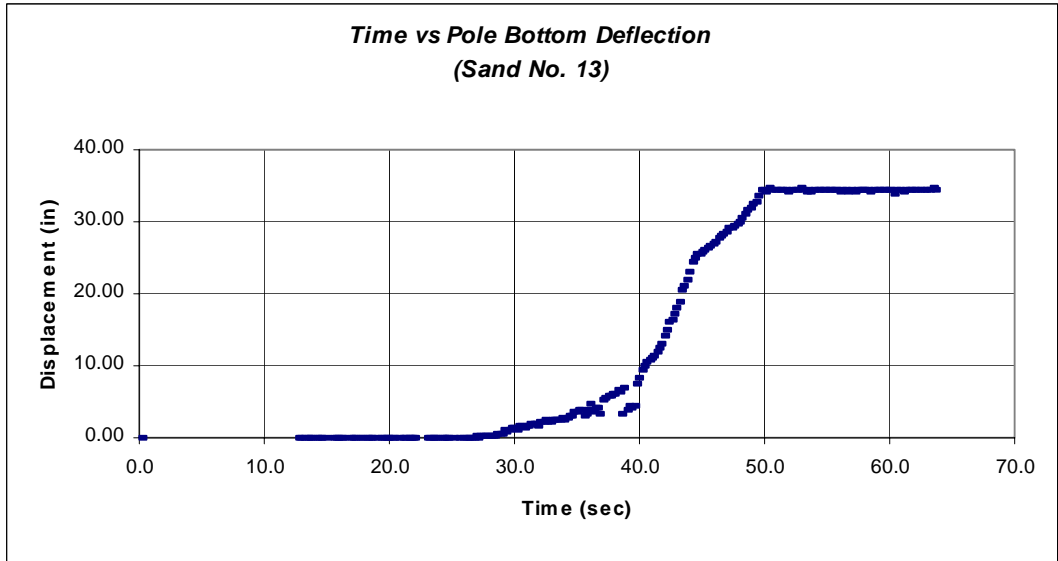
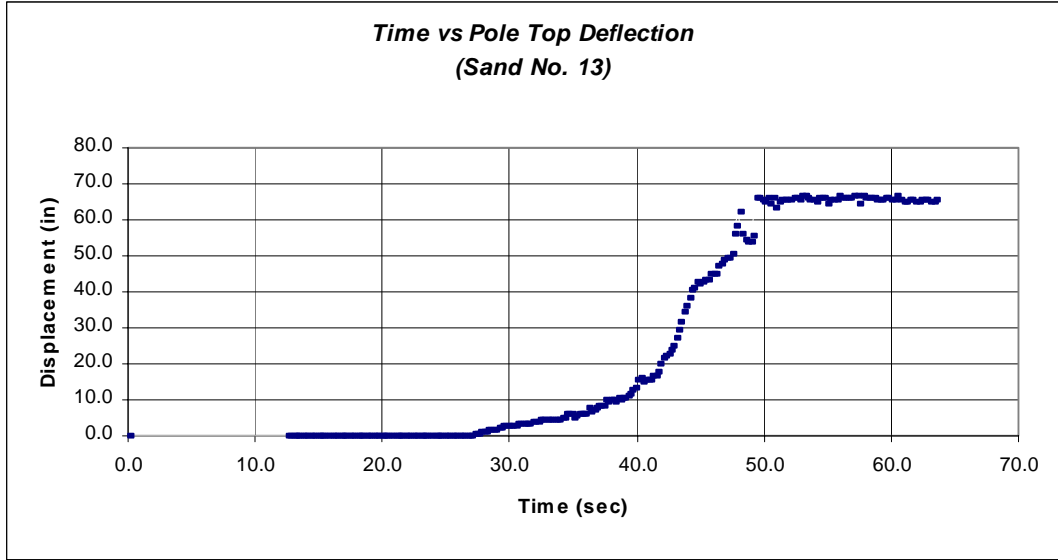


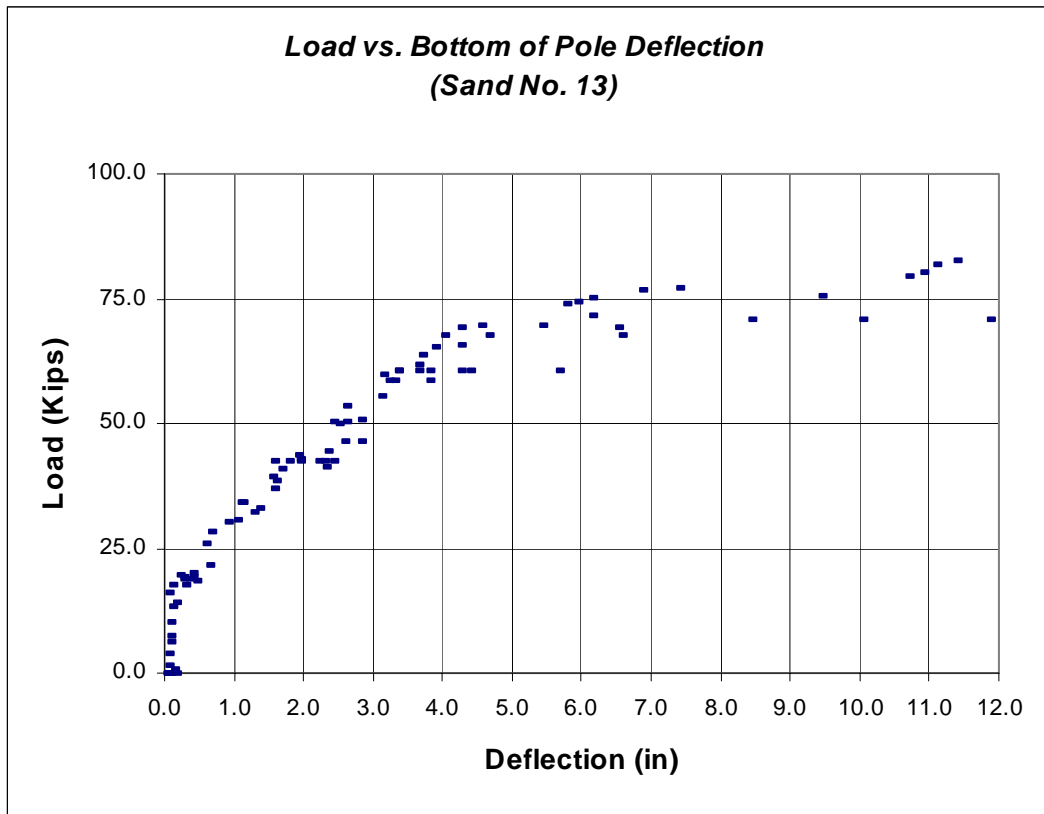
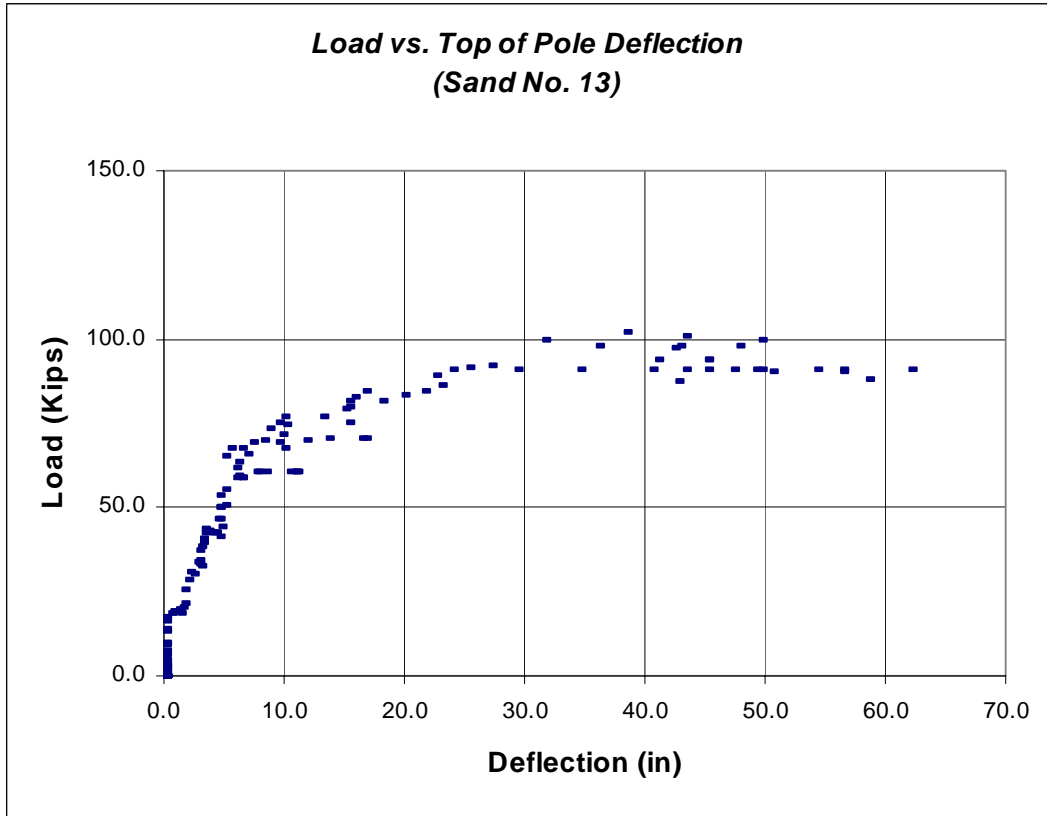


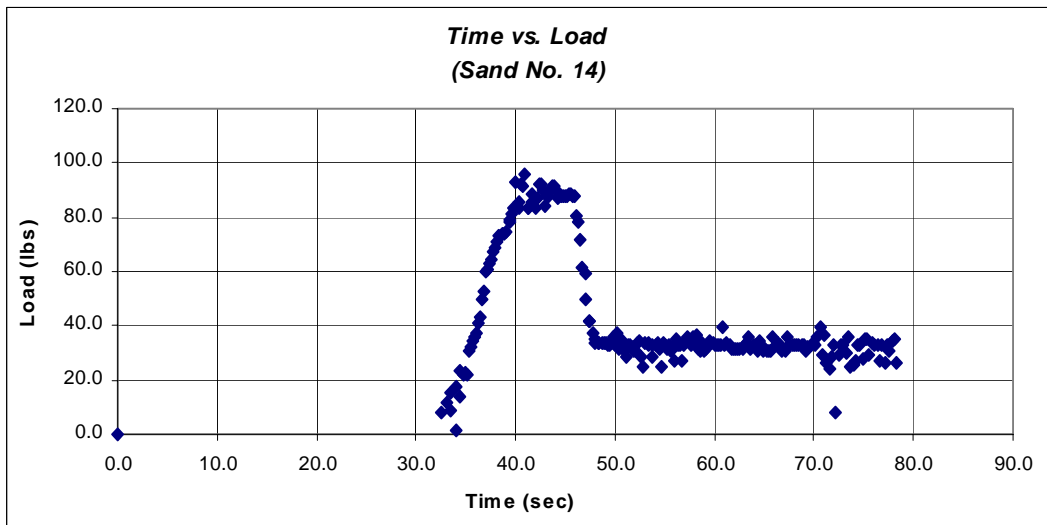
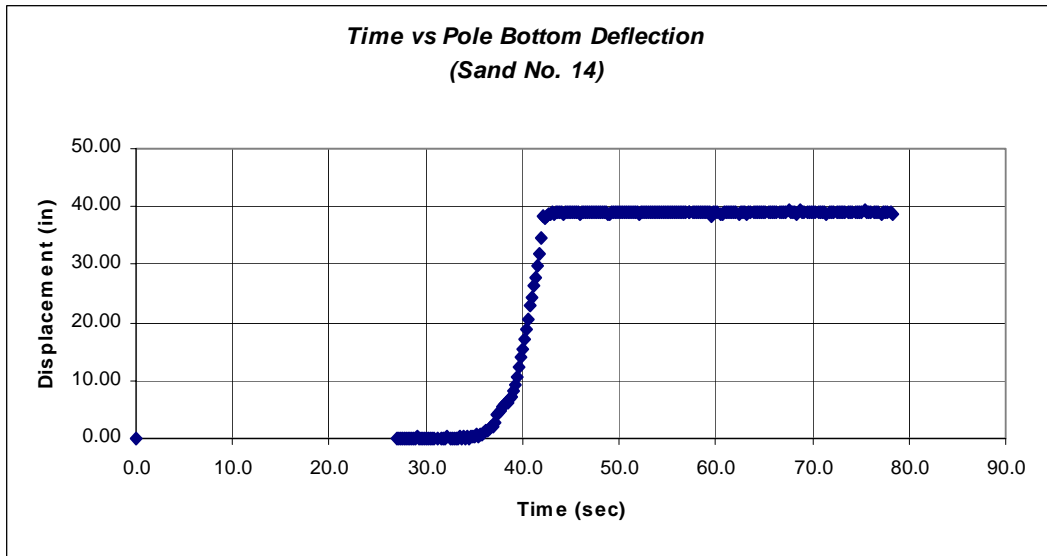
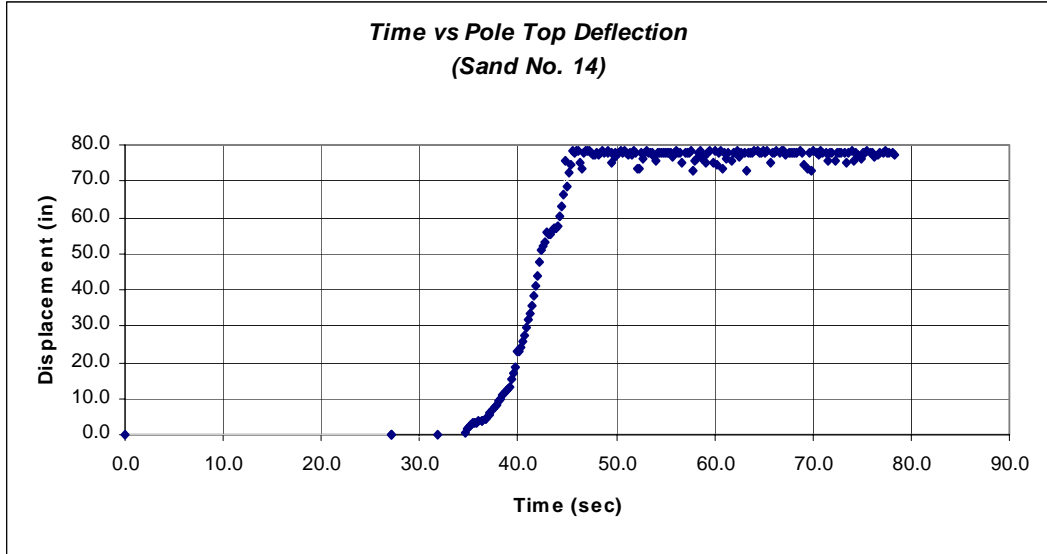


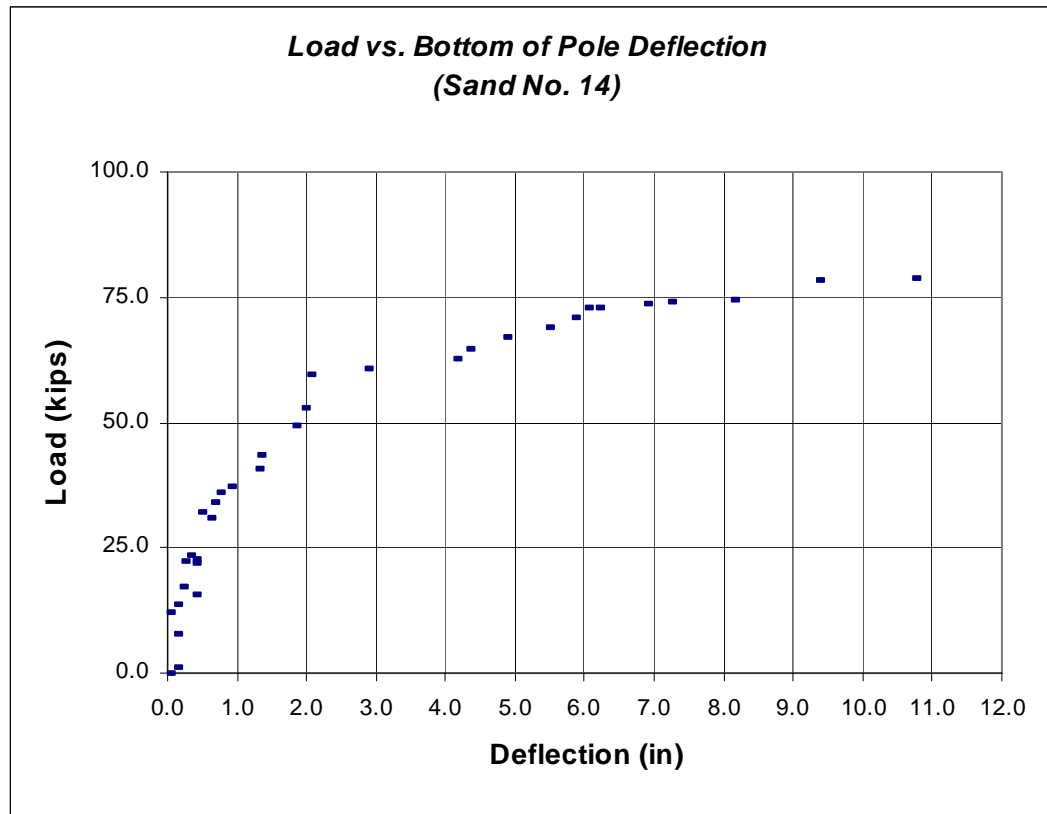
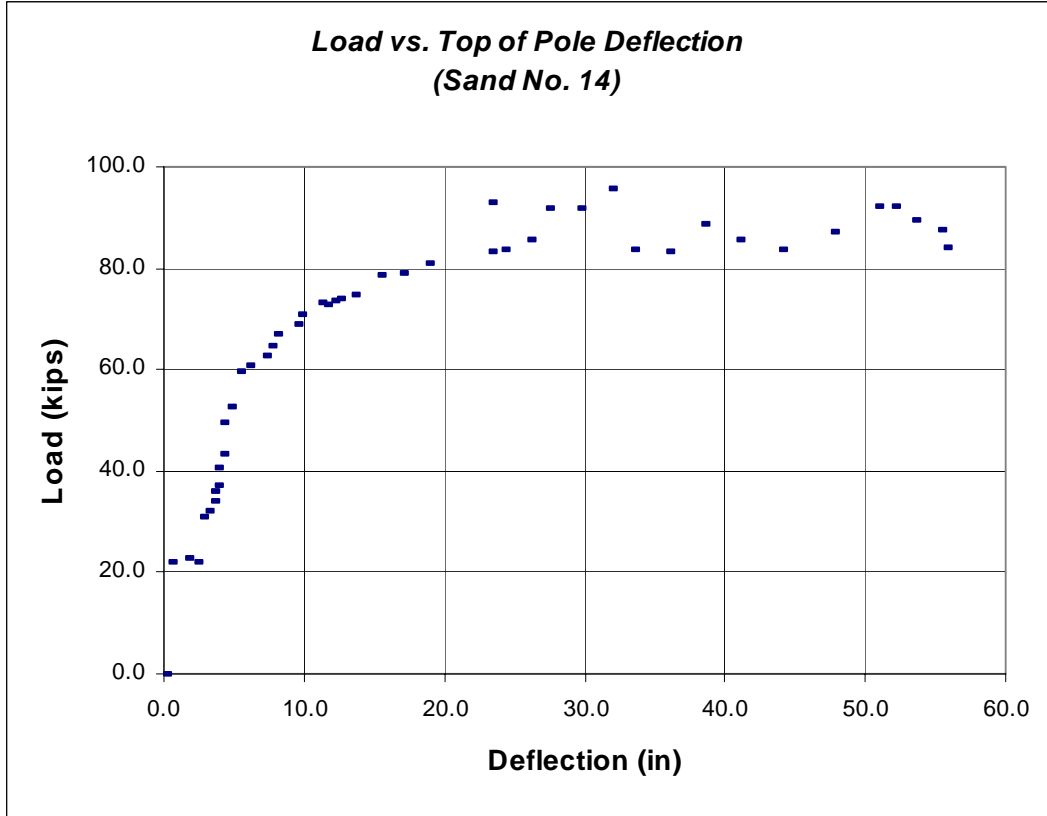


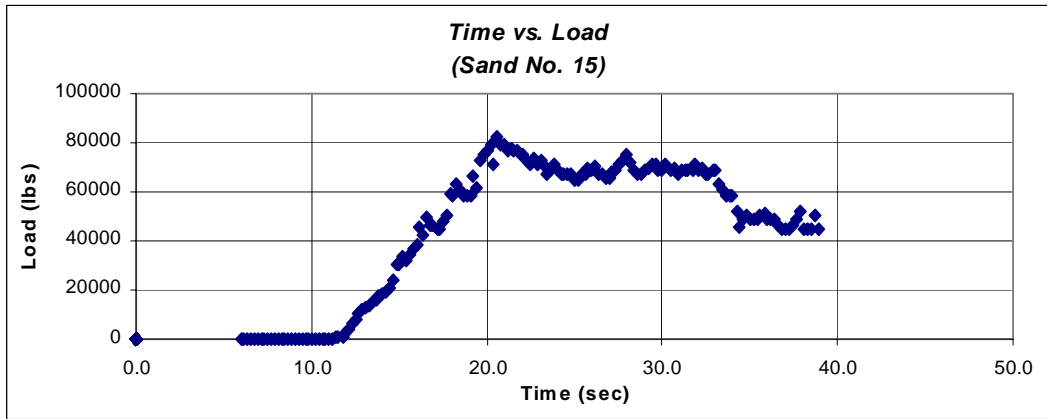
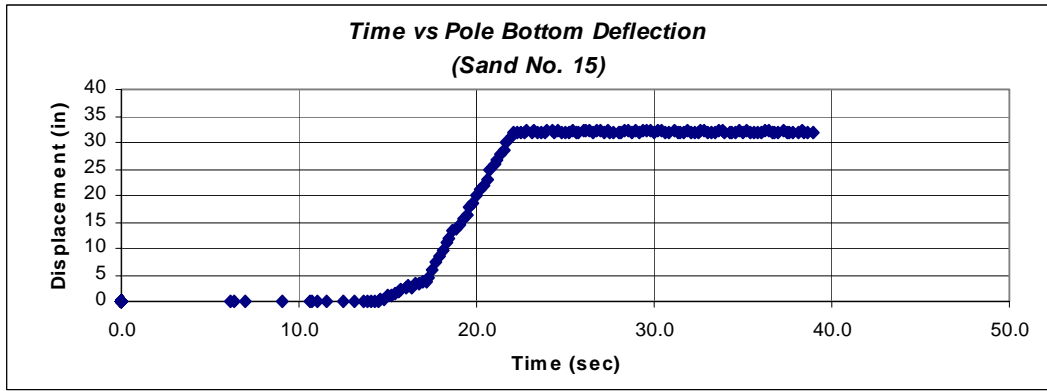
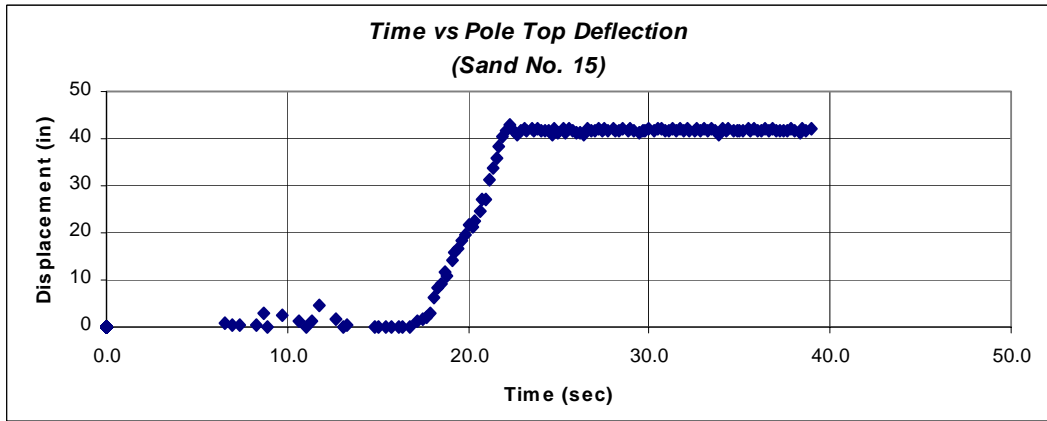
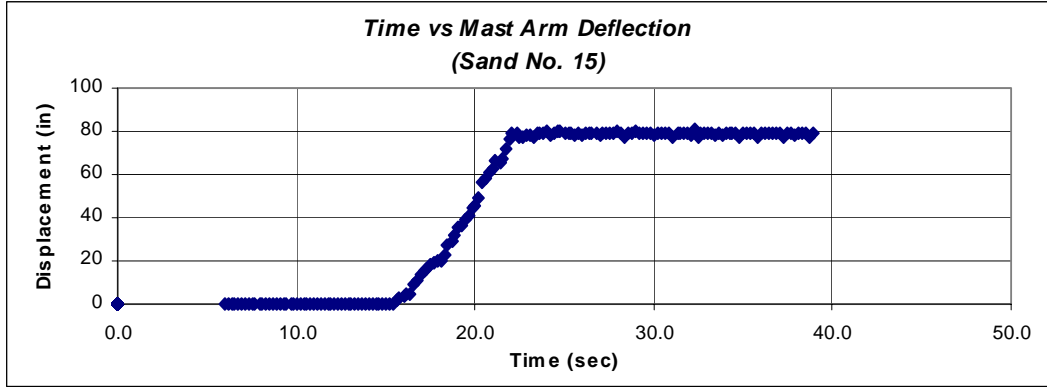


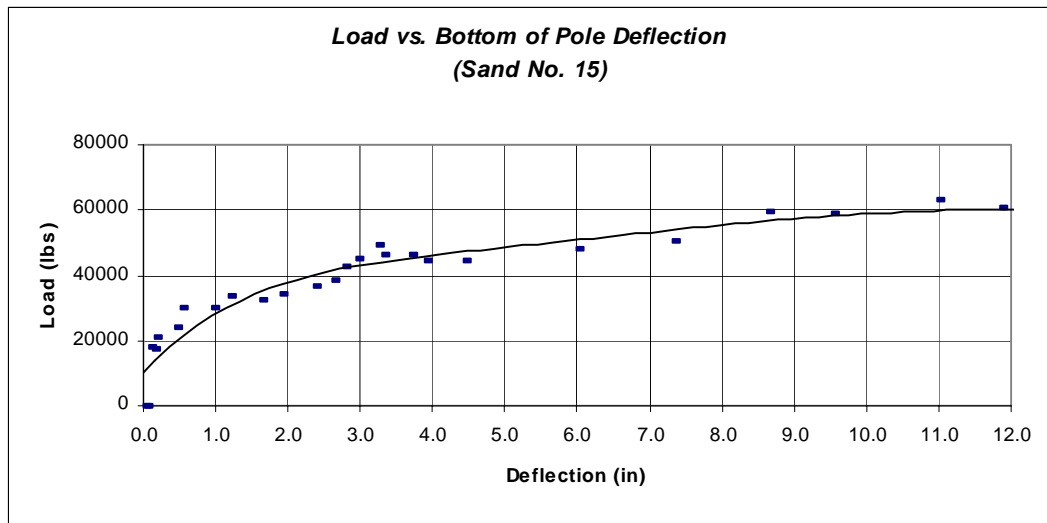
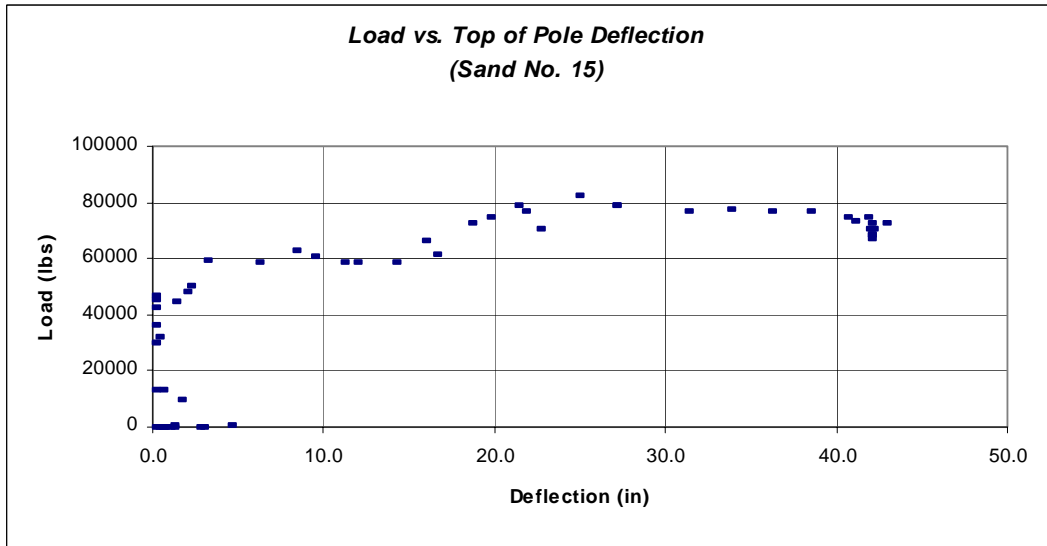
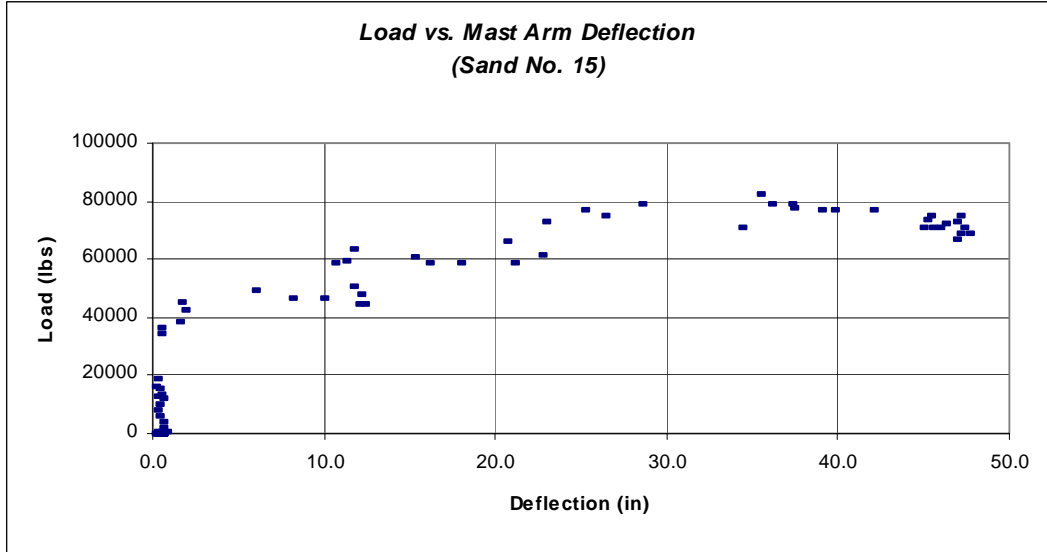


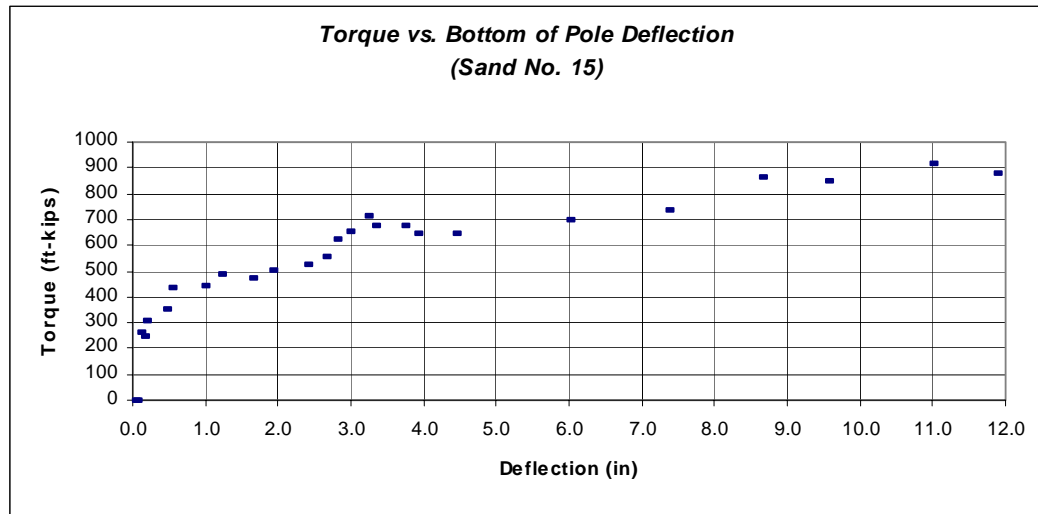
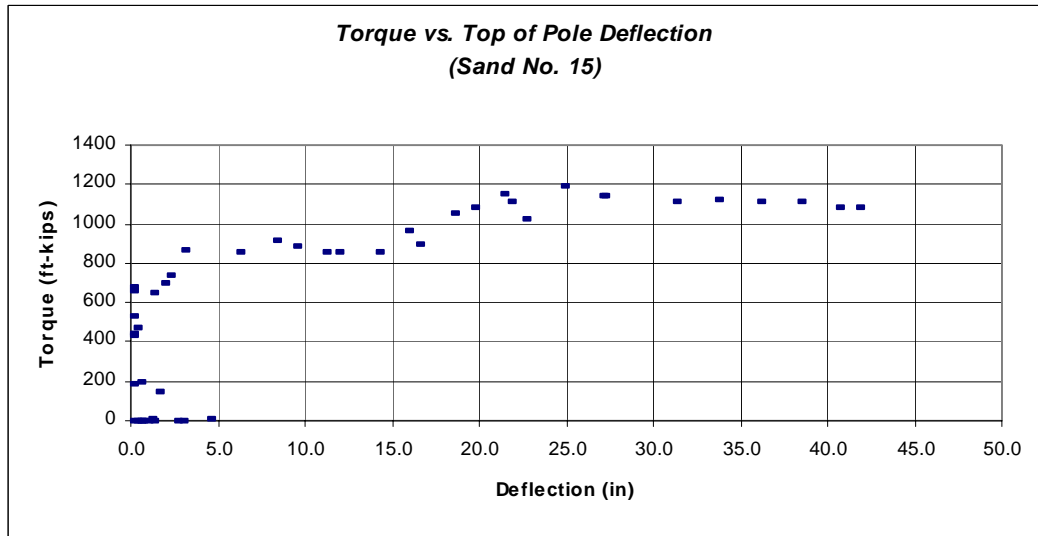
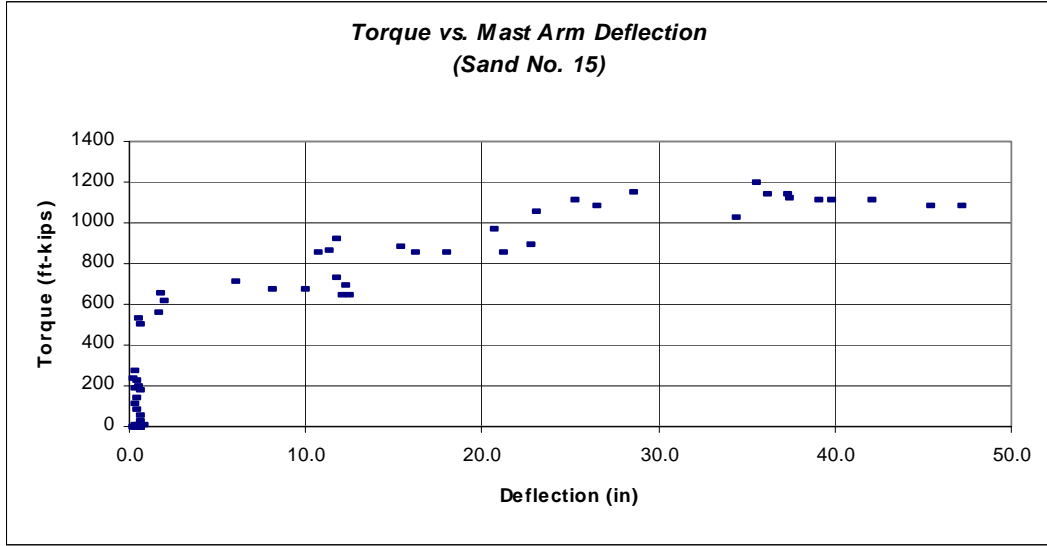


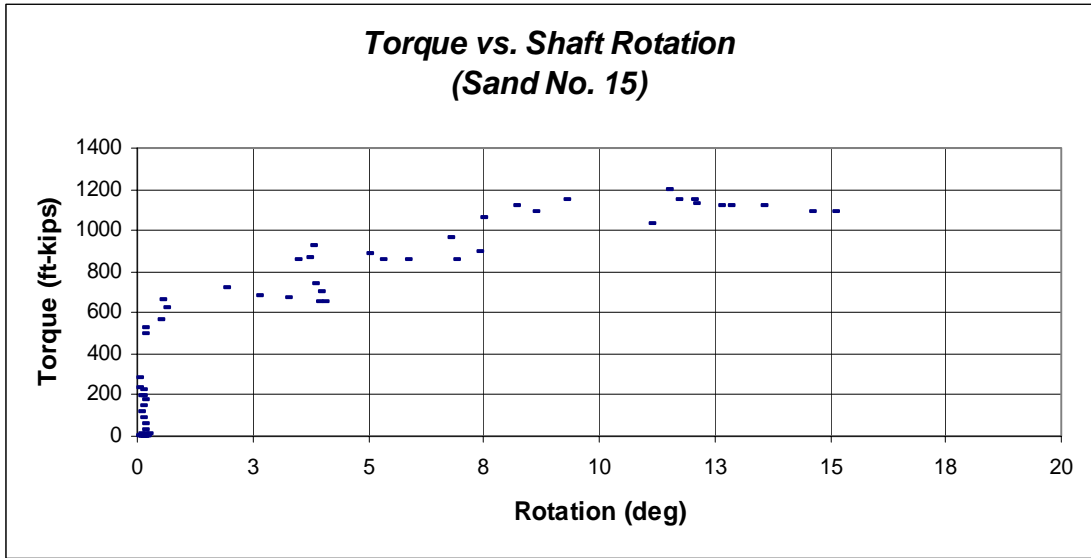


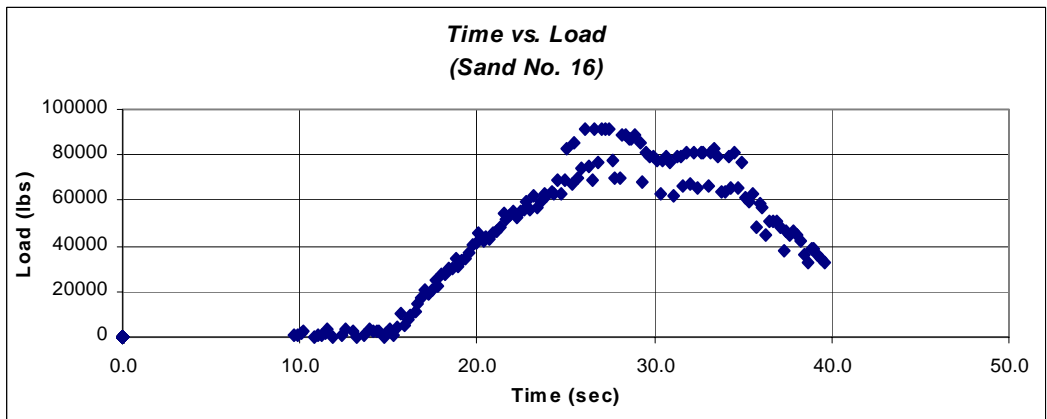
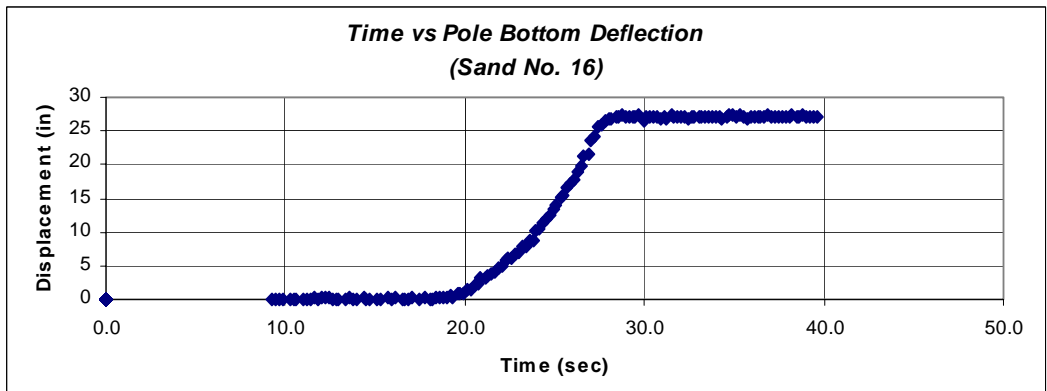
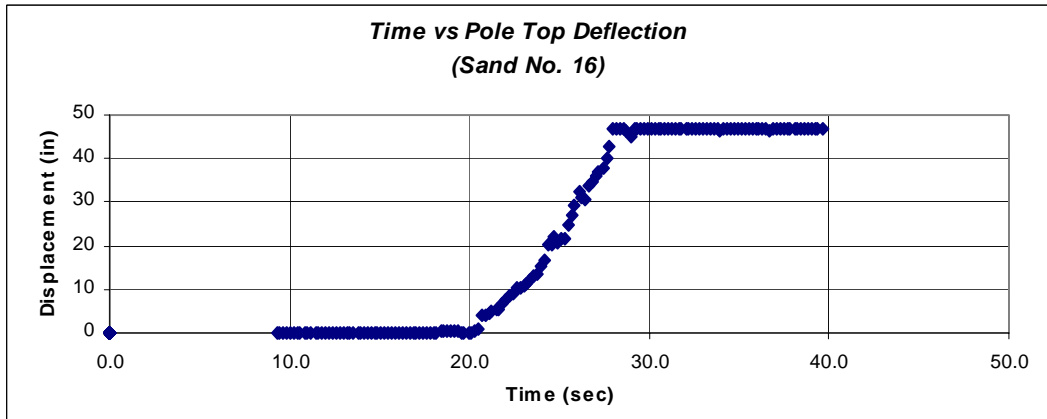
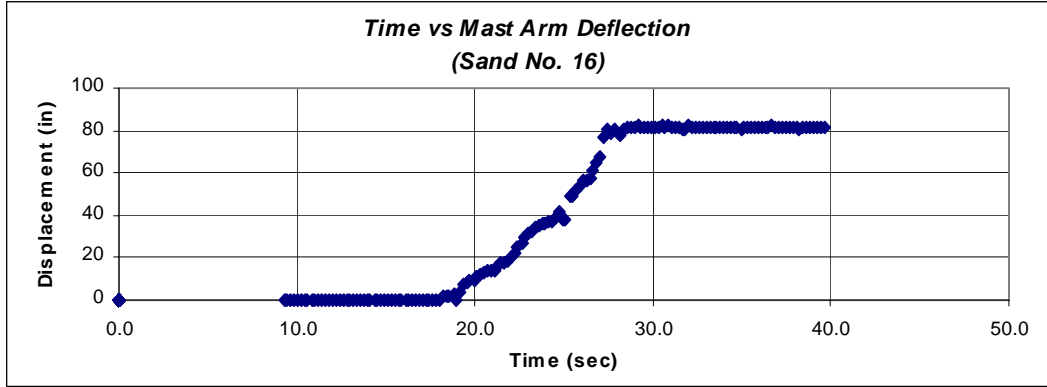


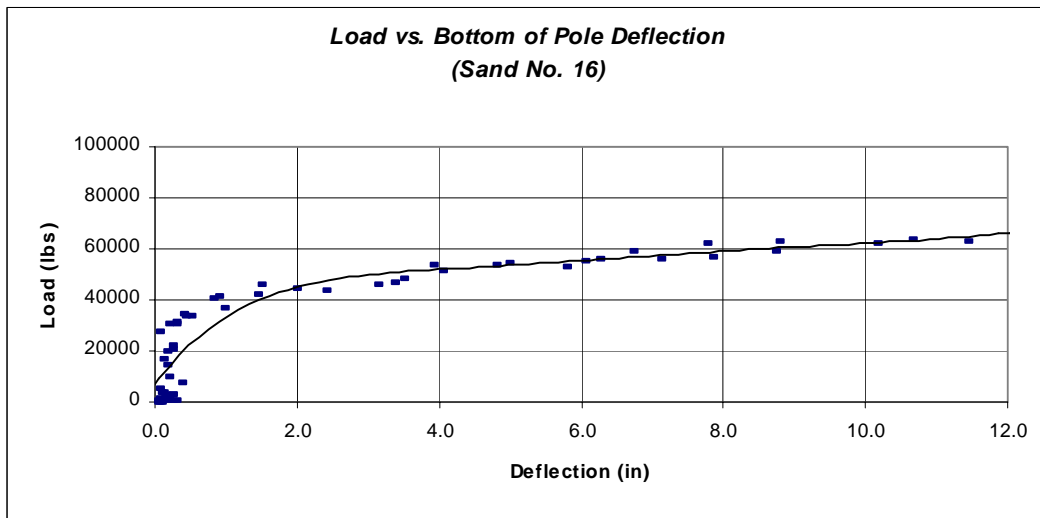
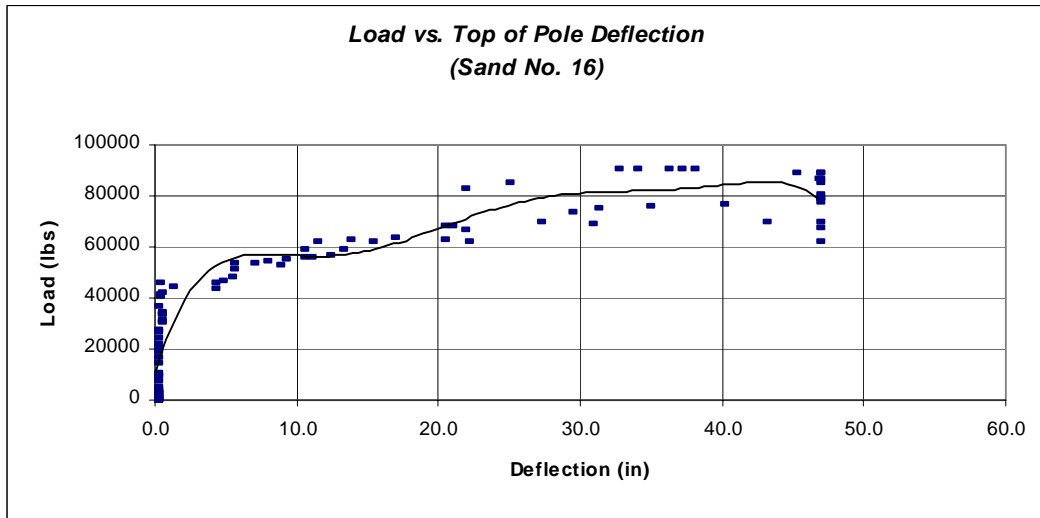
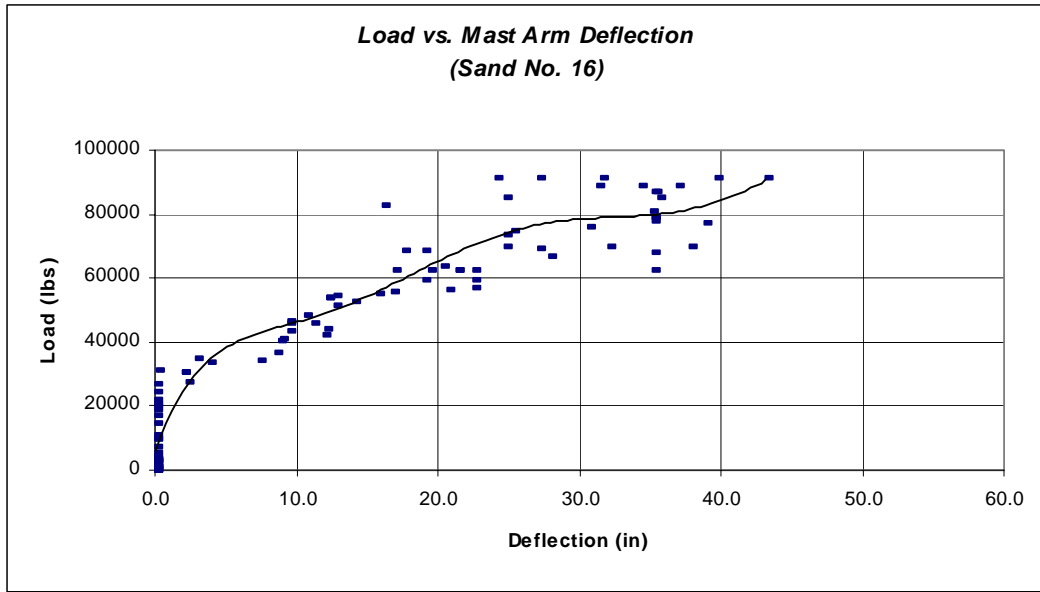


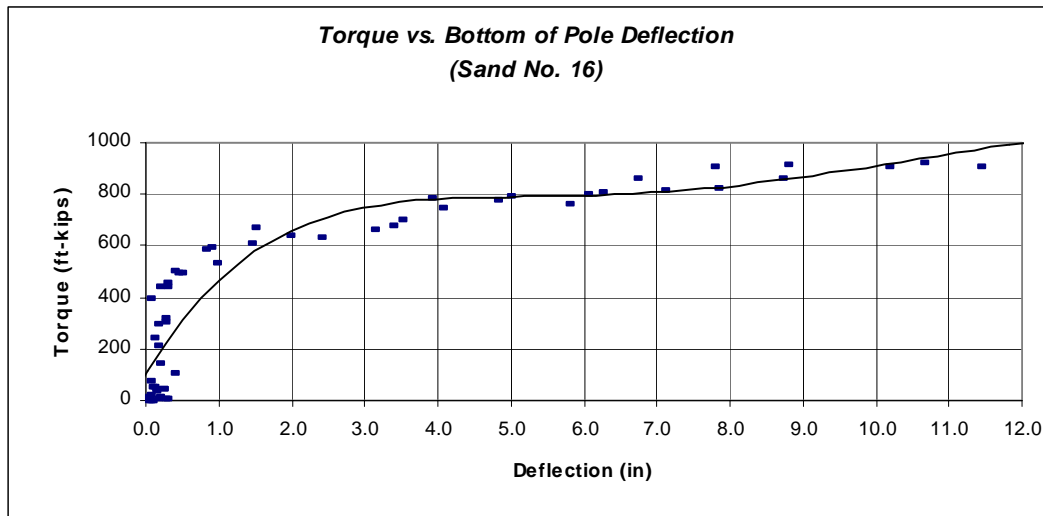
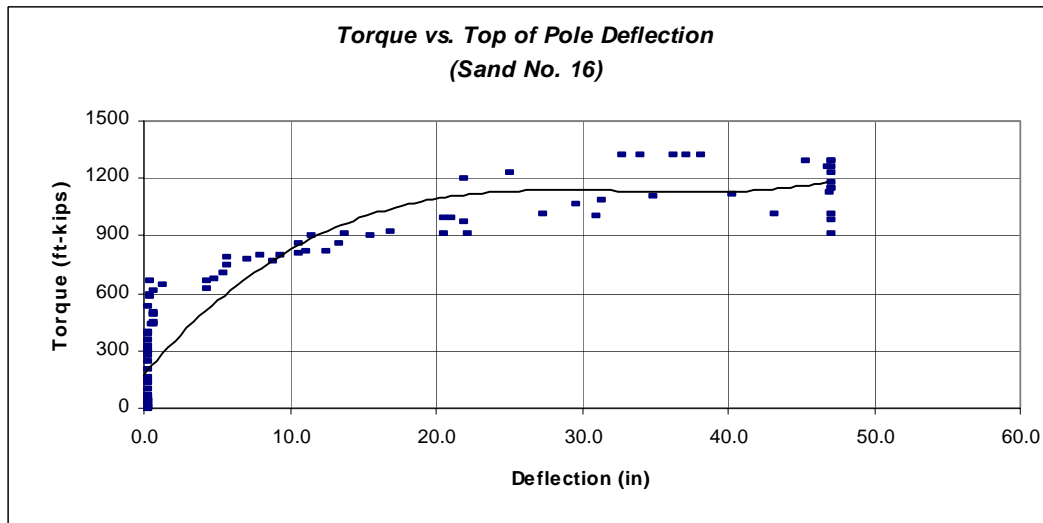
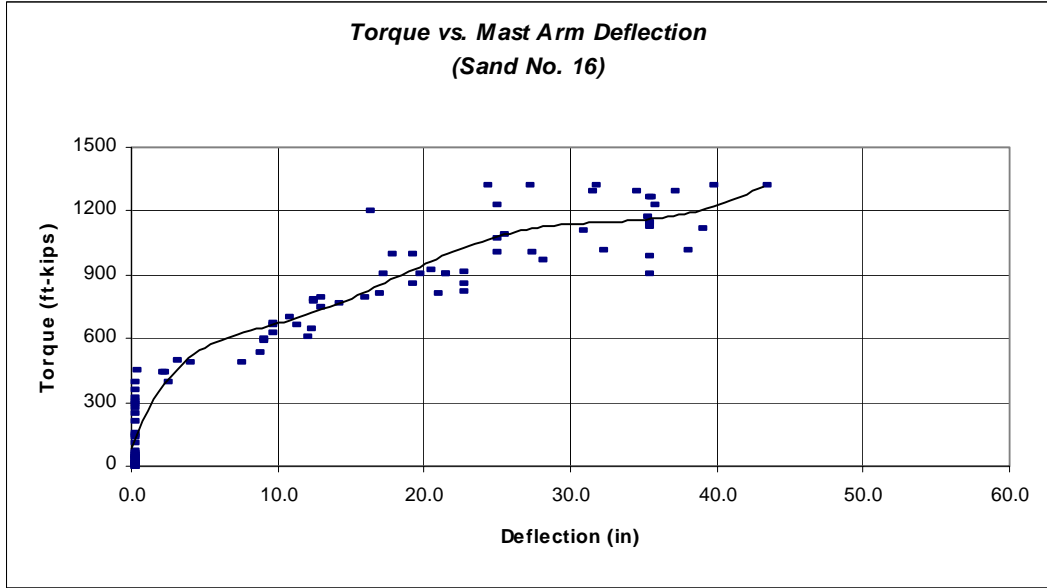


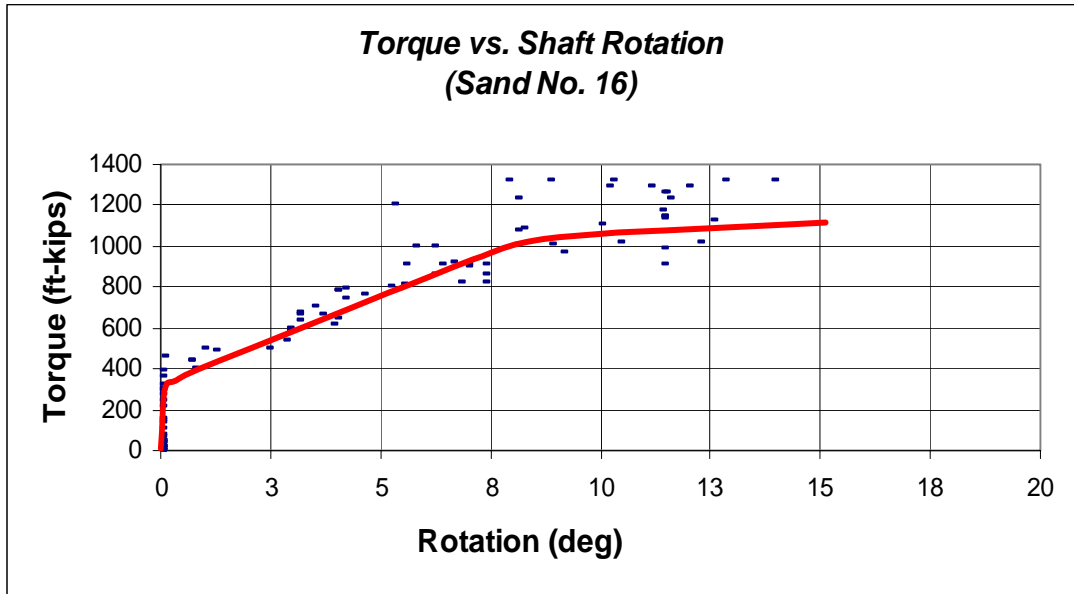


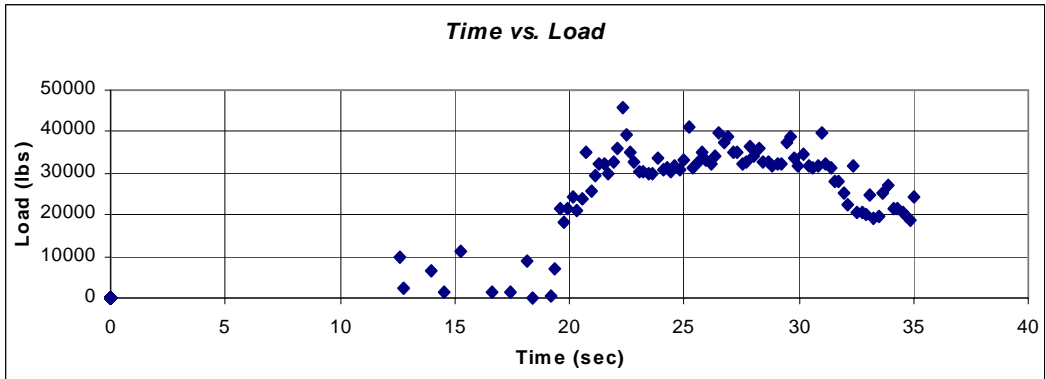
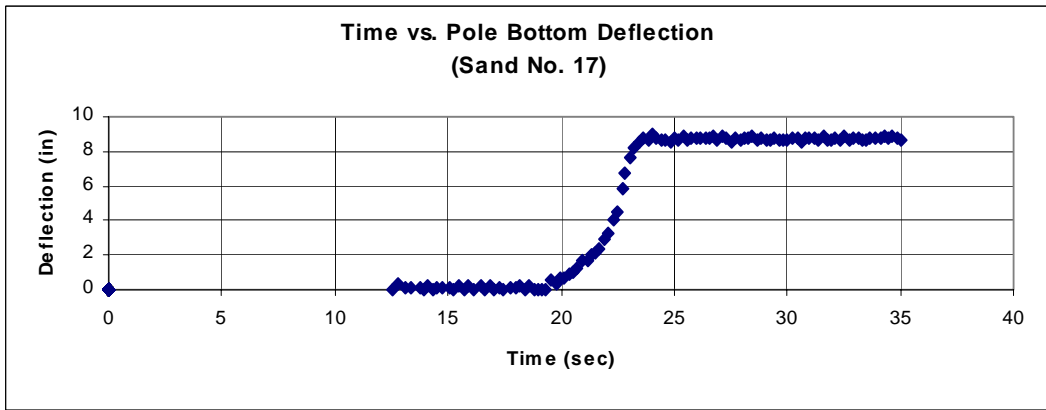
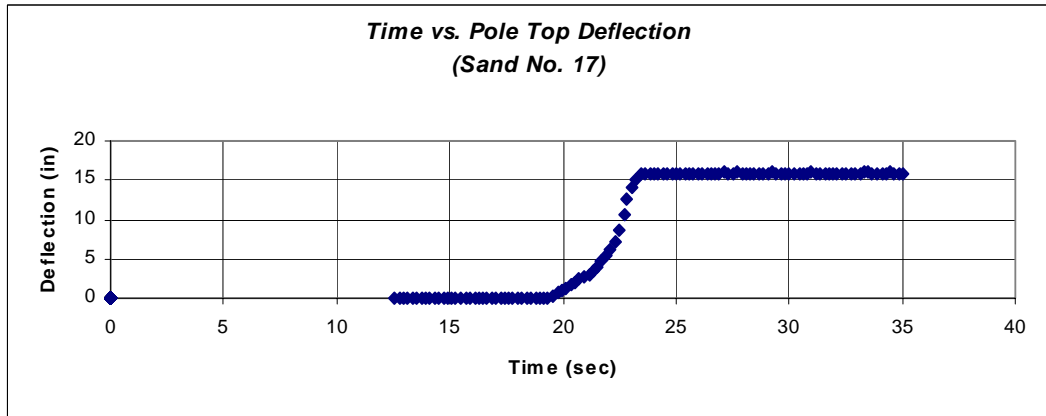
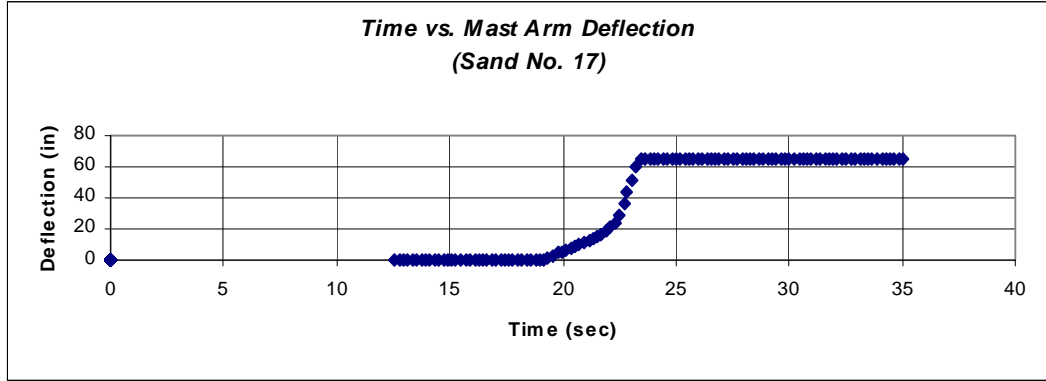


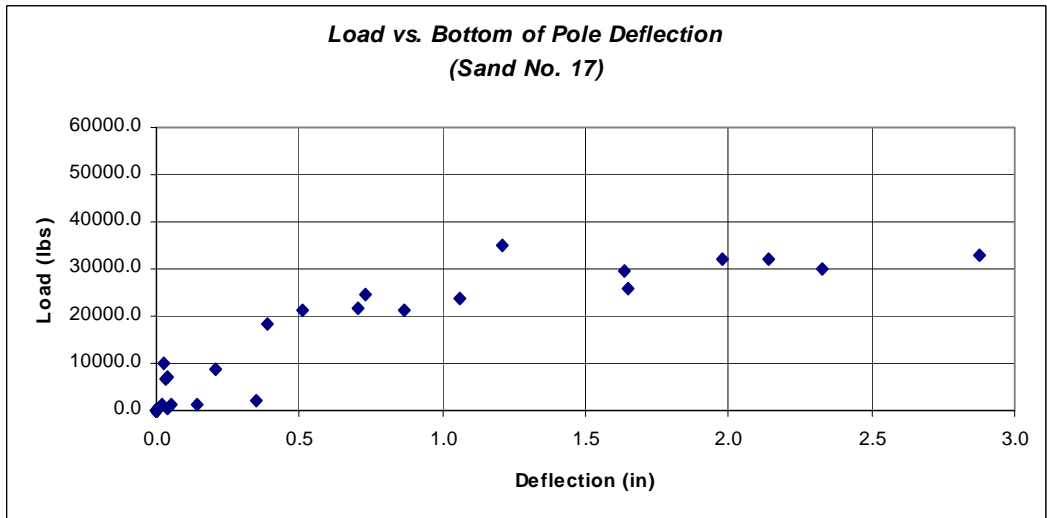
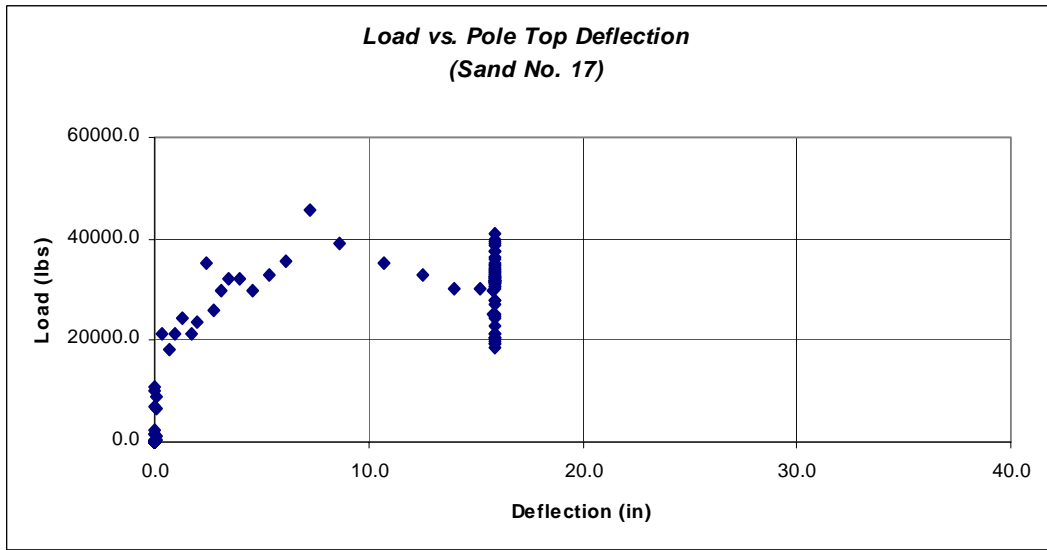
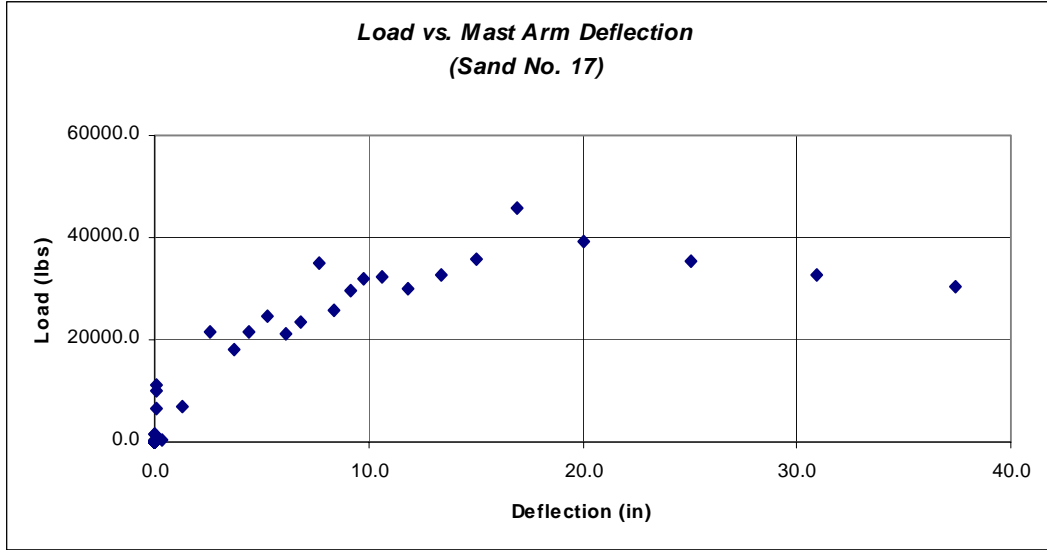


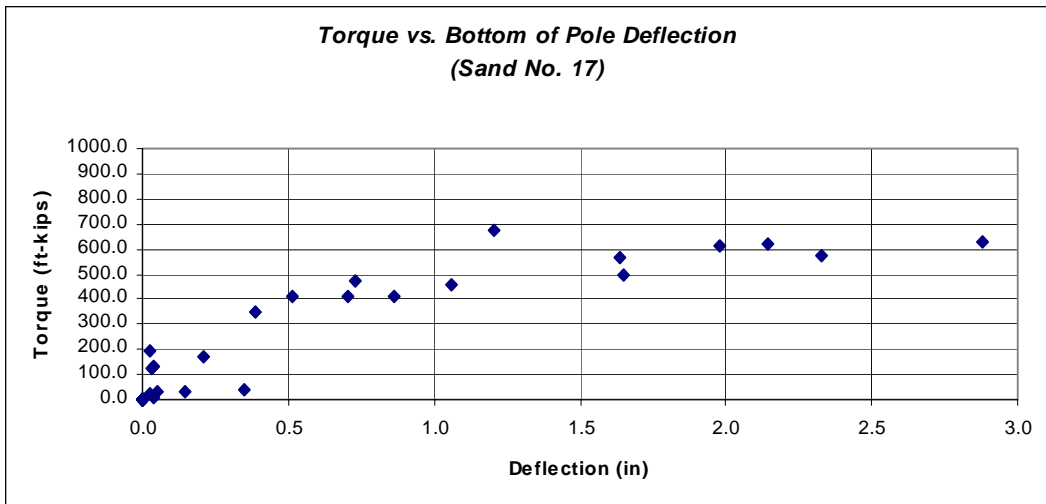
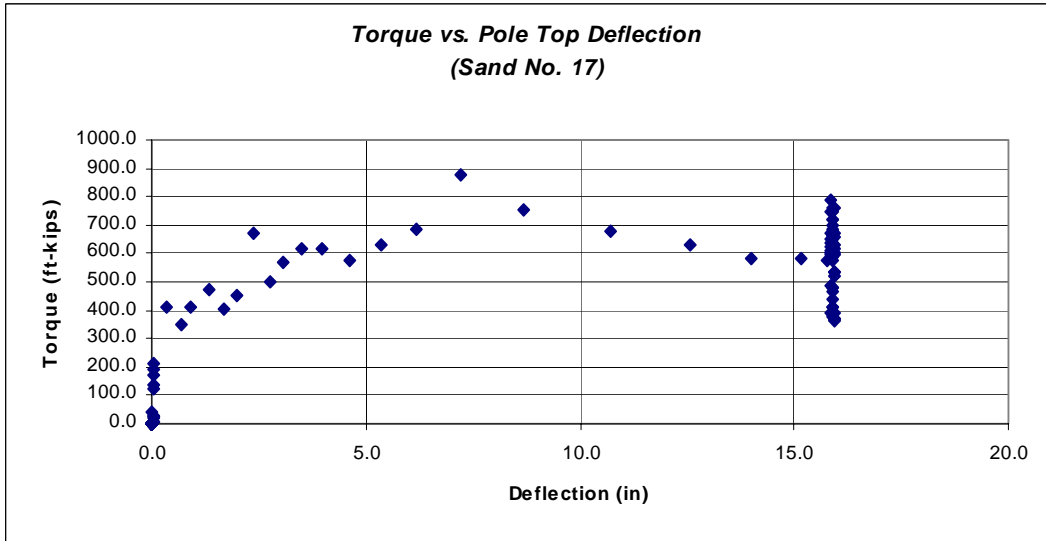
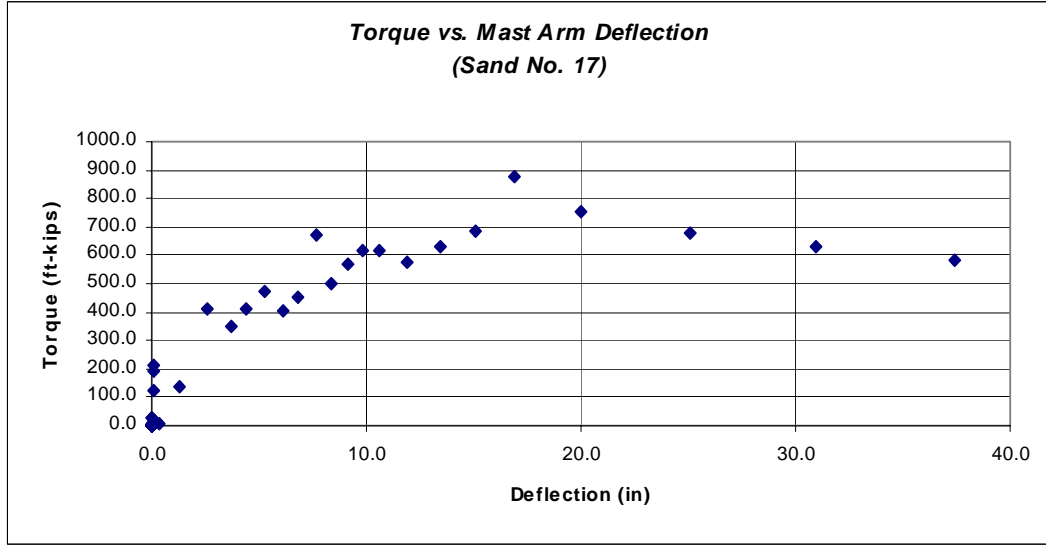


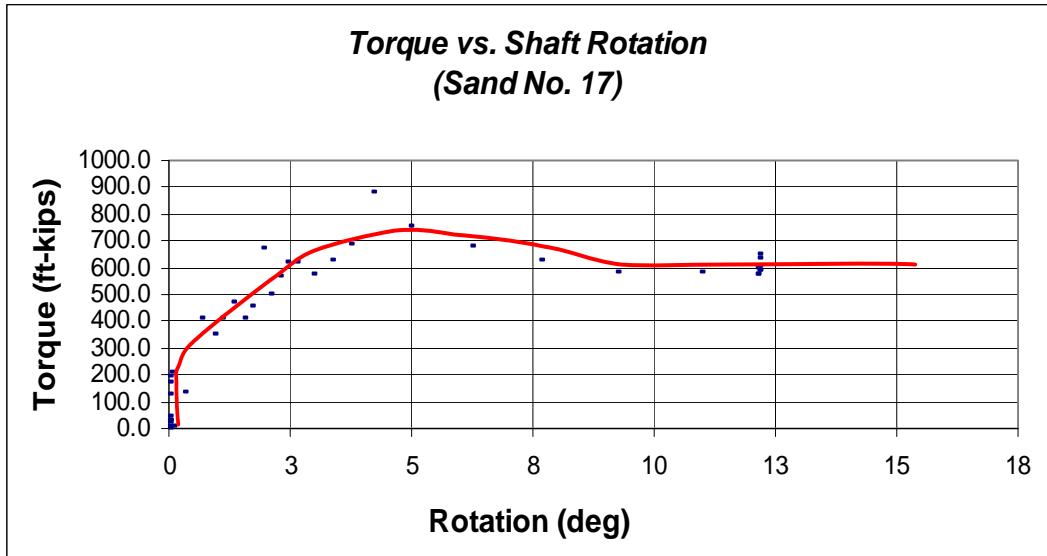


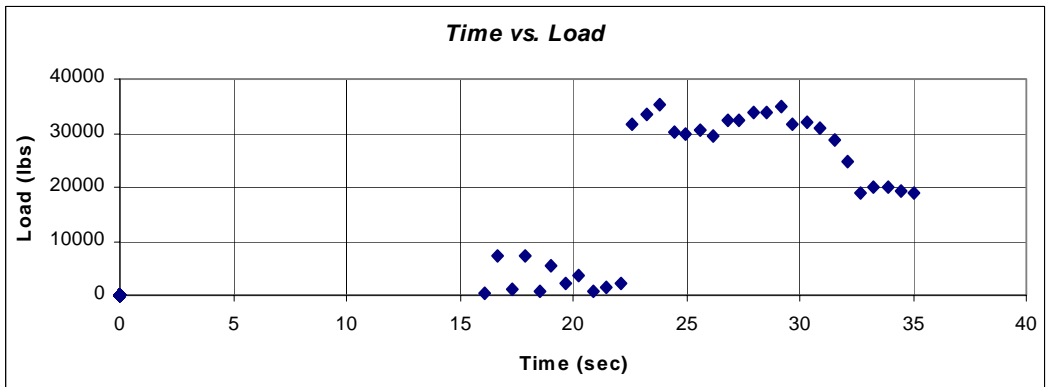
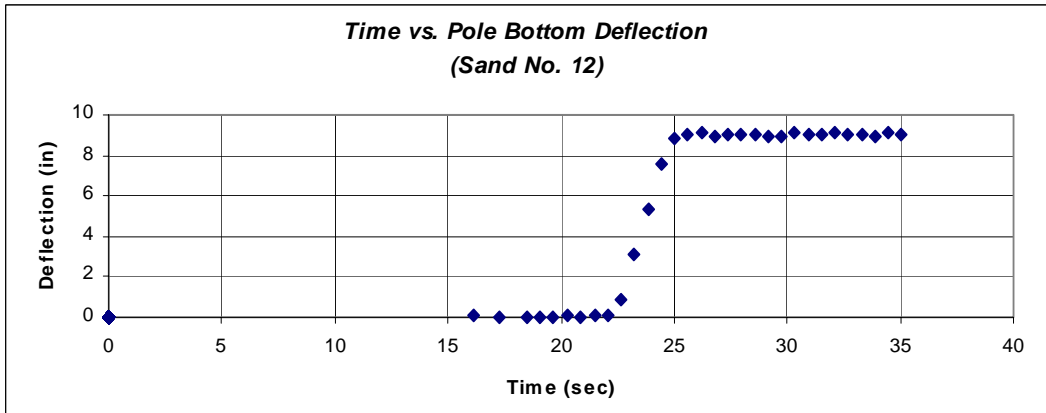
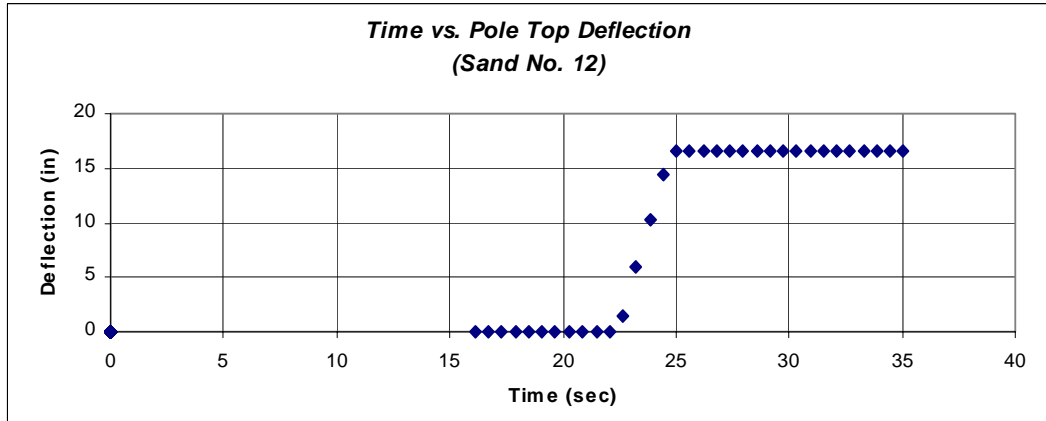
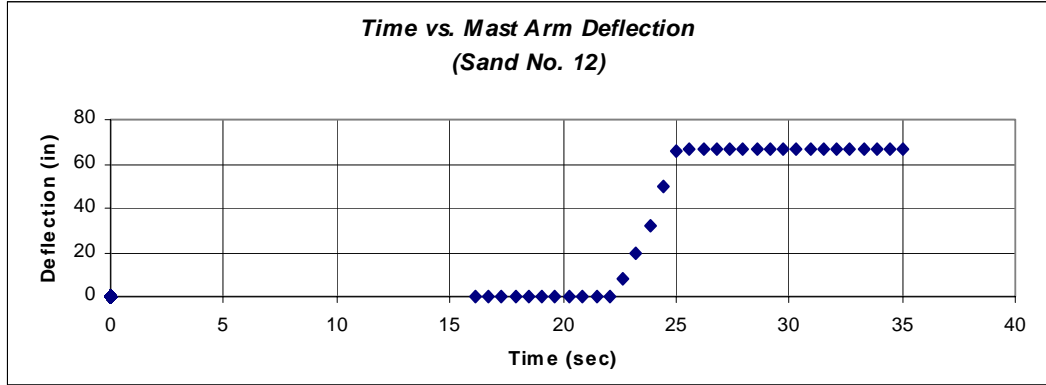


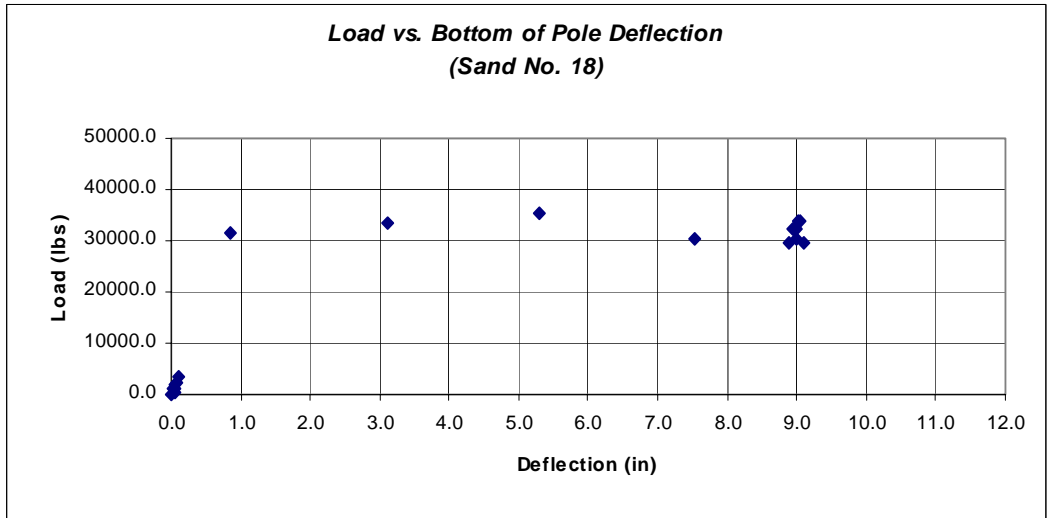
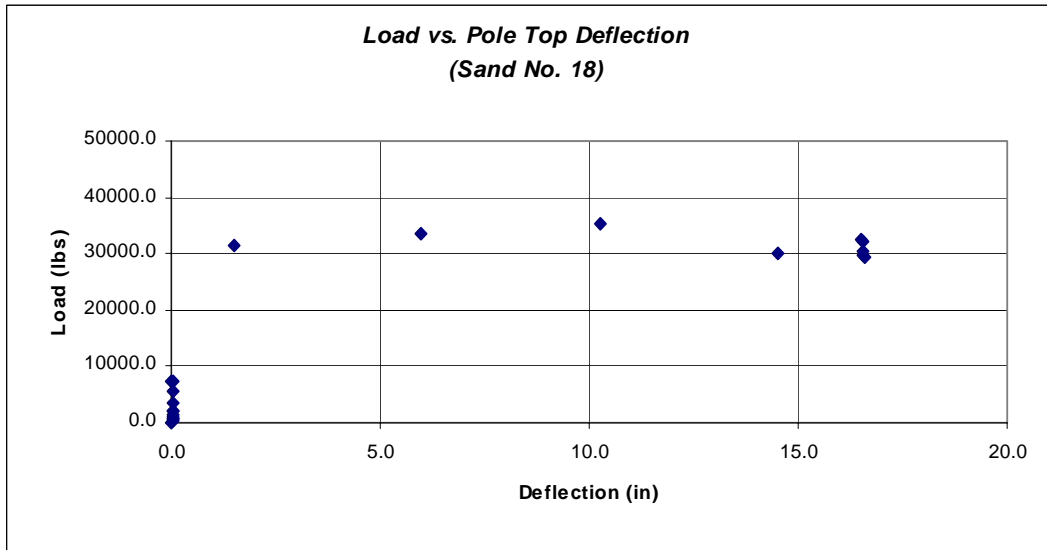
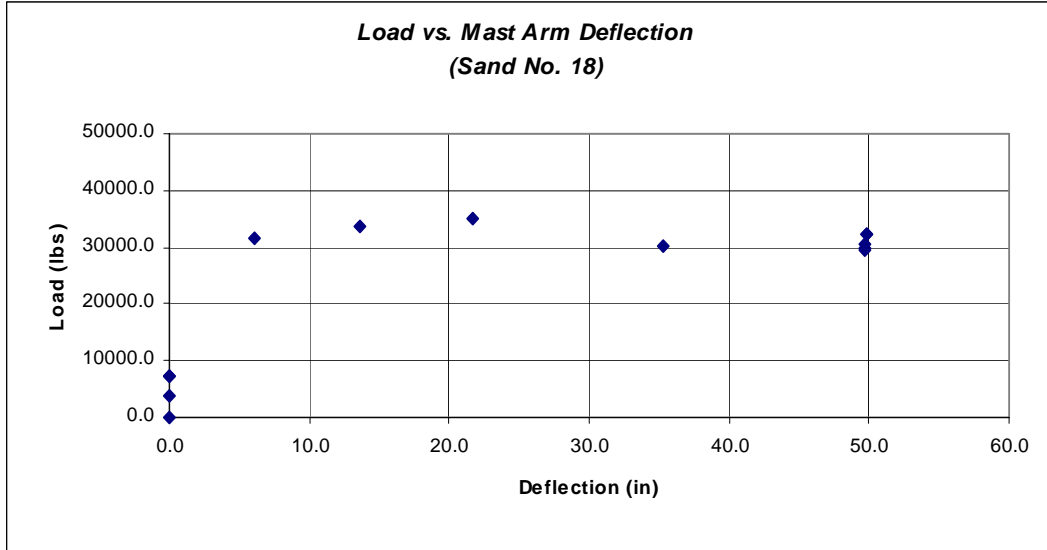


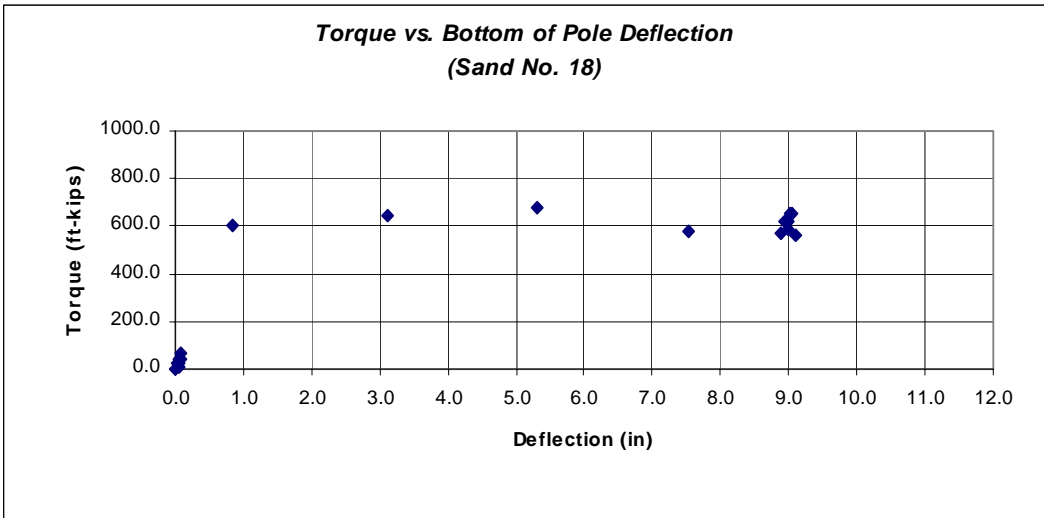
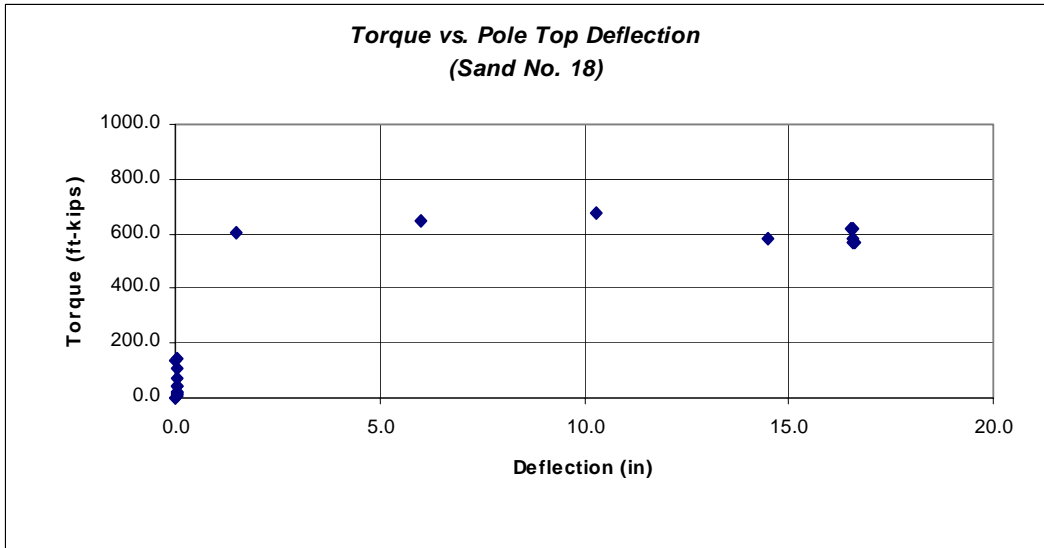
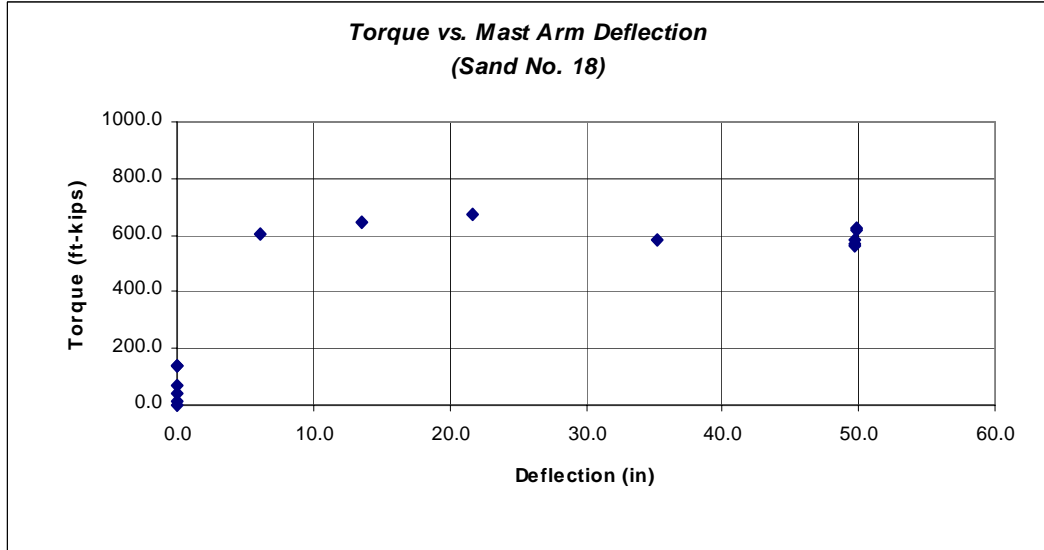


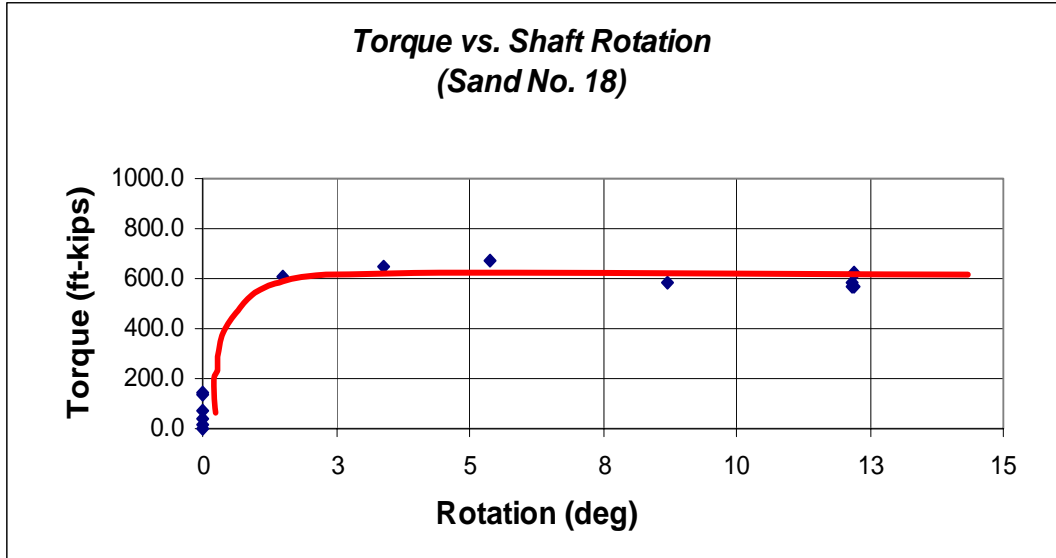


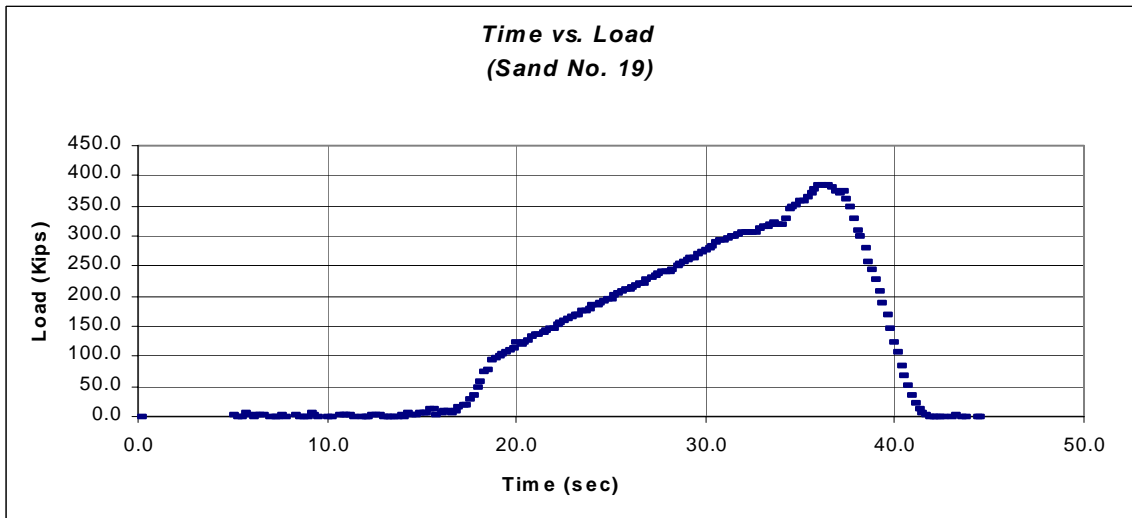
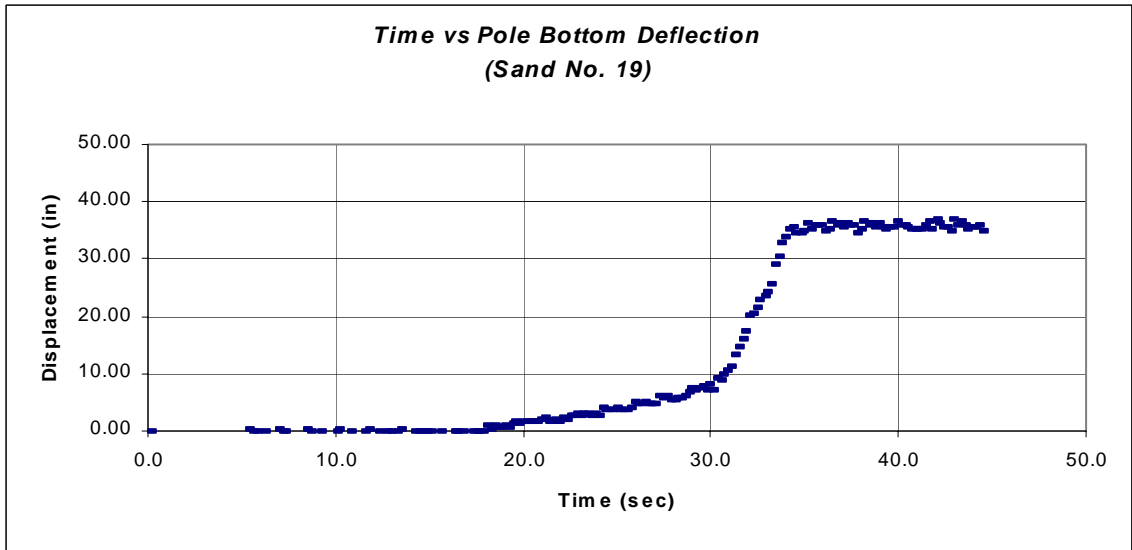
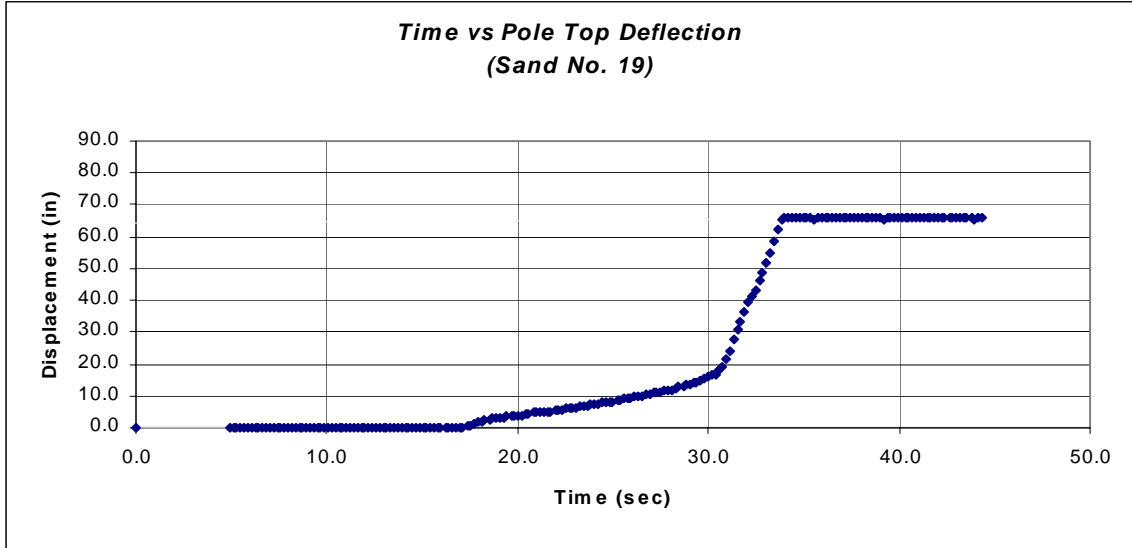


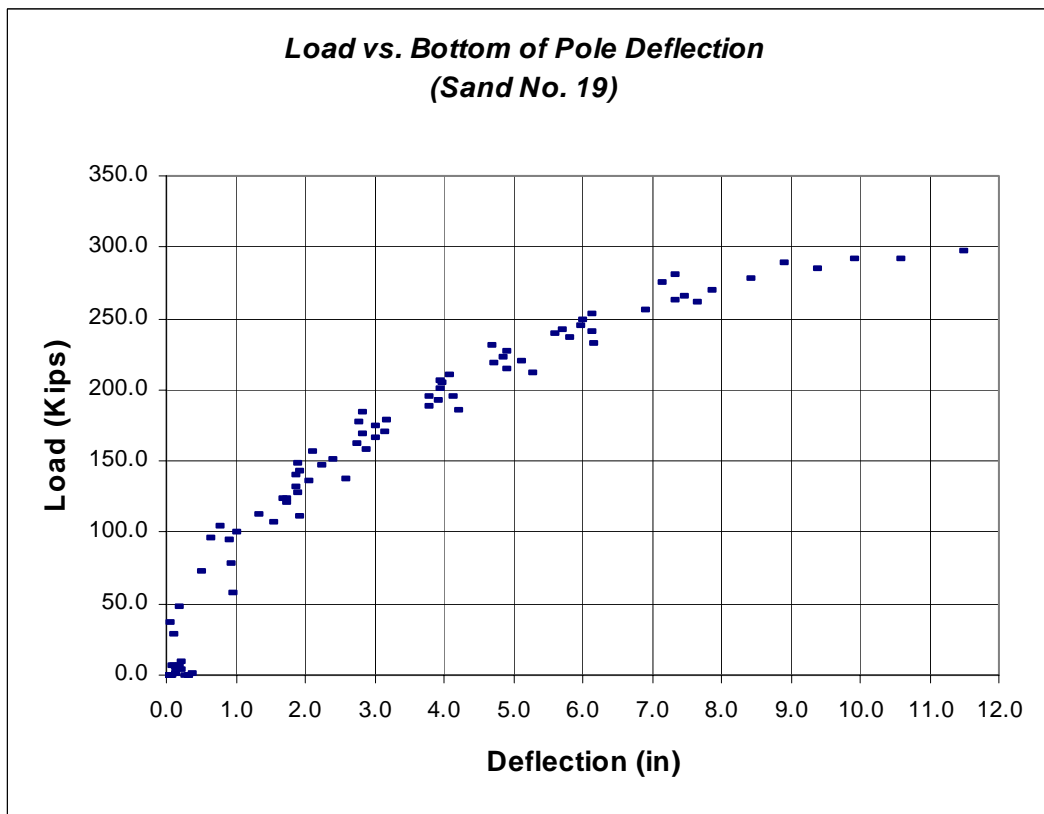
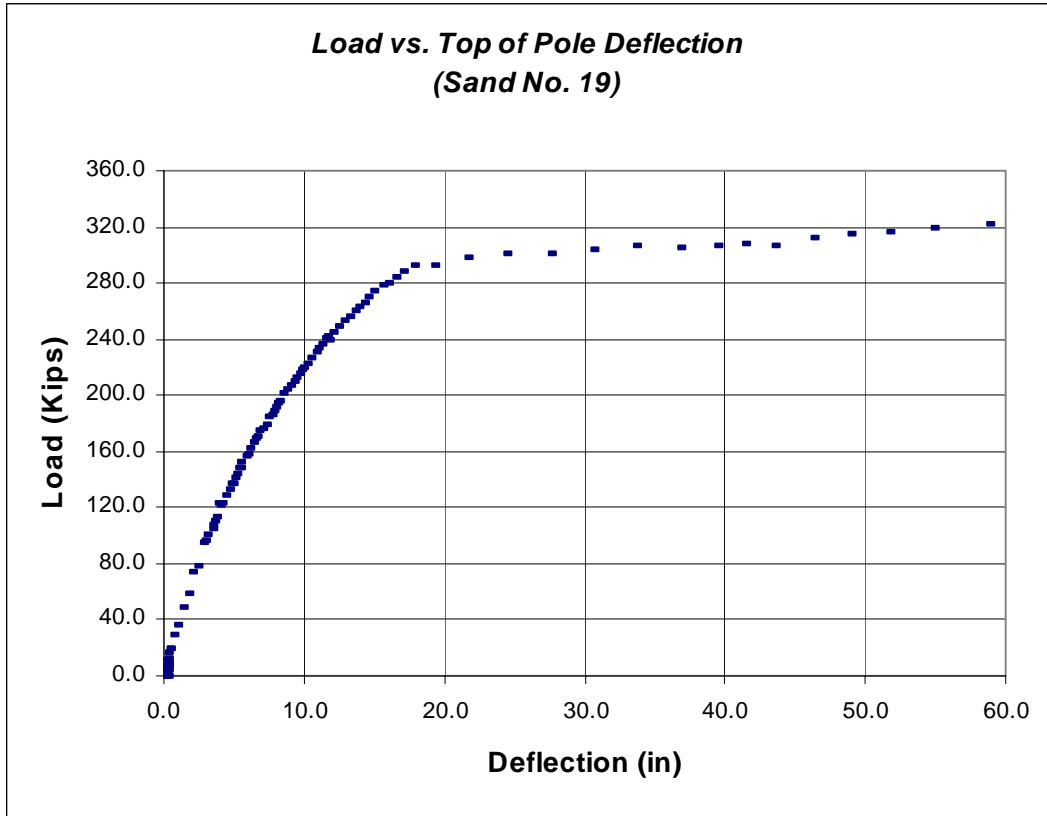


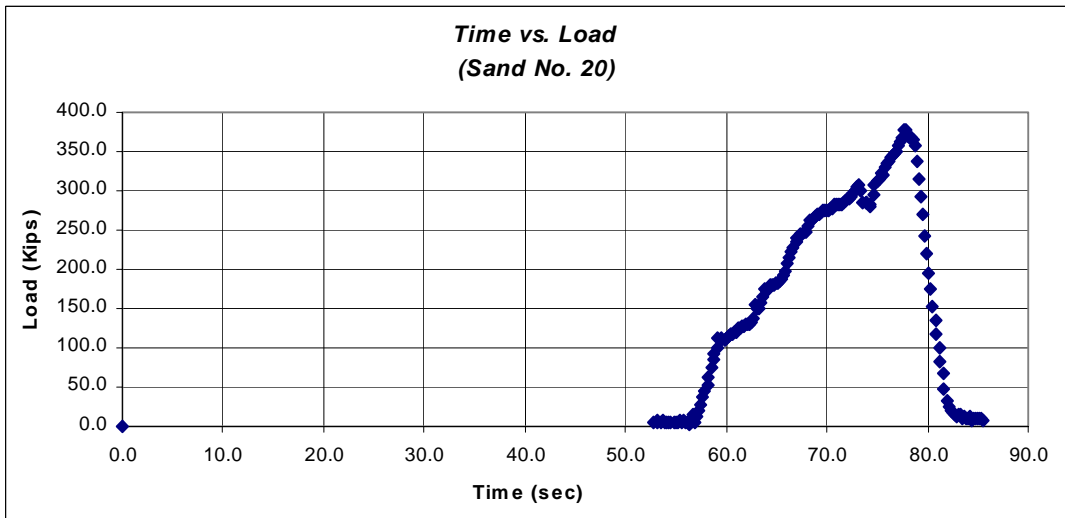
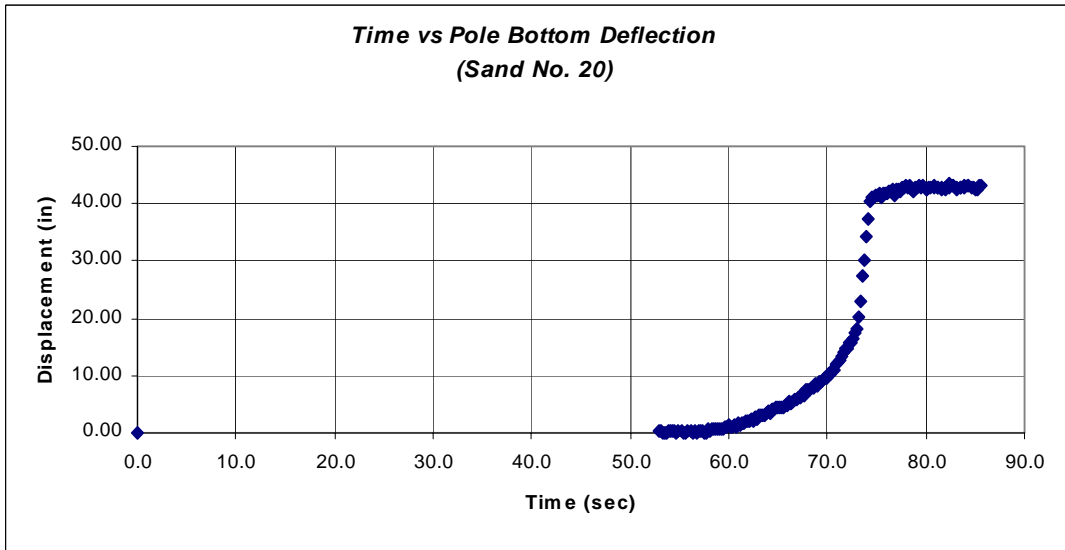
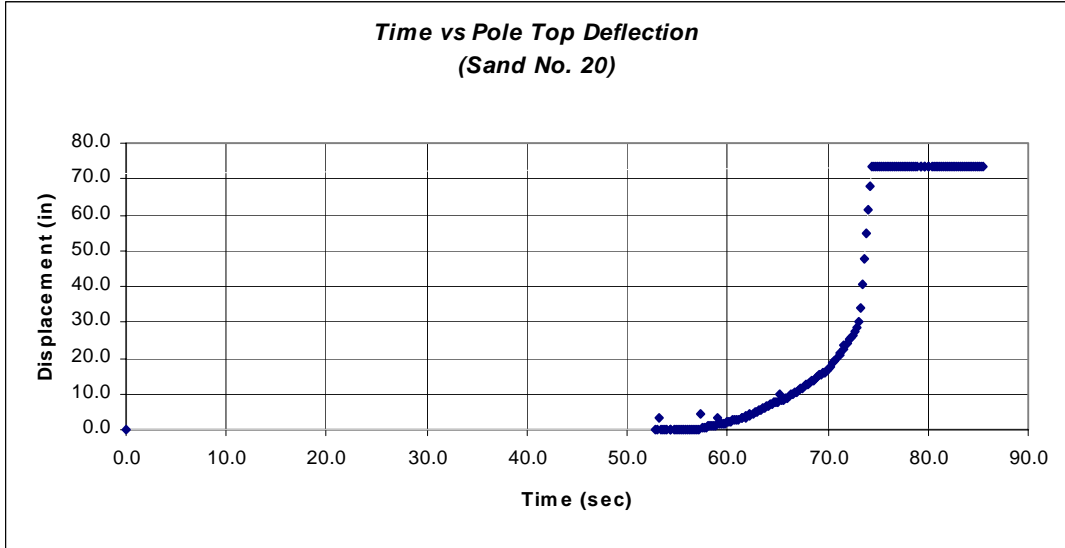


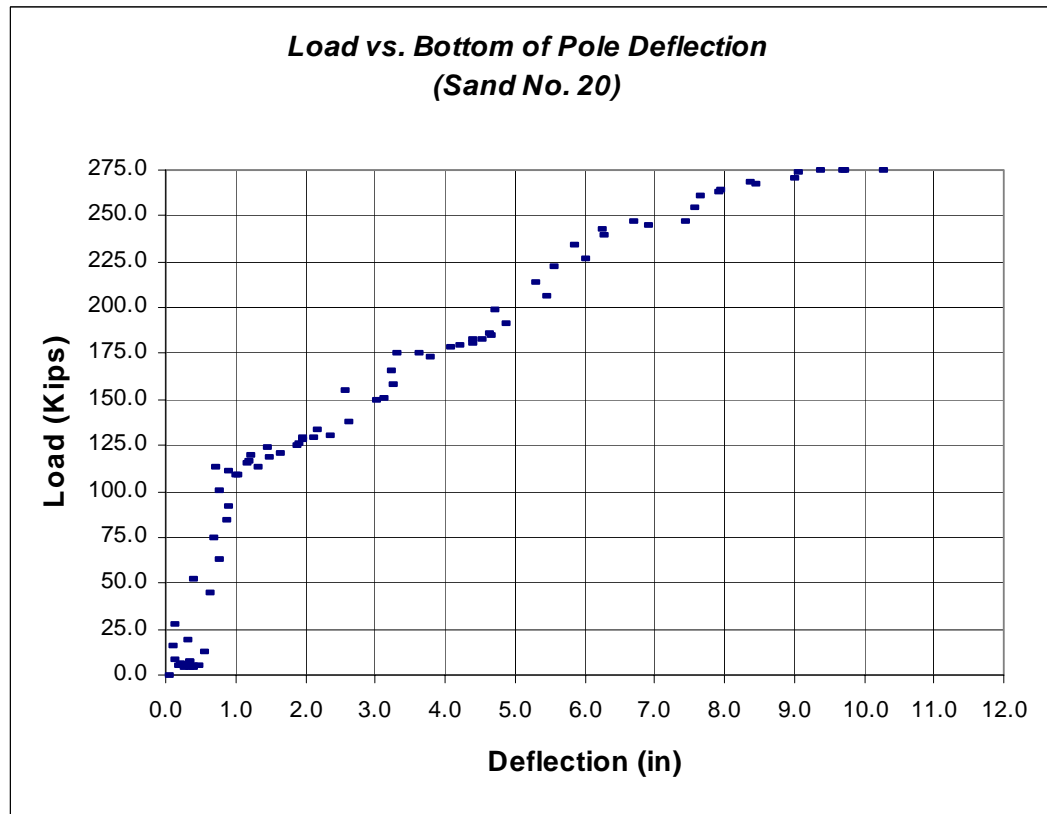
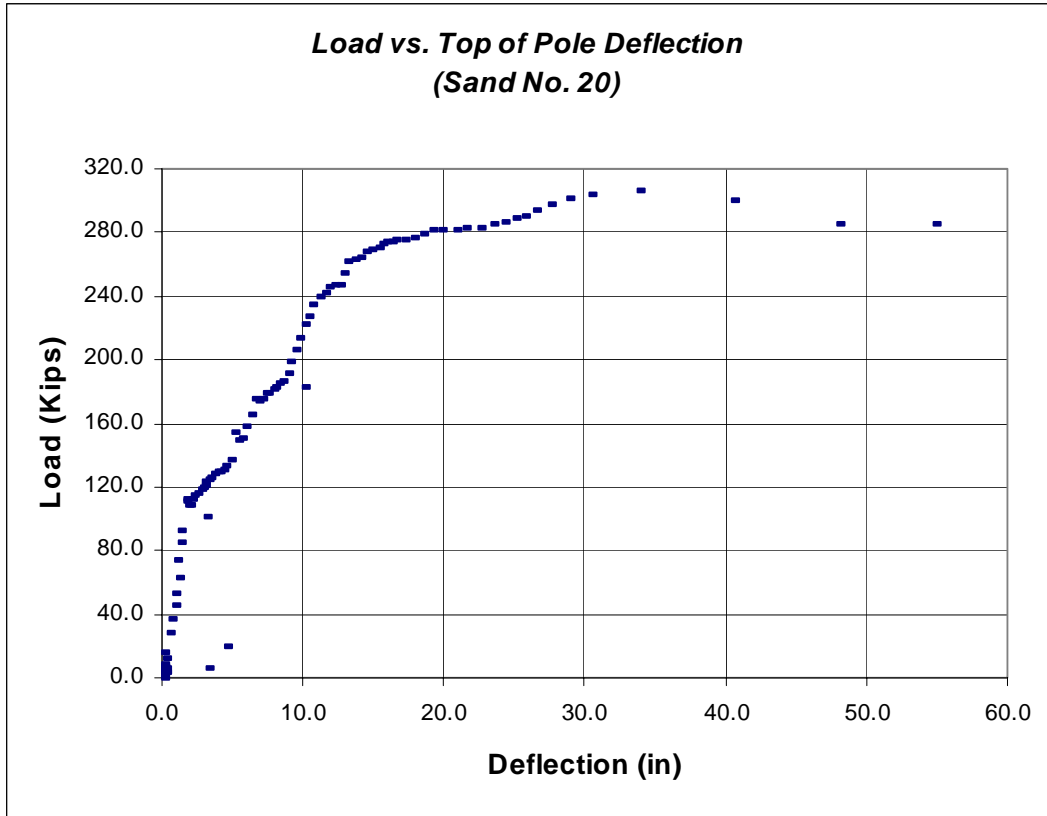


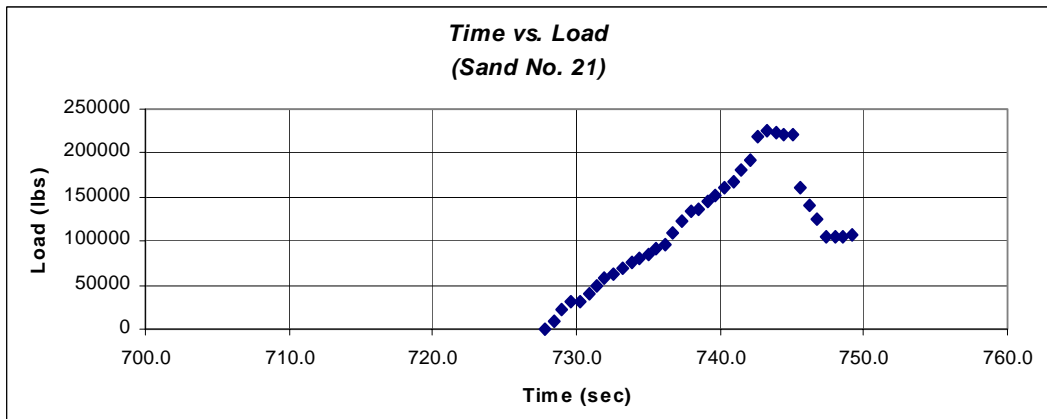
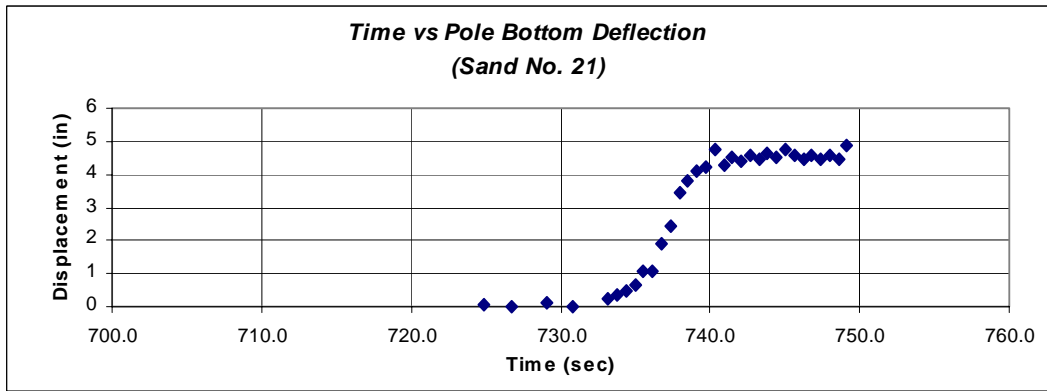
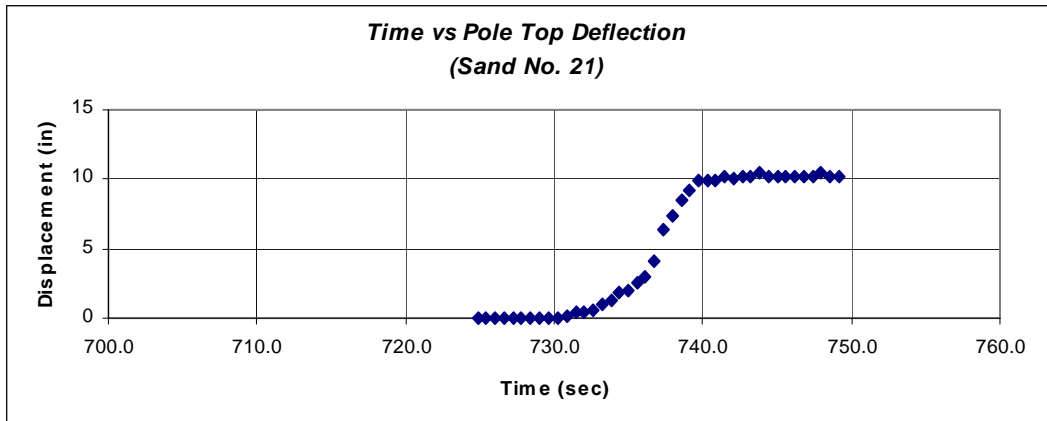
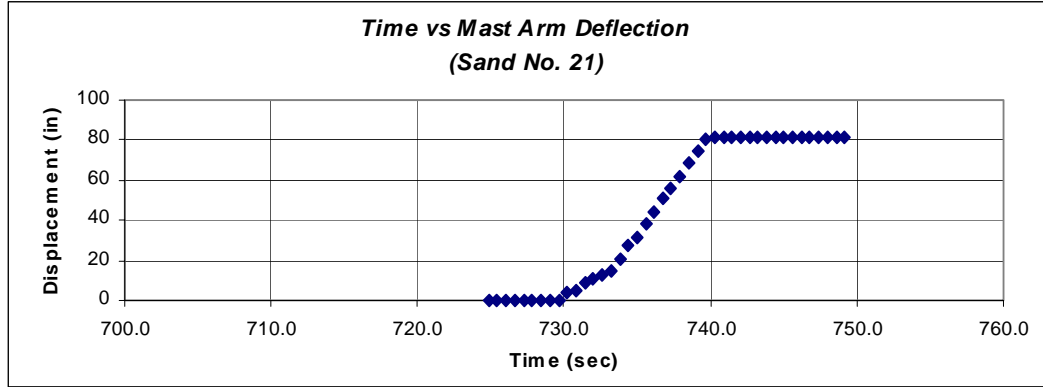


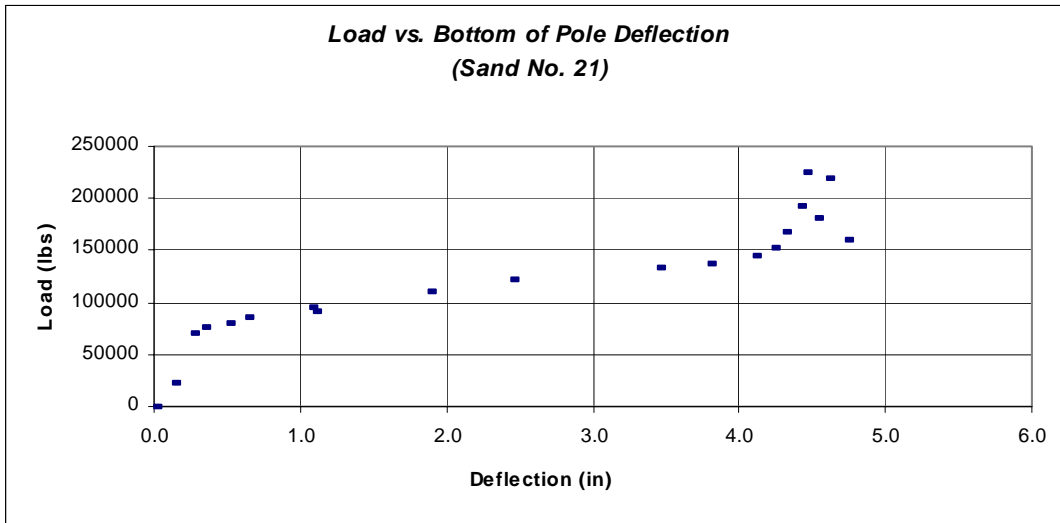
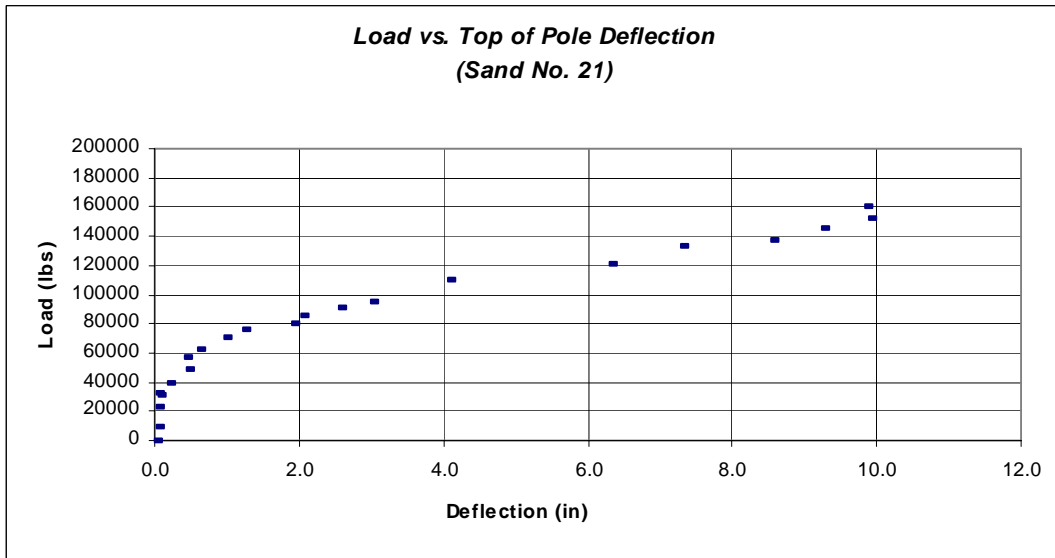
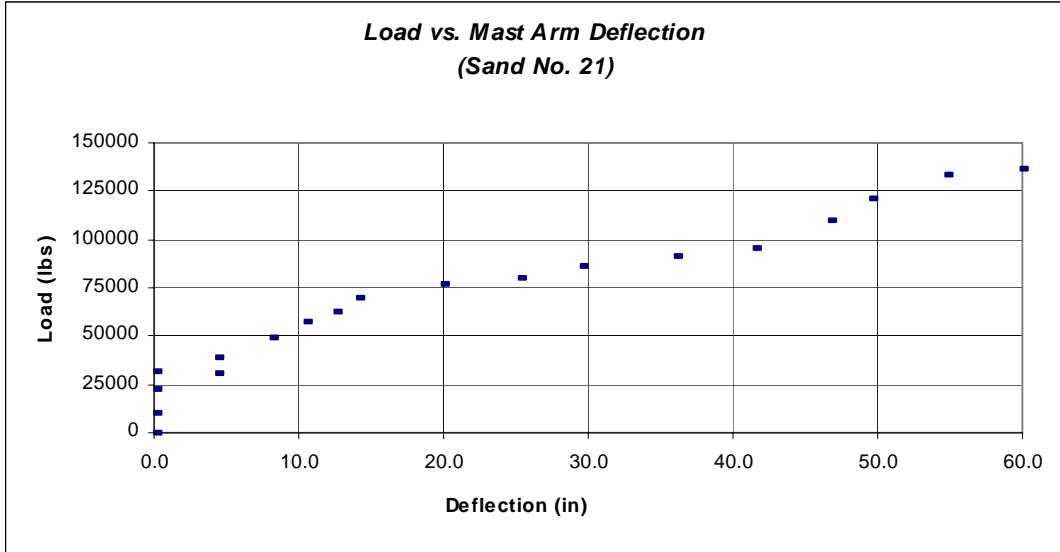


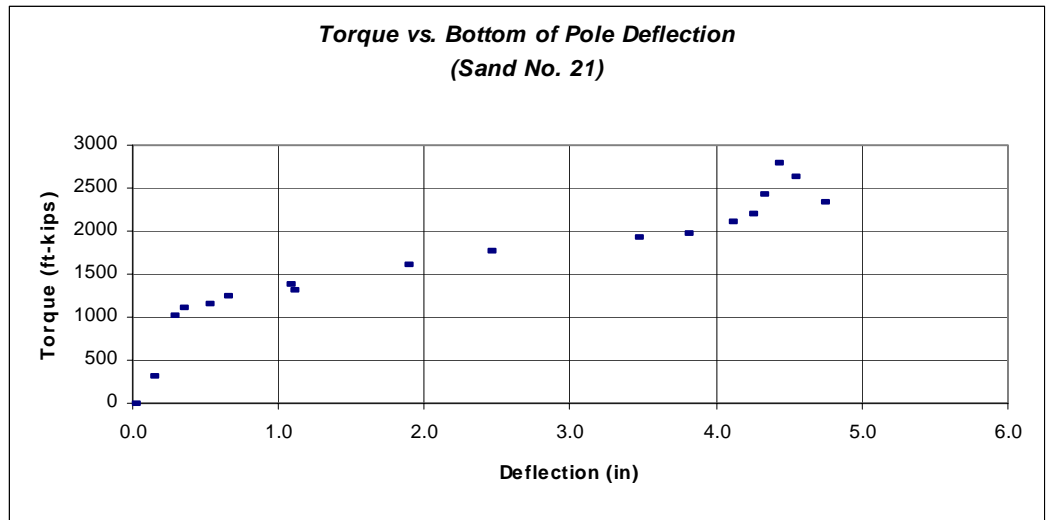
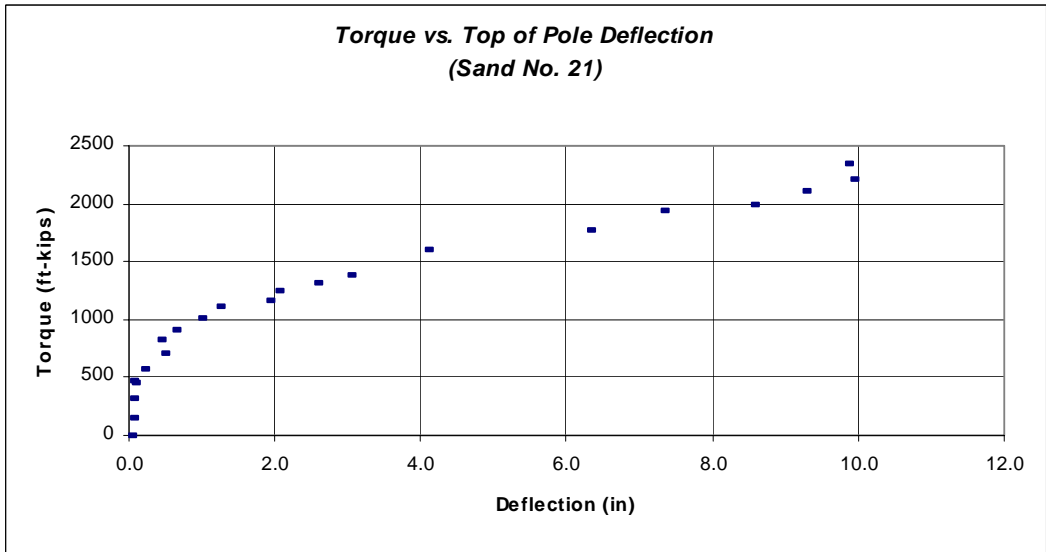
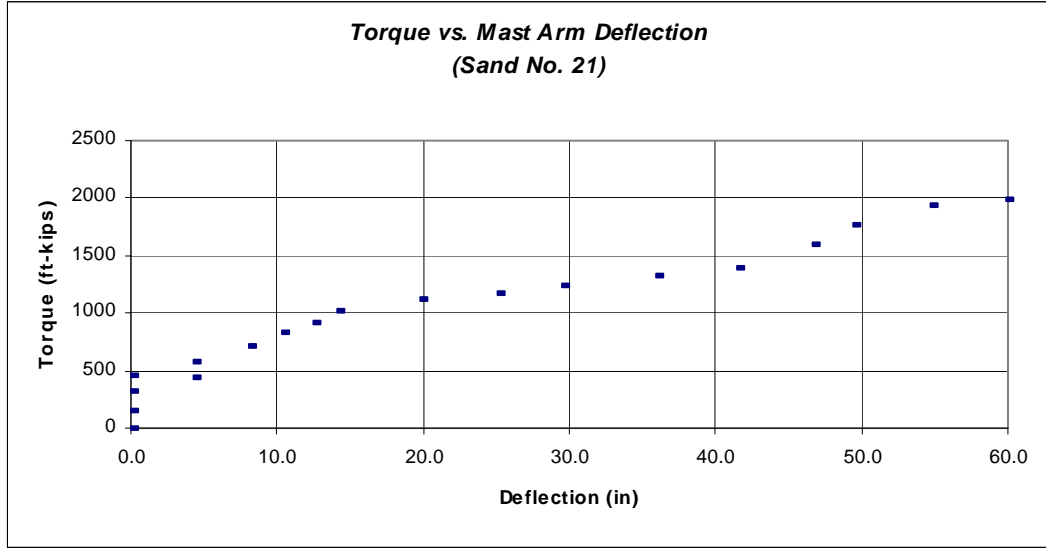


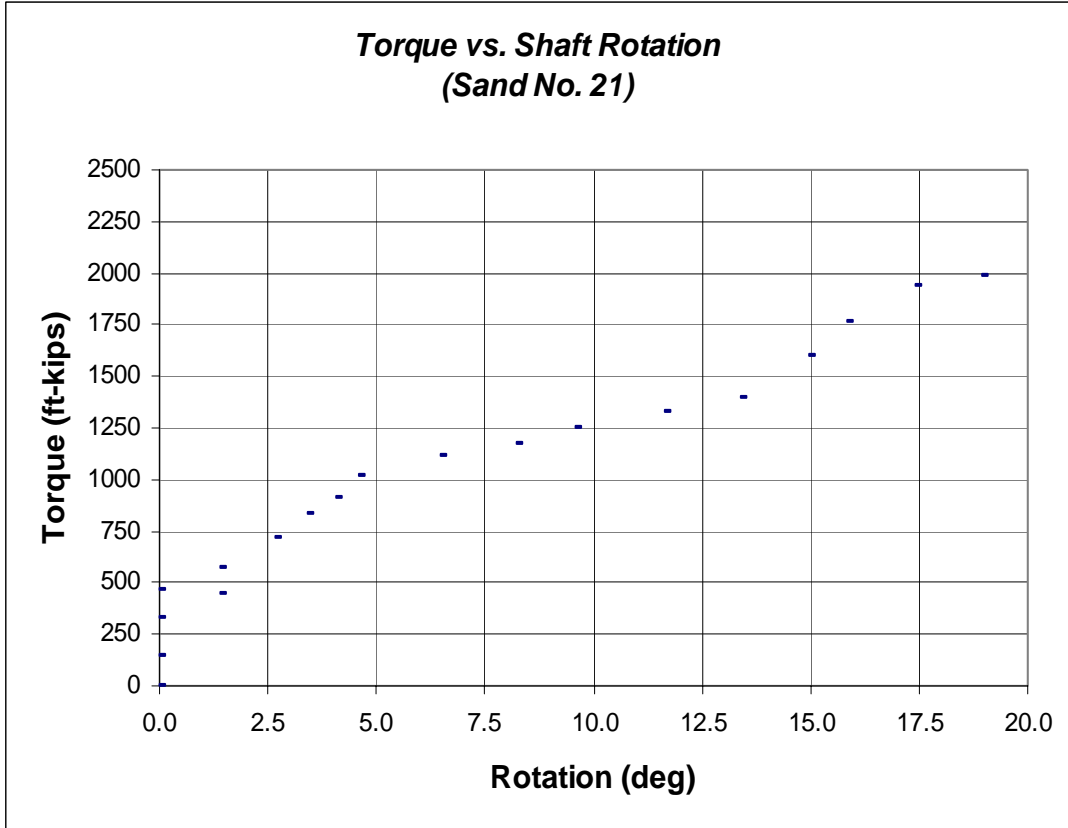


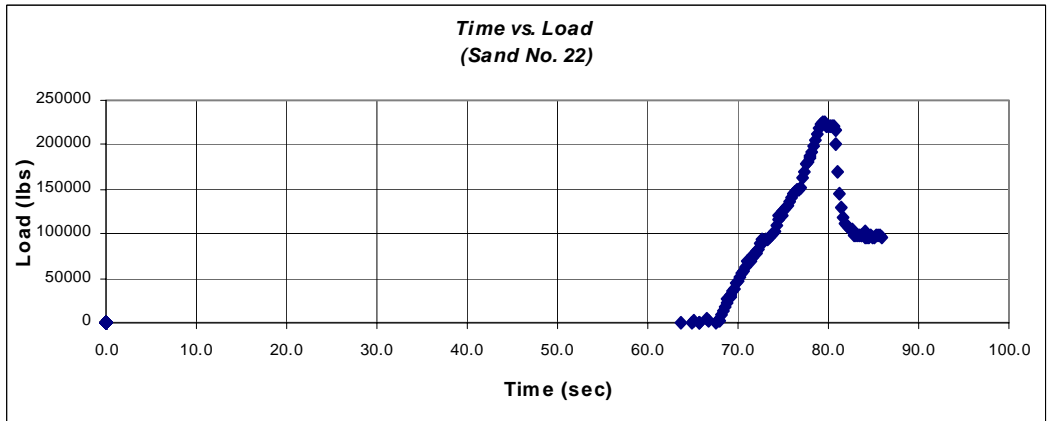
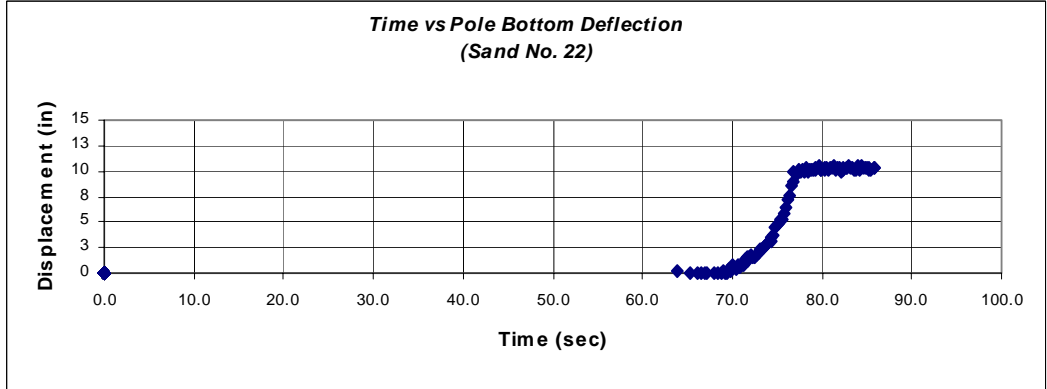
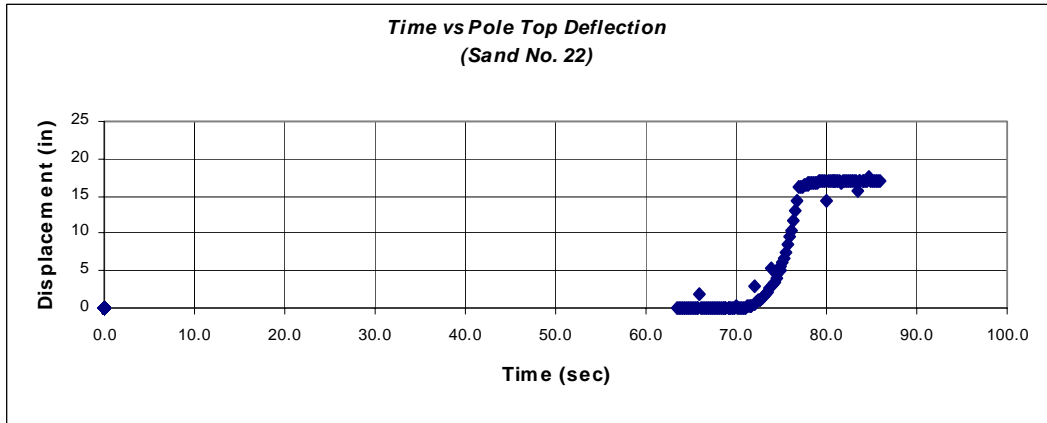
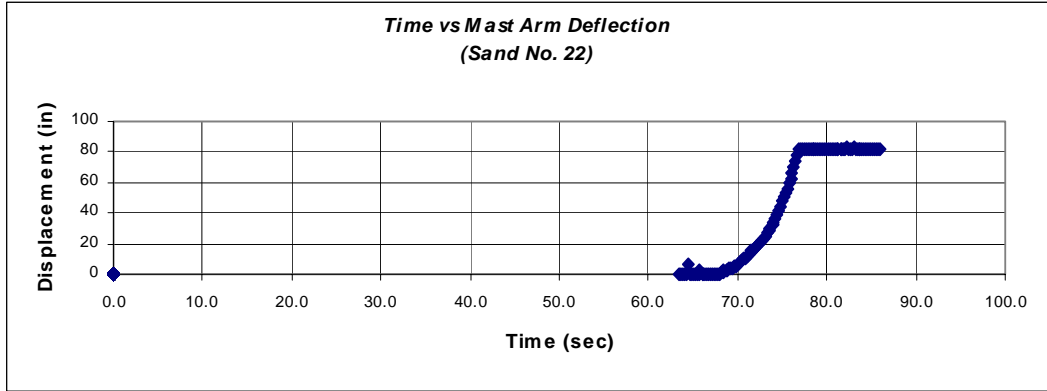


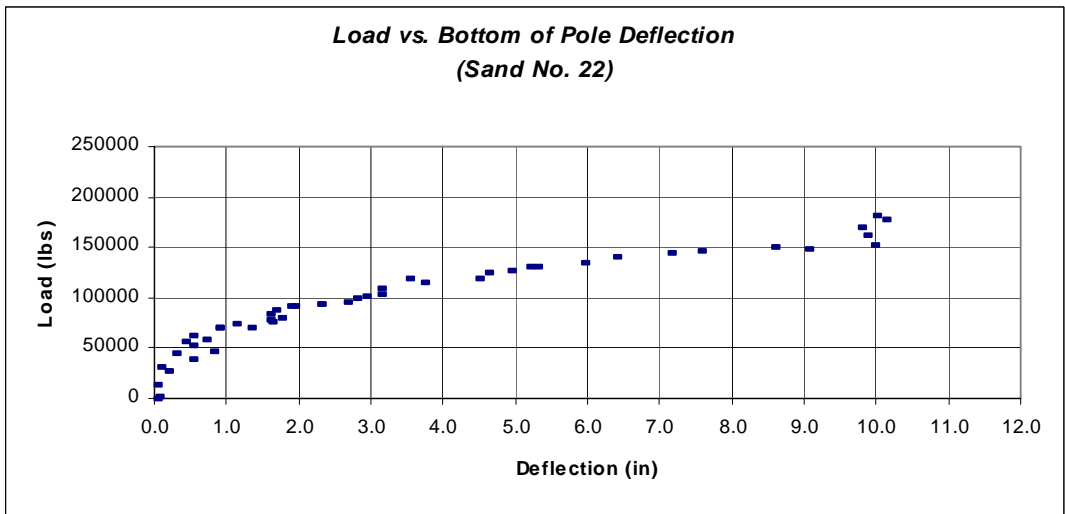
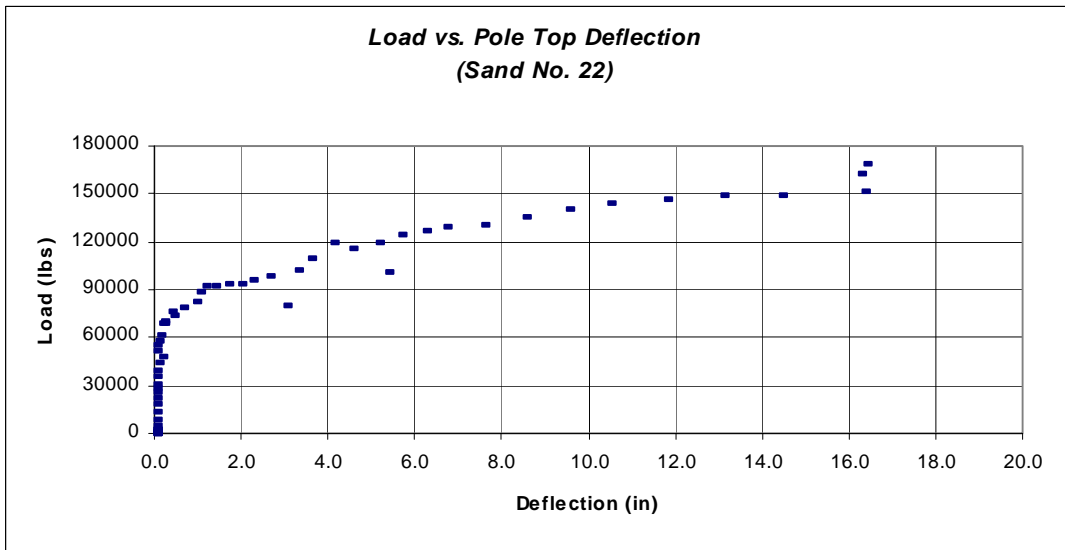
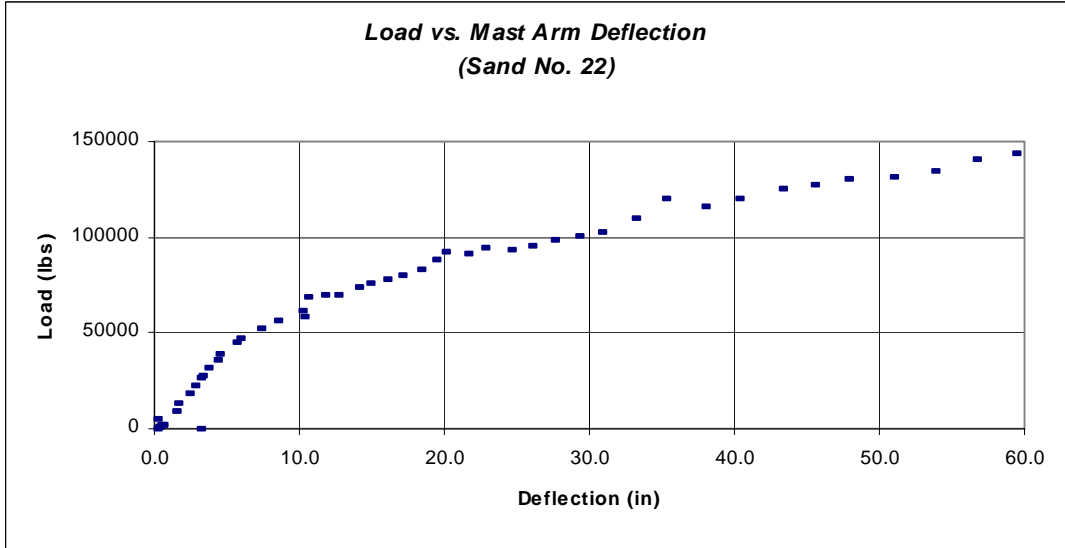


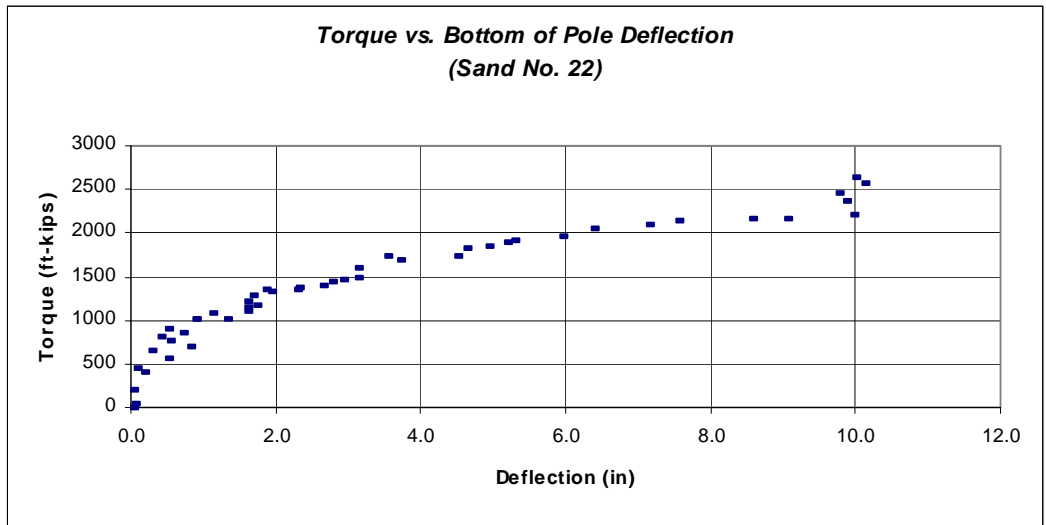
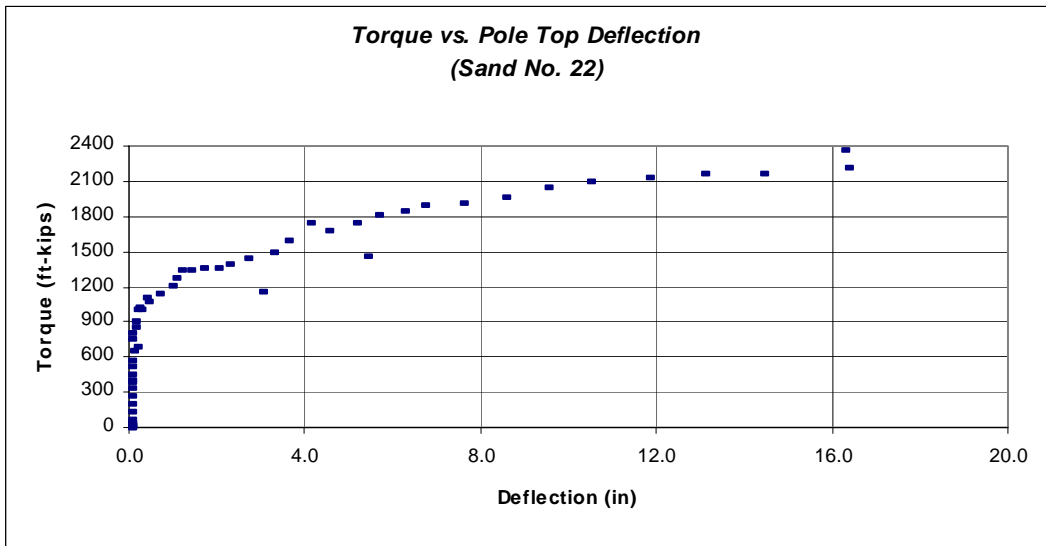
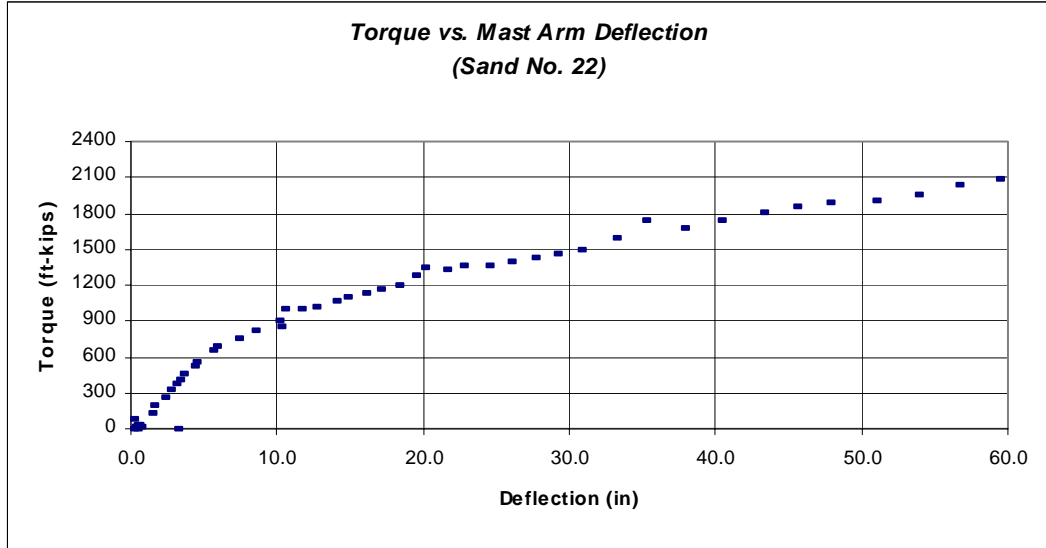


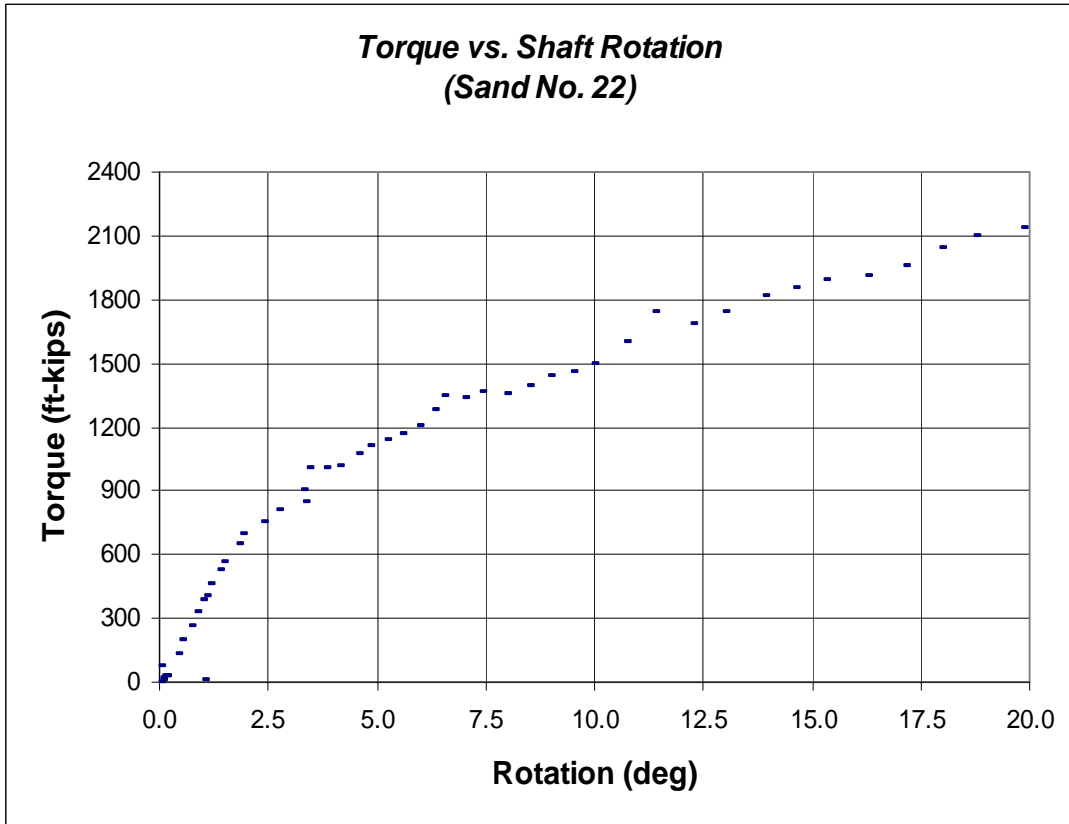


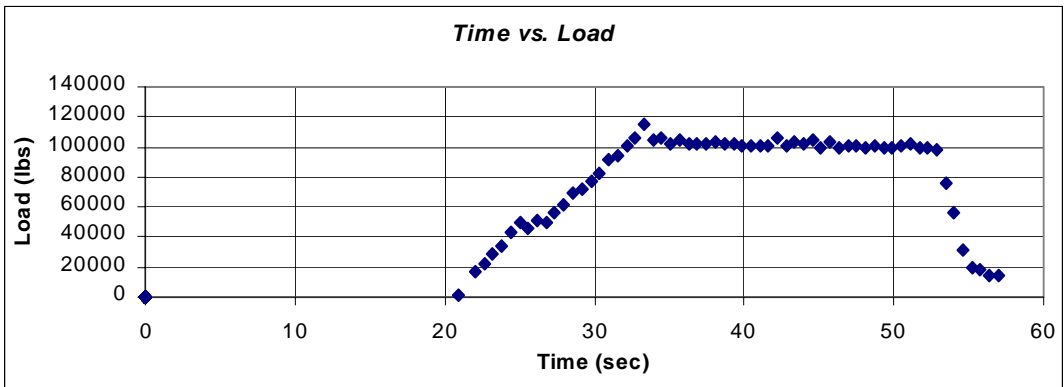
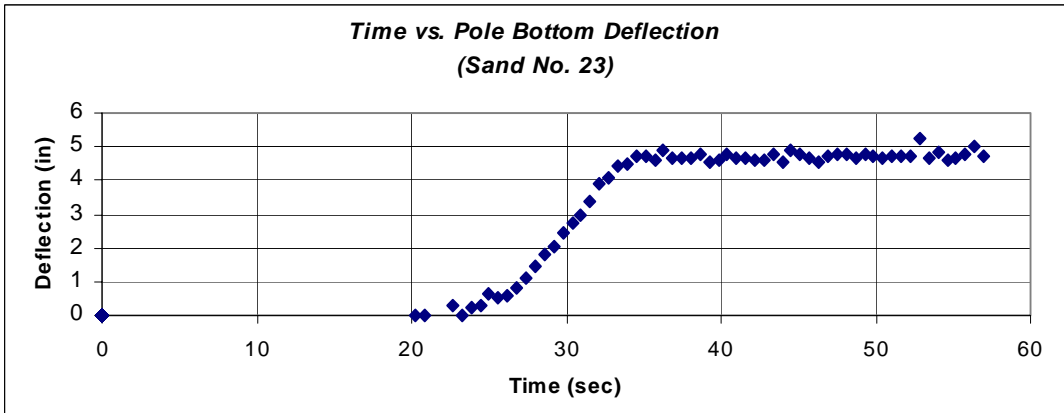
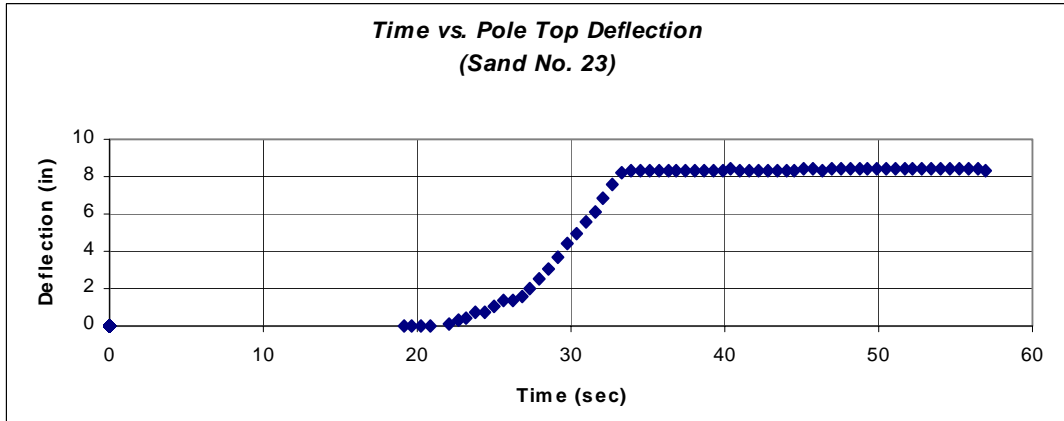
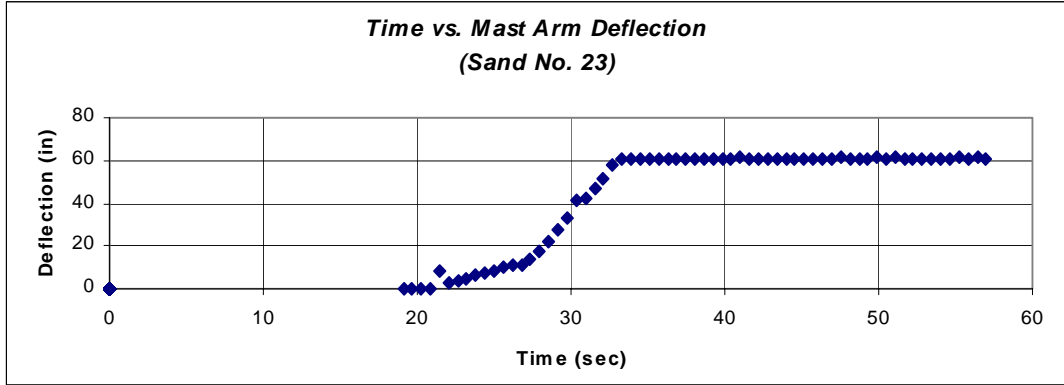


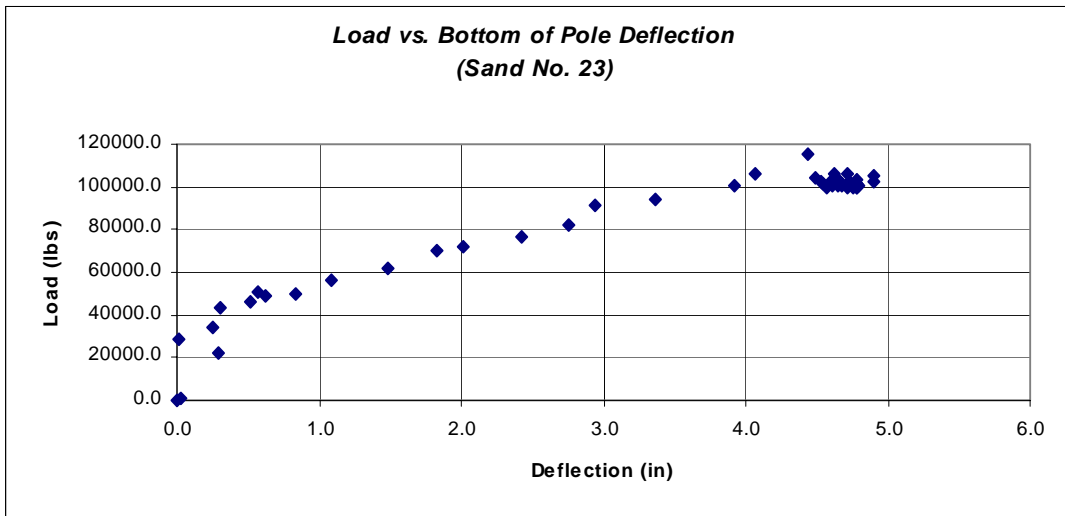
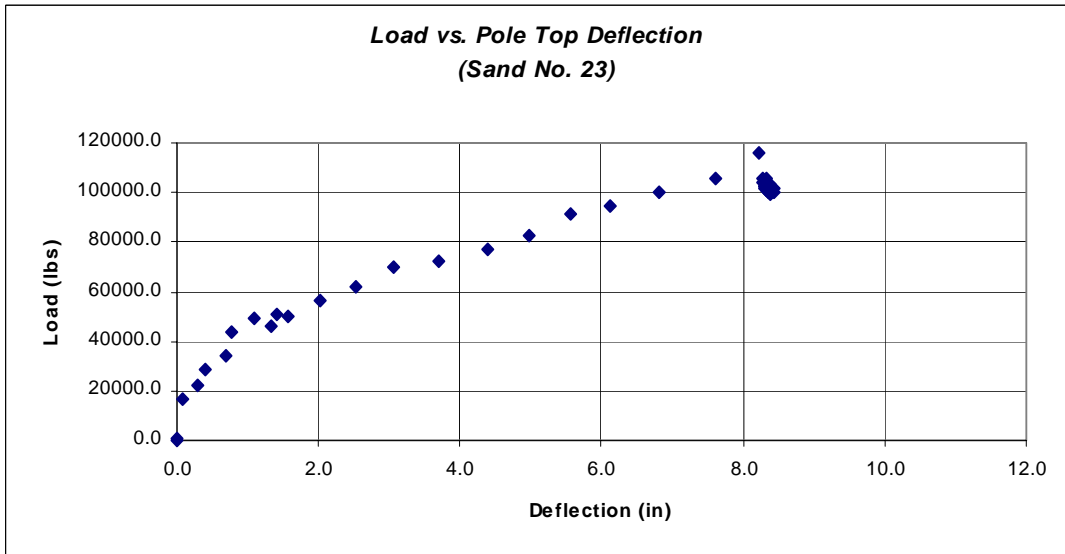
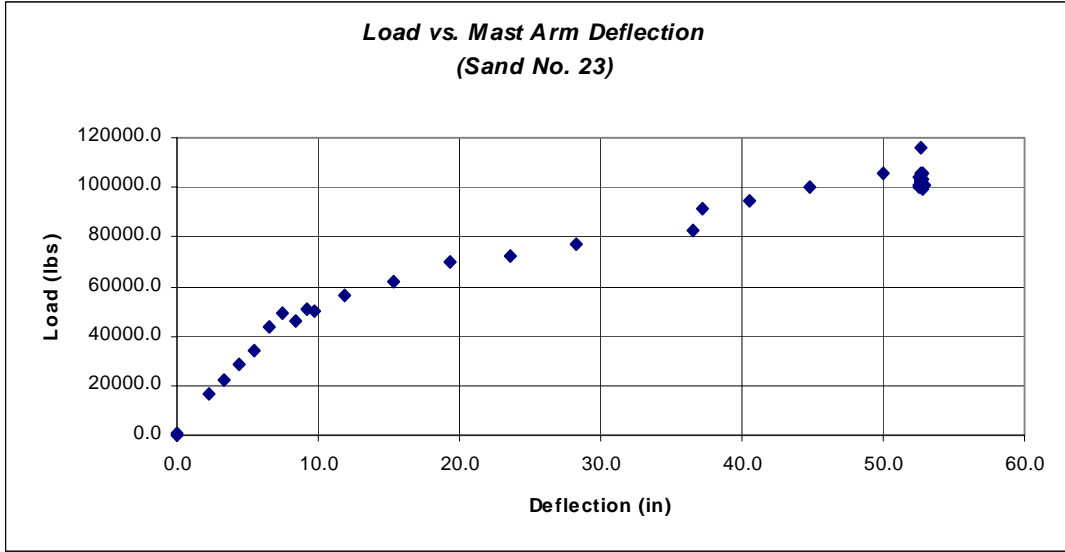


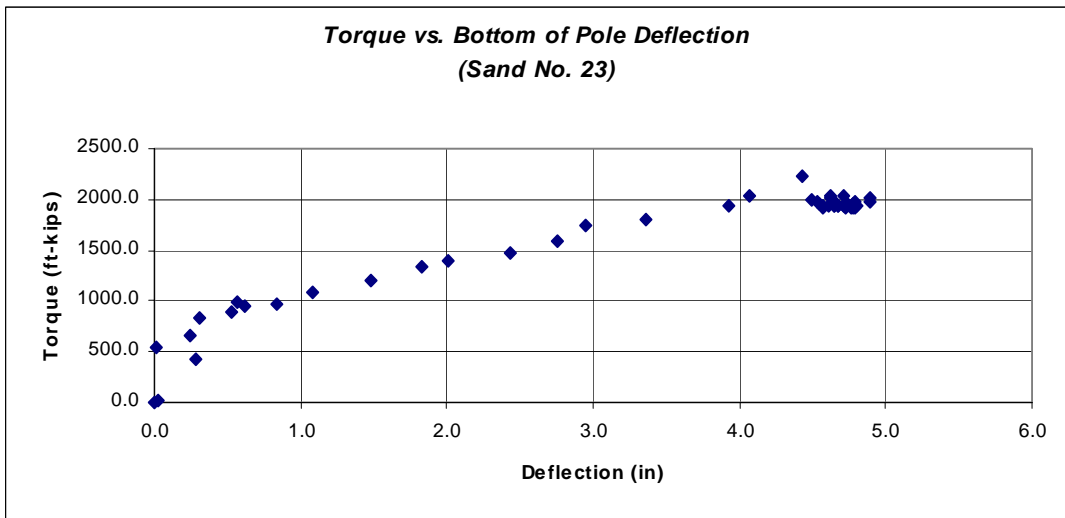
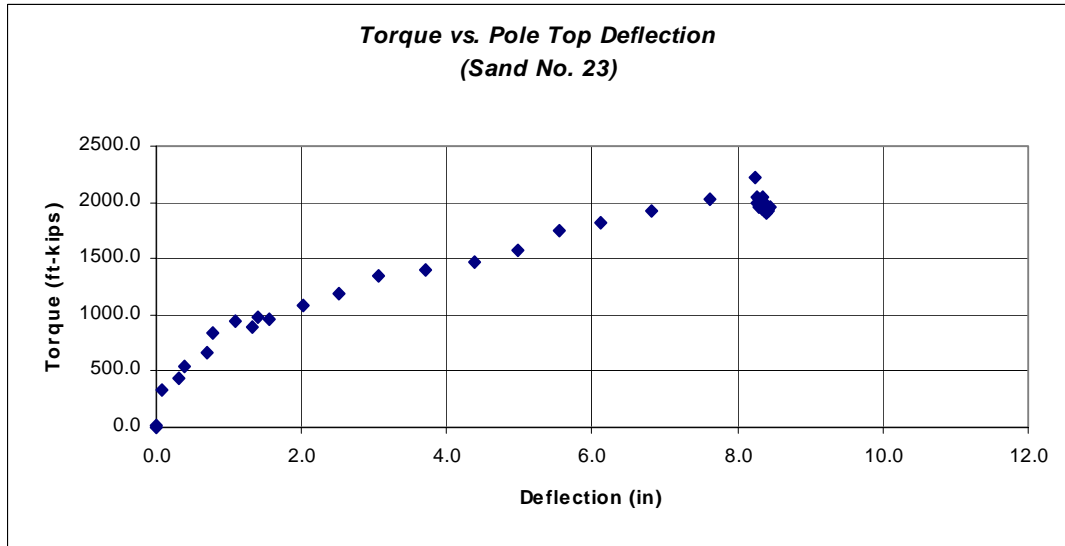
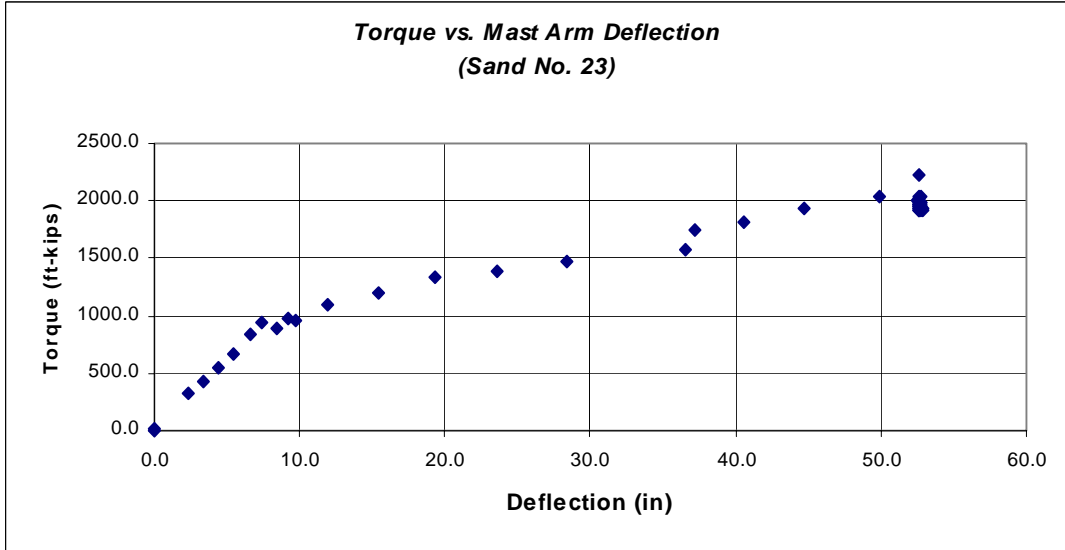


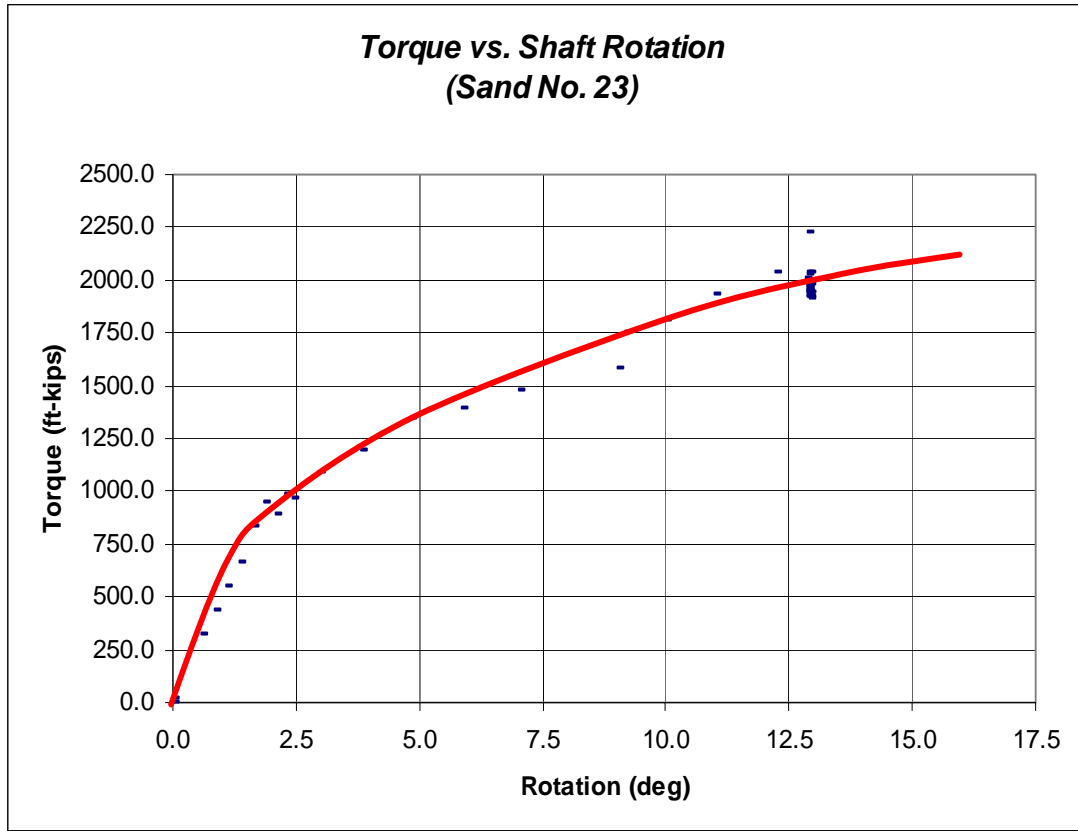


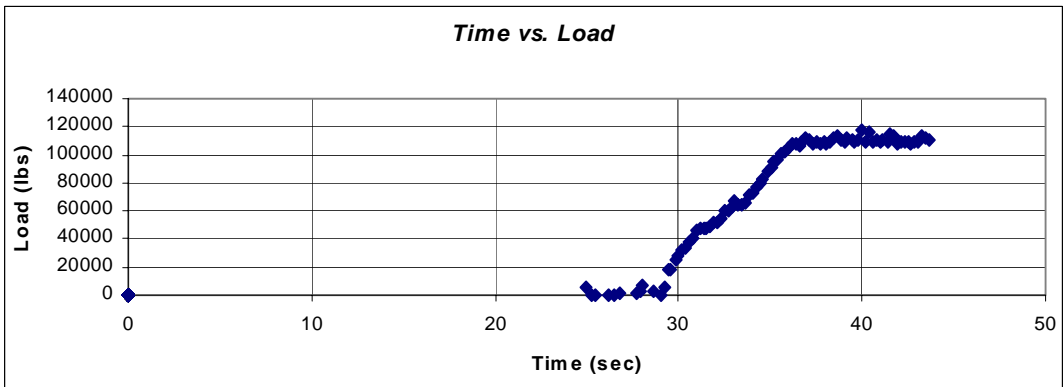
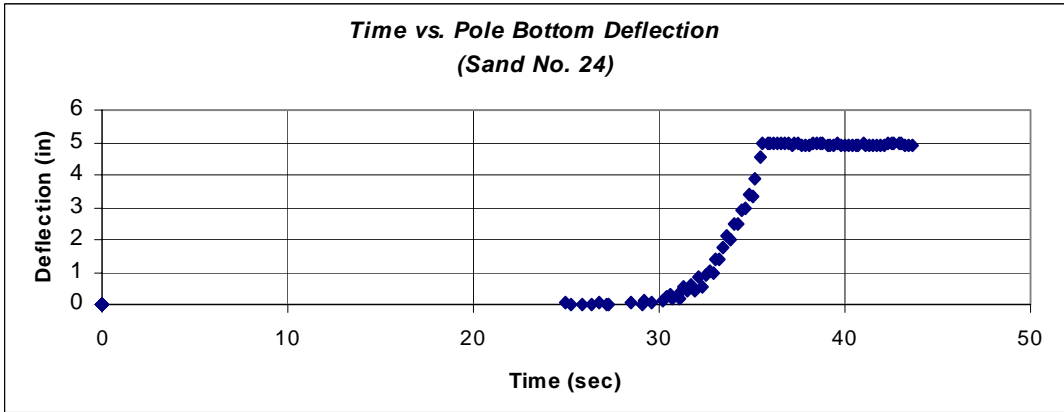
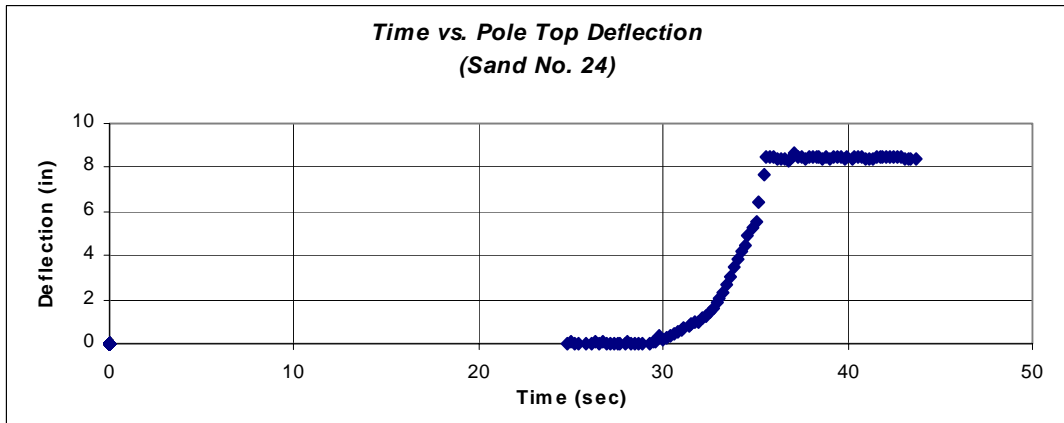
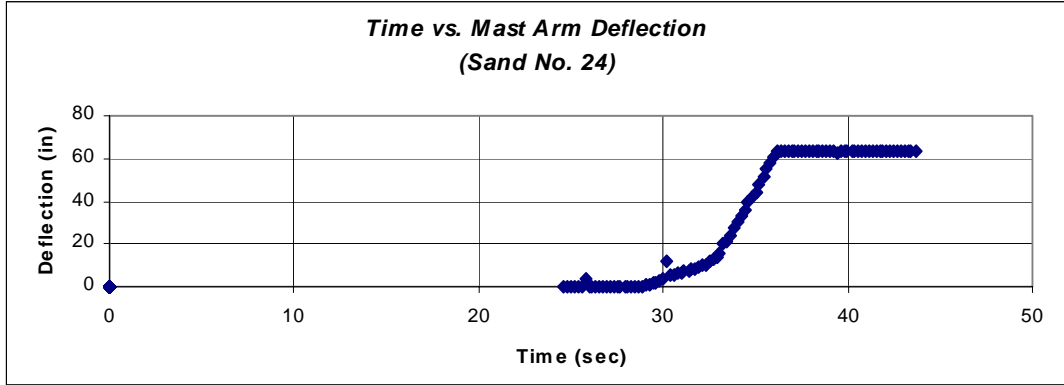


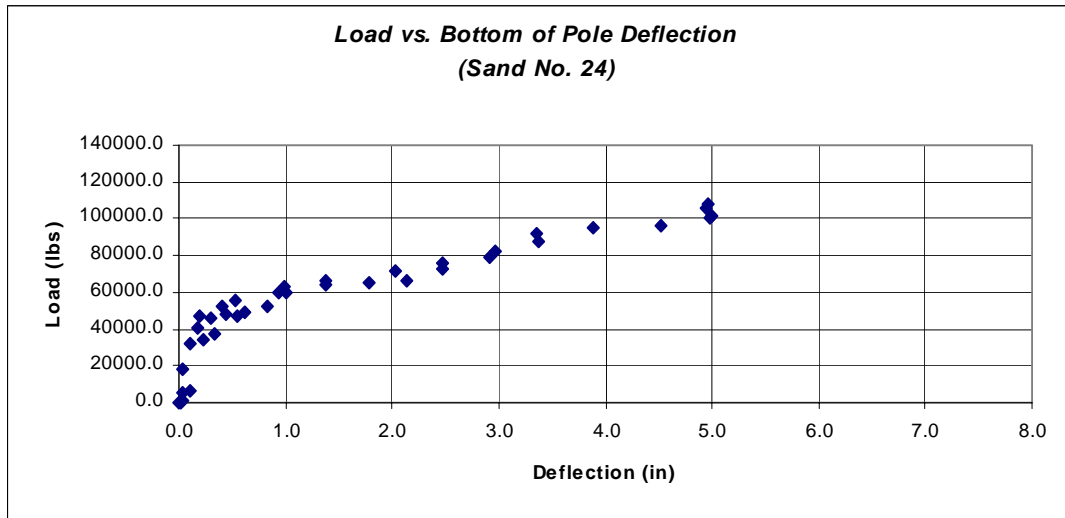
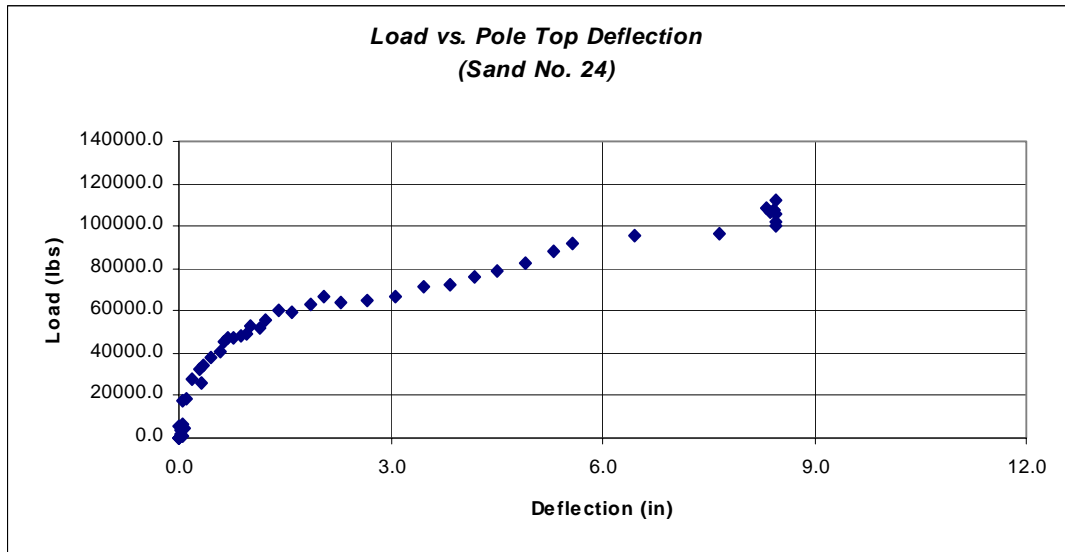
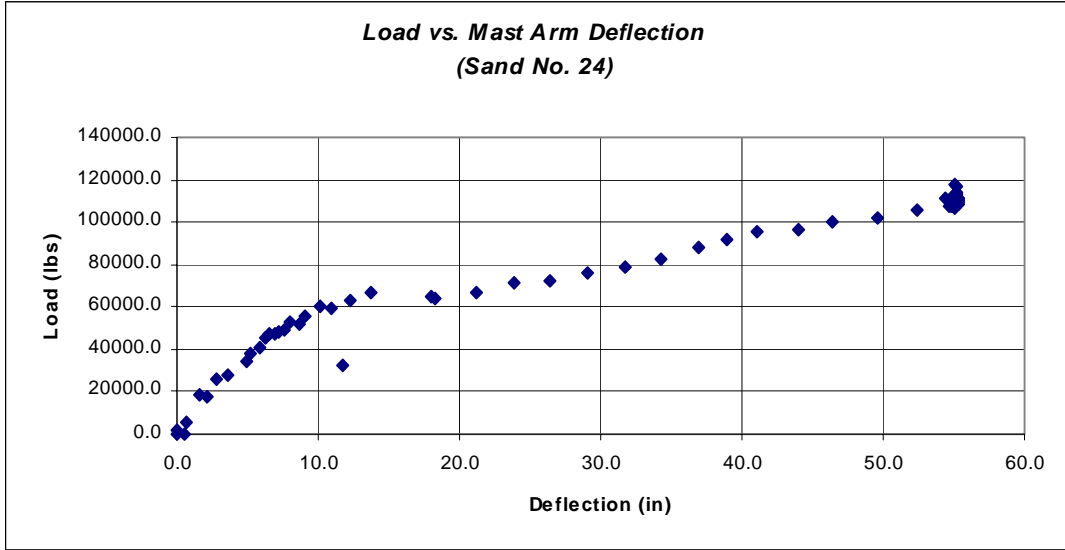


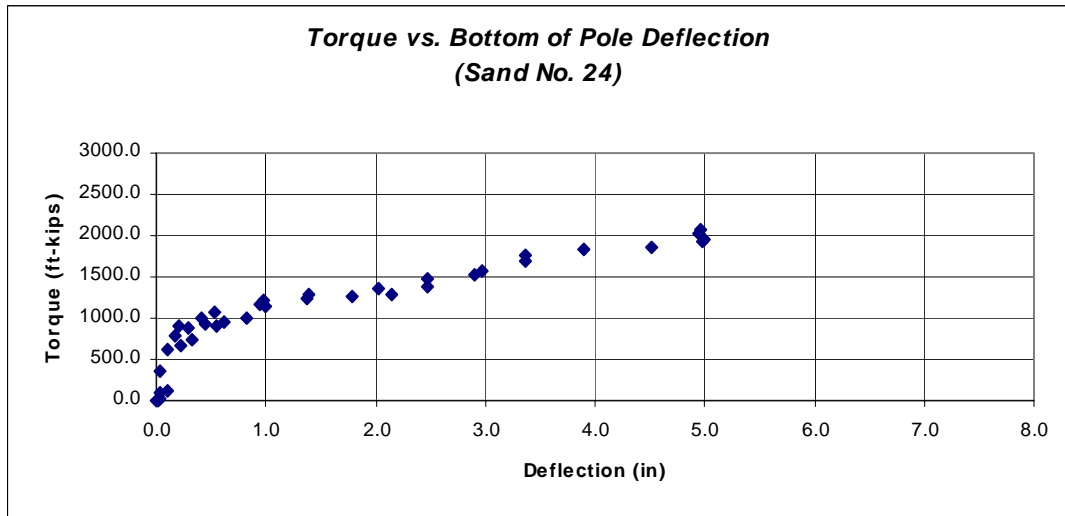
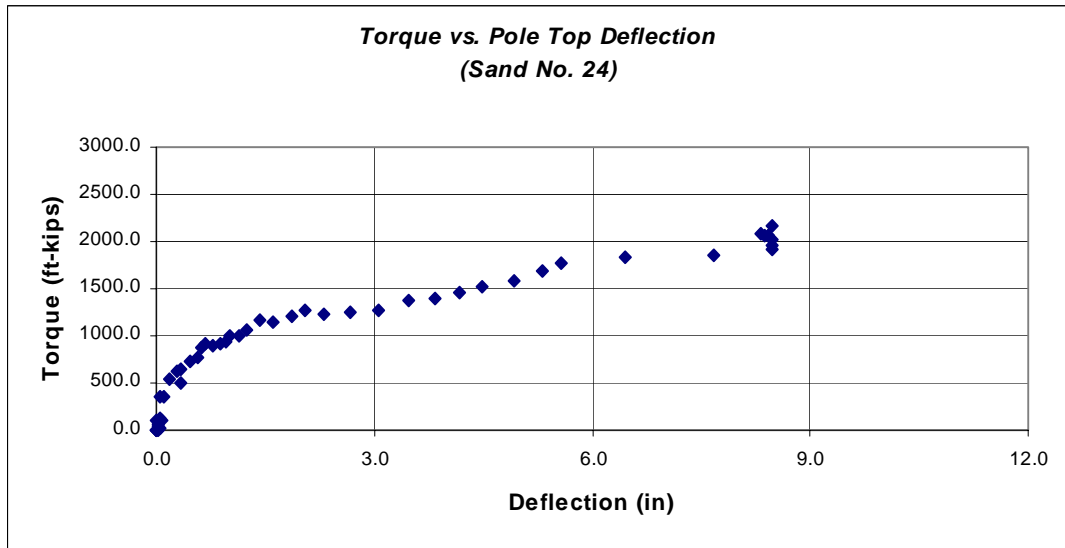
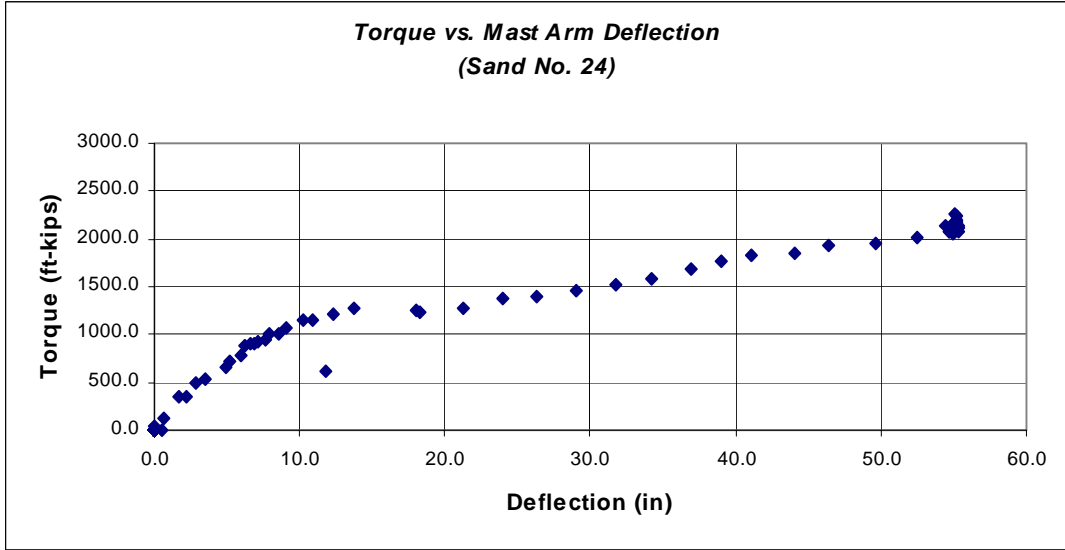


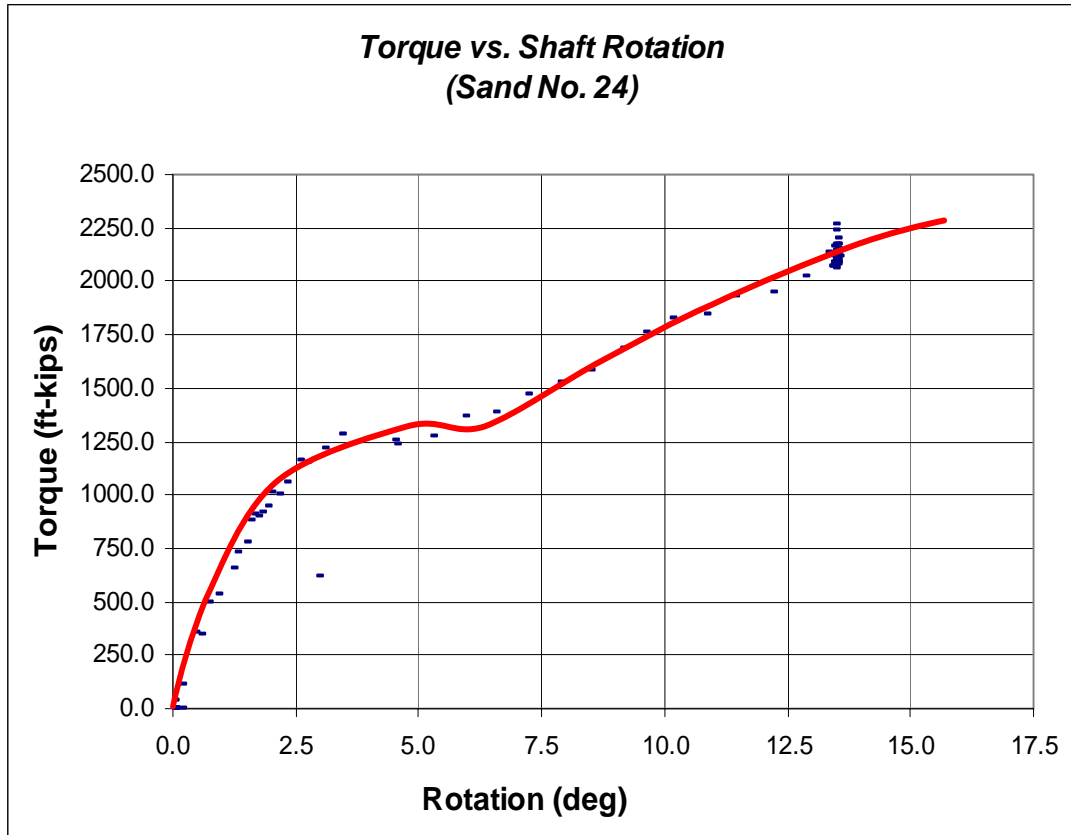


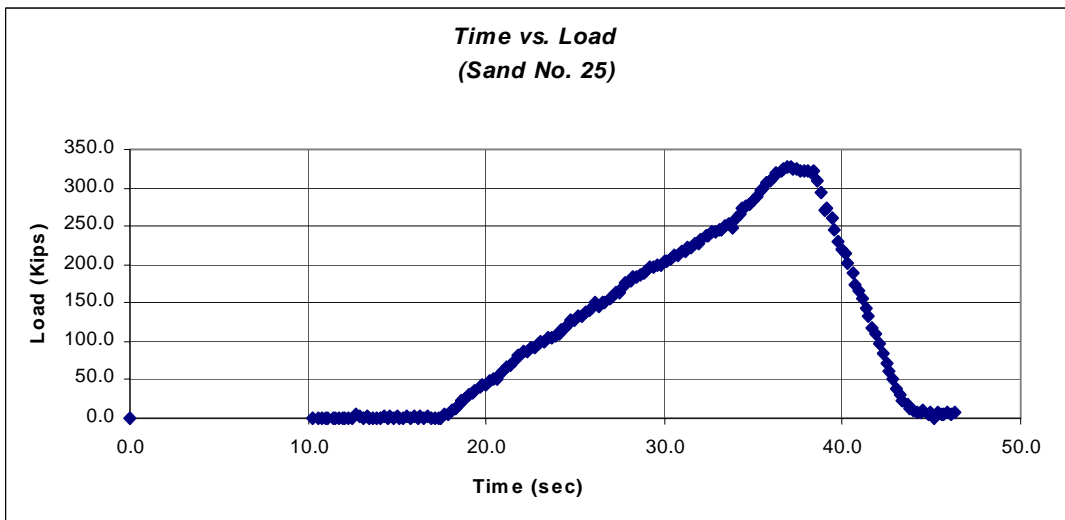
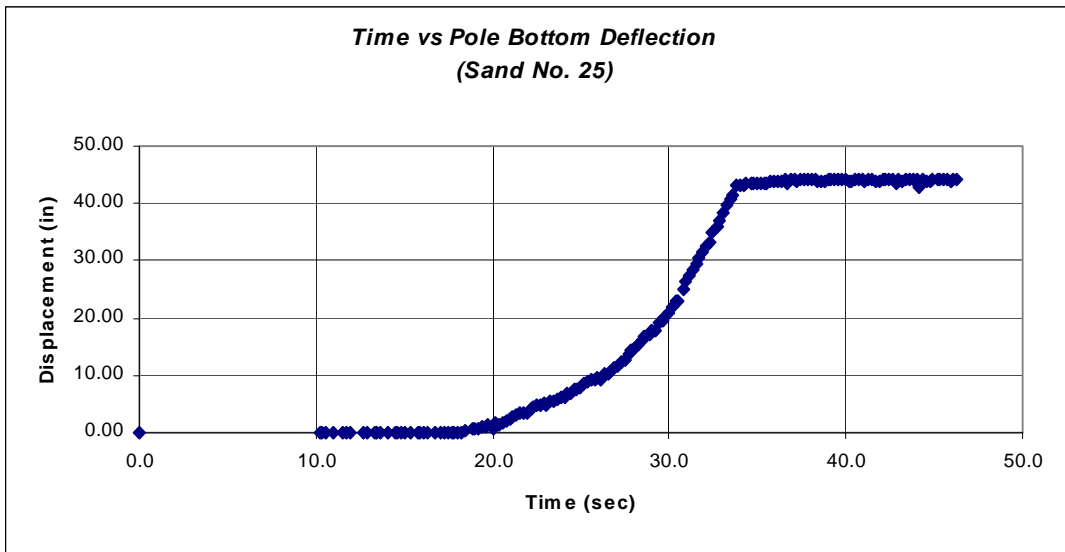
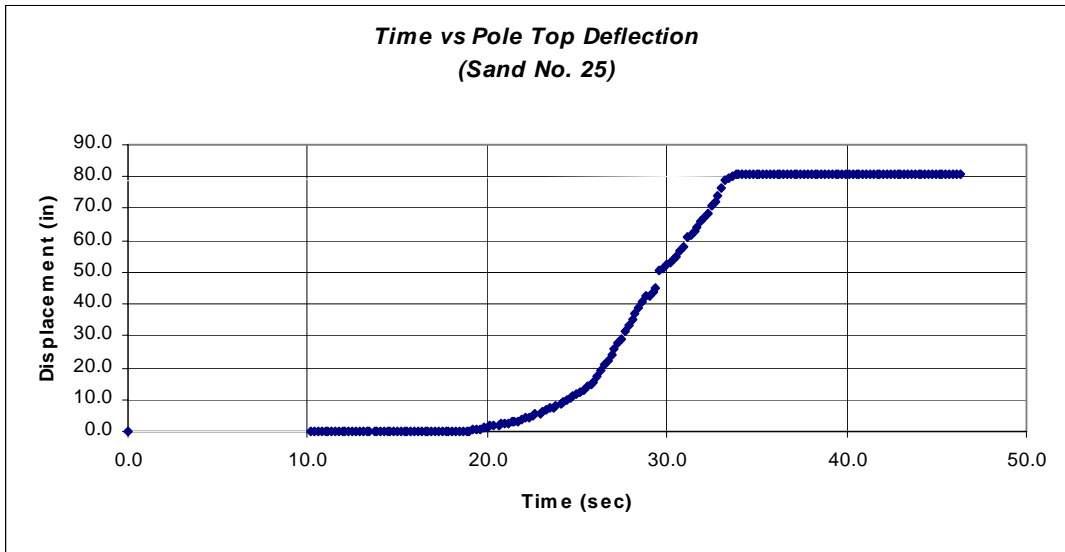


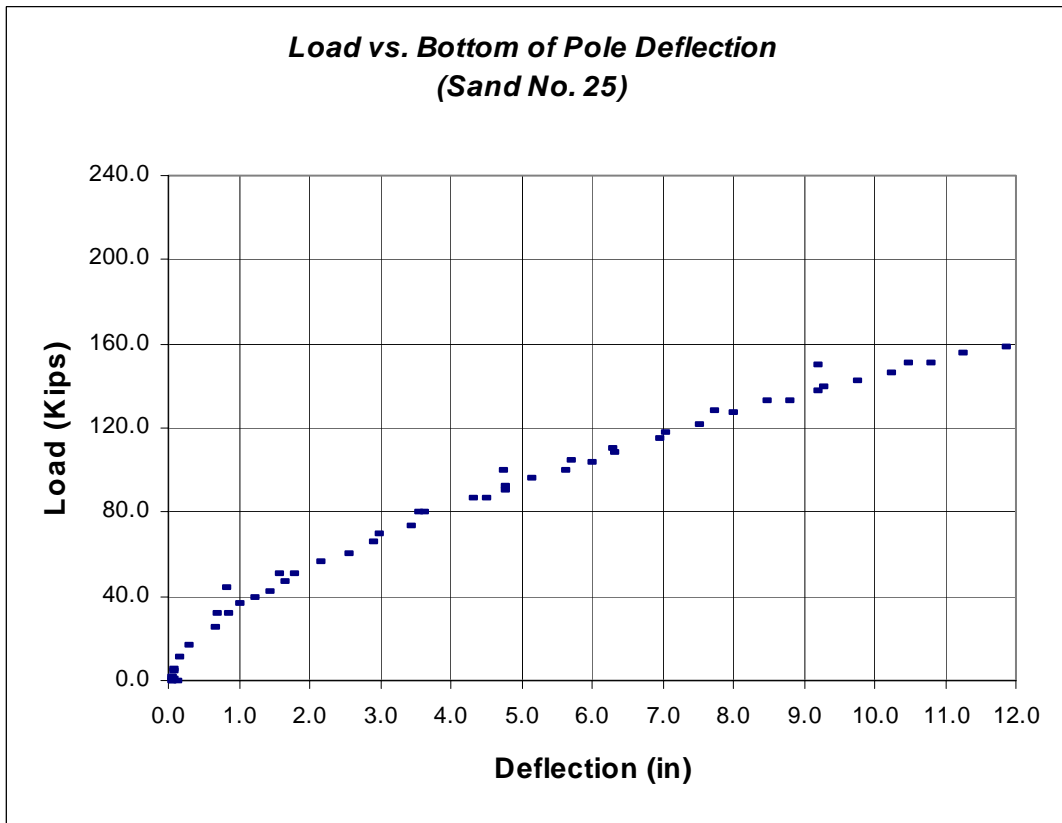
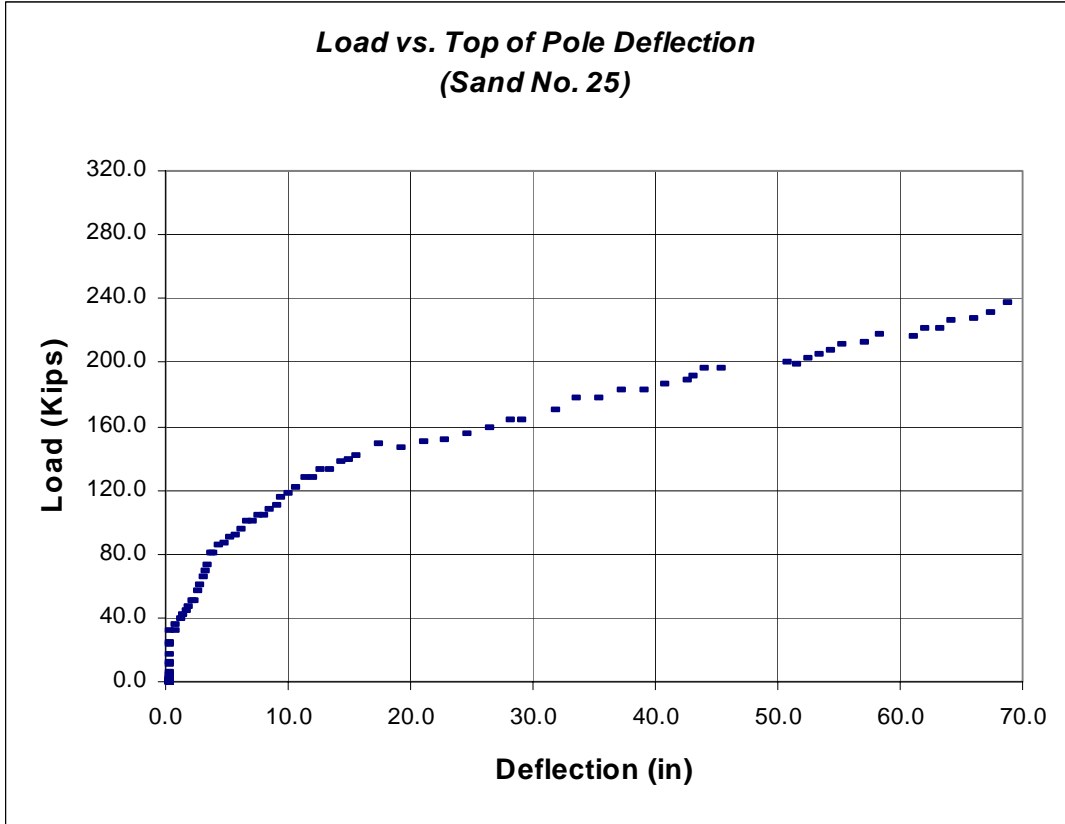


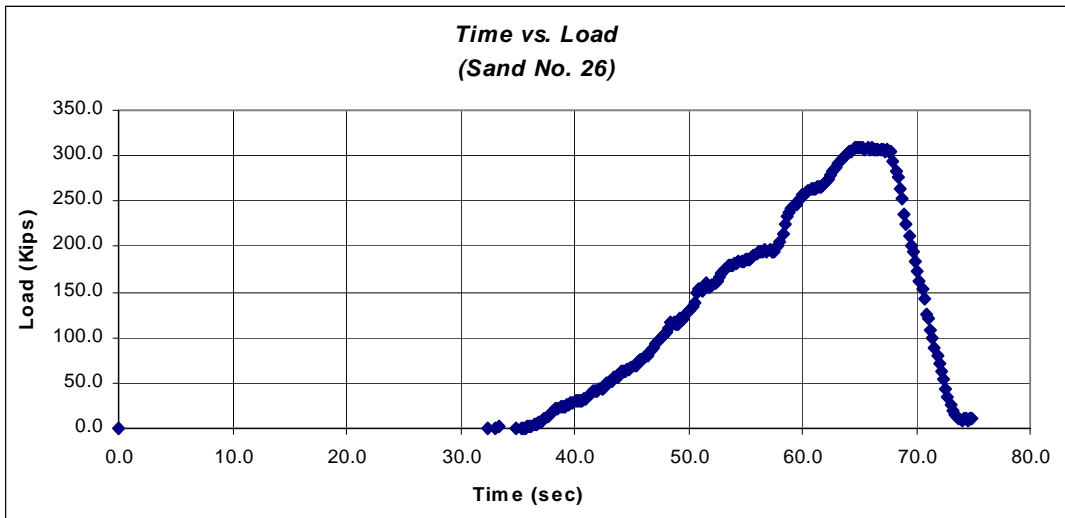
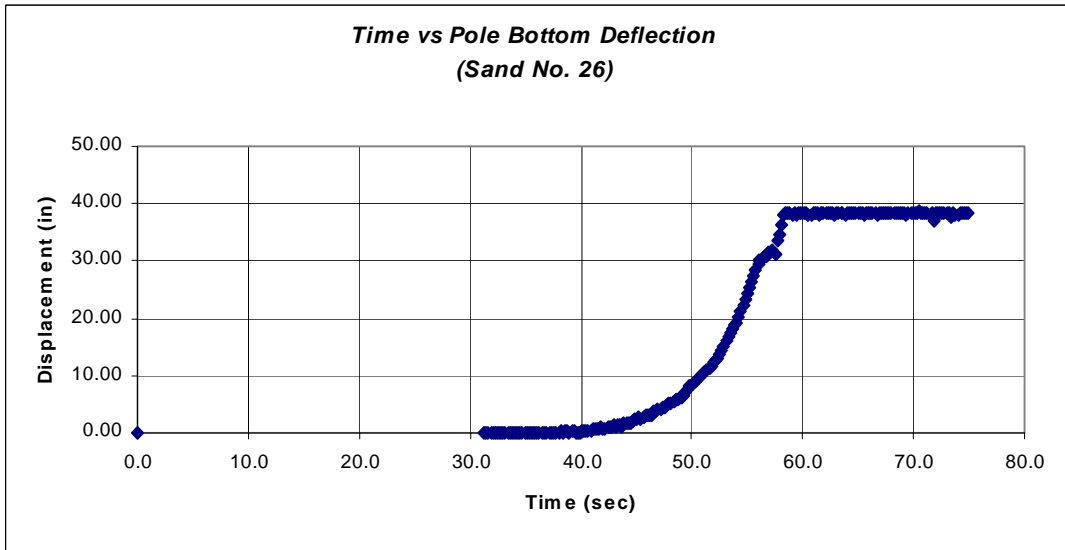
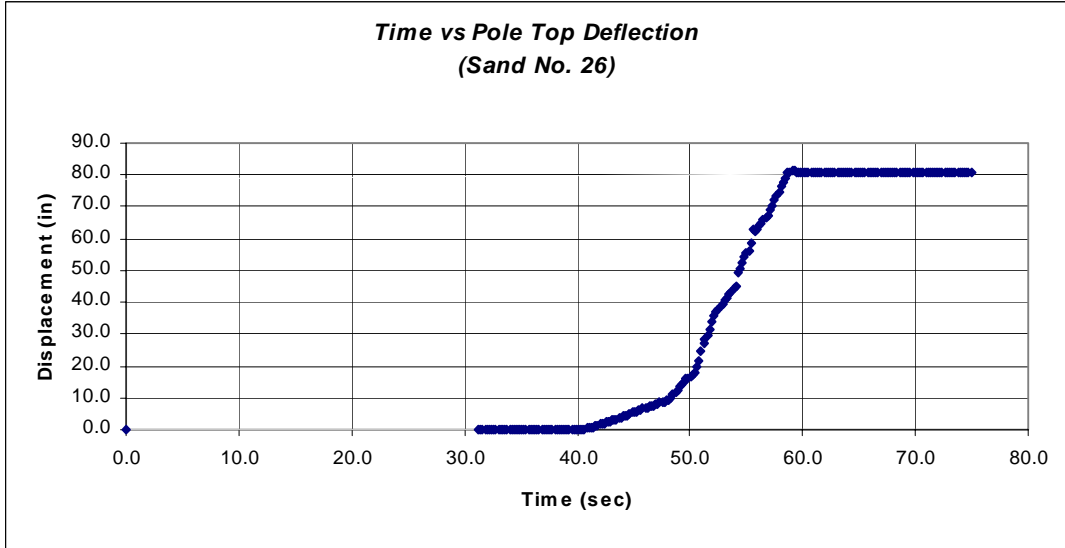


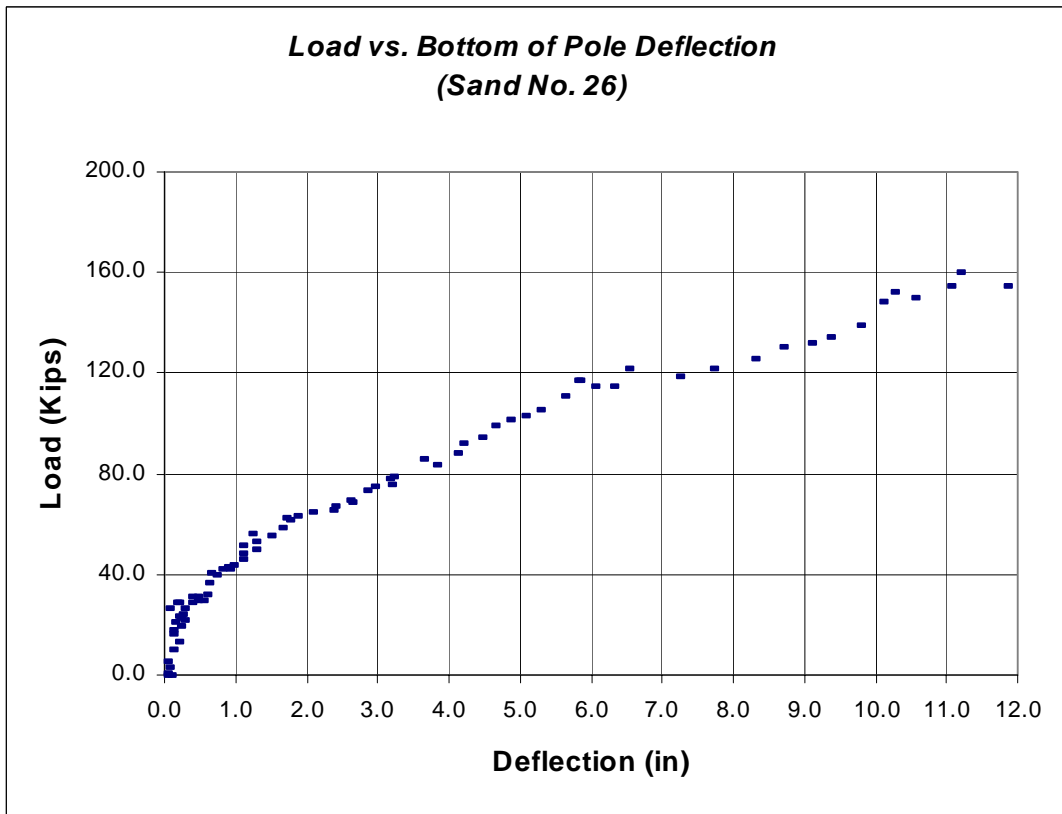
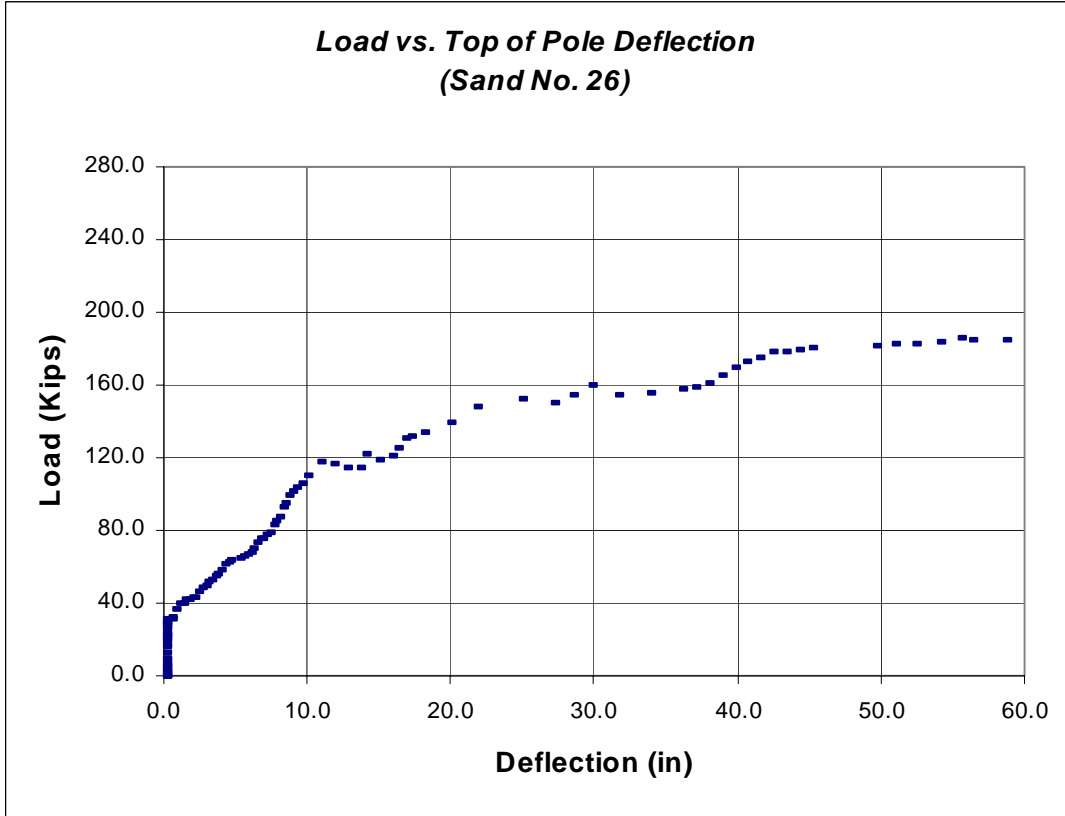


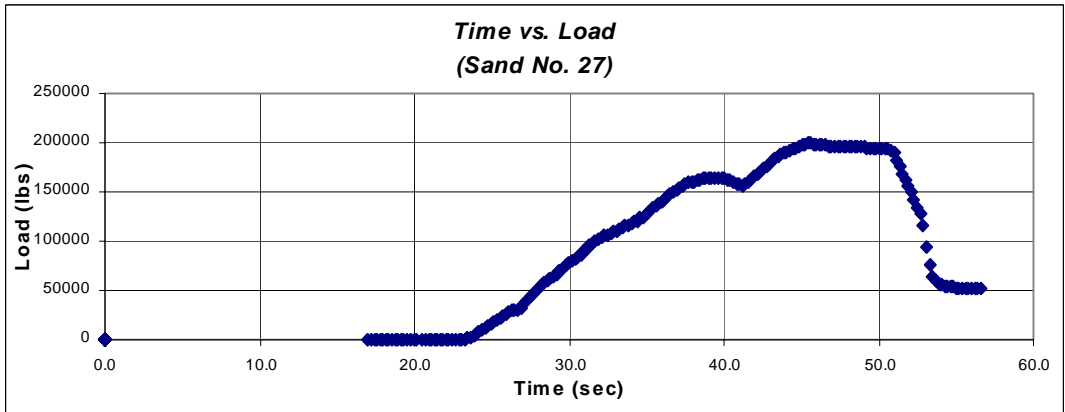
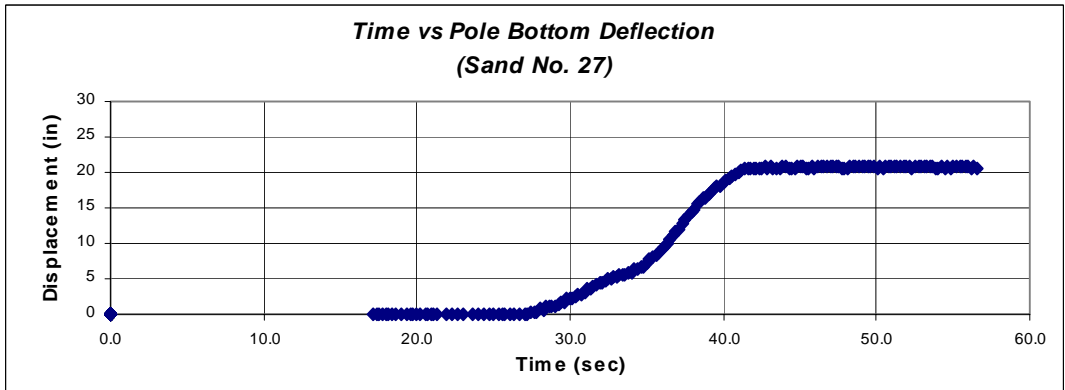
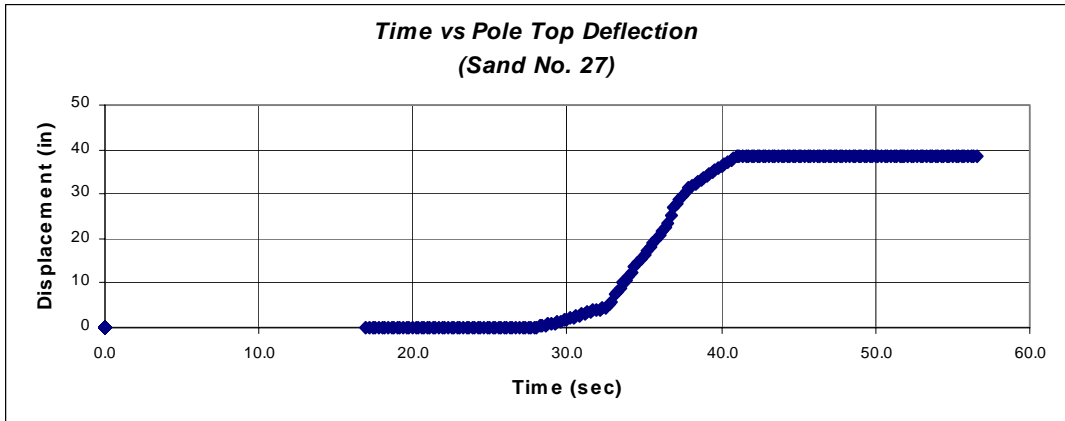
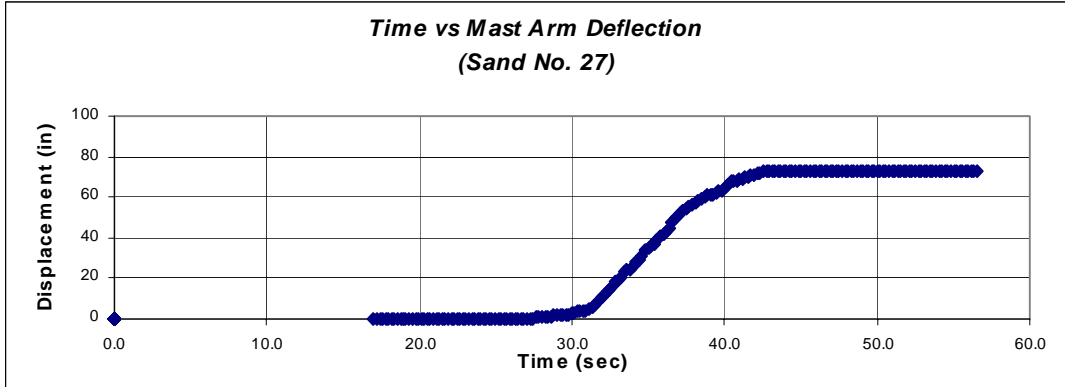


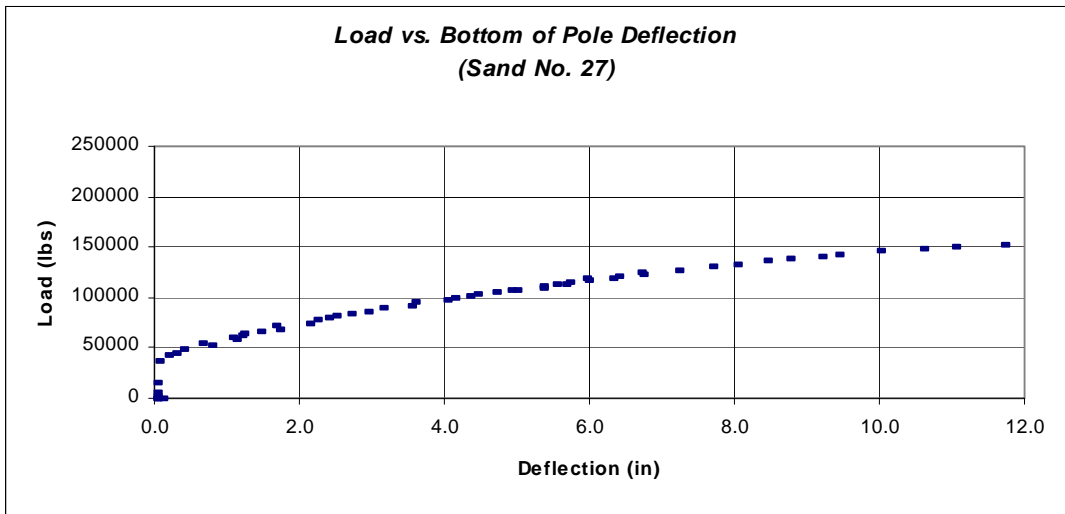
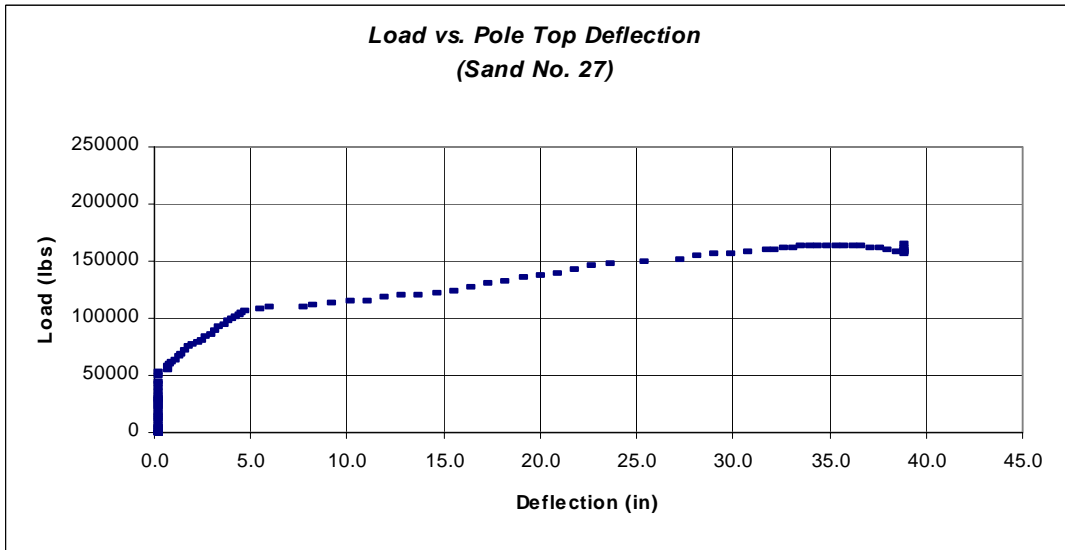
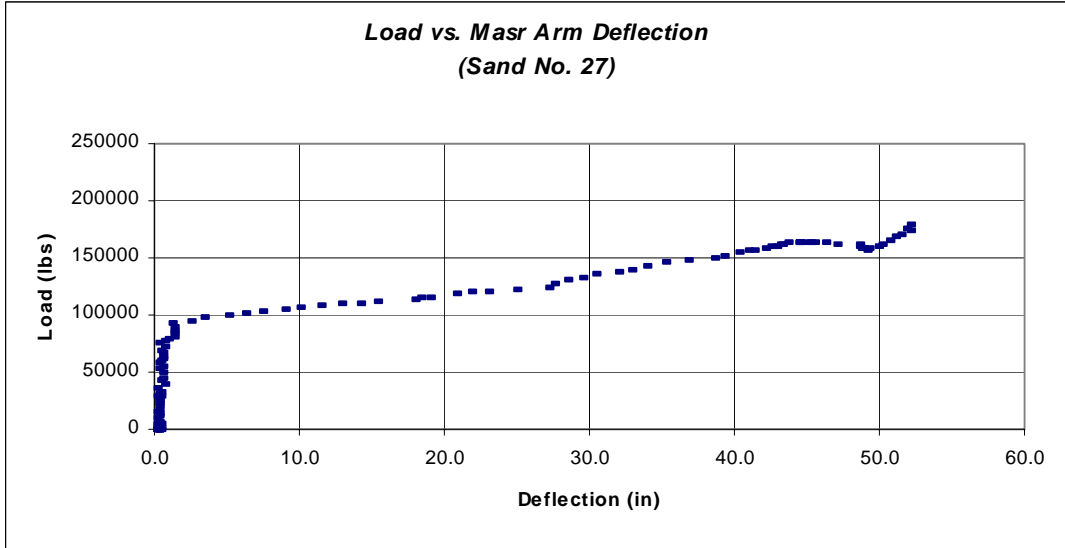


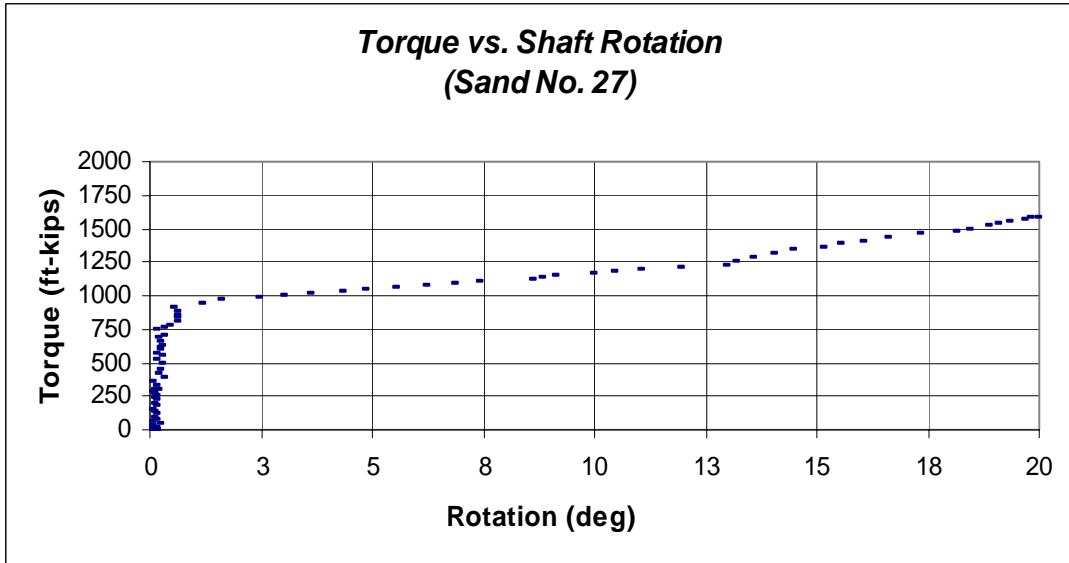


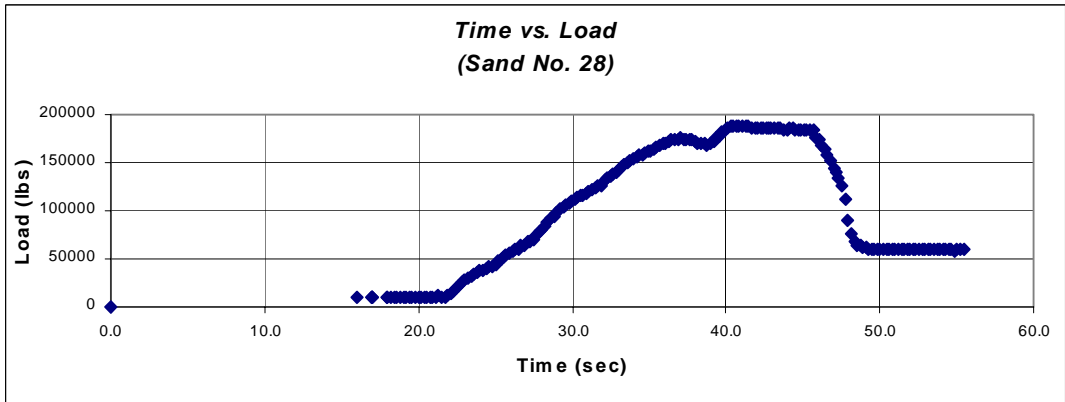
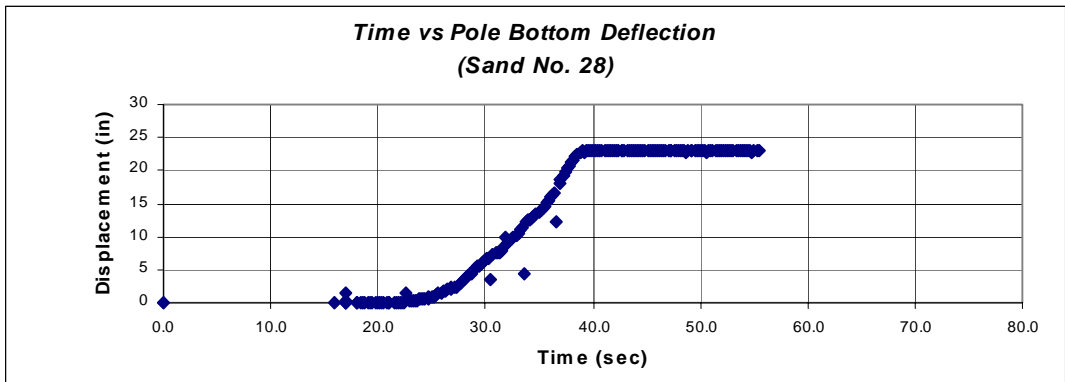
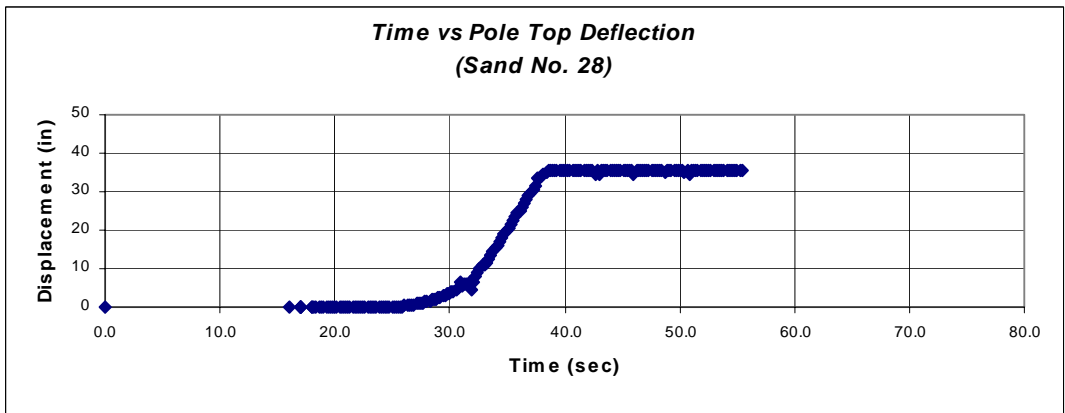
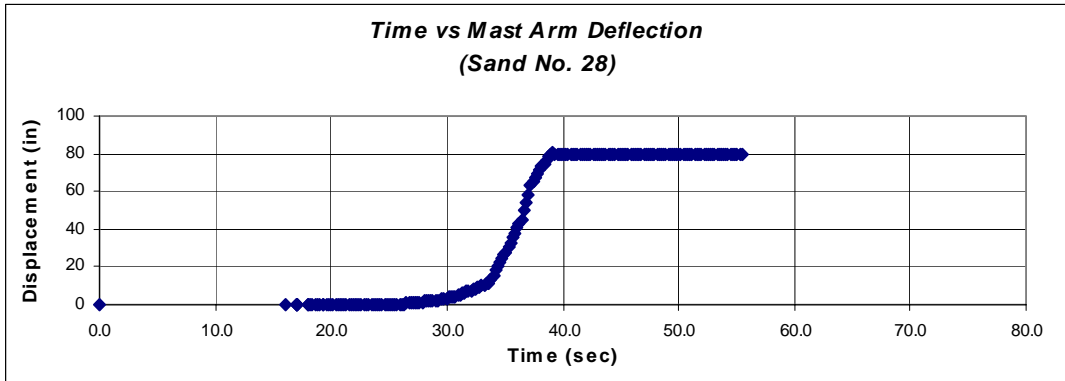


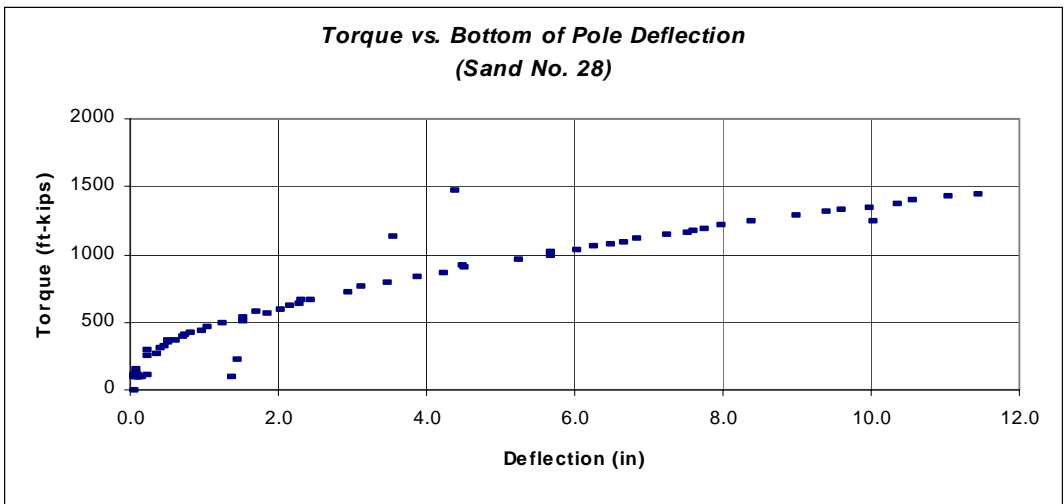
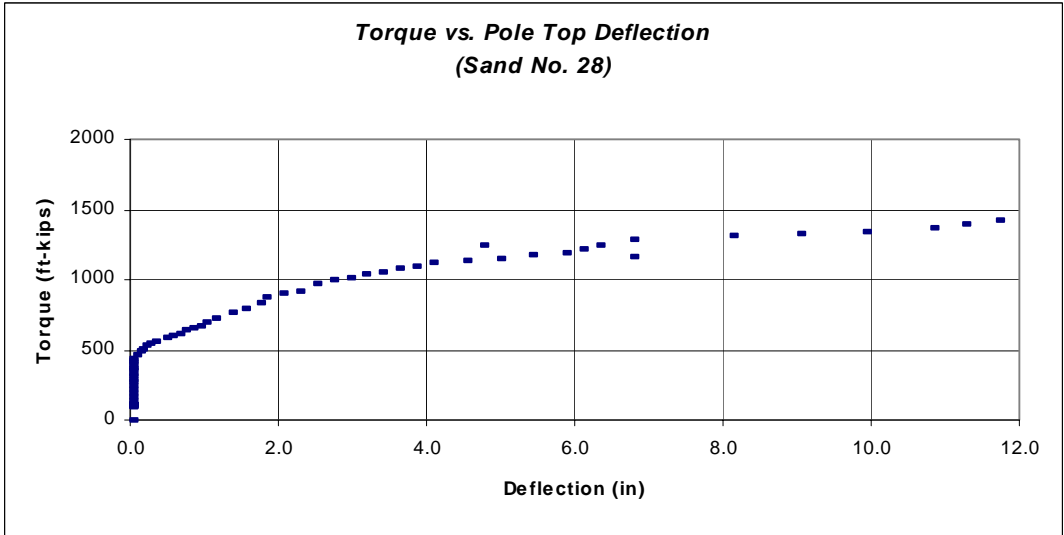
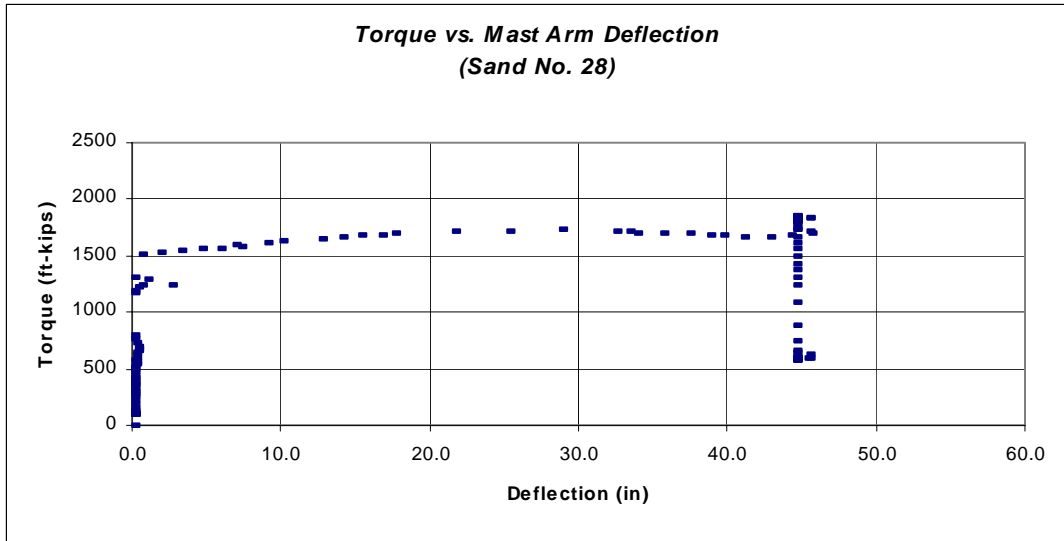


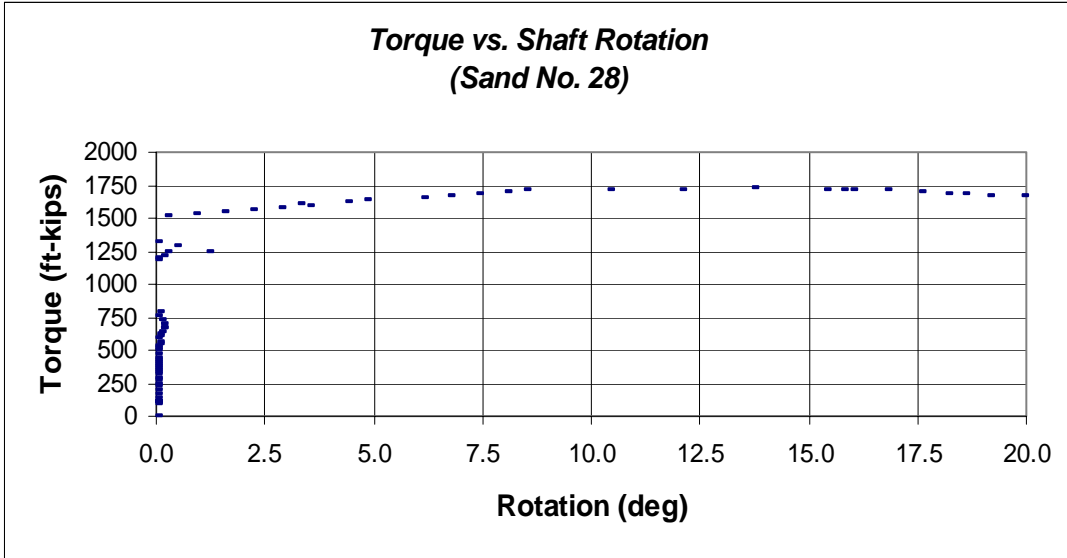


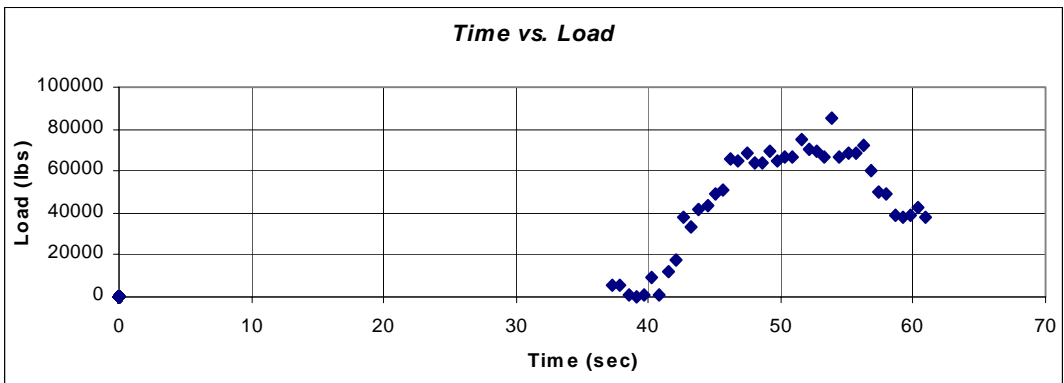
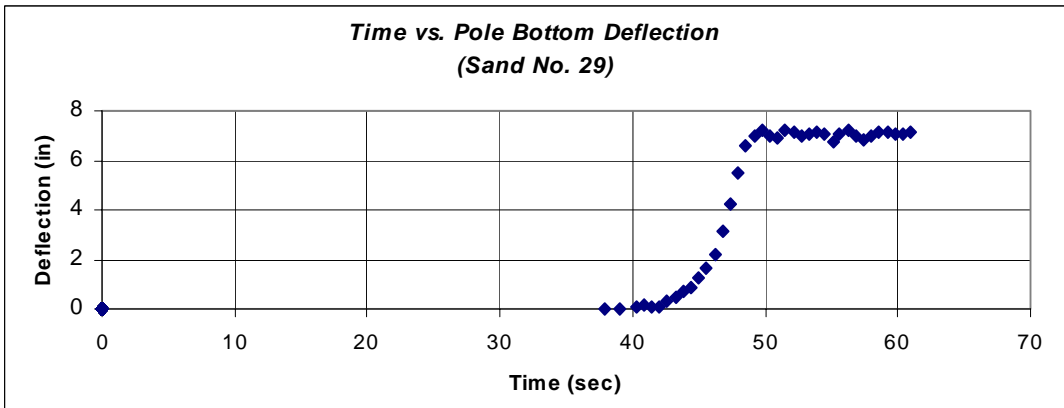
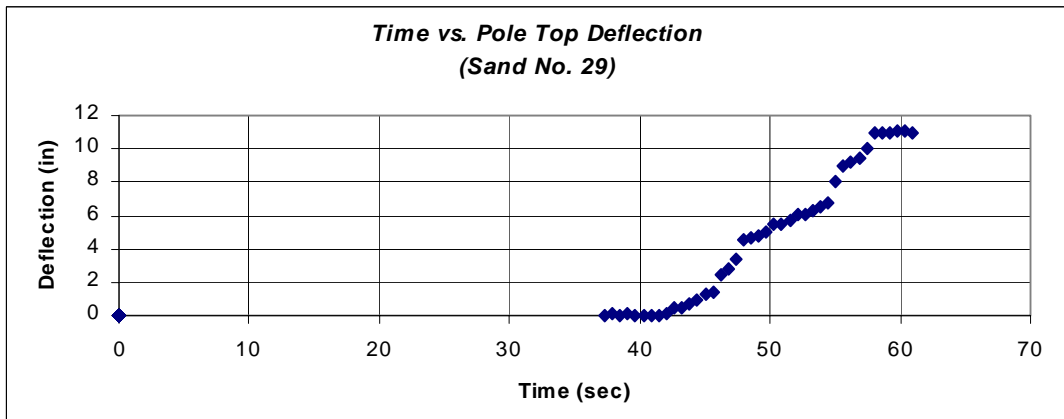
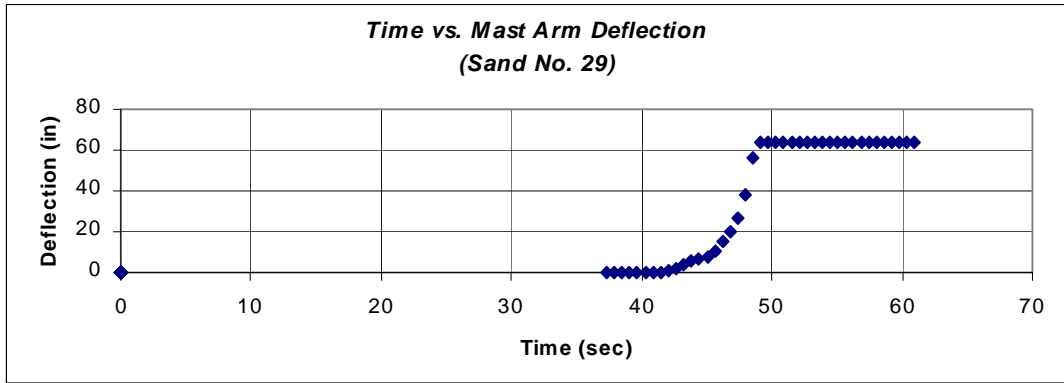


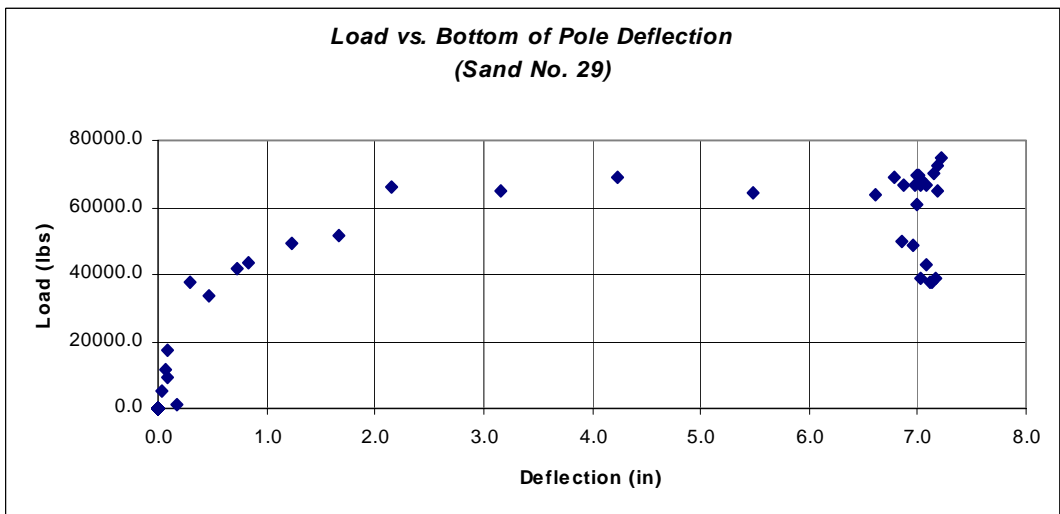
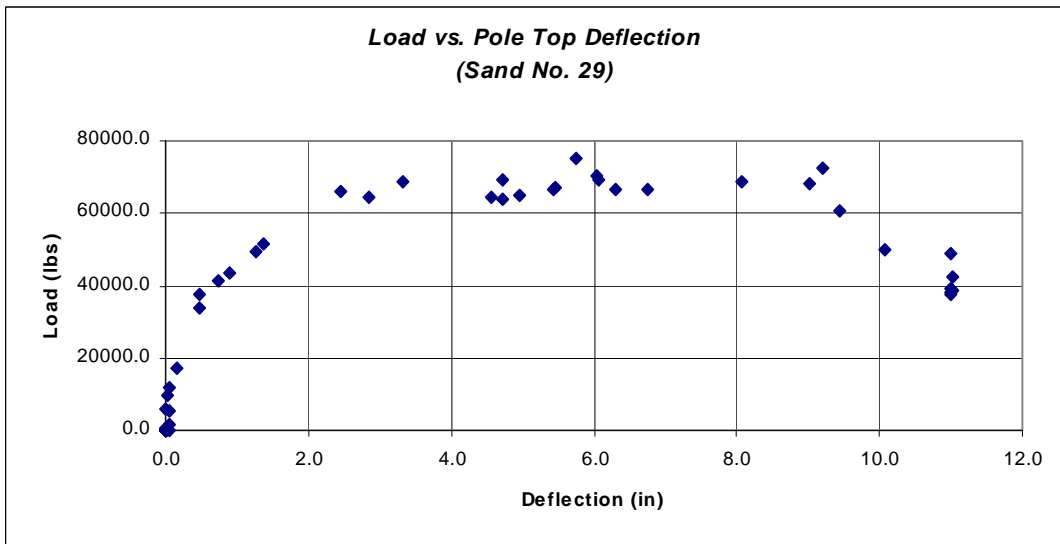
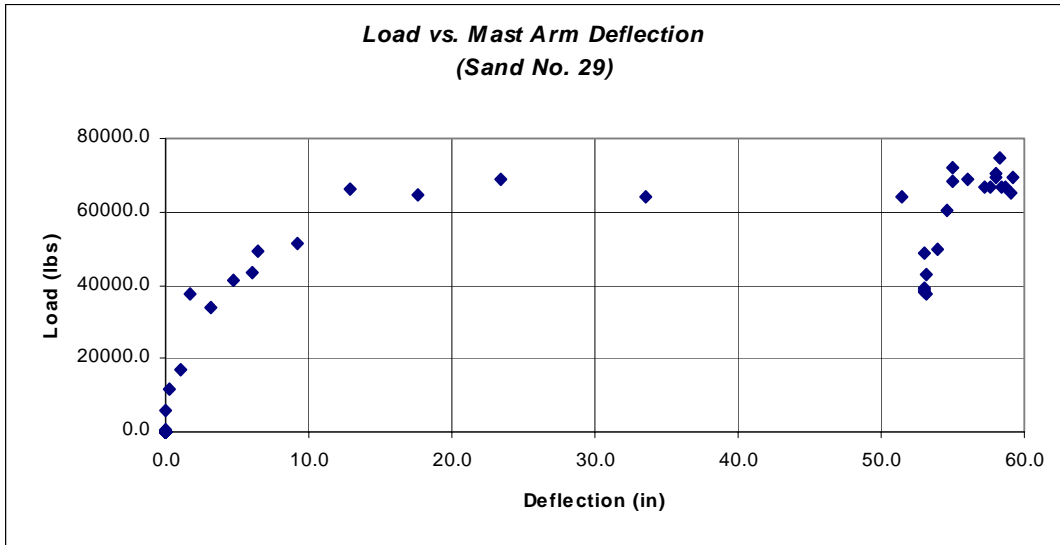


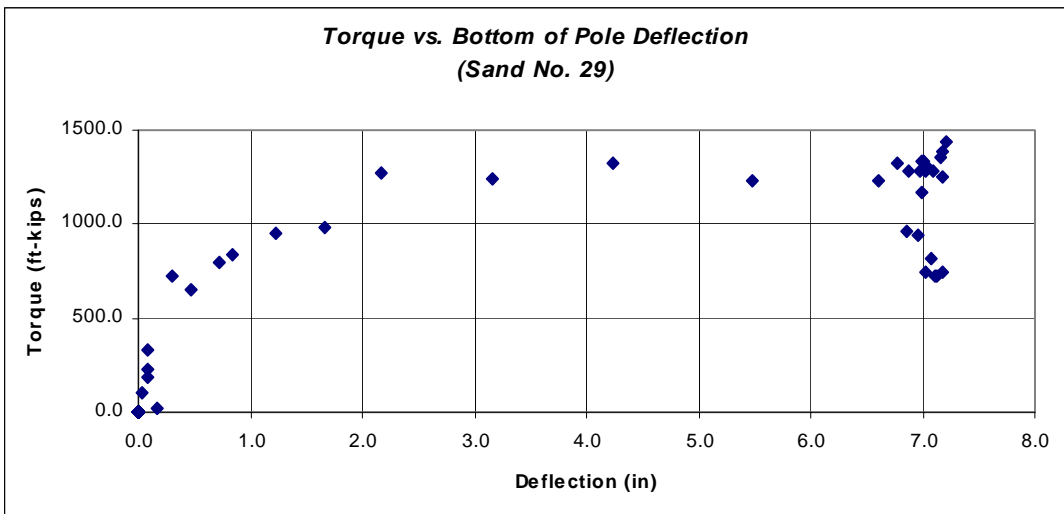
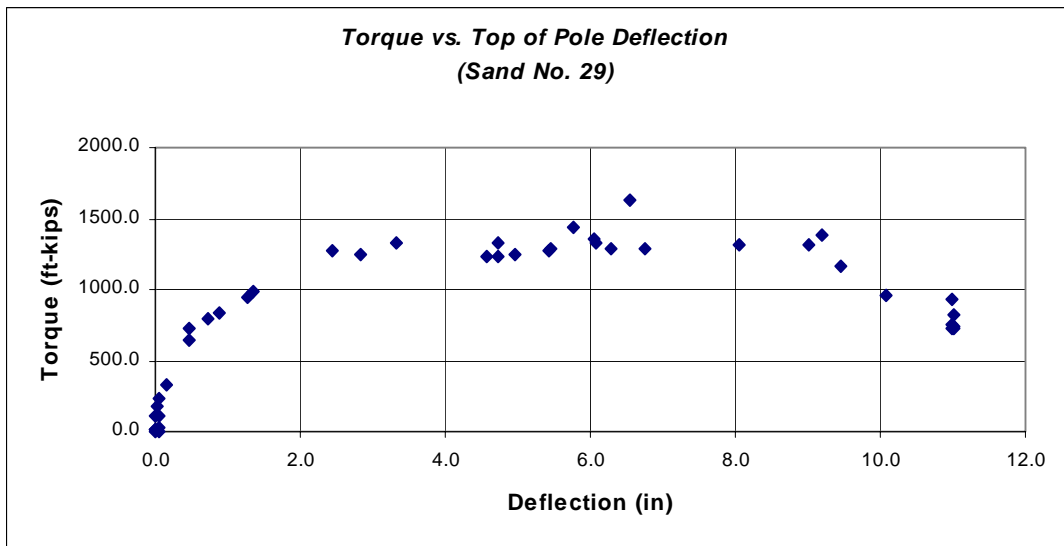
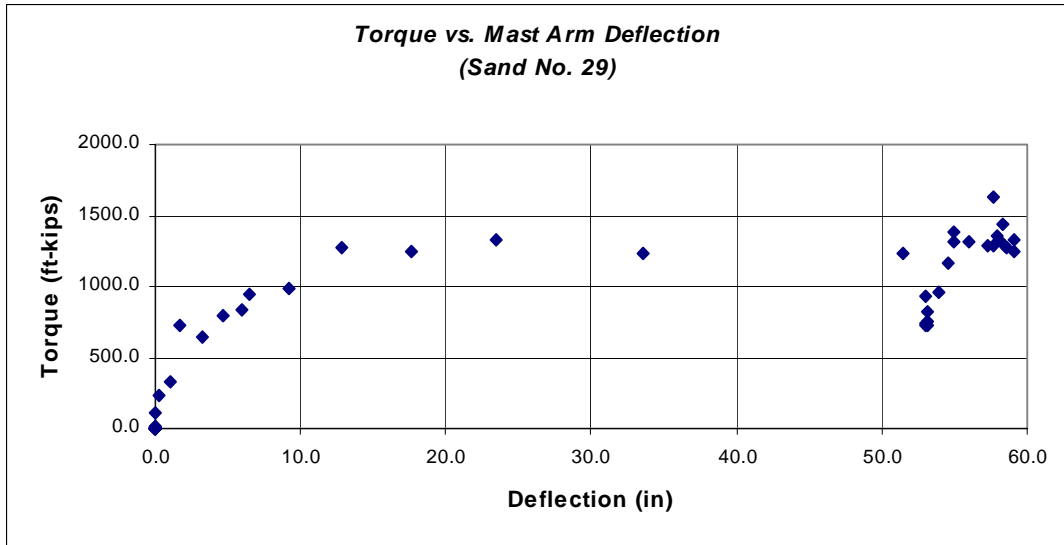


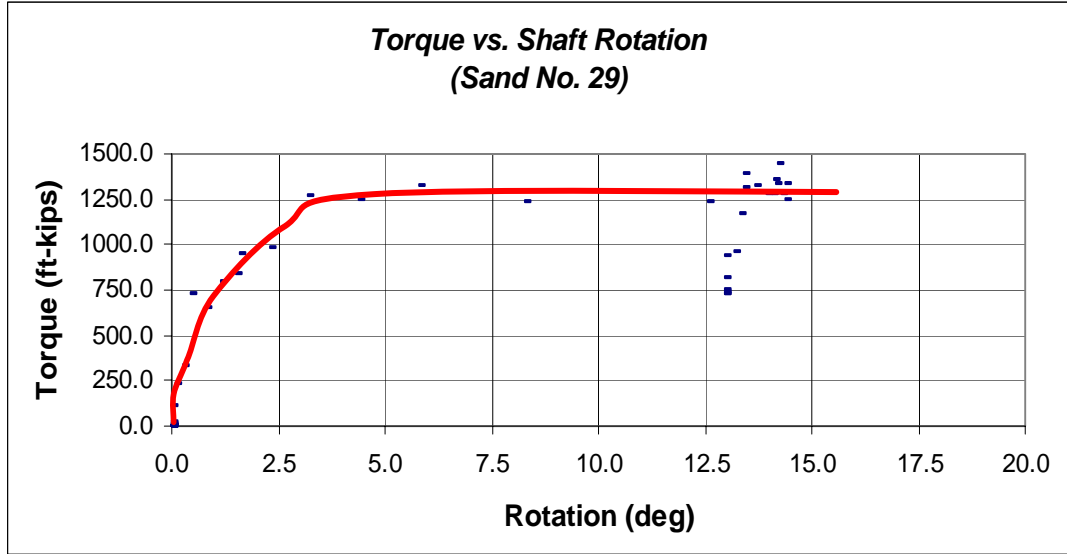


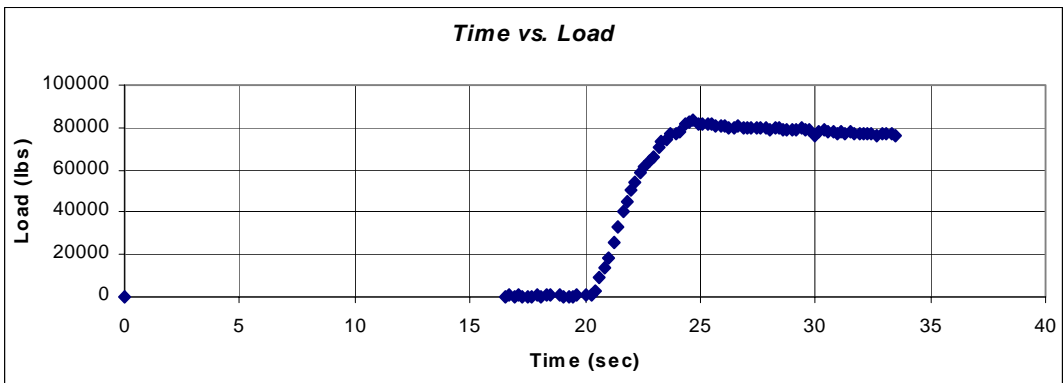
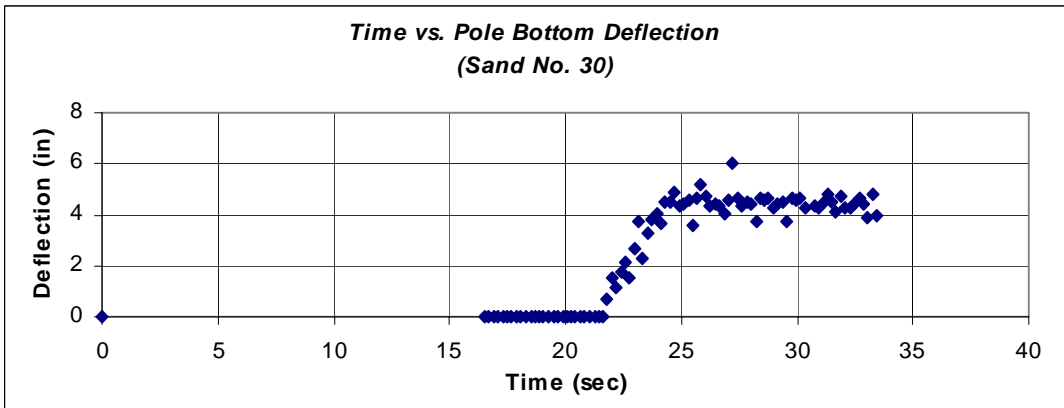
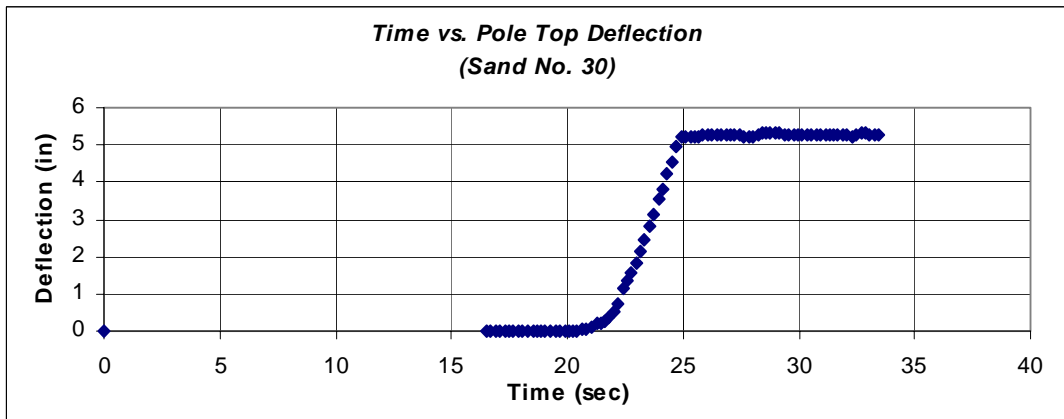
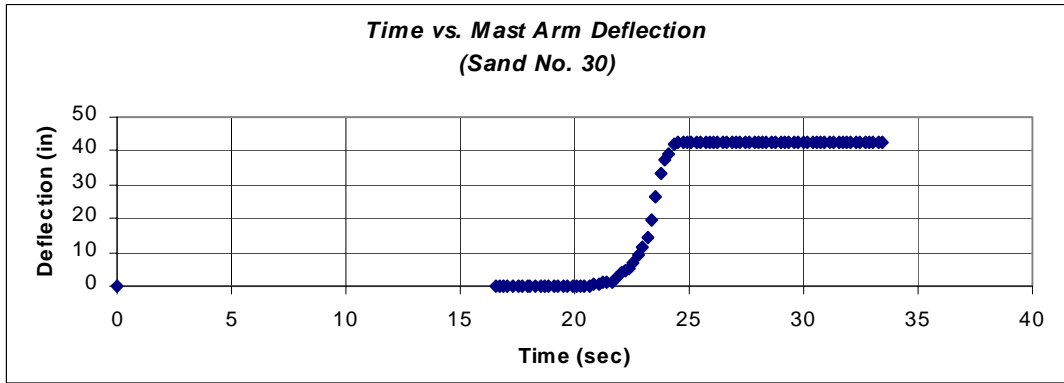


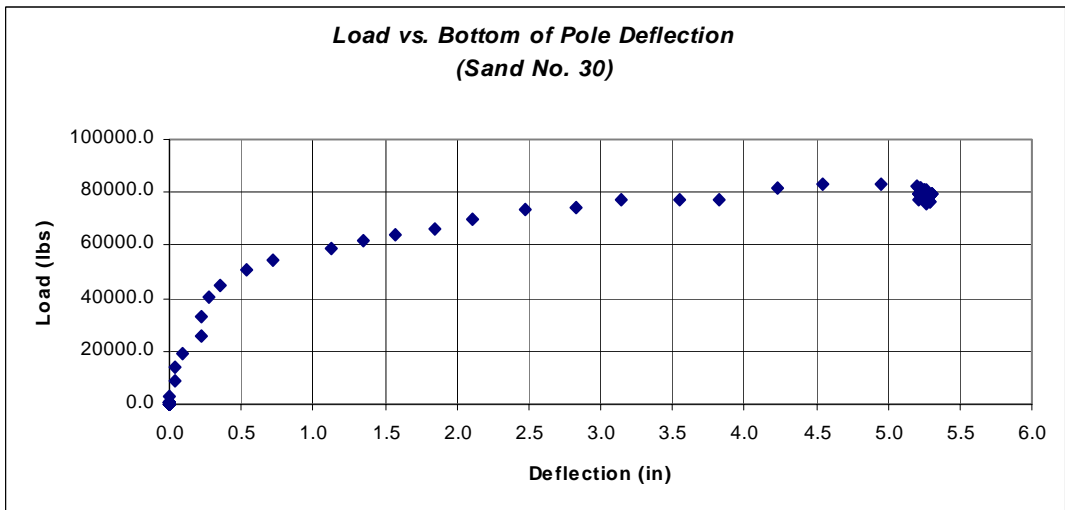
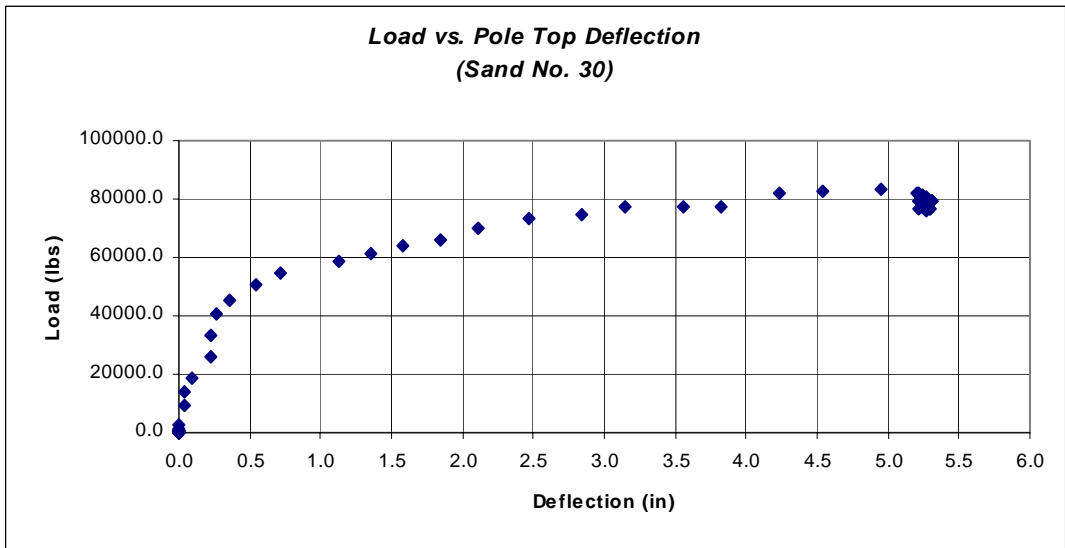
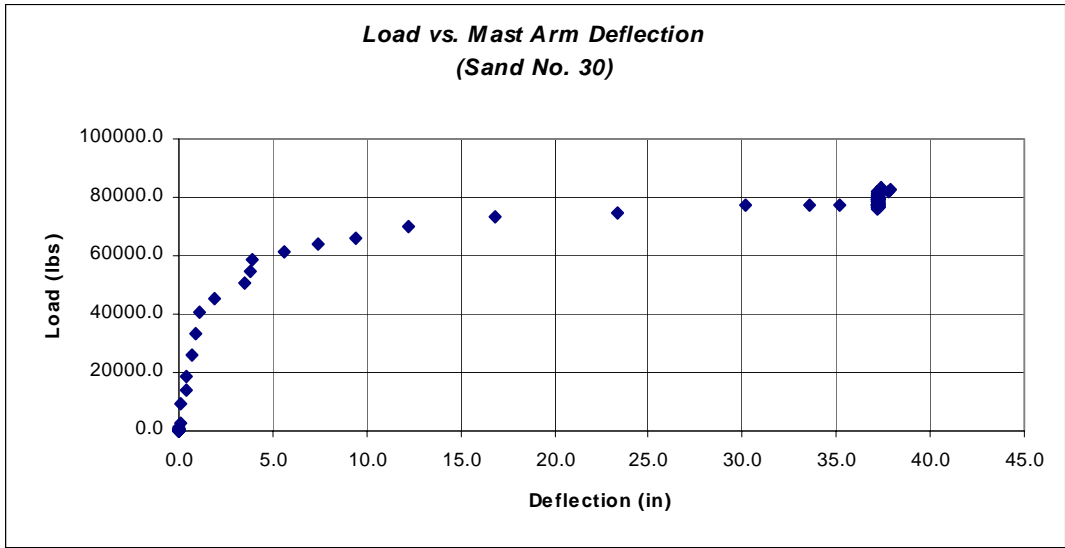


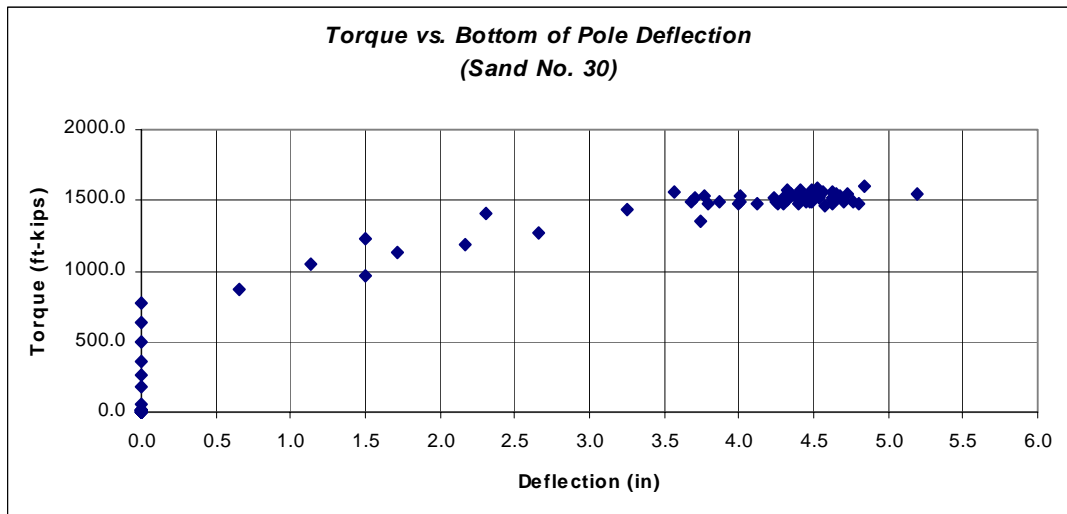
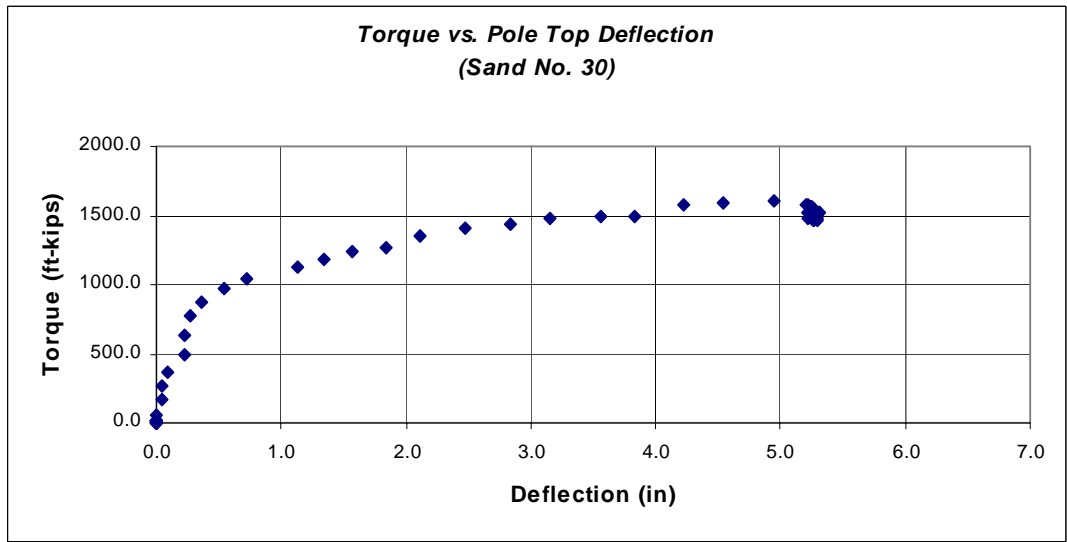
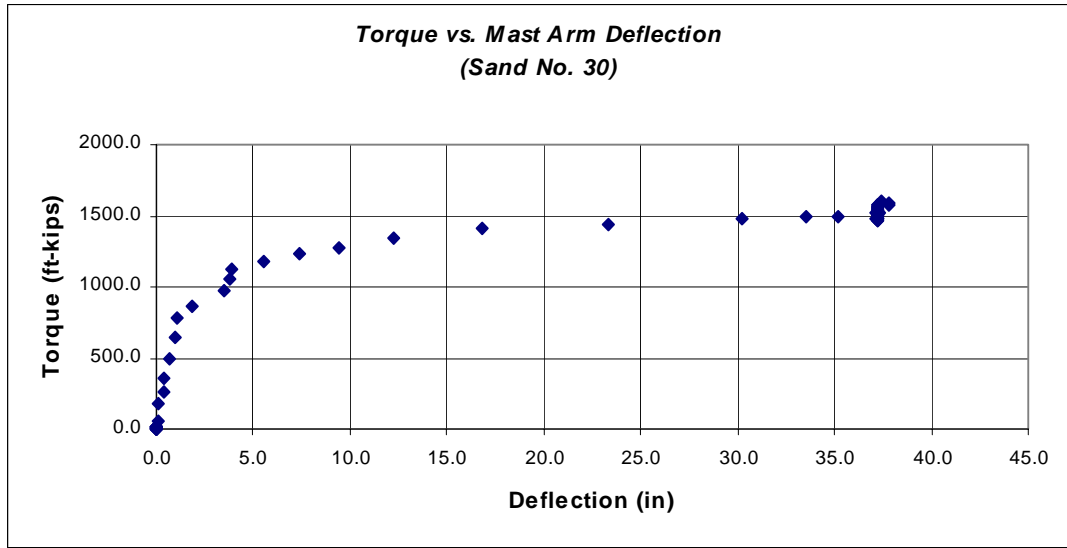


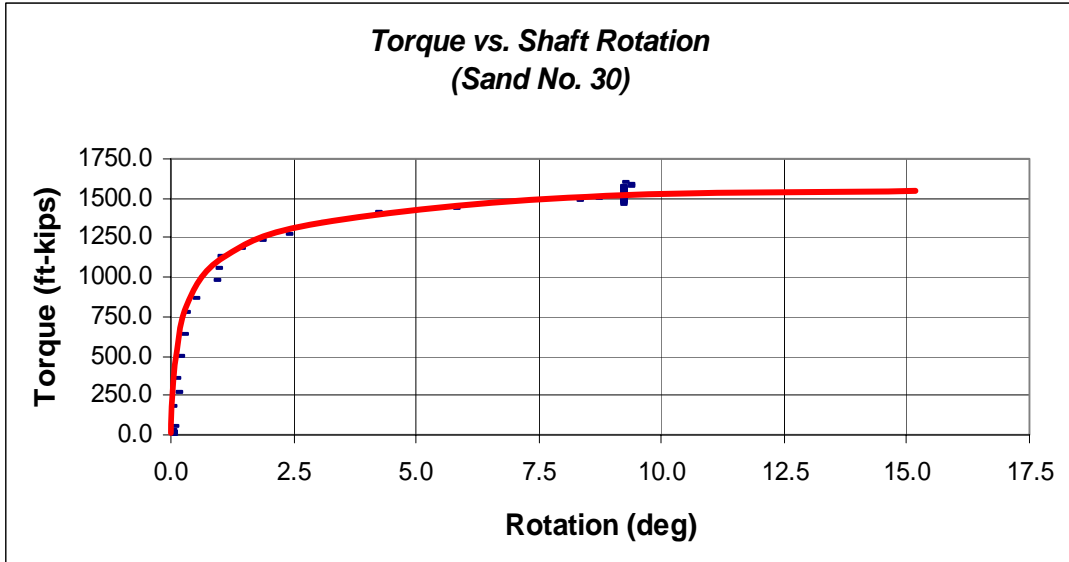


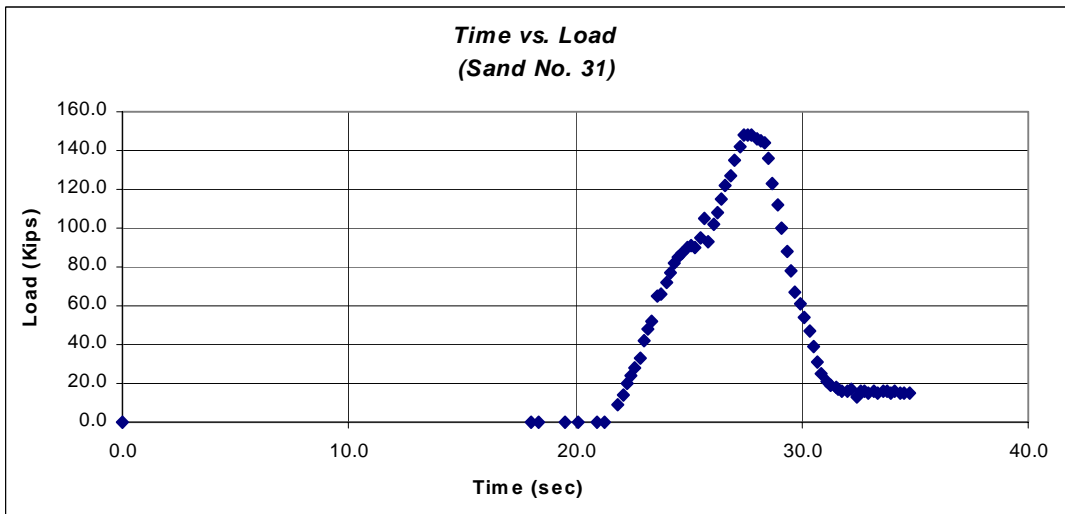
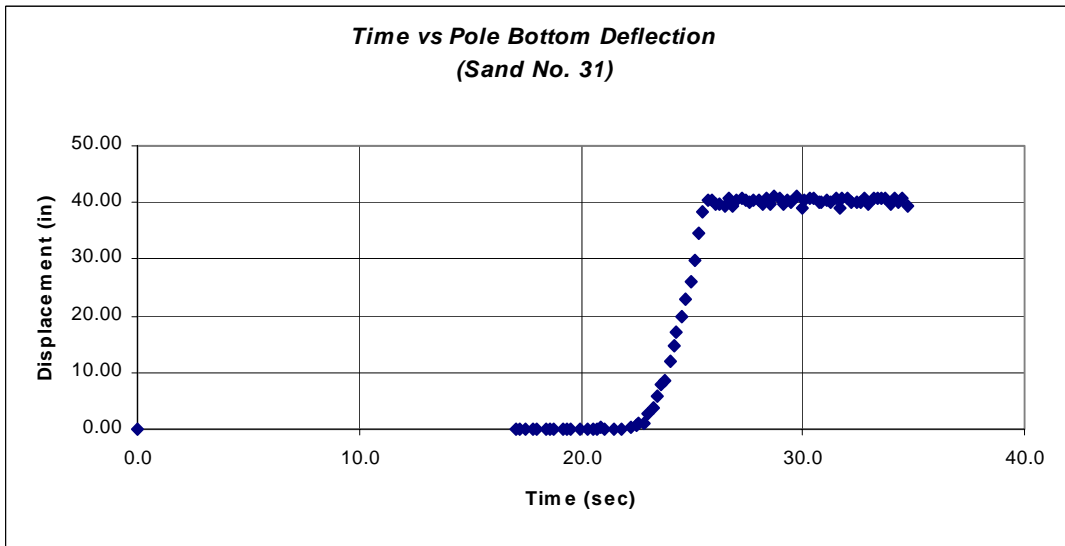
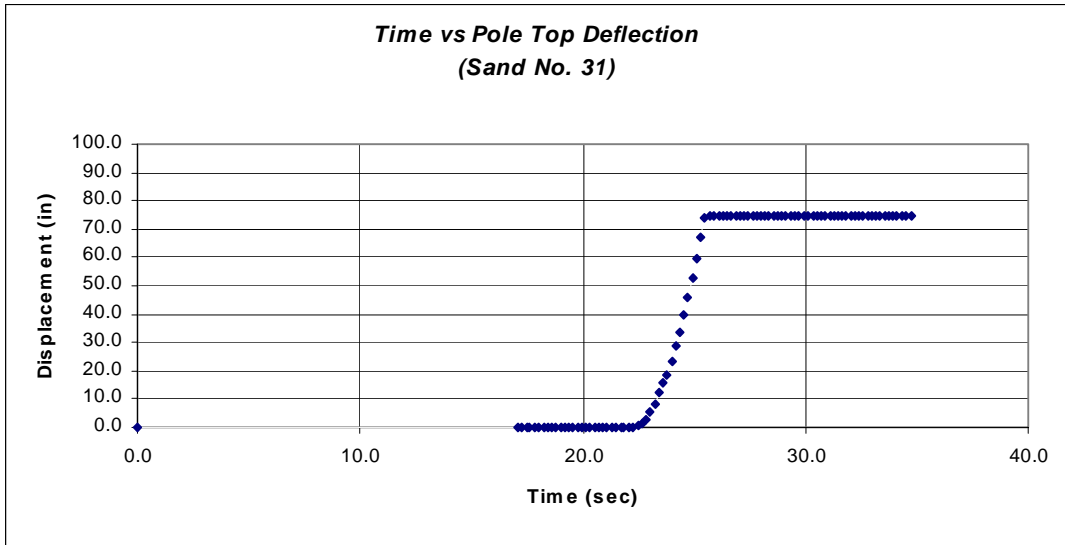


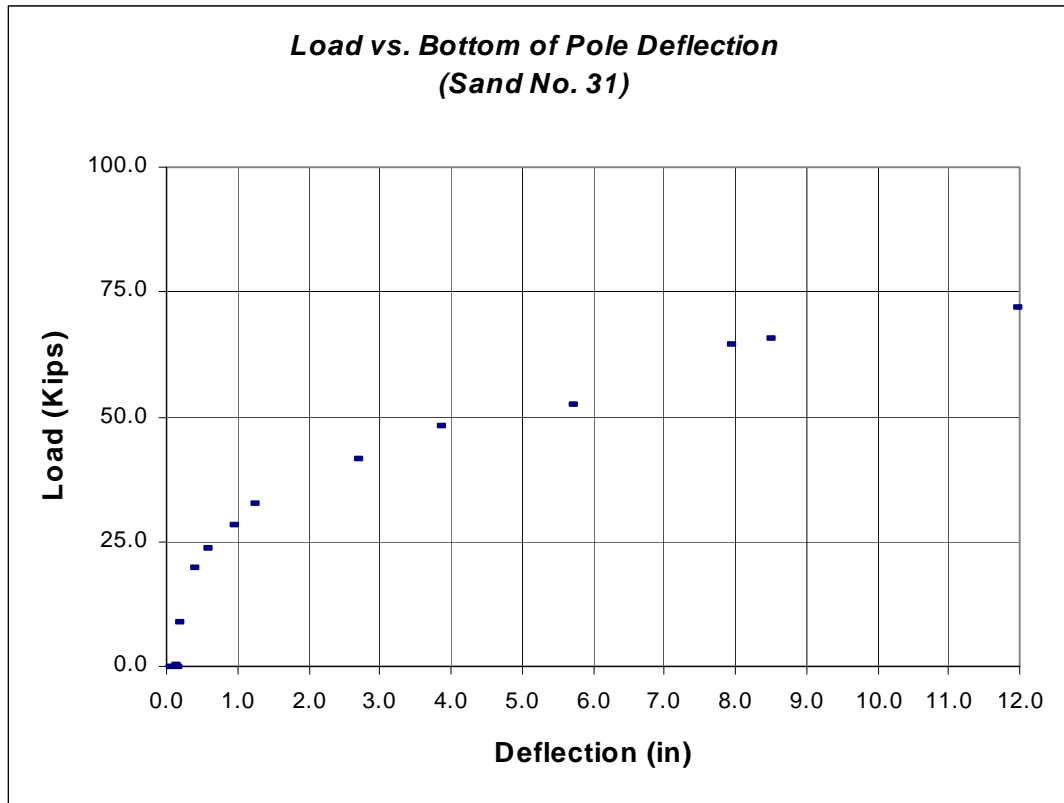
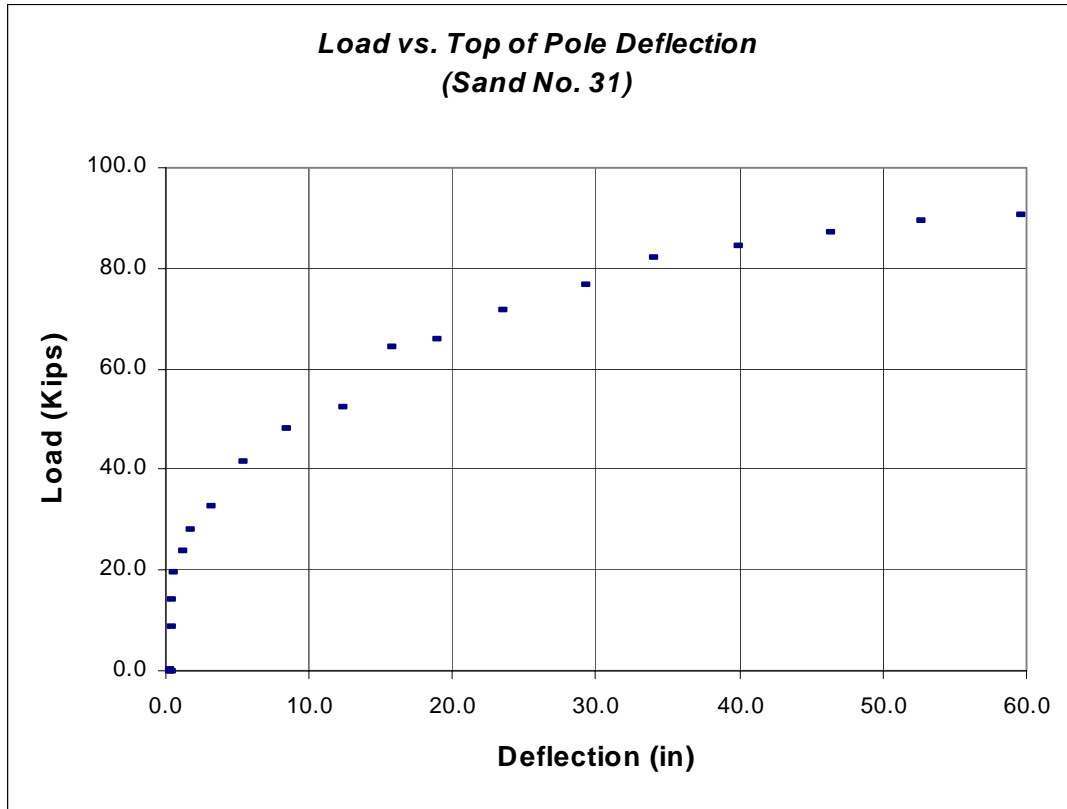


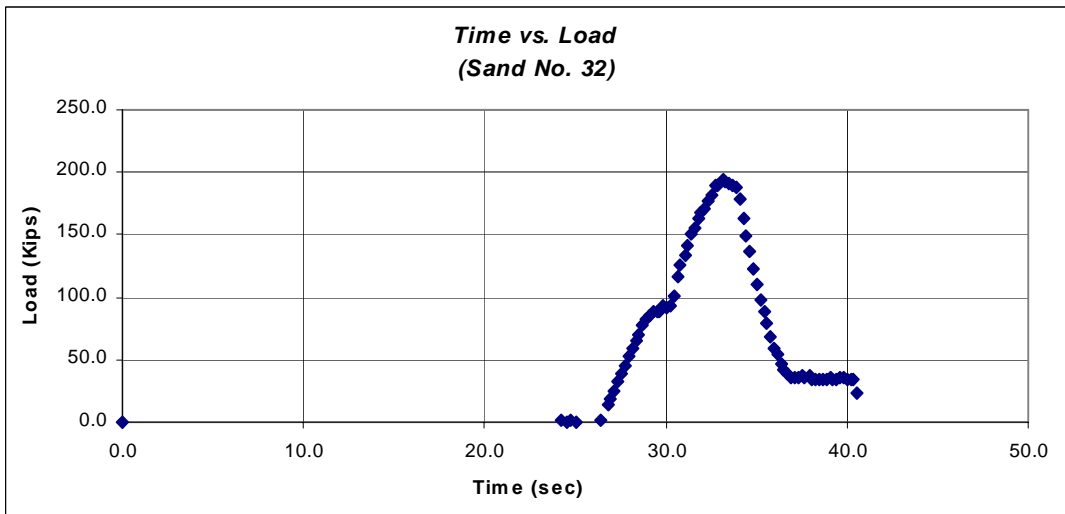
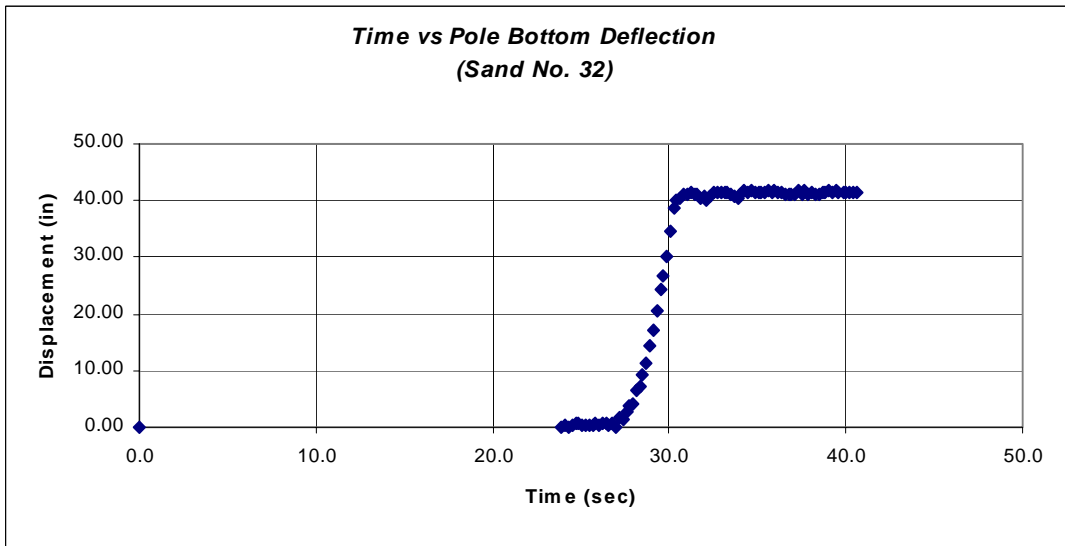
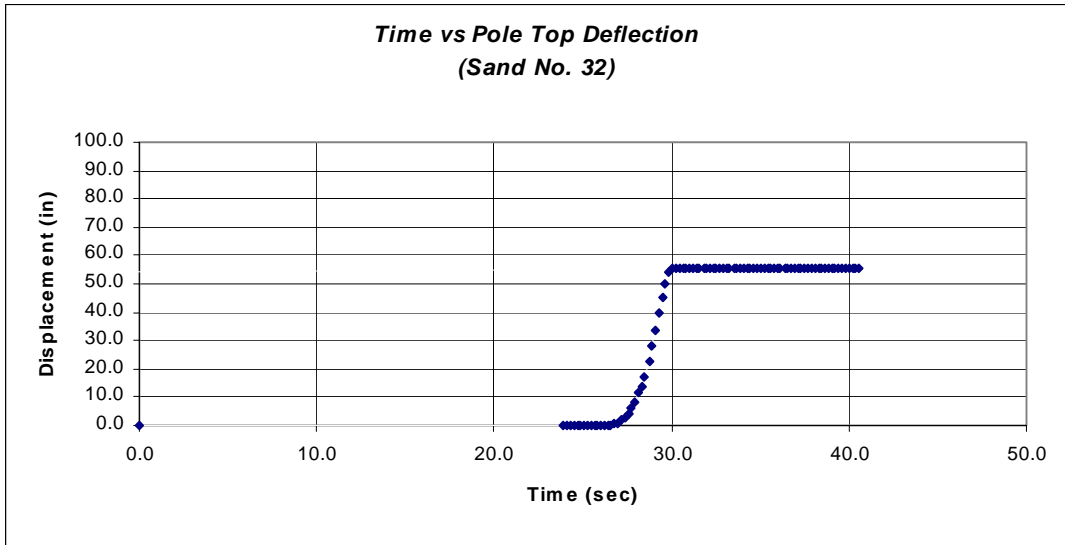


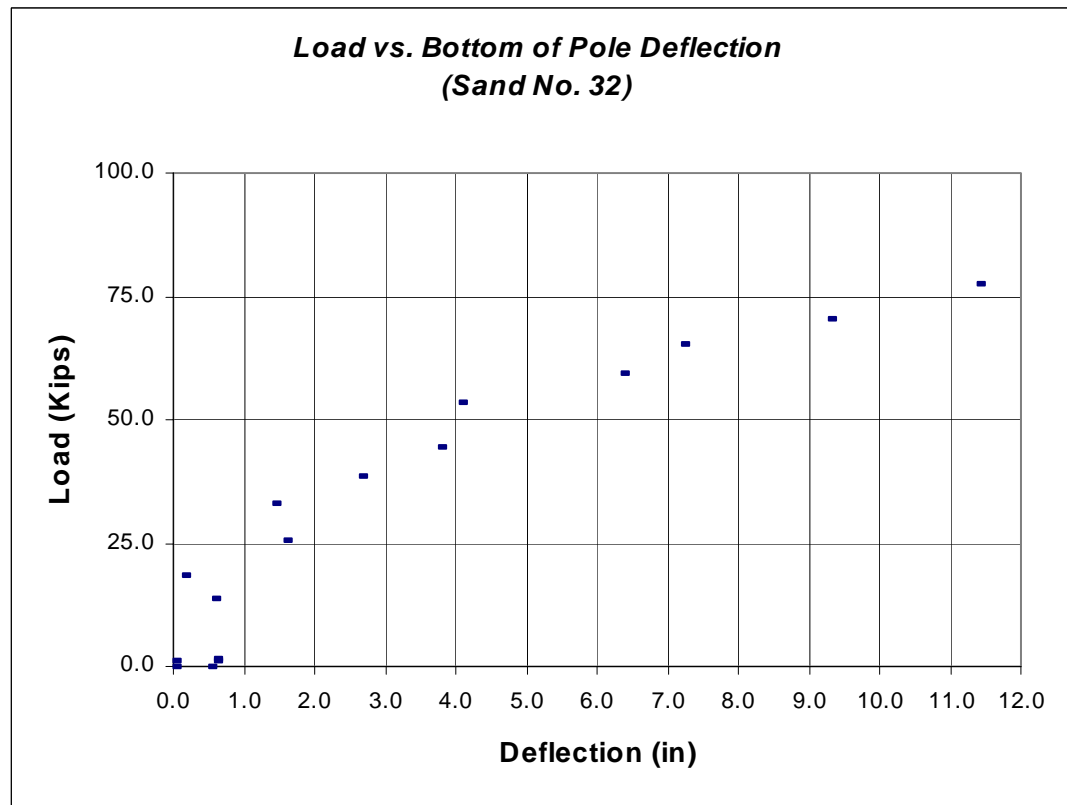
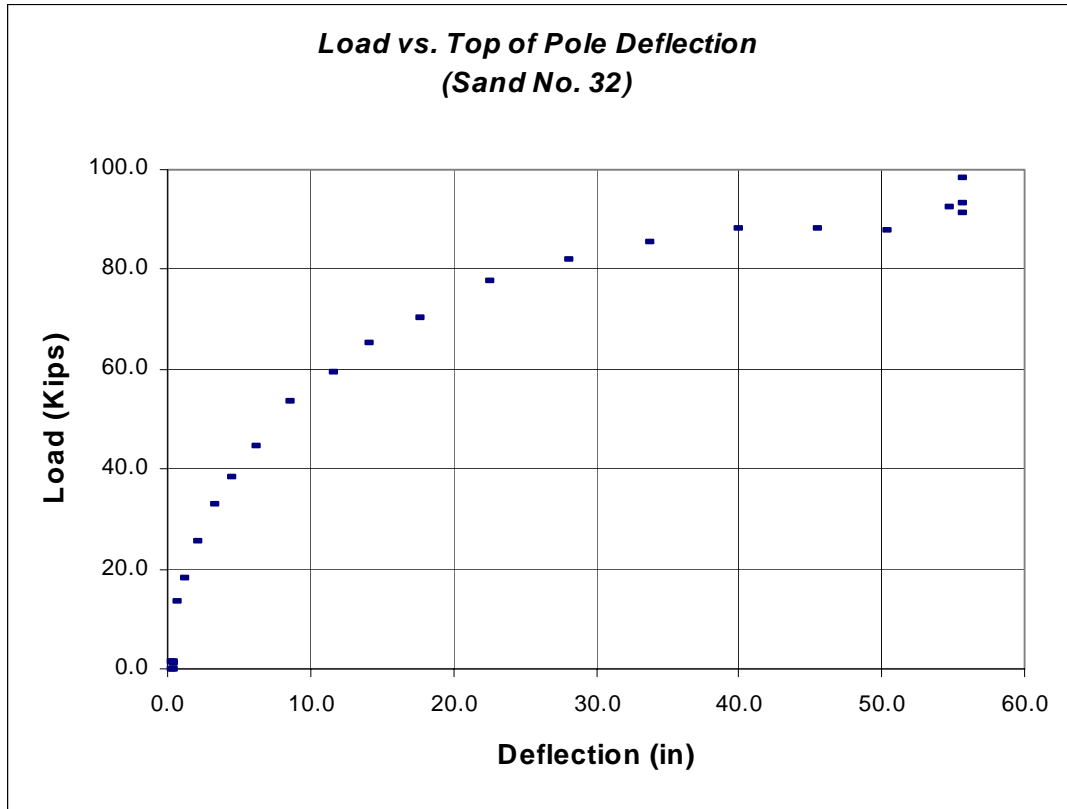


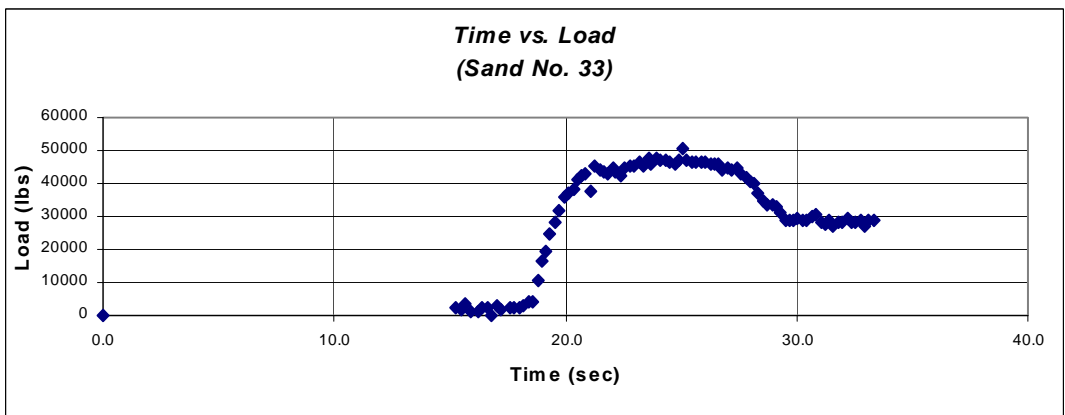
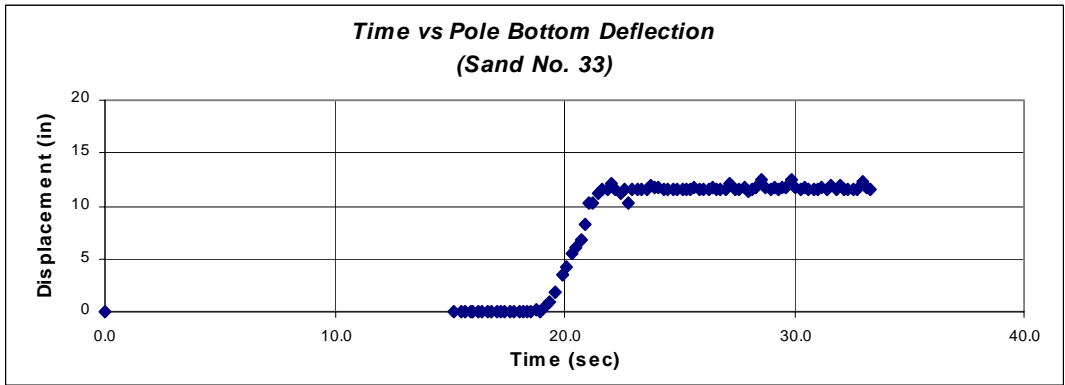
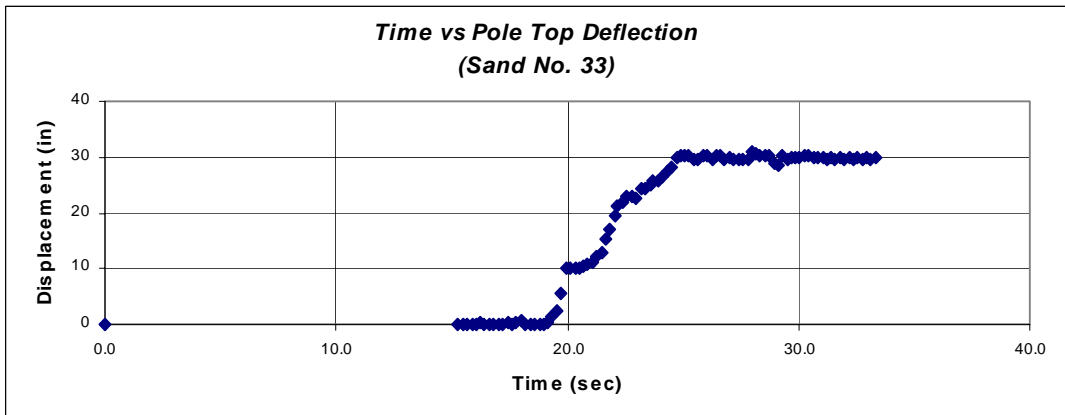
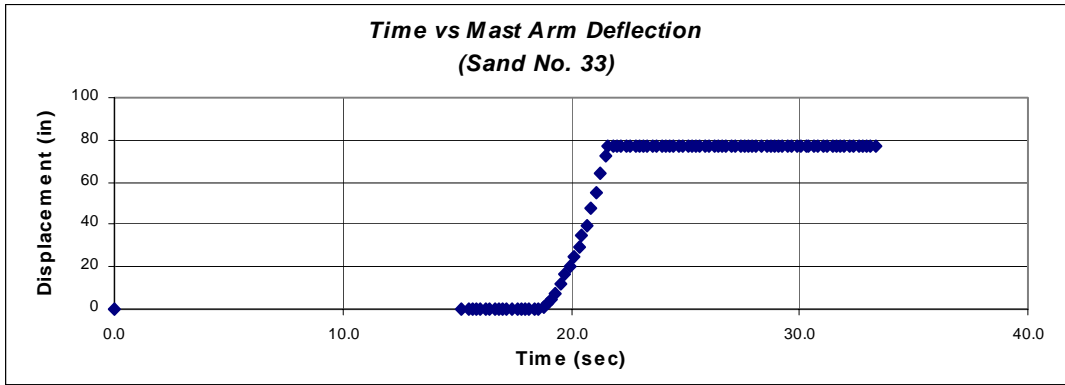


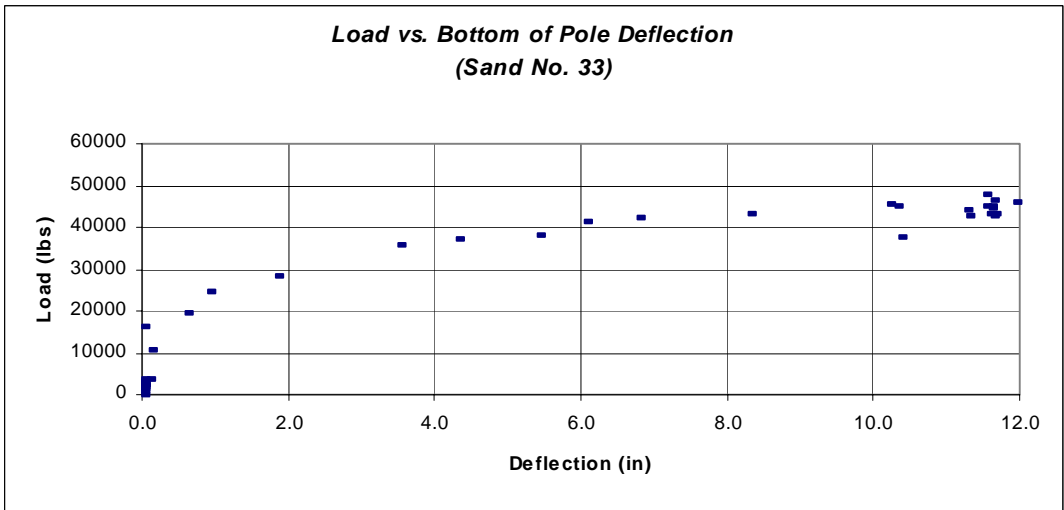
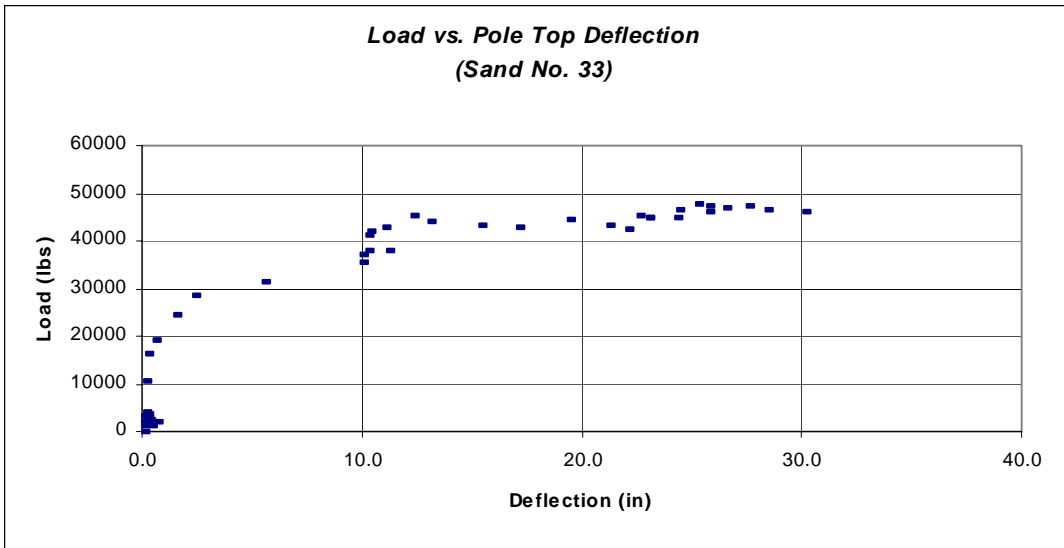
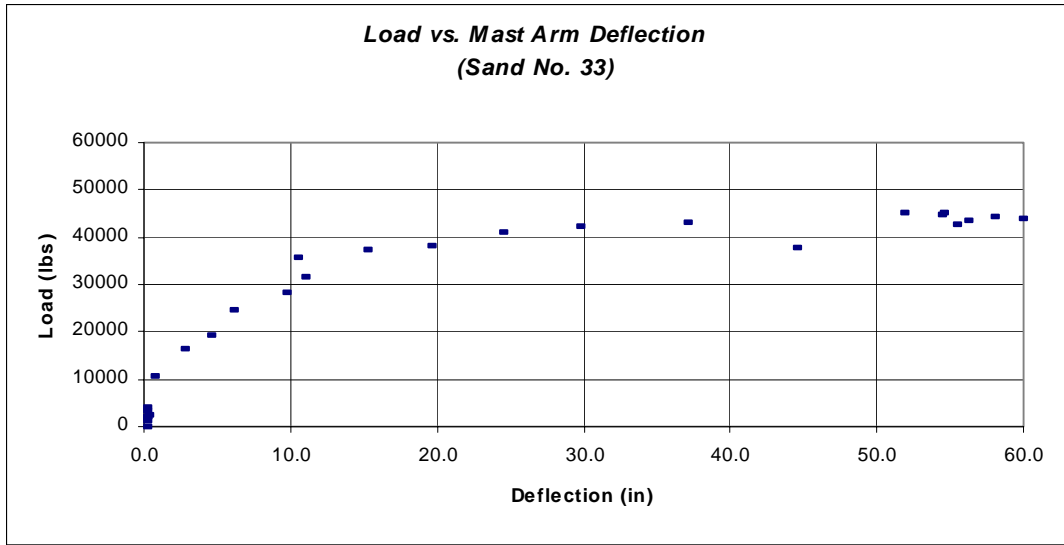


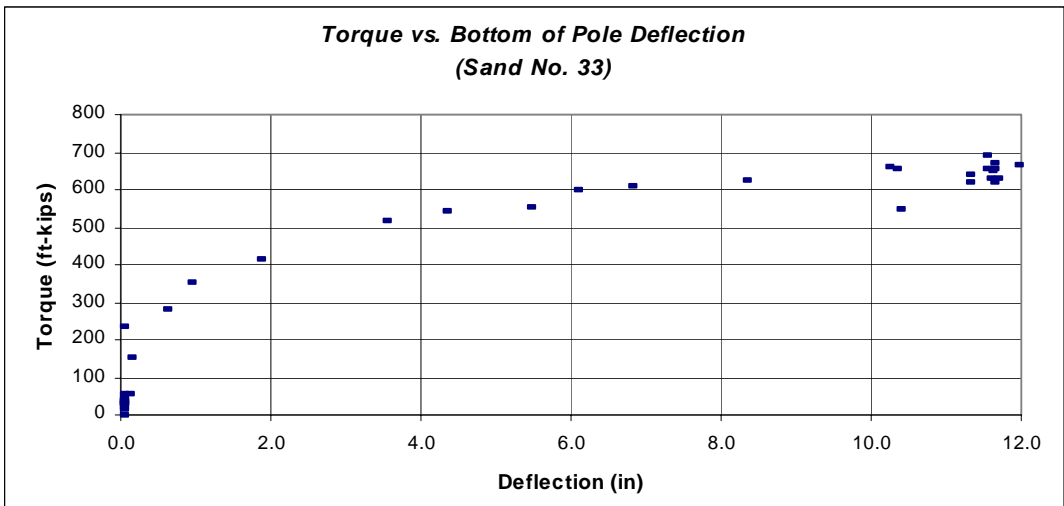
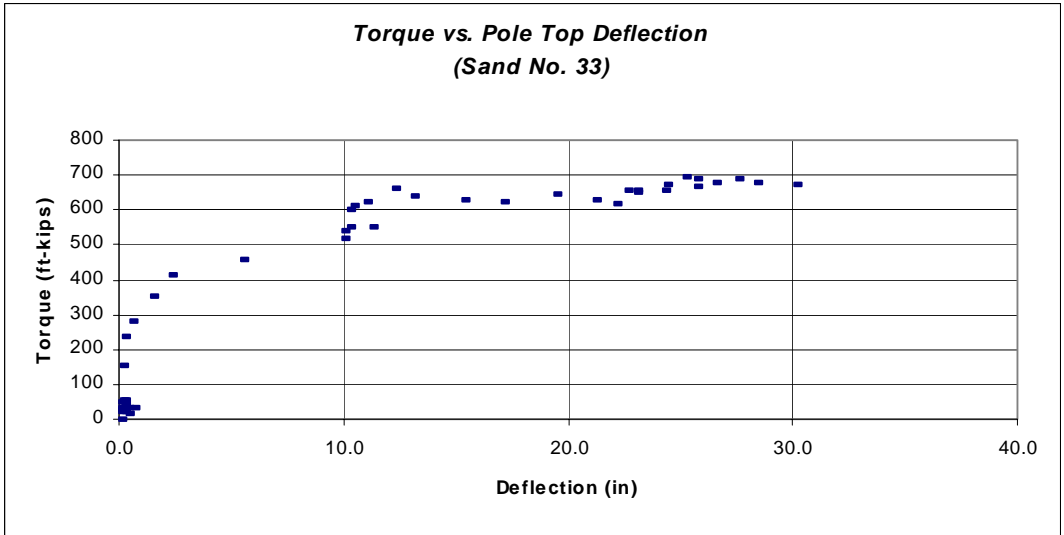
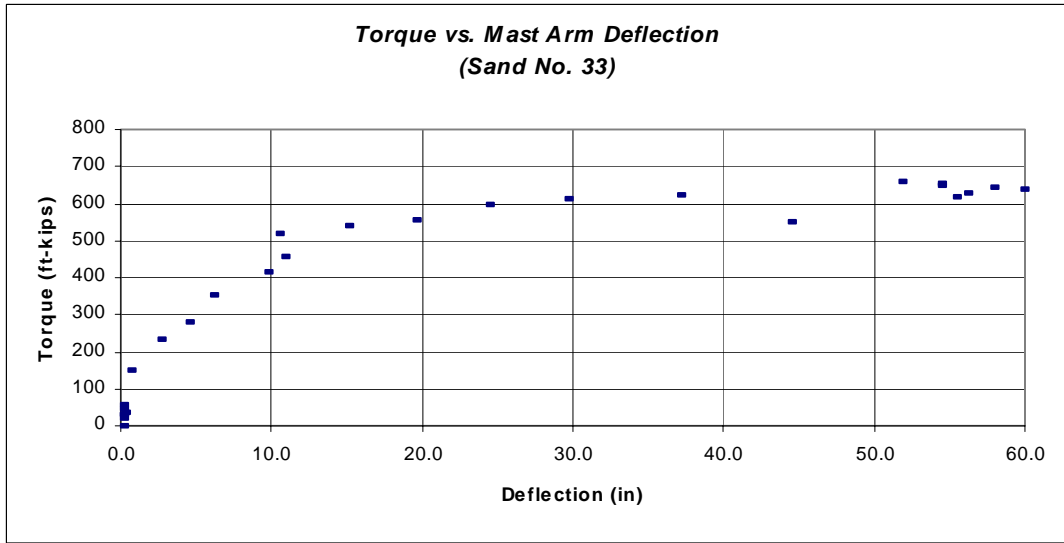


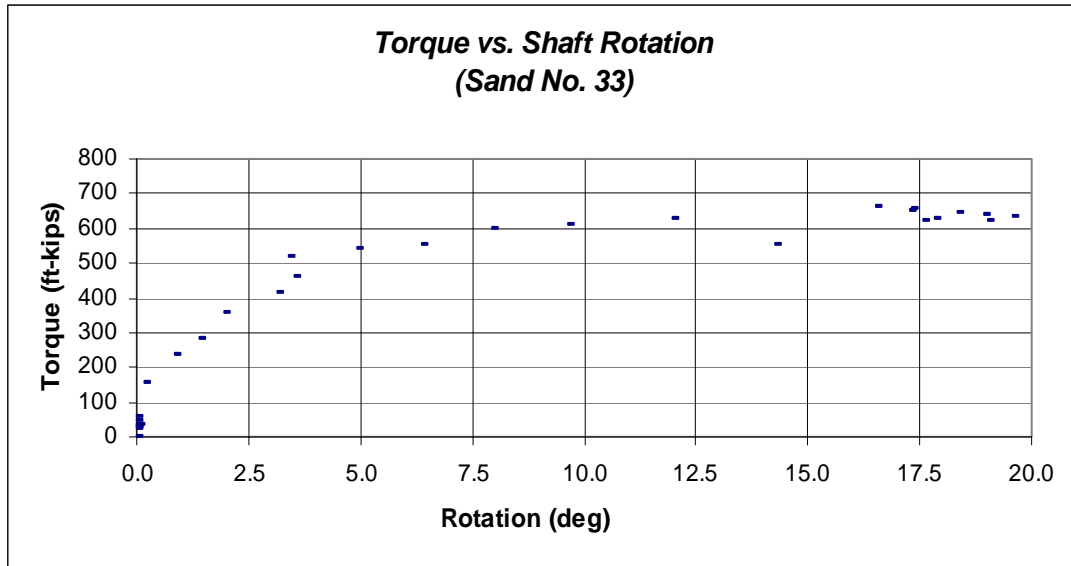


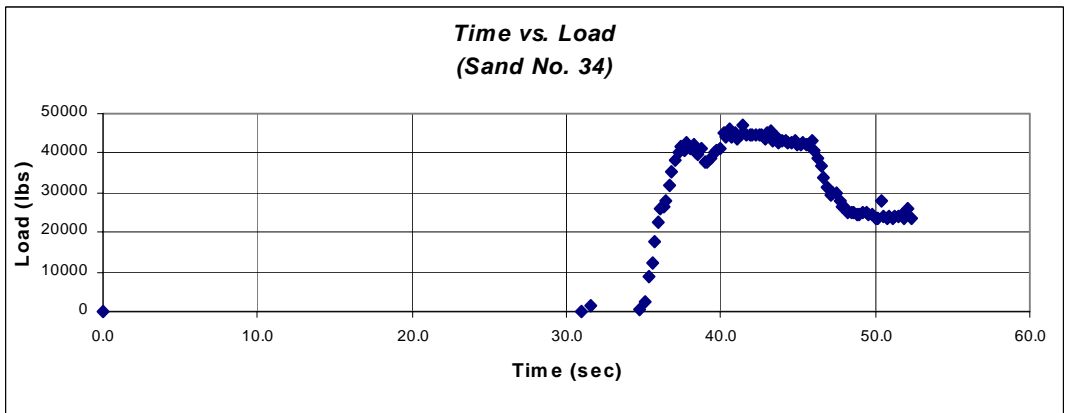
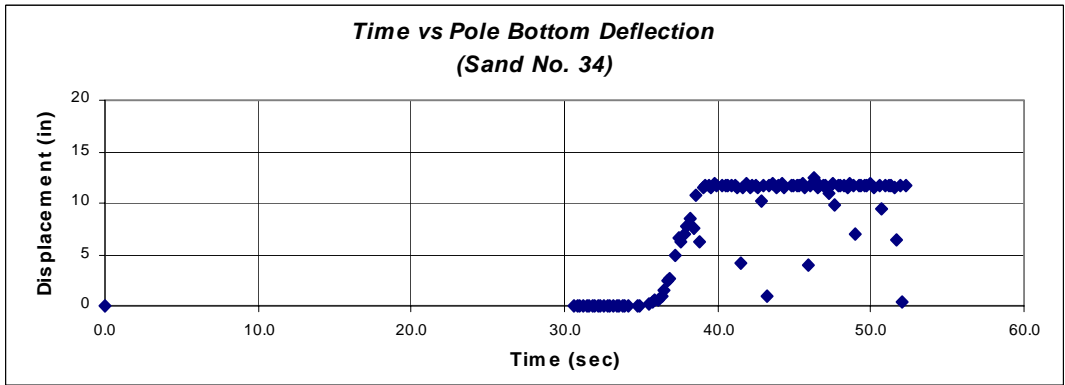
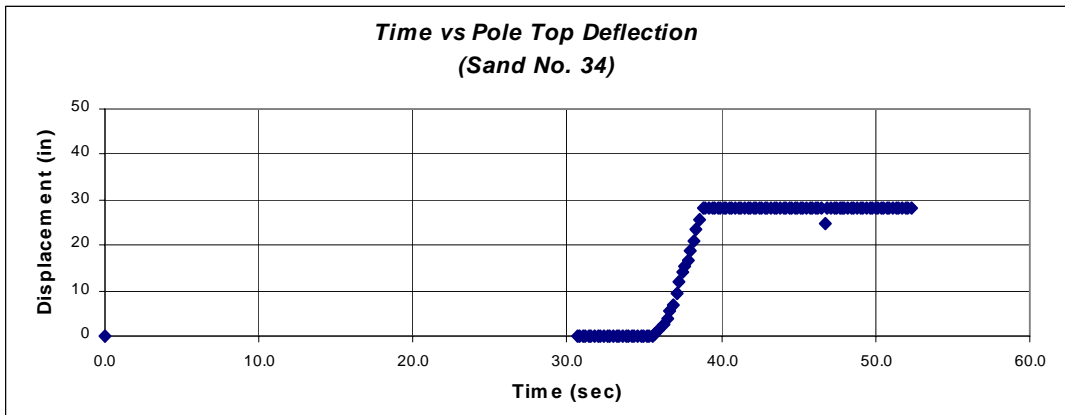
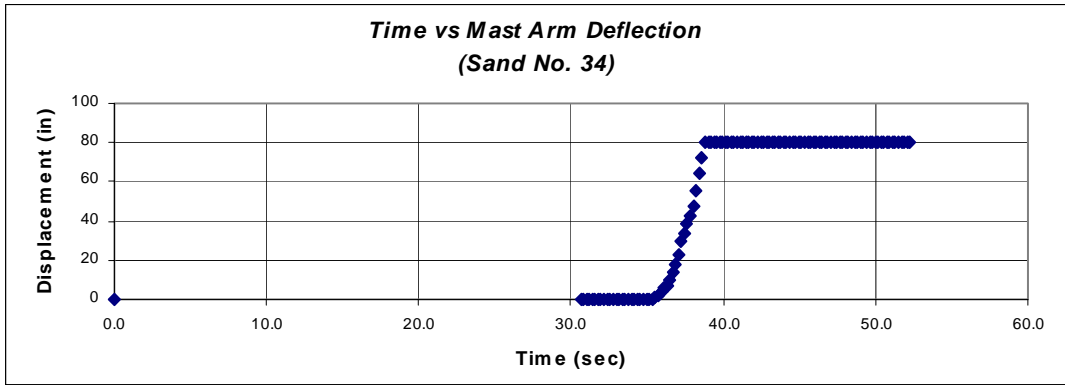


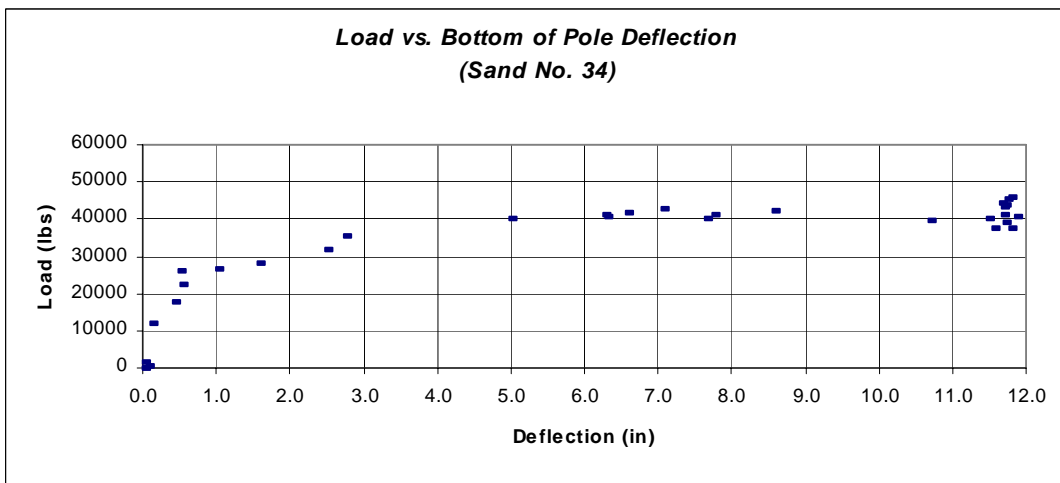
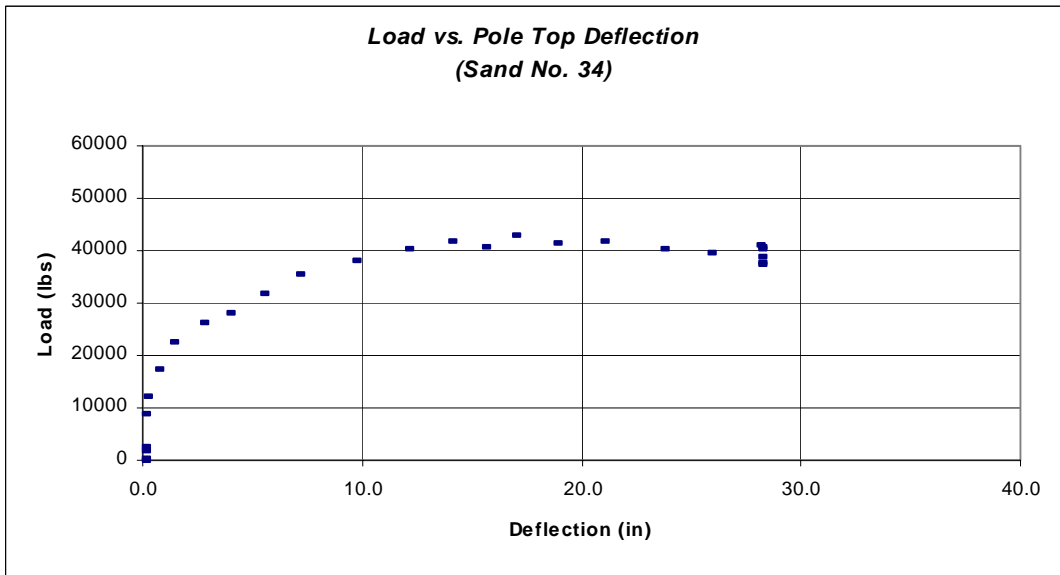
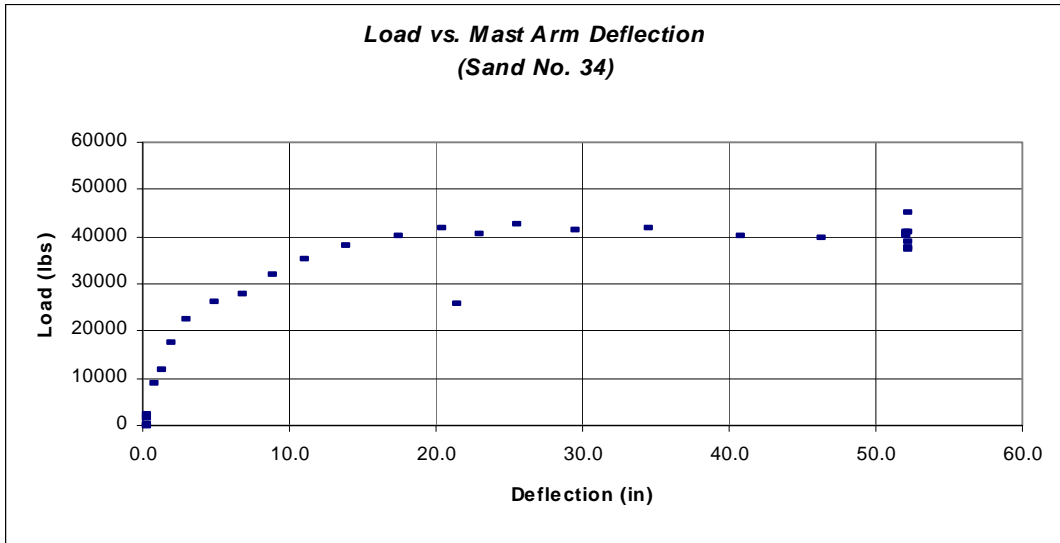


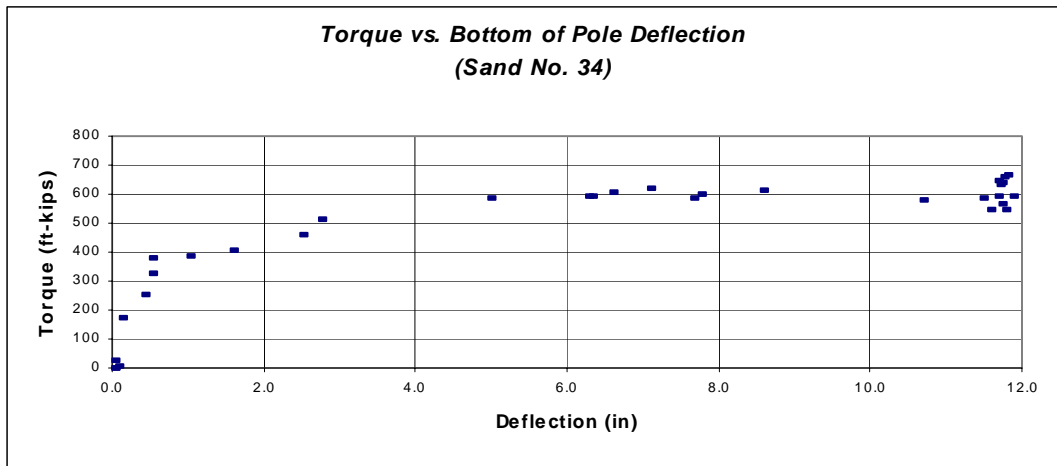
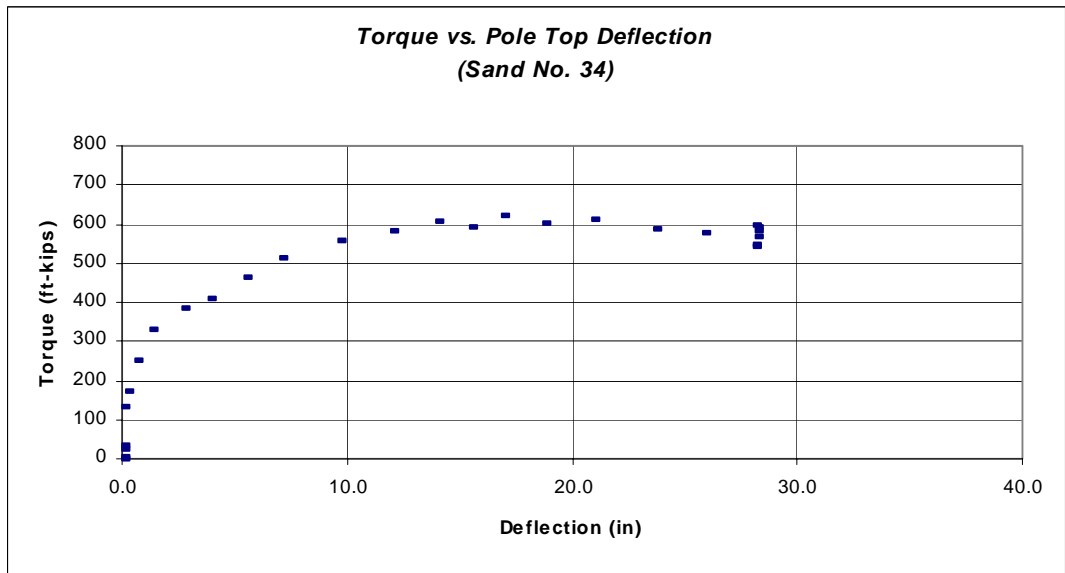
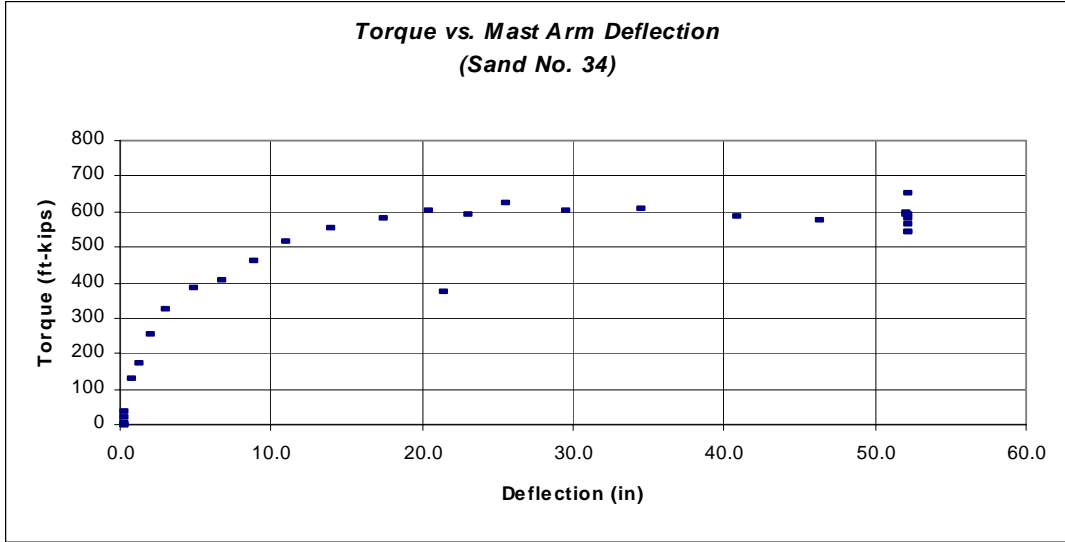


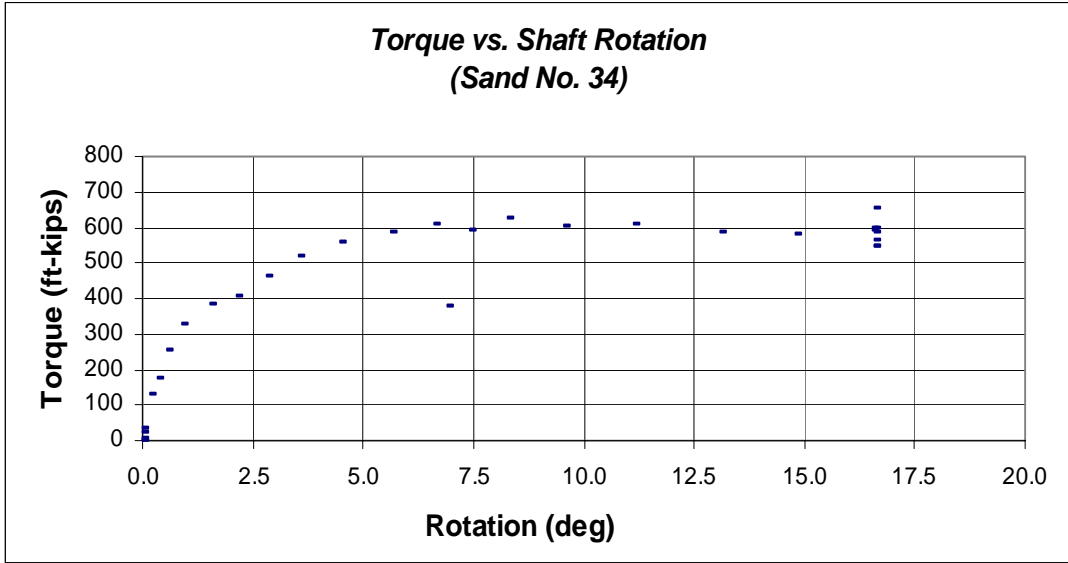


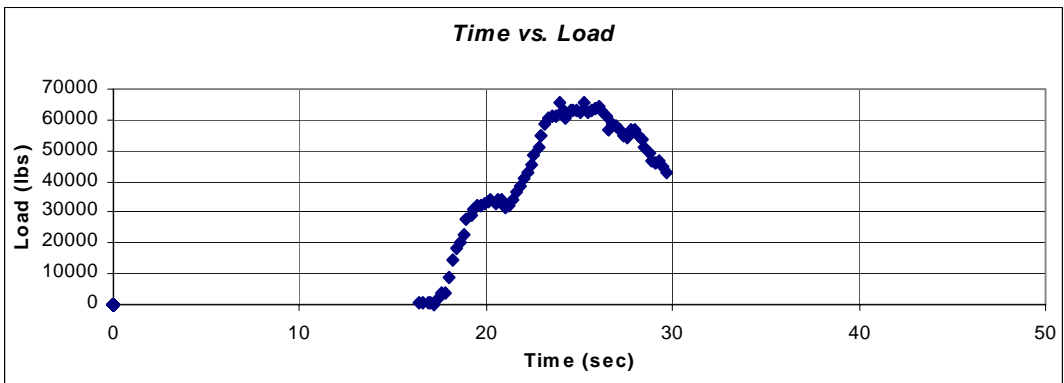
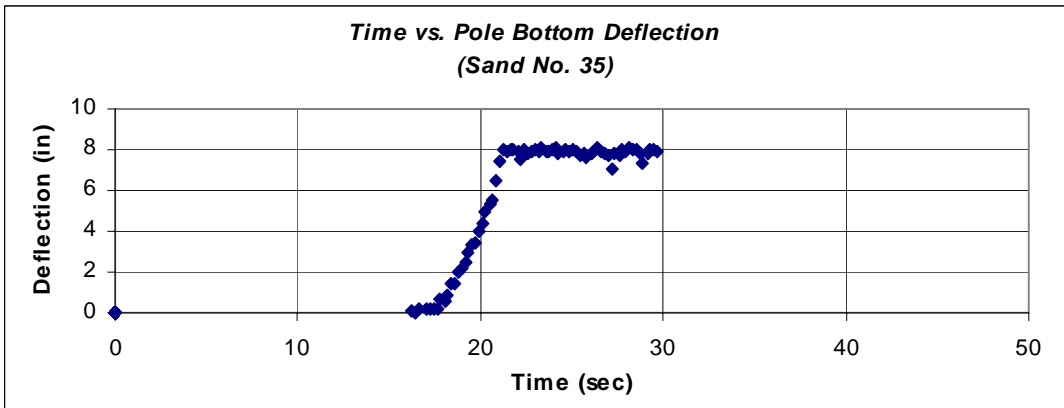
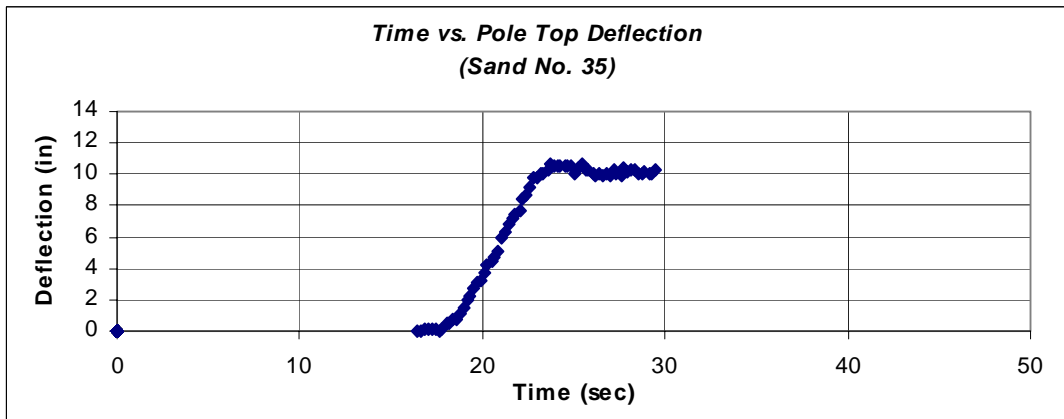
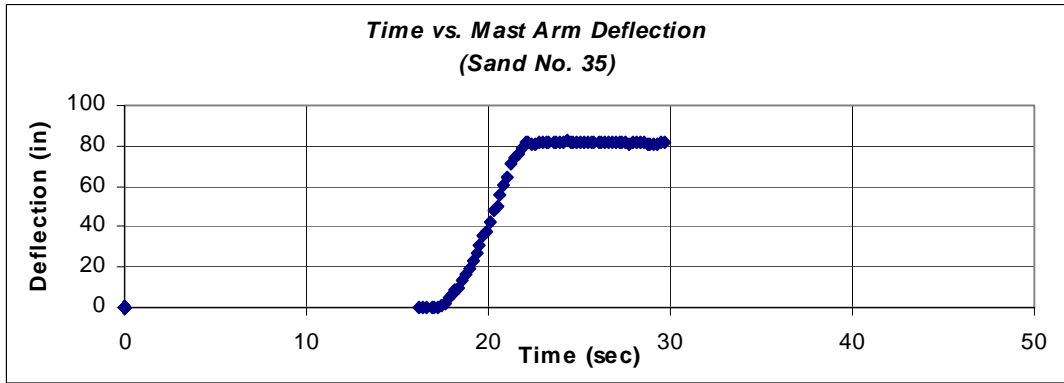


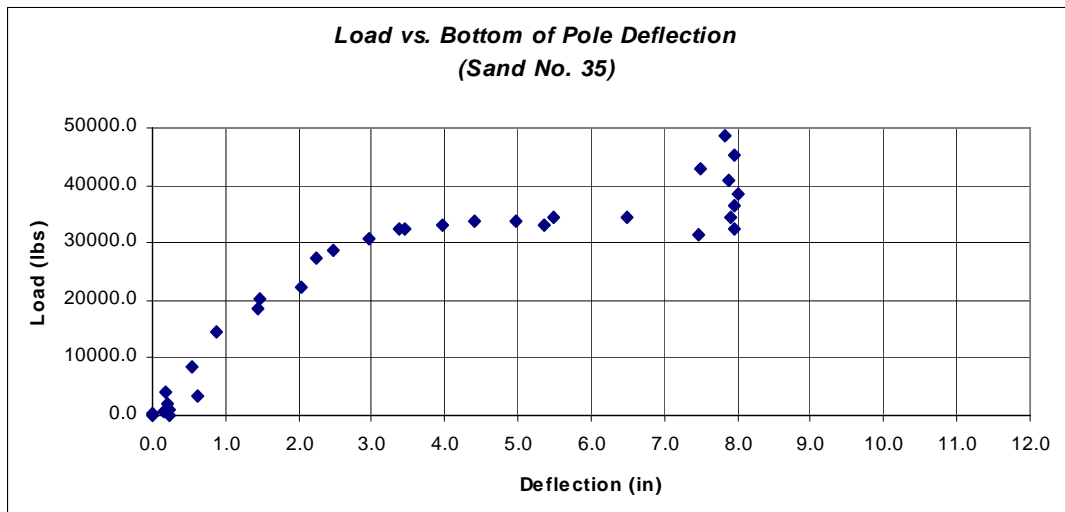
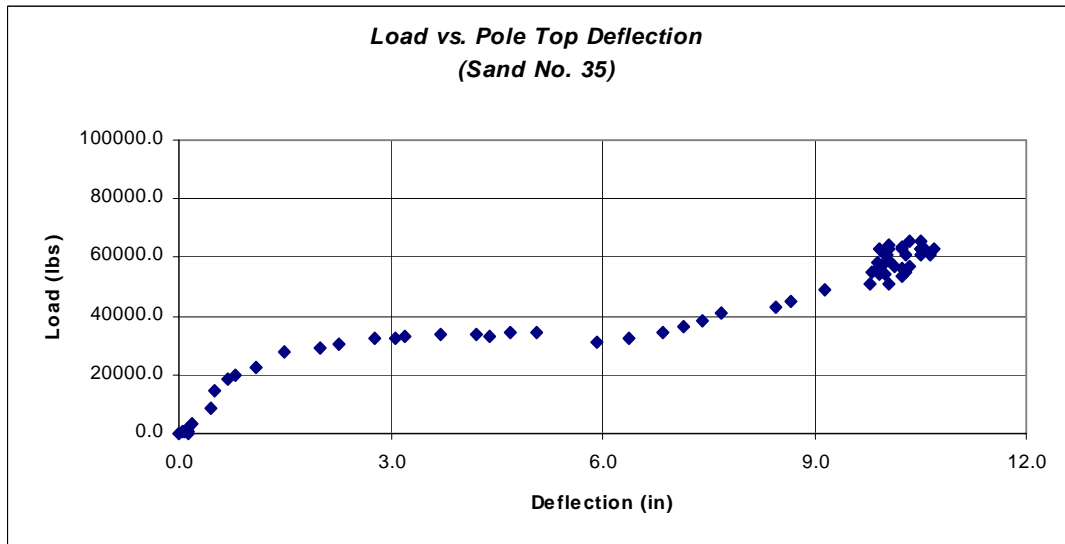
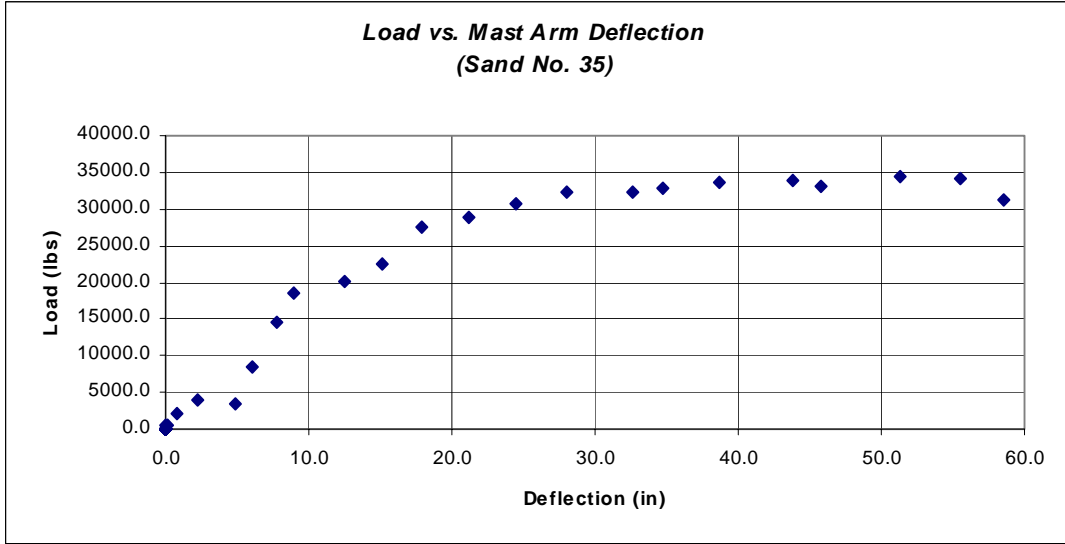


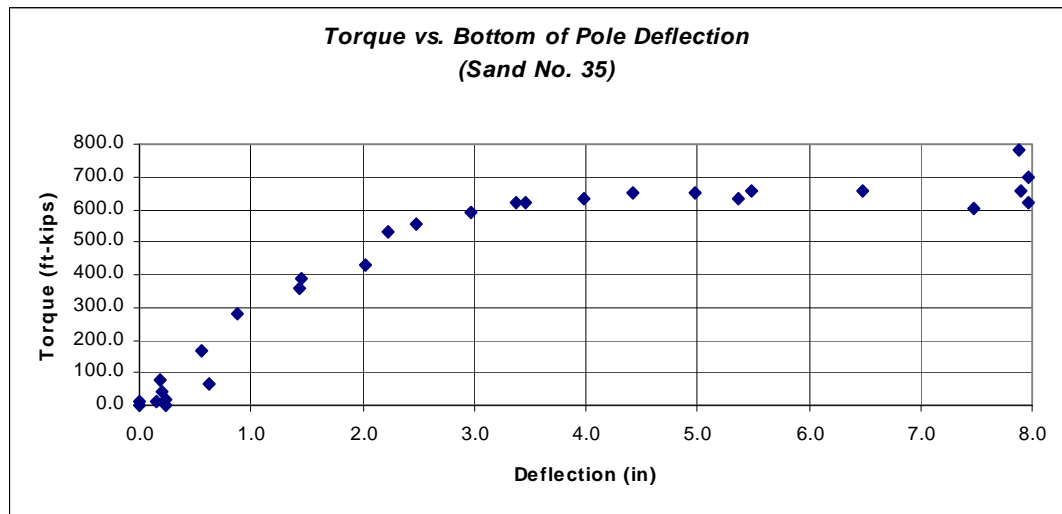
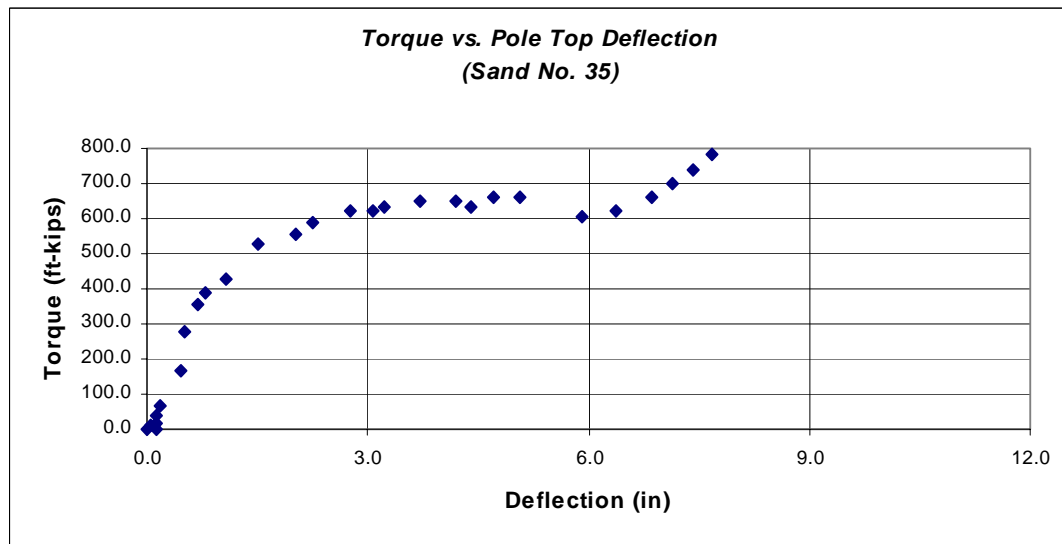
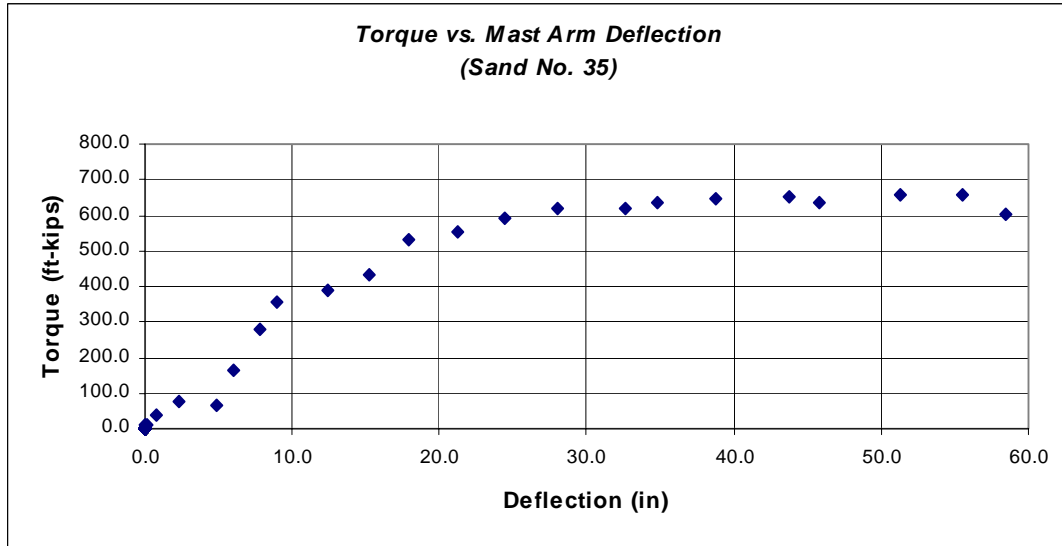


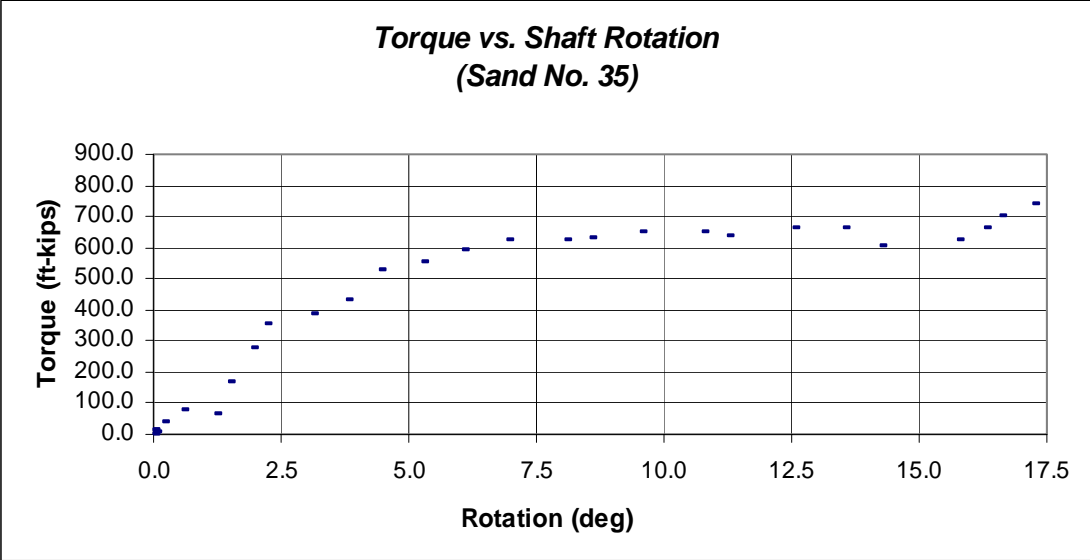


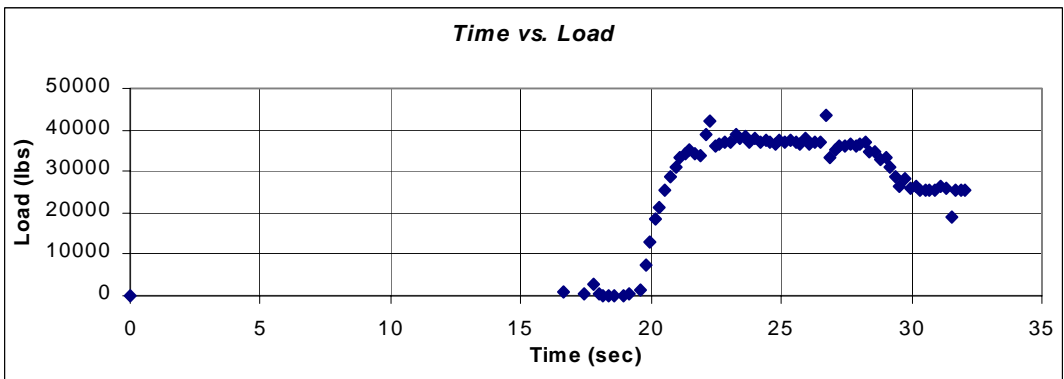
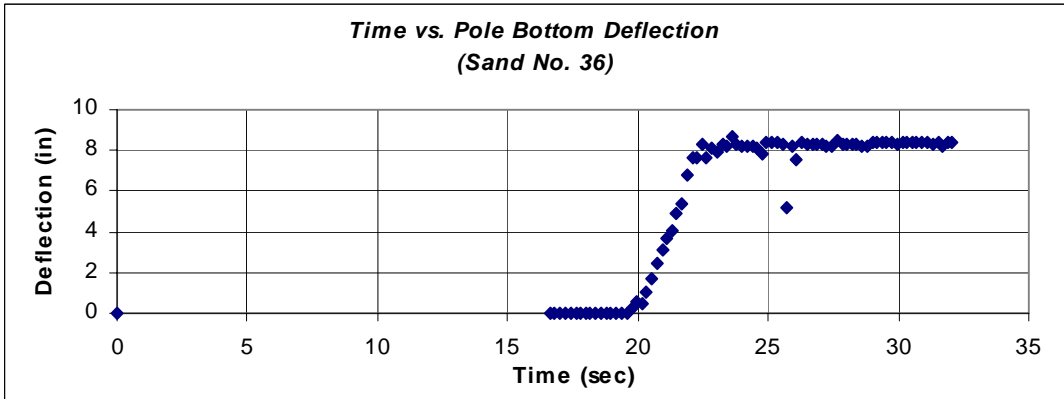
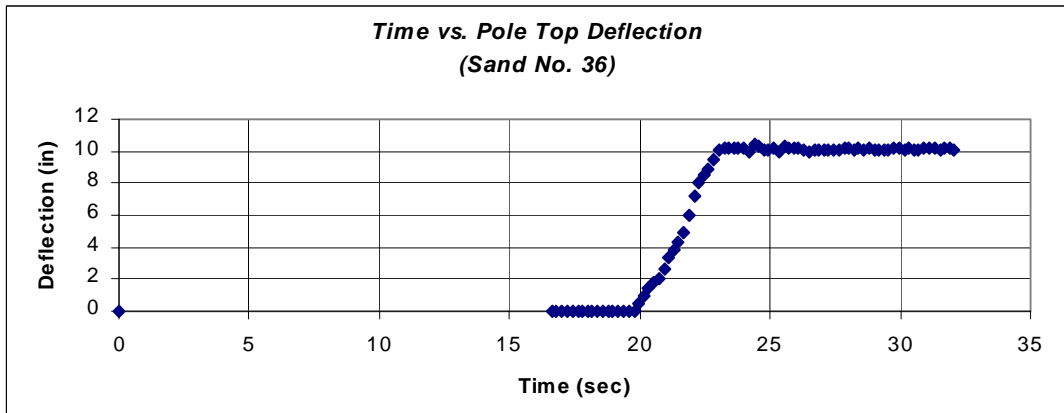
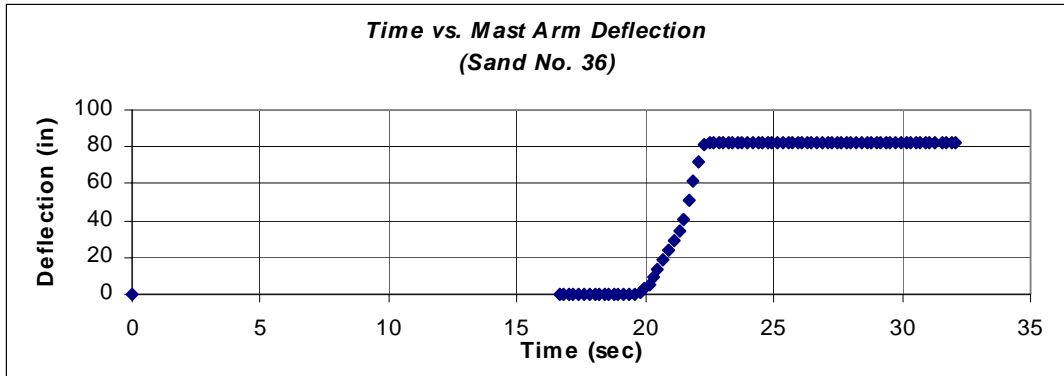


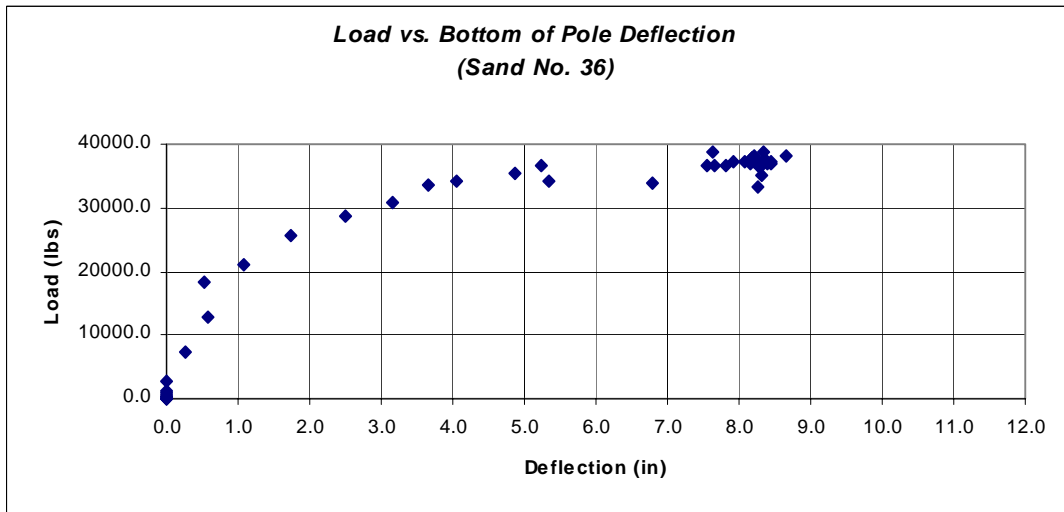
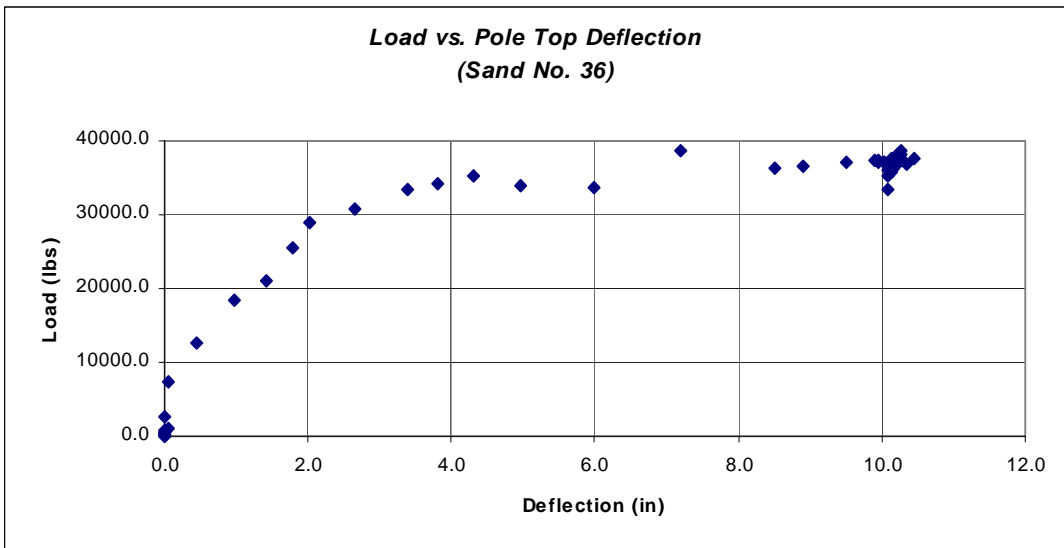
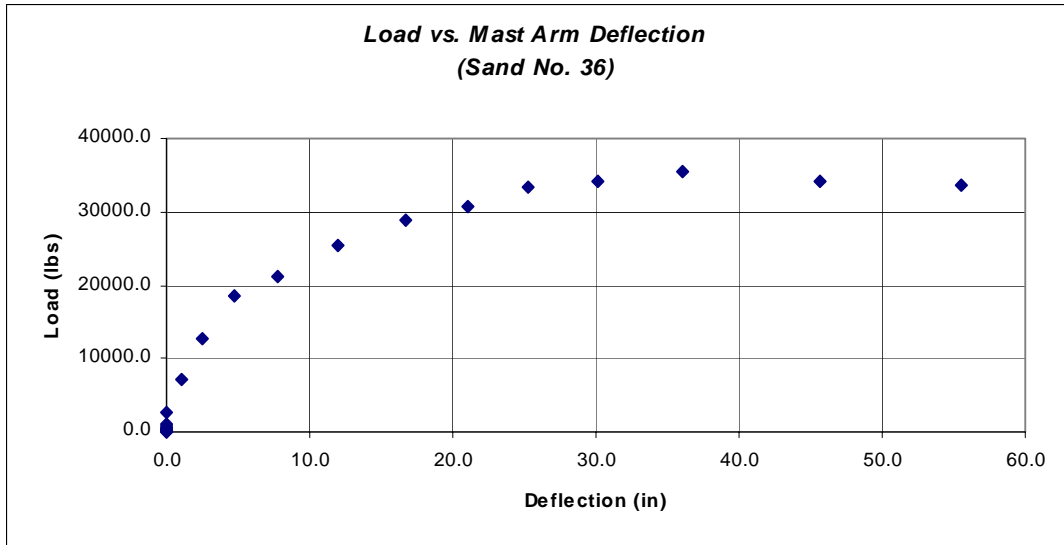


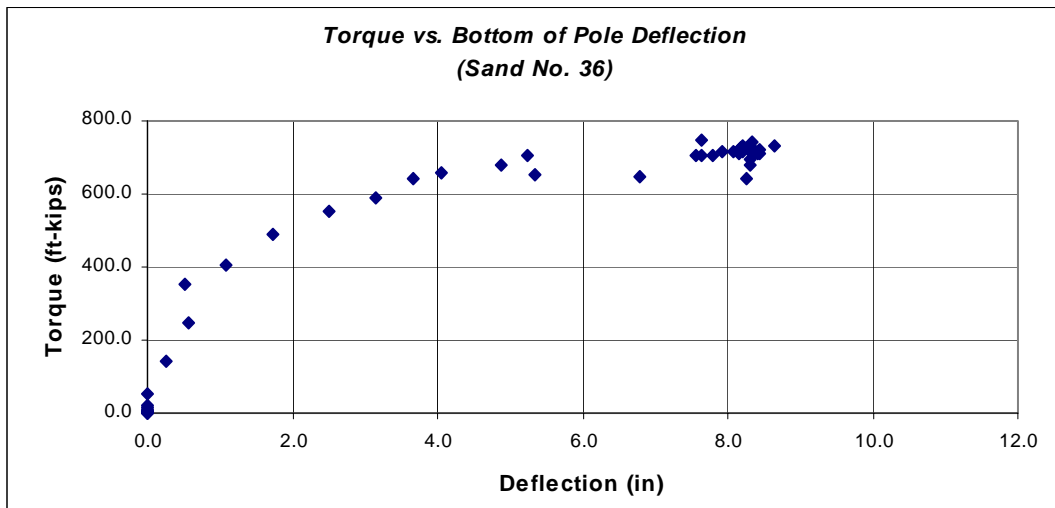
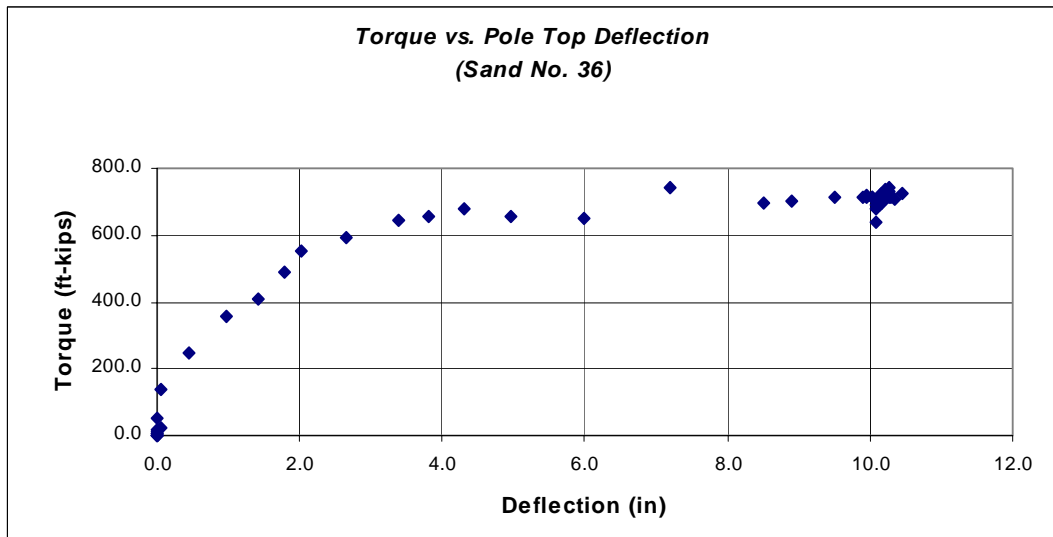
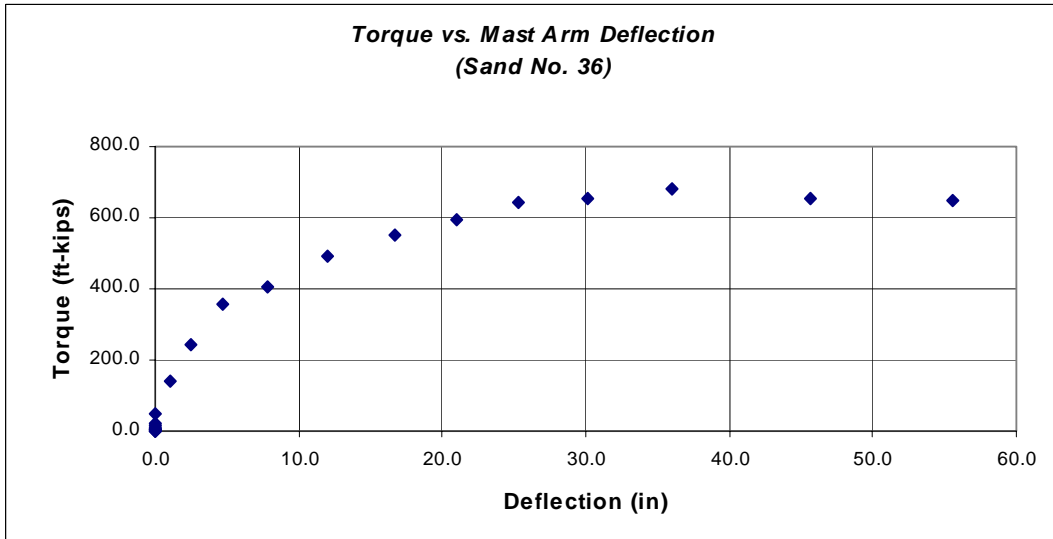


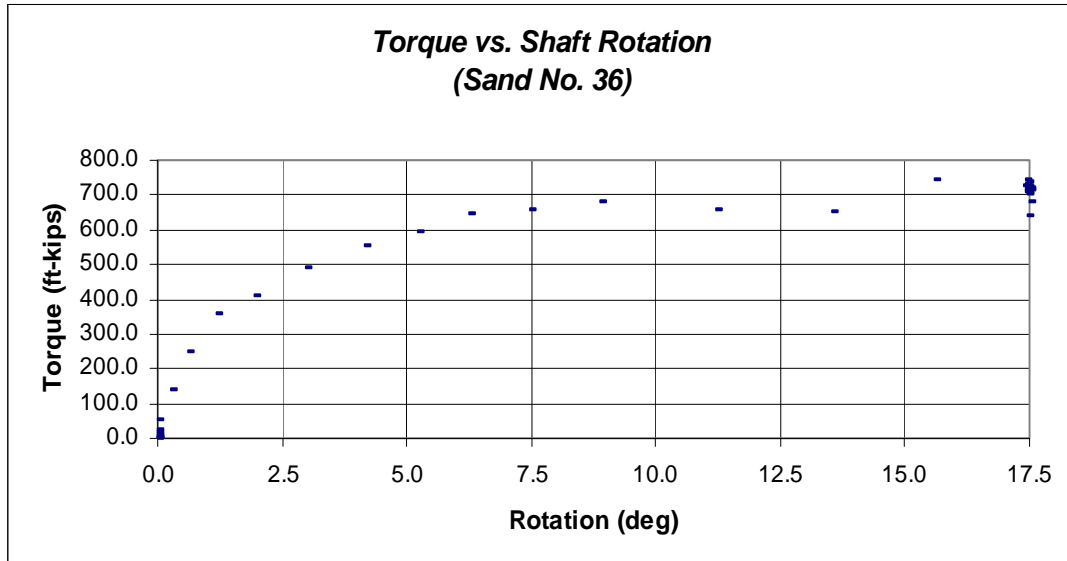


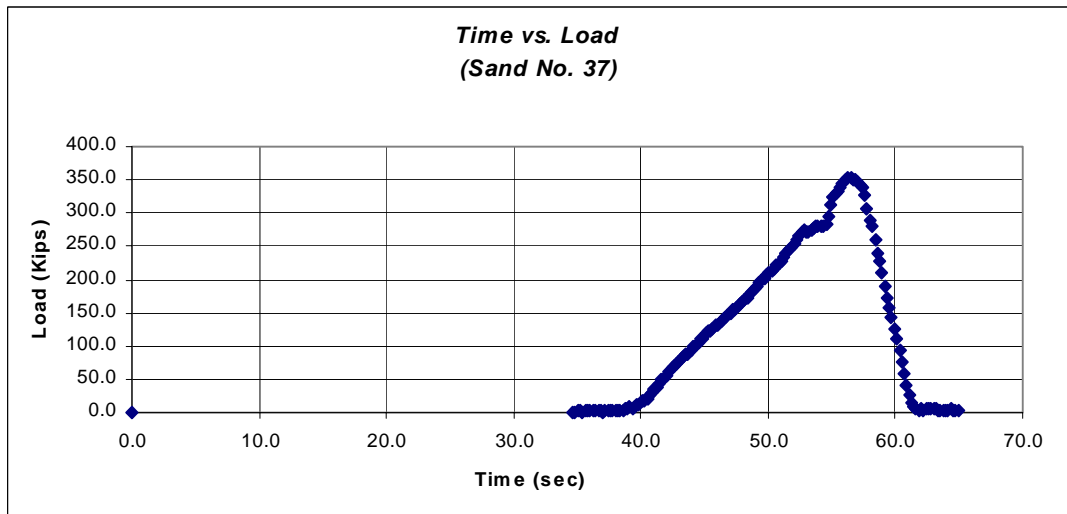
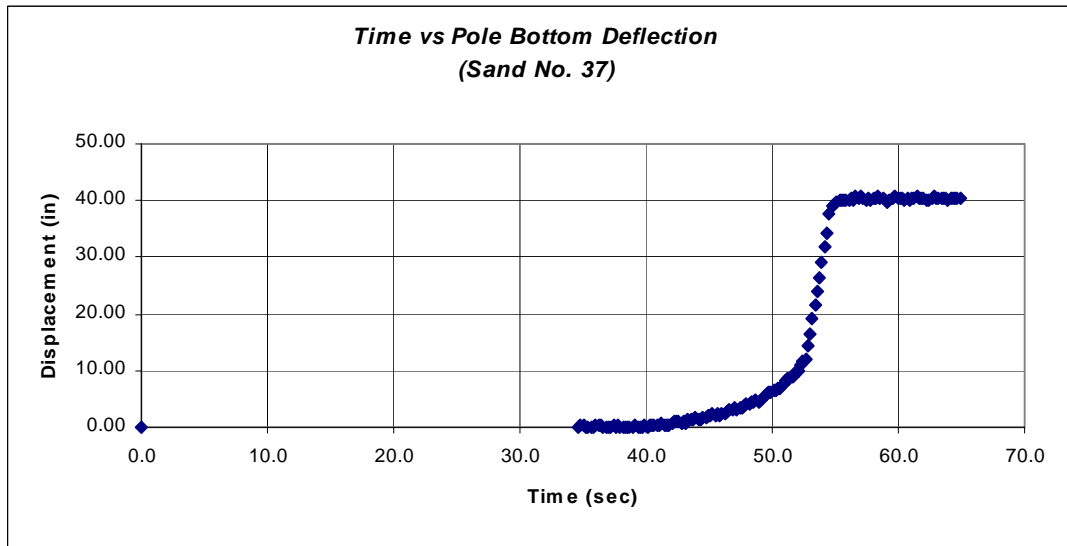
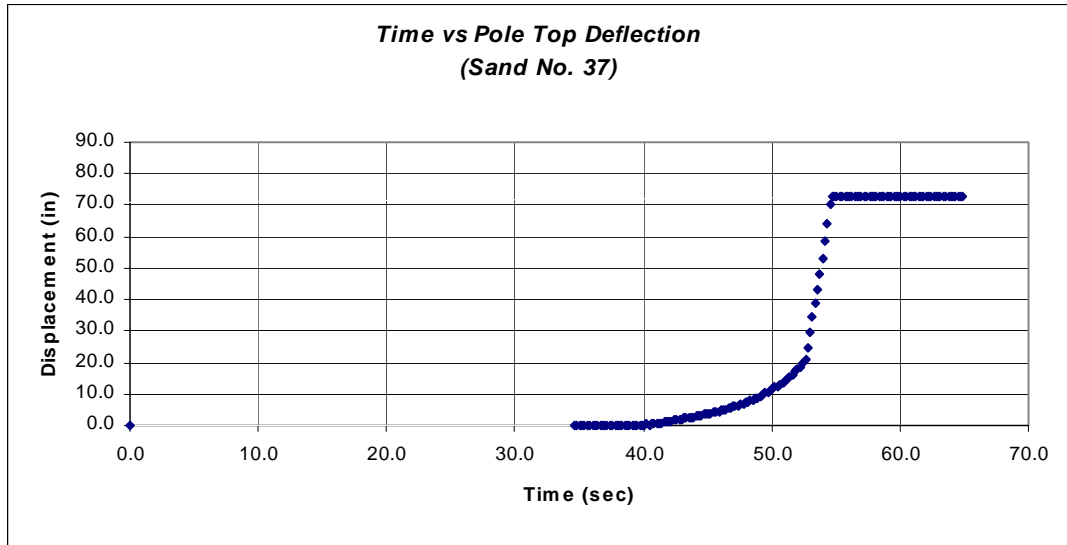


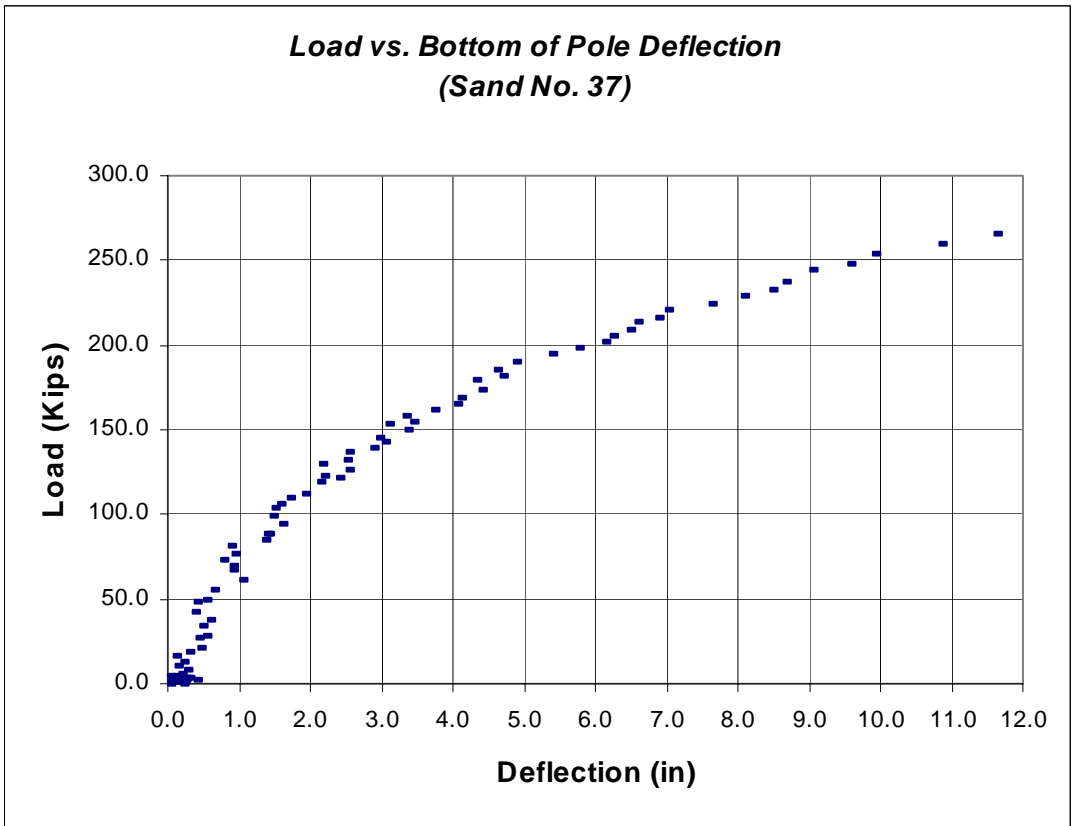
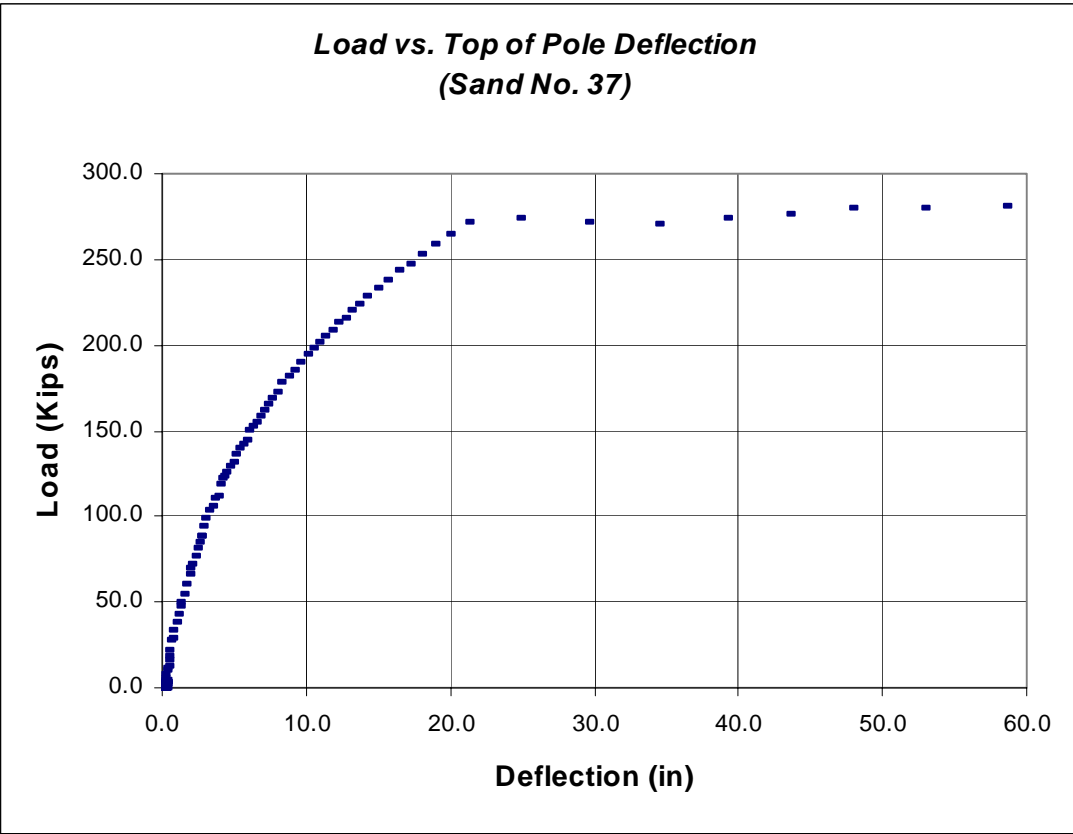


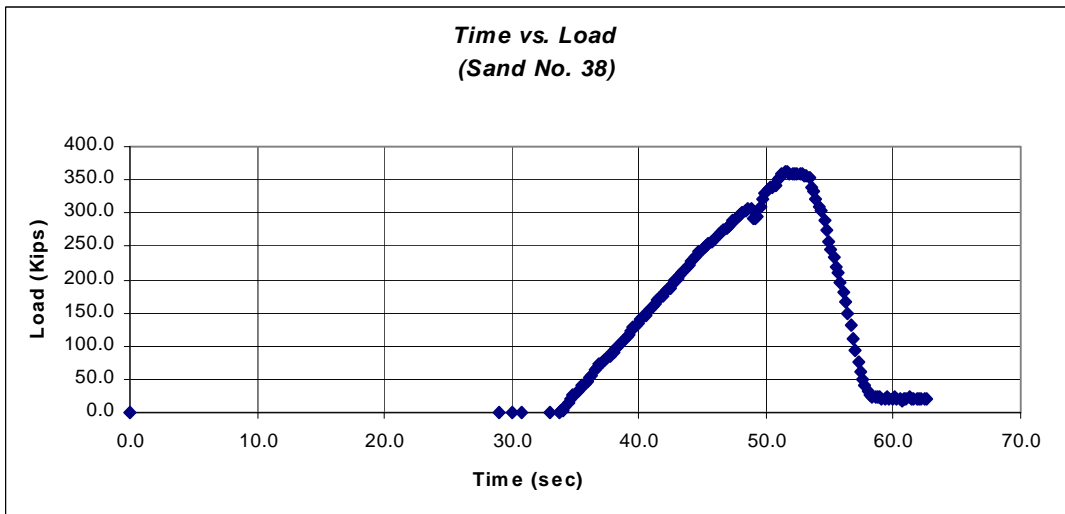
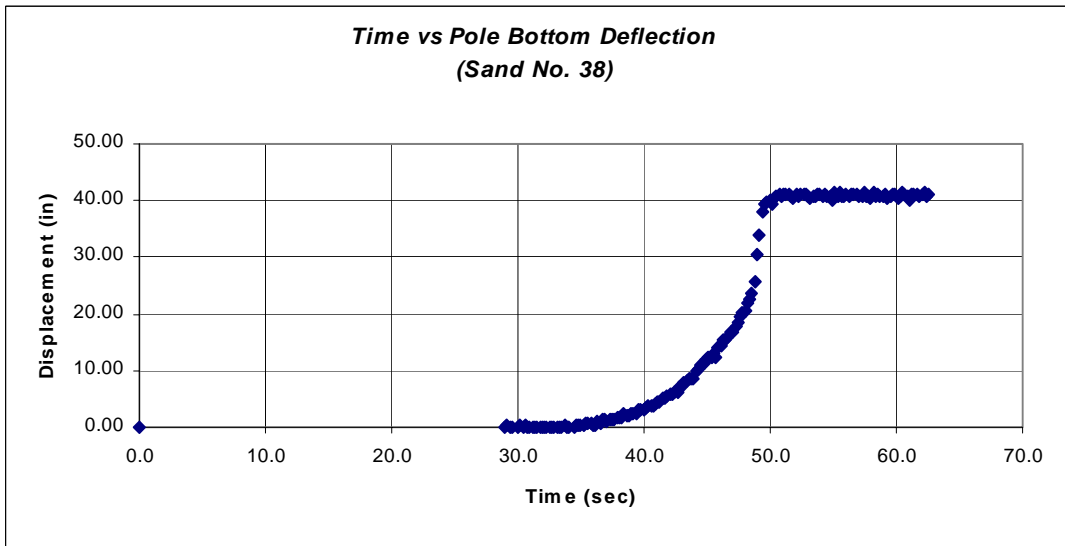
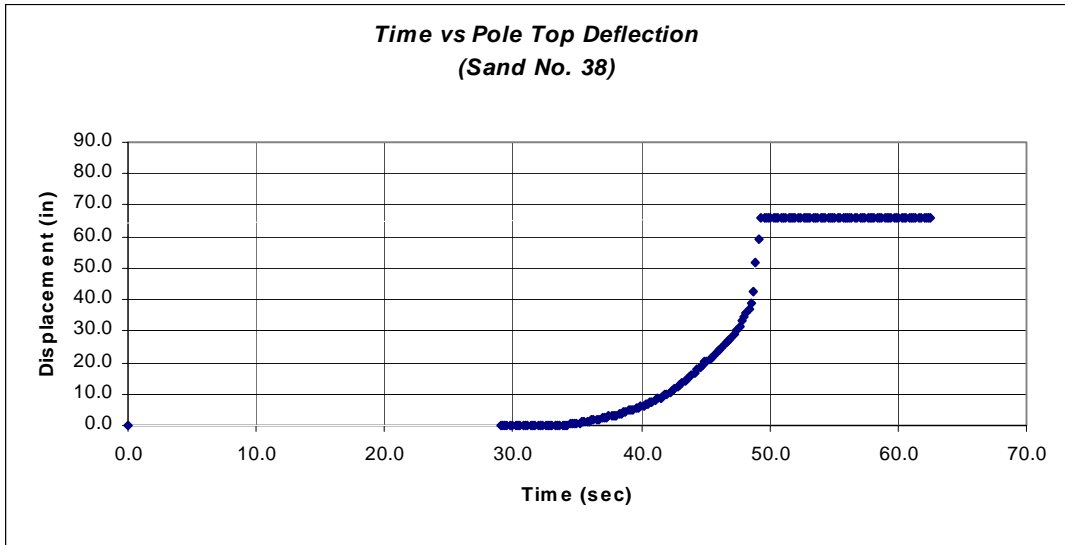


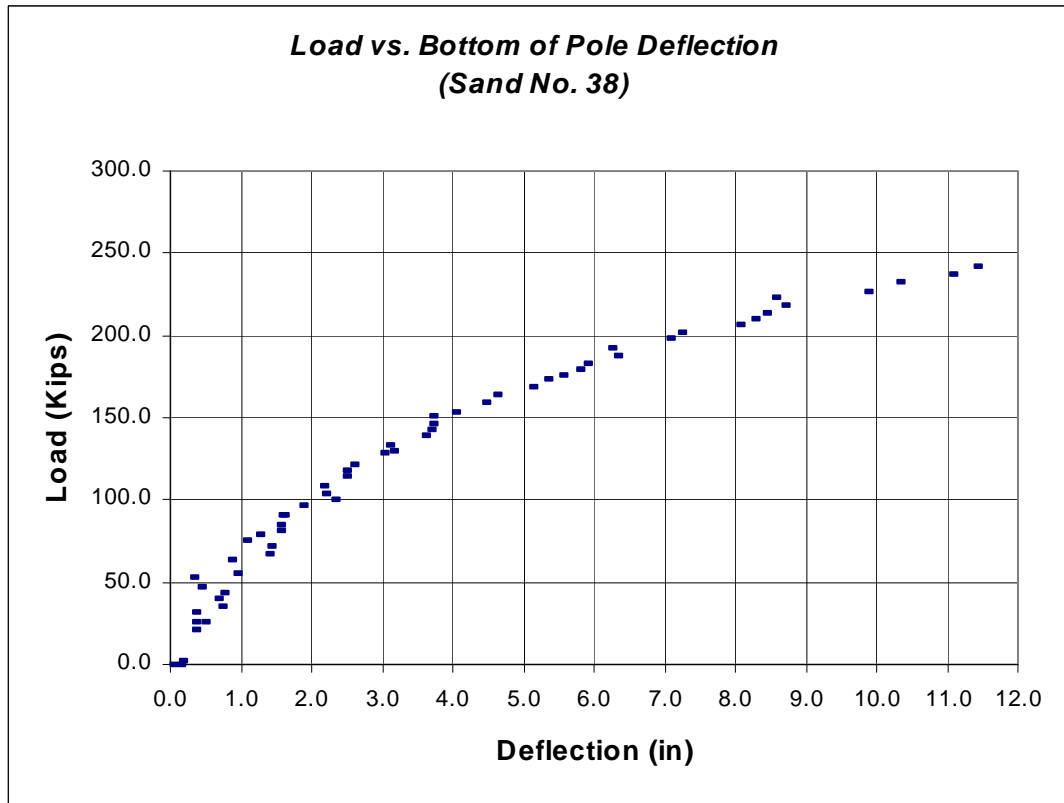
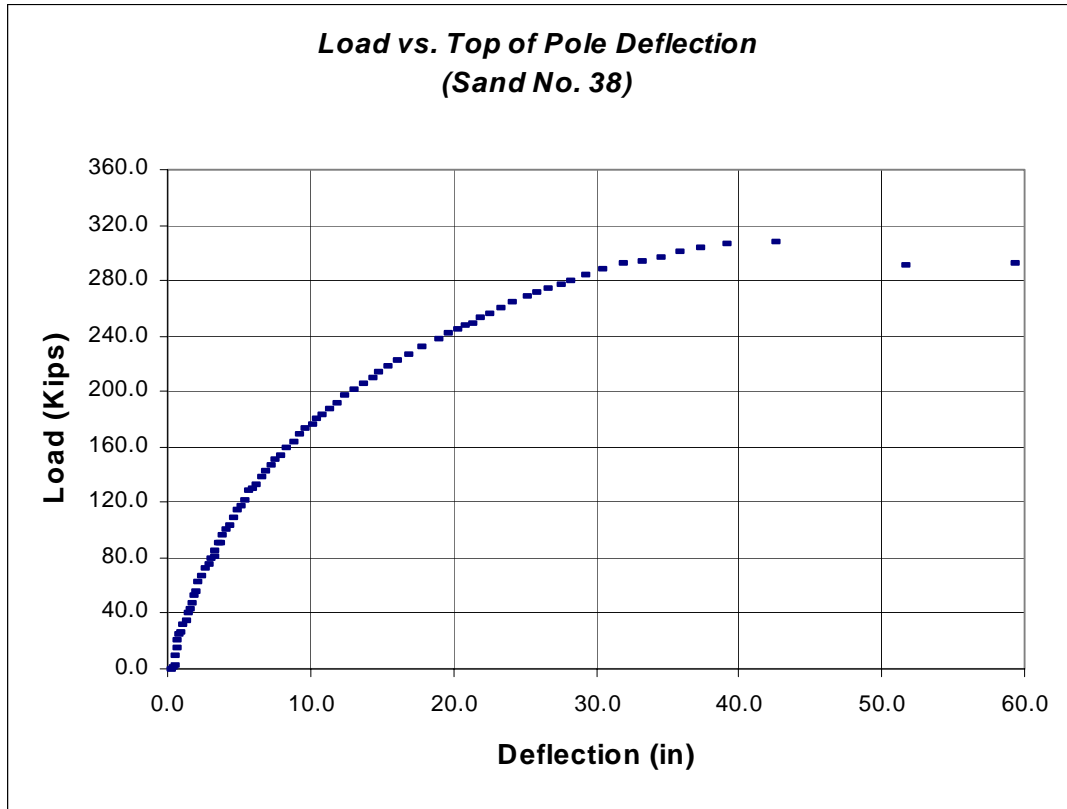


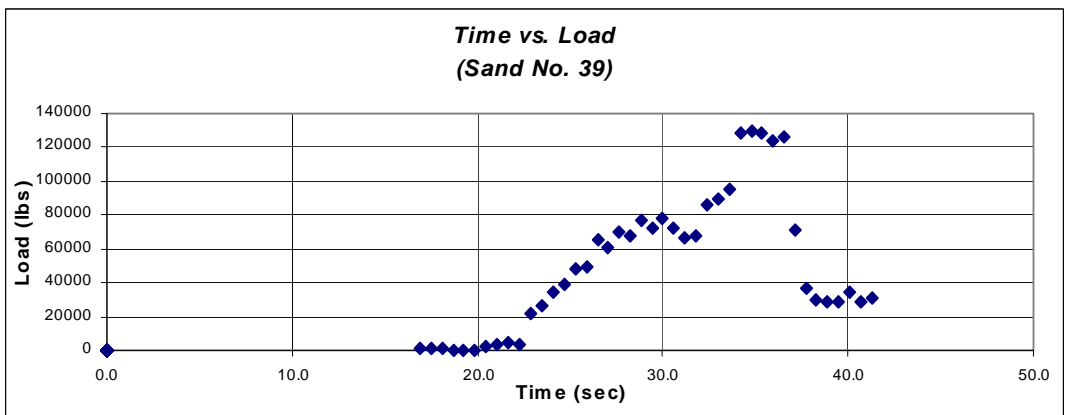
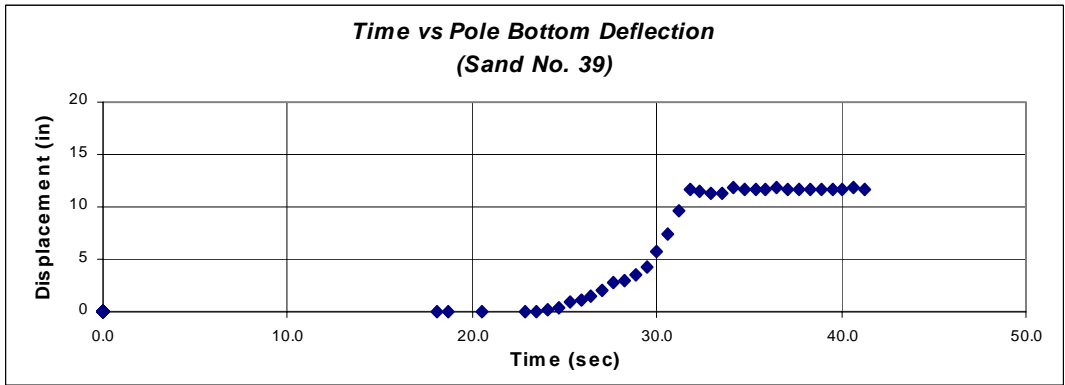
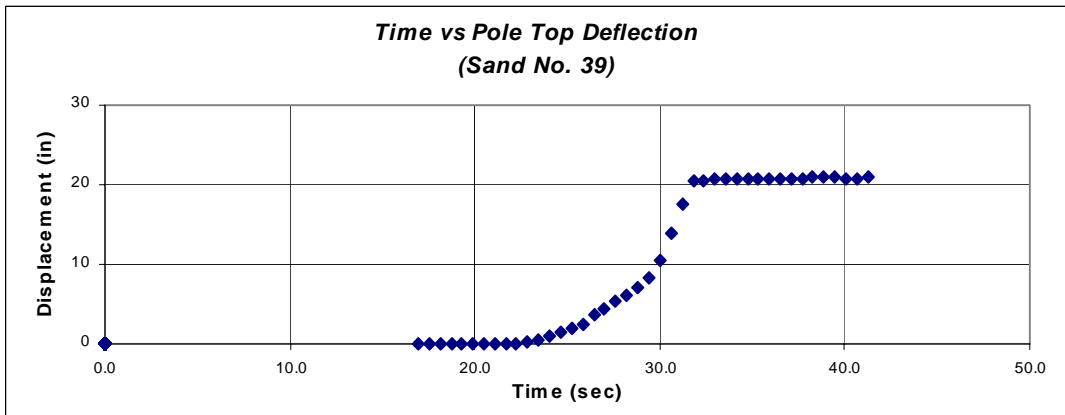
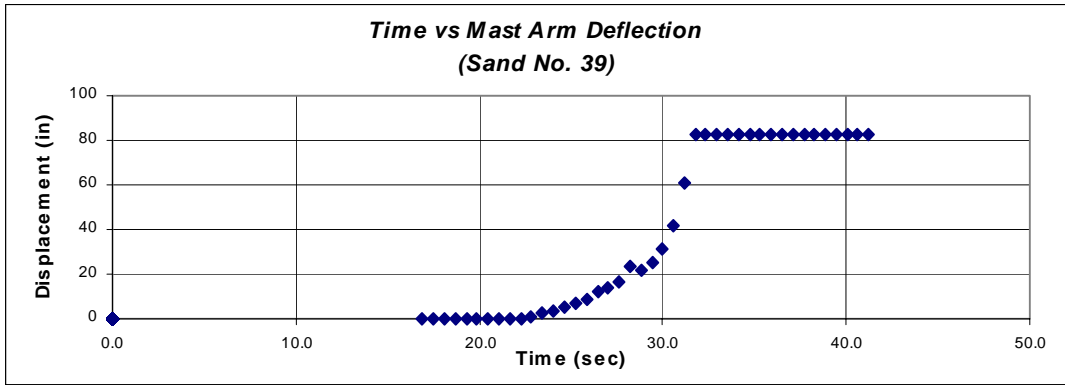


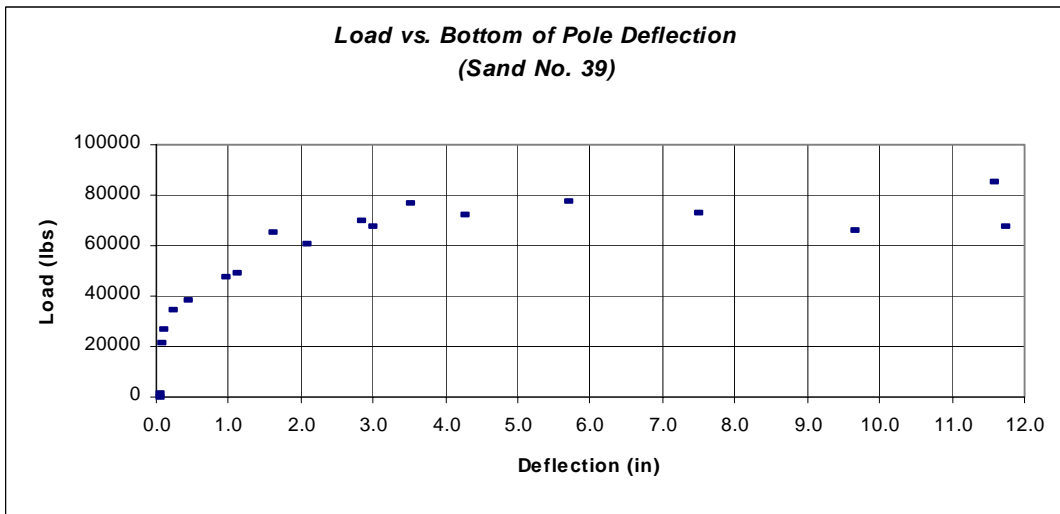
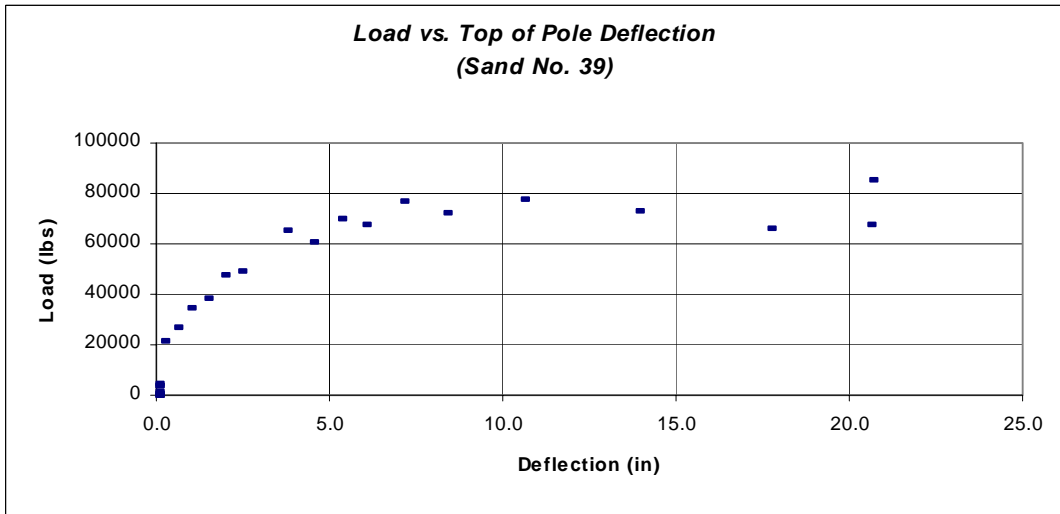
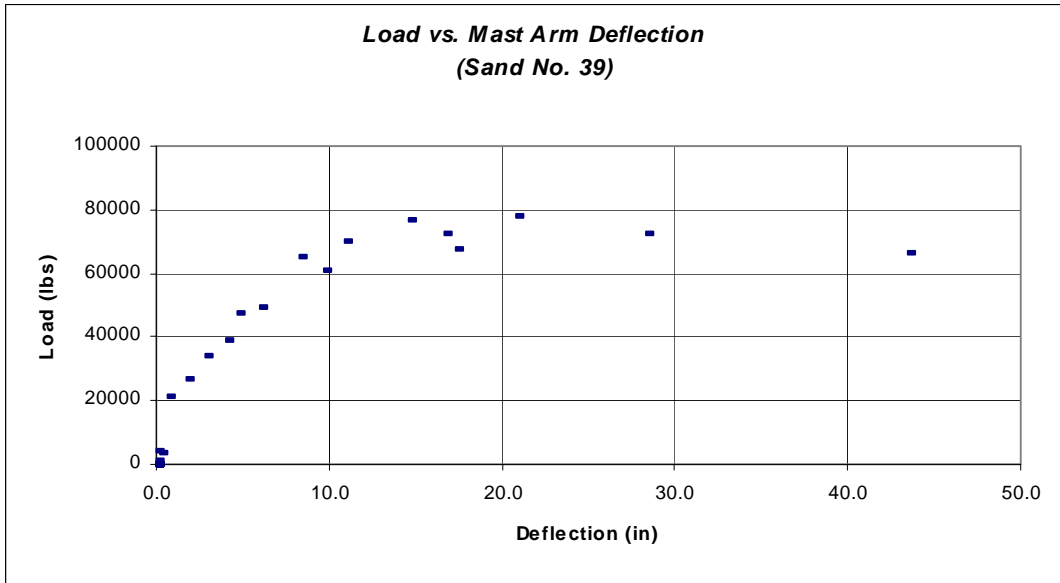


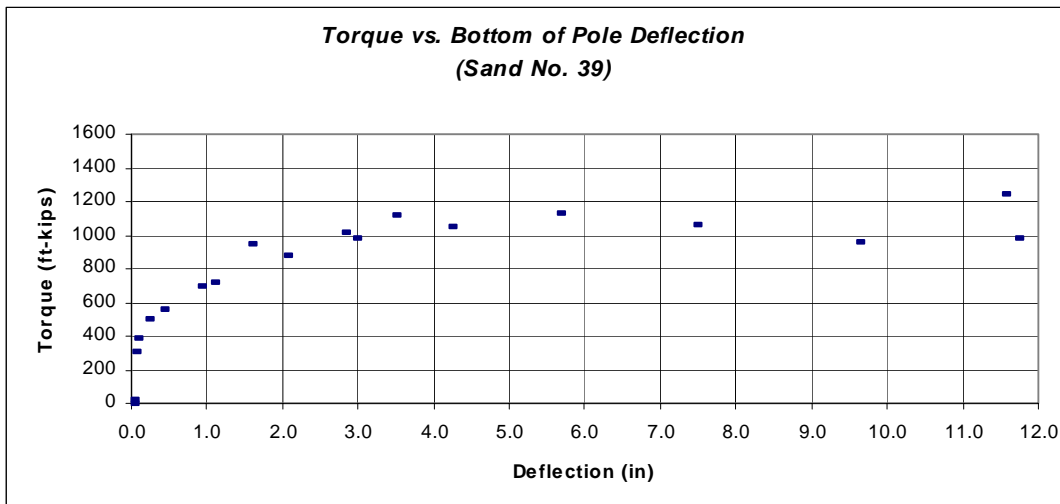
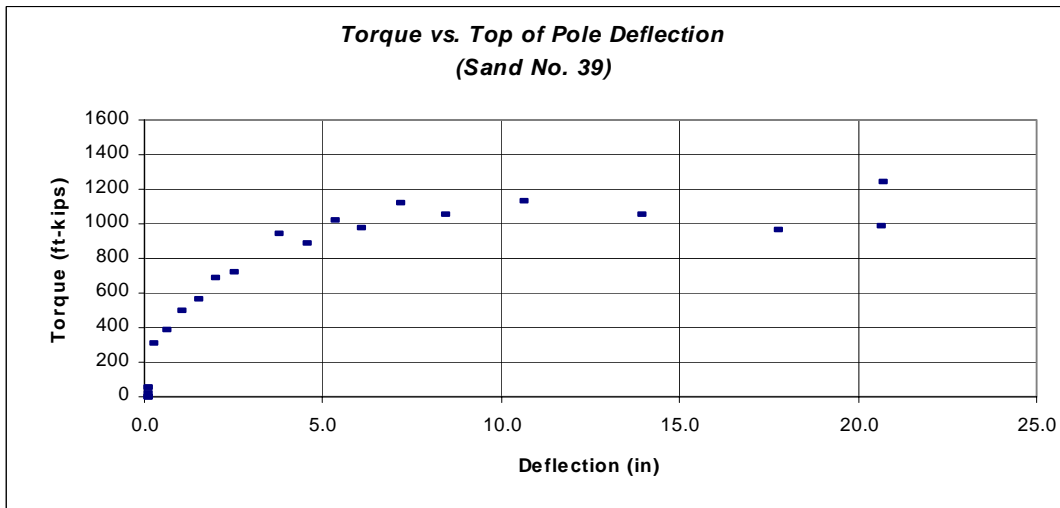
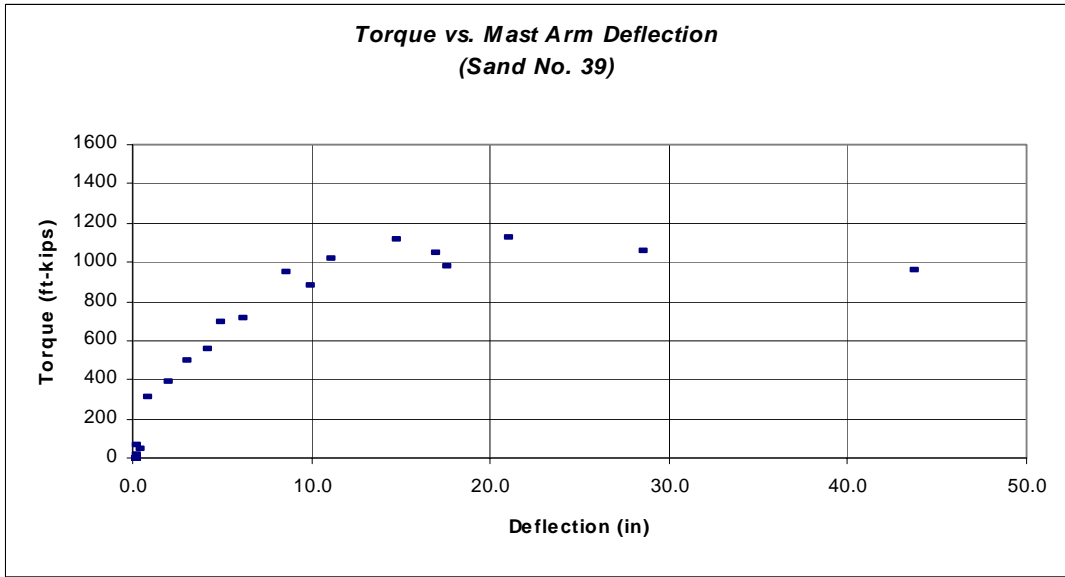


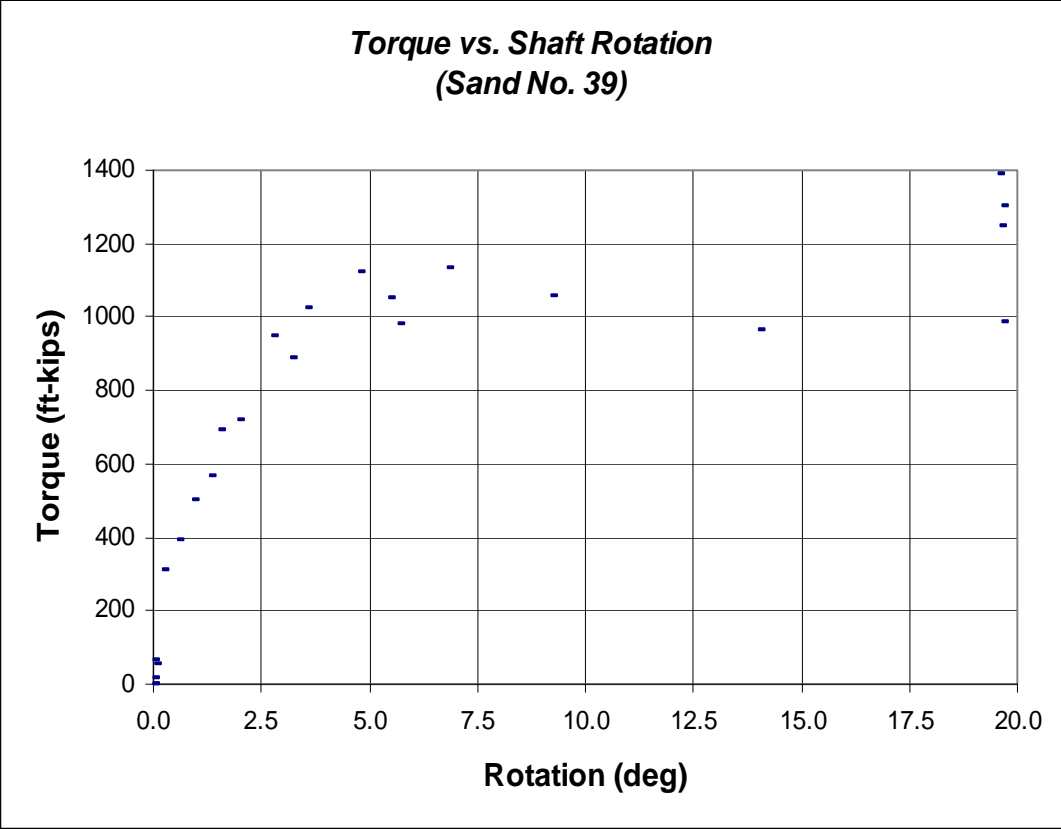


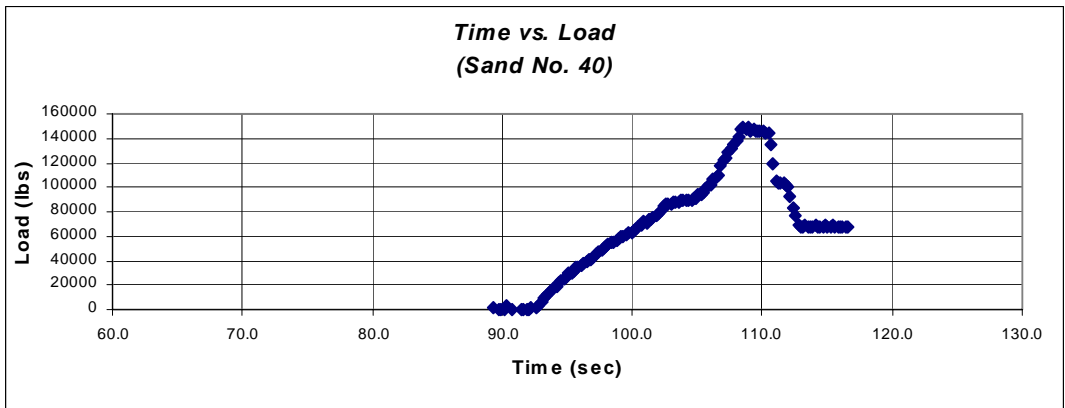
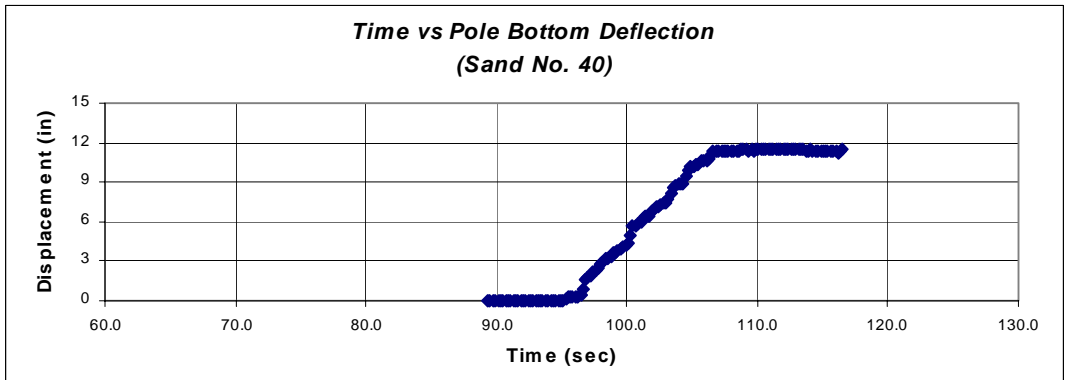
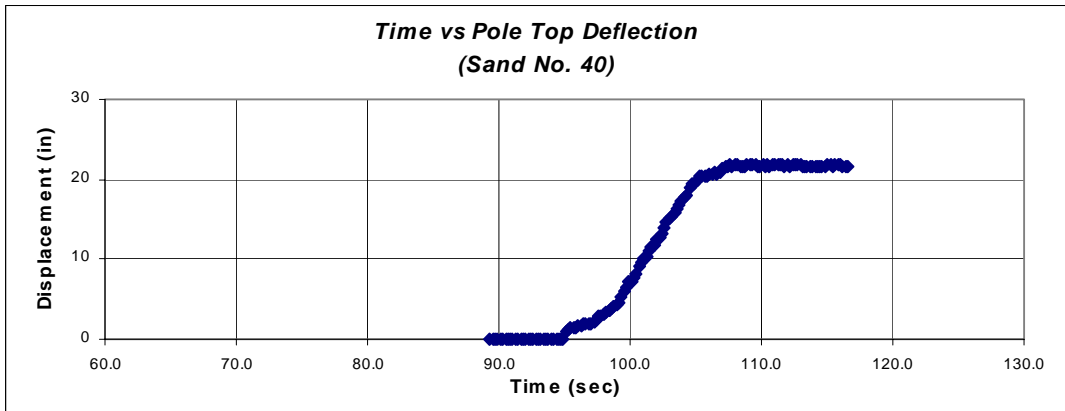
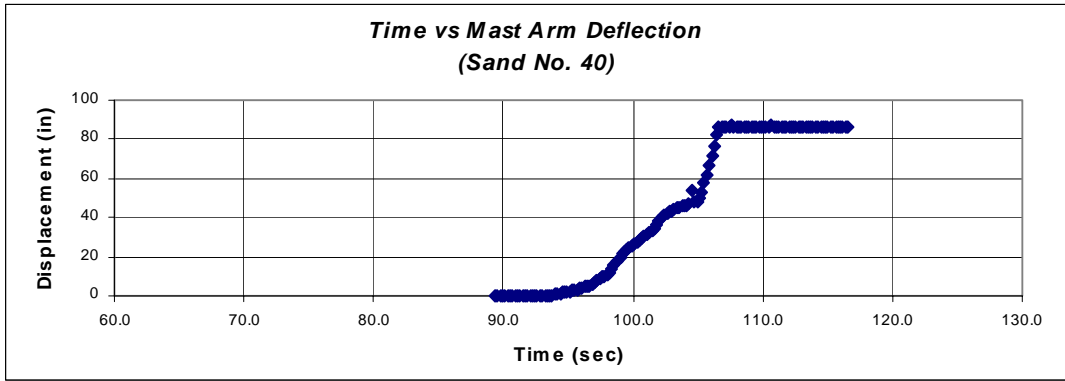


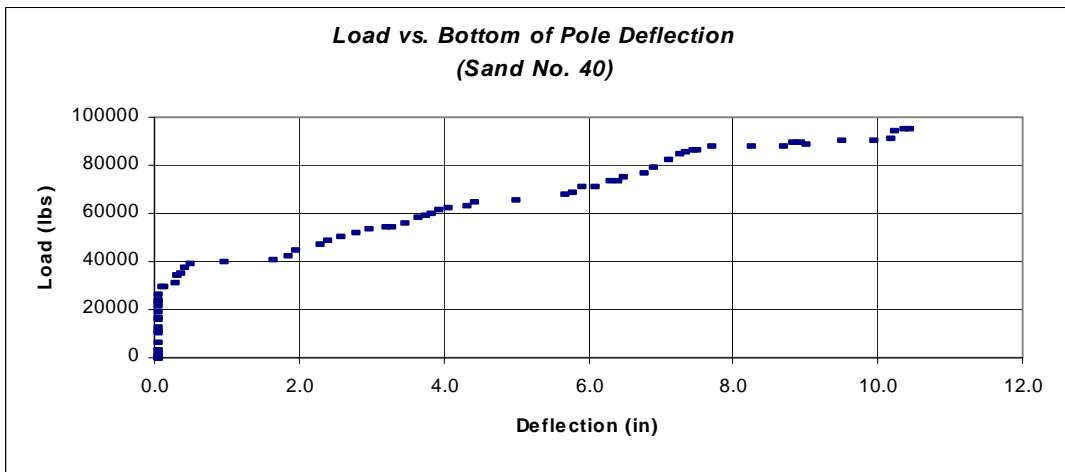
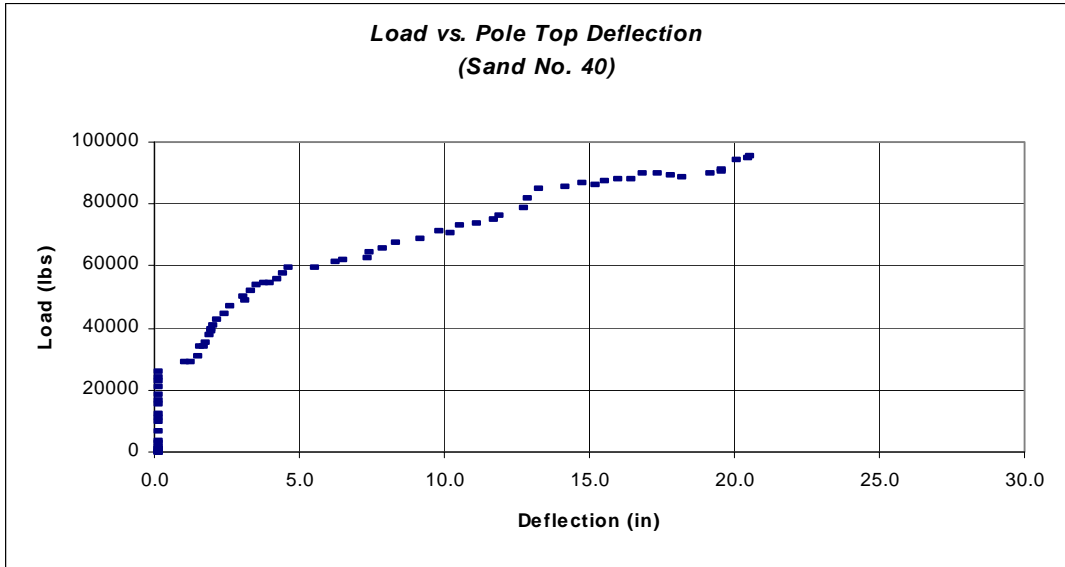
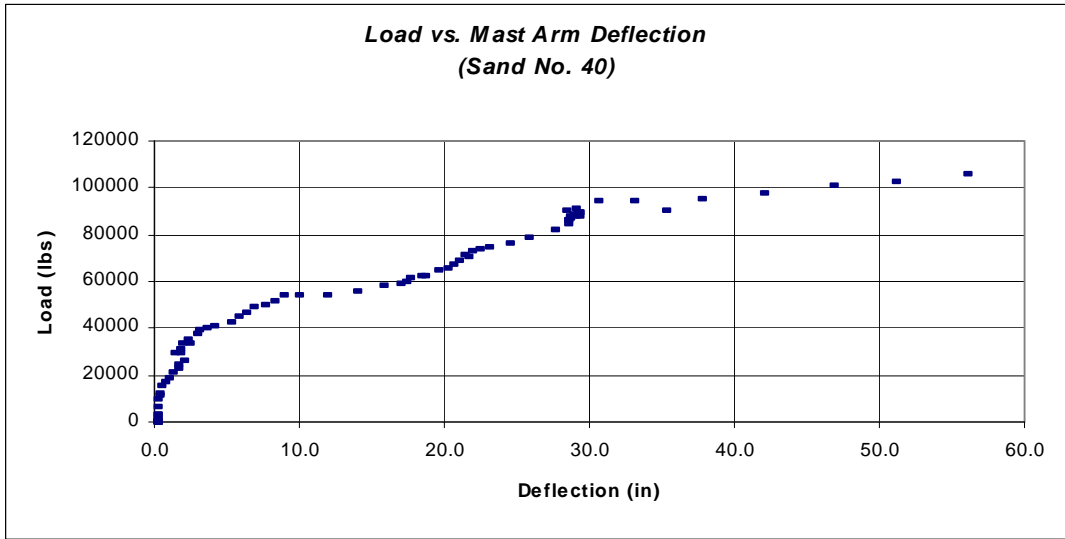


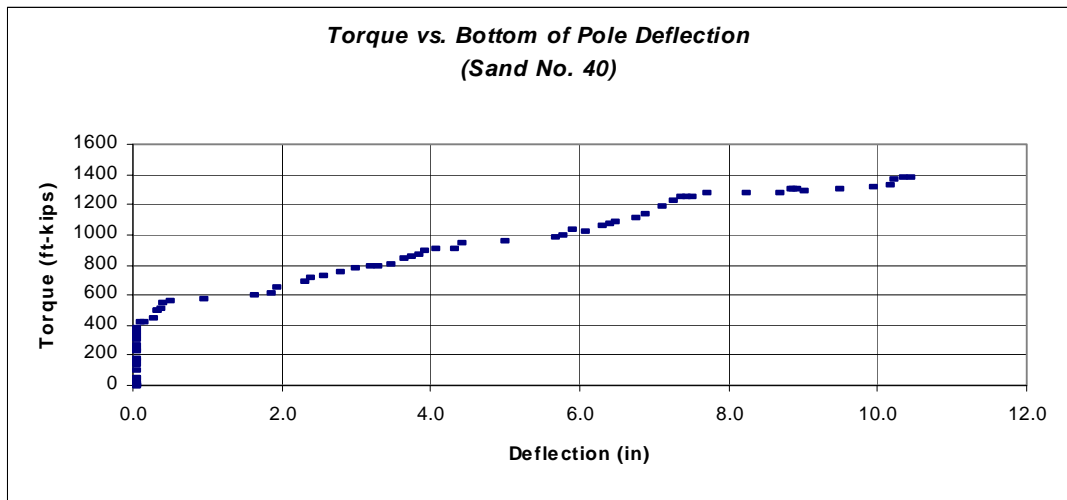
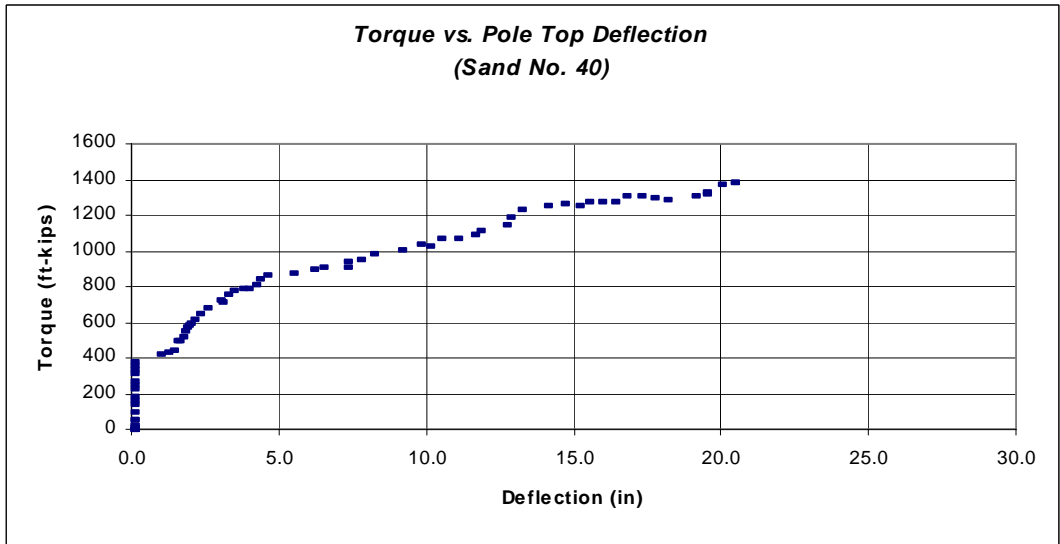
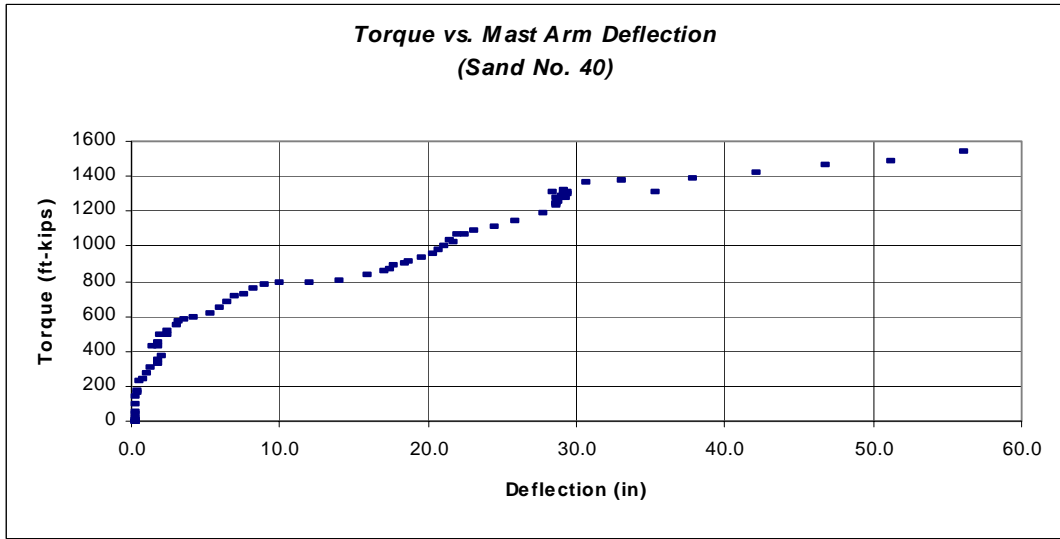


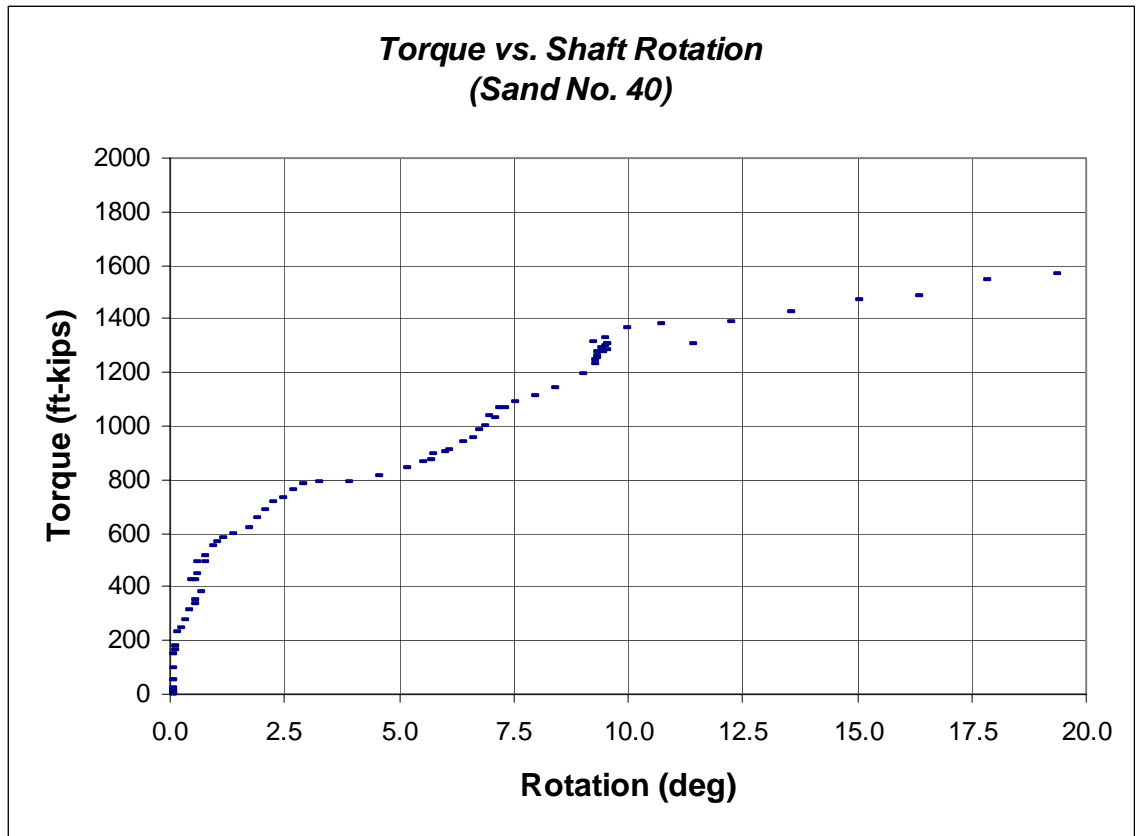


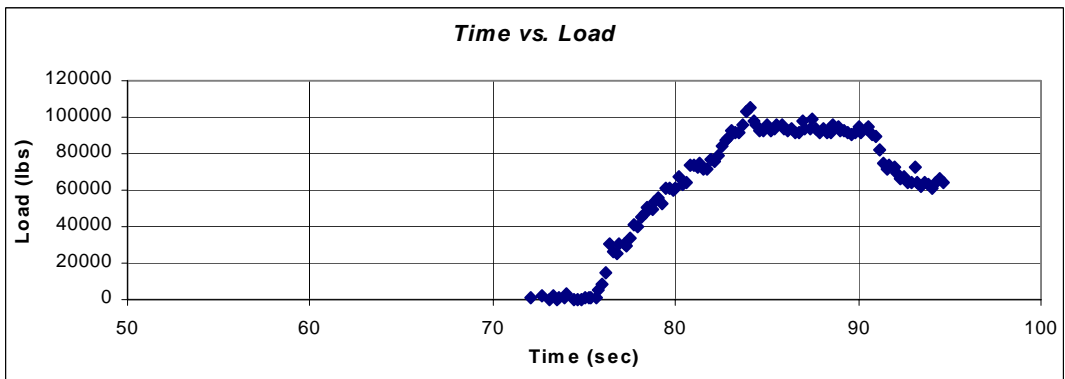
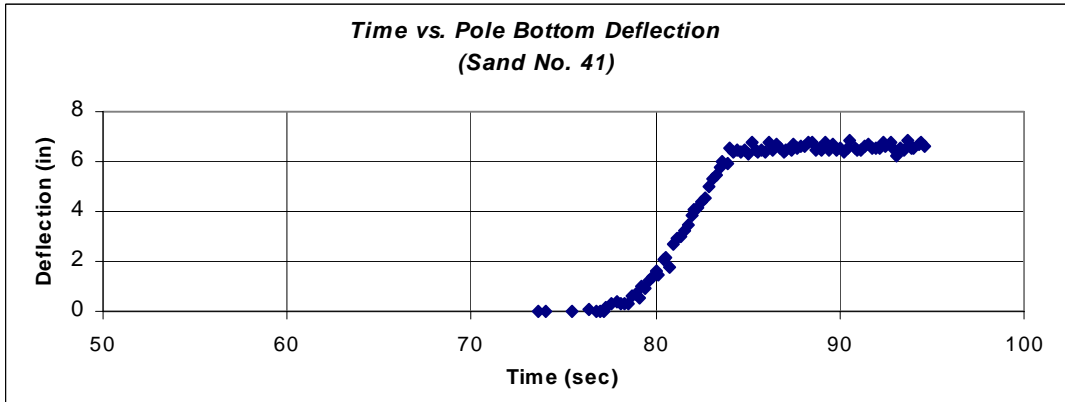
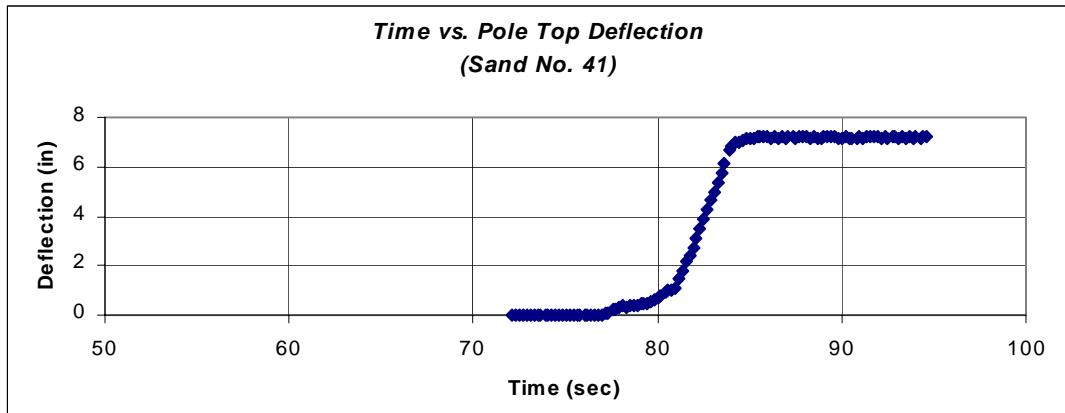
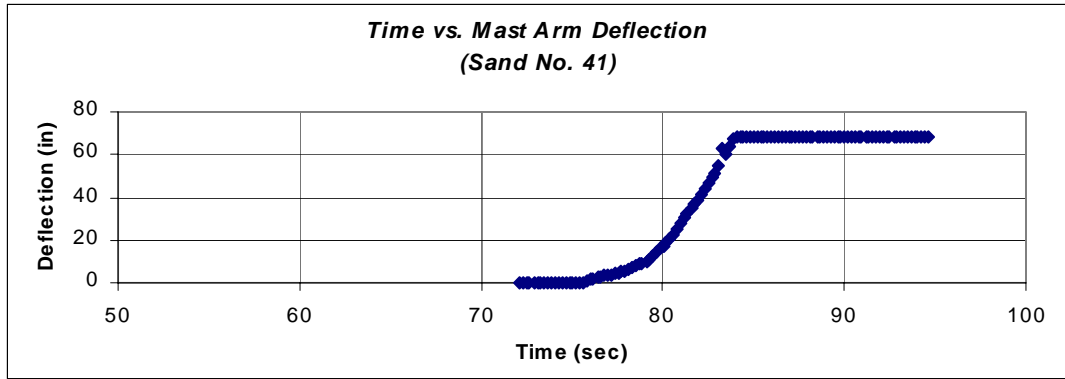


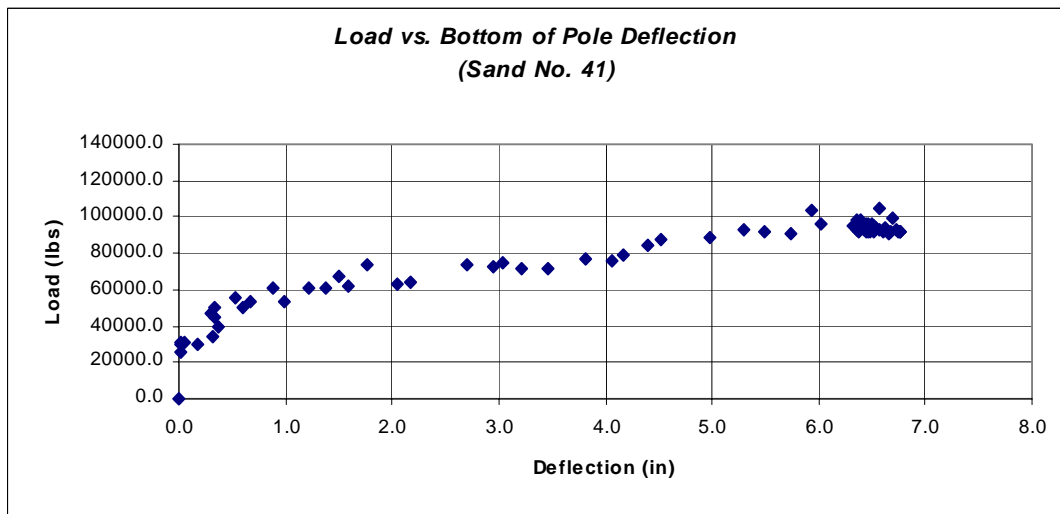
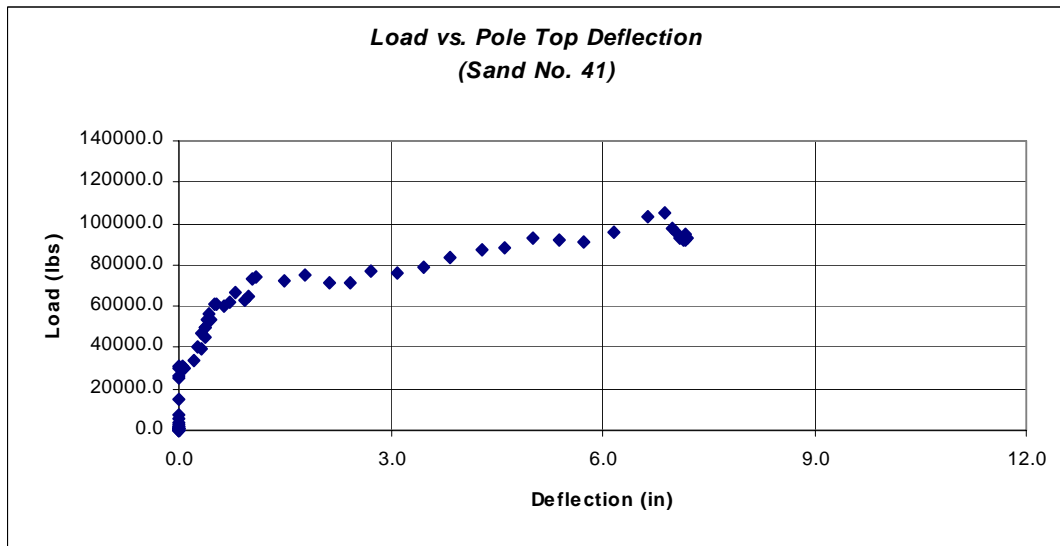
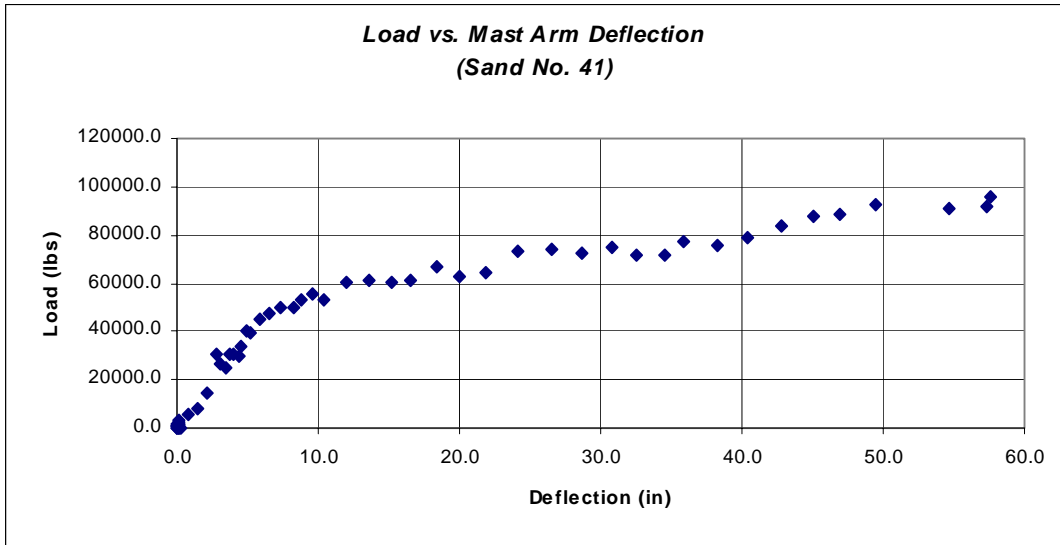


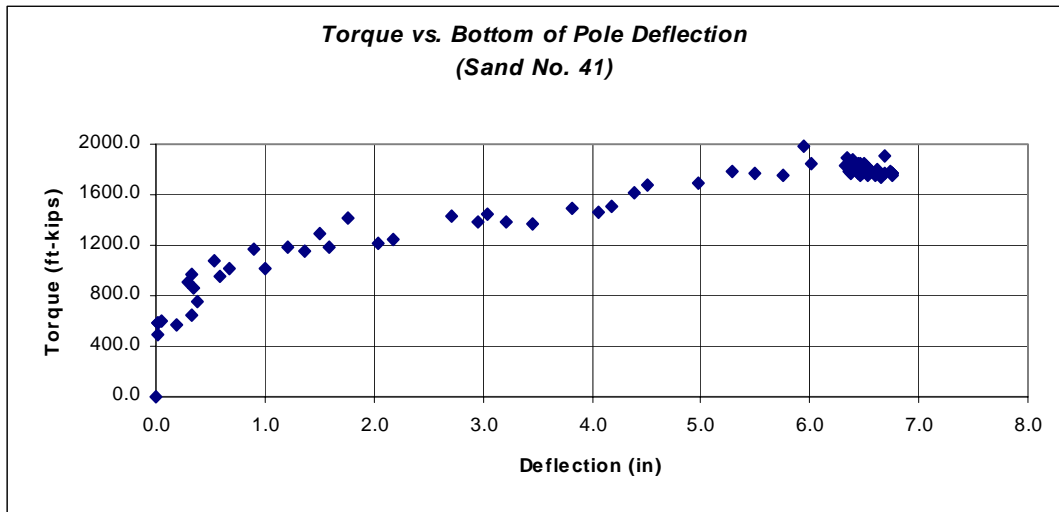
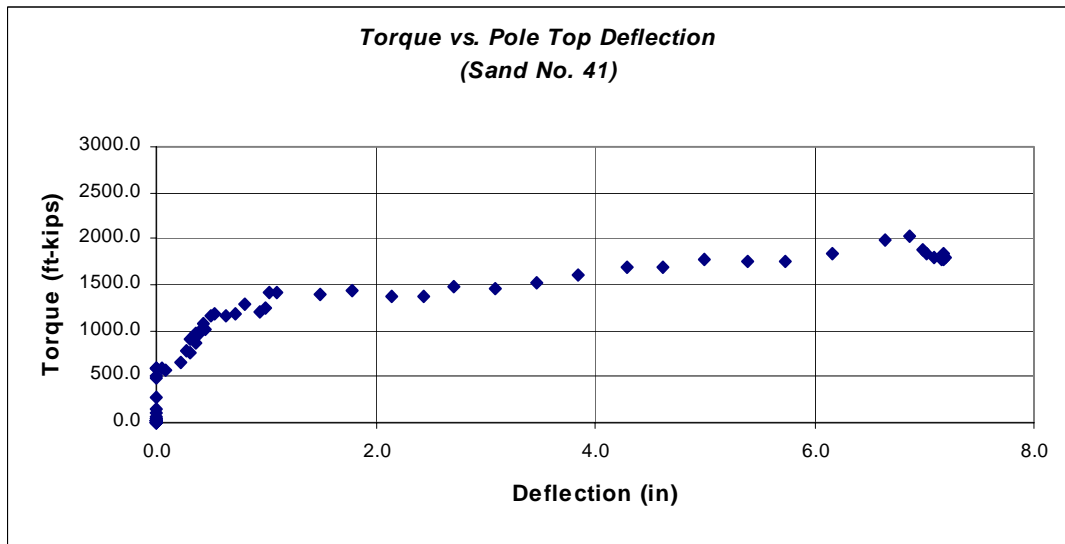
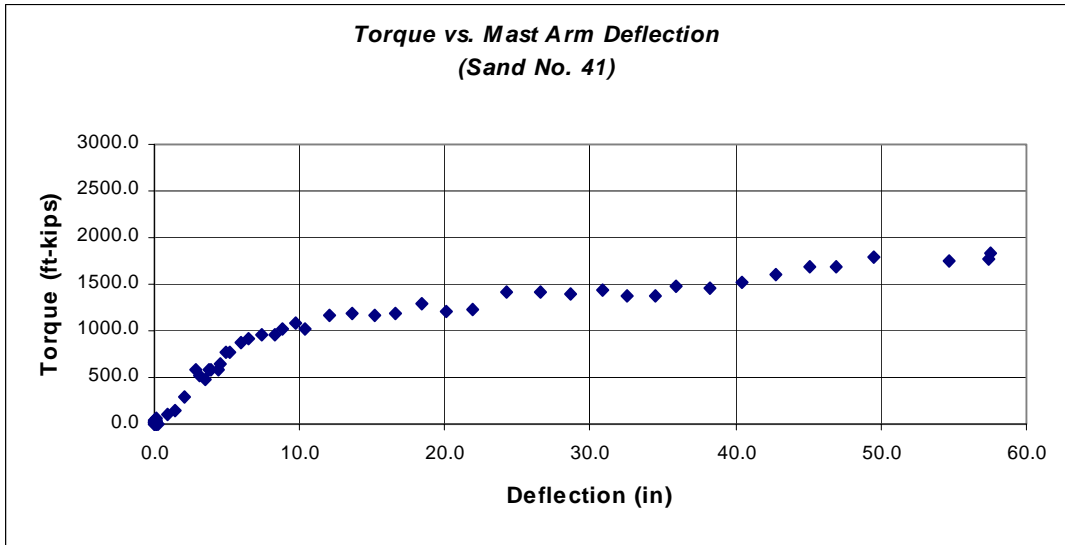


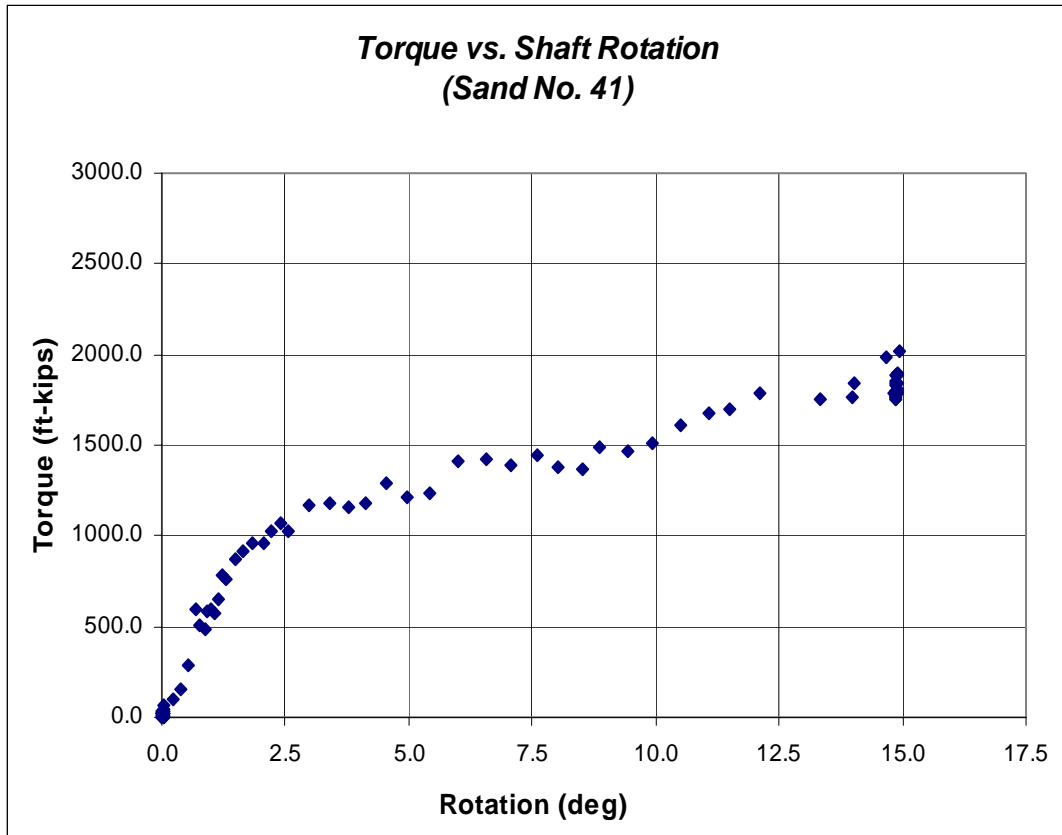


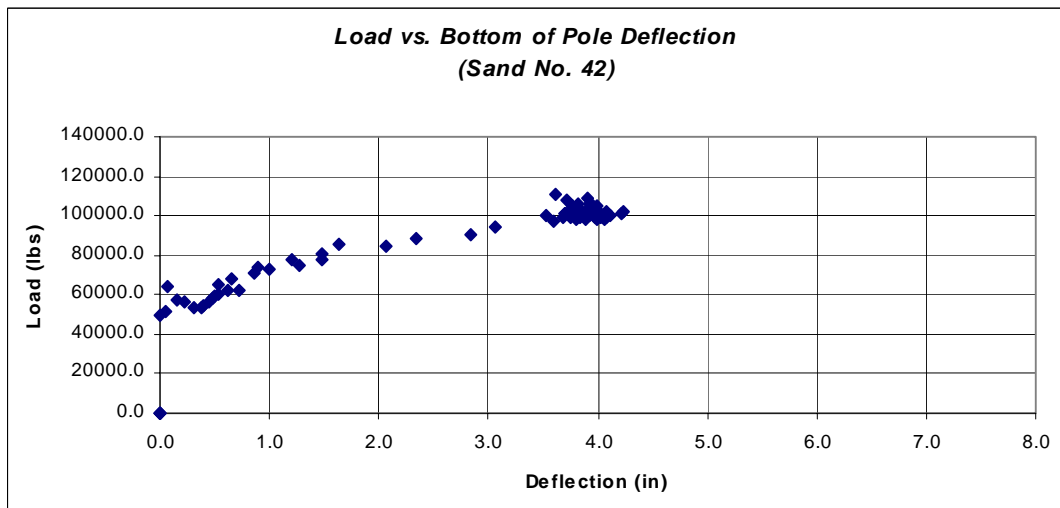
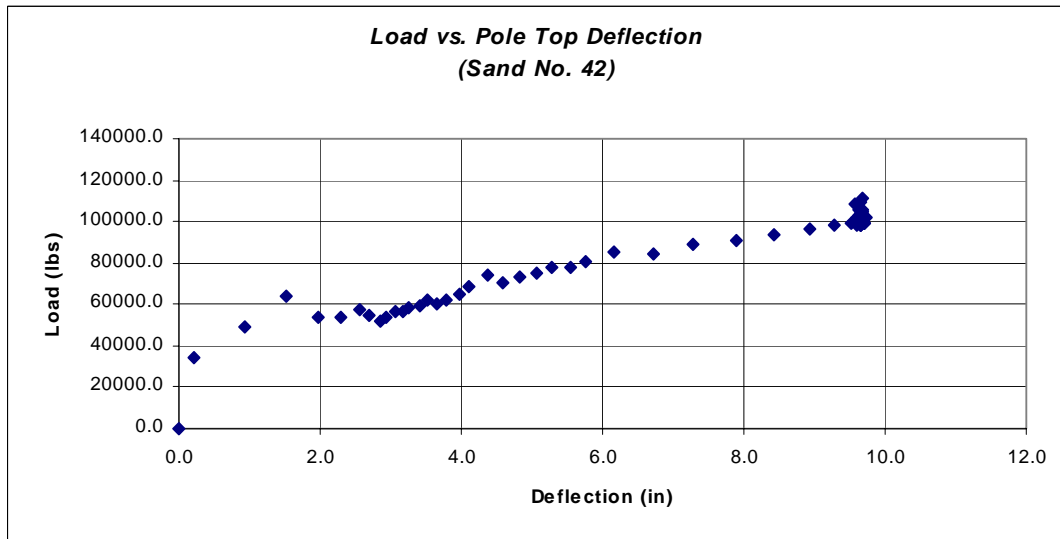
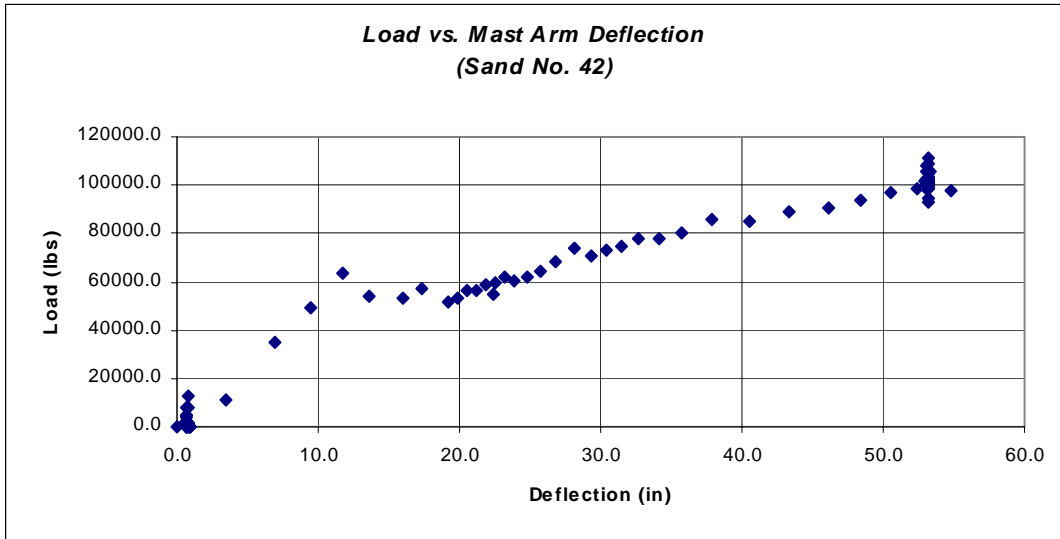


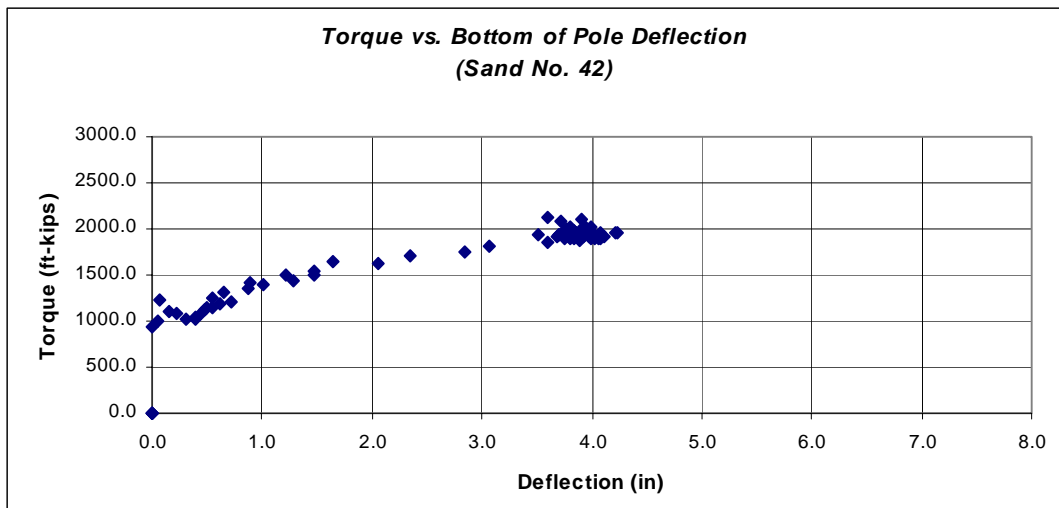
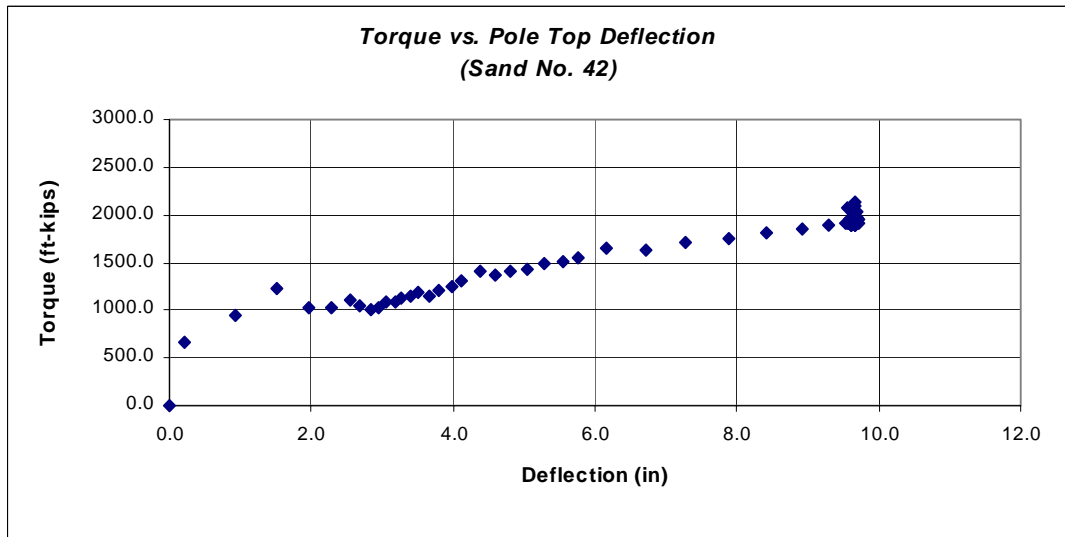
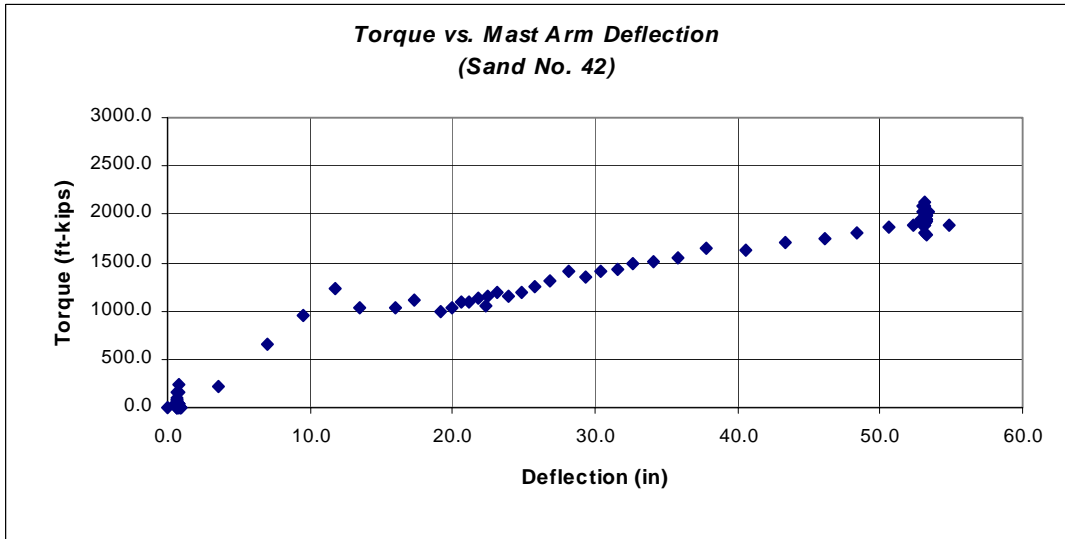


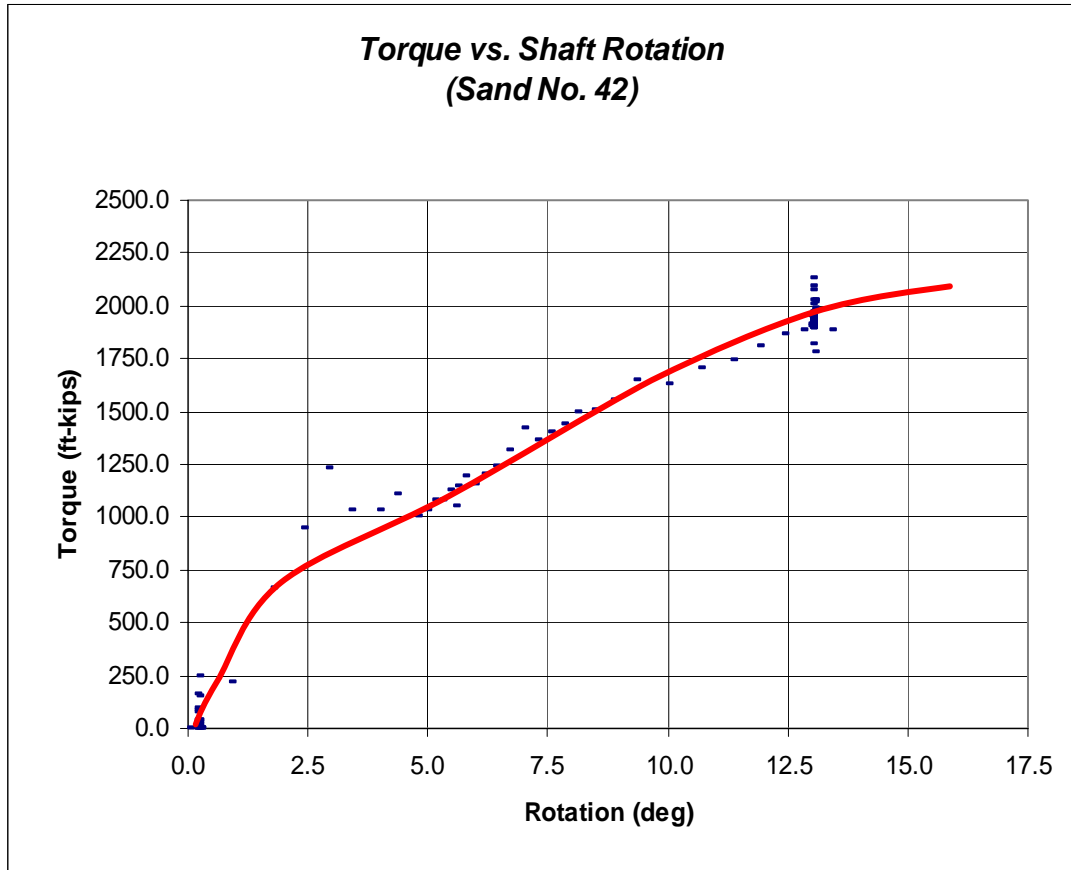


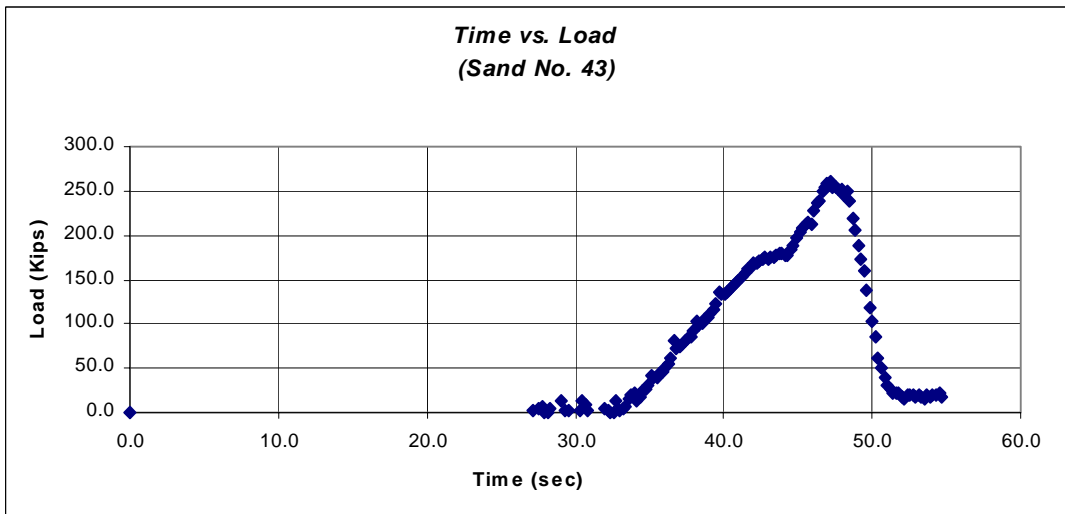
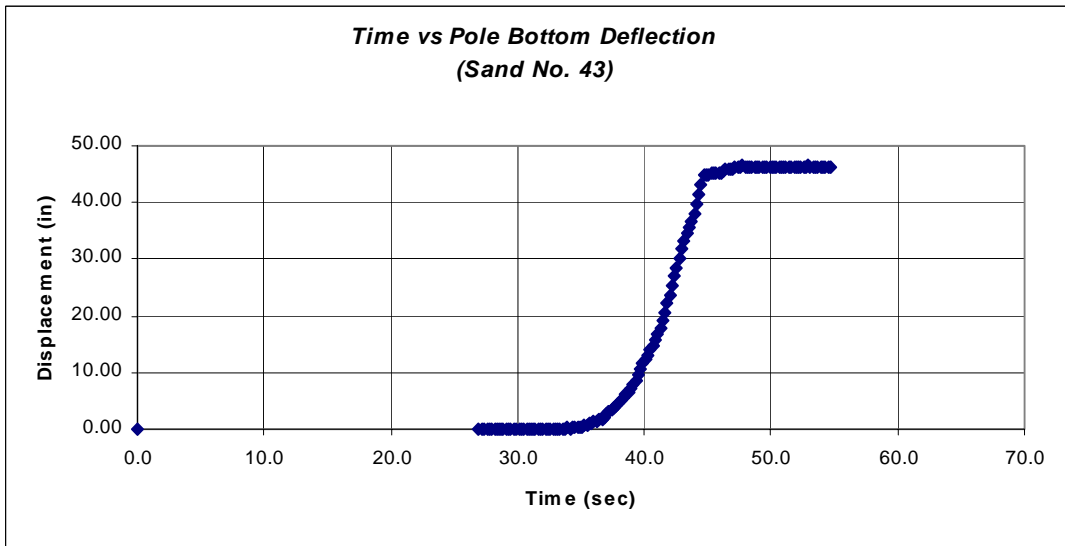
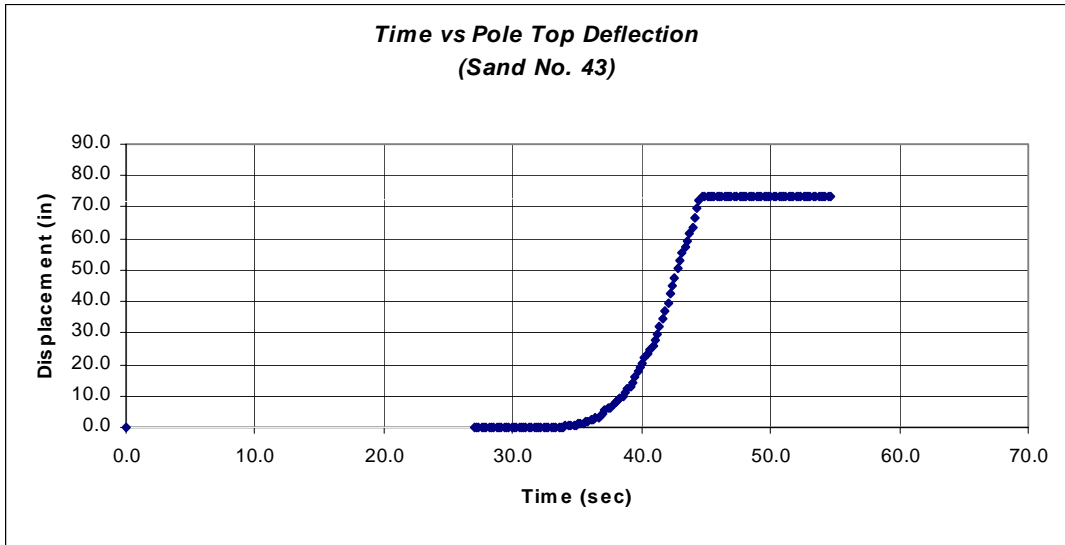


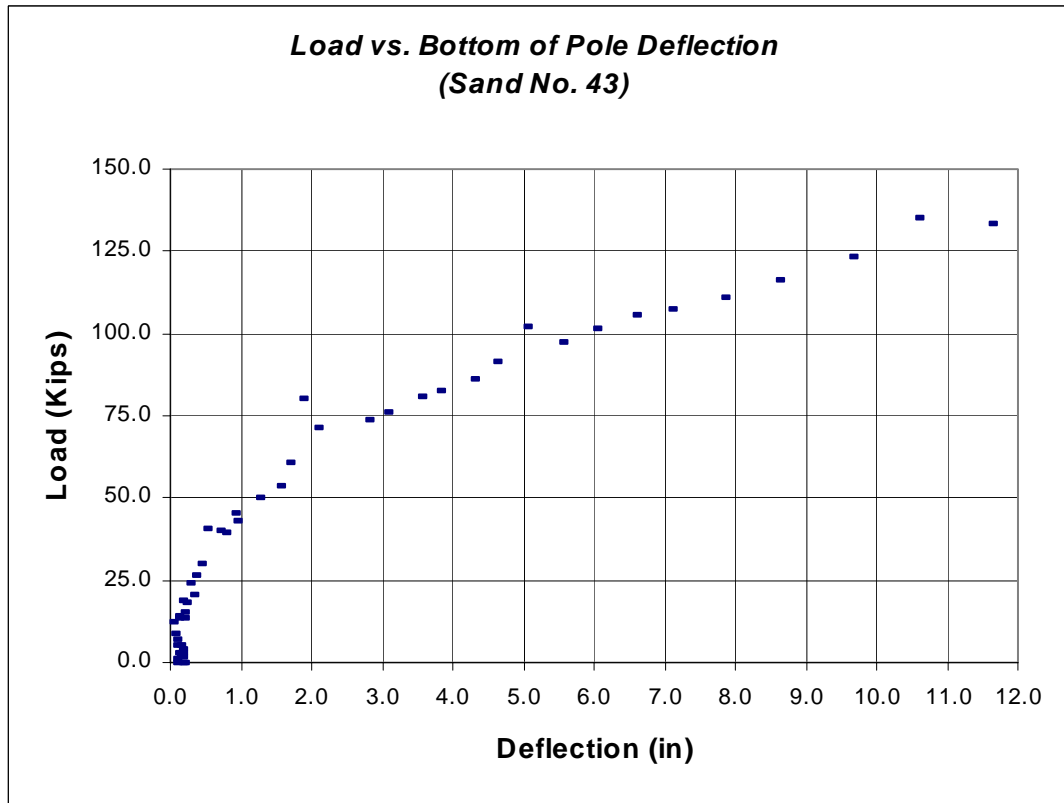
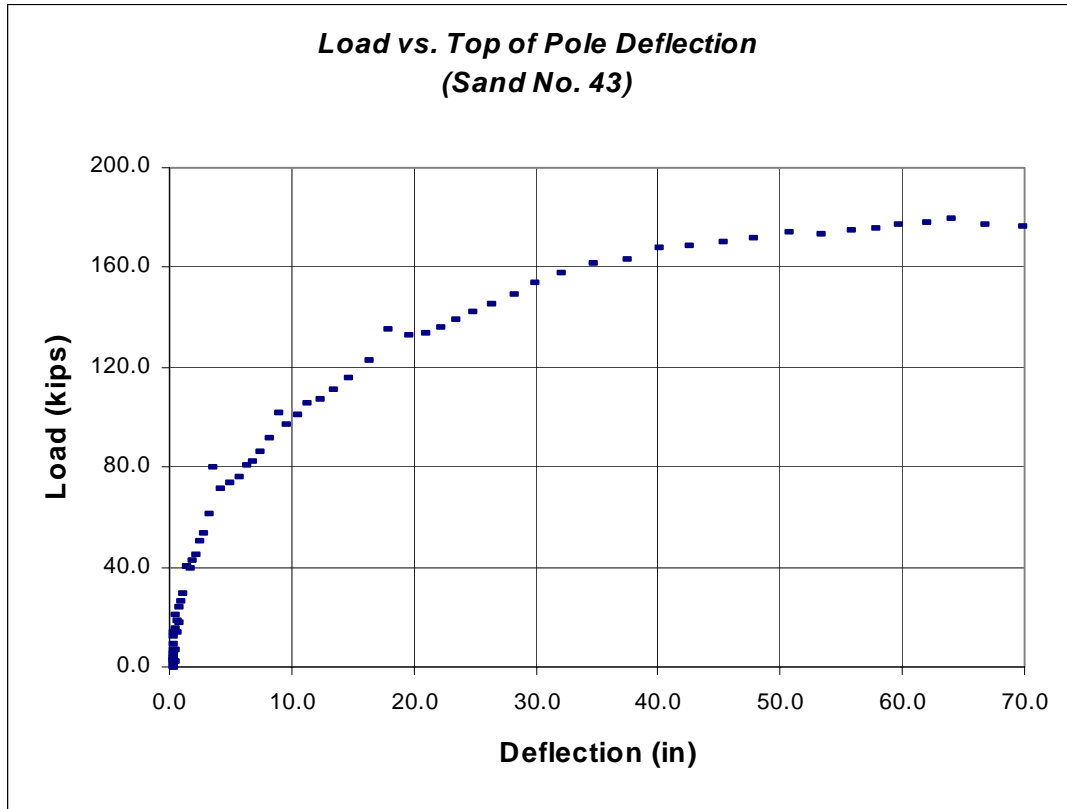


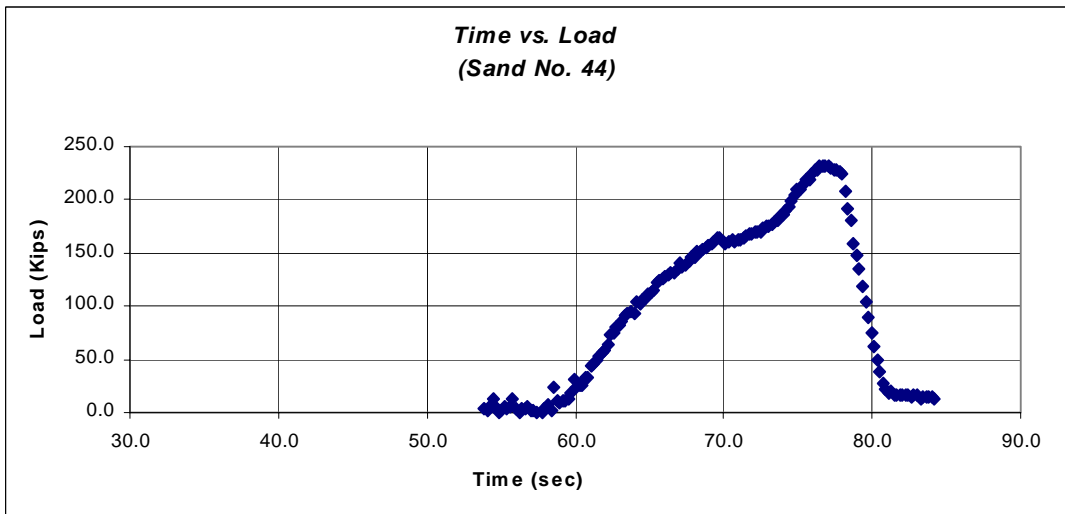
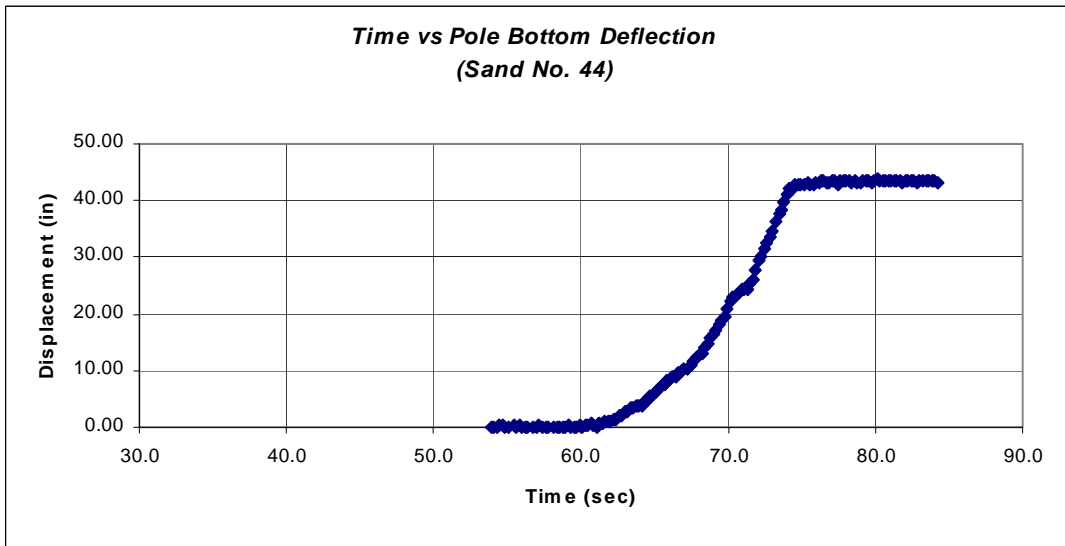
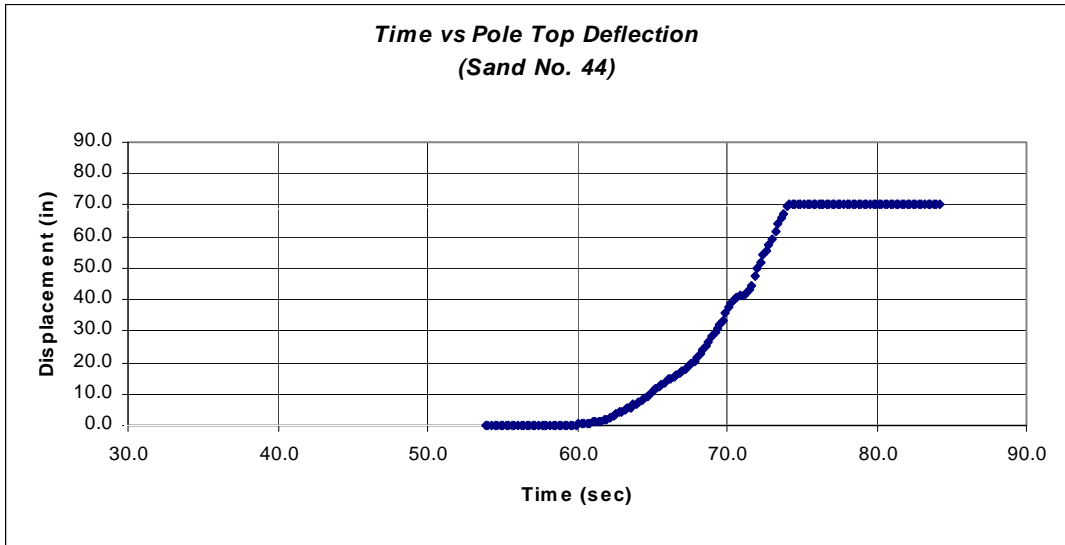


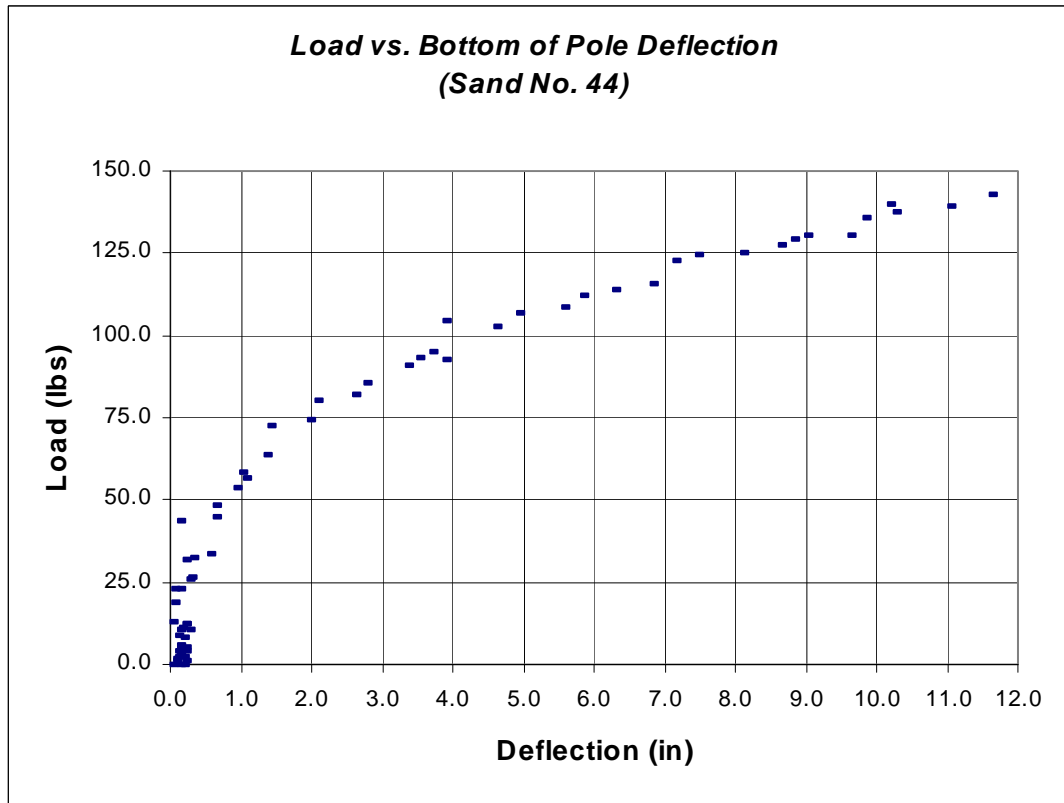
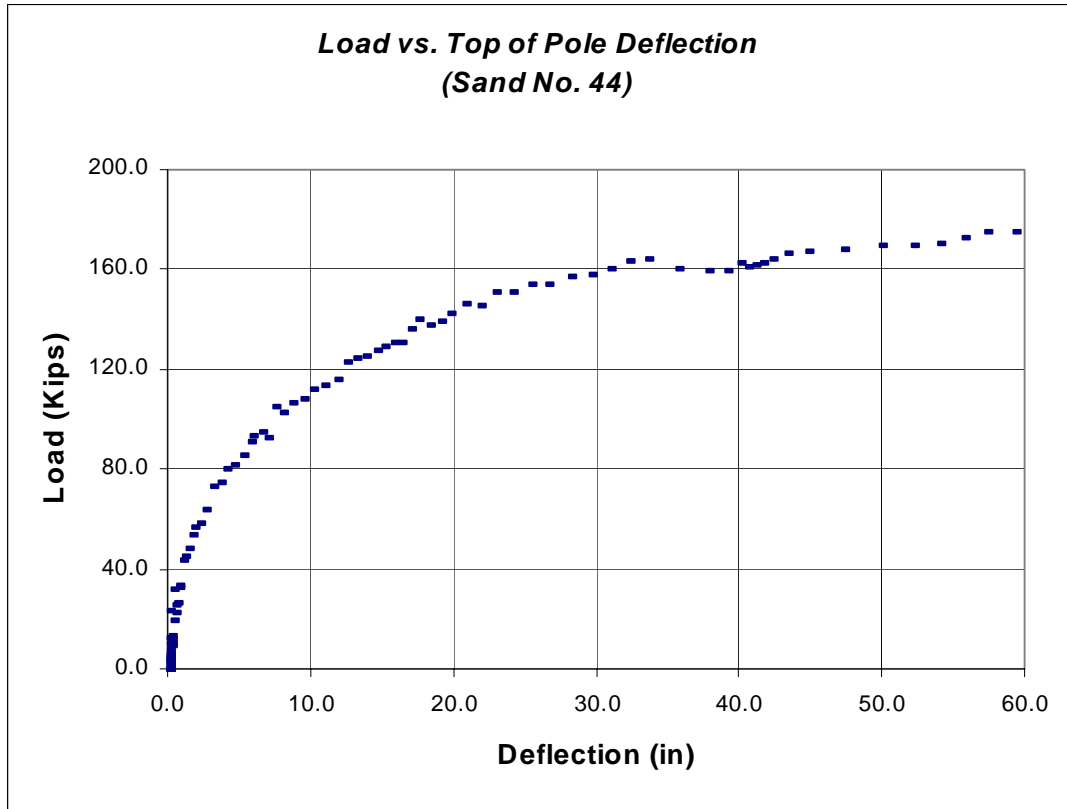


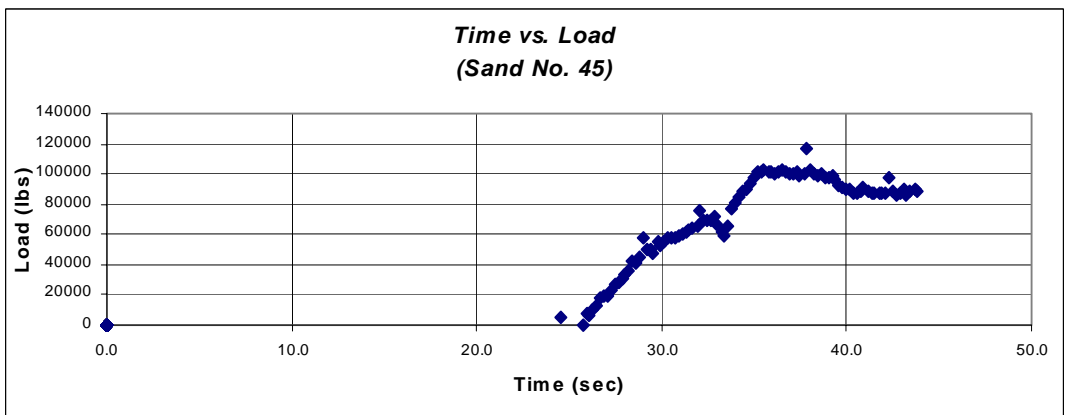
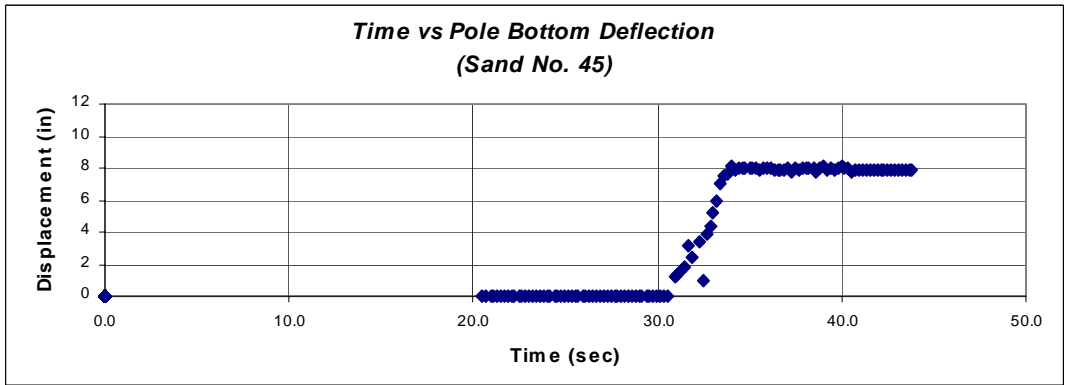
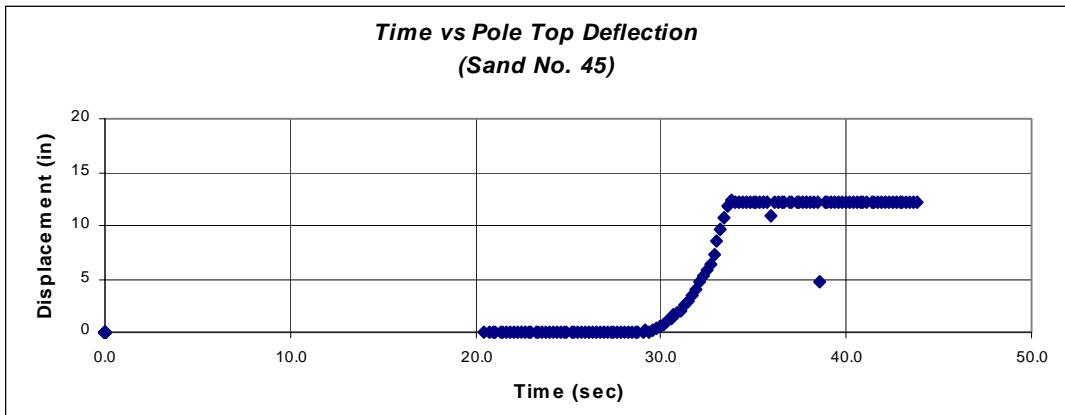
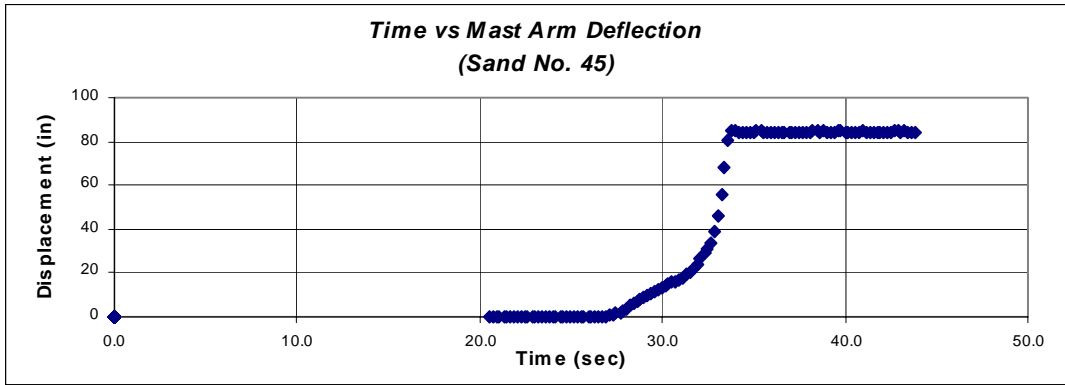


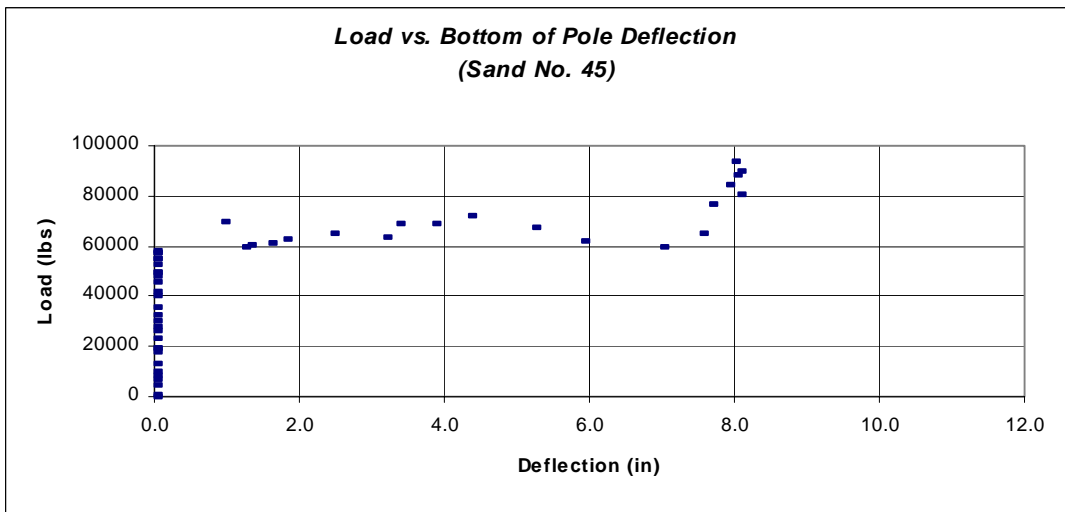
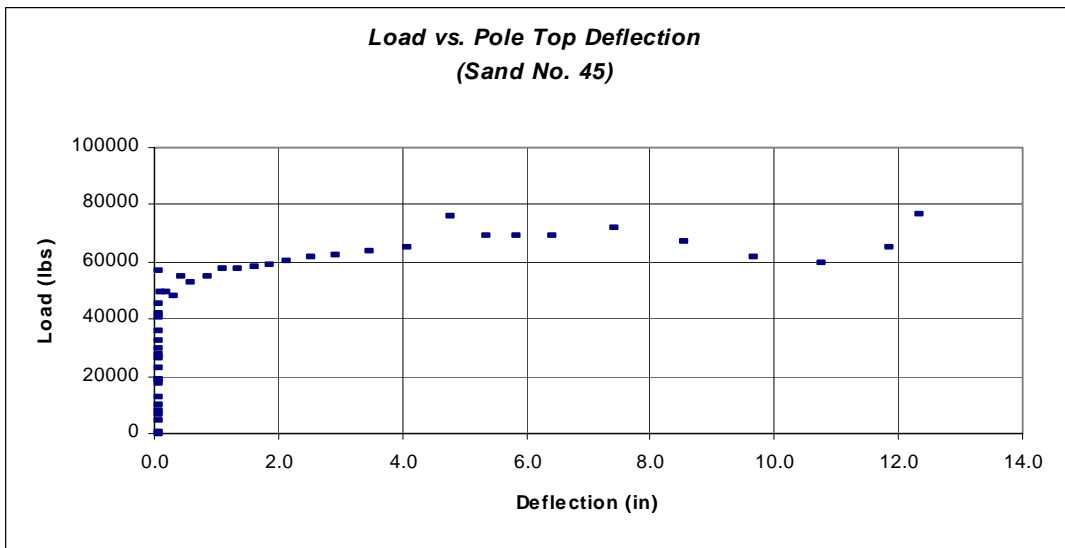
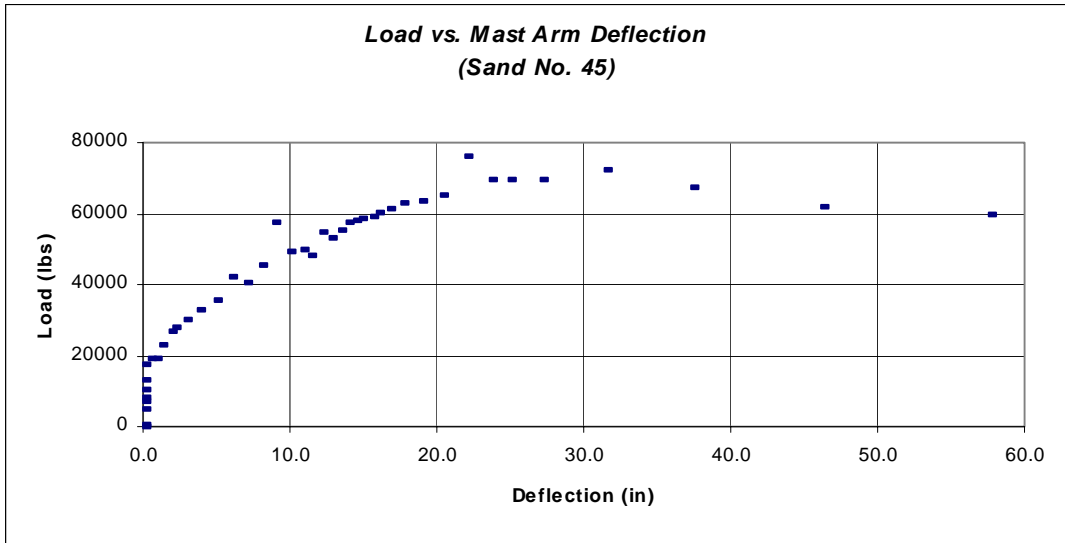


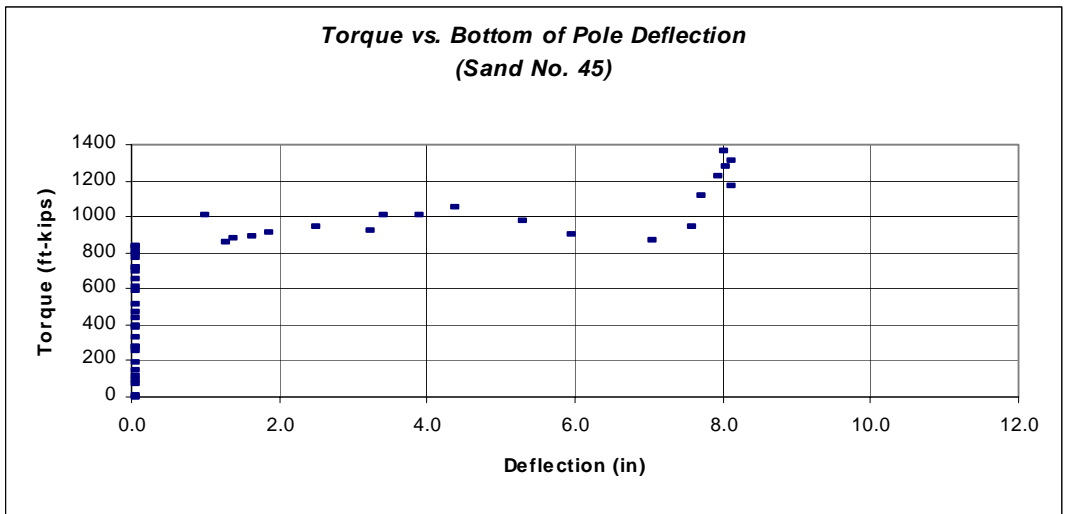
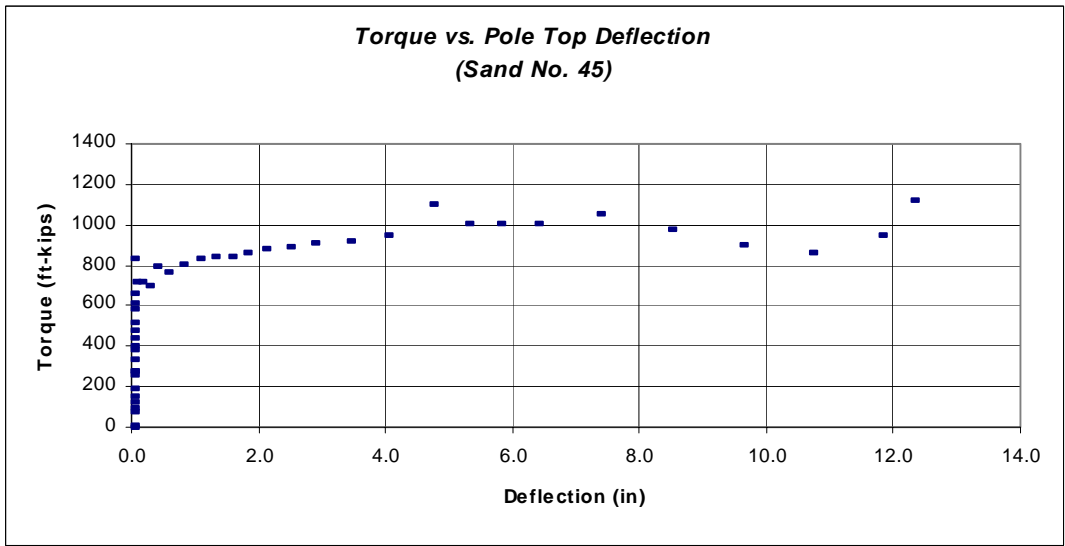
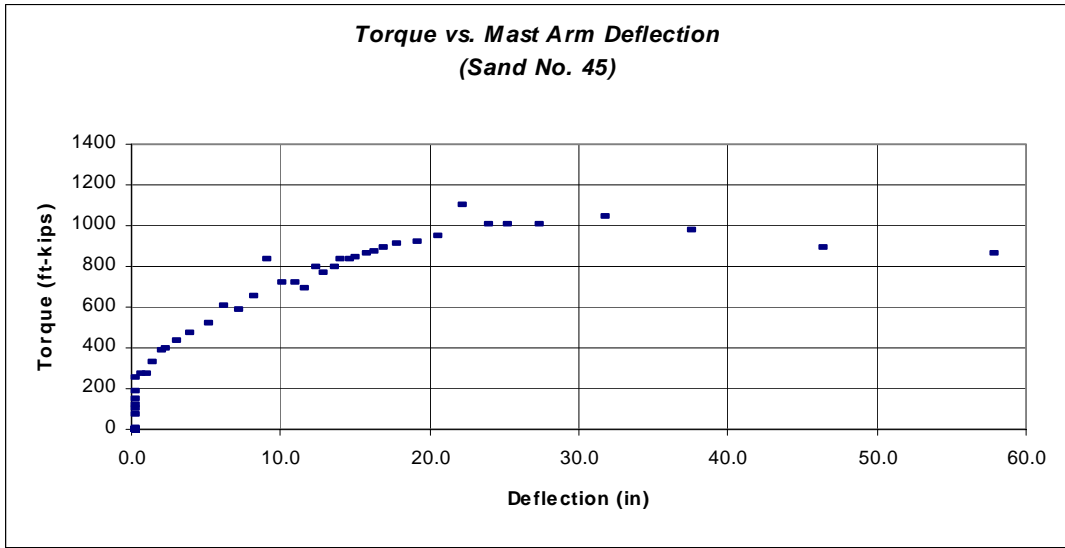


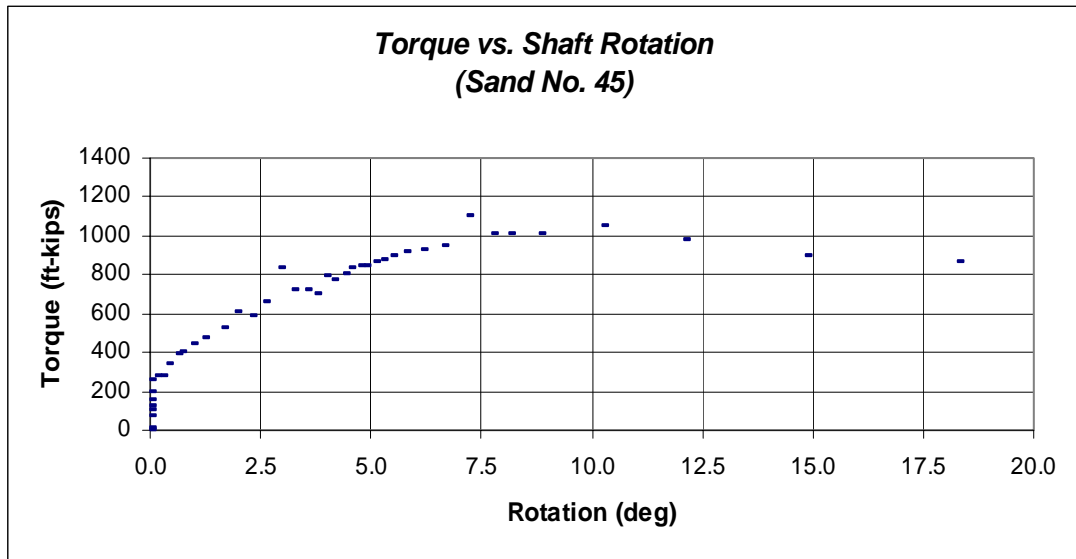


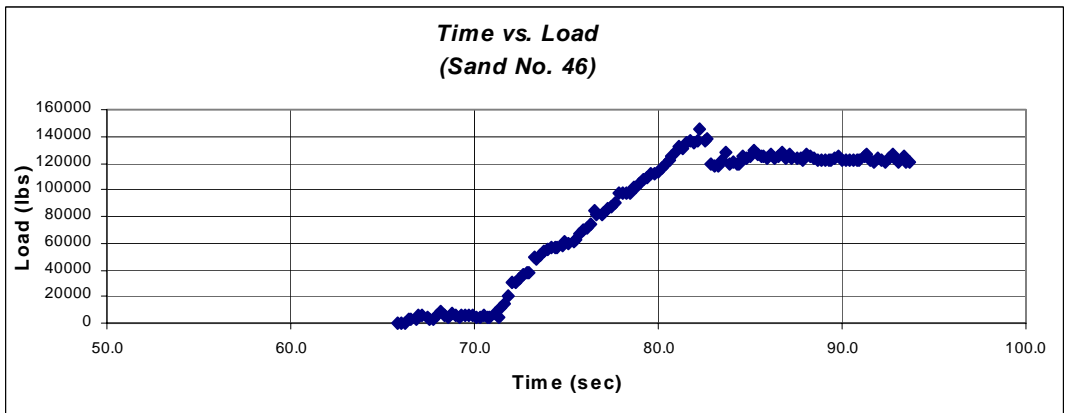
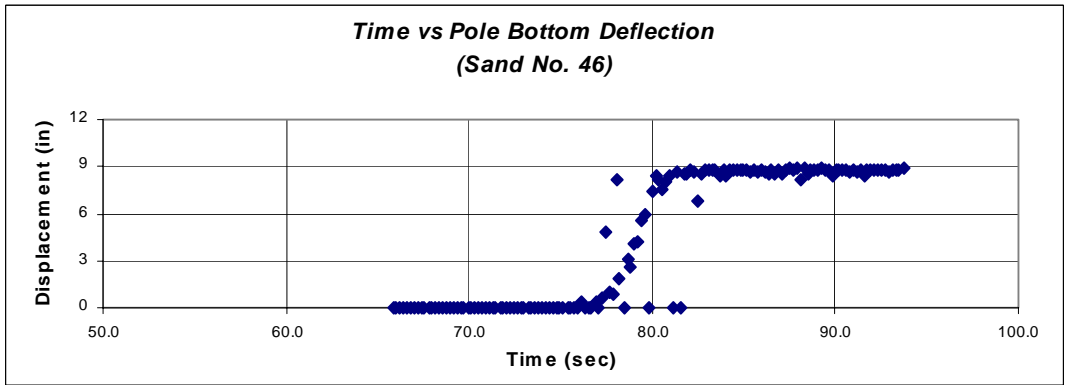
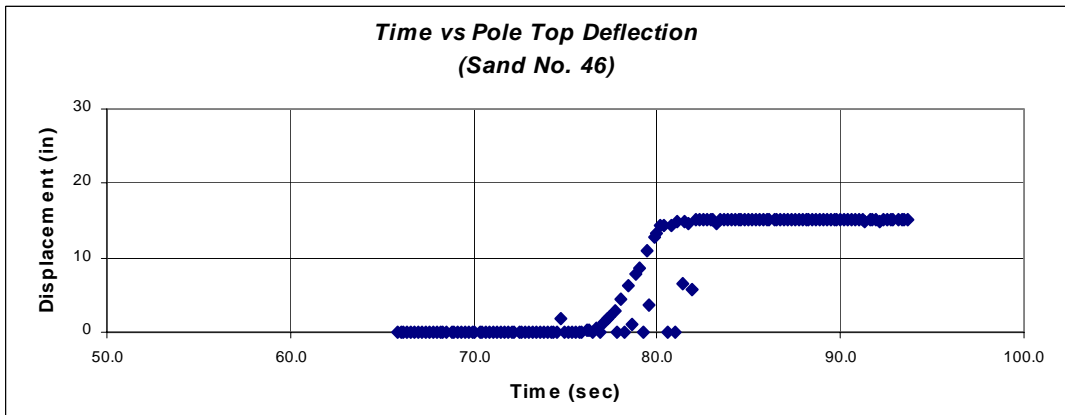
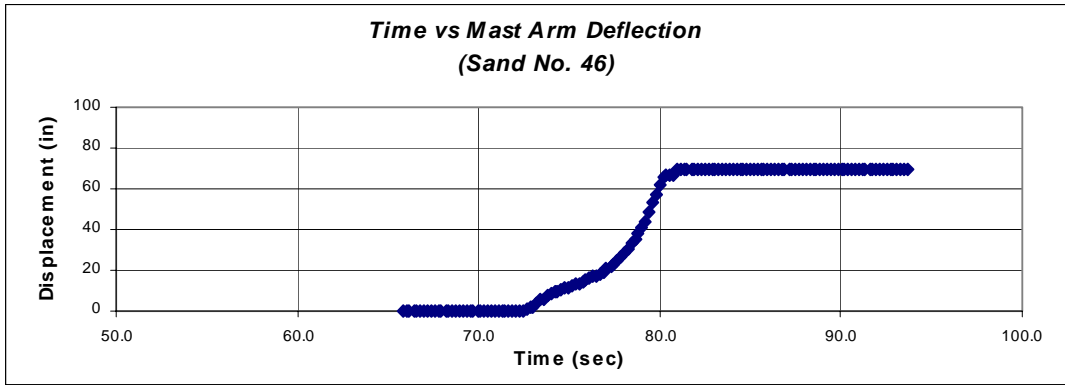


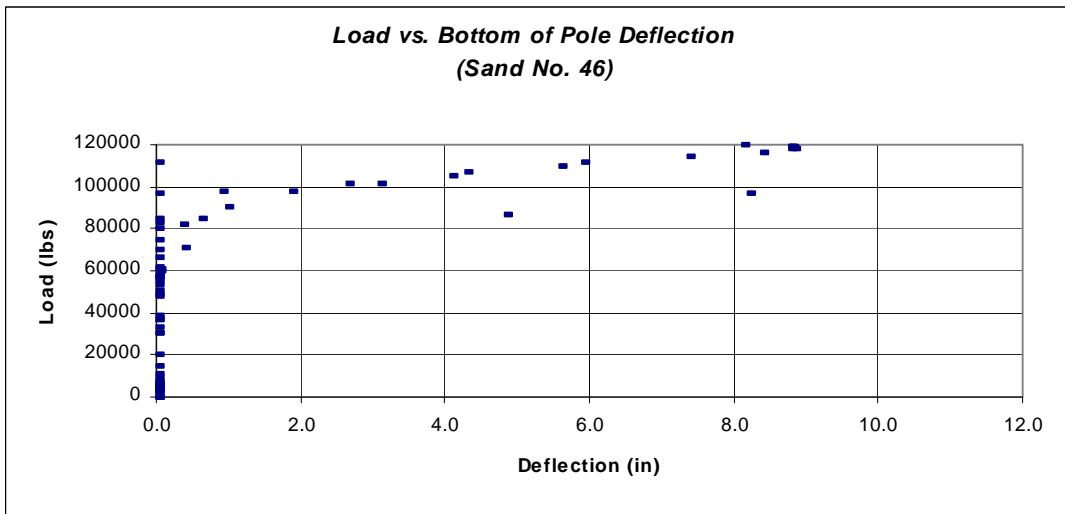
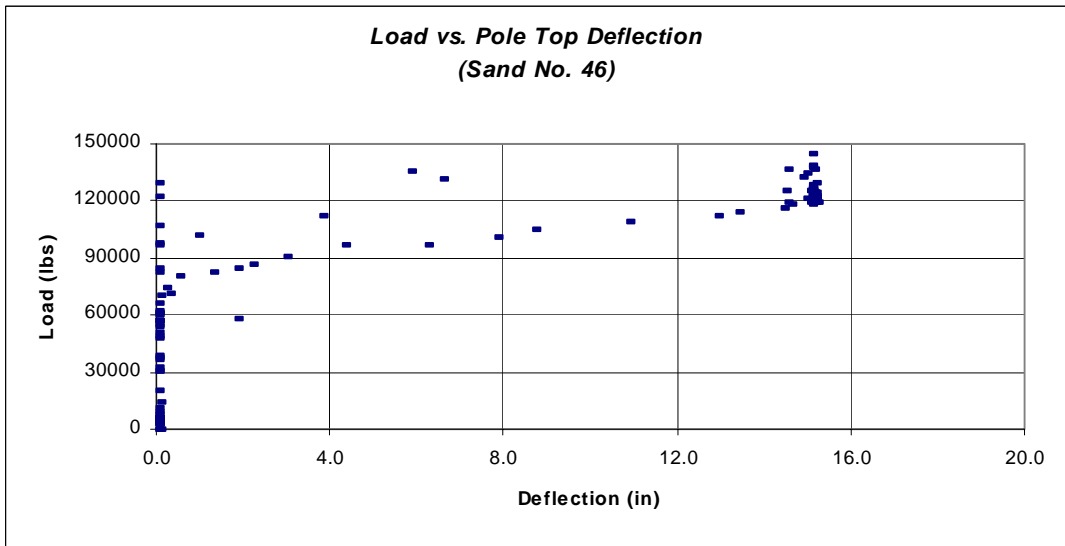
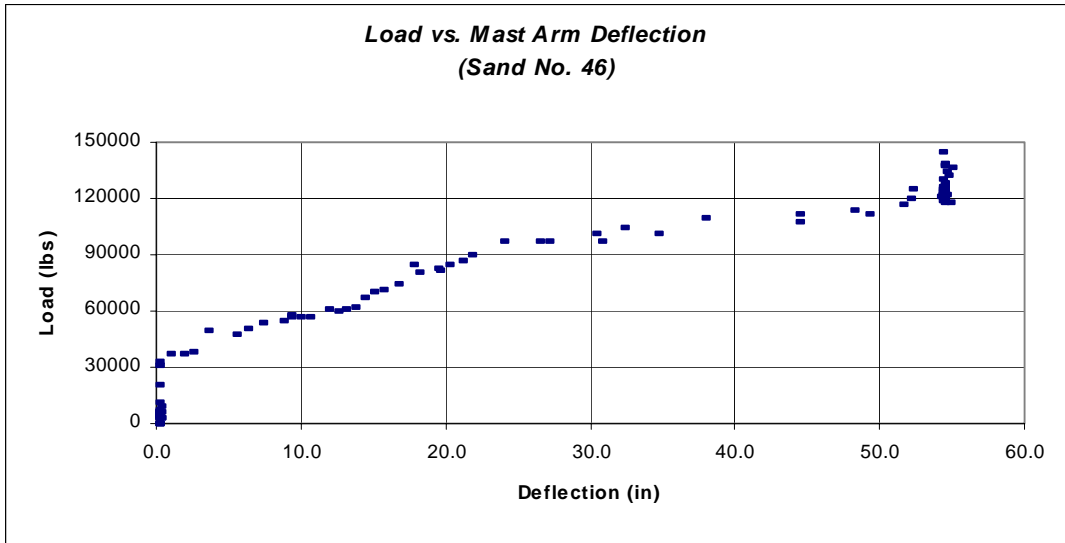


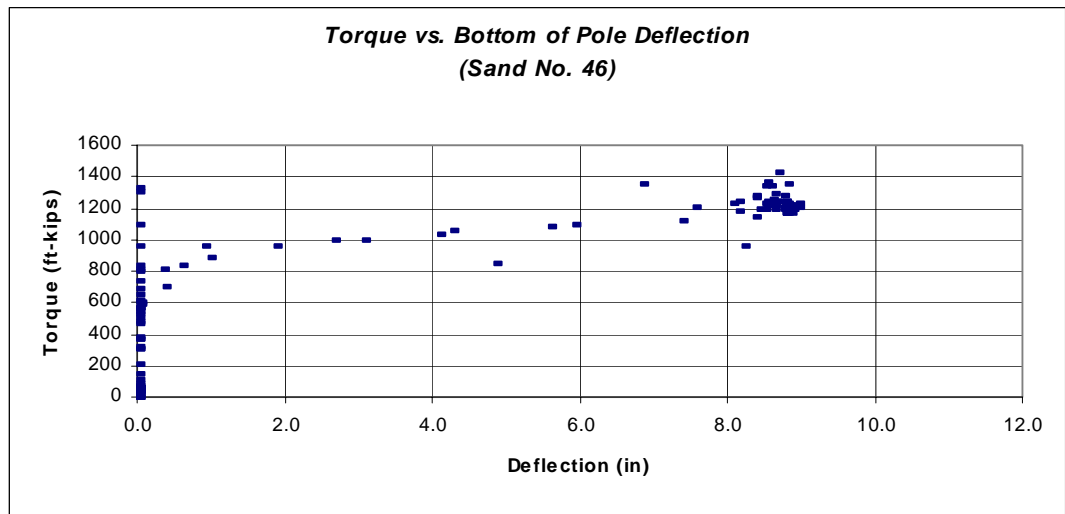
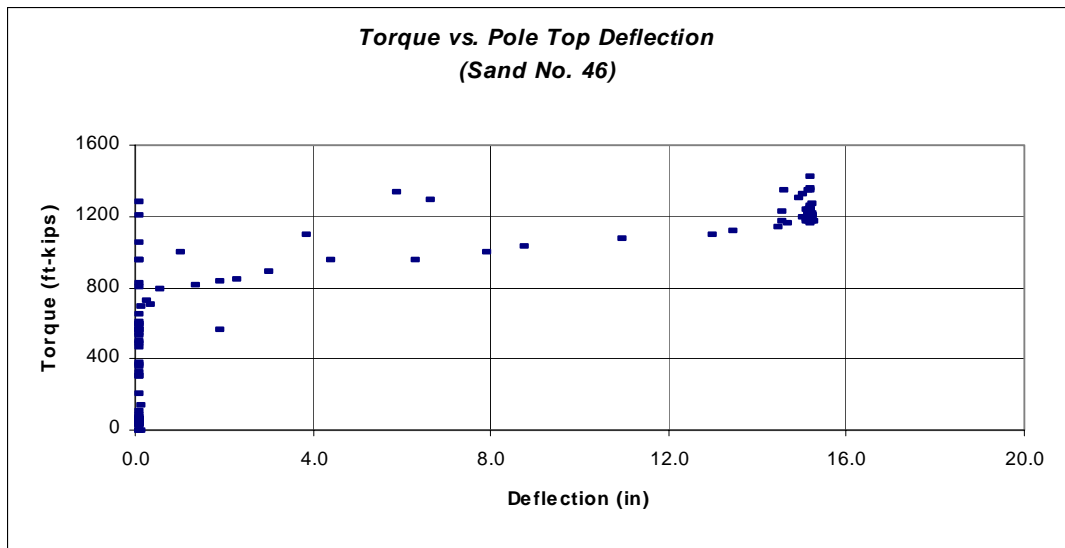
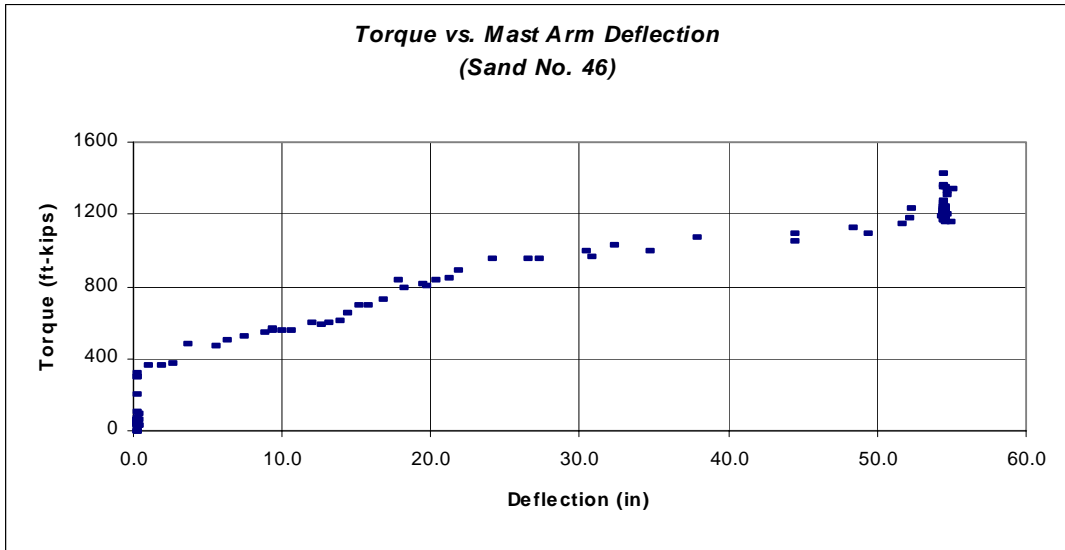


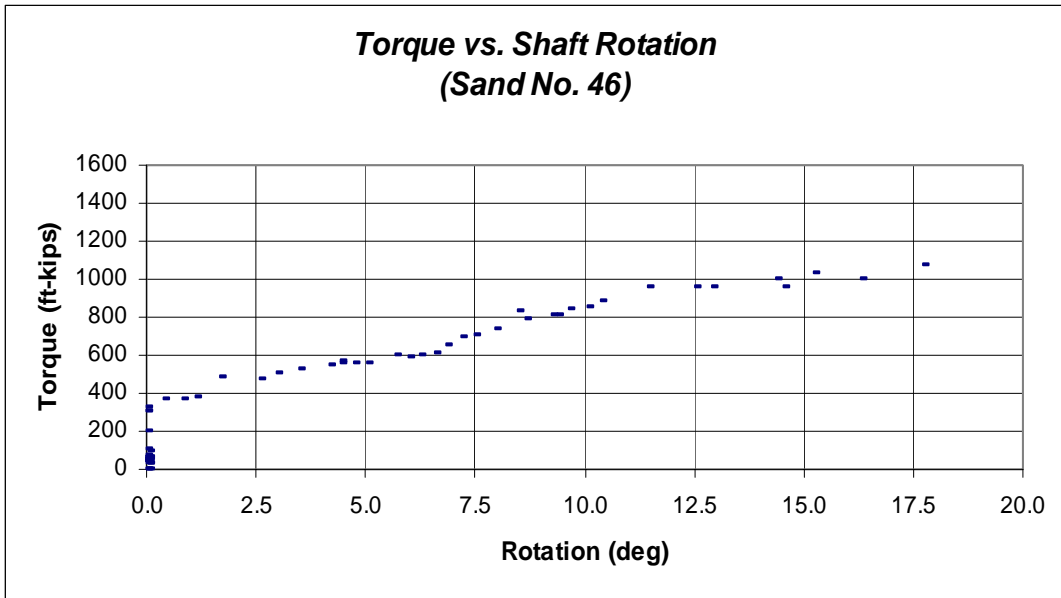


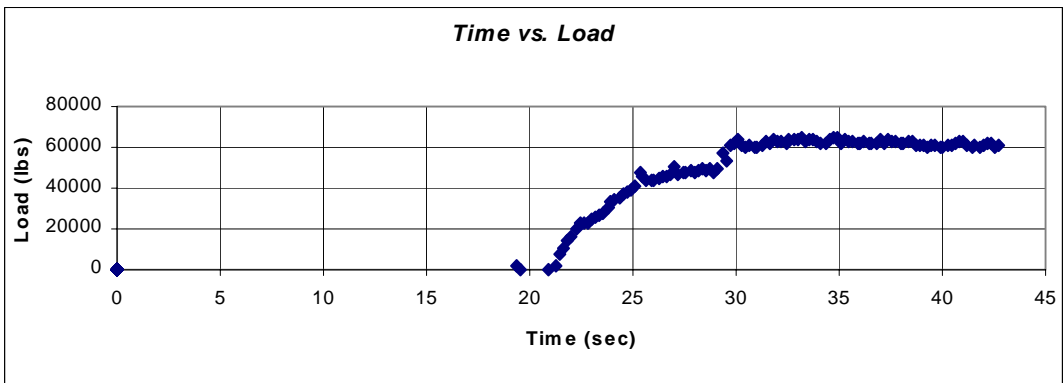
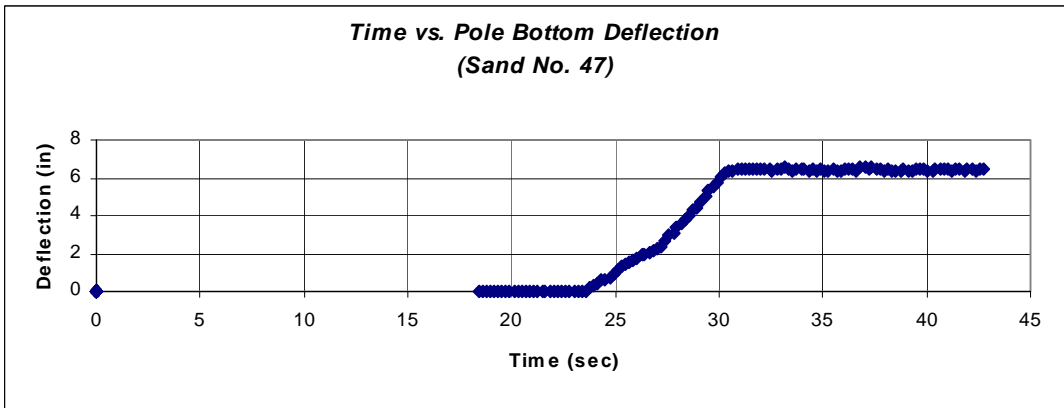
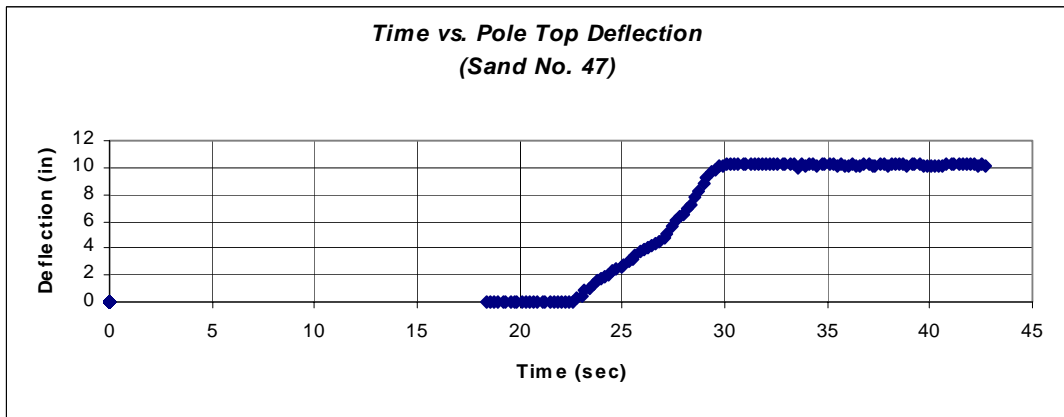
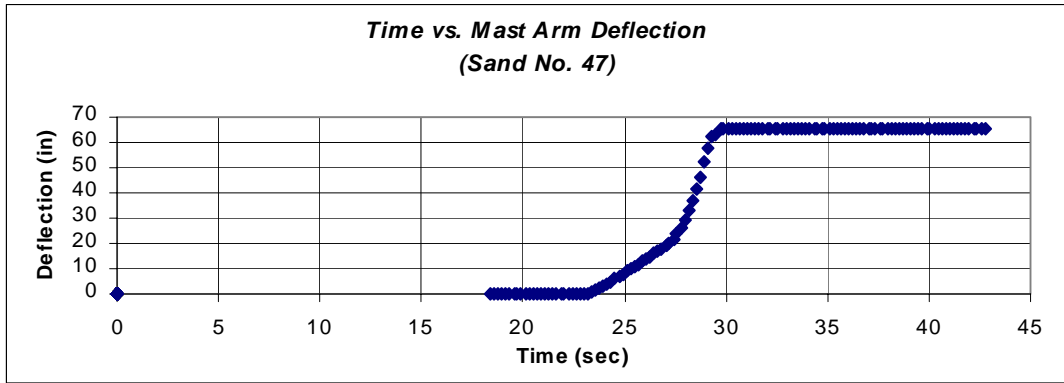


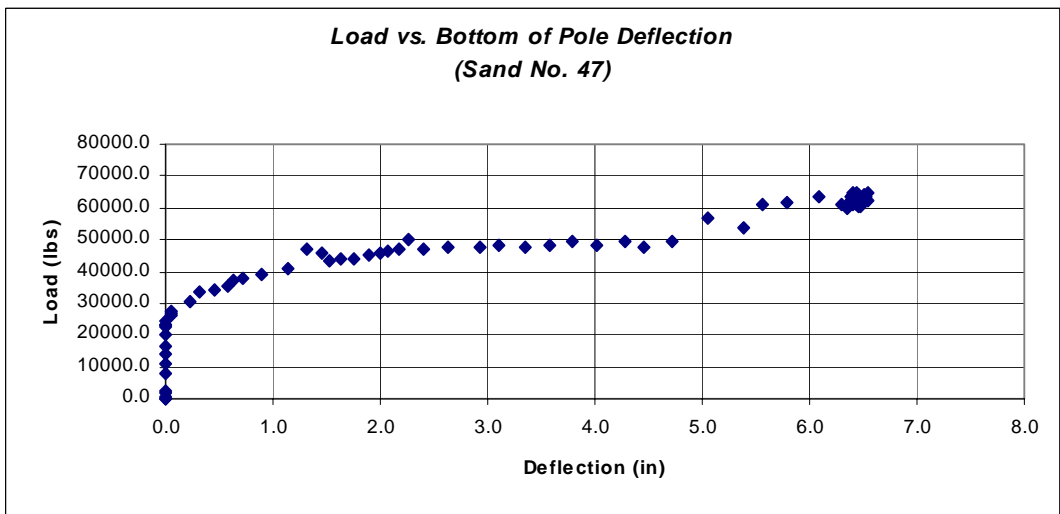
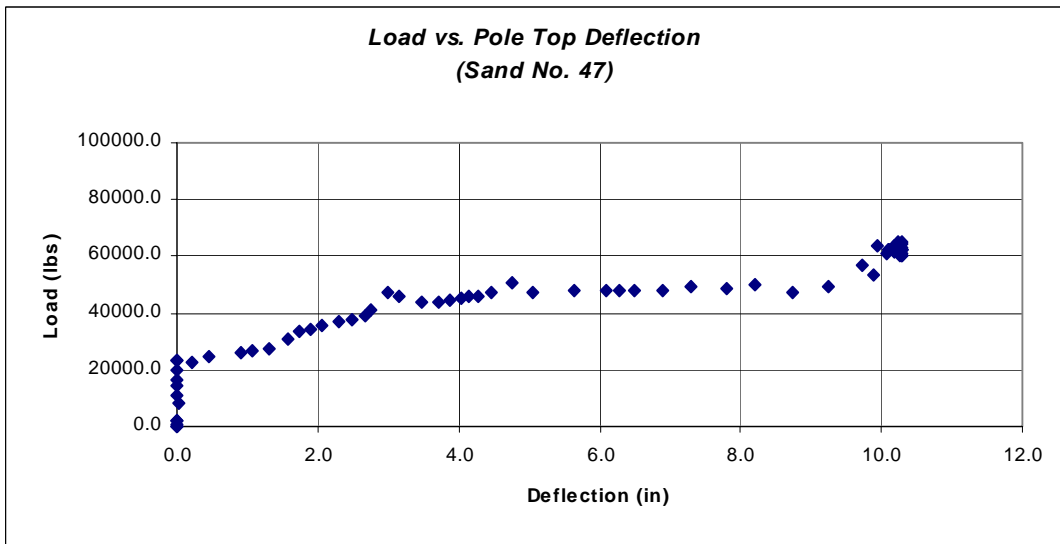
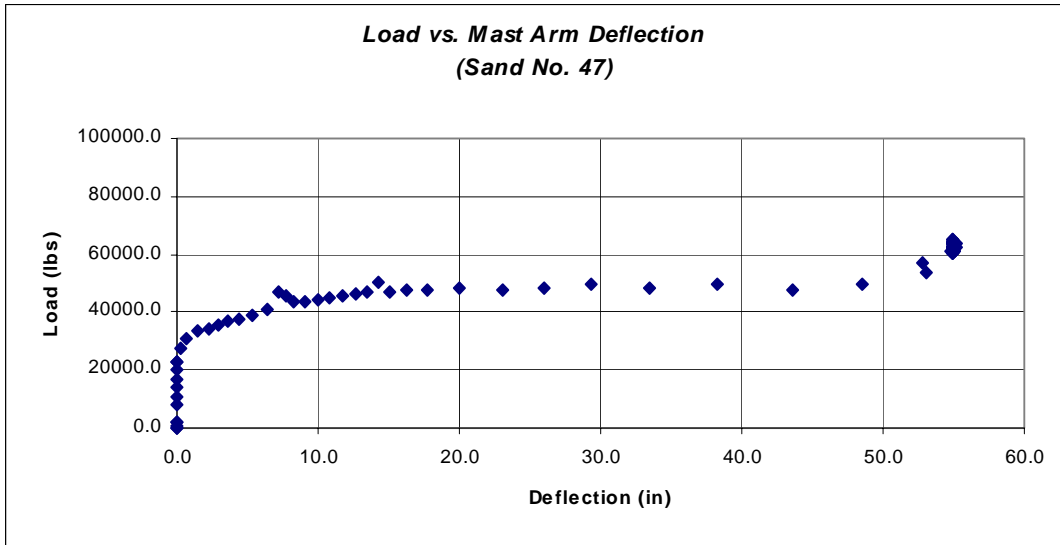


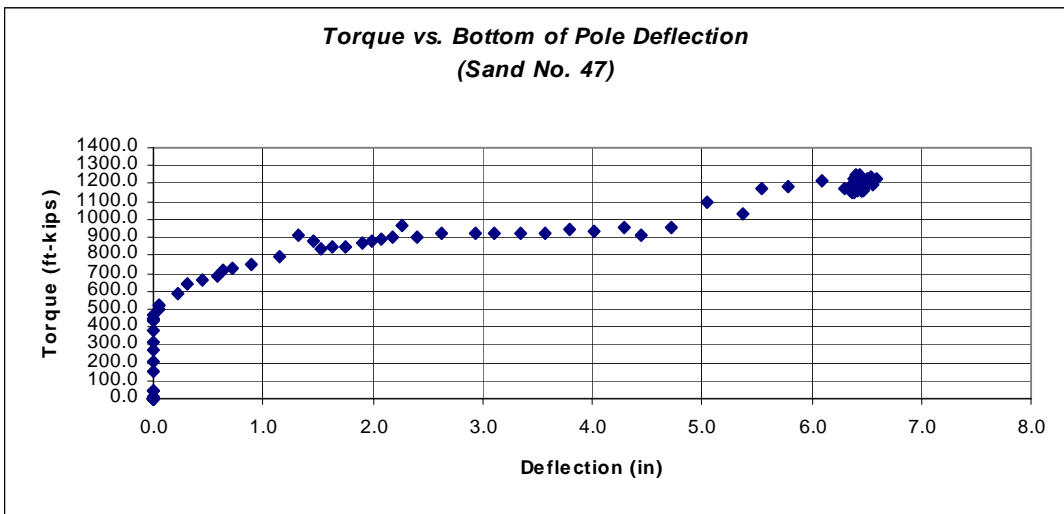
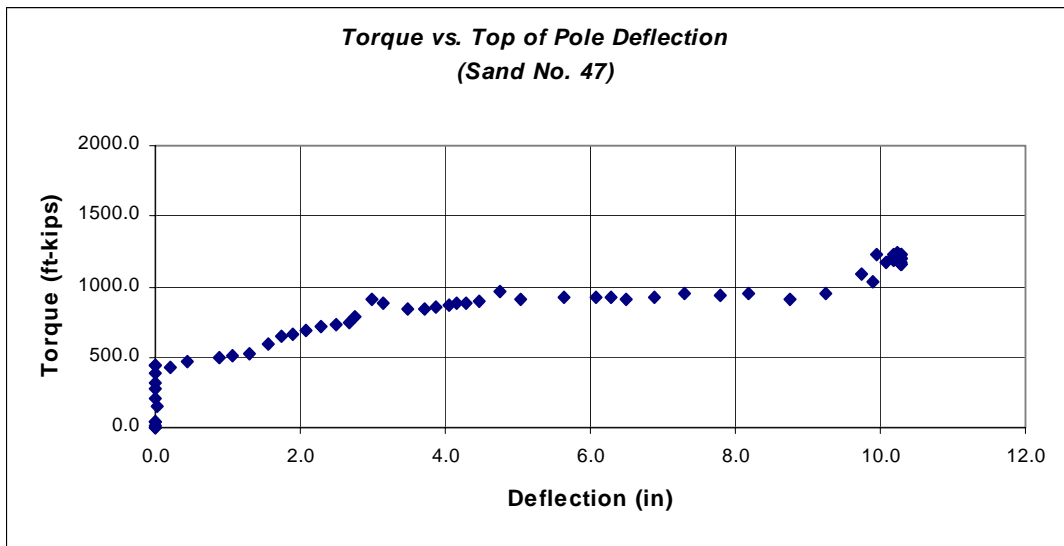
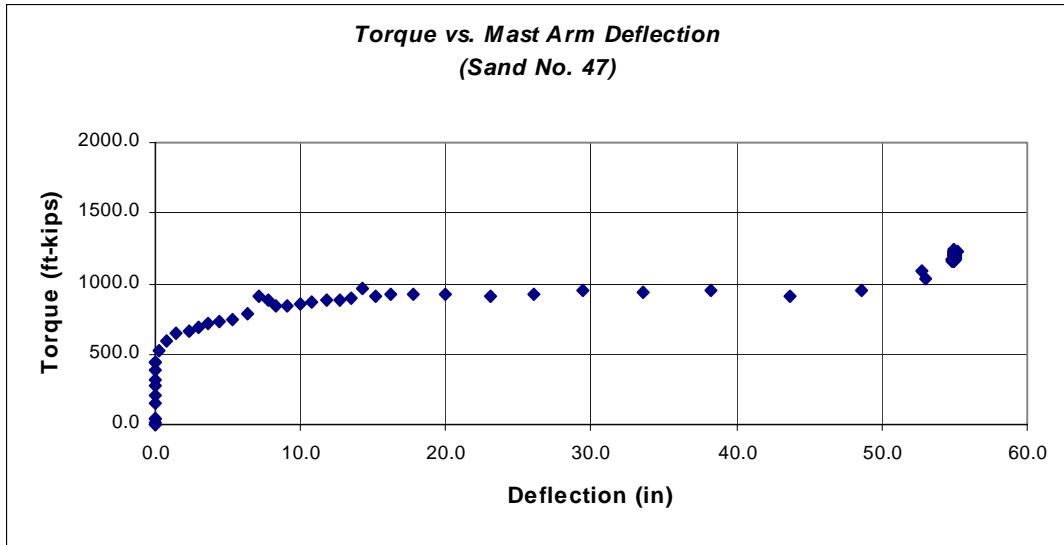


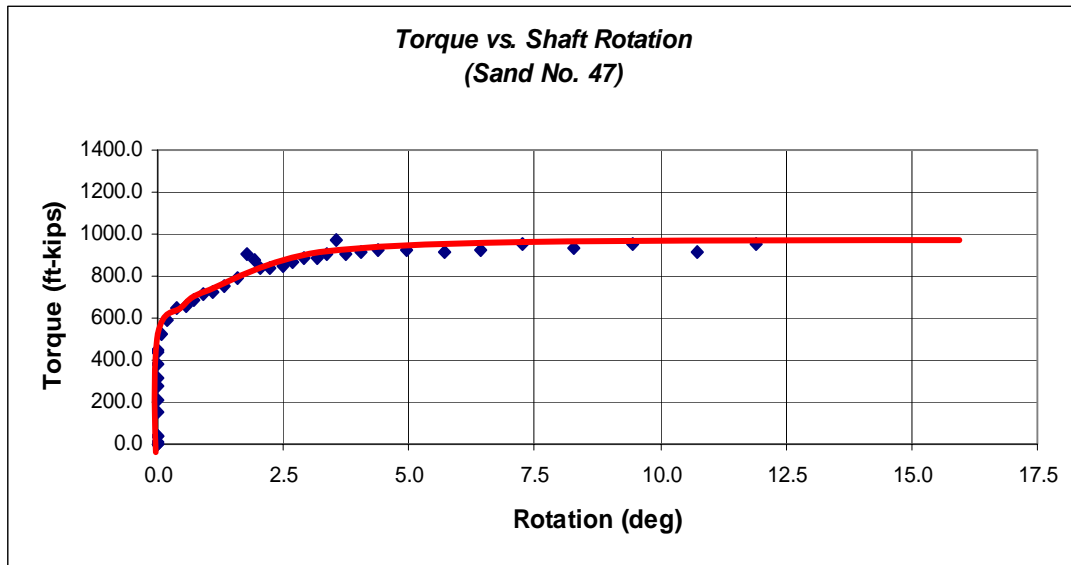


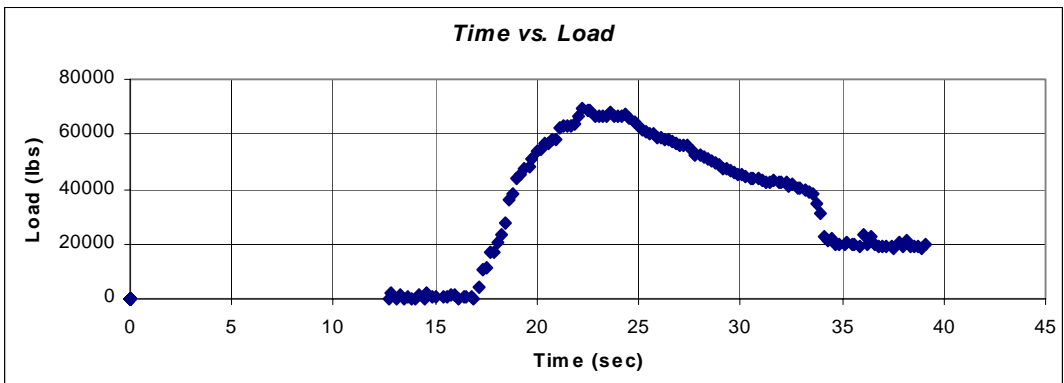
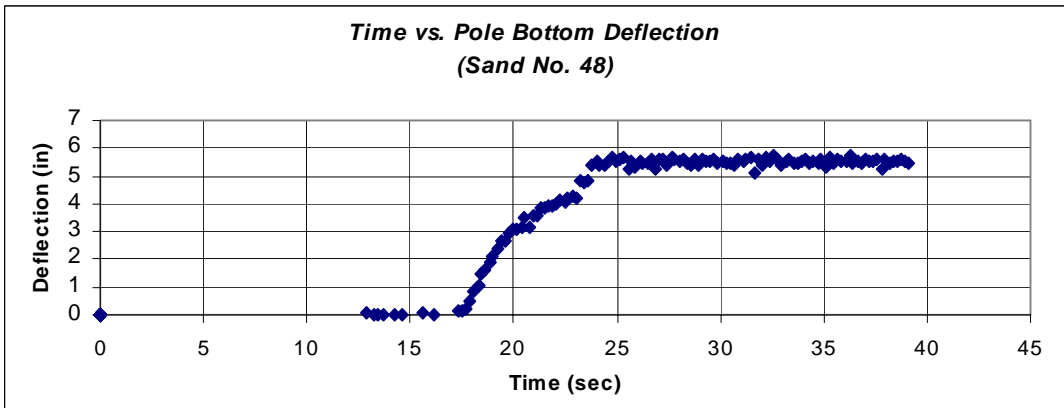
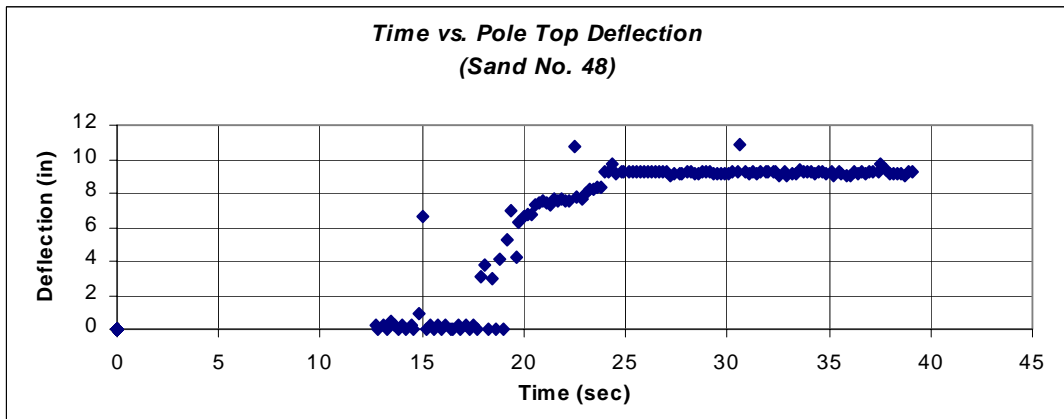
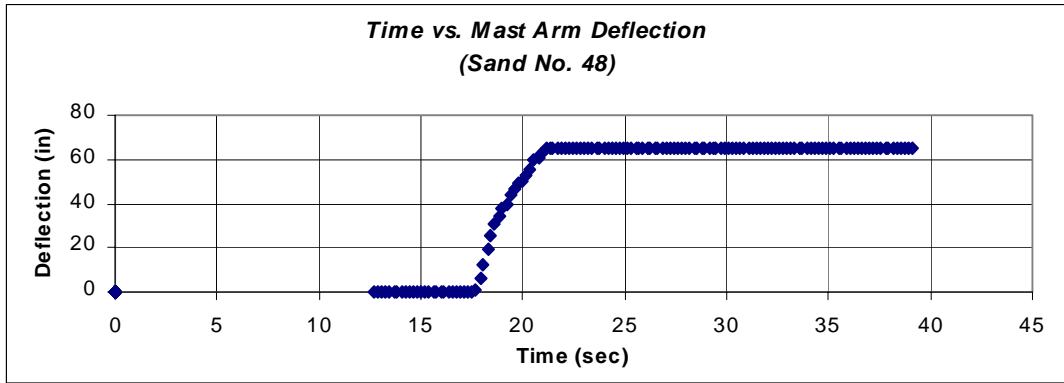


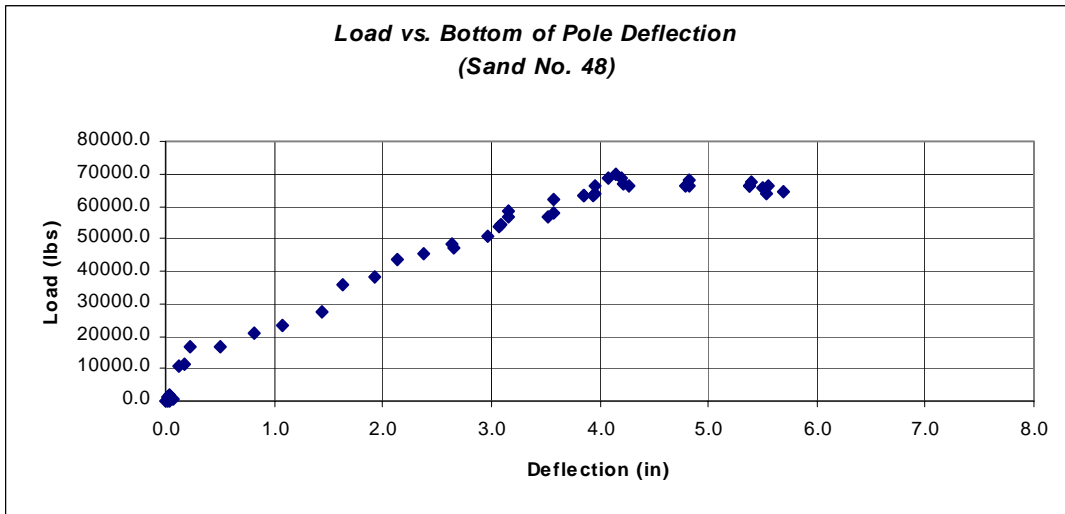
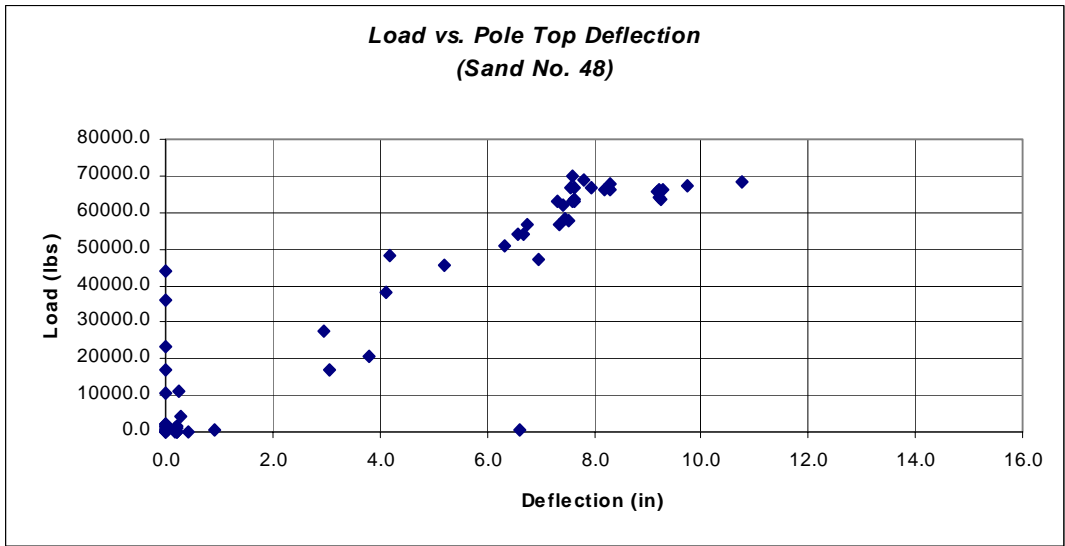
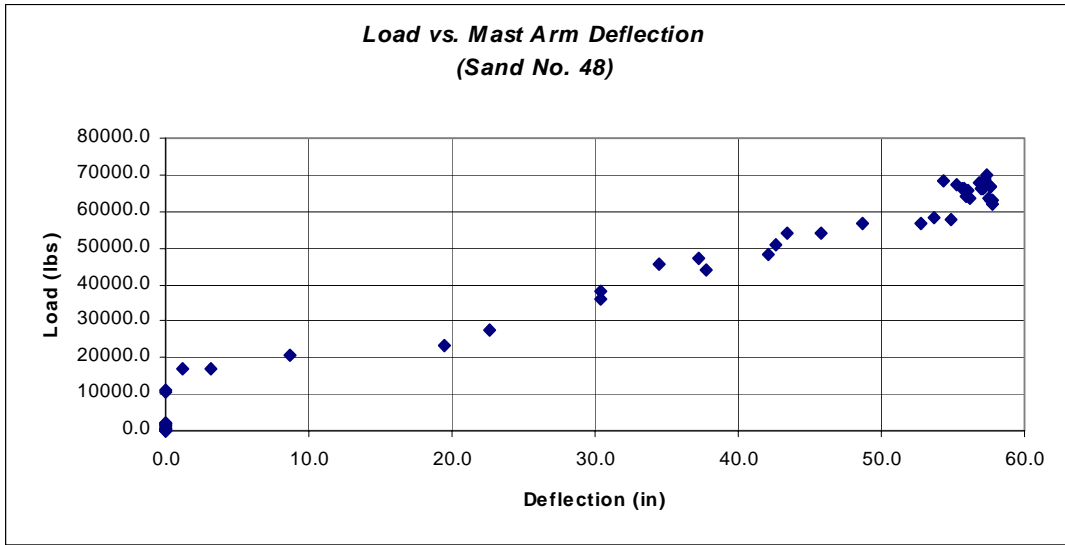


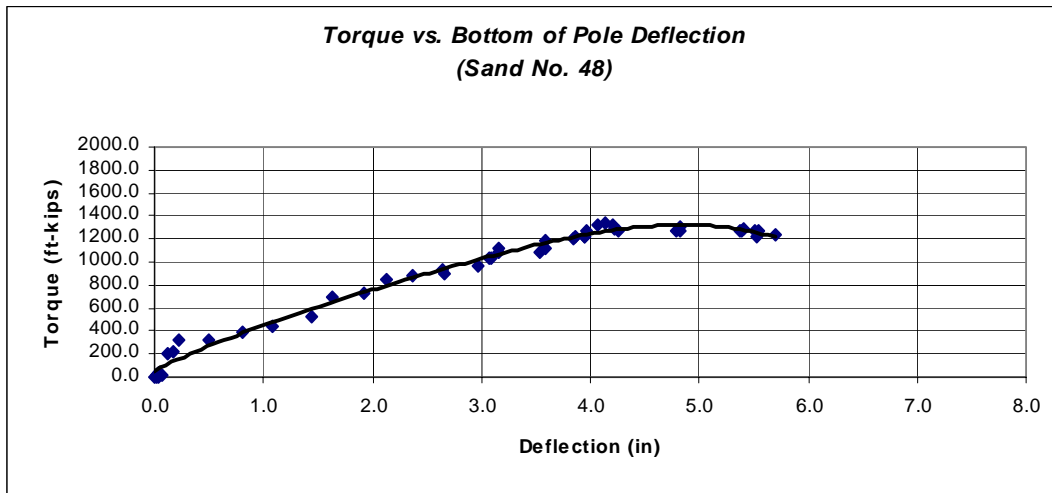
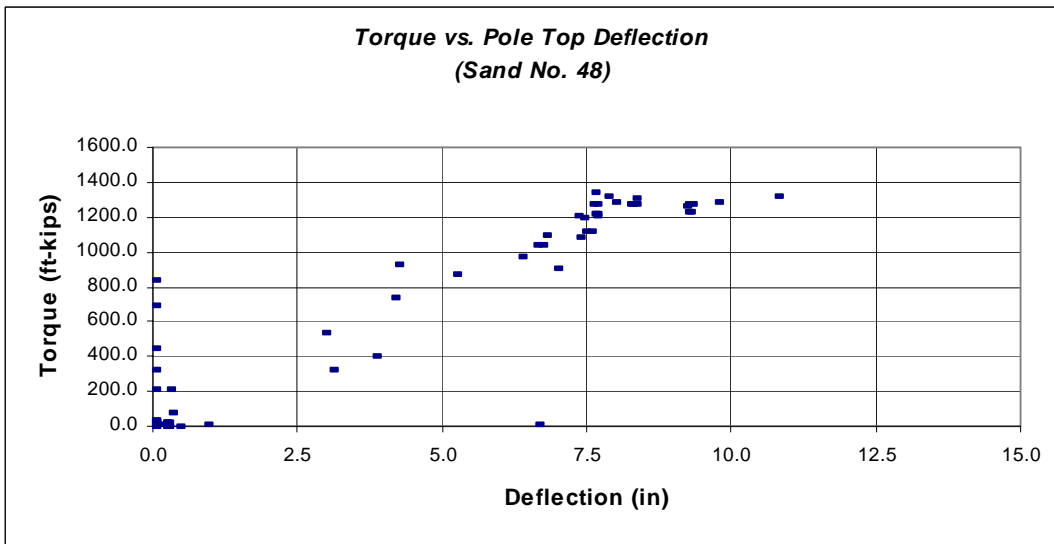
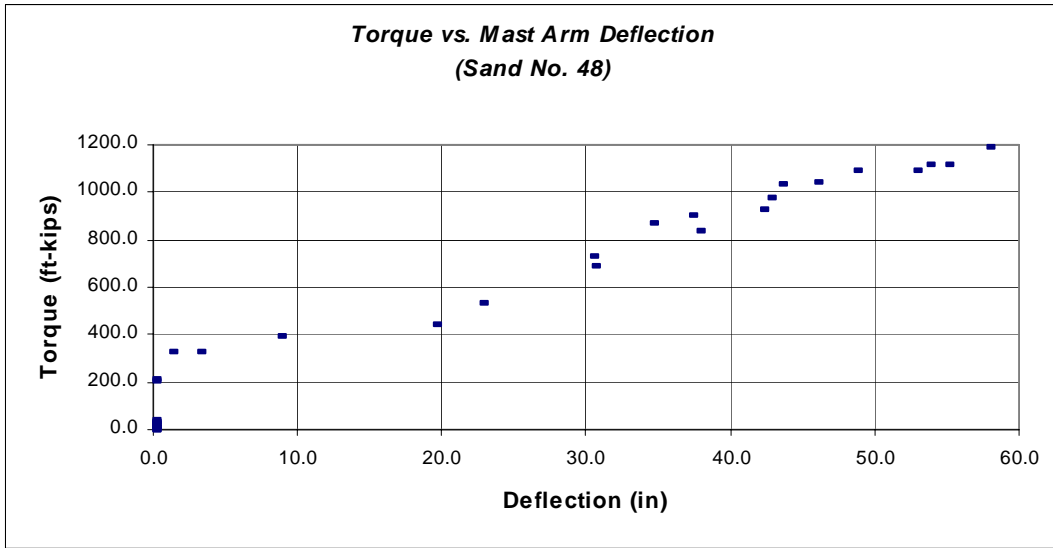


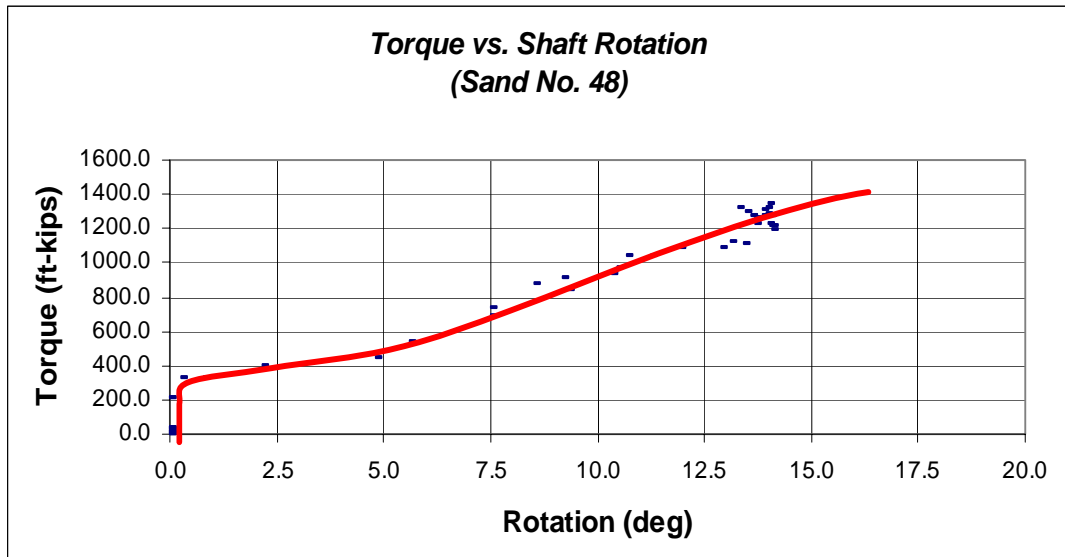


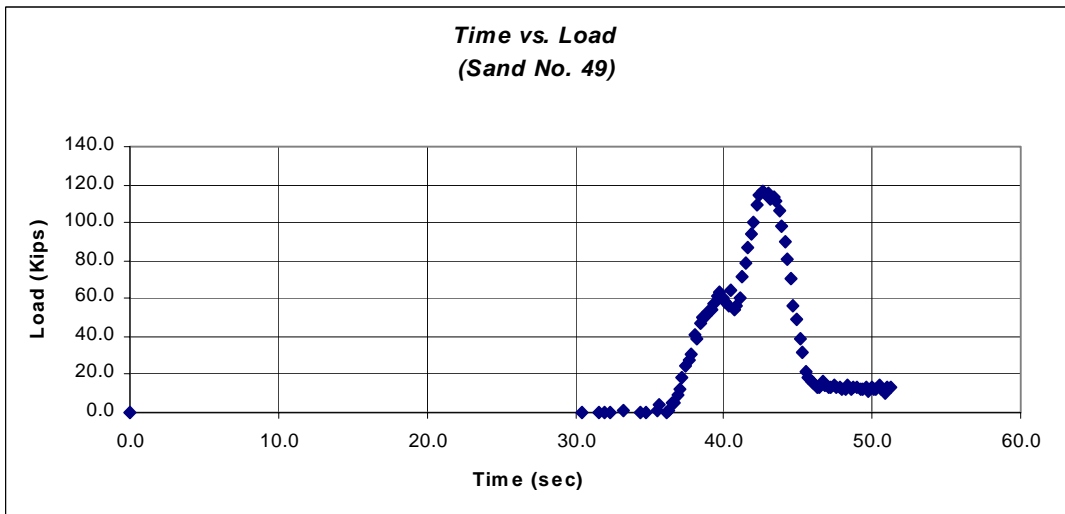
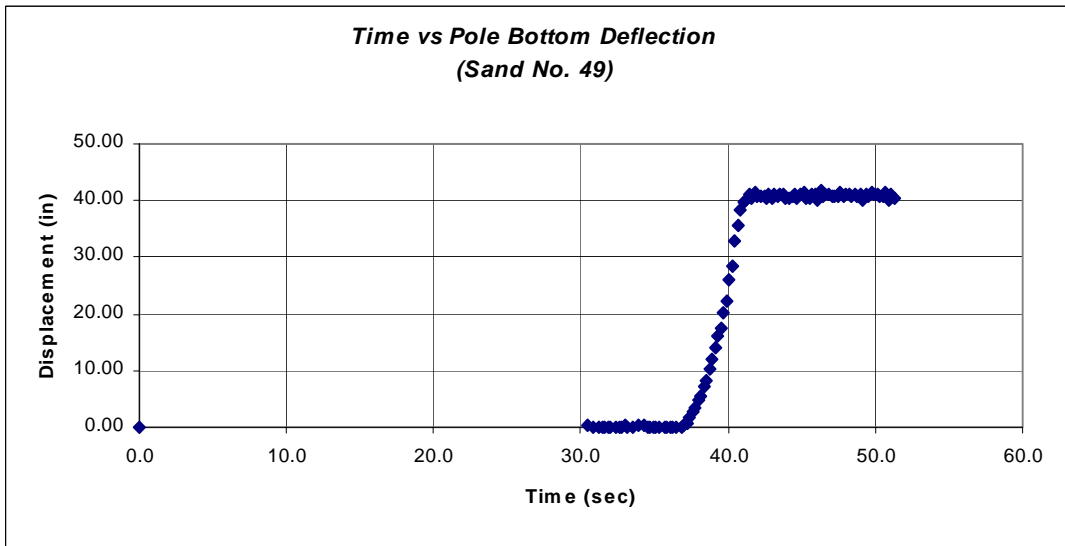
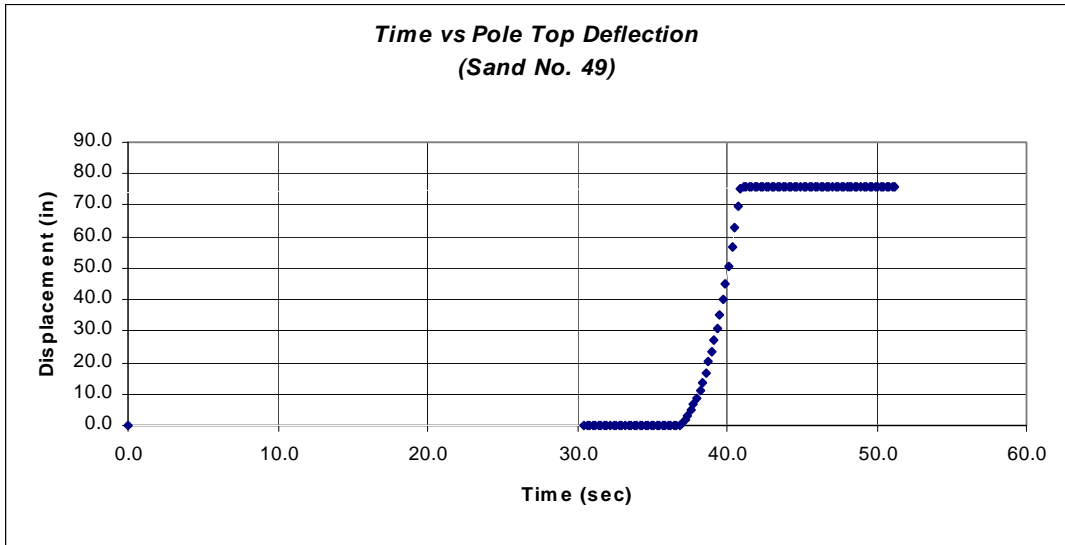


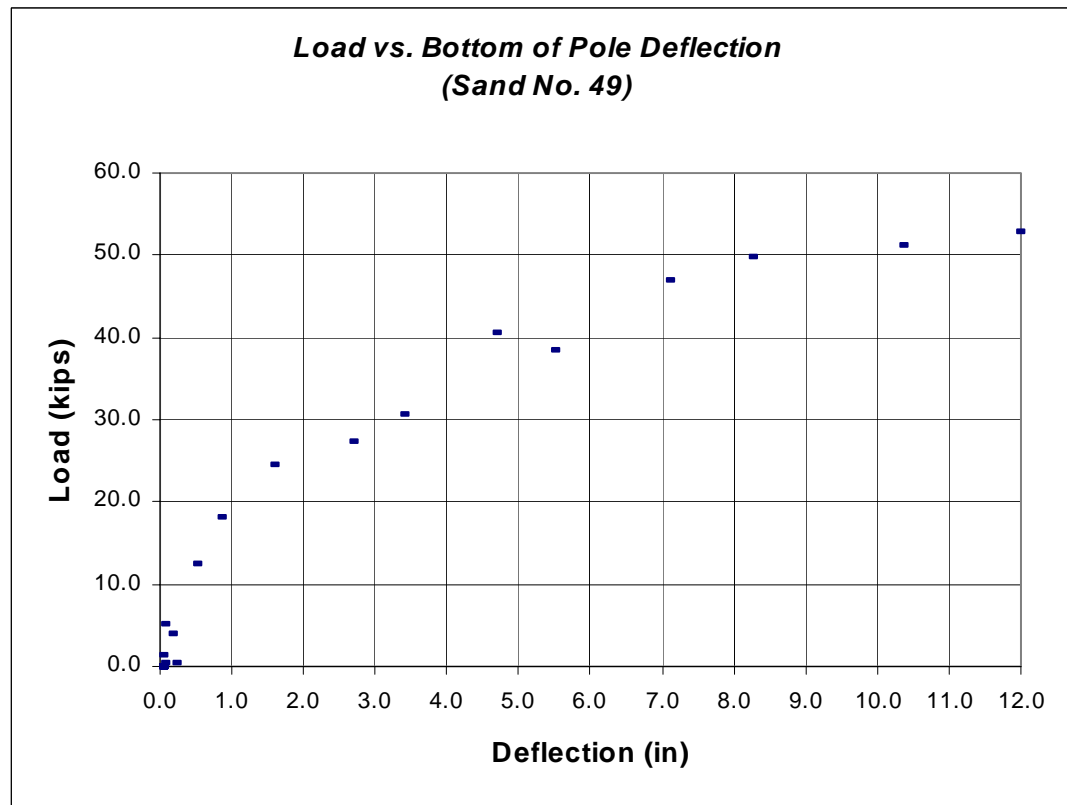
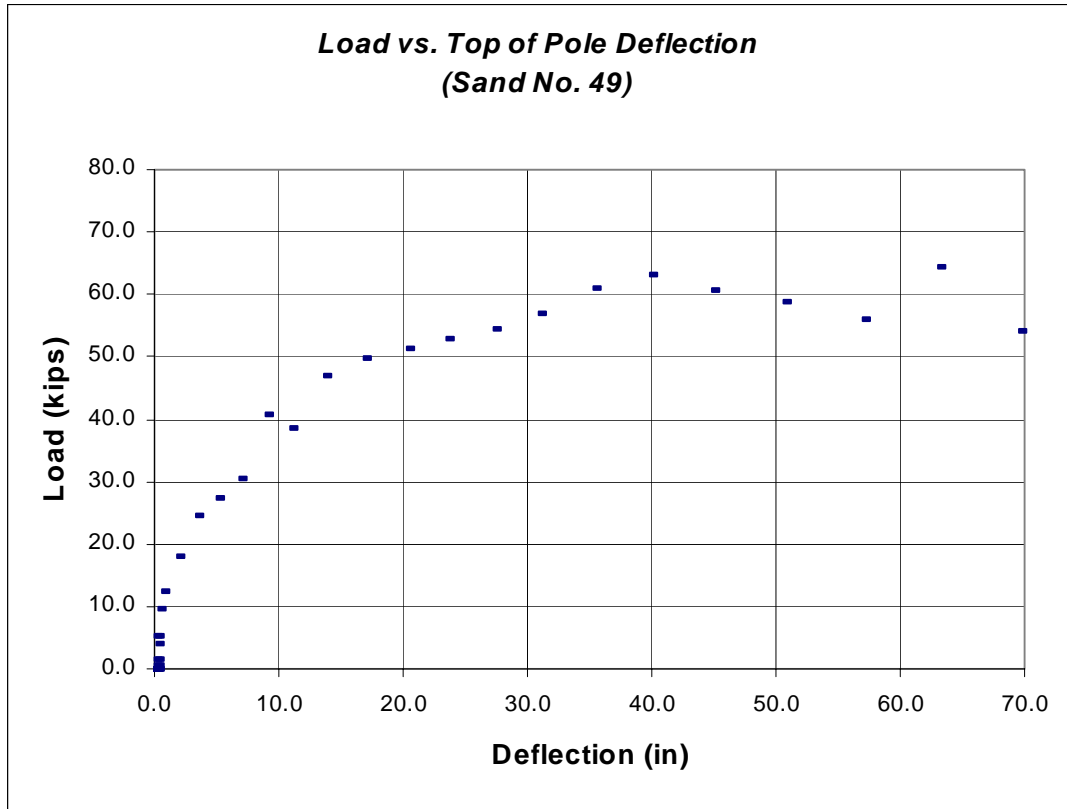


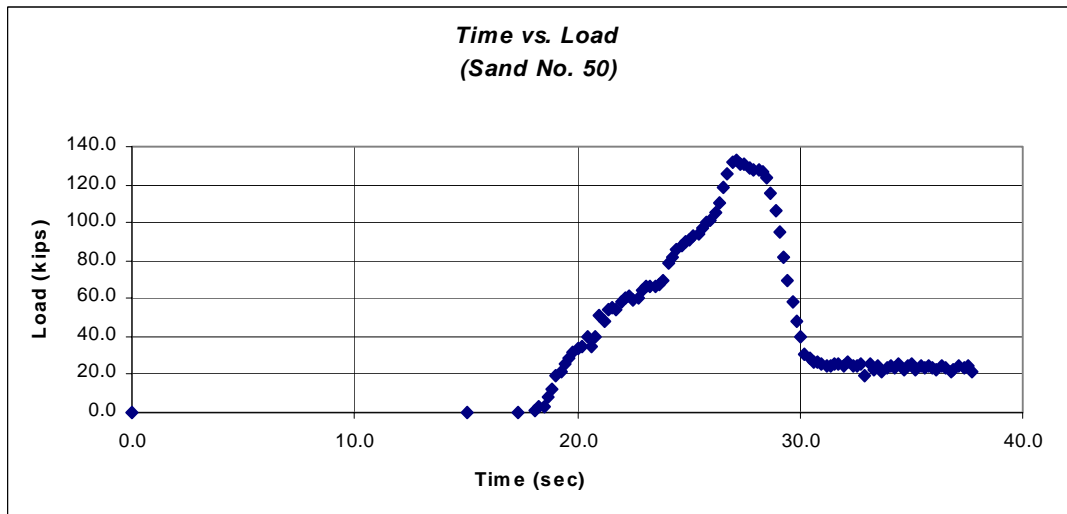
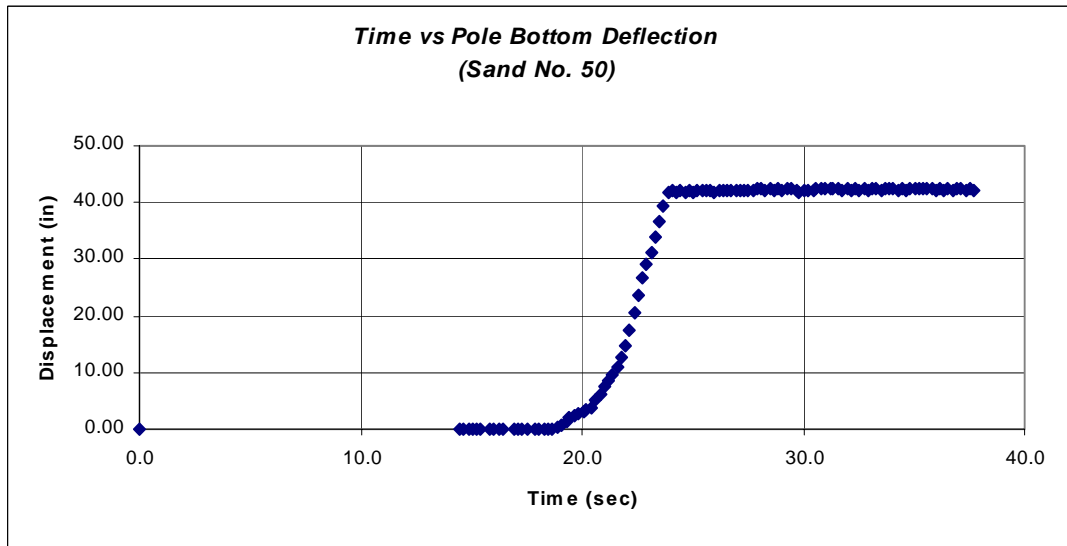
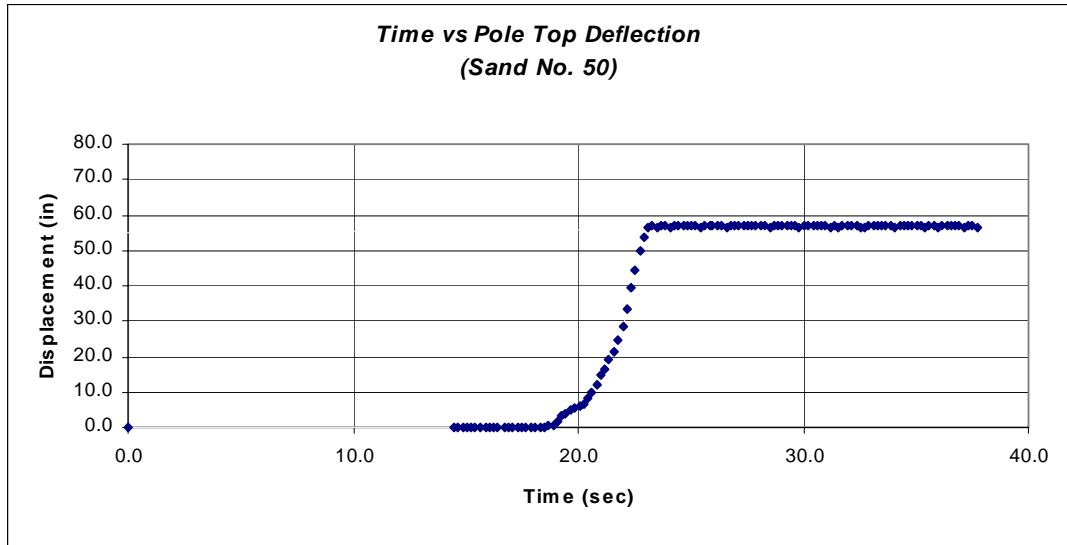


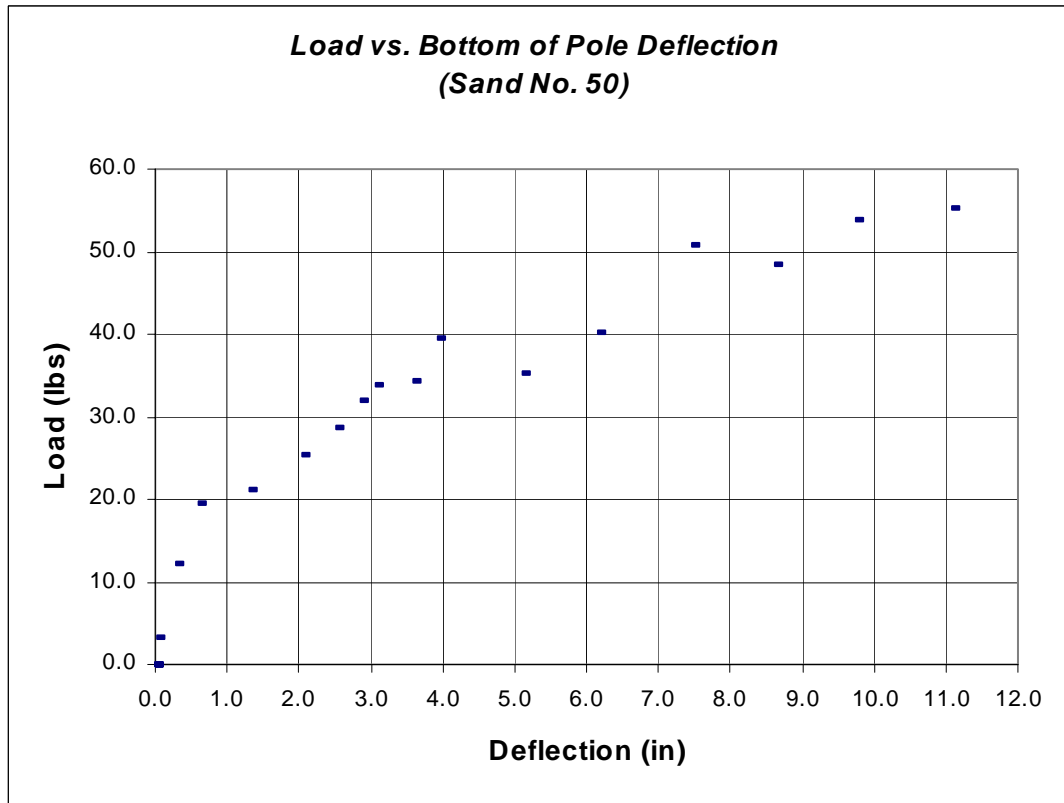
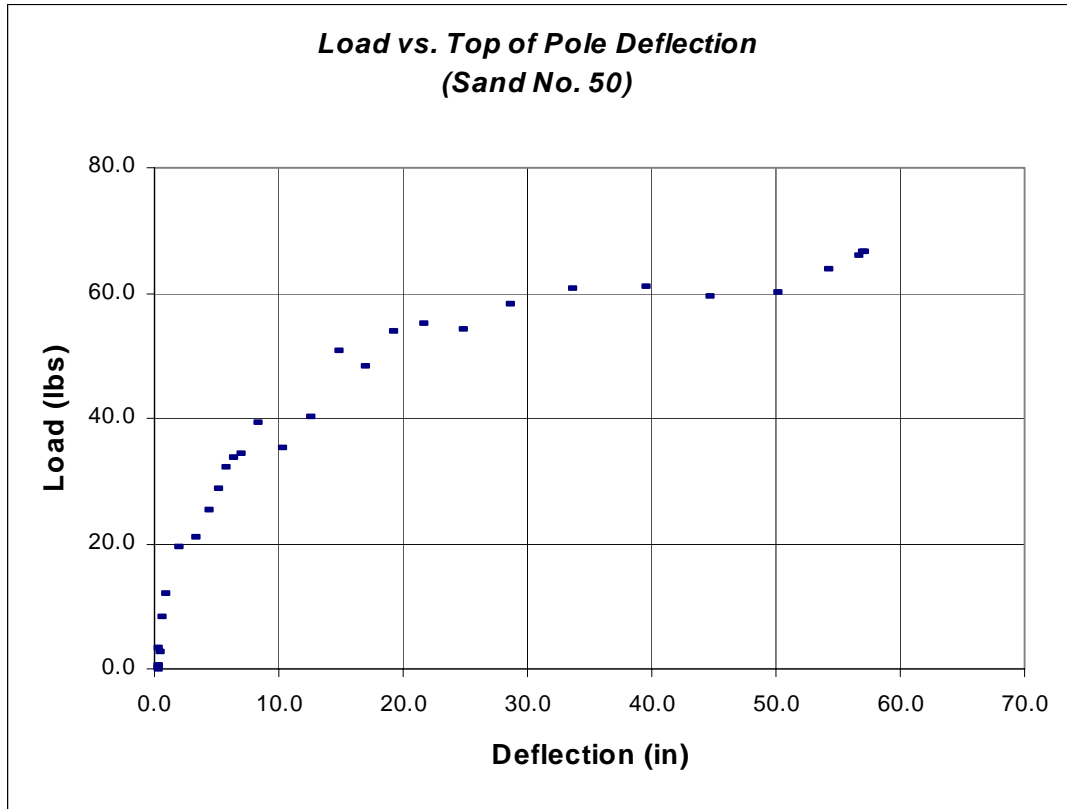


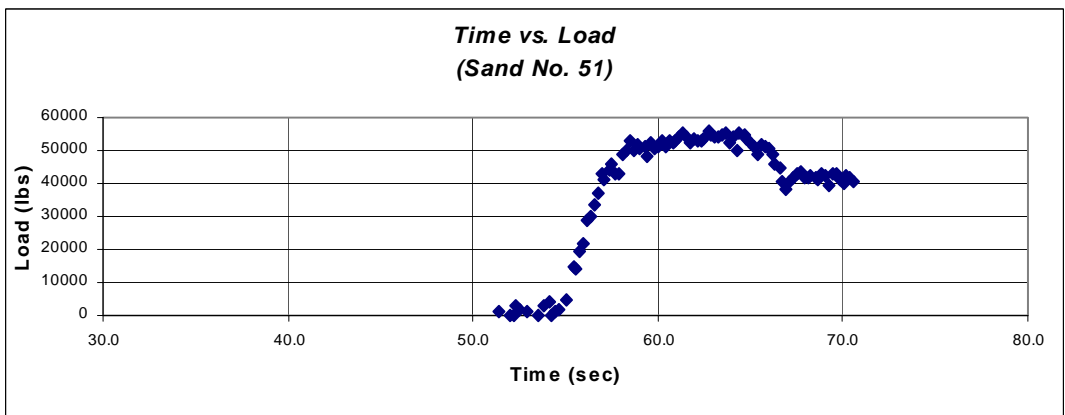
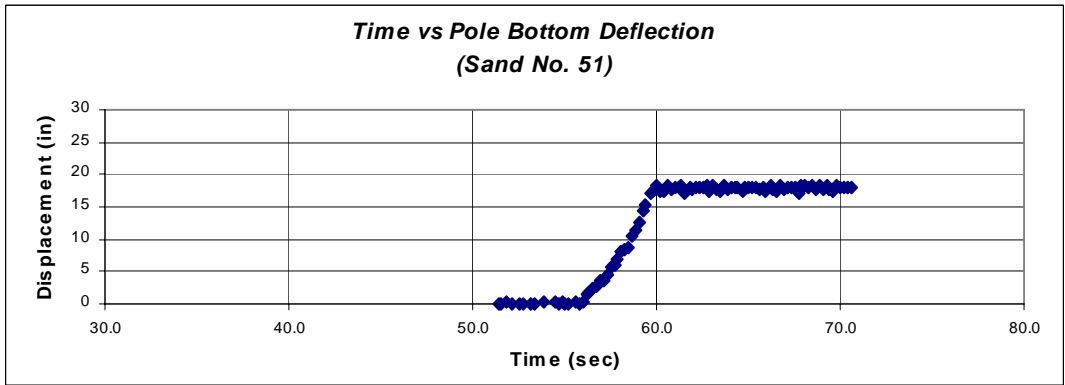
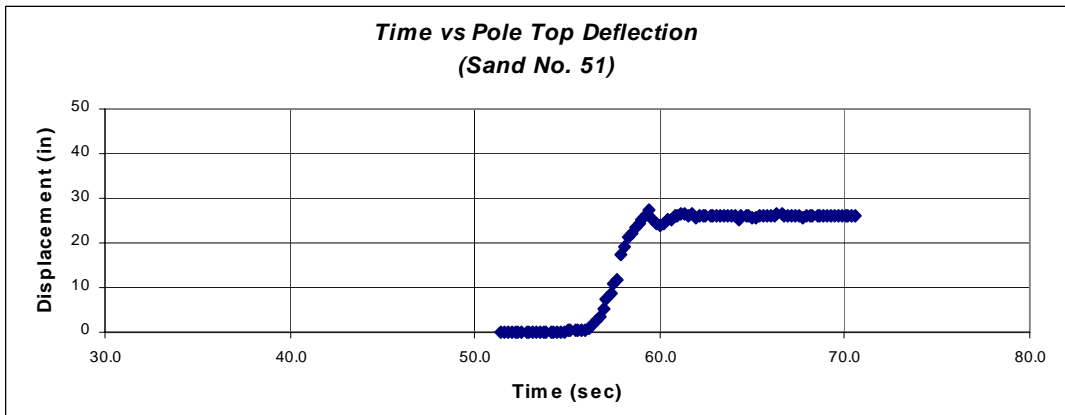
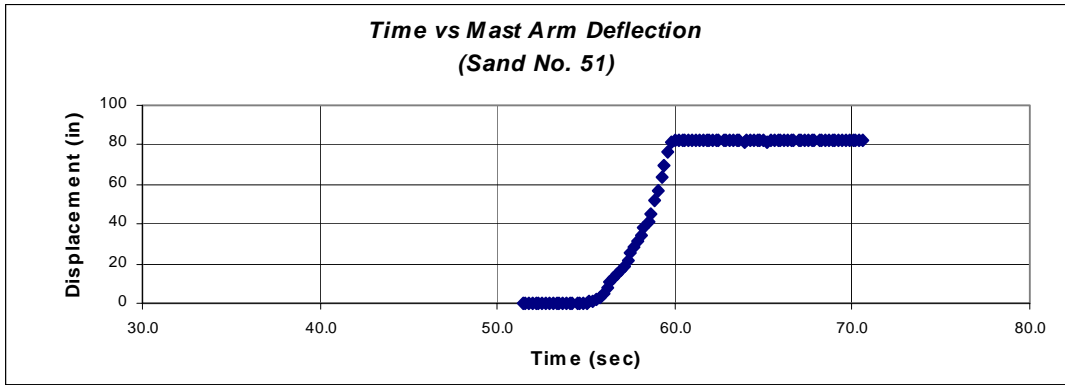


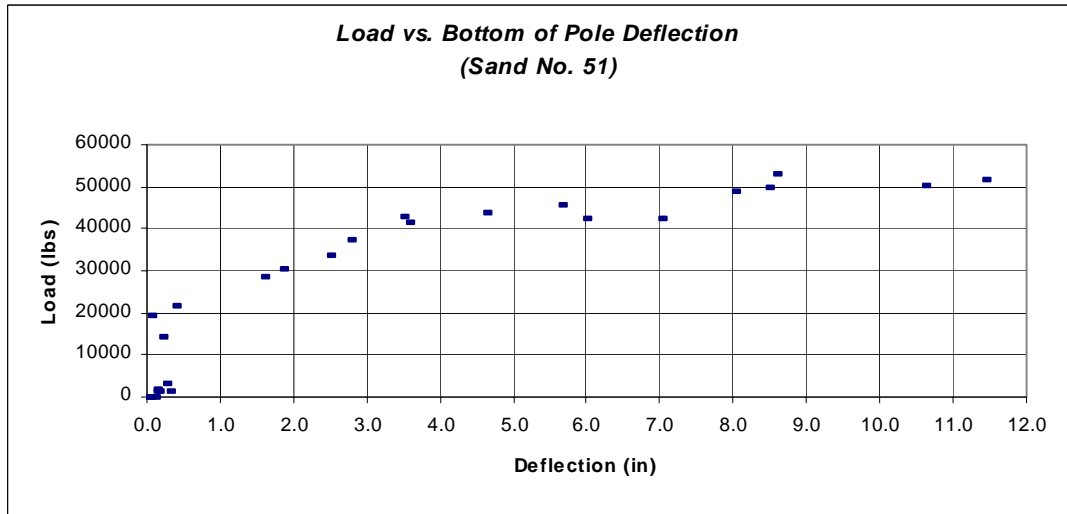
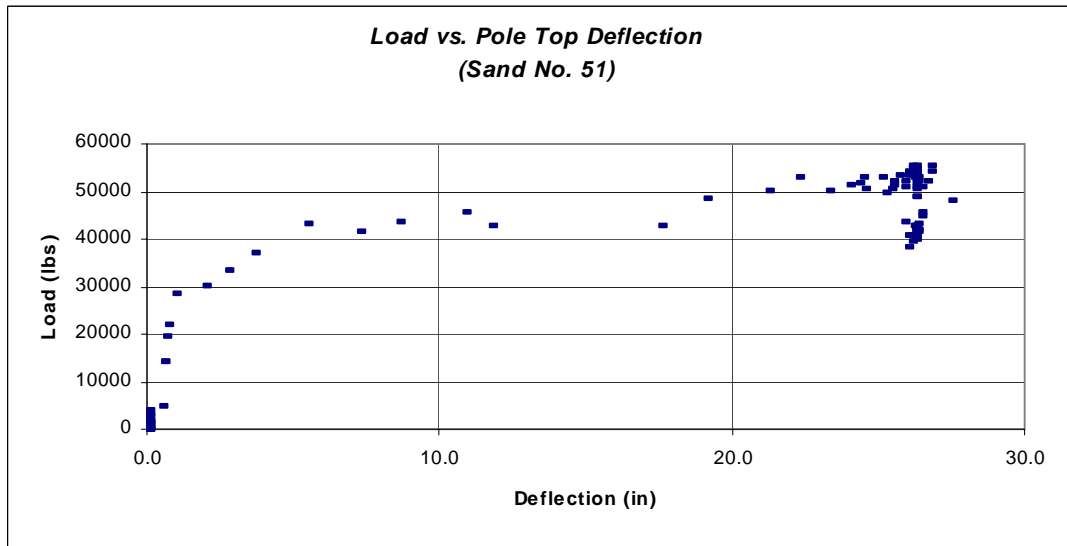
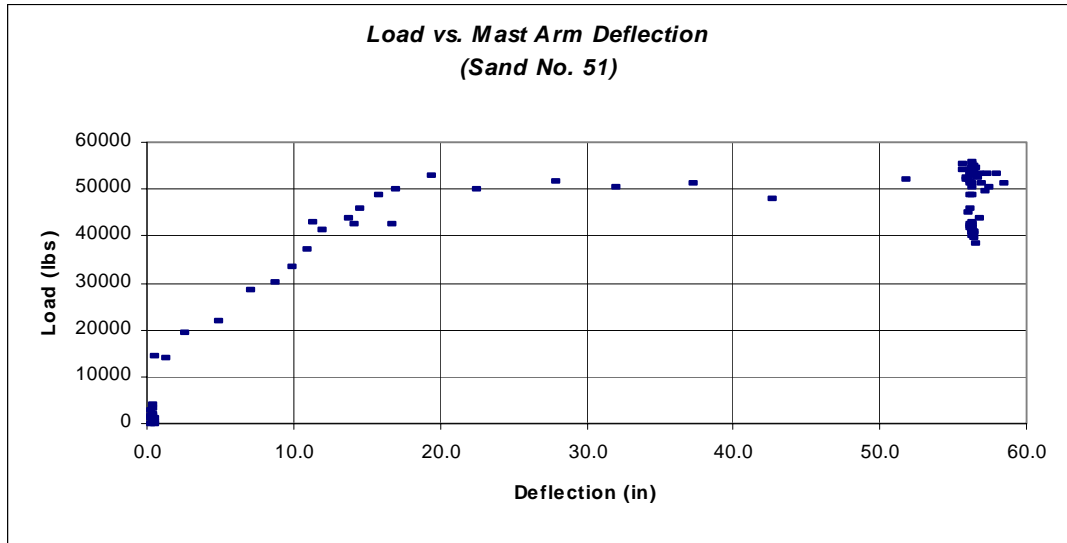


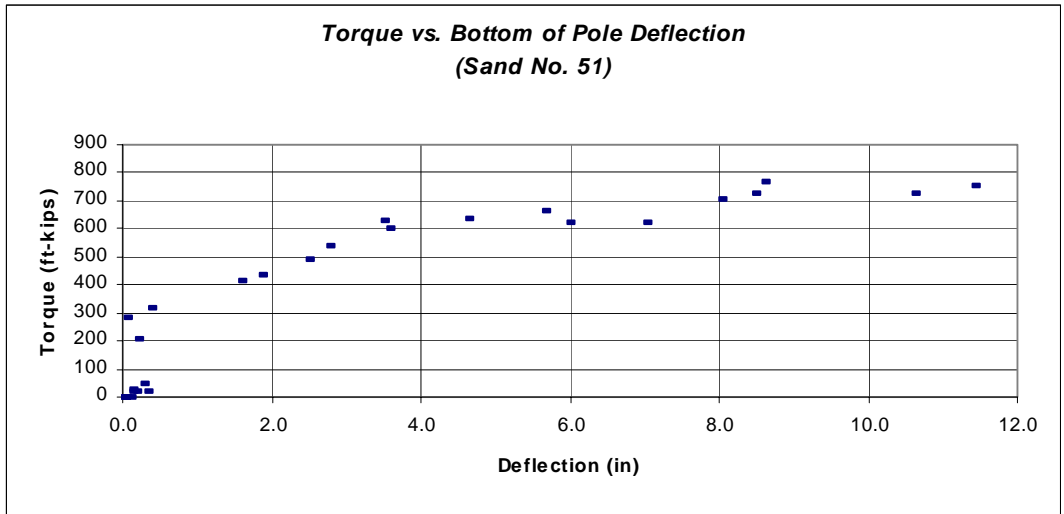
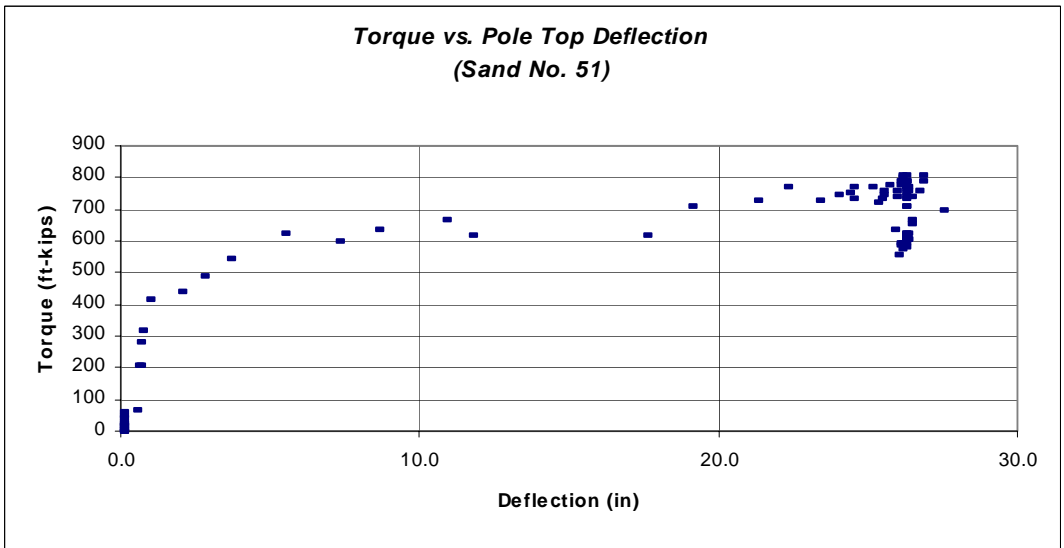
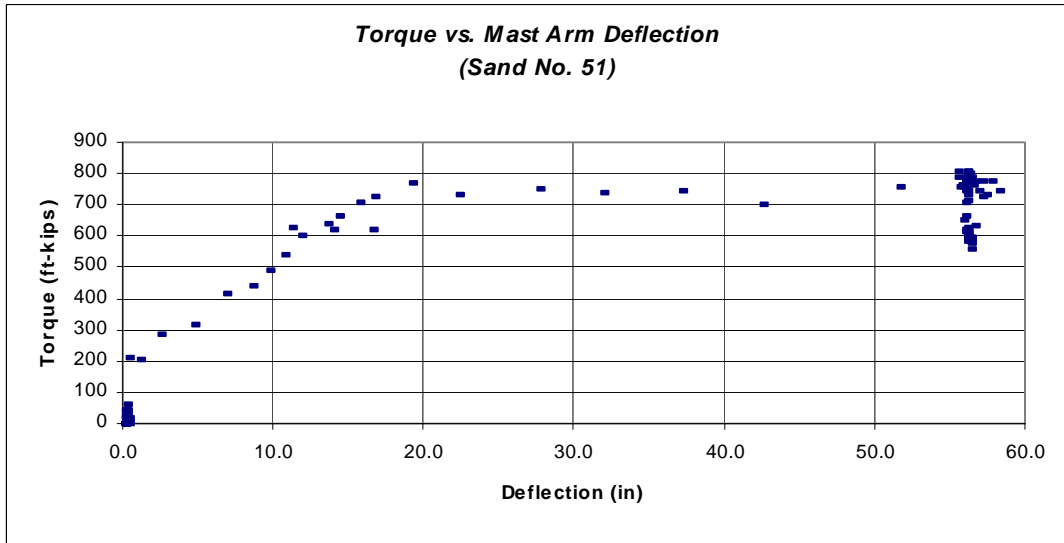


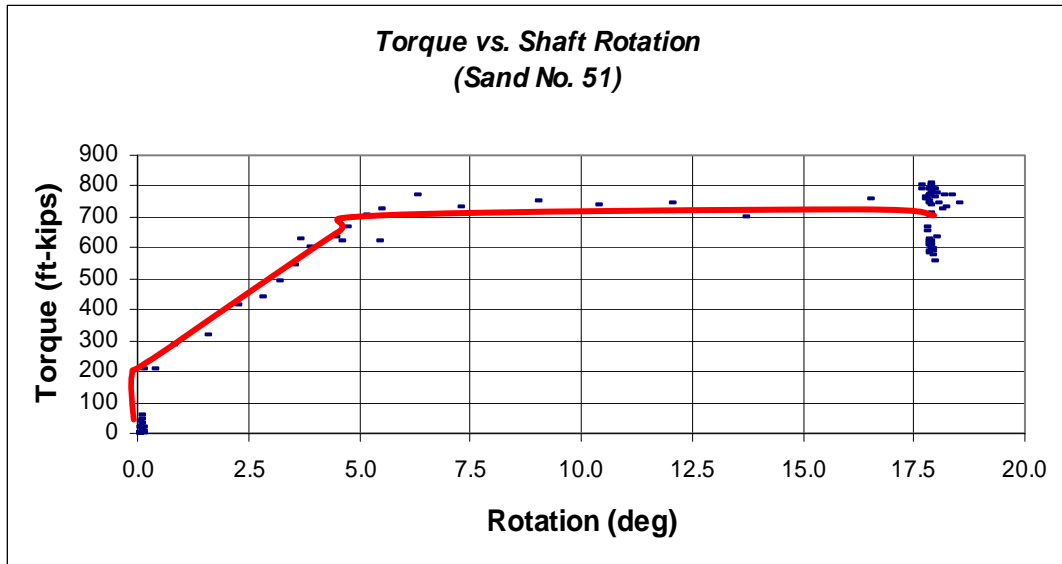


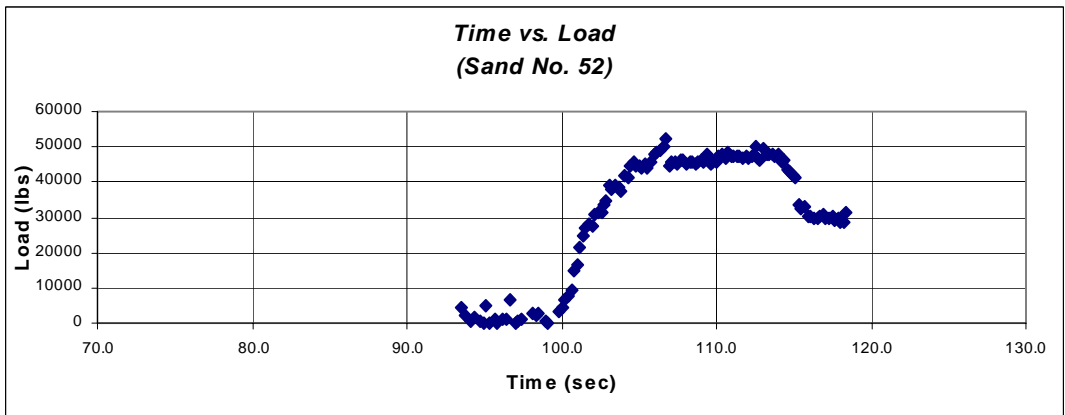
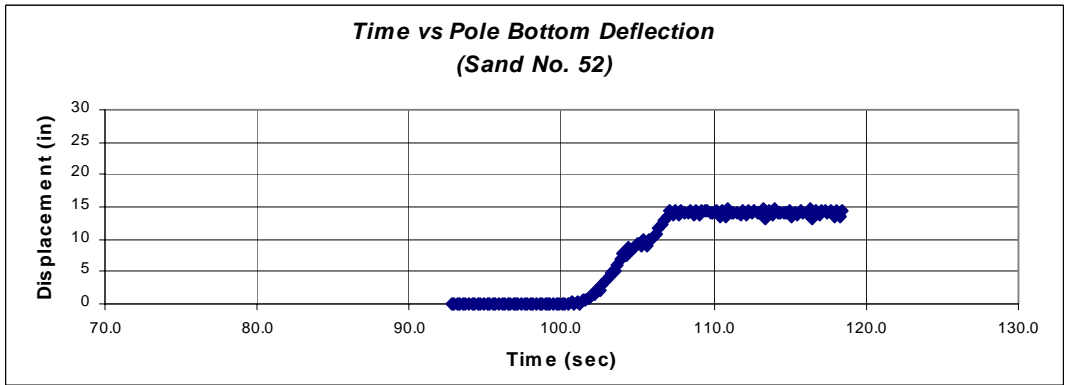
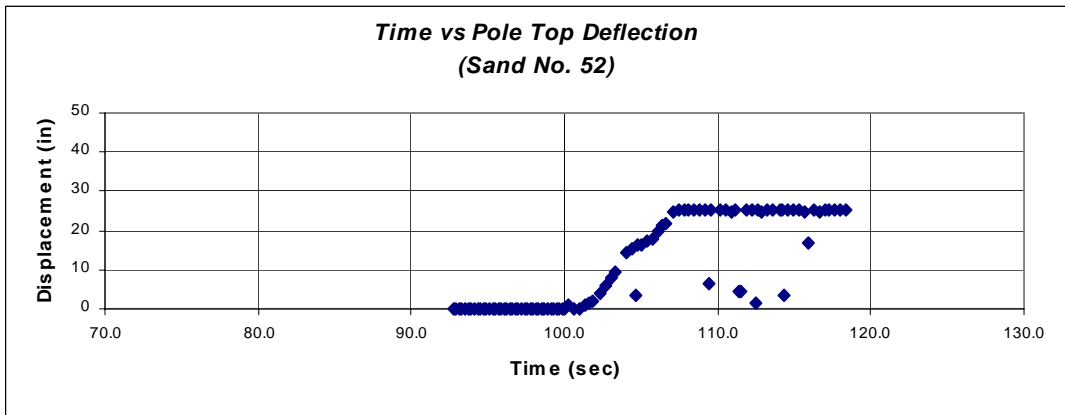
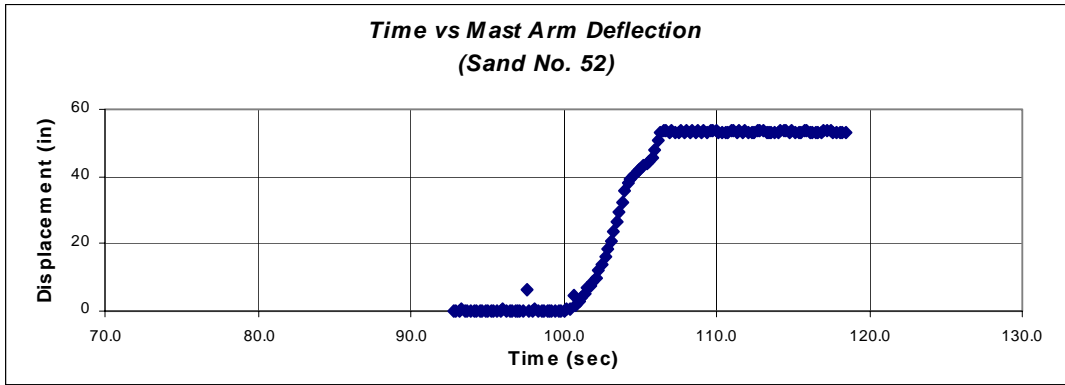


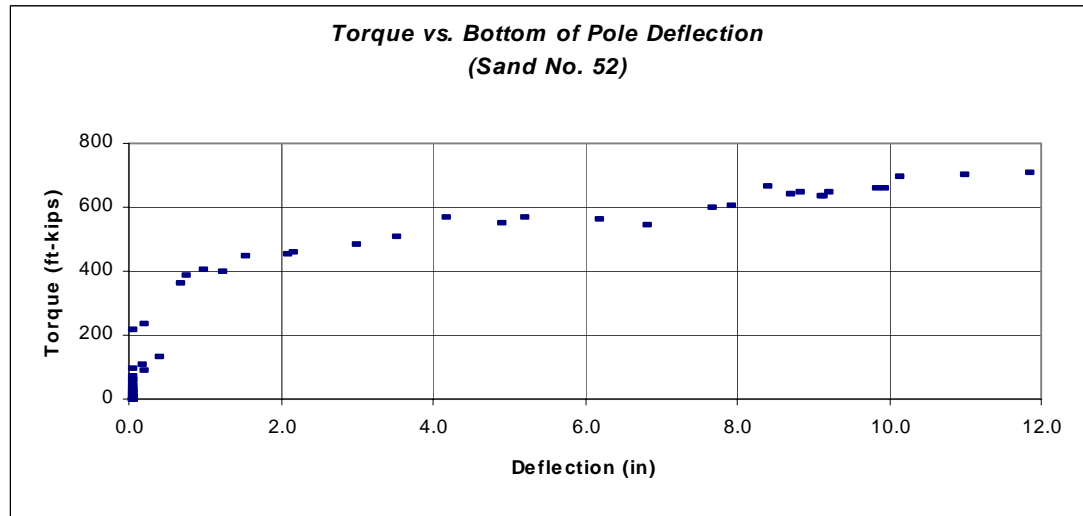
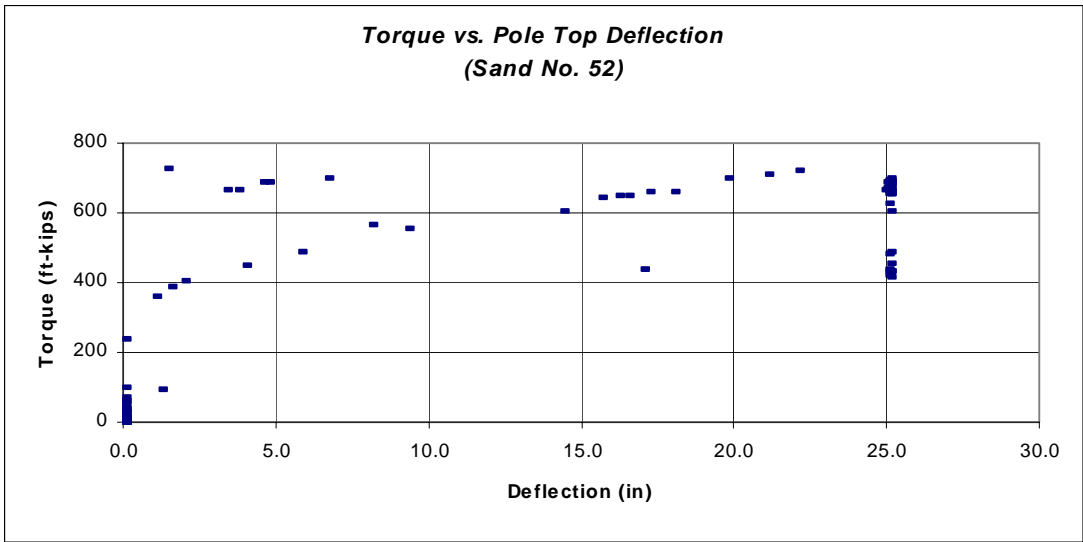
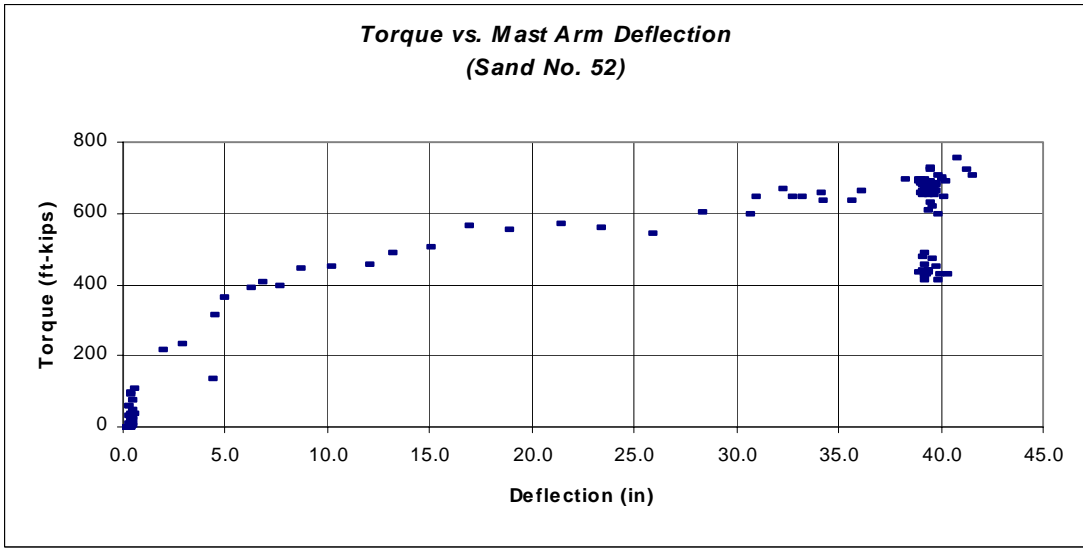


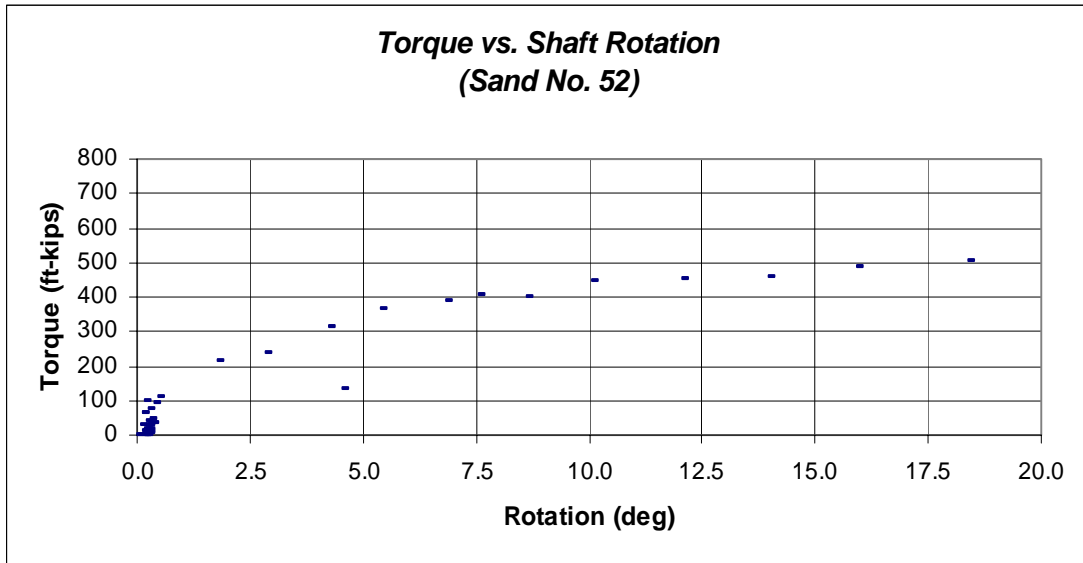


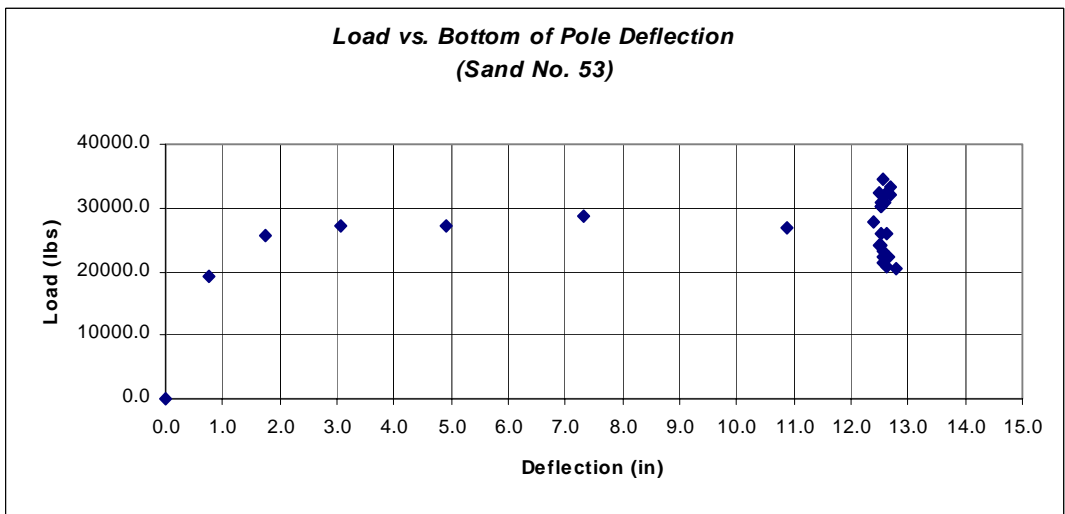
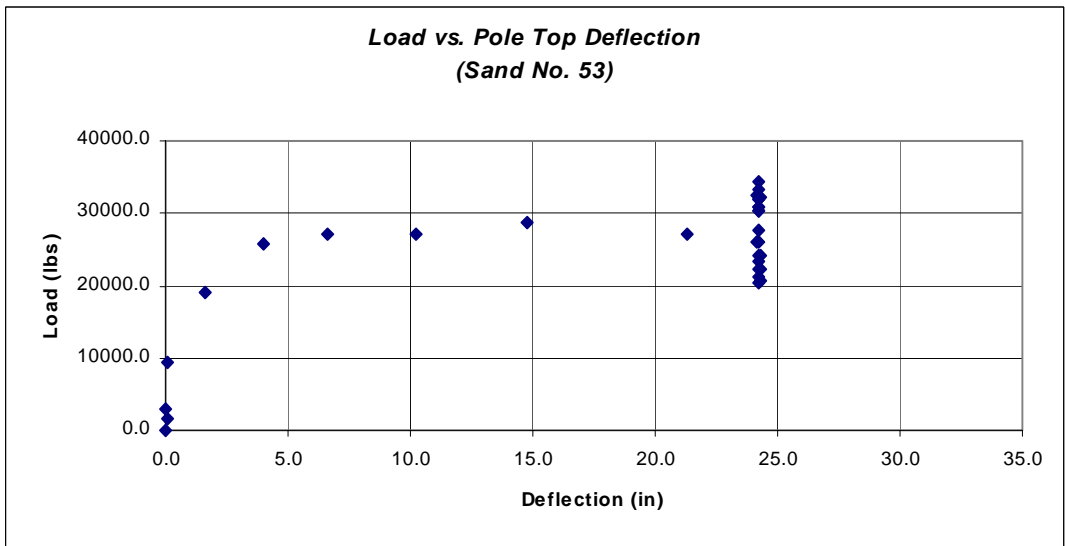
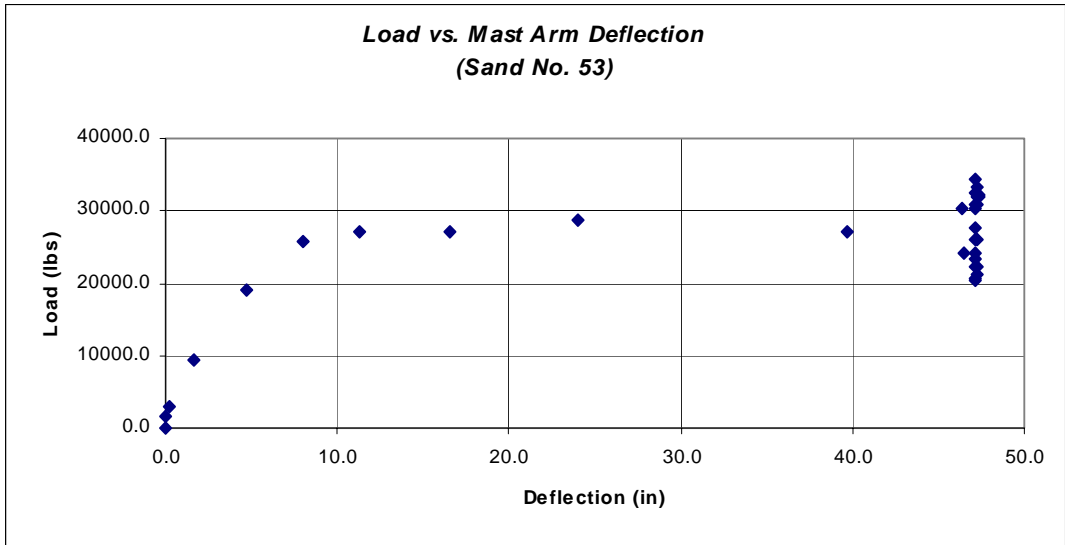


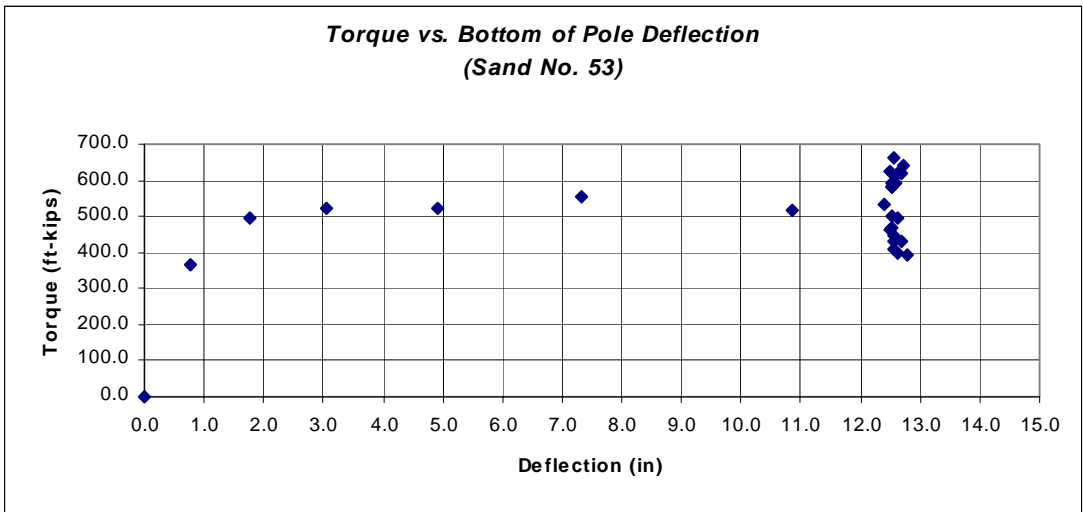
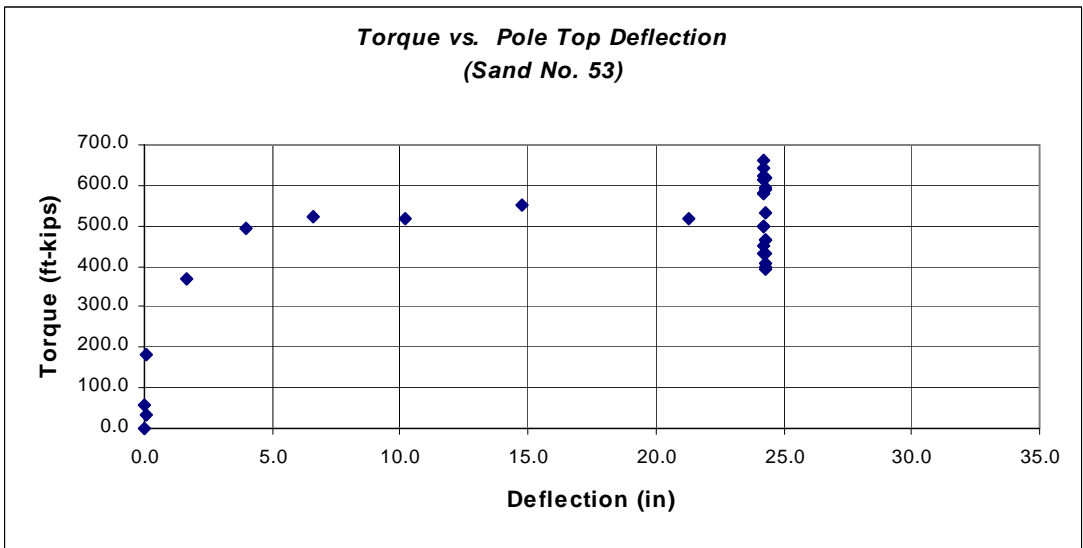
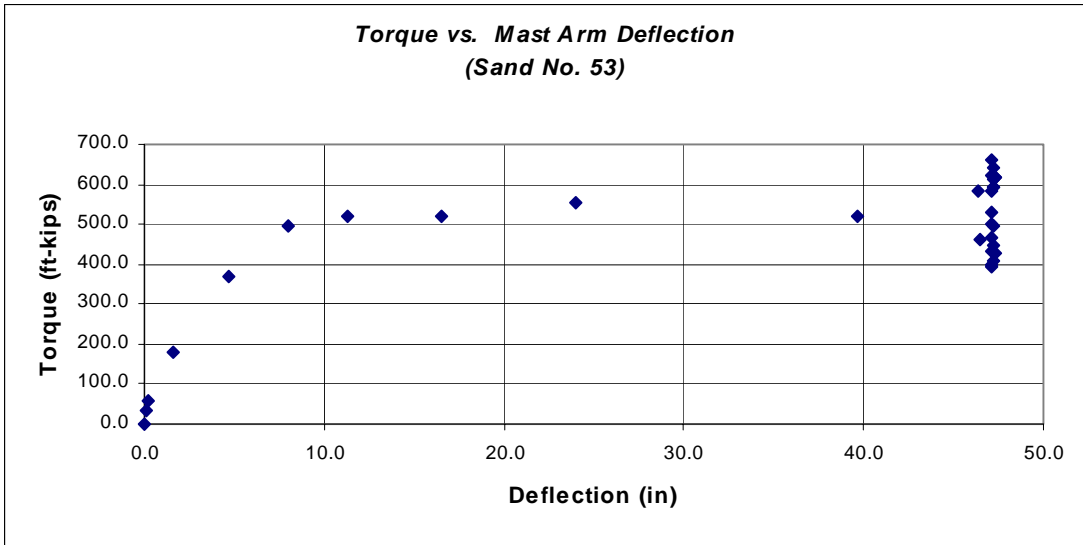


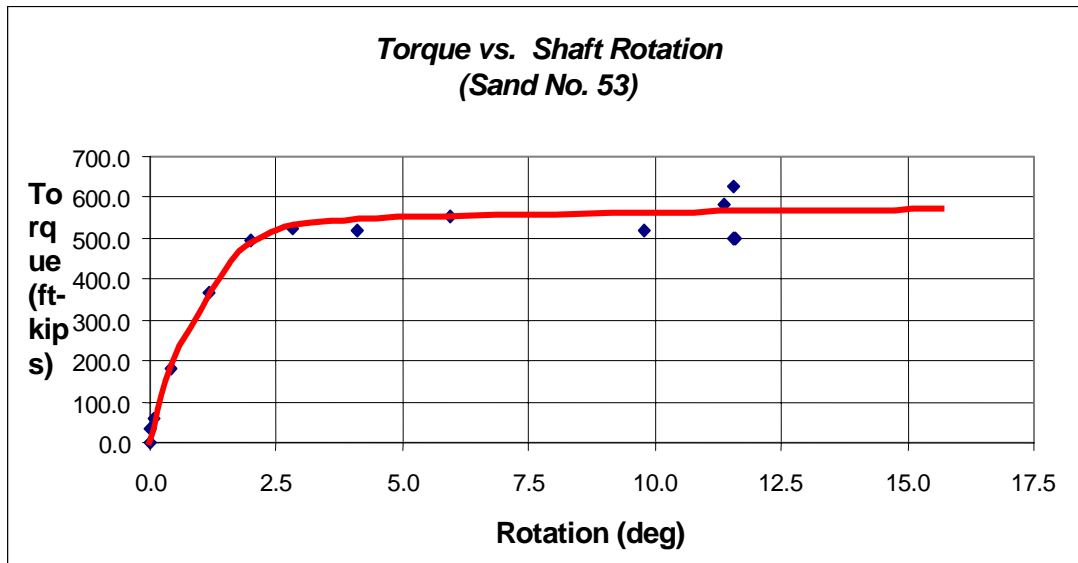


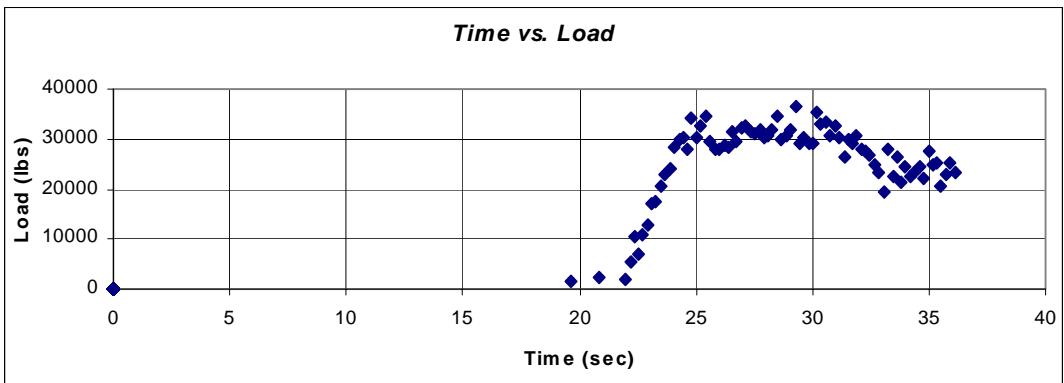
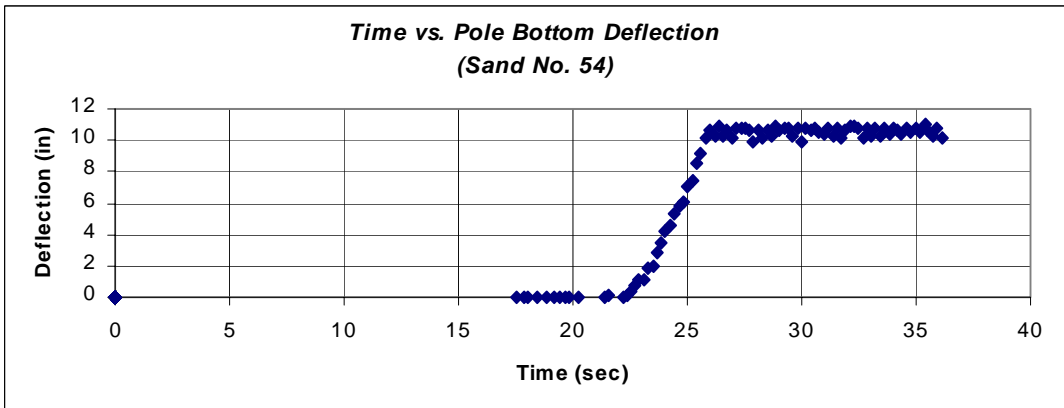
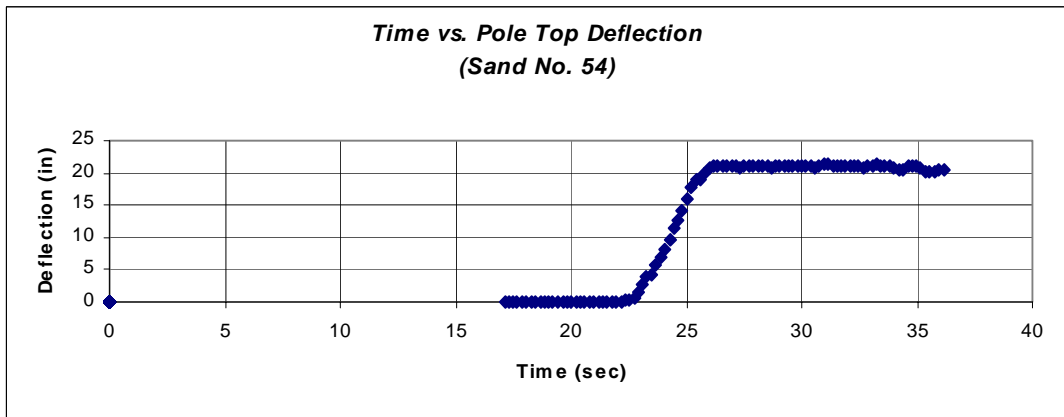
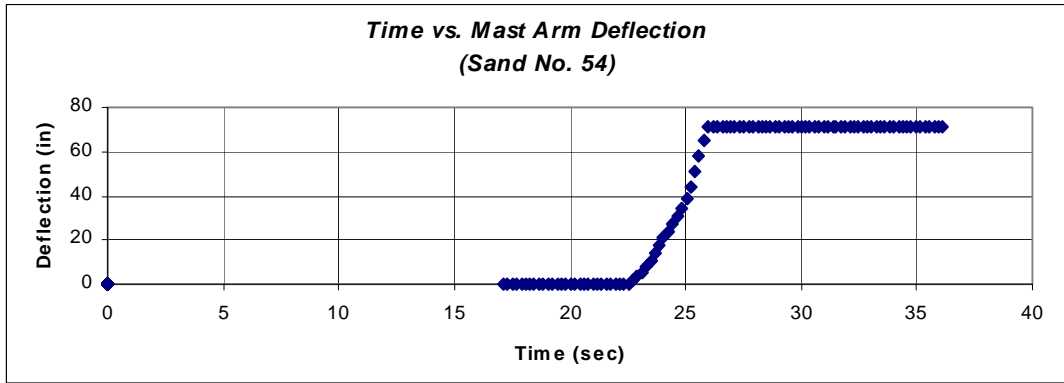


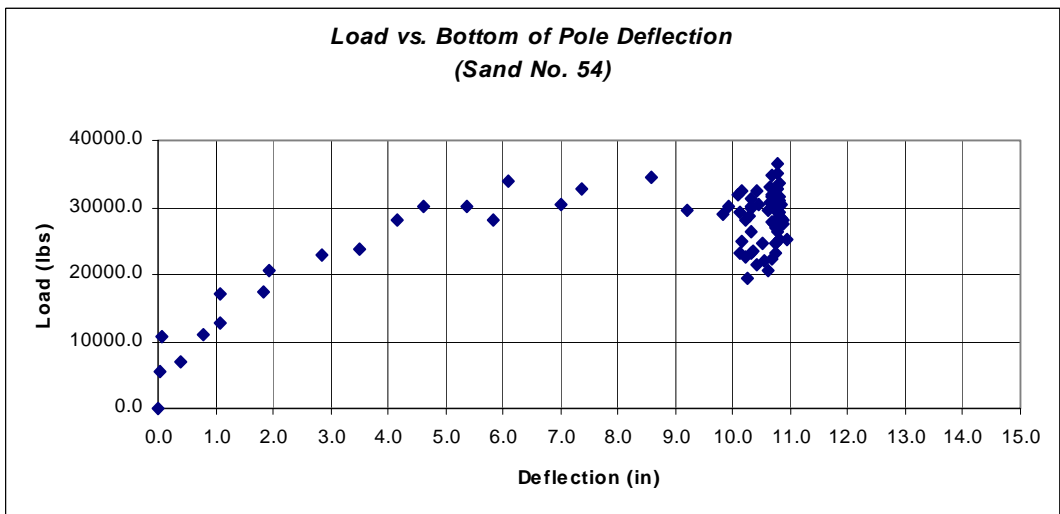
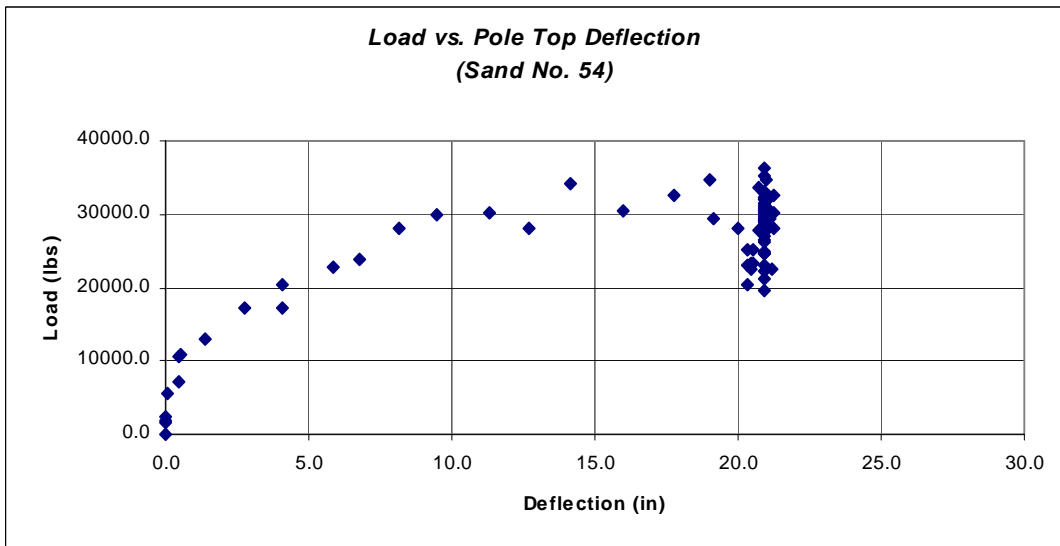
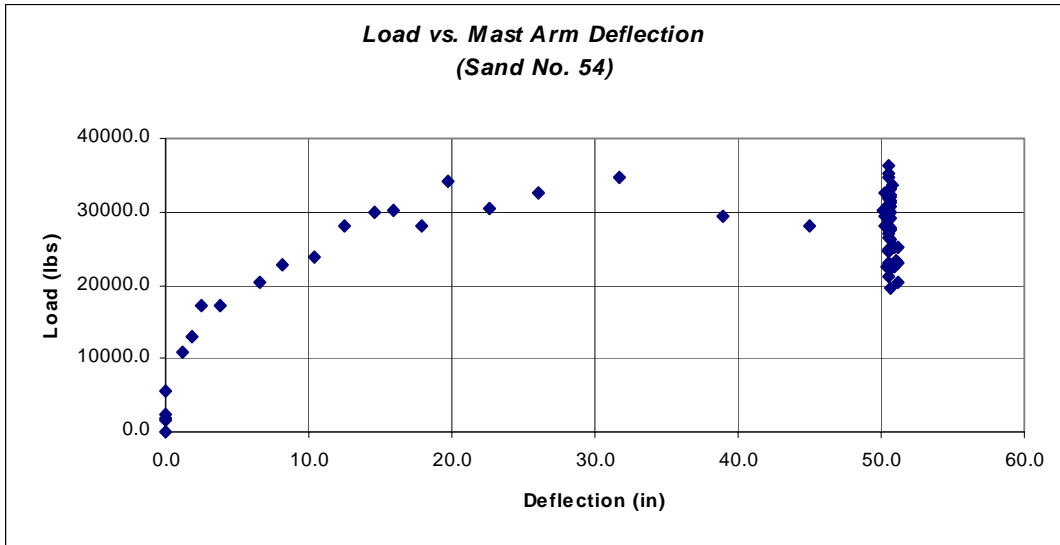


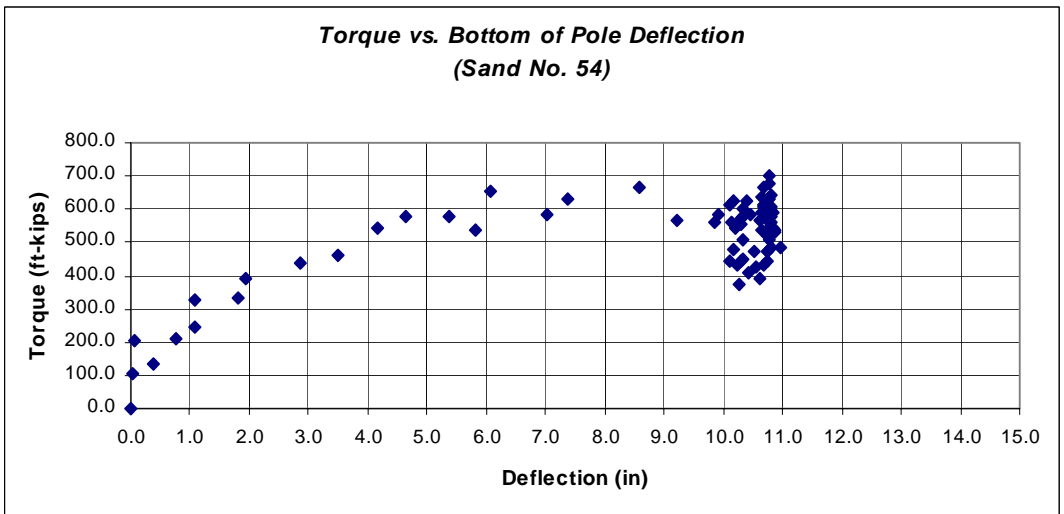
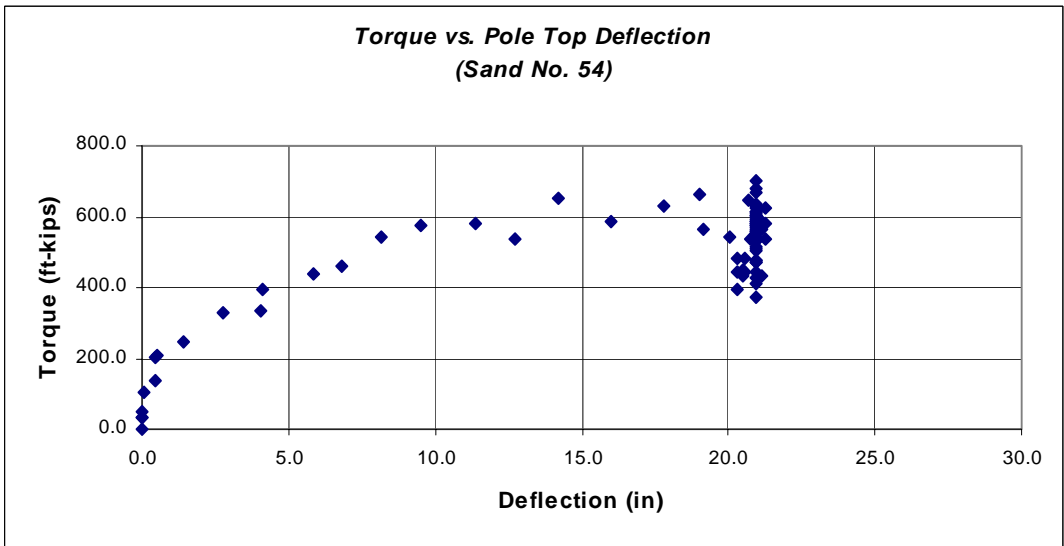
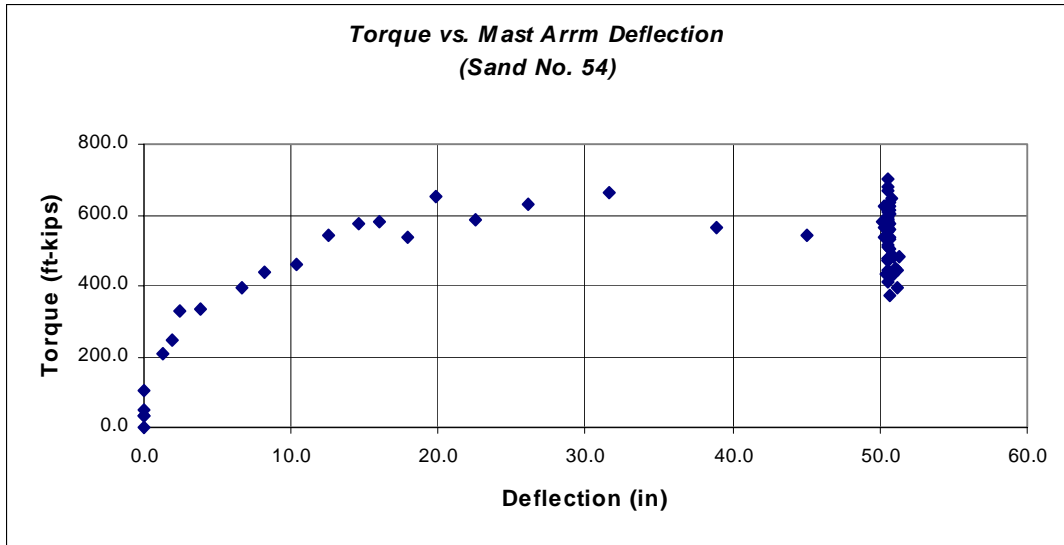


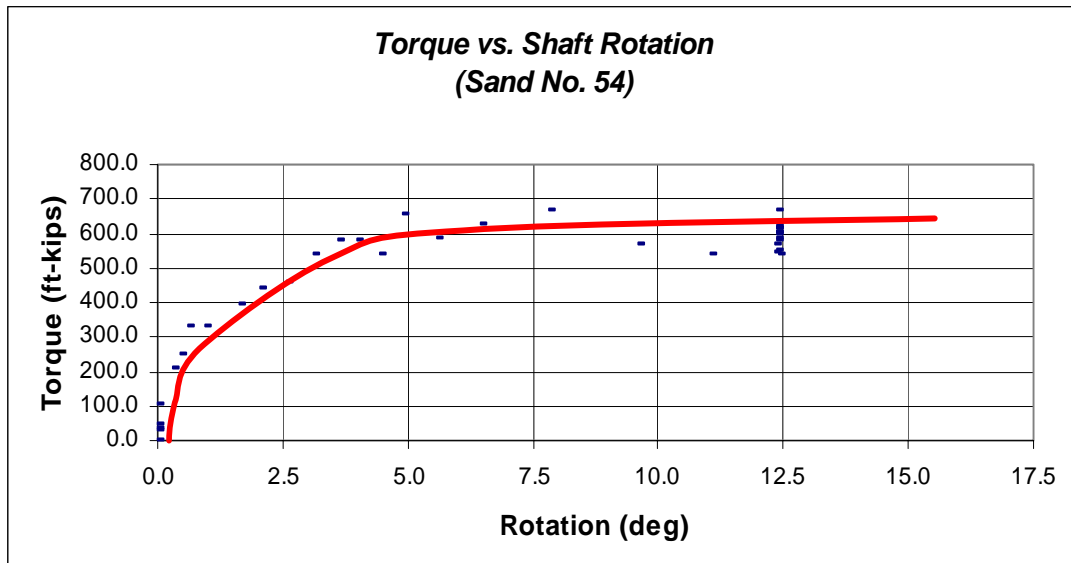




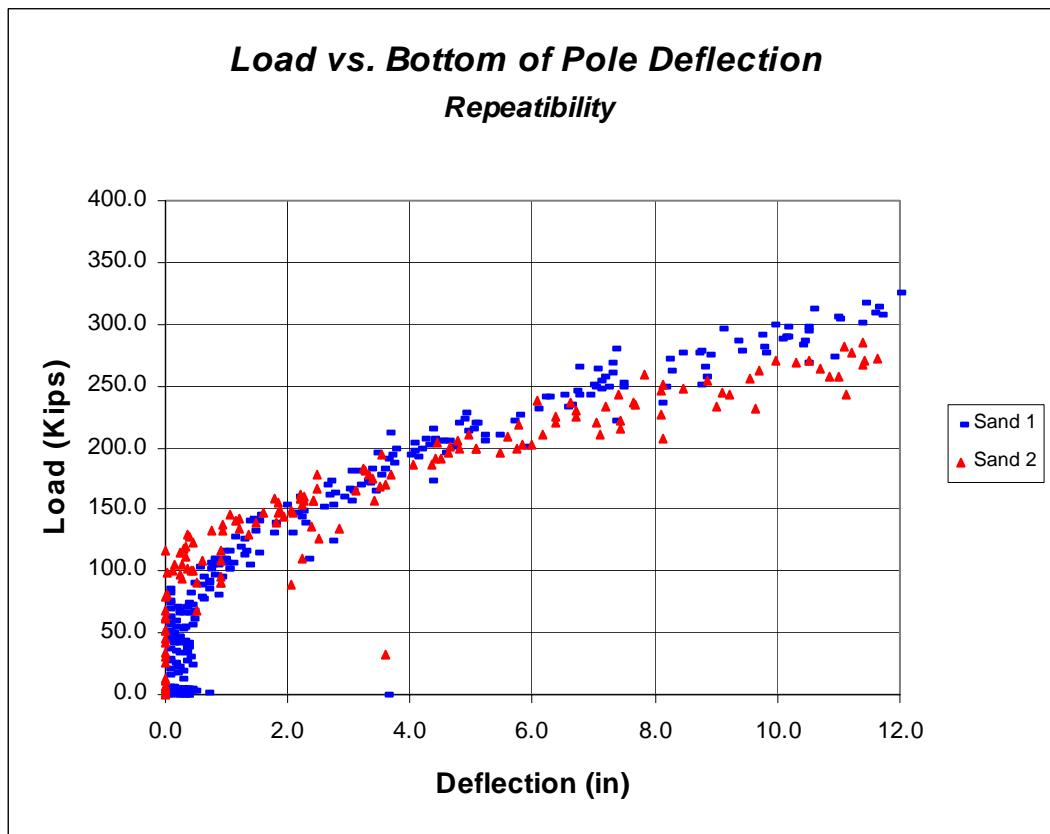
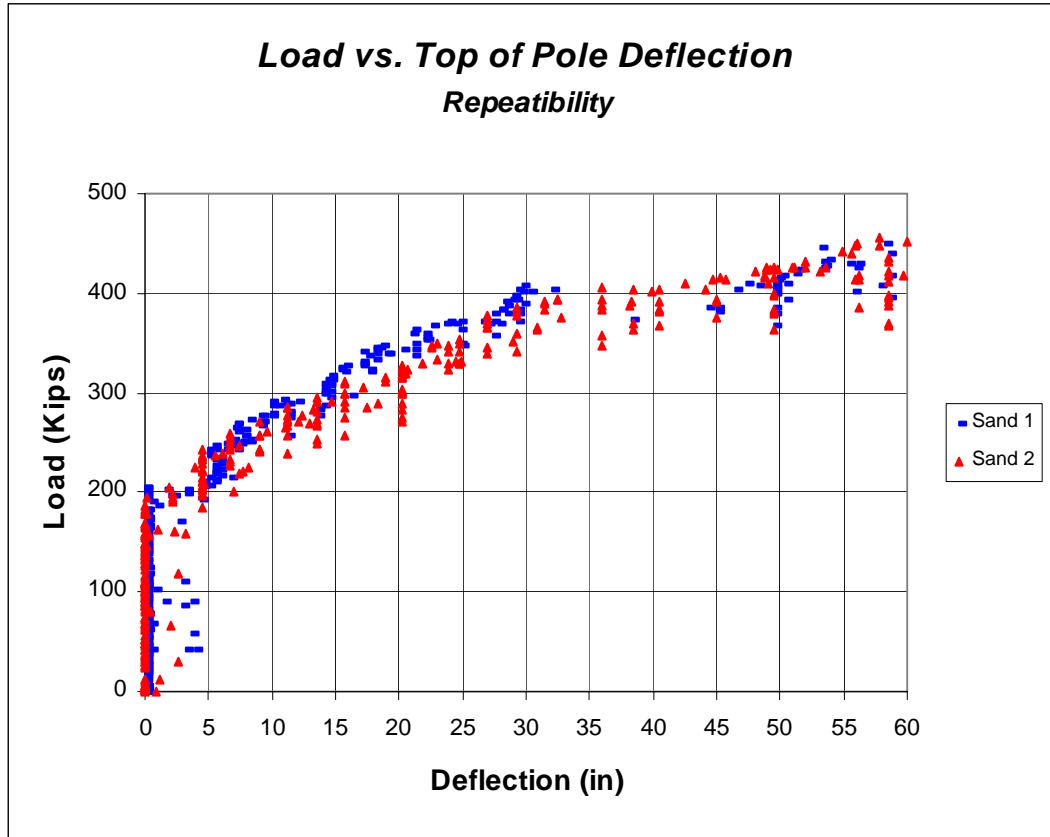


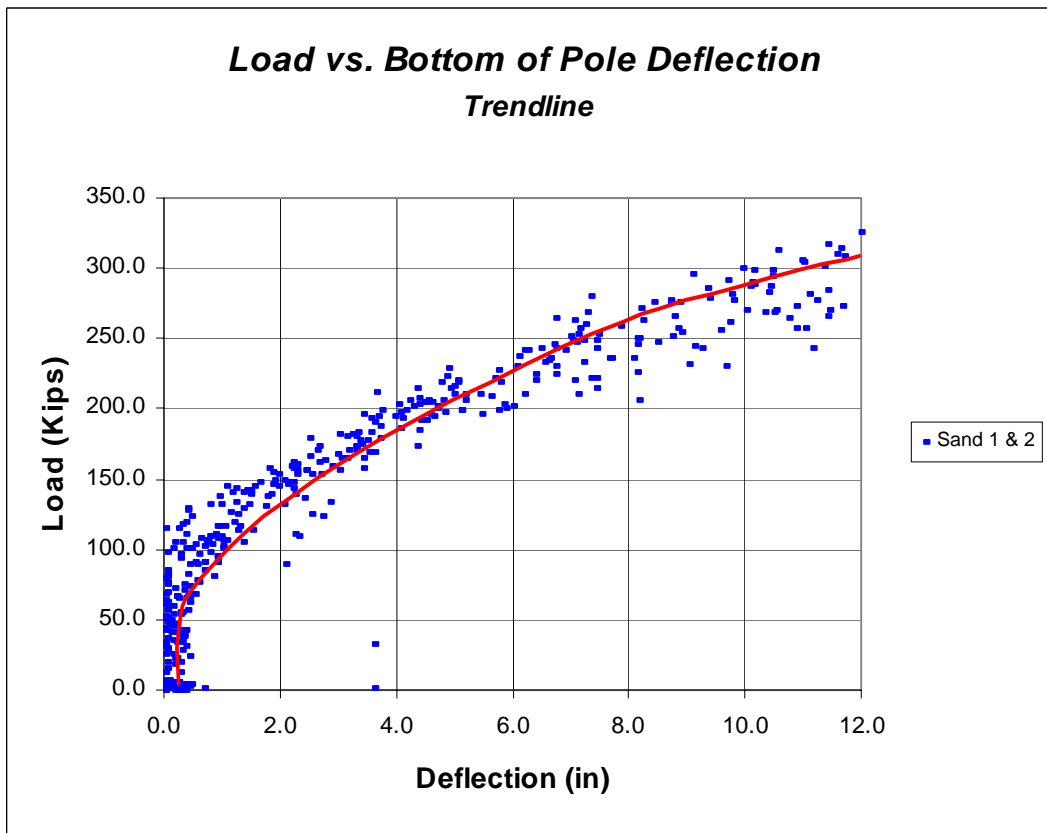
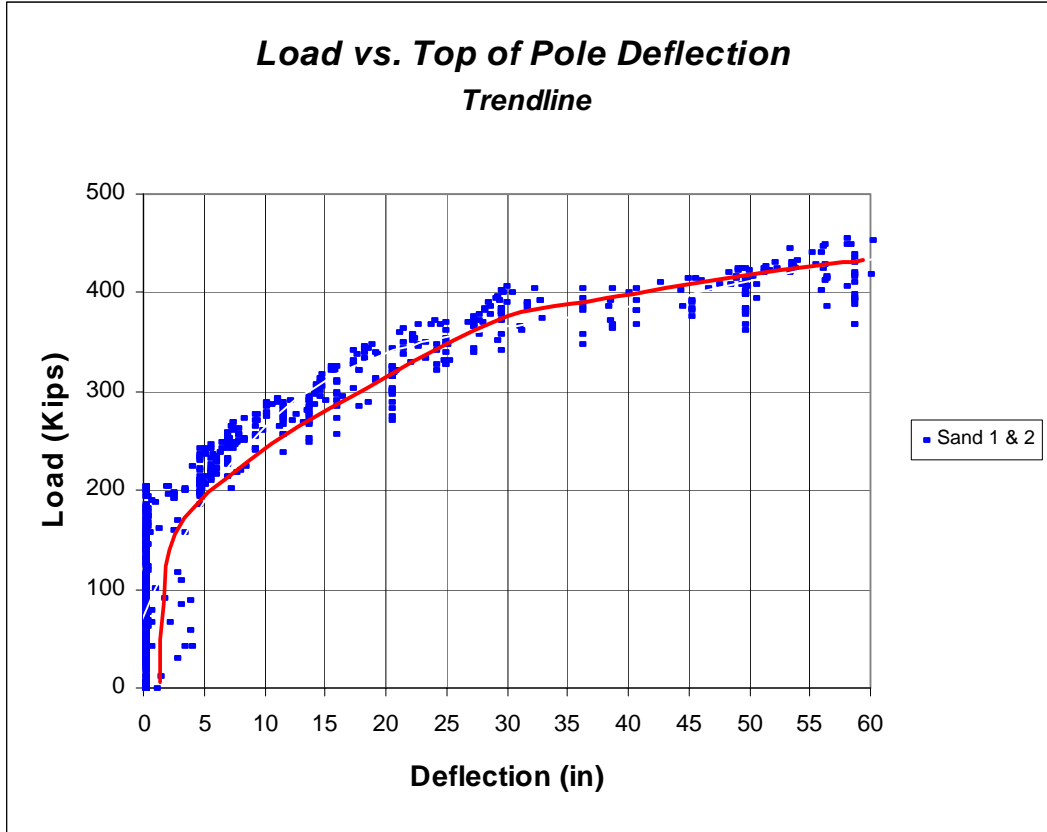


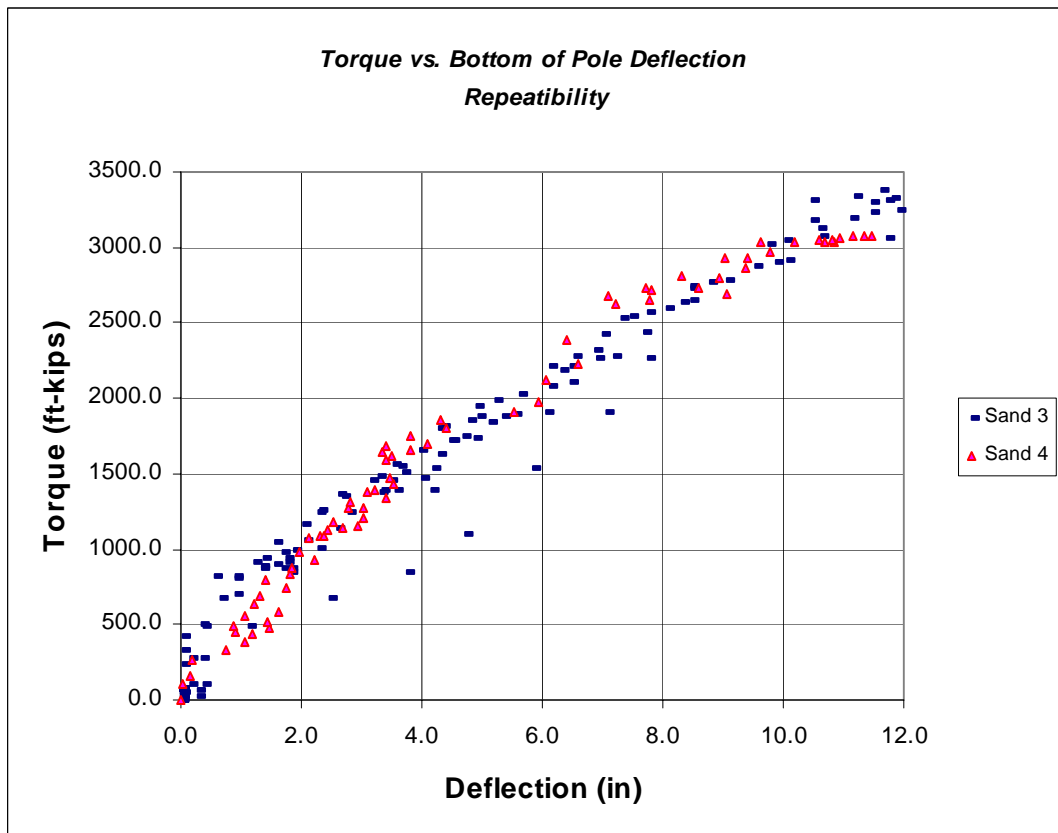
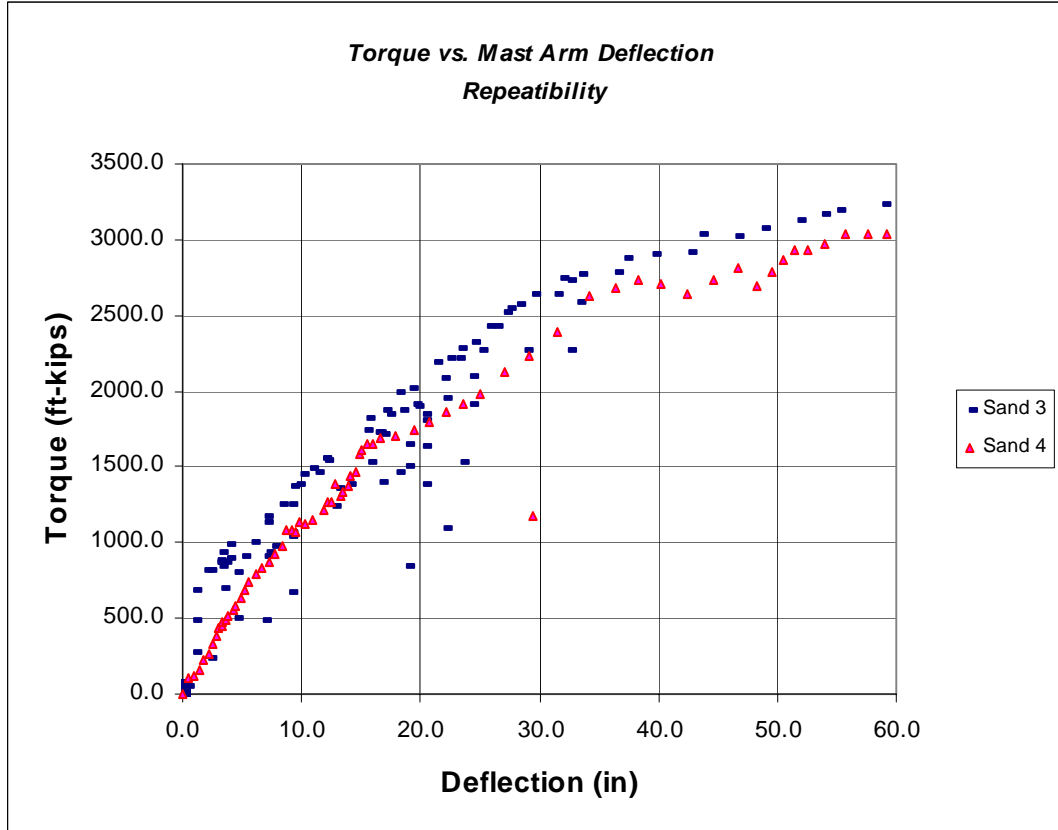


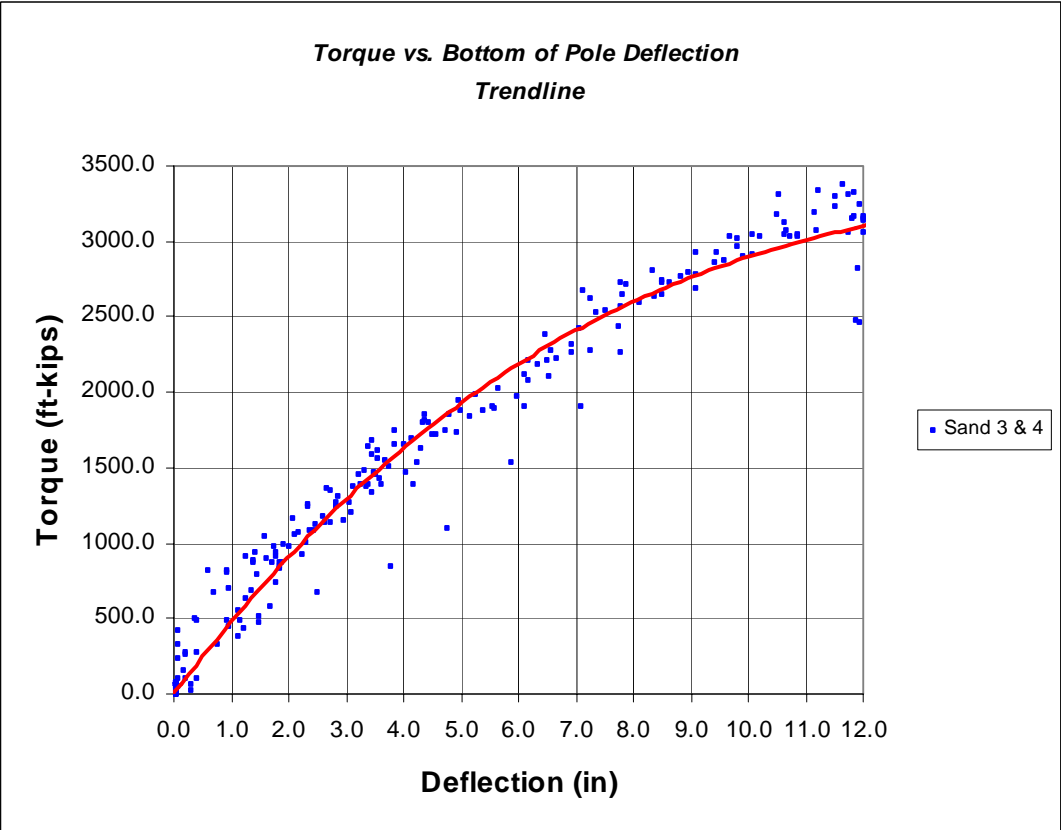
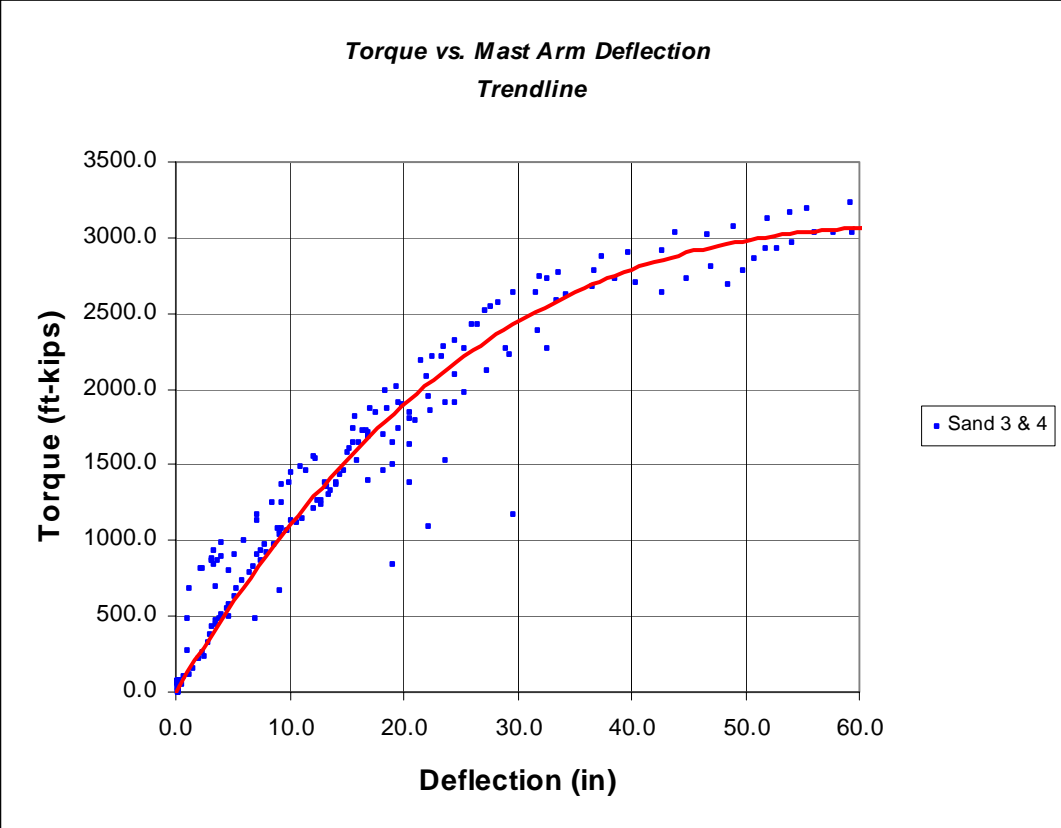


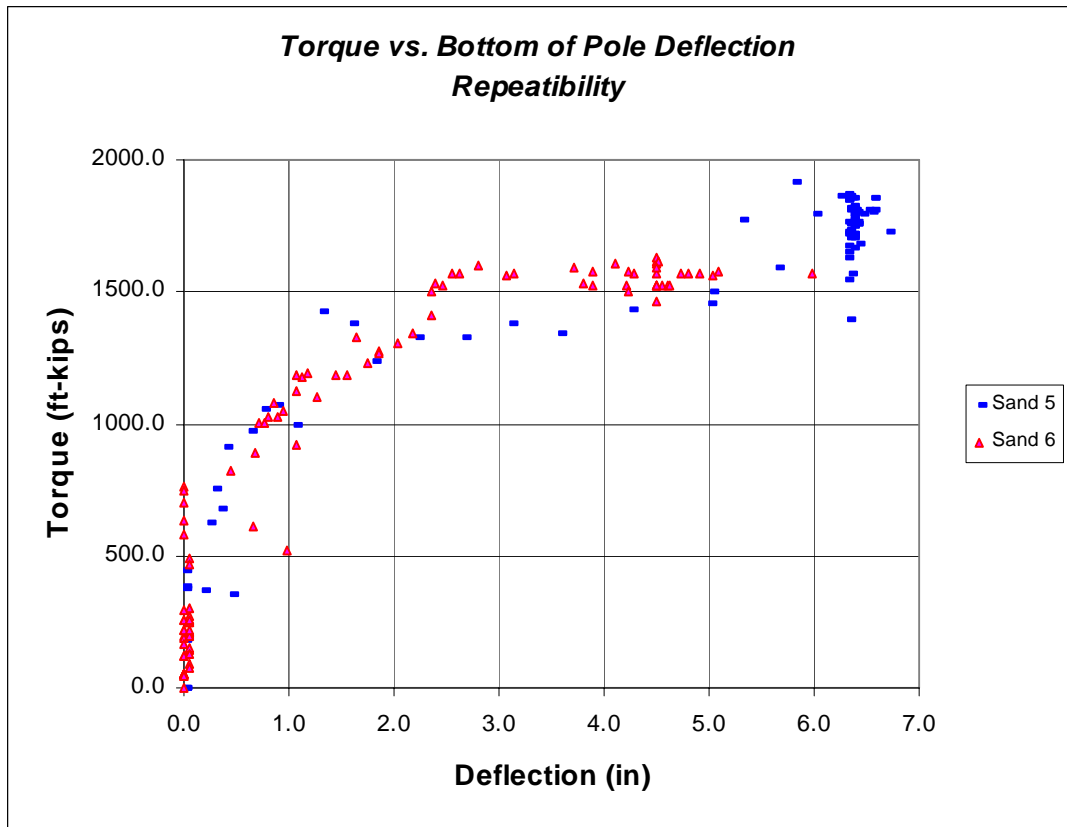
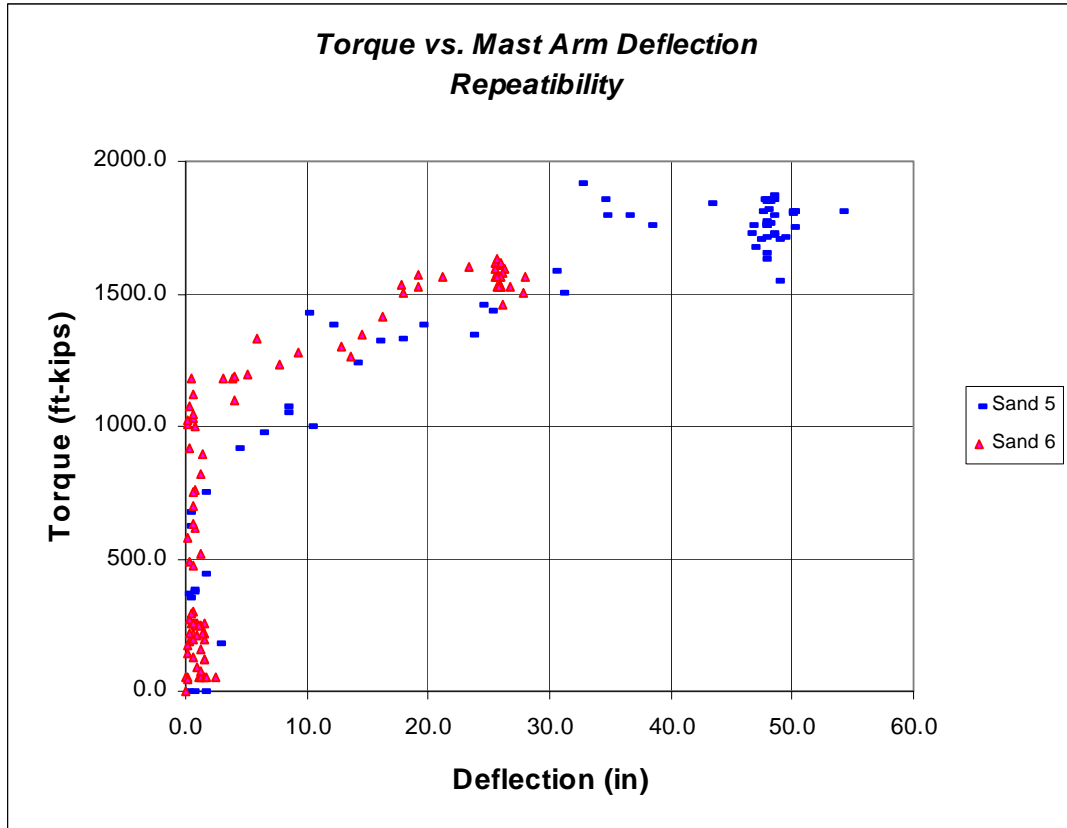
APPENDIX B
Centrifuge Test on Dry Sand (Reduced Data)

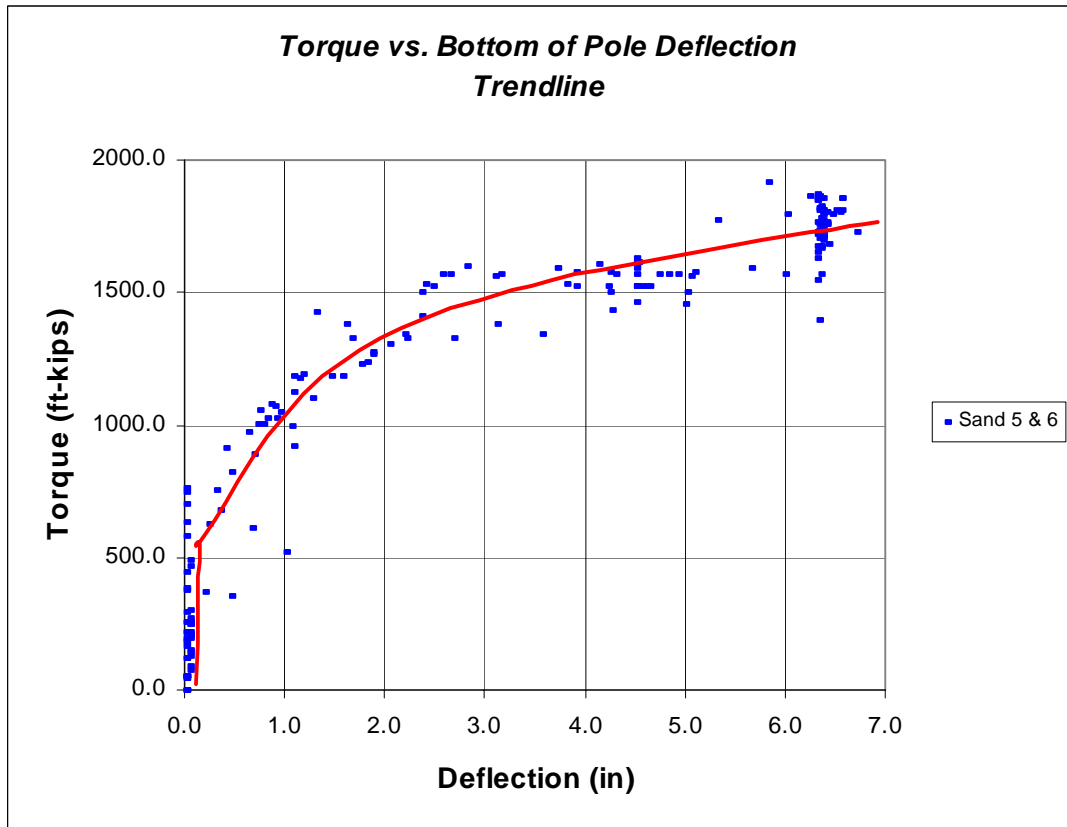
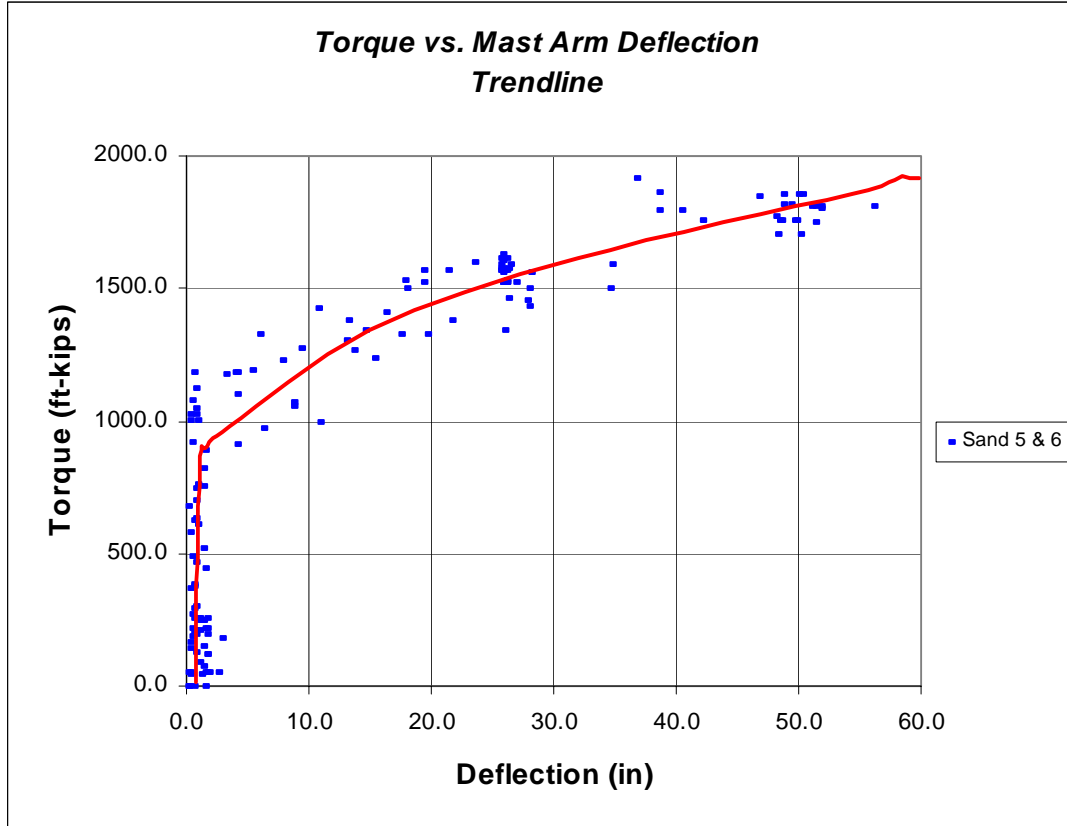


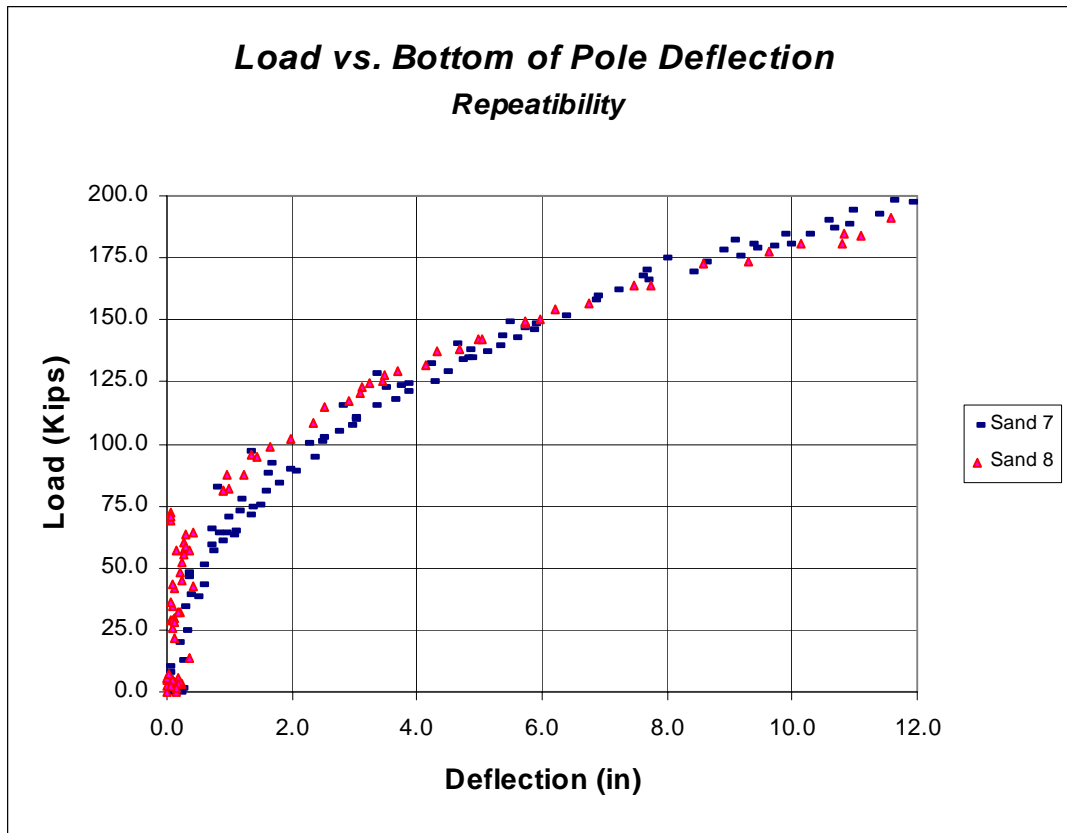
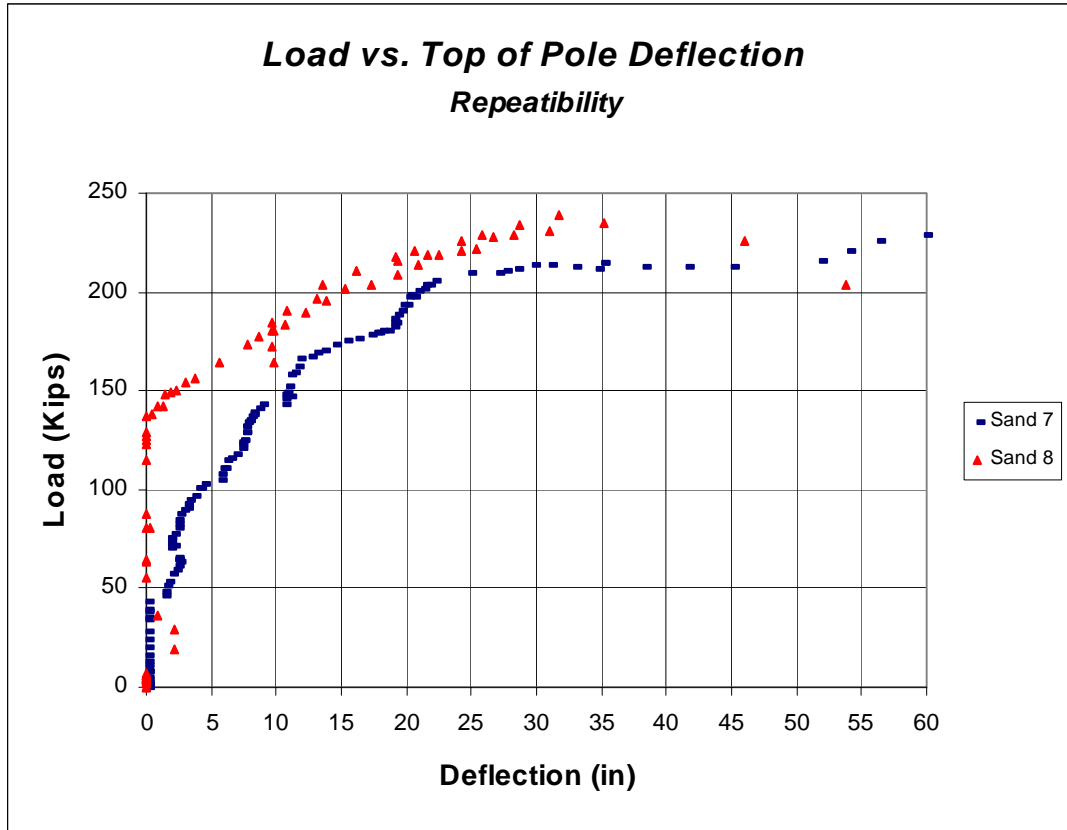


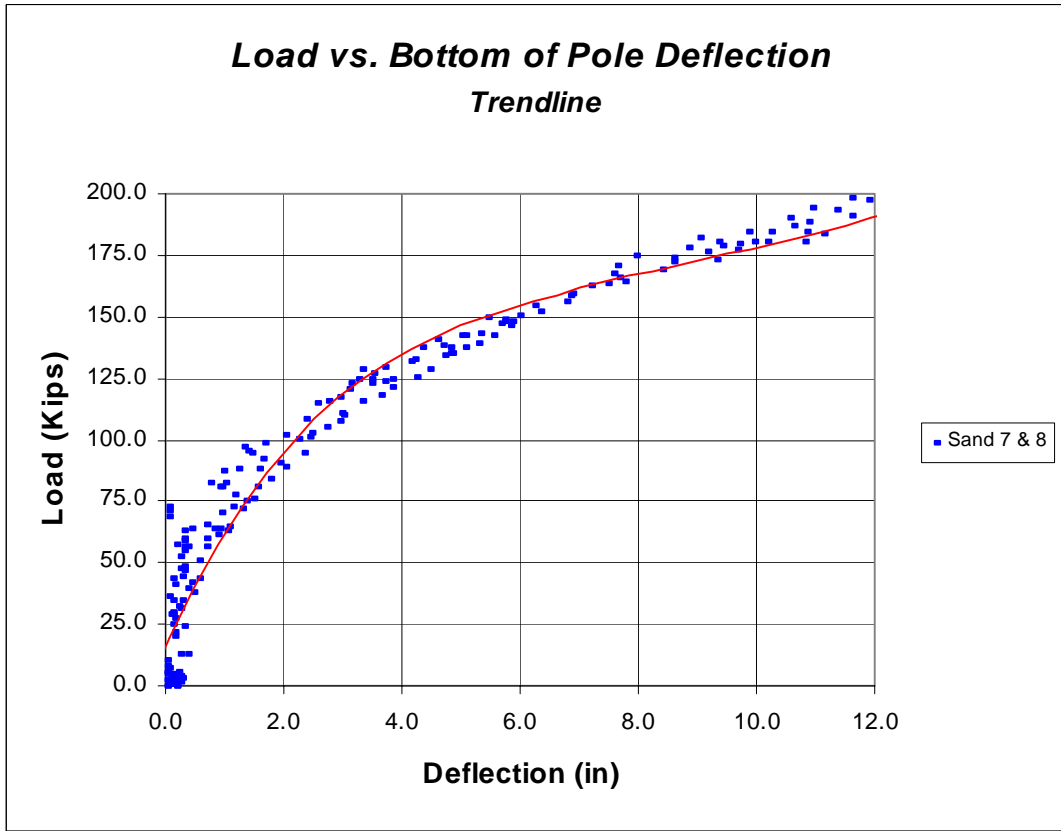
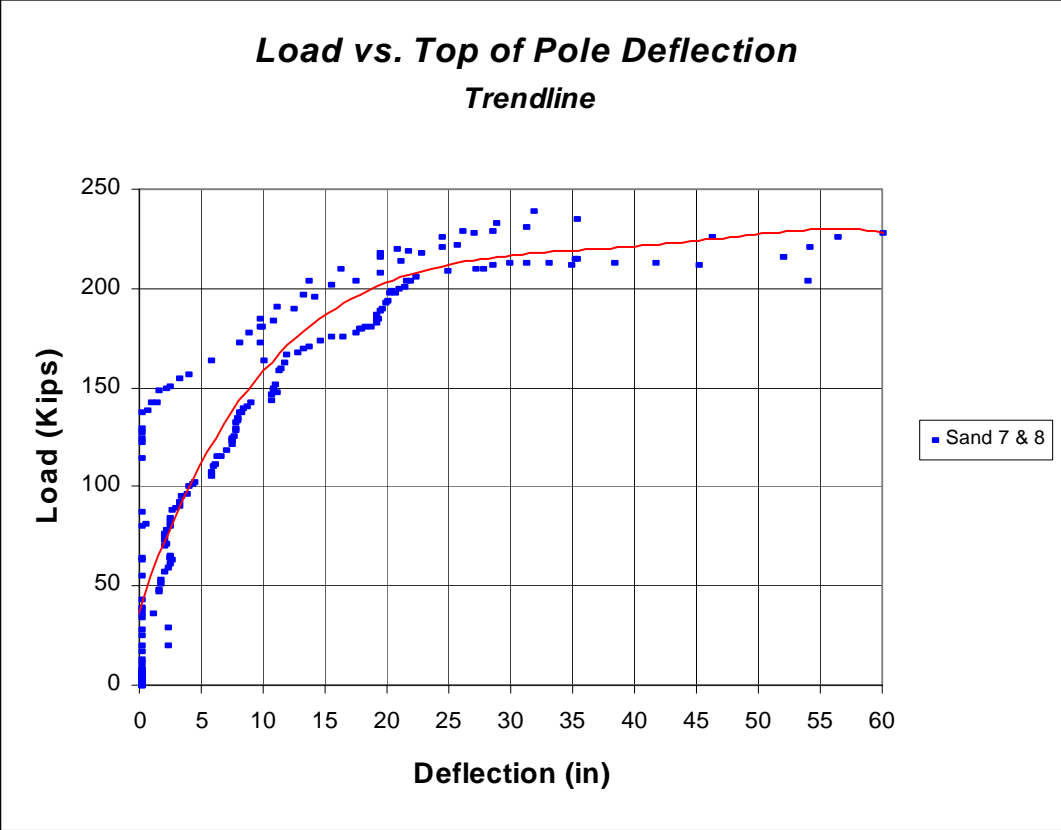


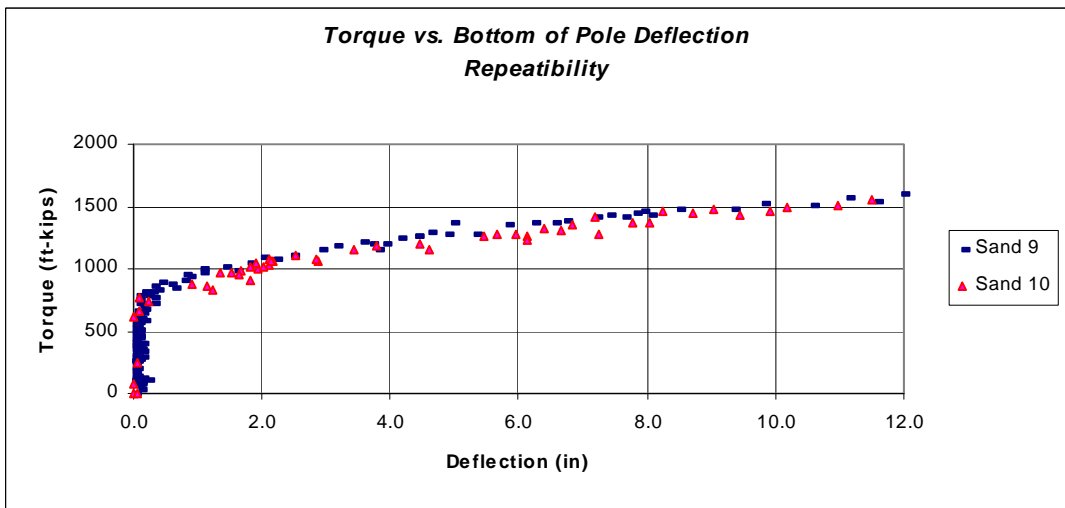
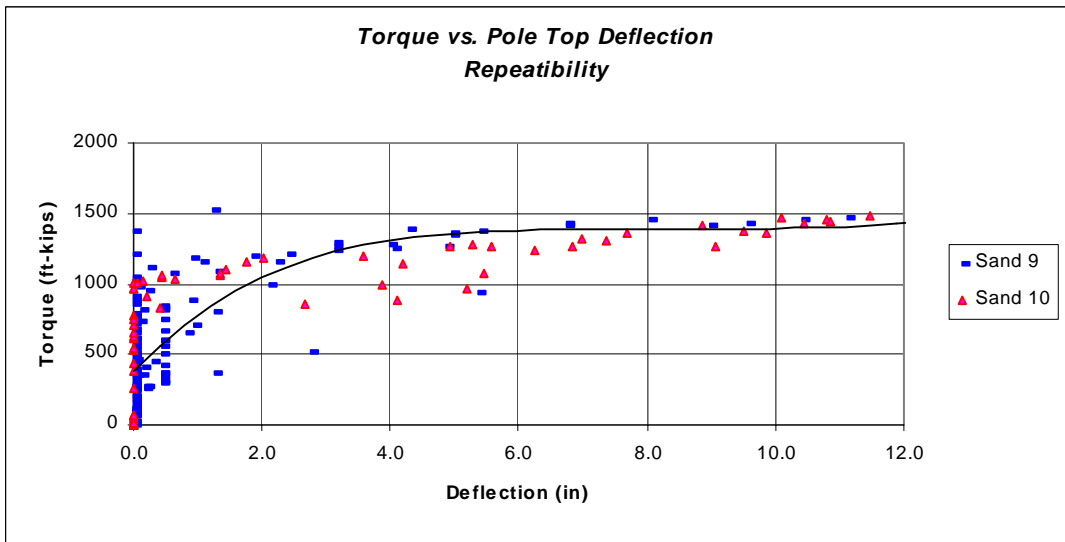
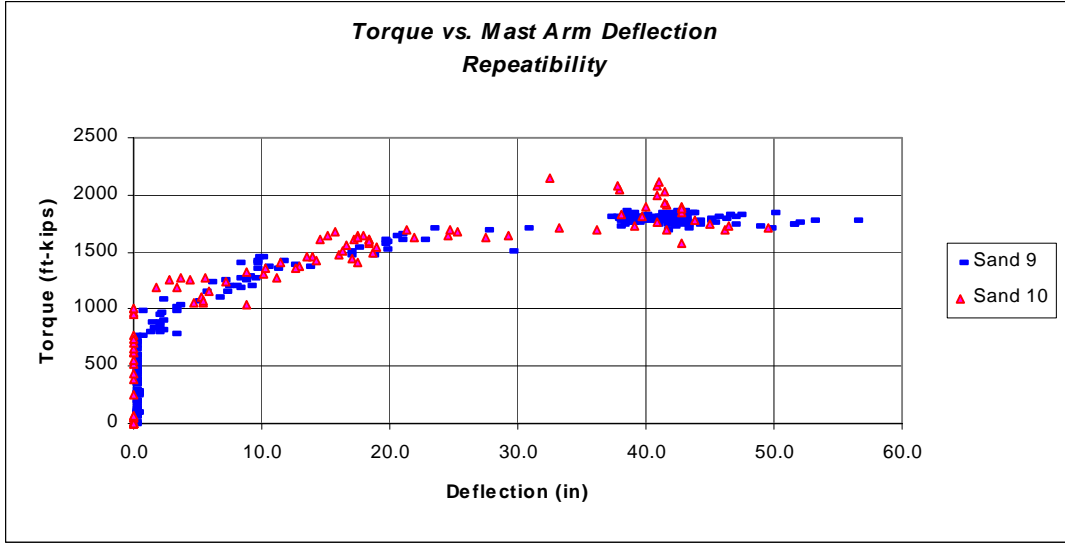


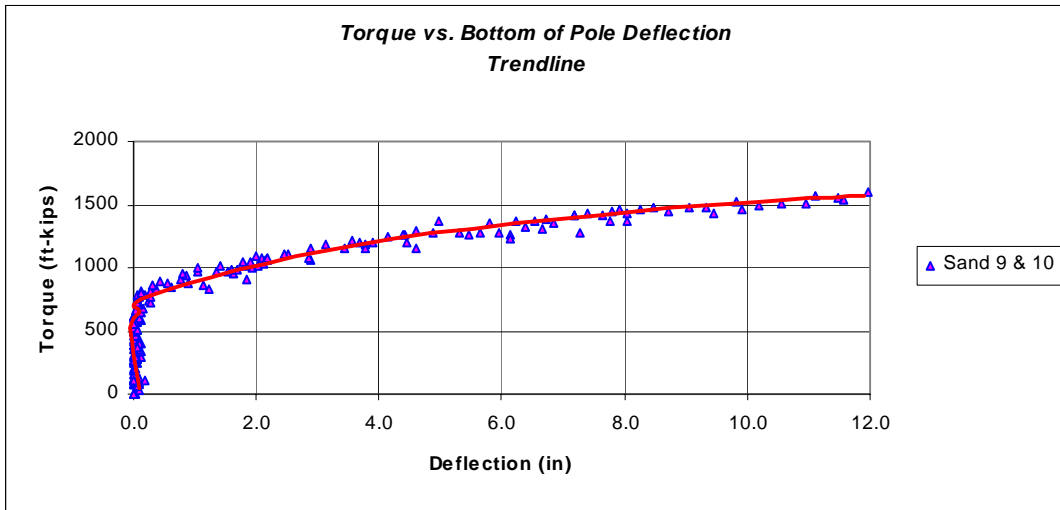
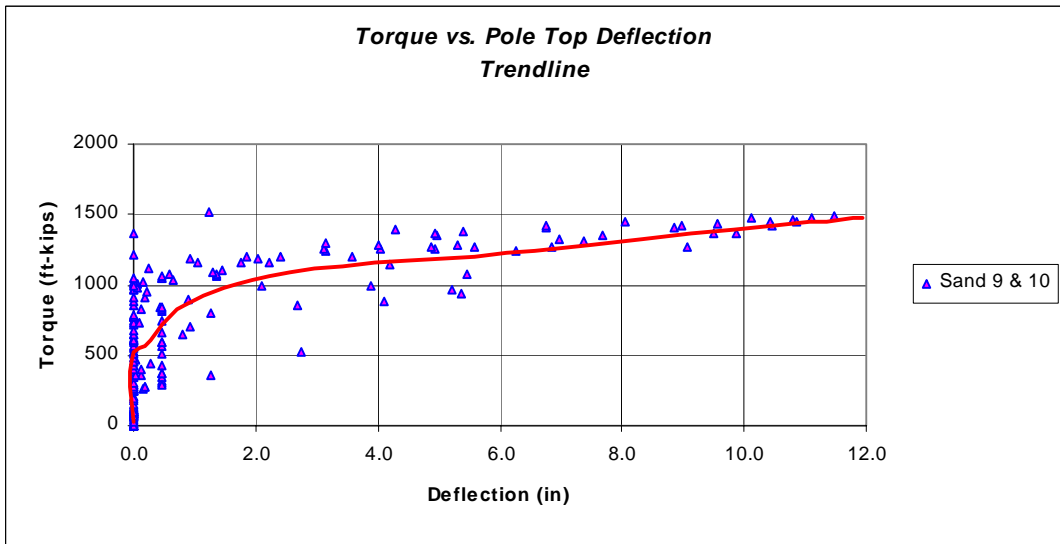
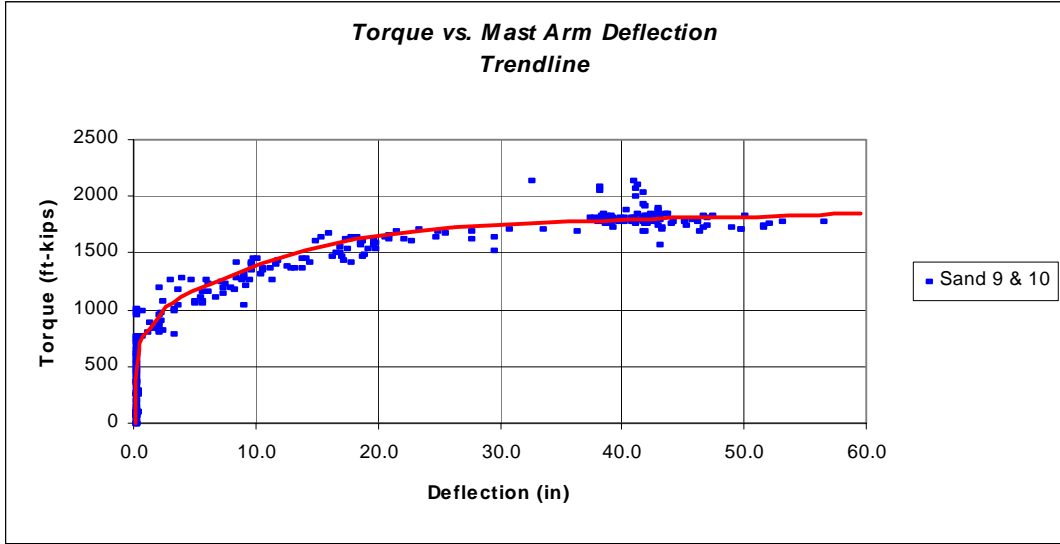


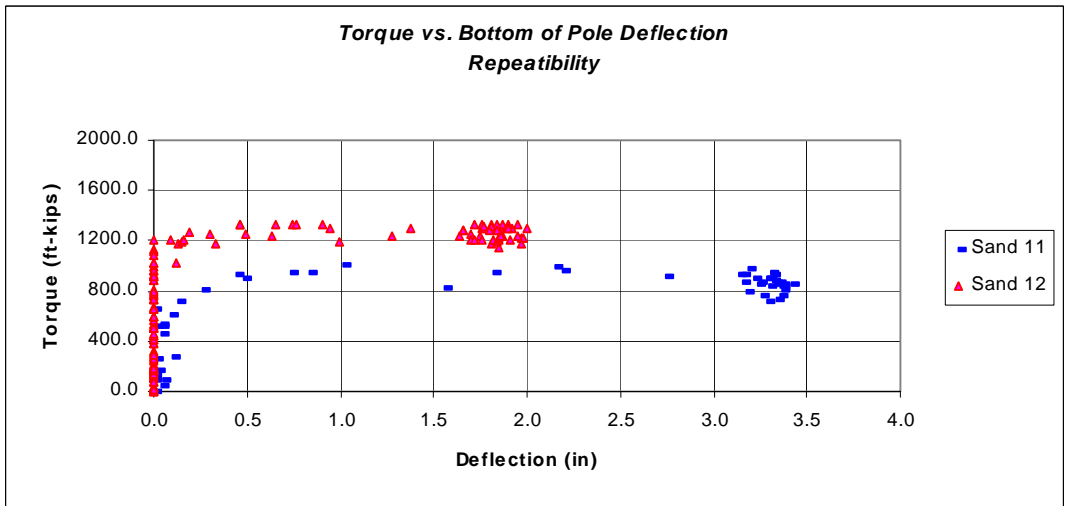
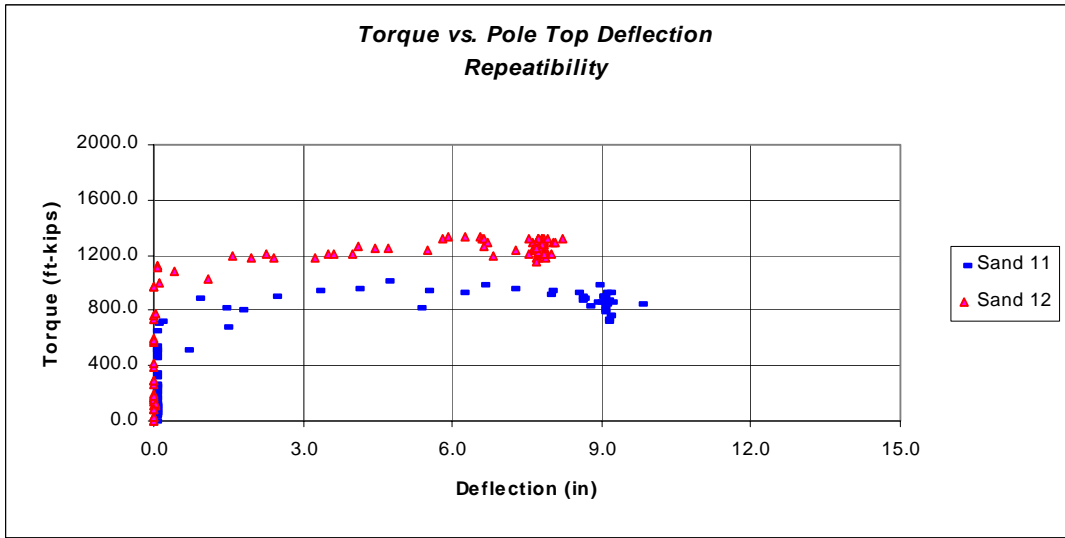
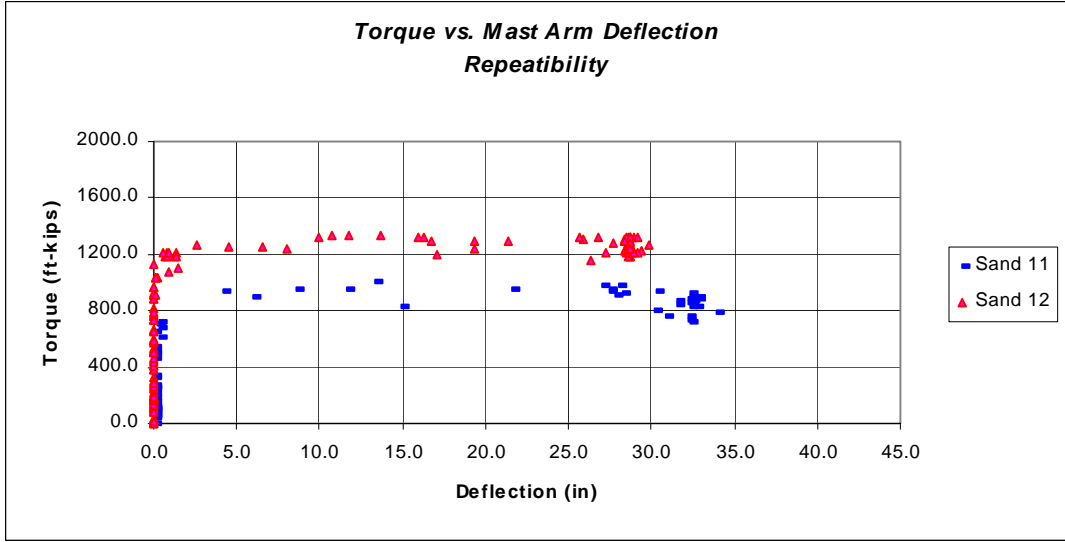


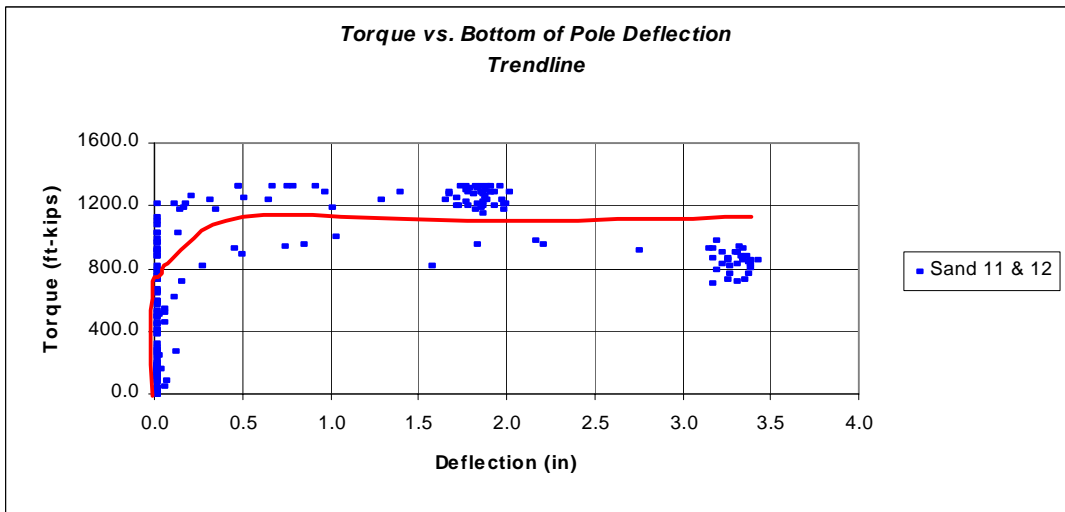
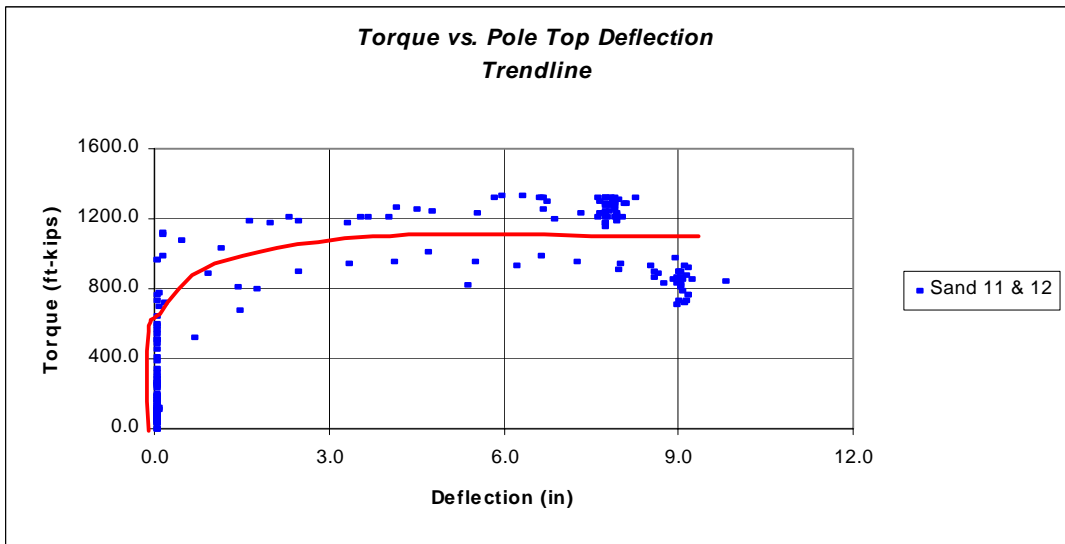
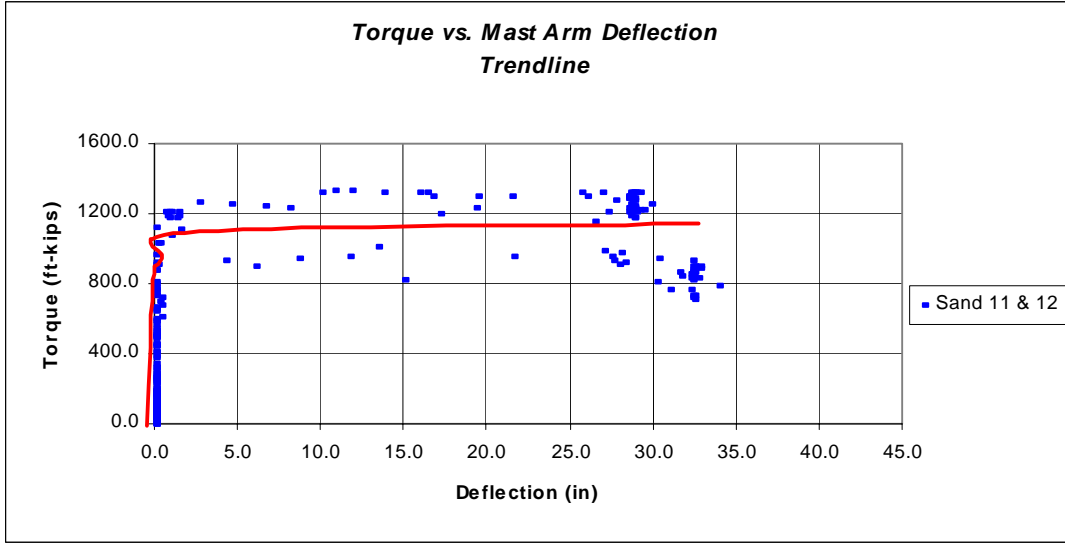


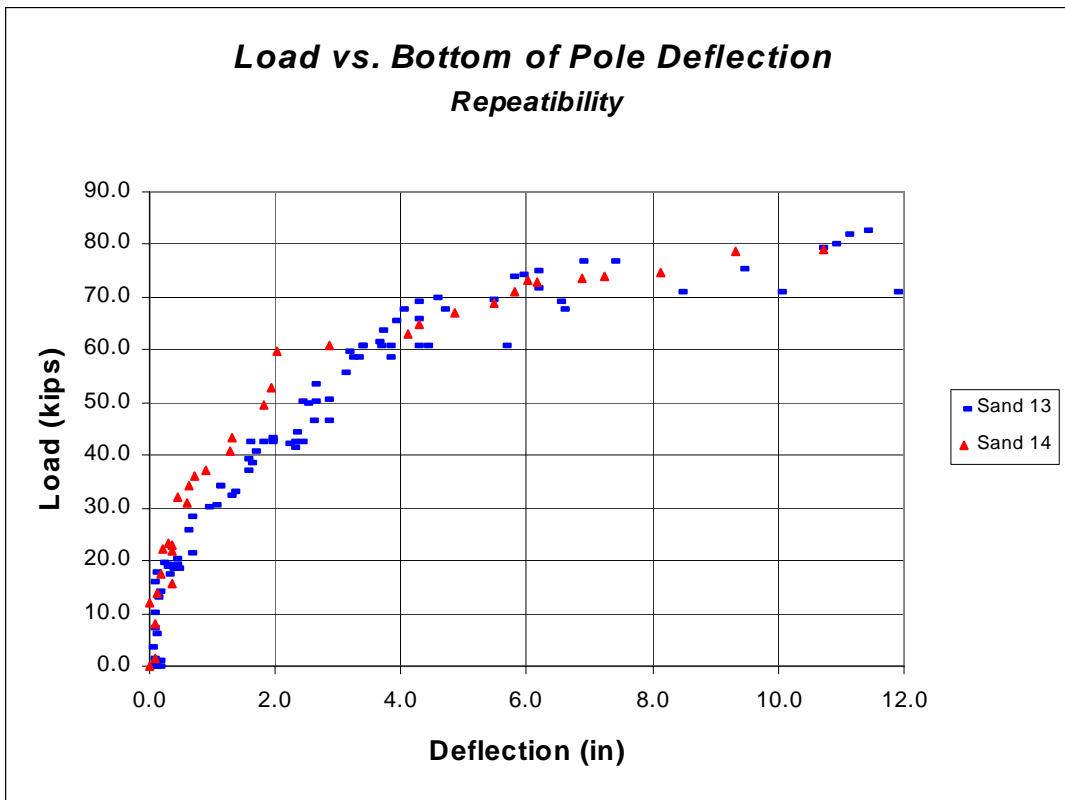
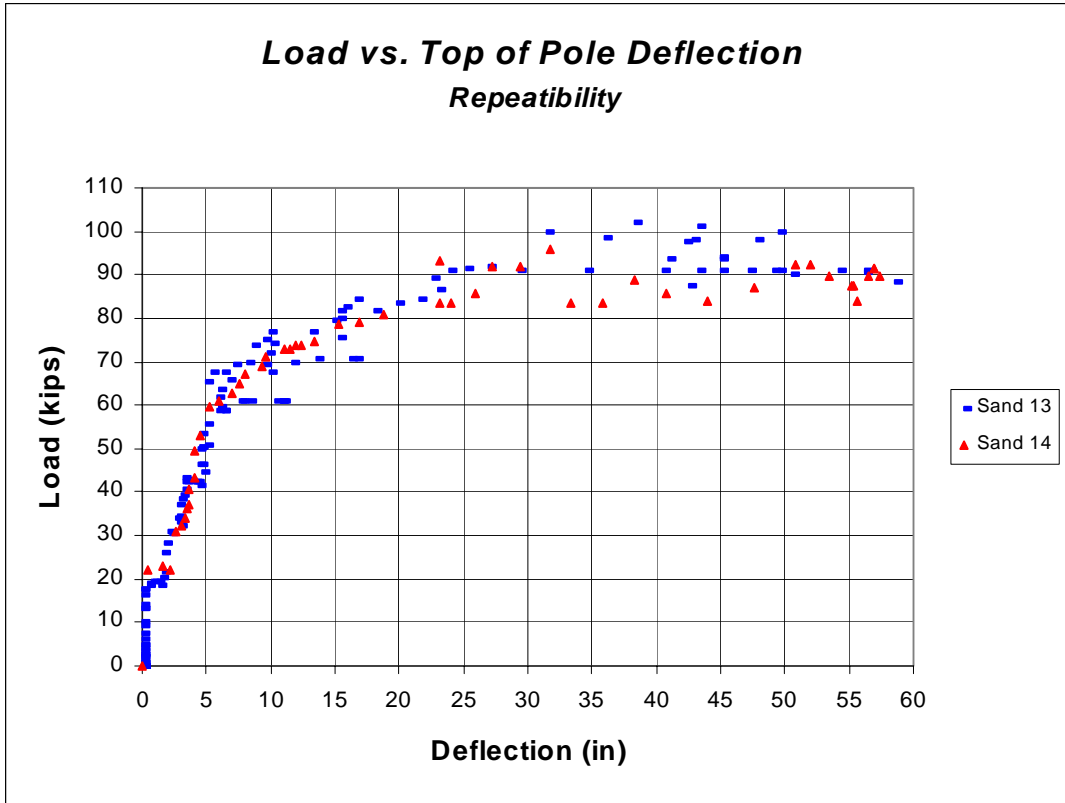




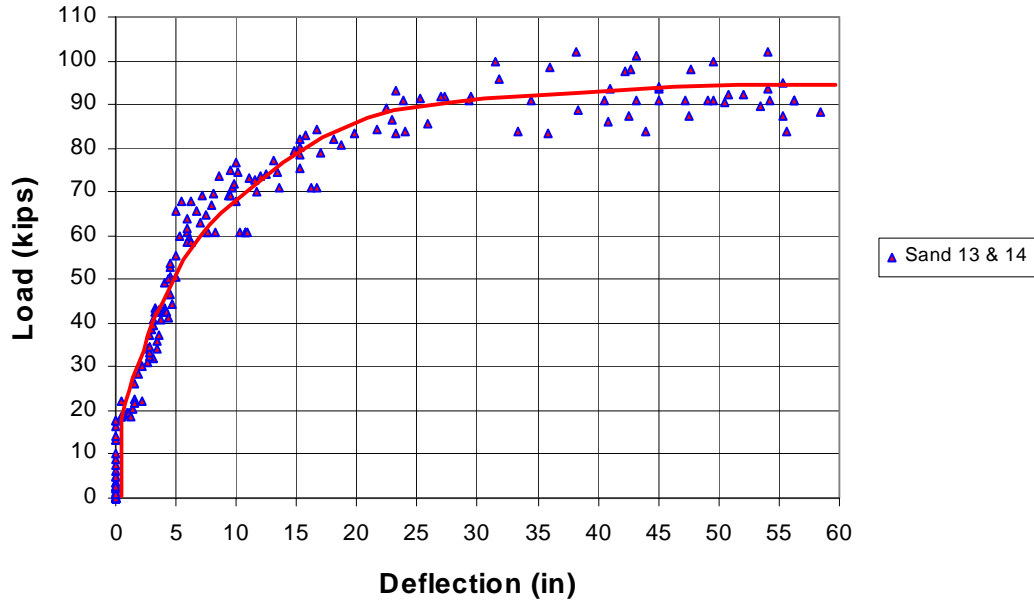




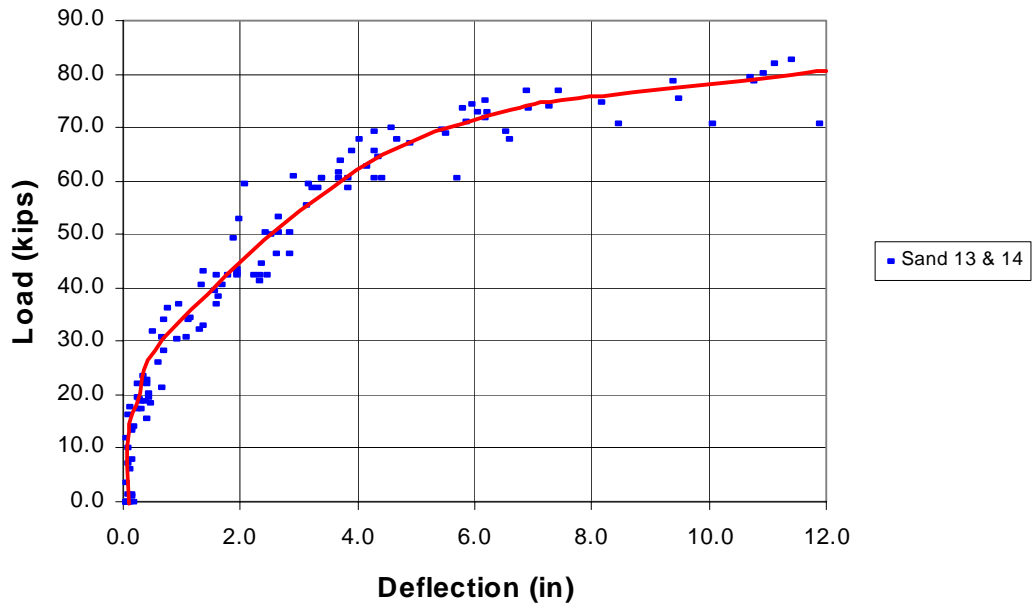


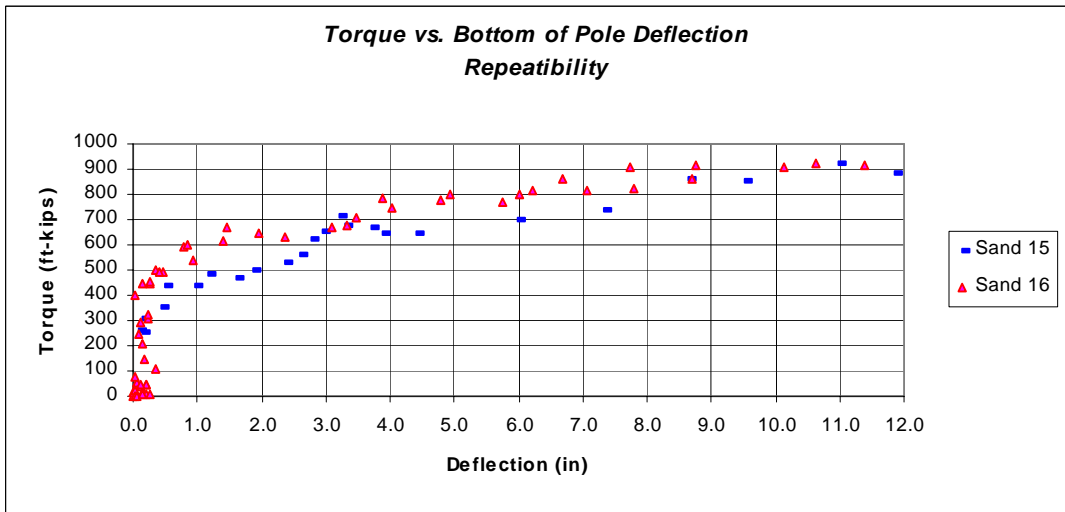
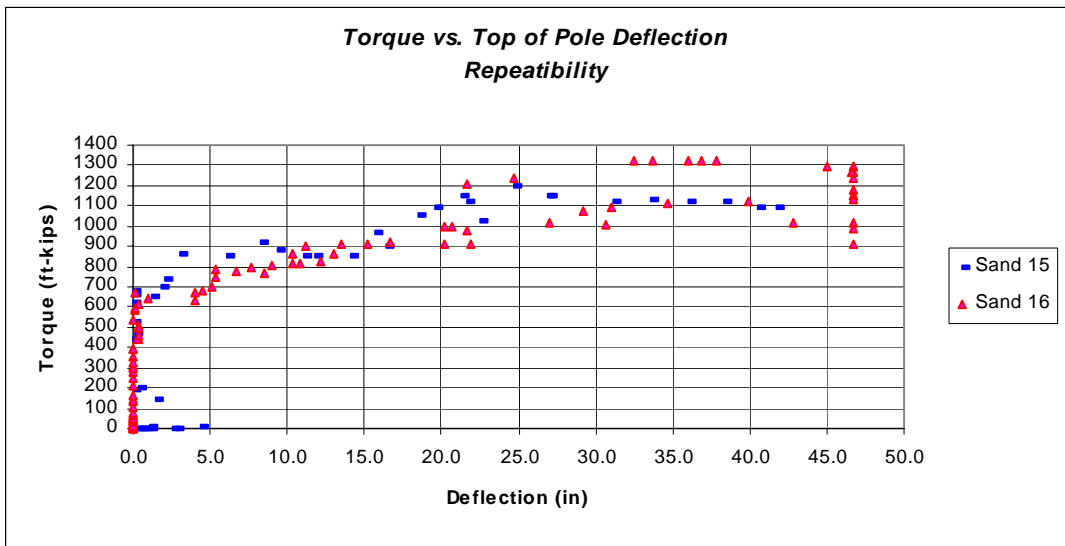
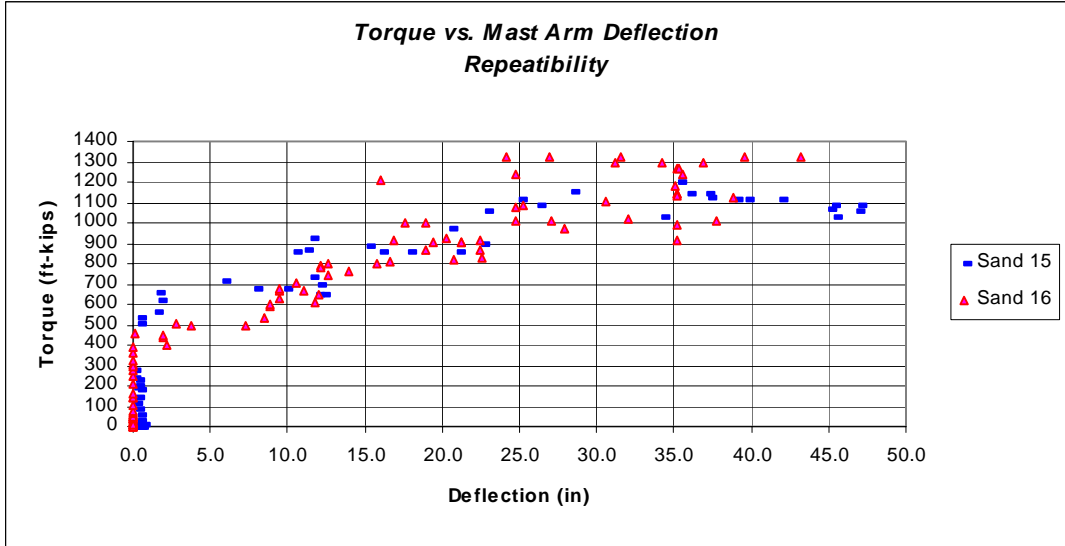


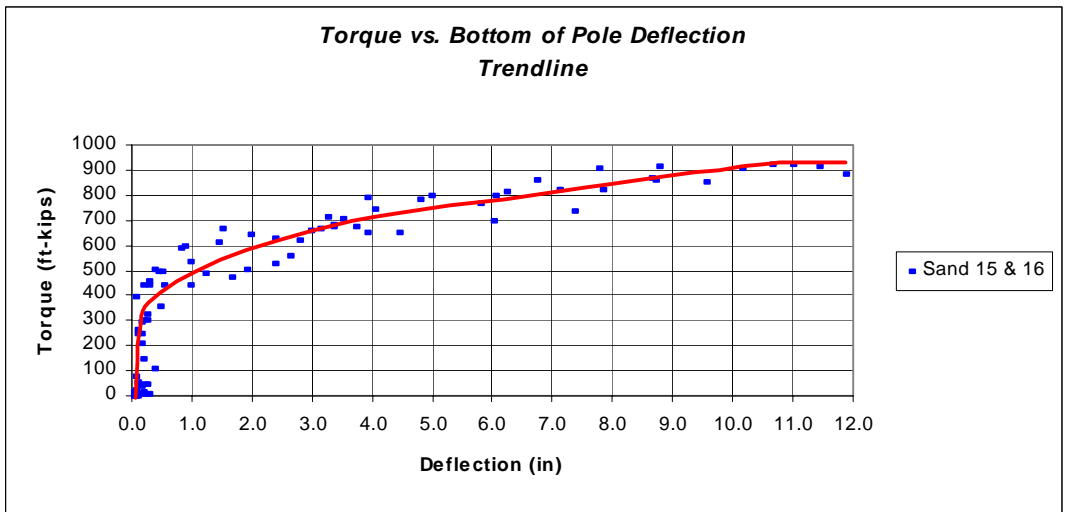
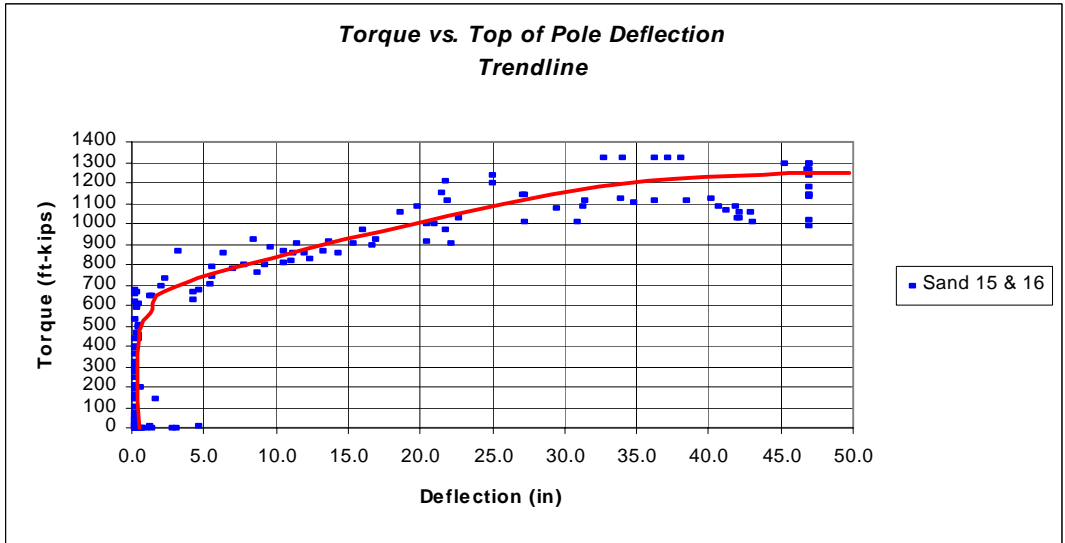
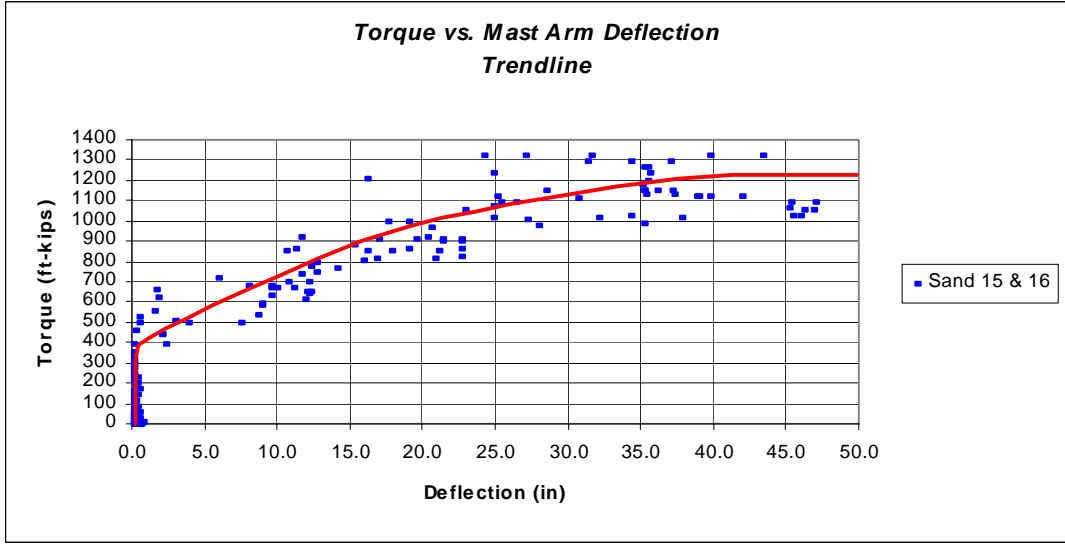
**Load vs. Top of Pole Deflection
Trendline**

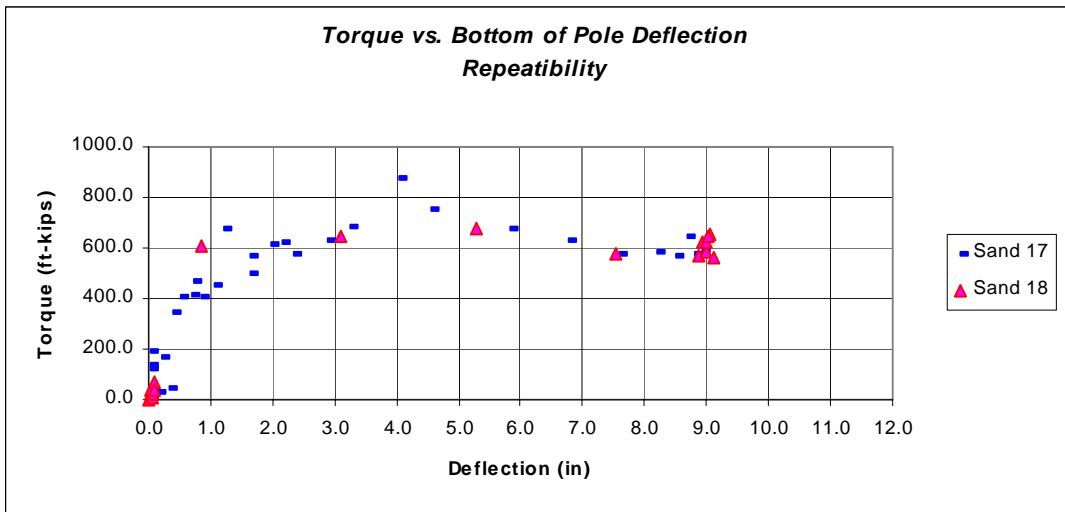
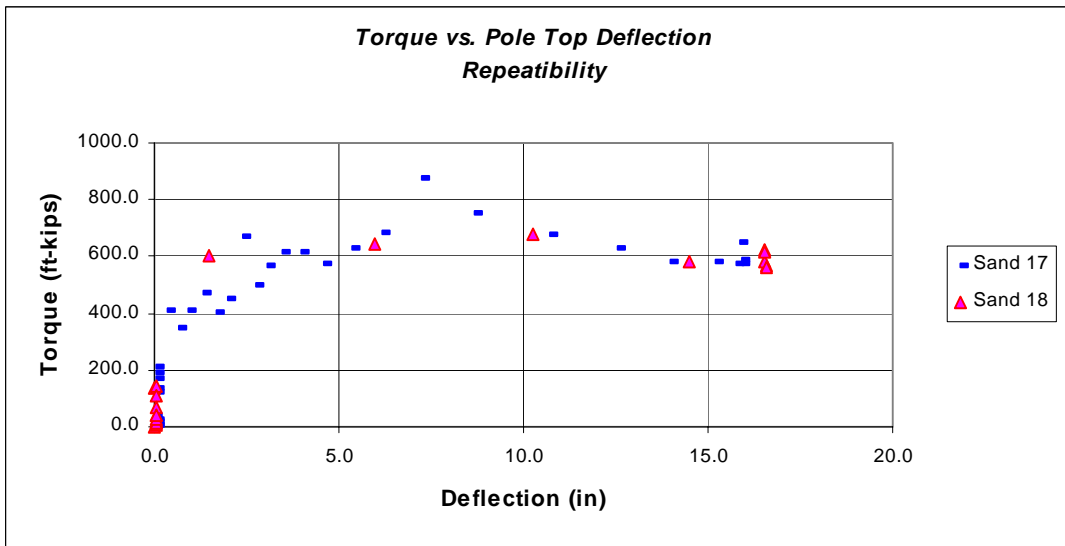
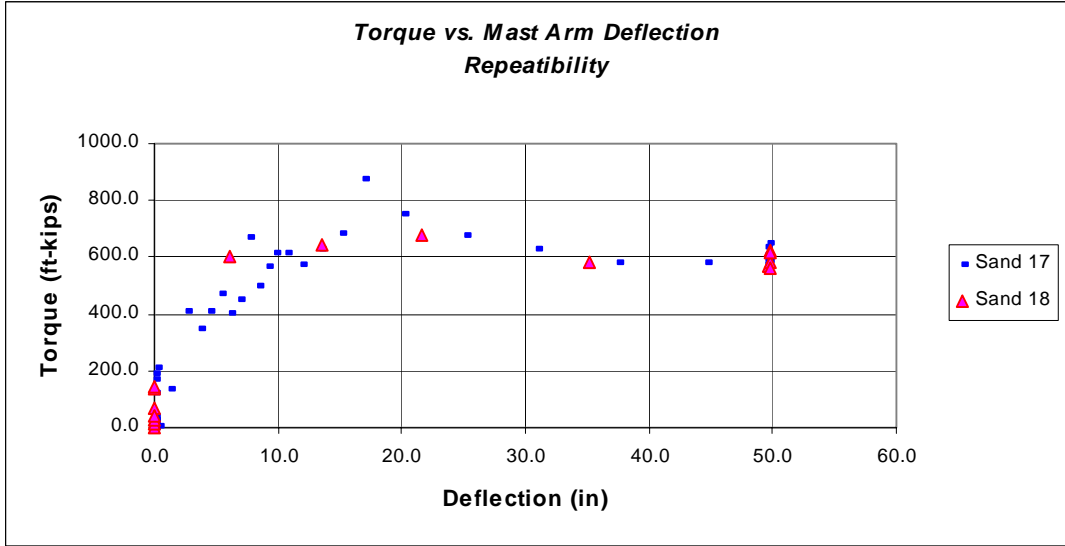


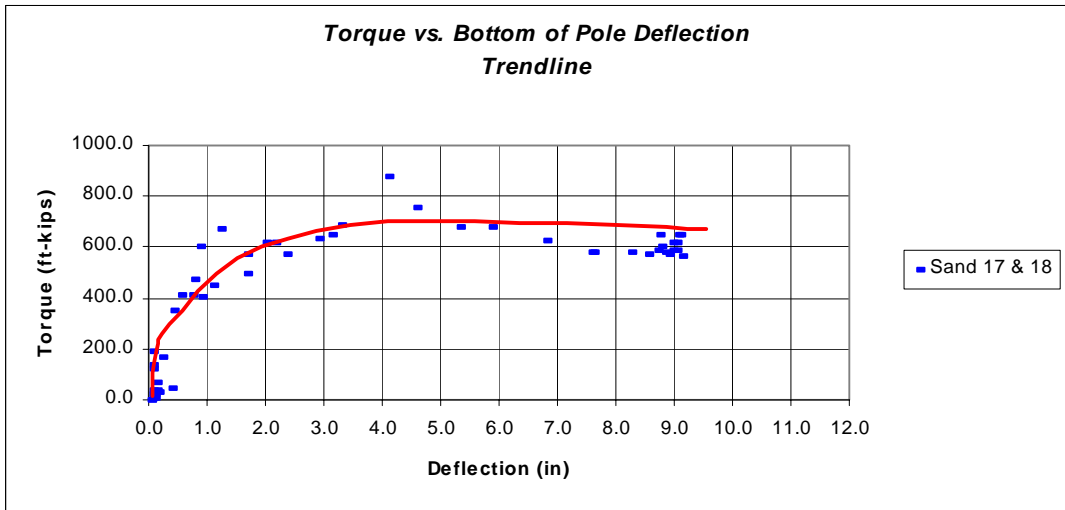
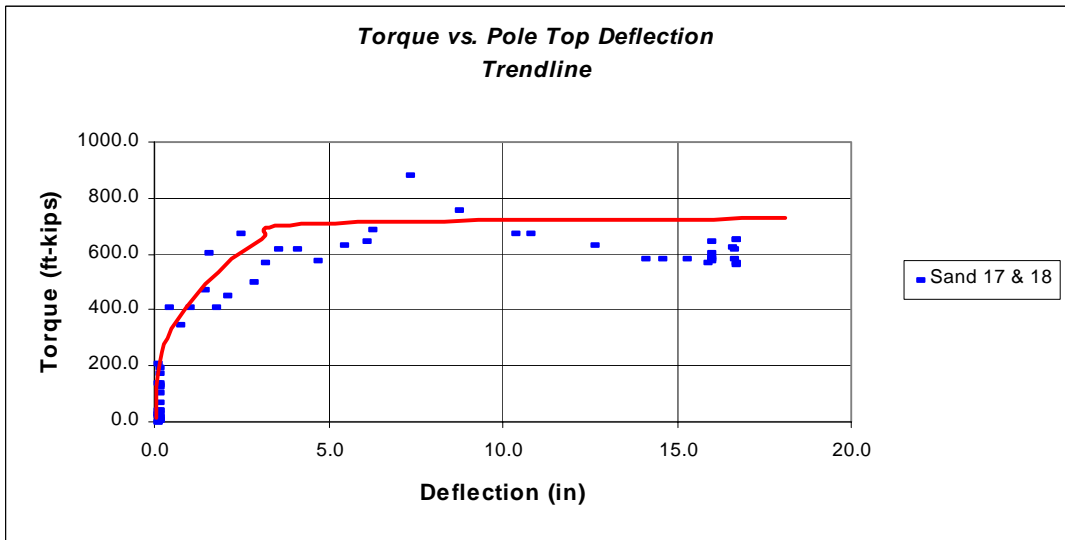
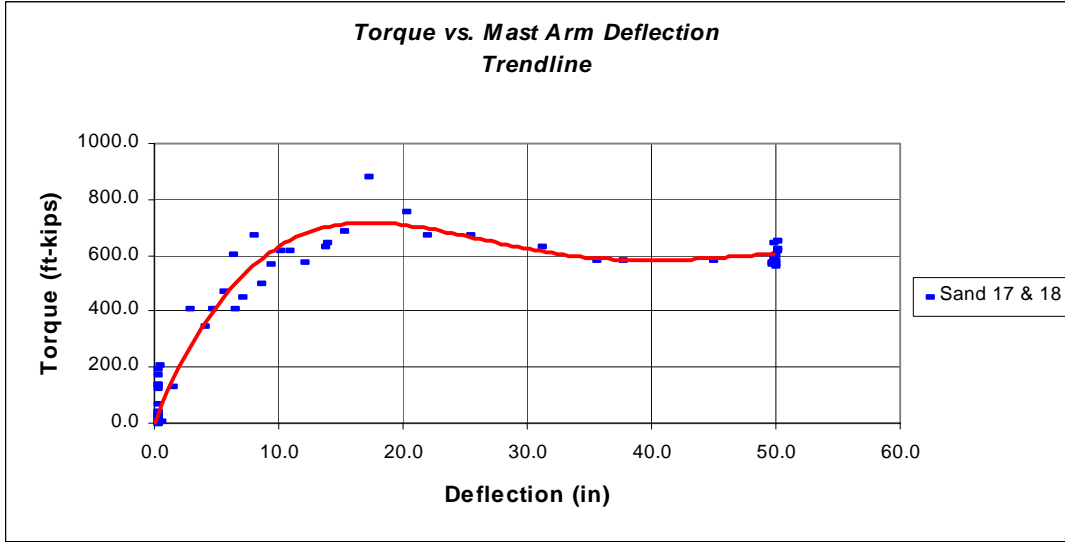
**Load vs. Bottom of Pole Deflection
Trendline**

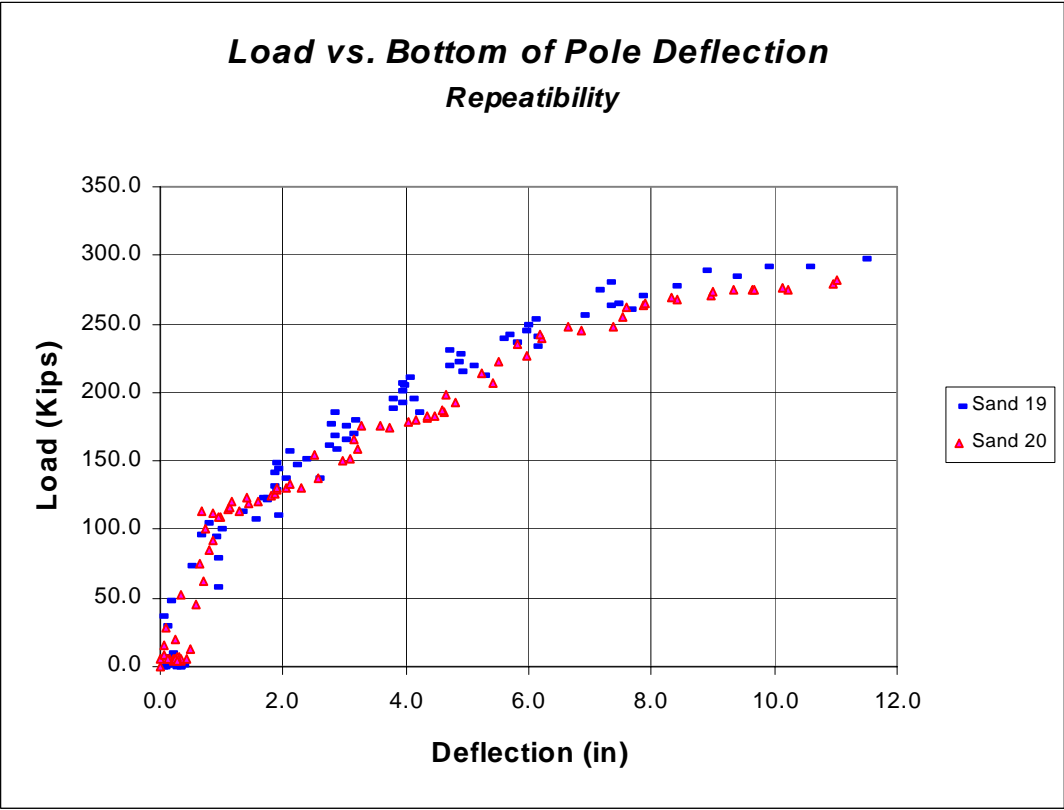
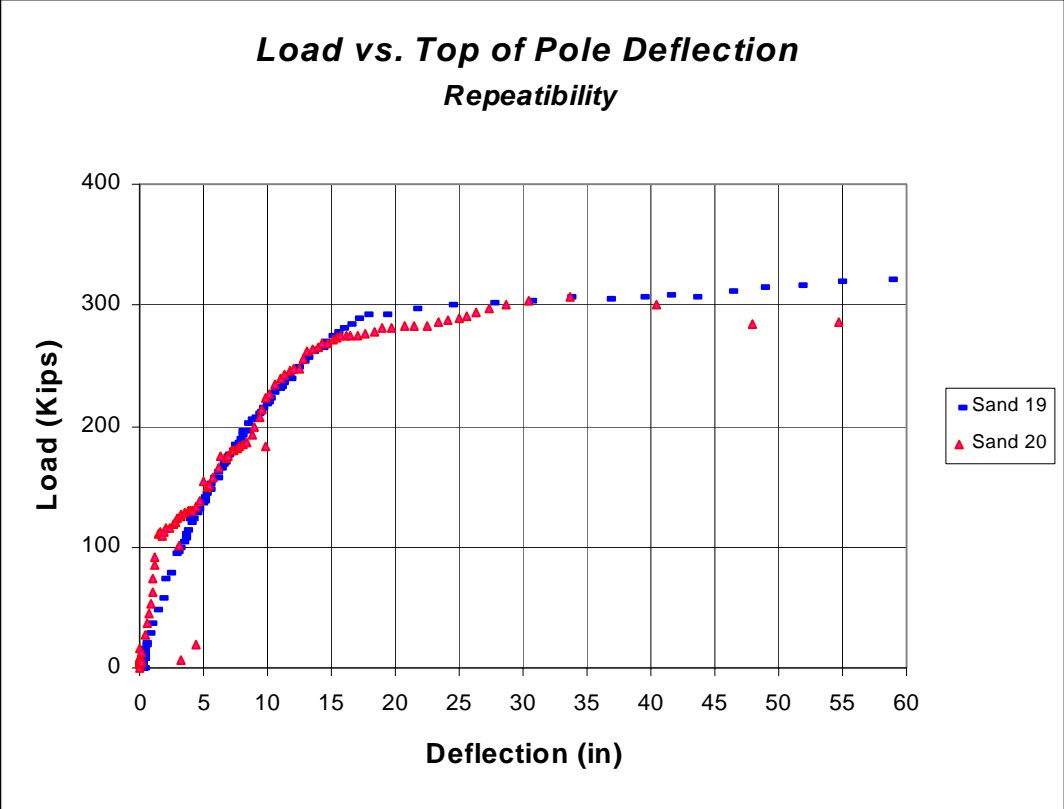


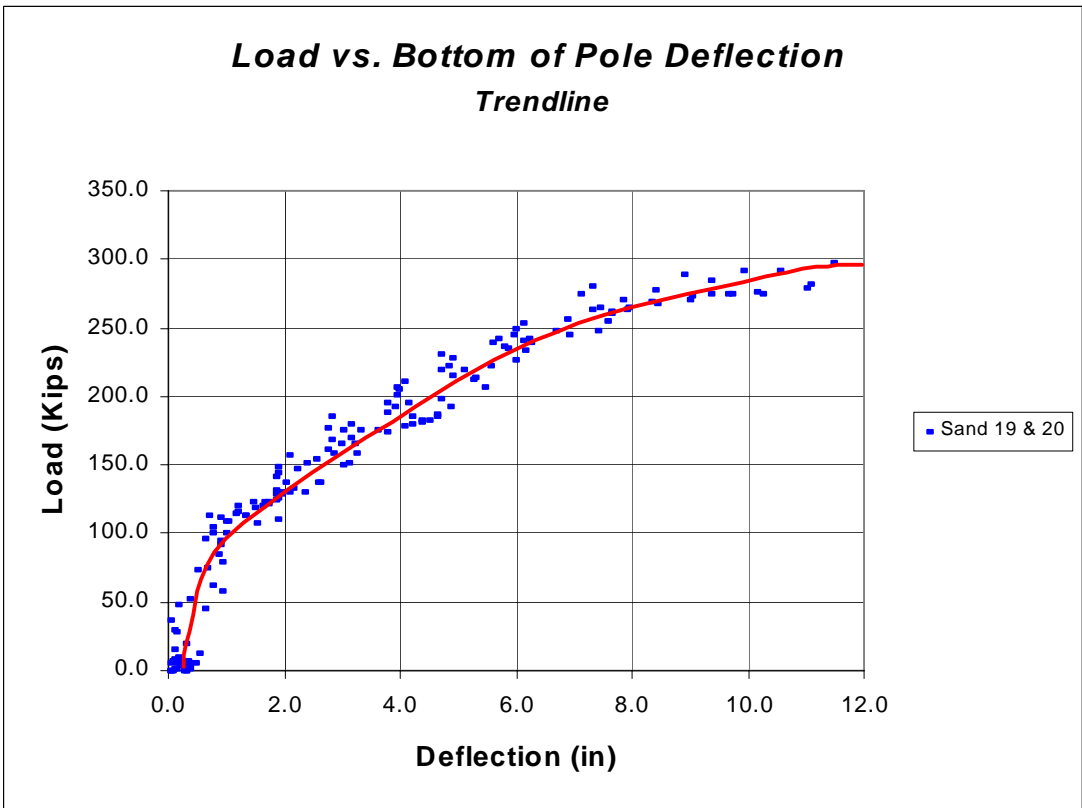
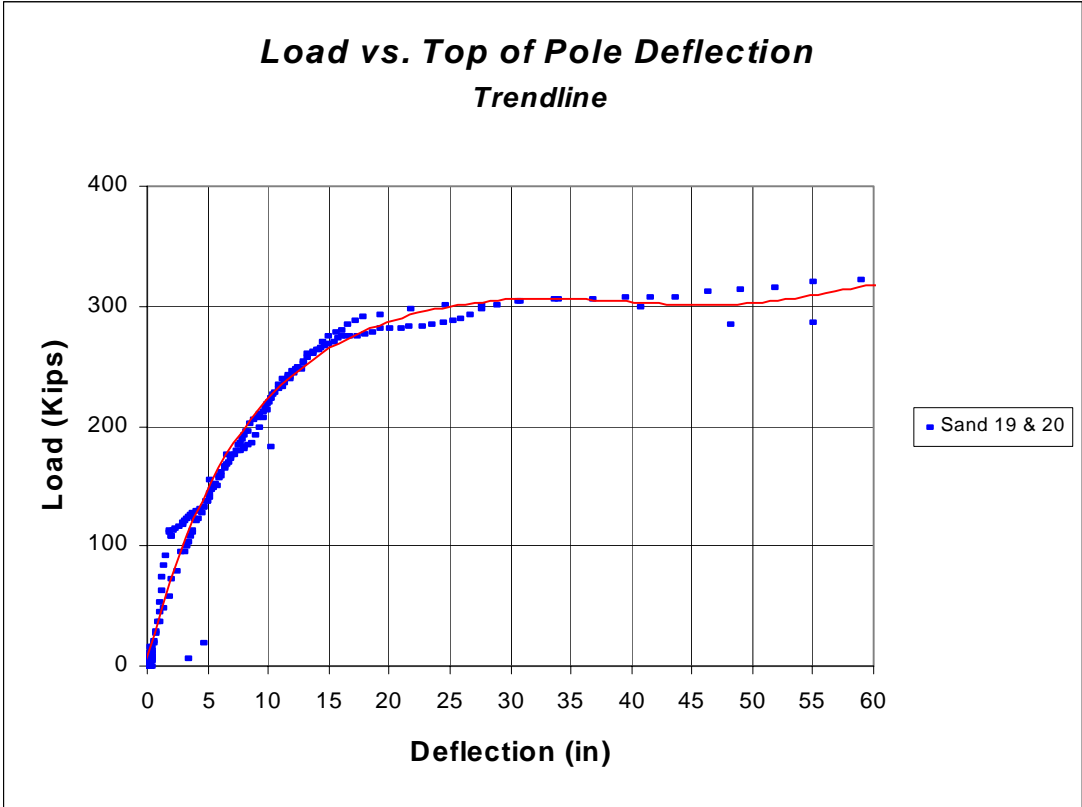


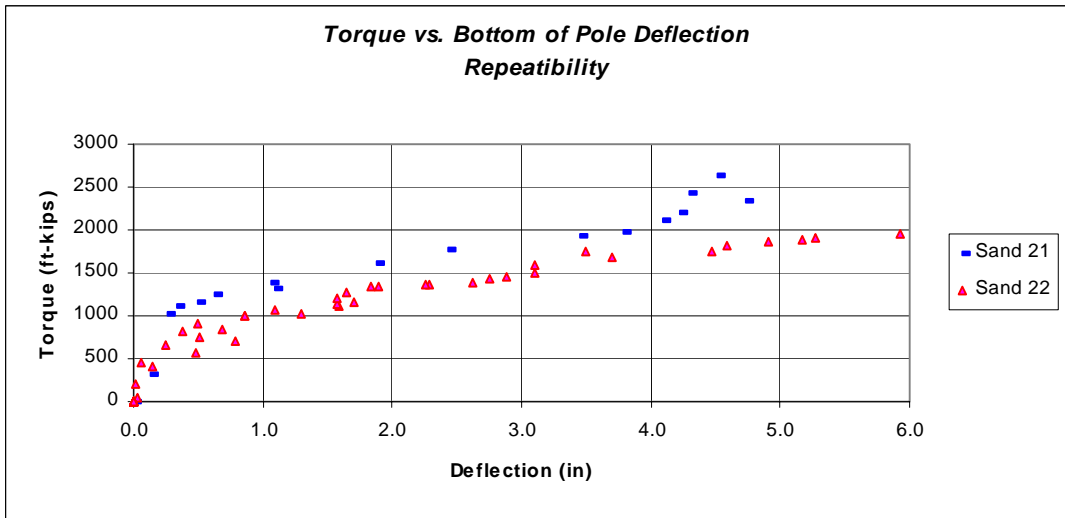
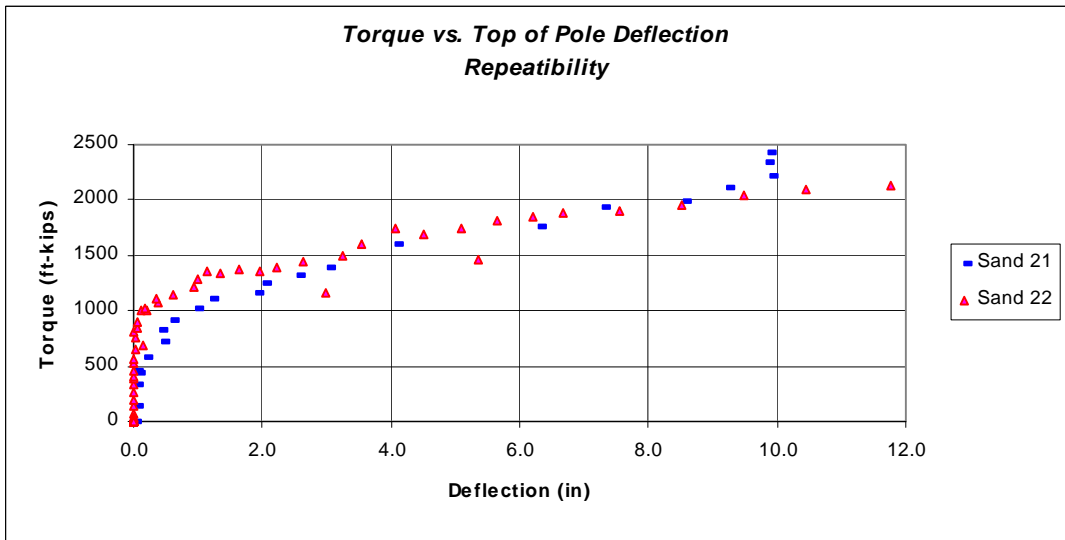
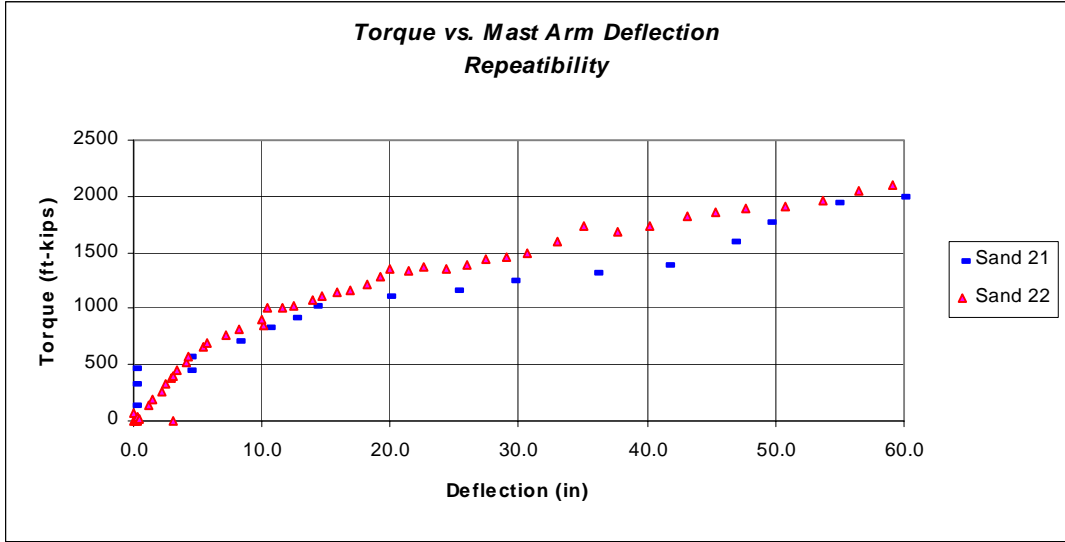


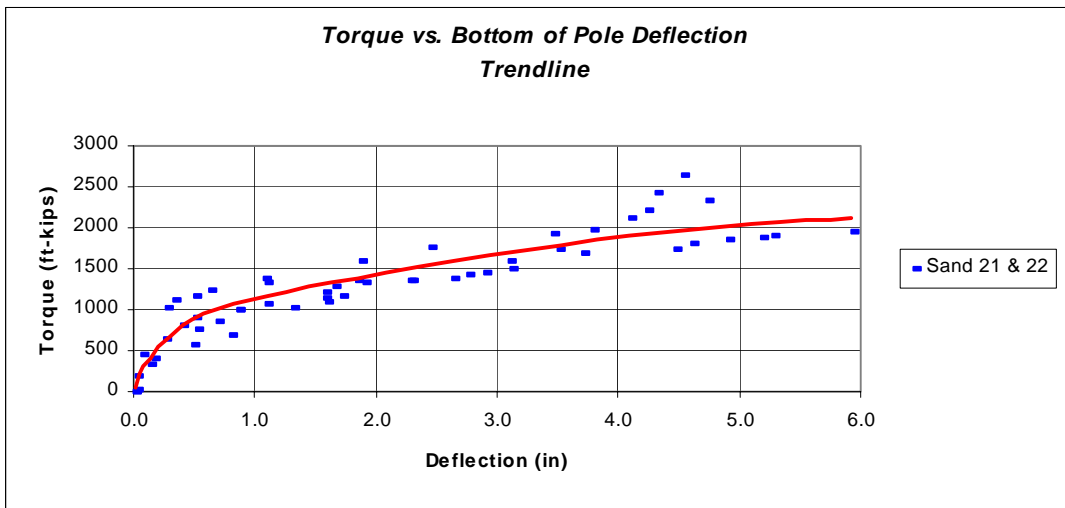
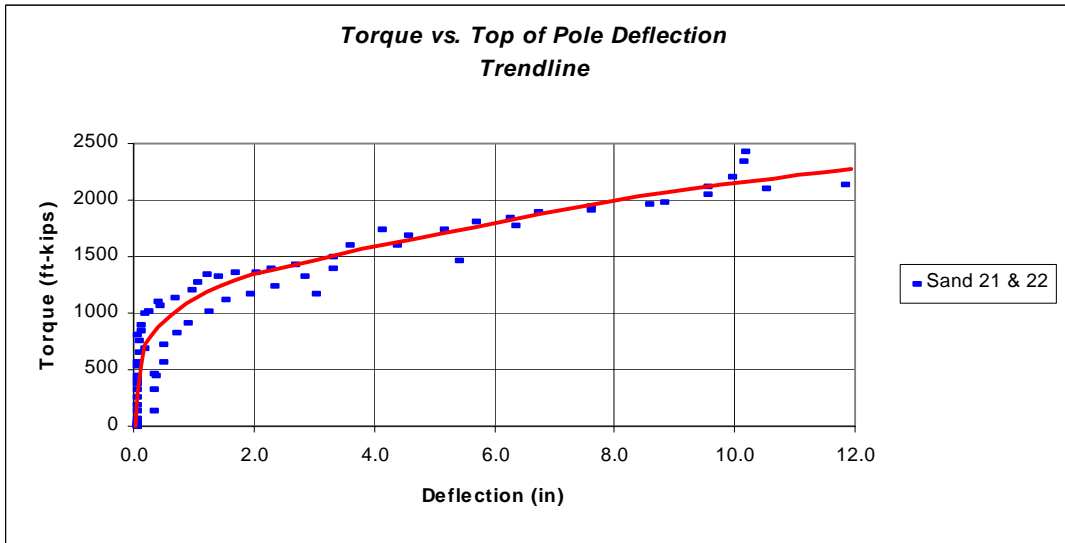
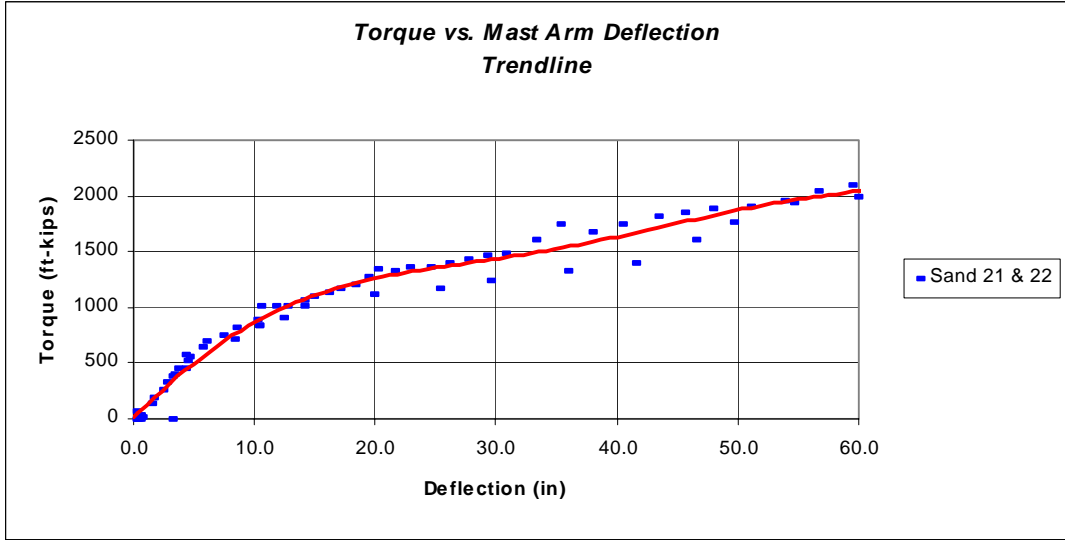


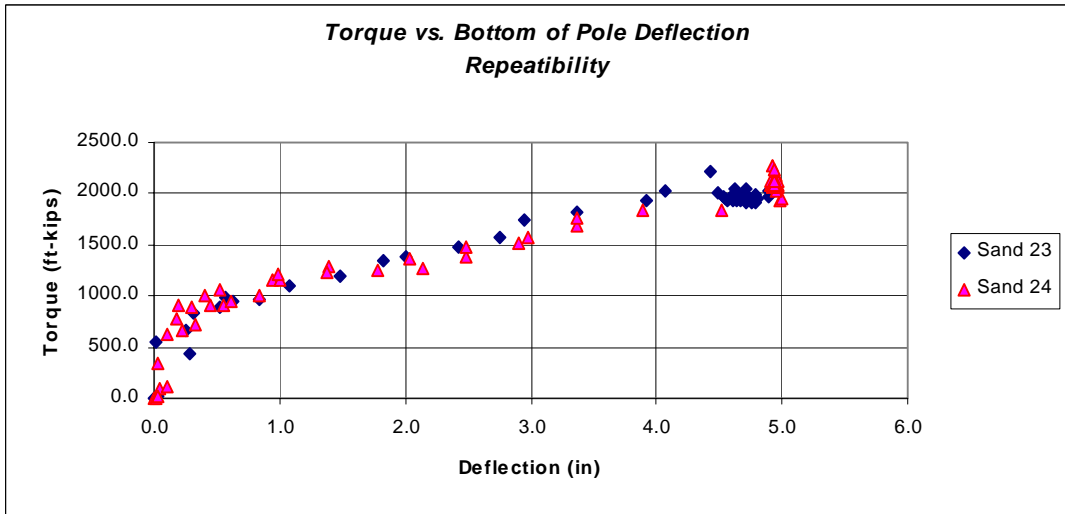
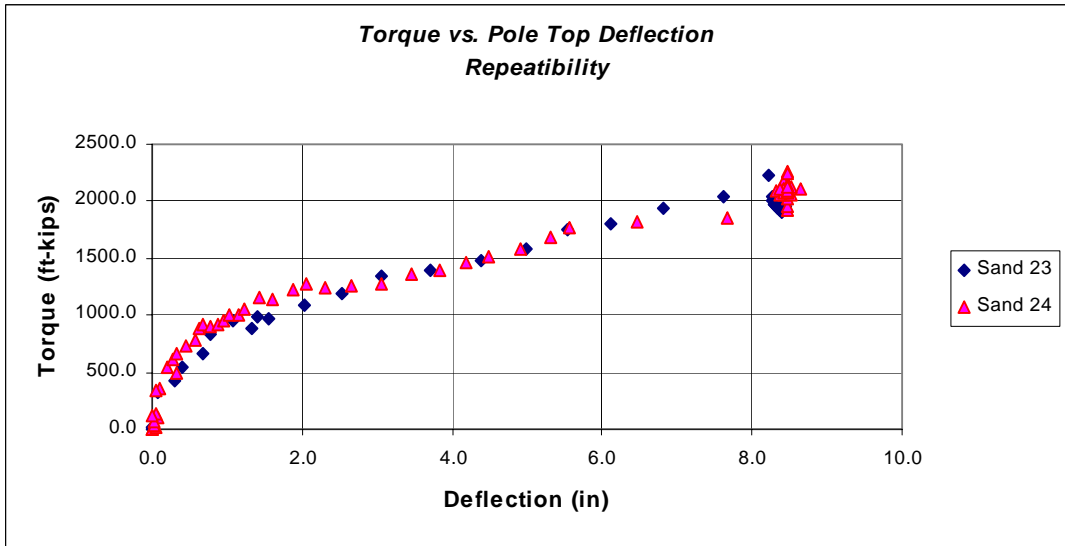
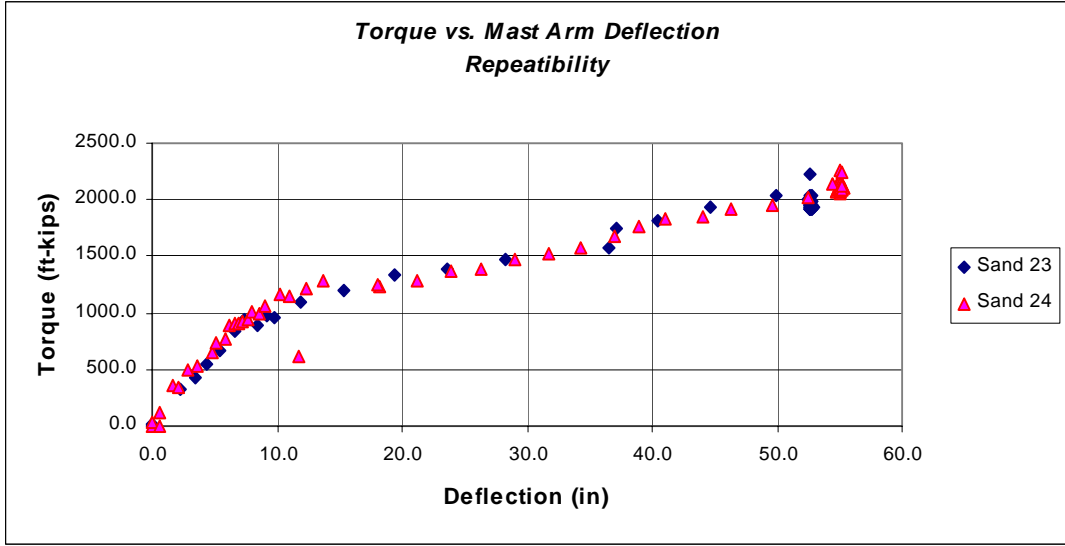


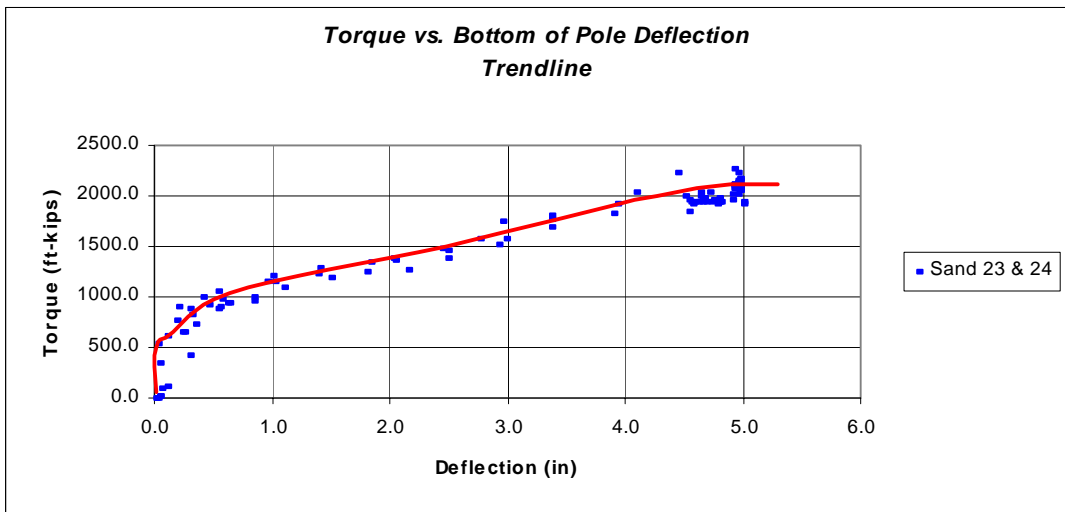
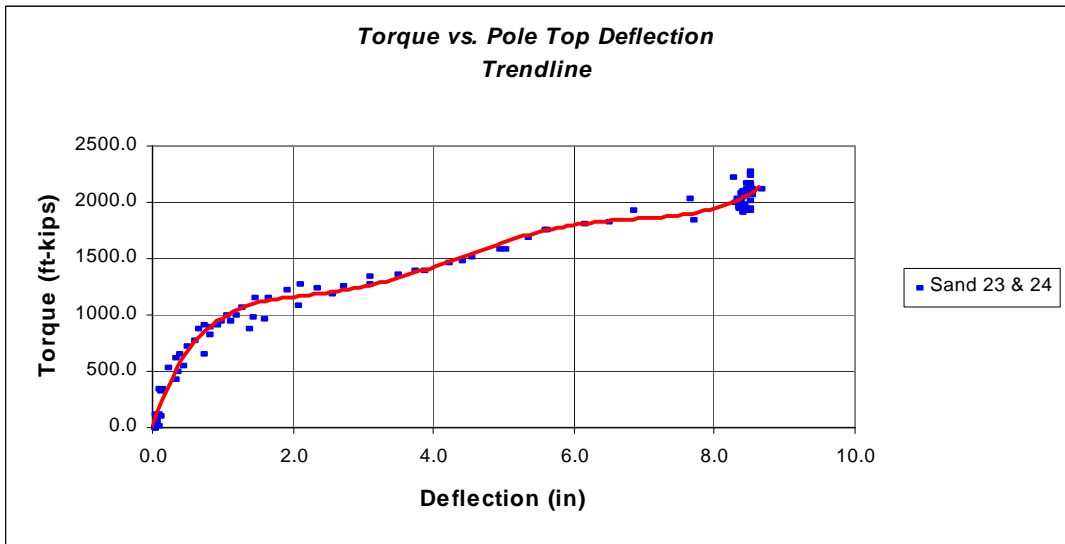
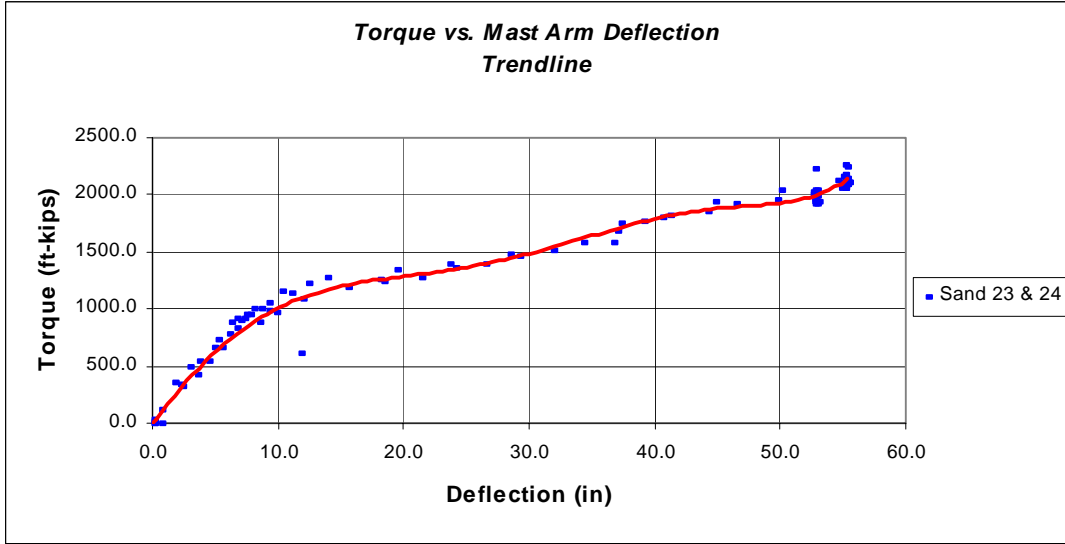




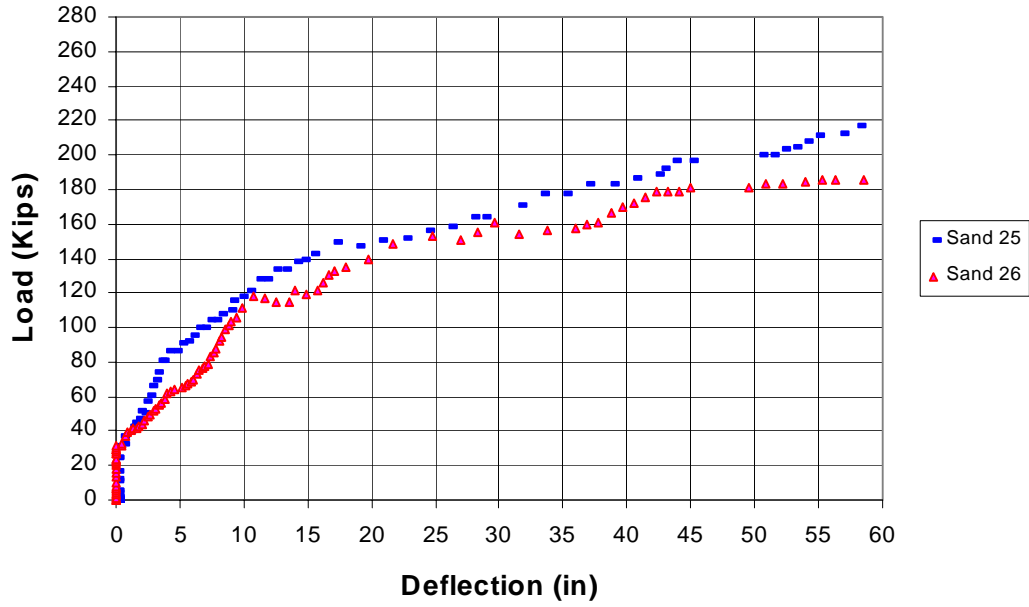




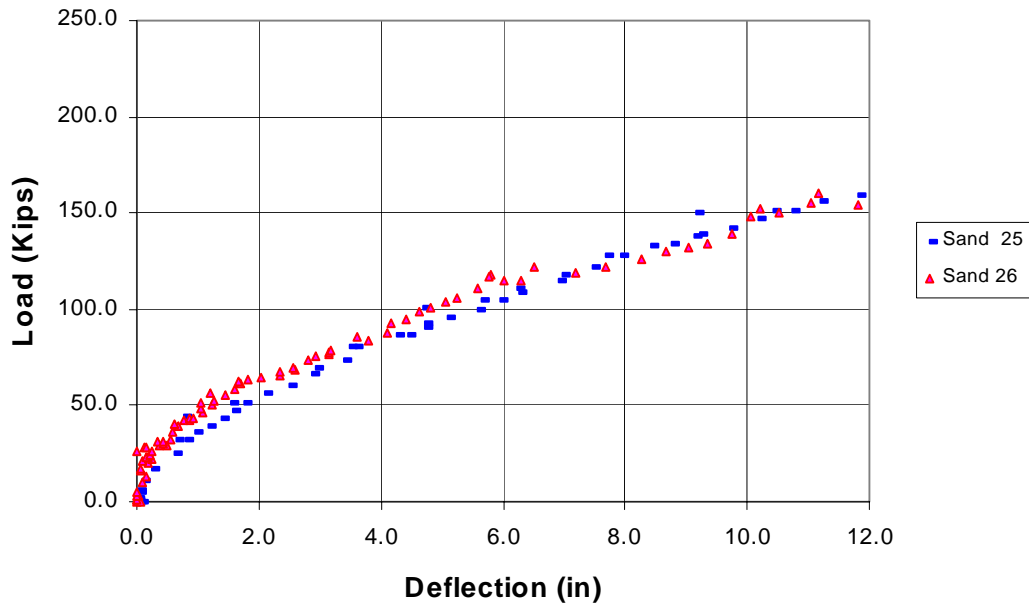


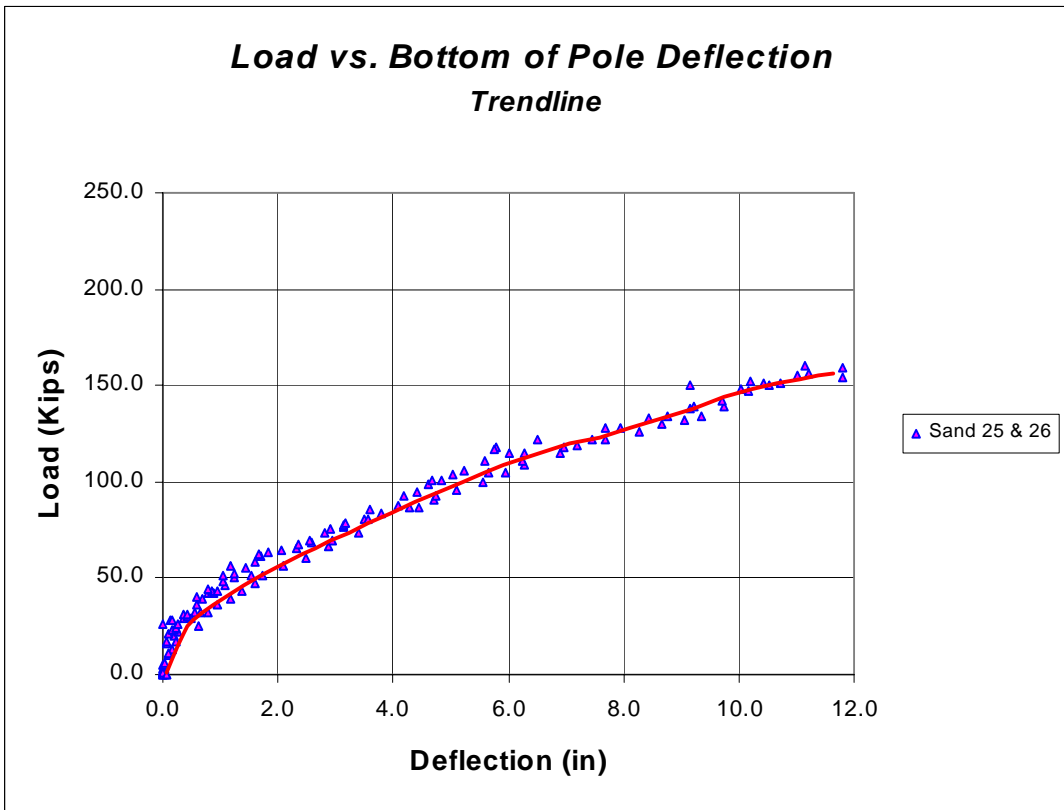
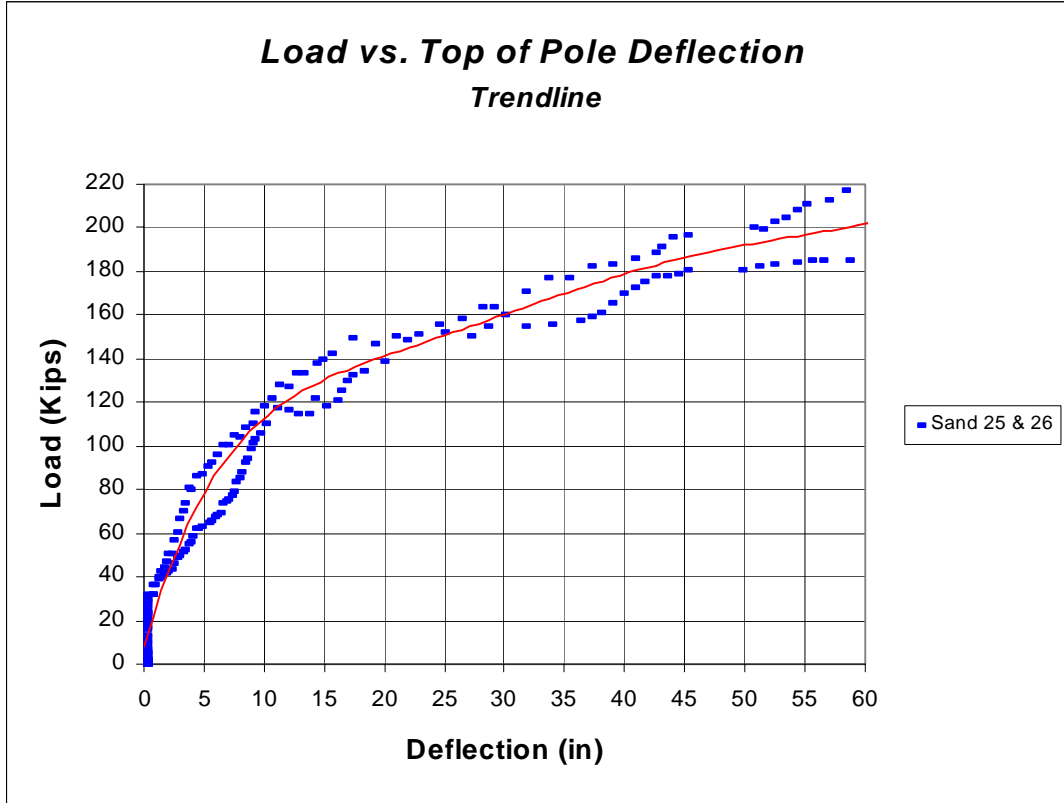


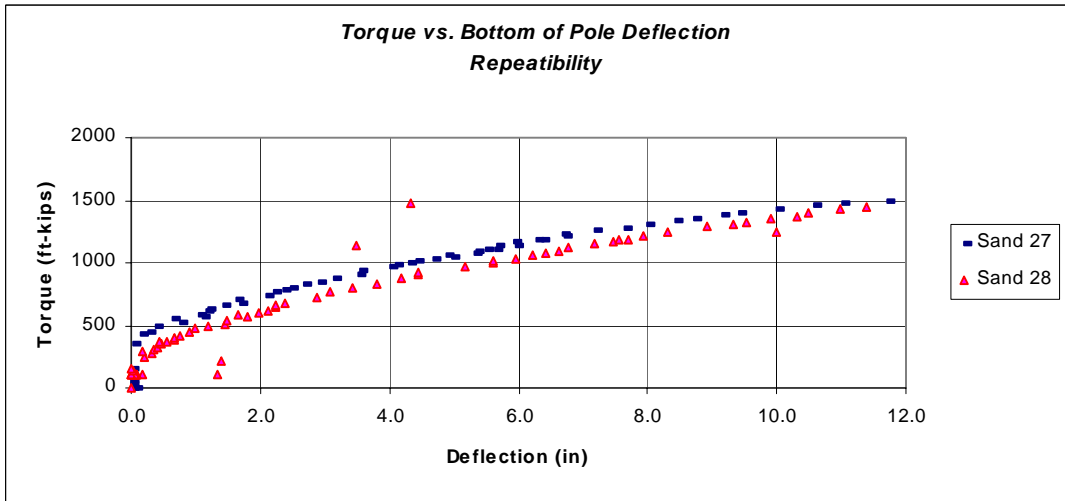
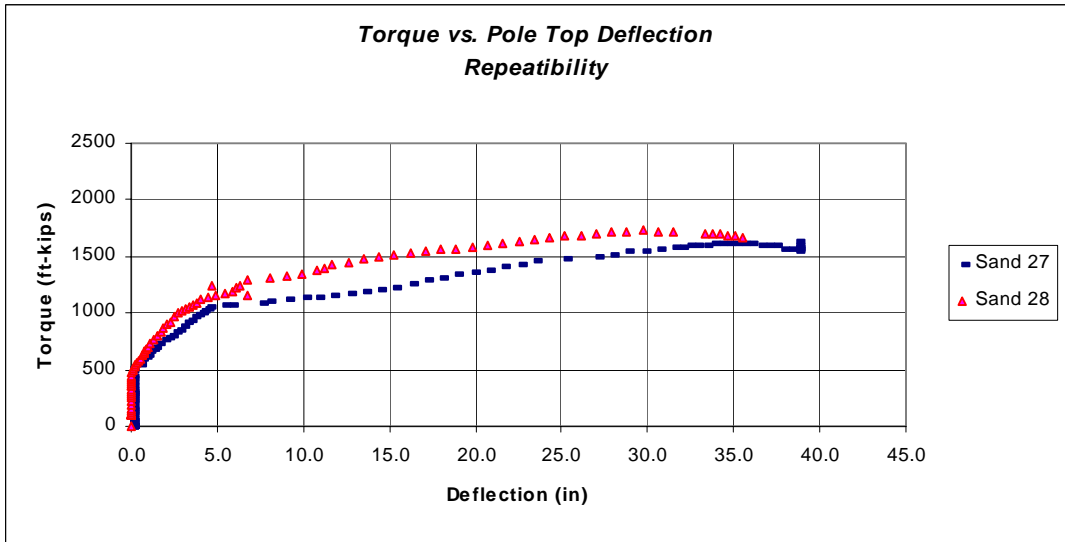
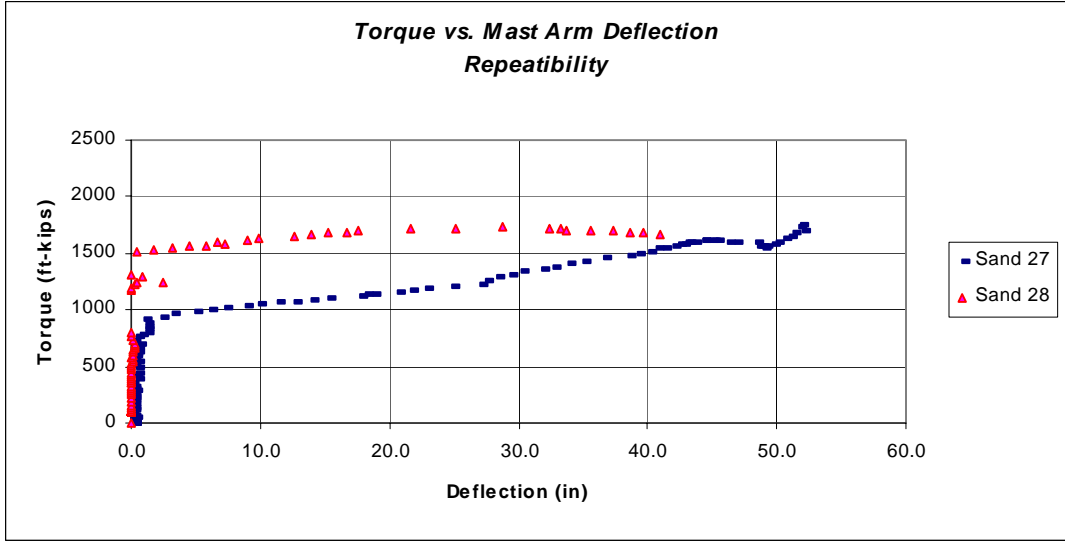
Load vs. Top of Pole Deflection
Repeatability

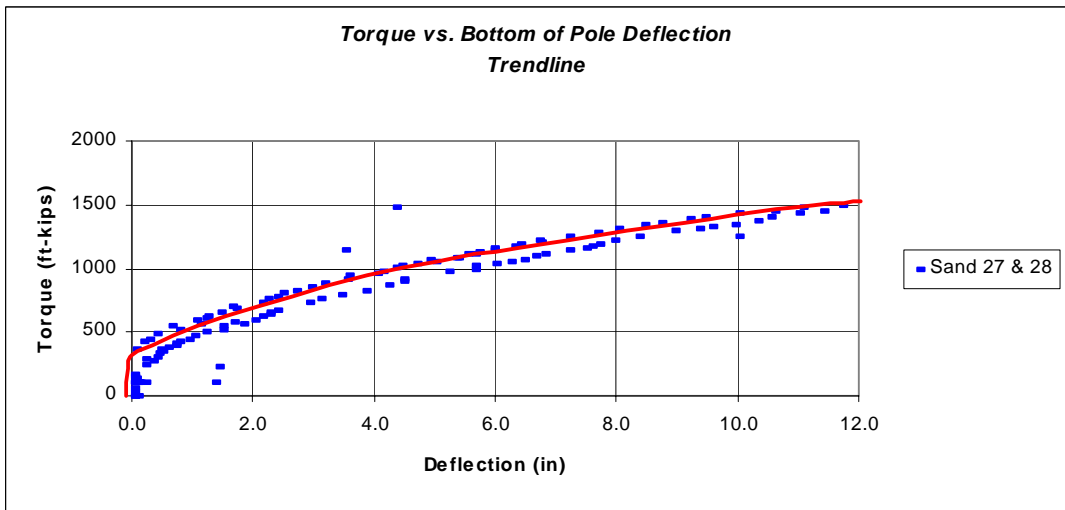
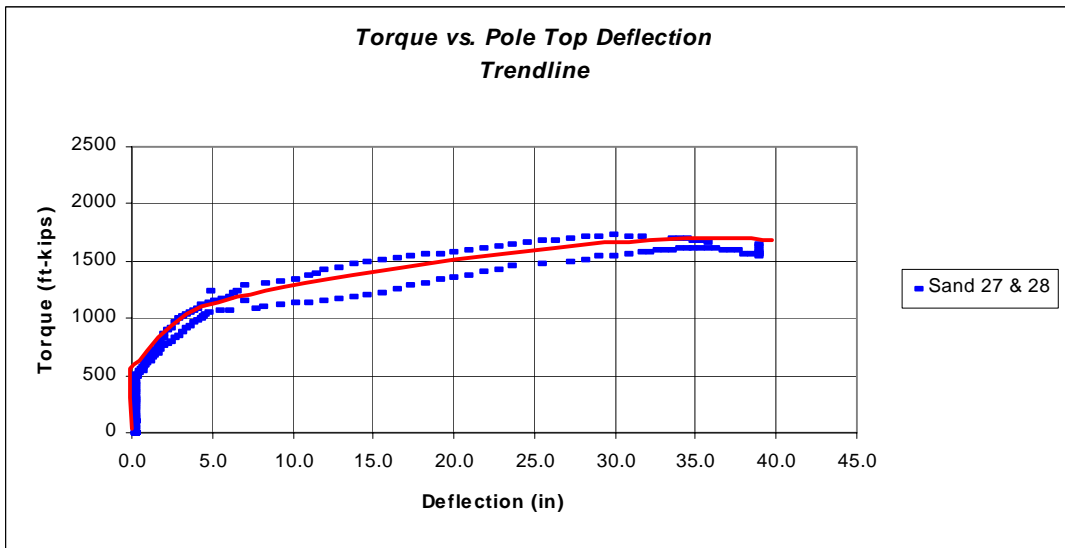
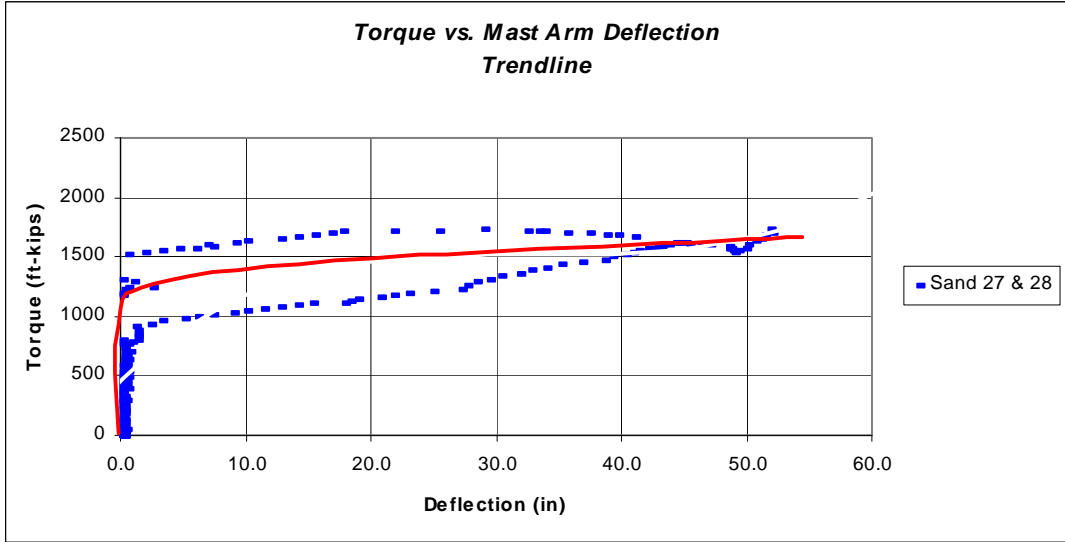


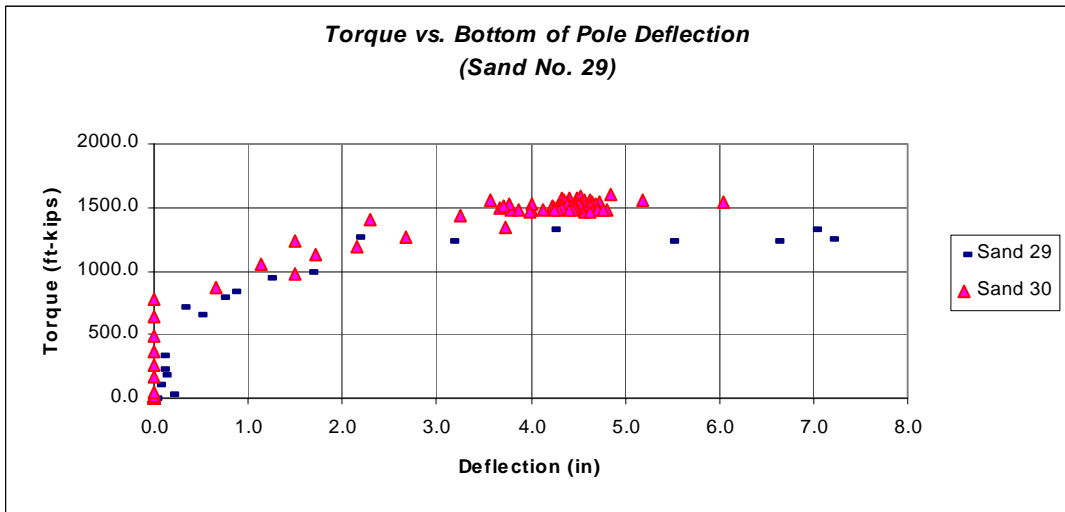
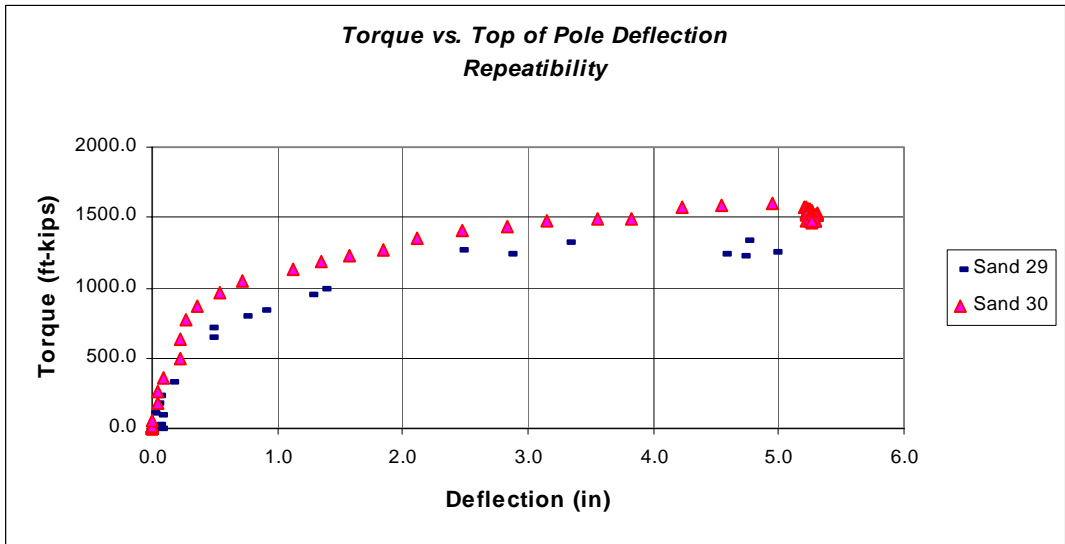
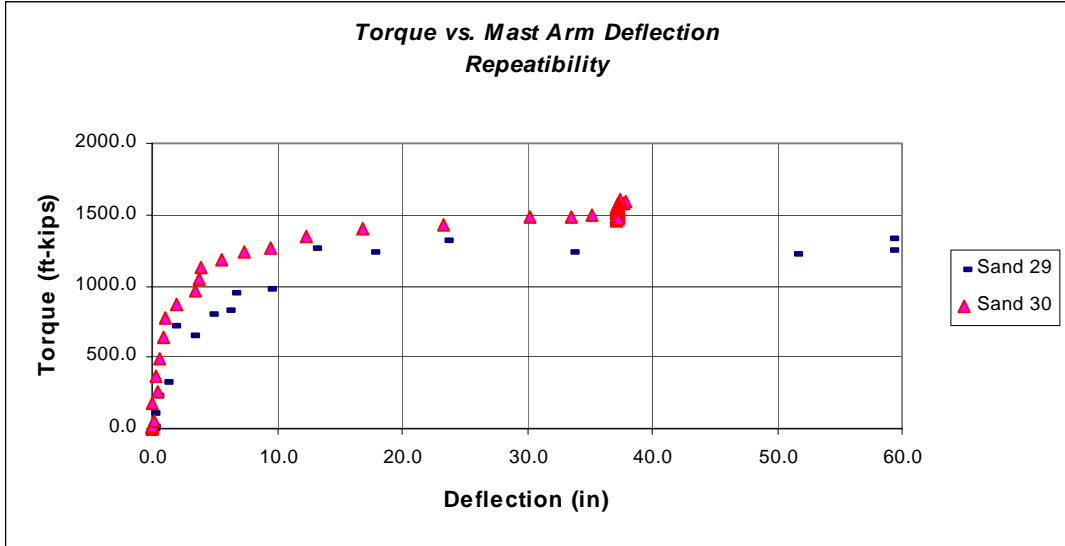
Load vs. Bottom of Pole Deflection
Repeatability

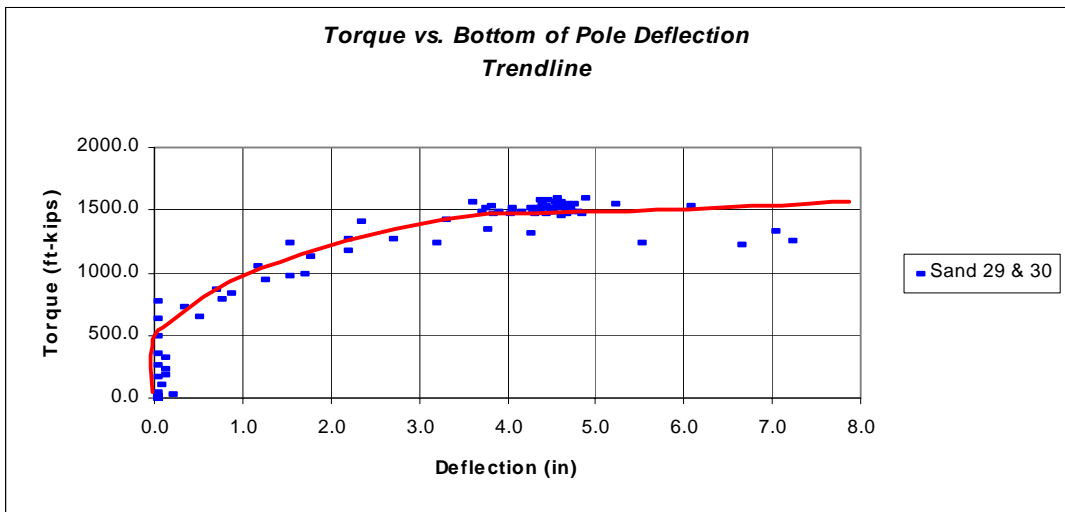
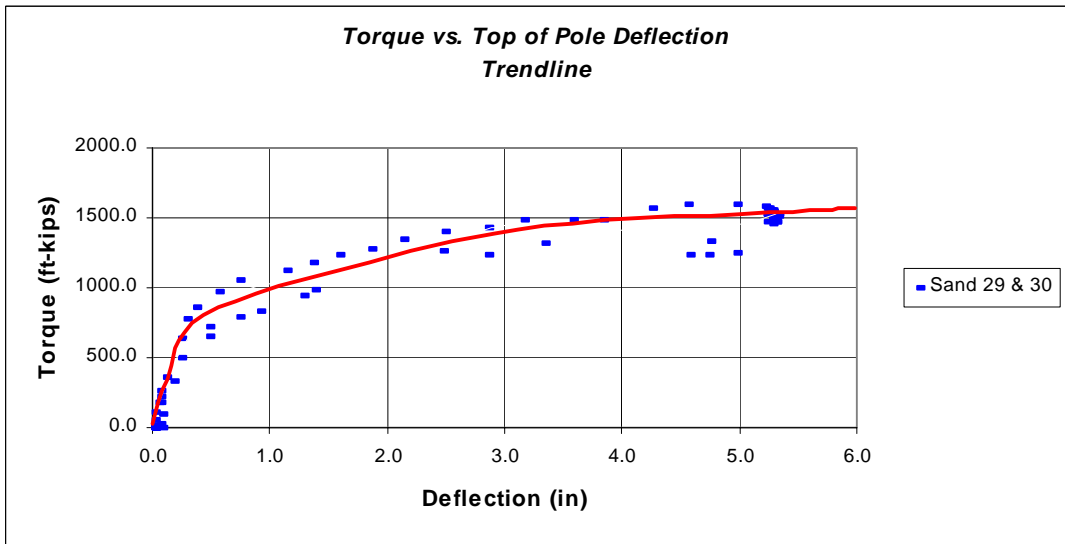
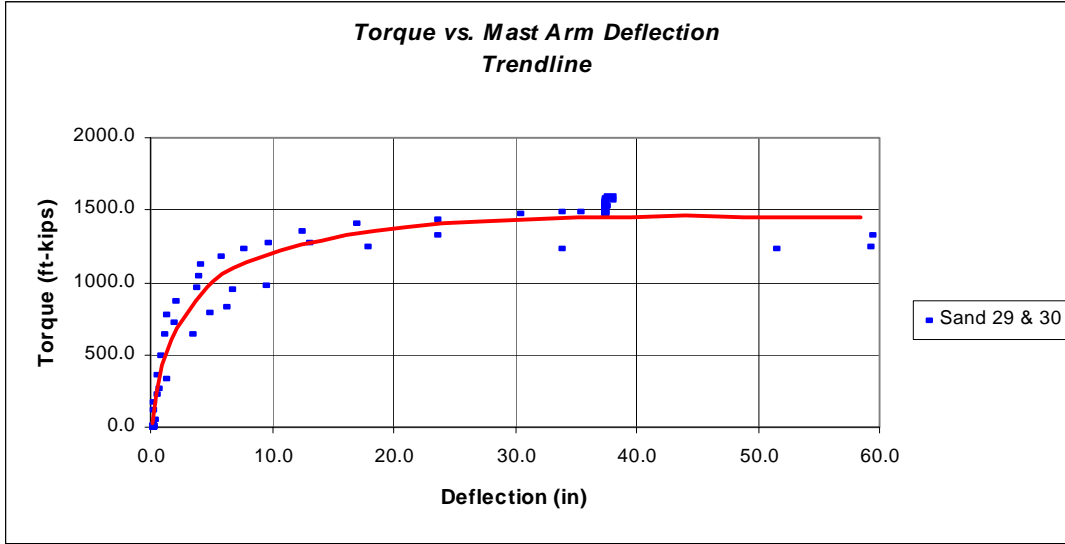


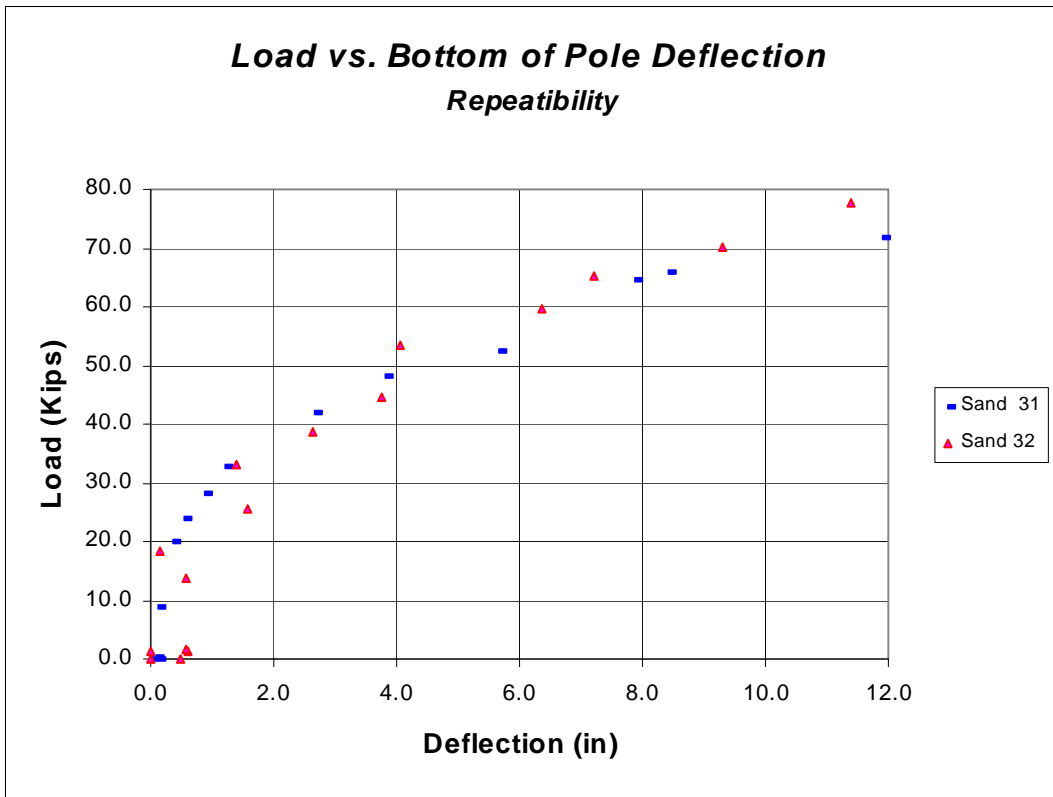
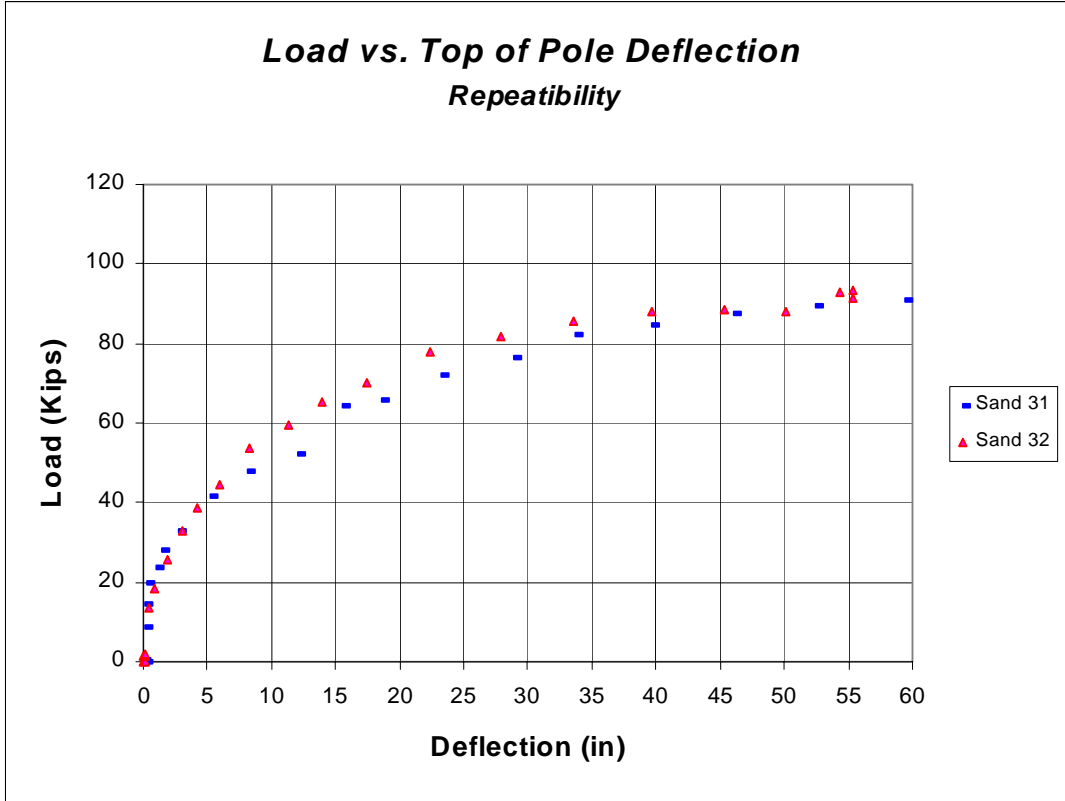




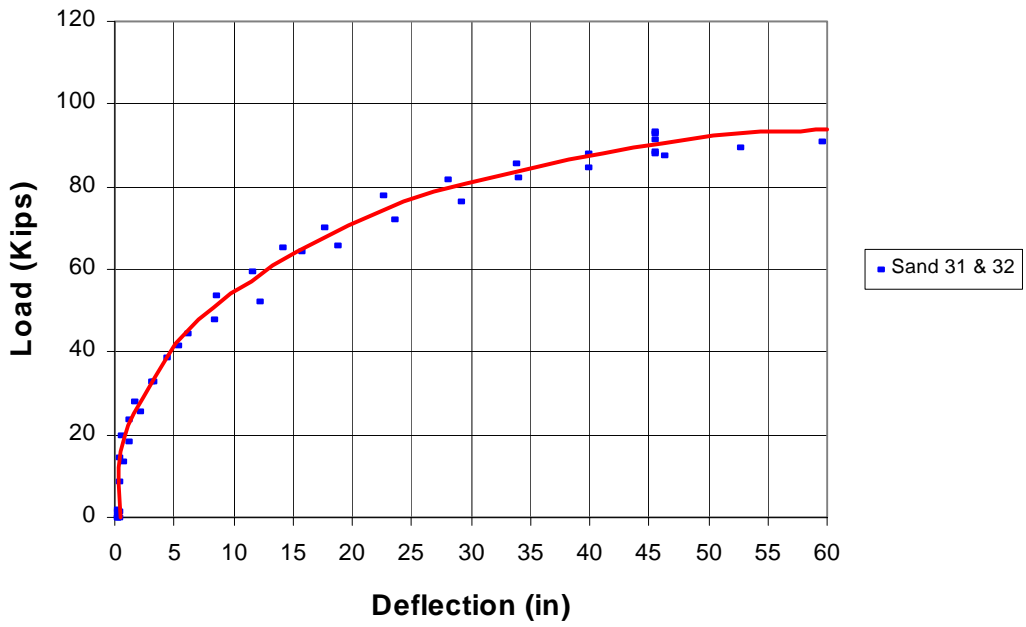








Load vs. Top of Pole Deflection
Trendline



Load vs. Bottom of Pole Deflection
Trendline

